Structural and Mechanistic Studies on Antimicrobial Lipopeptides

by

Stephen Albert Cochrane

A thesis submitted in partial fulfillment of the requirements for the degree of

Doctor of Philosophy

Department of Chemistry
University of Alberta

Abstract

The lipopeptides, tridecaptin A_1, tridecaptin B_1 and cerexin A_1 were isolated from *Paenibacillus terrae* NRRL B-30644, *Paenibacillus polymyxa* NRRL B-30507 and *Bacillus mycoides* ATCC 21929, respectively. A combination of chemical synthesis, peptide derivatization, high performance liquid chromatography and nuclear magnetic resonance was used to elucidate the absolute stereochemistry of these peptides, which were not known prior to this work. Furthermore, new cerexin analogues bearing a succinyl group on the lysine or 4-hydroxylysine residues were isolated from *B. mycoides* ATCC 21929 and fully characterized. A new synthesis of orthogonally protected Fmoc-L-*threo*-4-hydroxylysine has been designed, which is shorter than literature procedures, giving comparable yields and easy access to both the *threo*- and *erythro*-isomers.

Tridecaptin A_1 was found to have strong activity against Gram-negative bacteria. Structural studies revealed the lipid tail could be replaced with octanoic acid, yielding Oct-TriA_1, which is synthetically more accessible and retains all antimicrobial activity. Oct-TriA_1 has strong activity against strains of multidrug resistant Gram-negative bacteria, including *Klebsiella pneumoniae* and *Acinetobacter baumannii*. This peptide is stable to proteases and has low cytotoxicity and hemolytic activity. Activity is retained *in vivo*, increasing the survival rate of mice infected with *Klebsiella pneumoniae*.

An unacylated analogue of tridecaptin A_1, H-TriA_1, has low antimicrobial, hemolytic and cytotoxic activity, but was found to sensitize Gram-negative bacteria to antibiotics typically used for Gram-positive infections. In particular, the activity of rifampicin and vancomycin are increased 512- and 256-fold against *Klebsiella pneumoniae*. It was found that covalently linking H-TriA_1 to erythromycin led to

enhanced activity *in vitro*, greater than that of the synergistic mixture. In contrast to the tridecaptins, the cerexins were found to have poor antimicrobial activity against most bacteria.

An alanine scan was used to identify critical residues in Oct-TriA_1 for antimicrobial activity. We found that D-Dab8 is essential for activity and substitution of this residue destroys the ability of the peptide to adopt a stable defined secondary structure in a model membrane environment. We identified the mode of action of the tridecaptins as disruption of the proton-motive force on the inner-membrane of Gram-negative bacteria. This halts the synthesis of adenosine triphosphate, the essential energy source of the cell, and kills Gram-negative bacteria in approximately 30 min. The tridecaptins bind to lipopolysaccharide on the surface of the outer-membrane and use this anchor to traverse the outer-membrane and enter the periplasm. We also identified the selective binding of tridecaptin A_1 to the Gram-negative analogue of peptidoglycan precursor lipid II, which contains diaminopimelic acid, rather than lysine found in the Gram-positive version. *In vitro* assays were used to show that Gram-negative lipid II significantly enhances the ability of the tridecaptins to disrupt a proton gradient compared to Gram-positive lipid II. This explains the selective activity of the tridecaptins against Gram-negative bacteria. Finally, a solution structure of Oct-TriA_1 was determined by nuclear magnetic resonance, and Gram-negative lipid II modeled into this structure. This preliminary model shows a key interaction between D-Dab8 on Oct-TriA_1 and diaminopimelic acid on lipid II, which is only present in the Gram-negative version.

Preface

The work on tridecaptin A_1 and B_1 in Chapter 2 of this thesis has been published as Lohans et al. *ChemBioChem* **2014**, *15*, 243-249 and Cochrane et al. *Org. Biomol. Chem.* **2015**, *13*, 6073-6081. In both manuscripts, I was responsible for the chemical synthesis of small molecules and peptides, structural elucidation of the lipid tail stereochemistry and most antimicrobial testing. The other authors isolated the peptides, characterized them, sequenced the genomes of the producer strains and performed bioinformatic analyses. I performed approximately 30% of the work in the tridecaptin A_1 manuscript and 70% of the work in the tridecaptin B_1 manuscript, which I also wrote. The structural elucidation of the cerexin analogues has recently been published as Cochrane et al. *Org. Lett.* **2015**, *17*, 5428-5431. Richard Surgenor synthesized orthogonally protected 4-hydroxlysine, activated lipids and the cerexin C analogues and Kevin Khey performed the new synthesis of orthogonally protected 4-hydroxylysine. I conceived the research project, synthesized cerexin A analogues, performed all structural elucidation experiments and prepared the manuscript.

Work described in chapter 3 of this thesis have been published as Cochrane et al. *Int. J. Antimicrobial Agents* **2014**, *44*, 493-499, Cochrane et al. *ChemBioChem* **2014**, *15*, 1295-1299, Cochrane et al. *J. Med. Chem.* **2014**, *57*, 1127-1131 and Cochrane et al. *J. Med. Chem.* DOI:10.1021/acs.jmedchem.5b01578. I was responsible for 100%, 70%, 90% and 90% of the work described in these respective manuscripts. In the *Int. J. Antimicrobial Agents* article on H-TriA_1 synergy, I performed all experiments and wrote the manuscript. In the *ChemBioChem* article on a tridecaptin A_1 alanine scan, I synthesized some peptides, performed circular dichroism experiments and wrote the

manuscript. Other authors performed antimicrobial testing and synthesized the remaining peptides. In the *J. Med. Chem.* article on lipid tail analogues of tridecaptin A_1, I synthesized all peptides, performed most of the antimicrobial testing and wrote the manuscript. Other authors performed antimicrobial testing and hemolytic assays. In the *J. Med. Chem.* article on tridecaptin-antibiotic conjugates, I conceived the project, synthesized all compounds and performed the *in vitro* testing. The other authors performed *in vivo* testing.

A manuscript is currently being prepared based on the work presented in Chapter 4. I performed isothermal titration calorimetry studies, most chemical synthesis, some mode-of-action assays and all nuclear magnetic resonance experiments and docking studies. Dr. Brandon Findlay performed most mode-of-action assays whilst Ms. Eva Rodriguez-Lopez and Mr. Alireza Bakhtiary assisted me in chemical synthesis.

Acknowledgements

Having arrived at the end of a five and a bit year journey, it is somewhat of an understatement to say I have multiple people to thank for their help during this time. Without the amazing support staff in our department, my research certainly would not have progressed at the speed it did. Therefore I would like to thank Wayne Moffat and his staff from the Analytical Laboratory, Gareth Lambkin of Biological Services, Dr. Randy Whittal, Dr. Angie Morales, Bela Reiz and Jing Zheng from the Mass Spec lab, Dr. Ryan McKay and Mark Miskolzie from the NMR facilities, all of the general office staff and the stores guys for their invaluable assistance over the years.

I have had the pleasure of collaborating with several amazing Vederas group members and summer students, and would like to thank Dr. Zedu Huang, Dr. Chris Lohans, Dr. Marco van Belkum, Dr. Brandon Findlay, Manon Bels, Richard Surgenor and Kevin Khey for helping me with my research. I would also like to thank Jeella Acedo, Randy Sanichar and Dr. Conrad Fischer for reading this mountain of a thesis. A special mention goes to Dr. David Dietrich, whose infectious appetite for science was contagious during his time in our group. I thank Dr. Justin Thuss, Shaun McKinnie and Rachel Cochrane for walking this path with me, and the countless ideas and suggestions they have contributed throughout my PhD.

It goes without saying that I am indebted to my supervisor Dr. John Vederas for providing me with a platform to build from and the freedom to pursue my research. His help and guidance has proved invaluable during my years as a graduate student and as a scientist he has inspired me to succeed.

Outside of work there have been multiple people supporting me reach my hopes

and dreams. Obviously I thank my family for all of their support, but In particular I want to thank my mother, who showed me the meaning of hard work through her sacrifices over the years to provide for her family. I thank my life-long friends, Steven McGuinness and Niall Dalton for all the banter over the years, and my old undergraduate housemates Daniel Critchlow, Alex Mateer, Kyle Hepburn and Eoin Duffy for making my undergraduate years so enjoyable.

Without a doubt, the person I owe the most gratitude too in my life is my beautiful wife, Rachel Cochrane. As a fellow graduate student, she has walked this path with me every step of the way, supporting me constantly through all the challenges and difficulties I have faced. Everyday she continues to make me a better person and I look forward to her constant support through the rest of my life. I also want to thank my beautiful son Caleb for lighting up my world. In those days and weeks where nothing seemed to work in the lab, your smile and laugh and unconditional love have lifted me up. You inspire me to succeed and I will work tirelessly to give you the best possible future I can.

Finally, I want to thank God for blessing me with such a wonderful life and career. When I have walked, he has walked with me and when I have been too weak, he has carried me. All of my success and achievements are by his grace and I am honored to have a career in which I study his creation.

“For since the creation of the world God’s invisible qualities - his eternal power and divine nature - have been clearly seen, being understood from what has been made, so that people are without excuse.”

Table of contents

List of tables

List of figures

List of schemes

List of abbreviations

A-site	Aminoacyl site
Aaa	1-Adamantaneacetic acid
aaRS	Aminoacyl tRNA synthetase
ABC	Adenosine-binding cassette
Abu	Aminobutyric acid
Agl	Allylglycine
Alloc	Alloxycarbonyl
AM	Acetoxymethyl ester
ANS	8-Anilino-1-naphthalenesulfonic acid
Apa	1-Anthracenylpropionic acid
ATP	Adenosine triphosphate
ATTC	American Type Culture Collection
BaCWAN	Bacterial Cell Wall Biosynthesis Network
BCECF	2',7'-Bis(carboxyethyl)-5(6)-carboxyfluorescein
BCFA	Branched chain fatty acid
Bio	Biotin
Boc	*tert*-Butyloxycarbonyl
BSA	Bovine serum albumin
CDC	Centre for disease control and prevention
CDMT	2-Chloro-4,6-dimethoxy-1,3,5-triazine
CLSI	Clinical and laboratory standards institute
CRKP	Carbapenem resistant *Klebsiella pneumoniae*

CuAAC	Copper-catalyzed azide-alkyne cycloadditon
Cxn	Cerexin
CYANA	Combined assignment and dynamics algorithm for NMR applications
Dab	2,4-Diaminobutyric acid
DAP	Diaminopimelic acid
DBU	1,8-Diazabicycloundec-7-ene
DCC	*N*,*N*′-Dicyclohexylcarbodiimide
DdlA	D-Ala–D-Ala ligase
Dha	Dehydroalanine
DiBAC$_4$(3)	Bis-(1,3-dibutylbarbituric acid) trimethine oxonol
DIPEA	*N,N*-Diisopropylethylamine
DMAP	4-Dimethylaminopyridine
DMF	*N,N*-Dimethylformamide
DMSO	Dimethylsulfoxide
DNA	Deoxyribonucleic acid
DPC	Dodecylphosphocholine
E-site	Exit site
EDCI	1-Ethyl-3-(3-dimethylaminopropyl)carbodiimide
EDTA	Ethylenediaminetetraacetic acid
EF-G	Elongation factor G
Erm	Erythromycin ribosomal methylase
FDA	Food and Drug Administration

Fmoc	Fluorenylmethyloxycarbonyl
Fpa	Fluorenylpropionic acid
G-LII	Gram-negative lipid II
G+LII	Gram-positive lipid II
GCMS	Gas chromatography mass spectrometry
GI	Gastrointestinal
GlcNAc	*N*-Acetylglucosamine
H1N1	Influenza A virus subtype H1N1
HATU	1-[Bis(dimethylamino)methylene]-1*H*-1,2,3-triazolo[4,5-*b*]pyridinium 3-oxid hexafluorophosphate
HBTU	*N,N,N′,N′*-Tetramethyl-*O*-(1*H*-benzotriazol-1-yl)uronium hexafluorophosphate
HEK	Human embryonic kidney
HIC	Hydrophobic interactions chromatography
HOBt	1-Hydroxybenzotriazole
HPLC	High performance liquid chromatography
Hyl	Hydroxylysine
IPA	2-propanol
IR	Infrared
ITC	Isothermal titration calorimetry
kDa	Kilo daltons
LPS	Lipopolysaccharide
LUV	Large unilamellar vesicle

MDR	Multidrug resistant
MFS	Major facilitator superfamily
MHB	Mueller-Hinton broth
MIC	Minimum inhibitory concentration
MMD	Maximum MIC decrease
MraY	UDP-MurNAc-pentapeptide phosphotransferase
mRNA	Messenger RNA
MRSA	Methicillin resistant *Staphylococcus aureus*
MS	Mass spectrometry
Ms	Mesyl
MTT	3-(4,5-Dimethylthiazol-2-yl)-2,5-diphenyltetrazolium bromide
MurA	UDP-GlcNAc enolpyruvyl transferase
MurB	UDP-MurNAc dehydrogenase
MurC	UDP-MurNAc-L-Ala ligase
MurD	UDP-MurNAc-L-Ala-D-Glu ligase
MurE	UDP-MurNAc-L-Ala-D-Glu-*meso*-Dap ligase
MurF	UDP-MurNAc-tripeptide-D-alanyl-D-Ala ligase
MurG	UDP-GlcNAc-undecaprenyl-pyrophosphoryl-MurNAc-pentapeptide transferase
MurNAc	*N*-acetylmuramic acid
Mw	Molecular weight
NCTC	National Collection of Type Cultures
NMM	*N*-Methylmorpholine

NMP	*N*-Methyl-2-pyrrolidone
NMR	Nuclear magnetic resonance
NOE	Nuclear overhauser effect
NOESY	Nuclear overhauser effect spectroscopy
NRPS	Non-ribosomal peptide synthetase
NRRL	Northern Regional Research Laboratory
OD	Optical density
ONPG	*Ortho*-nitrophenyl-β-galactoside
P-site	Peptidyl site
PBP	Penicillin-binding protein
PBS	Phosphate buffered saline
PEG	Polyethylene glycol
PEP	Phosphoenolpyruvic acid
PMBN	Polymyxin B nonapeptide
PolyB	Polymyxin B
PyBOP	(Benzotriazol-1-yloxy)tripyrrolidinophosphonium hexafluorophosphate
RMSD	Root mean square deviation
RNA	Ribonucleic acid
rRNA	Ribosomal RNA
S	Svedberg
SAR	Structure activity relationship
SPPS	Solid-phase peptide synthesis

Su	Succinimide
TB	Tubercolosis
TBAF	Tetra-*n*-butylammonium fluoride
TCEP	Tris(2-carboxyethyl)phosphine hydrochloride
TFA	Trifluoroacetic acid
TIPS	Triisopropylsilane
TMS	Trimethylsilyl
TOCSY	Total correlation spectroscopy
TPS	*tert*-Butyldiphenylsilyl
Tri	Tridecaptin
tRNA	Transfer RNA
Troc	2,2,2-Trichlorethoxycarbonyl
Ts	Tosyl
UDP	Uracil diphosphate
UP	Undecaprenyl phosphate
UPP	Undecaprenyl pyrophosphate
UppP	Undecaprenyl pyrophosphate phosphatase
USDA	United States Department of Agriculture
UV	Ultraviolet
Vgl	Vinylglycine
VRE	Vancomycin-resistant Enterococci
XMR	Extremely multidrug resistant
ΔpH	Proton gradient

$\Delta\psi$	Electric potential

Chapter 1

Antibiotics – Types, targets and trails ahead

"If we are not careful, we will soon be in a post-antibiotic era… and for some patients and for some microbes, we are already there." – CDC, 2013

1. Introduction

1.1. Bacteria – The good and the bad

There are ten times more bacterial cells present in our bodies than human cells.[1] The human body is a complex ecosystem inhabited by trillions of bacteria and other microorganisms (known as the microbiome), mostly found in our mouth, skin and intestines. We begin life as sterile beings in our mother's womb but by late infancy have developed one of the most complex microbial ecosystems on the planet. In fact, genetic analysis has revealed that no two individuals have the same microbiome, not even identical twins.[2] These bacteria are essential to many of our physiological processes, including digestion, growth and our immune response. One such example is the bacterial species *Bacteroides thetaiotaomicron*, which is found in our intestinal tract.[3] It produces enzymes not encoded in the human genome that allow us to digest complex carbohydrates from many plant-based foods. We have a long and happy symbiotic relationship with many types of bacteria; however, there are unwelcomed guests to the party.

Pathogenic microorganisms are infectious microbes that cause disease in their host organism and include bacteria, fungi, protozoa, viruses and viroids. Less than 1 % of bacteria cause disease in humans, and illnesses can range from often minor

ailments, such as food poisoning, to deadly infections like tuberculosis (TB). Throughout human history, bacterial pandemics have decimated our population, with the Black Death being one of the most devastating. Caused by the Gram-negative bacterium *Yersinia pestis*, this disease killed between 75 million and 200 million people between 1346 and 1353.[4] Another example is the 1918 flu pandemic (Spanish Flu), which killed 50 to 100 million people. Recent research has shown that the H1N1 influenza virus was not the main cause of these deaths, and that most victims died from bacterial pneumoniae.[5] As society progressed, so did our ability to treat these infections. Popular treatments during the time of the black plague included bloodletting with leeches to remove bad blood, washing in urine, and strapping a shaved (and still clucking) chicken to one's neck to remove the infection. Other cultures had more effective treatments for bacterial infections, including the use of molds, soils and plants, which we now know produced antibiotic compounds.

1.2. Antibiotics

Antibiotic literally means "life-killing," although it is now used synonymously with antibacterial and refers to a compound that kills bacteria. In 1928 Alexander Fleming serendipitously discovered the first antibiotic on a discarded *Staphylococcus* culture plate.[6] He found that a *Penicillium notatum* mold had grown on this plate overnight and that the areas surrounding the mold were devoid of bacteria. This was due to the production of Penicillin G, whose structure was later determined by Dorothy Hodgkin in 1945. The discovery of penicillin initiated a golden era in antibiotic development that lasted for 40 years and produced a large majority of the antibiotic classes we use today.

However, by the early 1970s this golden era ended, and since then there have only been six new classes of antibiotics approved for clinical use.[7] Two of these, mupirocin (1985) and retapamulin (2007) are topical, meaning they can only be used for treating open wounds and skin conditions. The remaining four classes, linezolid (2000), daptomycin (2003), fidaxomicin (2010) and bedaquiline (2012), are all capable of treating systemic infections, but are not effective in the treatment of infections by Gram-negative bacteria.

Gram-positive and Gram-negative bacteria differ in the composition of their cell walls and membranes, and can therefore be distinguished by a Gram stain.[8] Both types of bacteria have the same basic makeup, including a plasma membrane that encapsulates the nucleoid and other cytoplasmic components (Figure 1.1). Gram-positive bacteria have a thick layer of peptidoglycan, a sugar and amino acid polymer that contains many crosslinks. In contrast, Gram-negative bacteria have a much thinner layer of peptidoglycan. However, Gram-negative bacteria have an extra layer of defense in the form of the outer-membrane. This acts as an impermeable barrier to many negatively charged and hydrophobic antibiotics, and is a major hurdle that needs to be cleared for an antibiotic to be effective against Gram-negative bacteria. Furthermore, Gram-negative bacteria have multiple efflux pumps, which remove foreign compounds, as well as enzymes that modify antibiotics and their targets.[9,10,11] All of these factors make the design of antibiotics that target Gram-negative bacteria extremely difficult, and it is therefore no surprise that a large number of current antibiotics are only useful for infections caused by Gram-positive bacteria.

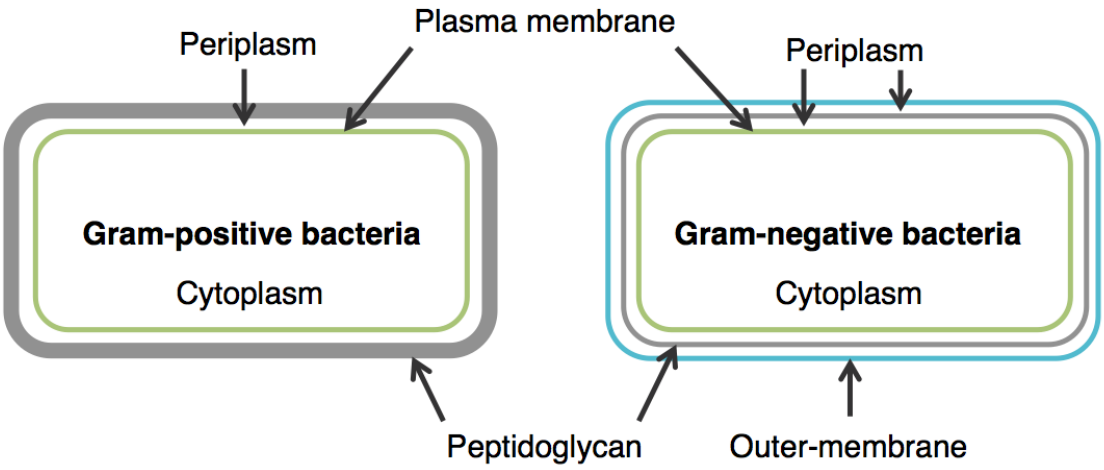

Figure 1.1. Some of the membrane differences between Gram-positive and Gram-negative bacteria.

1.3. Antibiotic Targets

Antibiotics can be bacteriostatic or bactericidal. Bacteriostatic agents halt the growth of bacteria but do not reduce the viable cell population. Bactericidal compounds kill bacteria, but do so at different rates depending on their mode of action. This allows antibiotics to be broadly classified according to the cellular processes that they inhibit. The major antibiotic targets are peptidoglycan biosynthesis, protein-synthesis, nucleic acid synthesis and the cell membrane. These classes can be further divided into structural classes of antibiotics and representative examples of antibiotics are summarized in table 1.

Cellular Target	Structural Classification	Representative Examples
Cell wall synthesis (Figure 1.2)	β-Lactams	Penicillins – Penicillin G (**1**) and ampicillin (**2**) Monobactems – Aztreonam (**3**) Carbapenems – Imipenem (**4**) Cephalosporins – Cephalexin (**5**)
	Cyclic peptides	Bacitracin (**6**)
	Glycopeptides	Dalbaheptides – Vancomycin (**7**)
	Lantibiotics	Nisin (**8**) and gallidermin (**9**)
	Others	Fosfomycin (**10**) D-cycloserine (**11**)
Protein synthesis (Figure 1.4)	Aminoglycosides	Streptomycin (**12**)
	Lincosamides	Lincomycin (**13**)
	Macrolactones	Macrolides – Erythromycin (**14**)
	Oxazolidinones	Linezolid (**15**)
	Pleuromutilins	Retapamulin (**16**)
	Tetracyclines	Tetracycline (**17**)
	Thiazoyl peptides	Thiostrepton (**18**)
	Monooxycarbolic acids	Mupirocin (**19**)
Nucleic acid synthesis (Figure 1.6)	Aminocoumarin	Novobiocin (**20**)
	Ansamycins	Rifampicin (**21**)
	Fluoroquinolones	Ciprofloxacin (**22**)
	Macrolactones	Fidaxomicin (**23**)
Cell membrane (Figure 1.7)	Cyclic peptides	Polymyxin B (**24**) and daptomycin (**25**)
Others (Figure 1.9)	Diarylquinolone	Bedaquiline (**26**)

Table 1.1. Examples of antibiotics according to the cellular process they target and their structural classification.

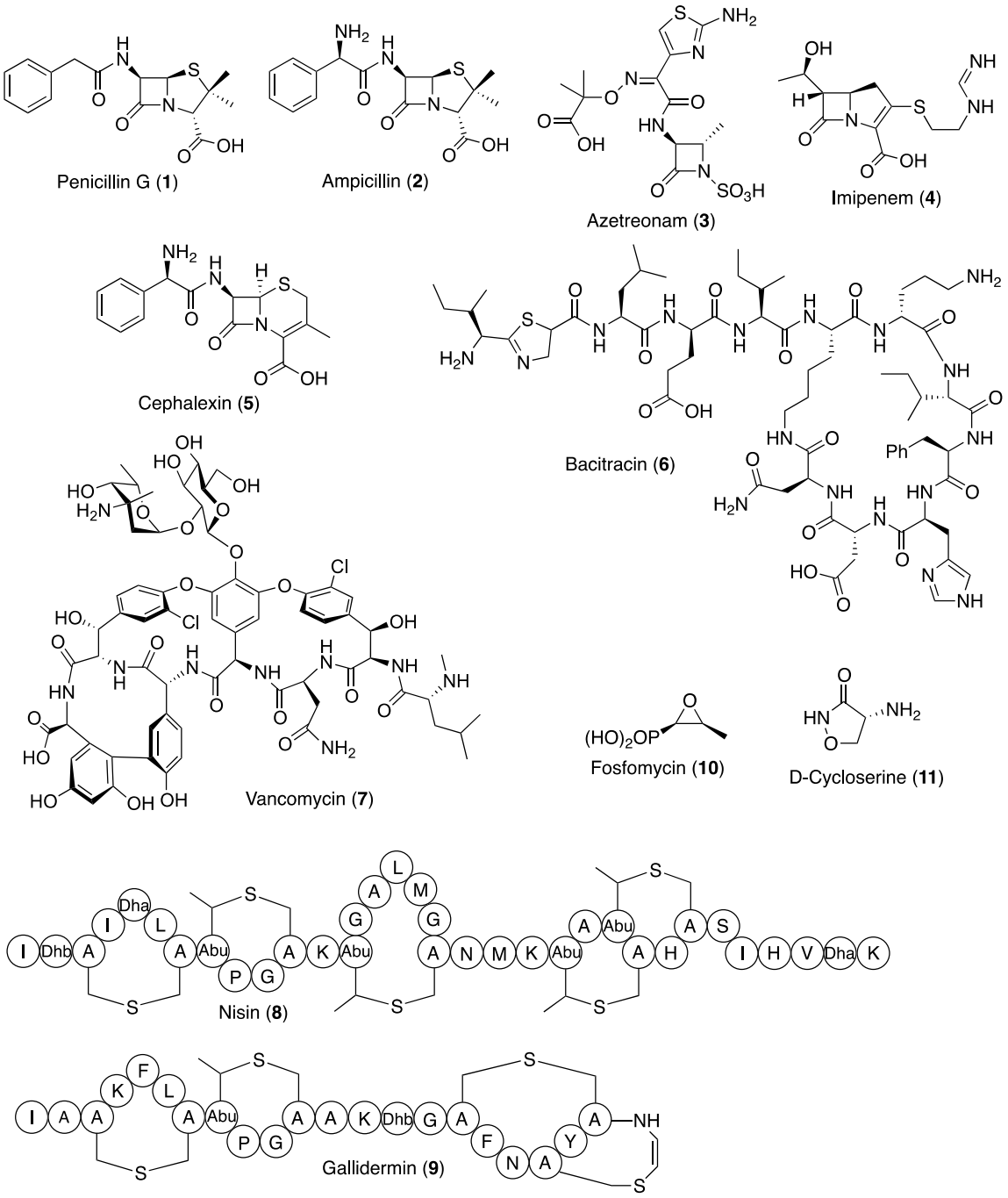

Figure 1.2. Clinically approved antibiotics that target cell wall biosynthesis.

1.3.1. Peptidoglycan biosynthesis inhibitors

Peptidoglycan is an essential component present in bacterial cell walls, and the enzymes and intermediates involved in its biosynthesis are common targets for antibiotics. Disruption of peptidoglycan biosynthesis diminishes the structural integrity of the cell, eventually leading to cell death. Furthermore, as human cells do not produce peptidoglycan, compounds that target this pathway are usually non-toxic to humans. Peptidoglycan biosynthesis begins in the cytoplasm with the biosynthesis of lipid II, a pentapeptidyl disaccharide (Figure 1.3). Uracil diphosphate (UDP) activated *N*-acetyl-D-glucosamine (GlcNAc) is converted into UDP activated *N*-acetyl-D-muramic acid (MurNAc) by the action of MurA and MurB.[12] MurC then ligates alanine to MurNAc, followed by the addition of D-glutamic acid by MurD. MurE ligates either lysine (most Gram-positive bacteria) or *meso*-diaminopimelic acid (DAP, Gram-negative bacteria) to the side chain of glutamic acid. Next, a D-Ala-D-Ala dipeptide, pre-synthesized by DdlA, is ligated onto the tripeptidyl monosaccharide to complete the pentapeptide chain. MraY anchors this intermediate to the interior of the inner-membrane yielding lipid I, which is then converted to lipid II by MurG. To continue peptidoglycan biosynthesis, lipid II is then flipped (by a flippase) to the exterior of the inner-membrane, where it is further processed by penicillin-binding proteins to produce peptidoglycan.

As peptidoglycan is essential for the structural integrity of bacteria, inhibiting its biosynthesis has a bactericidal effect, typically killing cells a few hours after treatment. Figure 1.3 summarizes peptidoglycan biosynthesis and shows the enzymes or intermediates inhibited by the antibiotics listed under the peptidoglycan section of Table 1.1. The β-lactams are a large class of antibiotics that can be subdivided into penicillins

(e.g. **1**), monobactems (e.g. **3**), carbapenems (e.g. **4**) and cephalosporins (e.g. **5**), according to their molecular structure.[13] Almost all β-lactams disrupt peptidoglycan biosynthesis by irreversibly binding to the active-site of penicillin-binding proteins (PBPs). The β-lactam core is recognized by DD-transpeptidases and bound to an active-site serine, preventing the crosslinking of peptidoglycan and eventually leading to cell death.[13] Most β-lactams are not active against Gram-negative organisms. Bacitracin (**6**) is a cyclic non-ribosomally synthesized peptide produced by *B. subtilus*. It is highly toxic if taken internally so is therefore used as a topical antibiotic.[14] Bacitracin disrupts peptidoglycan biosynthesis by binding to undecaprenyl pyrophosphate (UPP)

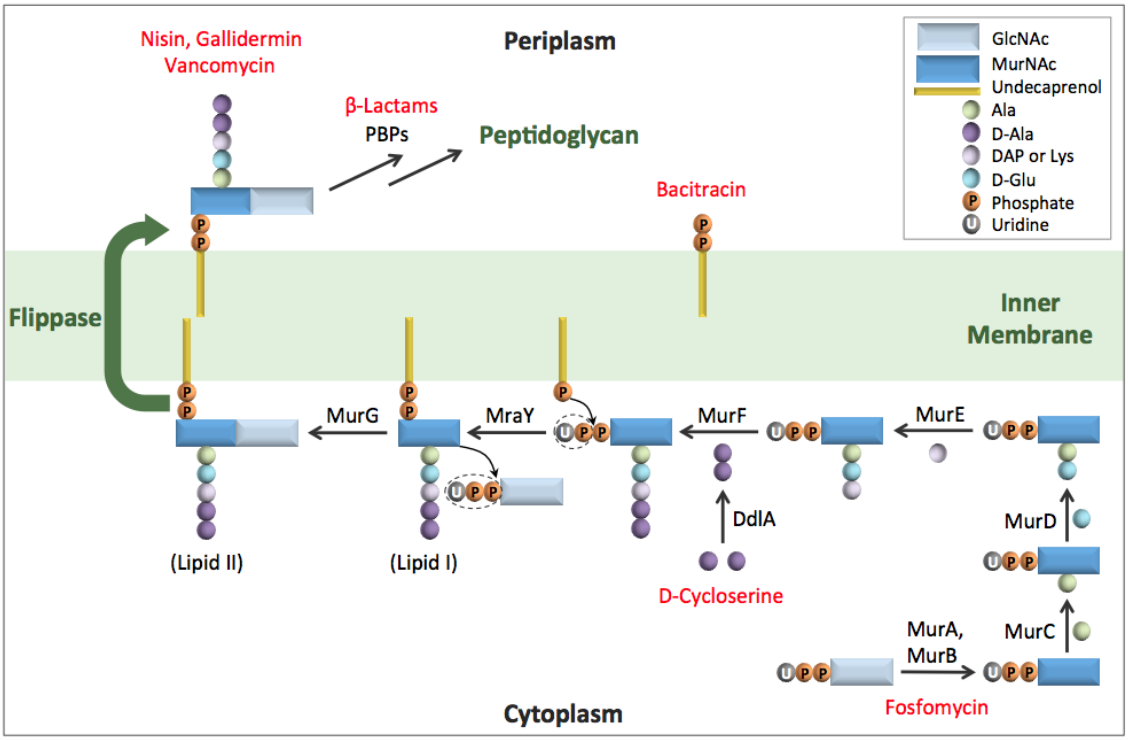

Figure 1.3. Peptidoglycan biosynthesis and the enzymes and intermediates targeted by antibiotics.

on the exterior surface of the inner-membrane.[15] This prevents the dephosphorylation of UPP to undecaprenol phosphate (UP) and its recycling back into the peptidoglycan pathway. UP is needed to anchor lipid I and lipid II to the bacterial membrane, therefore sequestering it is terminal to Gram-positive and Gram-negative bacteria. Glycopeptides are glycosylated cyclic non-ribosomal peptides produced by bacteria and can be further subdivided into Dalbaheptides (an acronym of **D-al**anyl-D-alanine **b**inding **a**ntibiotics having **hep**tapep**tide** structure).[16] Vancomycin (**7**) is the most common example of a Dalbaheptide and is isolated from the soil bacterium *Amycolatopsis orientalis*.[17] It cannot permeate the outer-membrane of Gram-negative bacteria but is active against Gram-positive bacteria. Vancomycin sequesters lipid II by binding to the D-Ala-D-Ala subunit on the pentapeptide chain.[18] This prevents further processing into peptidoglycan and leads to cell death. Lantibiotics, including nisin (**8**) and gallidermin (**9**), are post-translationally modified peptides produced by Gram-positive bacteria.[19] Owing to their large size, they are incapable of crossing the outer-membrane of Gram-negative strains. Like vancomycin, nisin and gallidermin sequester lipid II and prevent further processing into peptidoglycan. However, they make use of a "pyrophosphate cage" and bind to the pyrophosphate moiety on lipid II.[20,21] At lower concentrations, studies suggest these peptides form pores on the inner-membrane, killing cells.[22] Fosfomycin (**10**) is an analogue of phosphoenolpyruvate (PEP) and inhibits MurA.[23] MurA catalyzes the condensation of PEP onto the 3-OH group of UDP-GlcNAc, which is subsequently reduced by MurB to yield UDP-MurNAc. Fosfomycin irreversibly binds to the active-site cysteine (Cys115) on MurA, killing both Gram-positive and Gram-negative bacteria.[24] D-Cycloserine (**11**) is a cyclic analogue of D-alanine and binds to the ligase DdlA.[25] This

prevents the formation of the D-Ala-D-Ala dipeptide and inhibits peptidoglycan biosynthesis.

1.3.2. Protein-synthesis inhibitors

Protein-synthesis inhibitors disrupt translation in bacterial cells and most are bacteriostatic. Many of these antibiotics take advantage of the difference between eukaryotic and prokaryotic ribosomes, which read messenger ribonucleic acid (mRNA) and convert this information into proteins. The eukaryotic ribosome (80S) is made up of a 60S and 40S subunit and composed of 40% RNA and 60% proteins. The prokaryotic ribosome (70S) is made up of a 50S and 30S subunit and composed of 60% RNA and 40% proteins. The 50S subunit contains two ribosomal RNAs (rRNAs) (23S and 5S) complexed with ~34 proteins, whereas the 30S subunit has ~21 proteins and 16S rRNAs.[26] Other targets include aminoacyl tRNA synthetases and elongation factors (Figure 1.5).[27]

Translation has four main stages and synthesizes peptides from their *N*-terminus to C-terminus by reading mRNA 5' to 3'. In the activation stage, tRNA synthetases load the appropriate amino acid onto a complementary transfer RNA (tRNA) molecule using adenosine triphosphate (ATP). In the initiation stage, the 30S subunit of the ribosome binds to the 5' end of mRNA with the assistance of initiation factors. A loaded tRNA molecule then recognizes the codon in the A-site and binds using its complimentary anti-codon. The ribosome then moves 5' to 3' by one codon and another loaded tRNA binds to its complementary codon, so that now a loaded tRNA molecule is in both the A-

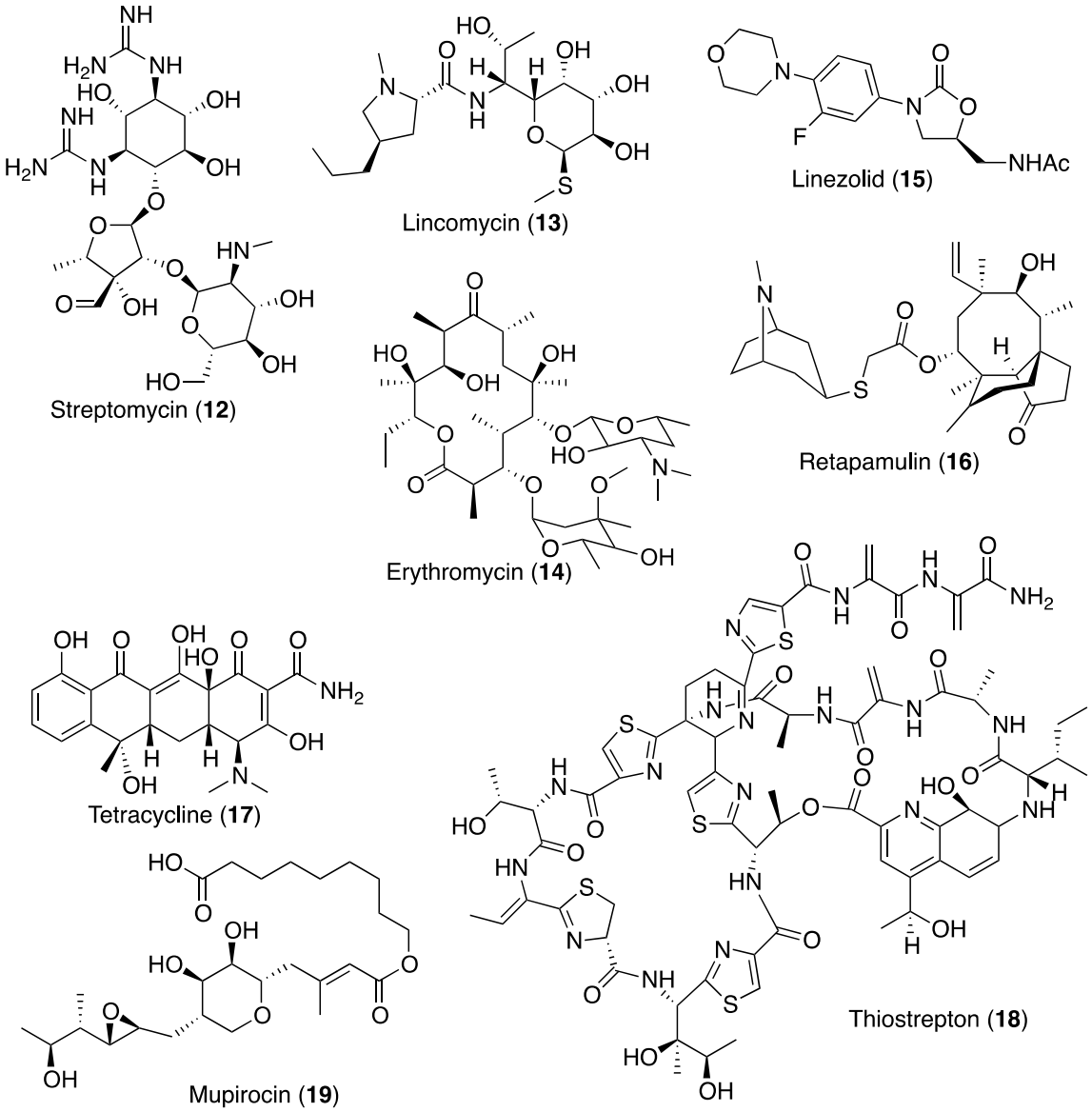

Figure 1.4. Clinically approved antibiotics that target protein biosynthesis.

site and P-site. The amino acid in the P-site then reacts with the amino acid in the A-site, forming a dipeptide on the A-site tRNA. The ribosome once again shifts one codon in the 3' direction and the empty tRNA molecule, now in the E-site, leaves. This process continues until the termination stage, when a stop codon is read in the A-site and the protein is hydrolyzed at the C-terminus.

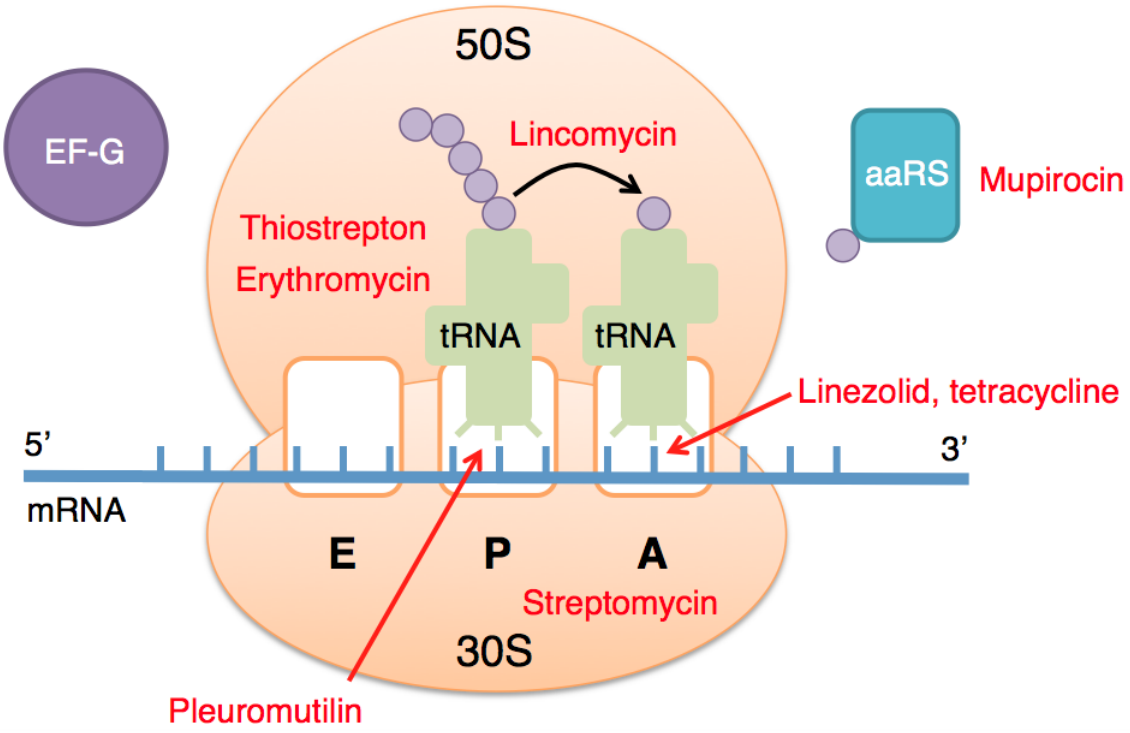

Figure 1.5. Binding sites of some antibiotics on the bacterial ribosome.

Streptomycin (**12**) is an aminoglycoside produced by *Streptomyces griseus* and was the first antibiotic found to be effective against *Mycobacterium tuberculosis*. It is active against both Gram-positive and Gram-negative organisms. Streptomycin binds to the 30S subunit, interacting with ribosomal protein S12 and 16S rRNA helices 1, 18, 27 and 44.[28] This induces a structural change in the ribosome and causes mRNA misreading, inhibiting protein-synthesis. Lincomycin (**13**) is a lincosamide class antibiotic isolated from *Streptomyces lincolnensis* that targets Gram-positive organisms. However, due to its toxicity it is usually reserved for the treatment of patients allergic to penicillin. Lincomycin binds to 23S rRNA on the 50S subunit of the ribosome and inhibits peptide bond formation between the loaded tRNA molecules in the A- and P-sites.[29] Erythromycin (**14**) is a glycosylated polyketide isolated from *Streptomyces*

erythreus. It falls under the macrolide subdivision of the macrolactone class of antibiotics and is only effective against Gram-positive organisms. Like lincomycin, erythromycin binds to 23S rRNA on the 50S subunit of the ribosome, close to the P-site, and blocks the transfer of peptides from the P-site to the A-site, inhibiting protein-synthesis.[30] Linezolid (**15**) is a fully synthetic antibiotic, developed by Pharmacia and the Upjohn Company, that is active against Gram-positive bacteria. It exerts its bacteriostatic effect by binding close to the A-site on the 50S subunit of the ribosome and blocking incoming tRNA molecules.[31] Retapamulin (**16**) is a topical antibiotic and member of the pleuromutilin class that was developed by GlaxoSmithKline for use in humans. The pleuromutilins are diterpenes isolated from fungi that are active against Gram-positive bacteria. They inhibit protein-synthesis by binding to domain V on 23S rRNA in the 50S subunit of the ribosome, blocking the P-site and disrupting peptidyl transfer.[32] Tetracycline (**17**) is a broad spectrum polyketide antibiotic produced by the *Streptomyces* genus that is active against both Gram-positive and Gram-negative bacteria. It binds close to the A-site on the 30S subunit, blocking tRNA molecules from entering the ribosome.[33] Thiostrepton (**18**) is a non-ribosomally synthesized thiazoyl peptide isolated from *Streptomyces* species. It inhibits bacterial protein-synthesis by binding to a cleft formed by the ribosomal protein L11 and the 23S rRNA helices 43 and 44 on the 50S subunit and disrupting formation of a stable 70S complex.[34] Mupirocin (**19**) is a topical Gram-positive antibiotic originally isolated from *Pseudomonas fluorescens*. It is a member of the monoxycarbolic acid class and one of six new classes of antibiotics clinically approved in the last 50 years. Unlike the previously mentioned protein-synthesis inhibitors, mupirocin does not bind to the ribosome, but instead exerts

its bacteriostatic effect by binding to a tRNA synthetase. Specifically, it occupies the ATP-binding site on the isoleucyl-tRNA synthetase, inhibiting translation and killing the cell.[35]

1.3.3. Nucleic acid synthesis inhibitors

Antibiotics can inhibit the biosynthesis of deoxyribonucleic acid (DNA) or RNA. The most common targets of nucleic acid inhibitors are DNA gyrase (also known as DNA topoisomerase II) and RNA polymerase.[36,37] DNA gyrase moves along double stranded DNA as it is being unwound by a helicase during replication. It relieves torsional strain built up during this process by cleaving the DNA ahead of the helicase, unwinding it slightly and then resealing it. DNA gyrase is made up of two subunits, A and B. The A subunit cleaves and reseals doubly stranded DNA whereas the B subunit uncoils the cleaved DNA. DNA gyrase is not found in humans. RNA polymerase (also called DNA dependent RNA polymerase) produces primary transcript RNA, which is single stranded RNA that is used to make mRNA, tRNA and rRNA. Eukaryotes have multiple types of RNA polymerase but bacteria only have one, a 400 kDa enzyme made up of 5 subunits (α, α', β, β' and ω).

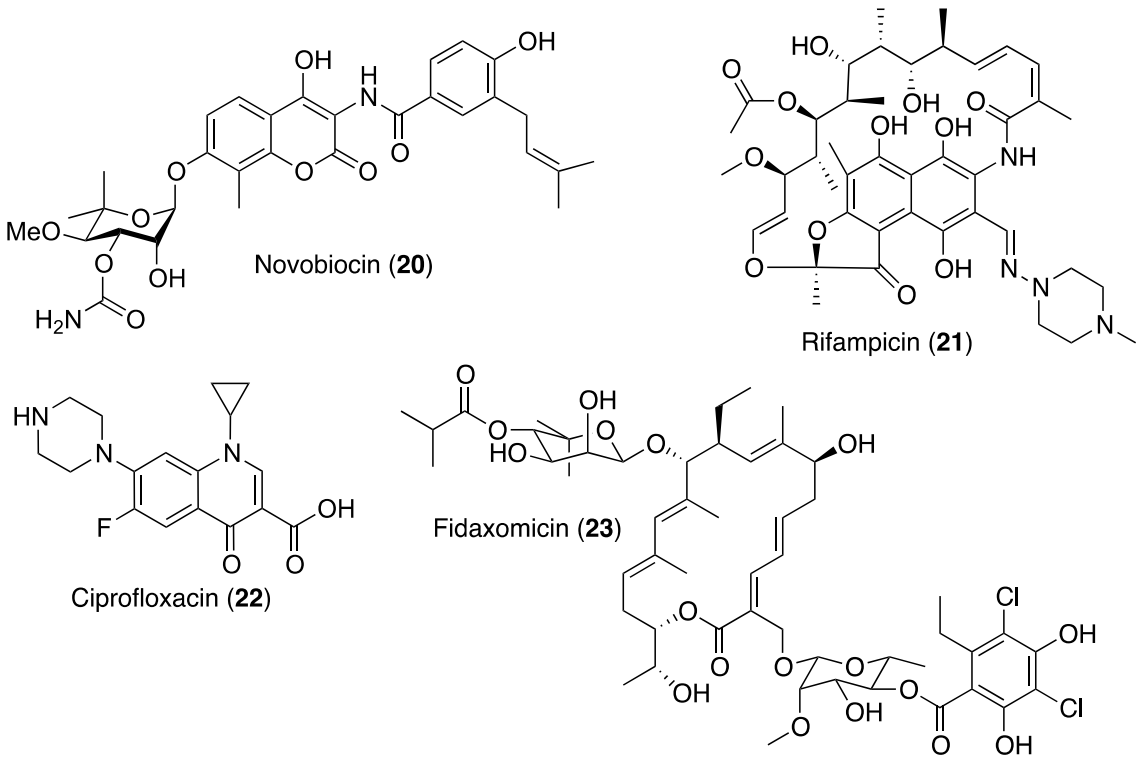

Figure 1.6. Clinically approved antibiotics that target nucleic acid biosynthesis.

Novobiocin (**20**) is a Gram-positive targeting antibiotic of the aminocoumarin class, isolated from species of *Streptomyces*. It exerts its bacteriostatic affect by occupying the ATP-binding site on the B subunit of DNA gyrase, blocking ATP hydrolysis and halting cell growth.[38] Rifampicin (**21**) is a semi-synthetic derivative of the polyketide natural product rifamycin B. It is a bactericidal antibiotic active against Gram-positive bacteria and shows weak activity against Gram-negative bacteria. Rifampicin binds in a pocket of the RNA polymerase β subunit 12 Å away from the active-site.[39] Therefore, it inhibits RNA synthesis by blocking the path of elongating RNA when it reaches 2-3 nucleotides in length. Ciprofloxacin (**23**) is a second generation fluoroquinolone antibiotic with potent activity against both Gram-positive and Gram-negative bacteria. It inhibits cell division by bridging the bound DNA and a transient non-

catalytic pocket on subunit A of DNA gyrase, close to the active-site.[40] Fidaxomicin (**24**), one of the newest classes of antibiotics (2010), is a macrolactone isolated from the actinomycete *Dactylosporangium aurantiacum* subspecies *hamdenesis*. It is marketed by Cubist Pharmaceuticals and used in the treatment of *Clostridium difficile* (Gram-positive) infections. Fidaxomicin kills *C. difficile* by binding to the sigma site of its RNA polymerase and inhibiting transcription.[41]

1.3.4. Cell membrane targeting antibiotics

The cell membrane is an essential part of every cell. It acts as a selective permeability barrier, protecting it from the outside environment, whilst regulating cellular homeostasis and metabolic energy transduction. It also encapsulates about one third of the cell's proteins, which perform vital physiological processes including the active transport of nutrients and waste, ATP generation, bacterial respiration, and establishment of the proton-motive force.[42] An often overlooked advantage to targeting the cell membrane is that these compounds can kill bacteria that are dormant or slow growing. As these bacteria have slower metabolic activities, the previously mentioned classes of antibiotics are often infective against them.[43] A major concern in developing membrane-targeting agents is selectivity towards bacteria, as compounds that target a phospholipid bilayer will likely be cytotoxic. However, differences in the composition of bacterial and mammalian membranes allow for selective targeting of bacteria. Bacterial membranes are overall negatively charged as they have a large amount of negatively charged phospholipids in their cytoplasmic membrane. In contrast, mammalian cell

membranes are abundant in cholesterol and zwitterionic phospholipids, and therefore more neutral.

There are a number of possible effects that membrane-targeting antibiotics can have on the bacterial membrane (Fig. 1.7).[44] They can operate through a membrane-lysis mechanism, forming large pores that release cytosolic components into the surrounding environment and rapidly killing the cell. Binding to essential trans-membrane proteins may also inhibit a vital cellular process and kill the cell, or act as an anchor for membrane lysis. Membrane targeting agents can disrupt the trans-membrane pH gradient, depolarize the cell or disrupt the electron transport chain, all of which are processes that are vital to cell survival and would lead to cell death.

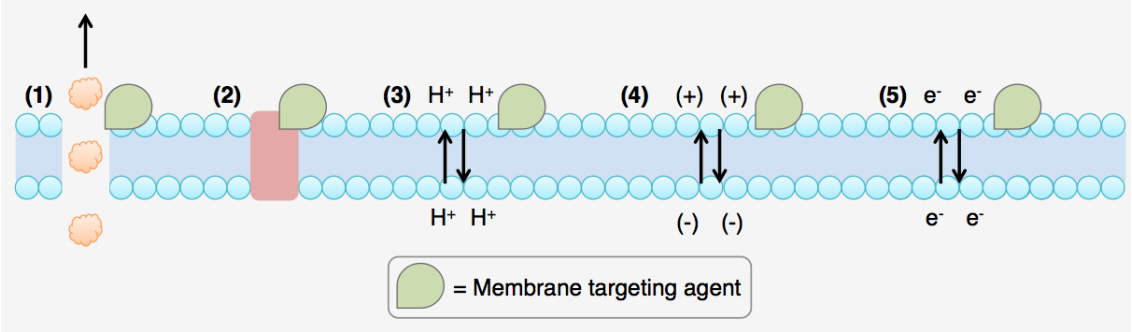

Figure 1.7. Effects of membrane targeting agents on the bacterial membrane. (1) Membrane lysis. (2) Trans-membrane protein inhibition. (3) Disruption of trans-membrane pH gradient. (4) Membrane depolarization. (5) Disruption of ETC.

Polymyxin B (**24**) is a member of the polymyxin family, a group of cyclic non-ribosomally synthesized lipopeptides produced by *Bacillus* and *Paenibacillus* species. They display strong activity against Gram-negative bacteria but as they operate by a

non-specific lysis mechanism, they are quite cytotoxic. Therefore they are often used as a last line of defense treatment.[45] Polymyxins bind to the phosphate groups of lipid A on lipopolysaccharide (LPS) and permeate the outer-membrane. They then insert into the inner-membrane and lyse the cell.[46]

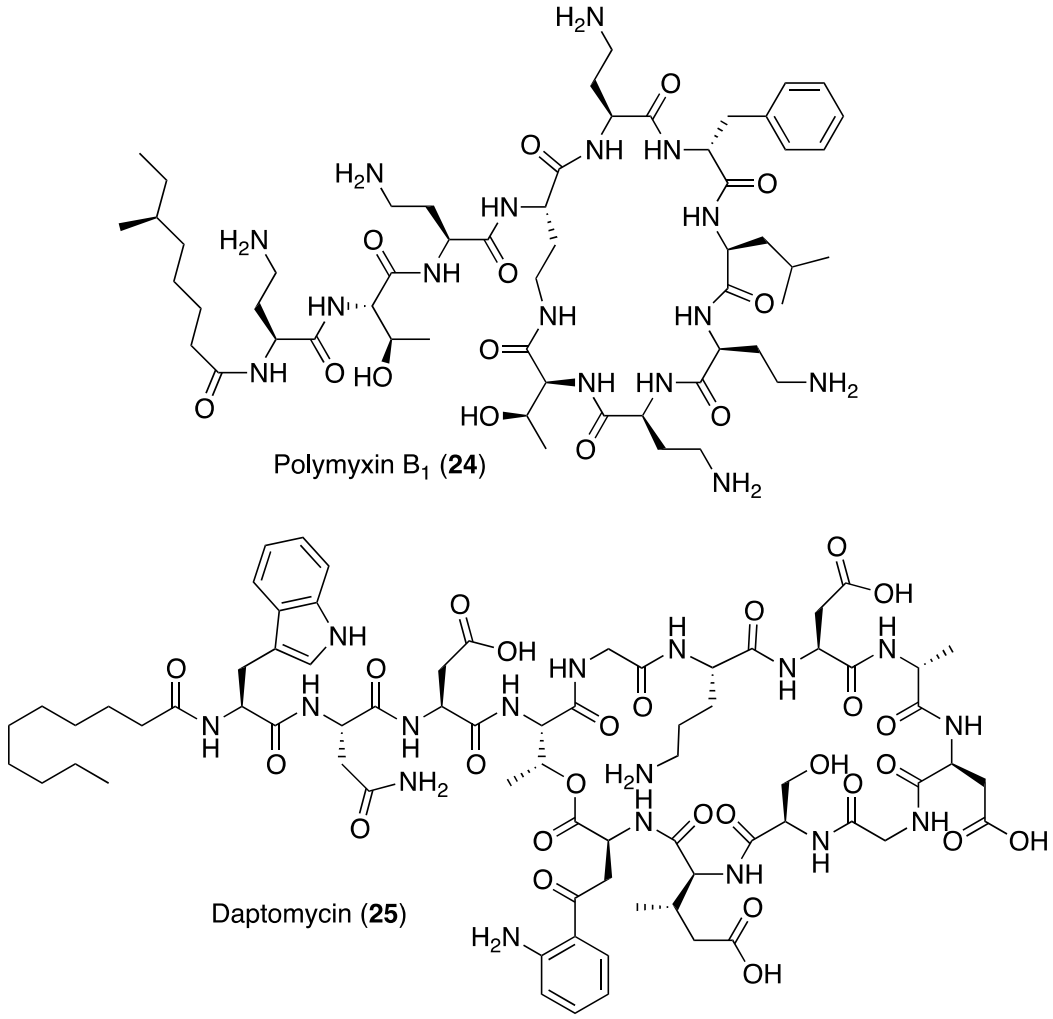

Figure 1.8. Clinically approved antibiotics that target the cell membrane.

Daptomycin (**25**) was originally isolated from *Streptomyces roseosporus* but is now marketed by Merck as cubicin. It is also a cyclic non-ribosomally synthesized lipopeptide, but in contrast to the polymyxins, which are polycationic, daptomycin is

polyanionic. Daptomycin is only active against Gram-positive bacteria as it cannot cross the outer-membrane. The overall negative charge is first sequestered by binding to calcium ions, which forms an oligomer with a micelle-like structure that is pseudopositively charged.[47] This pseudopositive structure is then drawn towards the negatively charged bacterial membrane, causing the micelle to dissociate and allowing the insertion of daptomycin's hydrophobic tail into the bacterial membrane, resulting in membrane lysis and killing the cell.

1.3.5. Bedaquiline

Bedaquiline (**26**) is the most recently approved new class of antibiotic (2012) and is used to treat multidrug resistant TB. It is a member of the diarylquinoline class of antibiotics and is only active against Gram-positive bacteria. Bedaquiline exerts its antimicrobial effect by binding to ATP synthase. This is an important enzyme that provides energy for the cell through the use of ATP, and its inhibition is terminal to bacteria.[48] Specifically, bedaquiline binds to the c-subunit of the F0 complex and interferes with its rotatory movement, leading to inadequate synthesis of ATP.

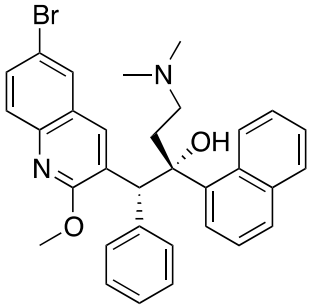

Bedaquiline (**26**)

Figure 1.9. The structure of Bedaquiline.

1.4 Antimicrobial Resistance

Bacteria reproduce very quickly. For example, *E. coli* cells have an average replication time of 24 hours, but can replicate every 20 min under optimal conditions. It is this rapid reproduction cycle that produces bacteria resistant to antibiotics. DNA replication in bacteria is extremely accurate, with a nucleotide mutation occurring only once every ten billion copies.[49] The *E. coli* genome has approximately 4.2 million nucleotides, therefore a mutation will arise about once every 1200 replications.[50] Taking the average replication time of *E. coli* cells (24 hours), in 11 days there will be enough DNA present amongst all the *E. coli* cells that mutations will occur every replication. In the laboratory, it only takes hours for this to occur, and the number of mutations increases exponentially as the cell population increases. Of course these are random mutations that may have a detrimental or beneficial effect to the survival of the bacterial cells. However, evolution is survival of the fittest, therefore positive outcomes from random mutations that give bacteria an advantage over their neighbors will lead to this mutation persisting in the population. This is the problem we face in the treatment of bacterial infections with antibiotics. Even if an antibiotic kills 99.9% of bacteria, the small amount it doesn't kill (due to some intrinsic resistance mechanism from a random mutation) will become dominant over time, eventually making the antibiotic worthless. The continued emergence of multidrug resistant (MDR) bacteria is a major global concern. Infections caused by MDR bacteria are twice as likely to end in death and place a significant physical and financial strain on health care systems worldwide.[51] A recent UK report predicts that by 2050, antibiotic resistance will cause 300 million premature deaths and result in a loss of up to $100 trillion from the global economy.[52]

Resistance is often reported shortly after the discovery of a new antibiotic, and typically happens within a few years but can be as rapid as a few weeks.[53] This is a serious problem that needs to be addressed, otherwise we face a post-antibiotic era in which routine illness could become deadly infections.

1.5. Resistance mechanisms

1.5.1. Resistance to peptidoglycan biosynthesis inhibitors

The modern antibiotic era and antibiotic resistance era began with penicillin, which was introduced in 1938. Resistant strains of *Staphylococcus* were first reported in 1948, and the mechanism of this resistance was quickly traced to the production of β-lactamases.[54,55] Mutated penicillin-binding proteins can also reduce the activity of β-lactam antibiotics. β-lactamases are enzymes produced by both Gram-positive and Gram-negative bacteria that hydrolyze the β-lactam ring, rendering the antibiotic inactive. There are four classes of β-lactamases; types A, C and D, which utilize an active-site serine to hydrolyze β-lactams; and type B (metallo-β-lactamases), which need zinc to exert their effect. The prevalence of β-lactamases has serious implications for the treatment of bacterial infections, and extremely multidrug resistant (XMR) strains of Gram-negative bacteria that produce carbapenemases are of particular concern.[56] Carbapenem-resistant *Klebsiella pneumoniae* (CRKP) strains are resistant to multiple classes of antibiotics, including aminoglycosides, fluoroquinolones and all available β-lactams.[57] The treatment of CRKP associated infections is often met with failure, and they have an associated mortality rate of over 50%. [58] Carbapenemase-producing XMR strains of *Acinetobacter baumannii* are attributed to many hospital-acquired infections

and show a worrying knack for the development of antibiotic resistance.[59] Carbapenemase-producing strains of *E. coli* also exist, which could have serious implications for future generations.

The existence of β-lactamases has lead to the development of β-lactamase inhibitors, which are used in conjunction with existing β-lactam antibiotics to increase their spectrum of activity. Clavulanic acid (**27**) is a naturally produced β-lactamase inhibitor that was discovered in 1976,[60] and is clinically administered with the penicillin amoxicillin (**28**), under the trade name augmentin (Fig. 1.10). Two of the three new structural classes of Gram-negative targeting antibiotics currently undergoing clinical trials are β-lactamase inhibitors, avibactam (**29**) (Forest Laboratories) and MK-7655 (**30**) (Merck).[61]

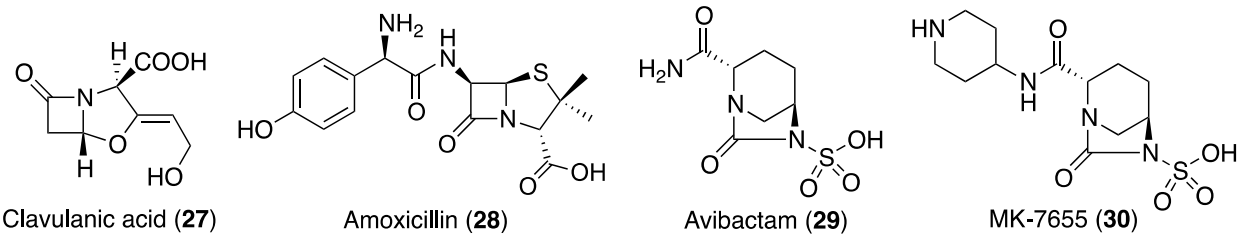

Fig. 1.10. Structures of β-lactamase inhibitors and amoxicillin.

Four major resistance mechanisms have been described for bacitracin. The first involves the production of an undecaprenyl pyrophosphate phosphatase (UppP), which converts UPP to UP and is not inhibited by bacitracin.[62,63,64] In the second mechanism of resistance, an adenosine-binding cassette (ABC) transporter is expressed that pumps bacitracin out of the cell.[65,66] The third mechanism is the overproduction of an undecaprenol kinase, which converts undecaprenol to UP, overcoming the effect of bacitracin.[67,68] Finally, mutations that inhibit the biosynthesis of non-essential

exopolysaccharides free up more UP for peptidoglycan biosynthesis, counteracting the effect of bacitracin.[69,70]

Almost all Gram-negative bacteria are resistant to vancomycin as it cannot cross the outer-membrane. Vancomycin-resistant Enterococci (VRE) are Gram-positive bacteria with a significantly reduced susceptibility to vancomycin. The main resistance mechanism involves modification of lipid II, specifically on the D-Ala-D-Ala dipeptide section.[71] Modification of D-Ala-D-Ala to D-Ala-D-Lac (replacement of an amide bond with an ester) results in the loss of one hydrogen-bonding interaction between vancomycin and lipid II, confering resistance.[72] Alternatively, changing the terminal D-alanine to a D-serine reduces the affinity between vancomycin and lipid II six-fold, likely due to increased sterics.[73]

Lantibiotics are also not active against Gram-negative bacteria as they cannot permeate the outer-membrane. Compared to other commercial antibiotics, there has been limited resistance development observed in Gram-positive species against the lantibiotics.[74] This is likely because they target the pyrophosphate moiety of lipid II, which is essential for recognition by several enzymes and cannot be as easily replaced as D-Ala5. Attempts have been made to deliberately induce resistance but most of the observed mechanisms are innate systems that react to the presence of any cationic peptides/proteins or ones which result from cell well damage, rather than being lantibiotic specific.[74]

There are three main resistance mechanisms to fosfomycin; reduced cell permeability to fosfomycin; modification of the target MurA and modification of fosfomycin *in vivo*.[75] Fosfomycin passes the outer-membrane in Gram-negative bacteria

through permeases and modification to these transporter enzymes has been shown to reduce the activity of fosfomycin against *E. coli*.[76,77] Modification of Cys115 to Glu in the fosfomycin-binding site on MurA yields a fully functional enzyme that is no longer inhibited by fosfomycin.[78] Several enzymes have also been found that open the epoxide on fosfomycin, rendering it inactive.[79]

D-Cycloserine resistance has been observed in *E. coli* and *M. tuberculosis*. In *E. coli*, mutations to the permease CycA, which is normally responsible for D-cycloserine uptake, make the organism resistant to this antibiotic.[80] Overexpression of the alanine racemase (AlrA) or D-alanine ligase (Ddl) in *M. tuberculosis* decreases the effectiveness of D-cycloserine against this organism.[81,82]

1.5.2. Resistance to protein-synthesis inhibitors

There are three main mechanisms of resistance against streptomycin and other aminoglycosides; mutation of the ribosome; reduced cell permeability to aminoglycosides and enzymatic inactivation of aminoglycosides. In the streptomycin interaction with the ribosome, this antibiotic binds to the S12 protein on the 30S subunit. There have been multiple mutations found on this protein that inhibit binding and confer resistance to streptomycin.[83] In *Pseudomonas* species and other Gram-negative bacteria, aminoglycoside resistance can be confered by making the membrane less permeable. This occurs by membrane protein mutations or active efflux of the antibiotics from the cell.[84,85] Several enzymes that inactivate the aminoglycosides through chemical modification have also been found, including acetyltransferases, adenyltransferases and phosphotransferases.[86] Like streptomycin, resistance to the

lincosamide lincomycin can also be achieved by modification of the ribosome or enzymatic inactivation of the antibiotic *in vivo*.[87] Enzymatic inactivation is the more prevalent resistance mechanism and is mostly due to nucleotidylation of one of the glycan hydroxyl groups.[88,89]

Erythromycin resistant bacterial strains have three main mechanisms of resistance to macrolide antibiotics. These are efflux of the drug, modification of the erythromycin-binding site on the ribosome or modification of the antibiotic.[90] Erythromycin ribosome methylases (ERMs) dimethylate adenine 2058, which is located in a conserved region of domain V of 23S rRNA, and prevent erythromycin-binding.[91] Gram-negative bacteria use chromosomally encoded efflux pumps to export hydrophobic compounds like erythromycin. In Gram-positive organisms, macrolide resistance by active efflux is due to two classes of pumps, ABC transporters and members of the major facilitator superfamily.[90] Erythromycin can also be chemically inactivated in enterobacteria by esterases and phosphotransferases, which confer resistance to erythromycin and other 14- and 15-membered ring macrolides.[90]

Almost all linezolid-resistance mechanisms involve small modifications to the linezolid-binding site on the ribosome.[92] These occur on the 23S RNA of the 50S subunit and several conserved residue mutations have been attributed to linezolid resistance. Retapumulin was clinically approved as a topical antibiotic in 2007 and limited resistance mechanisms have been reported. Studies on other pleuromutilin antibiotics have found that mutation of Asn149 to and Asp in the ribosomal protein L3 leads to a reduced susceptibility to these antibiotics.[93,94]

As with other protein inhibitors, tetracycline resistance can be due to efflux of the drug from cells, mutation of its ribosomal-binding site or chemical modification of the antibiotic itself.[95] Members of the MFS family that export tetracycline and protect the cell are found in both Gram-positive and Gram-negative bacteria.[96,97] Ribosomal protection proteins, which are homologous to elongation factors EF-Tu and EF-G, bind to the ribosome and prevent tetracycline from binding to the A-site.[98] A flavin dependent monoxygenase (TetX) has also been found that enzymatically inactivates tetracycline *in vivo*.[99] Studies have shown that TetX hydroxylates tetracycline at position 11a, inducing an intramolecular cyclization and non-enzymatic decomposition of the product.[100]

Resistance to the thiazoylpeptide thiostrepton can arise from ribosome mutation or the specific methylation of the rRNA that makes up the thiostrepton-RNA-binding interface.[101] In *S. aureus*, methylation of the 23S rRNA on the ribose 2-hydroxyl of adenosine 1067 by a methyltransferase (Tsr) inhibits binding and confers resistance.[102,103] Mutations on ribosomal protein L11, either at its *N*-terminus or its 23S RNA-binding site reduce the thiostrepton susceptibility of the organism.[104] The main resistance mechanism against mupirocin is the expression of an extra isoleucyl-tRNA synthetase (mupA or mupB).[105] This circumvents the inhibition of the native isoleucyl-tRNA synthetase by providing an alternative functional copy to take its place in protein-synthesis.

1.5.3. Resistance to nucleic acid synthesis inhibitors

The main targets of nucleic acid synthesis inhibitors are DNA gyrase and RNA polymerase, therefore it should come as no surprise that the main resistance

mechanisms are mutation of these target proteins. Resistance to novobiocin in staphylococci and other bacteria is predominantly due mutations in the gene *gyrB*, which encodes for subunit B of DNA gyrase, novobiocins target.[106] A similar mechanism of resistance exists for ciprofloxacin.[107] The primary mechanism of resistance to rifampicin is mutation of its target, the β-subunit of RNA polymerase.[108] Low levels of rifampicin resistance have also been attributed to the efflux pumps in mycobacteria.[109] Resistance to the RNA polymerase inhibitor fidaxomicin, which was clinically approved in 2010 for the treatment of *Clostridium difficile* infections, has yet to be reported. However, given the propensity for almost all bacteria to develop resistance to antibiotics by mutation of their protein targets, it is likely only a matter of time before resistance is observed.

1.5.4. Resistance to cell membrane targeting antibiotics

Polymyxin B is often a last line of defense treatment for serious Gram-negative infections, however Gram-negative organisms resistant to the polymyxins have been detected.[110] Polymyxins first bind to LPS on the outer-membrane, before entering the periplasm and lysing the inner-membrane. Therefore, modification of the polymyxin-binding site on LPS (lipid A) confers resistance to bacteria. This can be achieved by reducing the negative charge on lipid A through capping of the phosphate groups with ethanolamine or 4-amino-4-deoxy-L-arabinose.[111] Deacylation and hydroxylation have also been shown to confer polymyxin resistance,[111] and efflux pumps have been found that expel polymyxin B from the cell.[112]

The daptomycin-resistance mechanisms are not well understood, however daptomycin resistance in many cases is concurrent with single-nucleotide polymorphisms in the *mprF* gene.[113] This gene encodes MprF, a trans-membrane protein that caps phosphatidylglycerol in the cell membrane with lysine. It has been proposed that mutations to MprF lead to a reduction in the net negative charge of the cell membrane, making it less susceptible to the pseudopositively charged calcium bound daptomycin oligomer that initially binds to bacterial membranes.[114]

1.6. How do we fight antibiotic resistance?

Stopping the spread of antimicrobial resistance is of the utmost importance, and cannot be just a research and development problem. Resistance could typically develop against antibiotics in as short a time as a few months after their introduction, but the average time taken to move a drug from the lab to the clinic is 12 years.[115] Therefore, we cannot make new antibiotics fast enough to stem the development of resistance. Rapid diagnostic techniques that can quickly assign the bacterial strain responsible for an infection will prevent the use of antibiotics ineffective against that strain. Healthcare systems also need to crack down on the over prescription of antibiotics by medical doctors for the treatment of infections not caused by bacteria. This should give some breathing space for the development of new antibiotics, which will always be essential in our fight against bacterial infections.

The big question is can we make a resistance-proof antibiotic? The previous sections of this chapter gave a summary of the main classes of antibiotics, the cellular processes they target and the mechanisms by which bacteria become resistant to these

antibiotics. A few important lessons can be derived from this historical overview. For the most part, antibiotics that target large proteins (the ribosome, DNA gyrase, RNA polymerase, etc.) and bind at a specific site are prone to resistance development by mutations in the target protein and are not good targets. Also, small molecules with reactive sites are often enzymatically inactivated (e.g. β-lactamases) or removed from the cell by efflux pumps. Therefore, targeting the bacterial membrane, rather than peptidoglycan, protein or nucleic acid synthesis, offers some advantages when considering resistance development. Antibiotics that target the bacterial membrane can kill dormant or slowly growing bacteria, which are normally immune to other classes of antibiotics due to their slow metabolic activity. It is also the first point of contact between antibiotic compounds and a bacterial cell and circumvents the need to cross the membrane. An intact cell membrane is vital for cell survival and disrupting the cell membrane rapidly leads to cell death. Also, as the bacterial membrane is such a large fluid structure, it is difficult for bacteria to reorganize their membranes through mutations, which can significantly slow the development of resistance to membrane targeting antibiotics. Small molecule antibiotics that target trans-membrane proteins through a dedicated binding pocket can still be ruled ineffective by single-nucleotide mutations, however this may be less prevalent with larger molecules like antimicrobial lipopeptides.

1.7 Antimicrobial Lipopeptides

The term lipopeptide can be taken to mean any peptide that has lipophilic properties; however, it is more commonly used to describe non-ribosomally synthesized

linear or cyclic peptides that are *N*-terminally acylated with a lipid tail. These antimicrobial compounds have historically been overlooked as potential antibiotics due to worries about their systemic toxicity. Many antimicrobial lipopeptides have been known for over 50 years, but their clinical application has mostly been reserved for topical use. However, with the compounding problem of antimicrobial resistance, we have seen several lipopeptides gain FDA approval for the treatment of multidrug-resistant infections in recent years, including daptomycin and polymyxin B, and others are in various stages of clinical and preclinical trials.[116] Both bacteria and fungi produce lipopeptides, but a disproportionate amount of natural lipopeptides can be isolated from *Bacillus* and *Paenibacillus* species. These organisms produce a number of well-known examples, including the polymyxins. In addition, these organisms also generate a number of other classes of lipopeptides with potent antimicrobial activities.[117]

Lipopeptides are typically synthesized by non-ribosomal peptide synthases and can contain a mixture of D and L amino acids. This gives them enhanced stability to proteolytic enzymes and blood plasma proteases, which could enable effective patient treatment by oral administration or intravenous injection.[118] The *N*-termini of lipopeptides from these species are commonly acylated with branched chain fatty acids containing a β-hydroxyl group with the *R* stereochemical configuration.[119] In most cases, these lipopeptides are cyclized by an ester or amide linkage between a heteroatom on the side chain of an amino acid or lipid tail and the C-terminus (e.g. polymyxins), giving them a rigid structure. Non-proteogenic amino acids are often found in lipopeptides, providing further diversity and stability to this class of antibiotics. They usually target the cell membrane and resistance development is typically slower than for other antibiotic

classes. In the past 50 years, only four new classes of antibiotics have been developed that treat systemic infections, yet all of these are inactive against Gram-negative organisms. In an effort to develop new classes of antibiotics, this graduate work has focused on the study of two classes of linear lipopeptides, the cerexins and the tridecaptins, that have been known for decades but aside from early work on their isolation and structural characterization, have not been further studied.

1.8 Linear Antimicrobial Lipopeptides

From a synthetic perspective, linear lipopeptides are much easier to synthesize than cyclic lipopeptides like polymyxin B. Peptide synthesizers can rapidly synthesize most linear peptides on a solid-support, however cyclic peptides require the use of orthogonal side chain protecting groups and late stage cyclization procedures, increasing the cost and labor associated with their production. Therefore, they have the potential to be more accessible than their cyclic counterparts. The cerexins are a class of linear decapeptides isolated from *B. cereus*.[120,121,122,123,124,125,126] They contain more D-amino acids than L-amino acids and are acylated with a β-hydroxyl lipid tail (Fig. 1.11). Early studies suggest they have moderate antimicrobial activity against Gram-positive organisms, including *S. aureus* and *Streptococcus pneumoniae*. Aside from these early reports in the 1970's, no further work has been performed on the cerexins.

The tridecaptins are another class of linear lipopeptides, also isolated in the 1970's, from several strains of *P. polymyxa*.[127,128] They are tridecapeptides made up of a combination of L- and D-amino acids and acylated with a lipid tail that usually contains a β-hydroxyl group (Fig. 1.11). Of particular promise is that the tridecaptins are reported

to have strong activity against Gram-negative bacteria, but are less active against Gram-positive bacteria. This suggests that they do not operate by a general membrane-lysis mechanism and could therefore have reduced toxicity profiles.

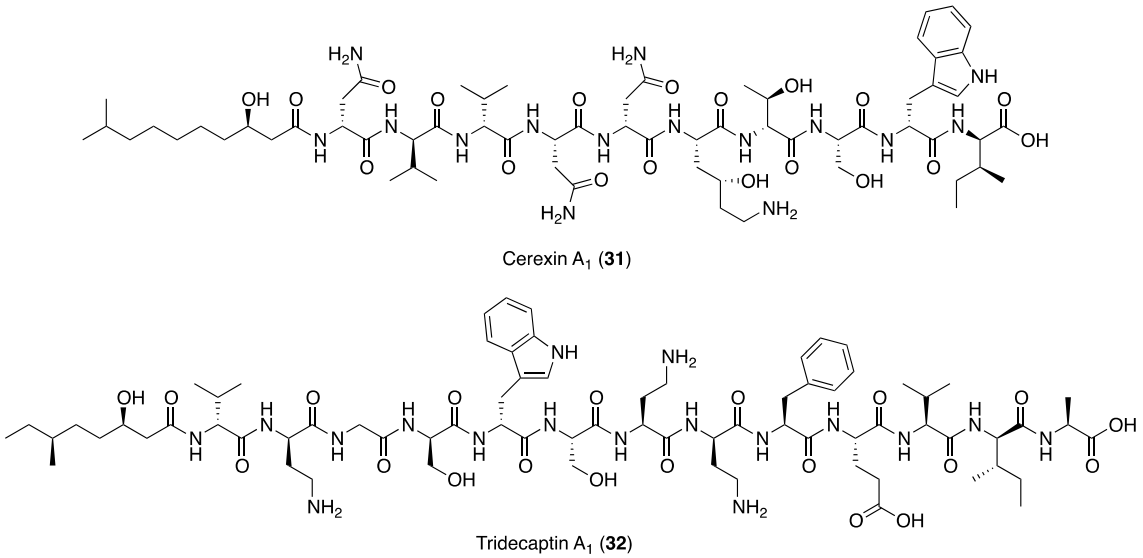

Figure 1.11. Examples of cerexin and tridecaptin lipopeptides.

Chapter 2

Isolation, synthesis and structural characterization of antimicrobial lipopeptides

2.1. Tridecaptins

2.1.1. Project background

2.1.1.1. Antimicrobial peptides and Gram-negative bacteria

In chapter 1, the main structural classes of antibiotic compounds are summarized and the difficulties associated in targeting Gram-negative bacteria highlighted. Although the presence of efflux pumps and target modifying enzymes play a role in resistance, the greatest hurdle is the outer-membrane. For large molecules like peptides and proteins, this blocks their entry into the cell. The cyclic lipopeptide polymyxin B is only capable of crossing the outer-membrane by interacting with LPS, and modification of the LPS structure in bacteria provides resistance to the polymyxins. The lantibiotics, produced by Gram-positive organisms, are too large and hydrophobic to cross the outer-membrane. The cyclic lipopeptide daptomycin, also produced by Gram-positive organisms, cannot permeate the outer-membrane. A general rule is that antimicrobial peptides produced by Gram-positive bacteria are not active against Gram-negative bacteria because they cannot cross the outer-membrane. This rule holds true for most bacteriocins produced by Gram-positive organisms.

Bacteriocins are ribosomally synthesized peptides excreted by both Gram-positive and Gram-negative bacteria.[129] The most studied bacteriocins (e.g. nisin) are produced by lactic acid bacteria and sometimes used as food preservatives due to their

low toxicity to humans. The bacteriocin class of antimicrobial peptides can be subdivided into four classes, type I, II, III and IV.[129] Type I bacteriocins are more commonly known as lantibiotics, and have previously been discussed in section 1.3.1. Type II bacteriocins are small, heat stable proteins (< 10 kDa) and can be further subdivided into five classes, of which type IIa is the largest. The *N*-terminal region of type IIa bacteriocins is highly conserved across all members of this class and contains two cysteines joined through a disulfide bond and a YGNG-V/L sequence, also known as the 'pediocin box' motif. Type III bacteriocins are large, heat sensitive proteins (> 10 kDa) and type IV are complex proteins containing lipids and/or carbohydrates. Most of these bacteriocins are inactive against Gram-negative bacteria.

2.1.1.2. Early reports of bacteriocins active against Gram-negative bacteria

In 2005, Svetoch and co-workers reported the isolation of three antimicrobial peptides, SRCAM 37, SRCAM 602 and SRCAM 1580 (Table 2.1) from *Bacillus* and *Paenibacillus* spp. This was an interesting discovery, given that the peptides were isolated from Gram-positive organisms, yet showed activity against the Gram-negative bacterium *Campylobacter jejuni*.[130] *C. jejuni* is one of the leading causes of foodborne illness and the development of antibiotic resistant strains has lead groups to search for new anti-*Campylobacter* agents.[131] This initially seemed an exciting discovery, given the rarity of antimicrobial peptides with activity against Gram-negative organisms, therefore our group sought to investigate this further.

Closer inspection of the proposed sequences of the antimicrobial peptides raised a number of red flags. All of the peptides contain the YGNG-V/L motif common to type

IIa bacteriocins, however, two lack the number of cysteines required for a disulfide bond (Table 2.1). Furthermore, the reported sequences of SRCAM 37, SRCAM 602 and SRCAM 1580 differ from the experimentally reported masses by 252 Da, 766 Da and 143 Da respectively.

Bacteriocin	Sequence
SRCAM 37	FV**YGNGV**TSILVQAQFLVNGQRRFFYTPDK
SRCAM 602	ATY**YGNGL**Y**C**NKQKHYTWVDWNKASREIGKITVNGWVQH
SRCAM 1580	VN**YGNGV**S**C**SKTK**C**SVNWGIITHQAFRVTSGVASG

Table 2.1. Sequences of bacteriocins reported by Svetoch and co-workers.

2.1.1.3. Genetic analysis of strains reported to produce SRCAM bacteriocins

The strains reported to produce SRCAM 37, 602 and 1580 (*P. polymyxa* NRRL B-30507, *P. polymyxa* NRRL B-30509 and *B. circulans* NRRL B-30644, respectively) were obtained from the US Department of Agriculture (USDA) Agricultural Research Service Patent Culture Collection. Previous Vederas group summer students, Maude Giroud and Erika Steels, fermented these organisms, and partially purified their supernatants. They found that the Gram-negative and Gram-positive activity could be separated, suggesting two or more different antimicrobial compounds. However, attempts to purify SRCAM peptides by previously reported methods were unsuccessful and no similar compounds were observed using mass spectrometry. Therefore, the genomes of the organisms were sequenced and analyzed, in an attempt to find the gene sequences encoding the SRCAM peptides.[132] A Vederas group research associate, Dr. Marco van Belkum, and former graduate student, Dr. Christopher Lohans, isolated the genomic DNA from these strains and submitted it for sequencing

using 454 pyrosequencing. In all cases, no genetic determinants for the proposed peptides were found. Genome sequencing also led to the reclassification of *B. circulans* NRRL B-30644 as *P. terrae* NRRL B-30644. Furthermore, polymerase chain reaction (PCR) experiments using degenerate oligonucleotide primers failed to identify any amplicons consistent with the reported sequences. Therefore, efforts were made by our group to isolate the compounds responsible for the observed Gram-negative activity, which was eventually attributed to tridecaptins and polymyxins. Dr. Lohans also determined that the lantibiotics paenicidin A and B were responsible for the observed activity against Gram-positive organisms.[133,134]

2.1.1.4. Isolation and partial characterization of tridecaptin A_1 and B_1

An activity-guided purification approach was used by Dr. Lohans to isolate compounds displaying Gram-negative activity from *P. terrae* NRRL B-30644 and *P. polymyxa* NRRL B-30507.[134,135] Large-scale cultures (4 L) of both organisms were grown and their supernatants separated by centrifugation. The supernatants were fractionated using hydrophobic interaction chromatography (HIC) and purified by reversed phase high-performance liquid chromatography (HPLC). At each stage, fractions containing compounds with activity against Gram-negative bacteria were identified using a spot-on-lawn assay with *E. coli* DH5α as the indicator strain. The major products responsible for the activity against Gram-negative bacteria from *P. terrae* NRRL B-30644 and *P. polymyxa* NRRL B-30507 were analyzed by mass spectrometry, nuclear magnetic resonance (NMR), total correlation spectroscopy (TOCSY) and nuclear overhauser effect spectroscopy (NOESY). This revealed that the

previously reported lipopeptide tridecaptin A_1 ($TriA_1$) was the active compound produced by *P. terrae* NRRL B-30644, and a new tridecaptin analogue, tridecaptin B_1 ($TriB_1$), was the active compound produced by *P. polymyxa* NRRL B-30507 (Fig. 2.1). However, using these techniques it was not possible to determine the stereochemistry on the lipid tails of both peptides.

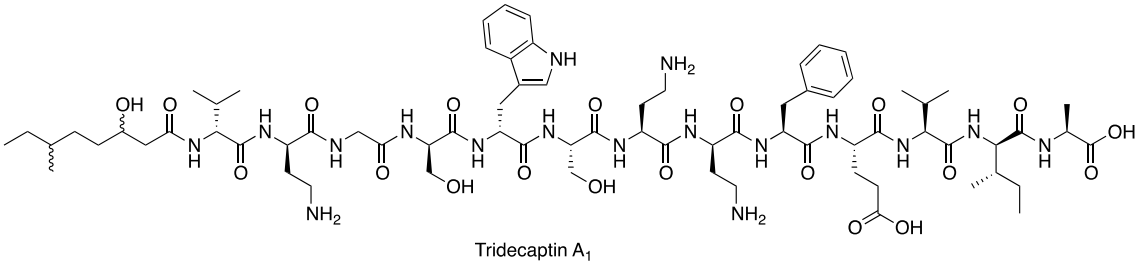

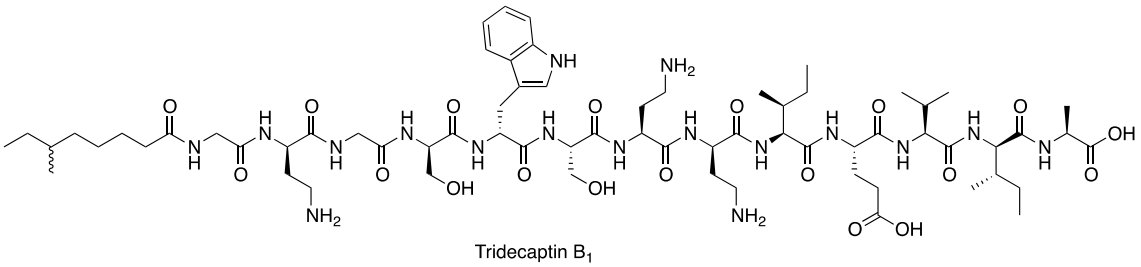

Figure 2.1. Preliminary structures of $TriA_1$ and $TriB_1$.

From the perspective of drug development, it is important to work with enantiomerically pure compounds. This helps avoid unknown side effects from an inactive enantiomer. The lipid tail from $TriA_1$ was hydrolyzed and derivatized for comparison with synthetic standards using chiral gas chromatography mass spectrometry (GCMS). However, this approach was unsuccessful and other groups have reported the difficulties associated with separating chiral fatty acids by GCMS.[136] It was at this stage that my involvement in the tridecaptins project began, and I used the power of chemical synthesis to solve this structural assignment problem.

2.1.2. Results and discussion – Tridecaptin A_1

2.1.2.1. Synthesis of the possible tridecaptin A_1 lipid tail isomers

Tridecaptin A_1 is *N*-terminally acylated with a 3-hydroxy-6-methyloctanoyl lipid tail, containing two chiral centres. Therefore, there are four possible configurations that the lipid on $TriA_1$ can have. I and a previous graduate student, Dr. Zedu Huang, synthesized compounds **41** – **43** to help elucidate the lipid tail stereochemistry using chiral GCMS (Scheme 2.1). Starting with (*S*)-citronellol (**33**) fixes the final 6-methyl stereochemistry as (*R*), whereas (*R*)-citronellol (**34**) yields the (6*S*)-product. Tosylation of citronellol, followed by detosylation by treatment with lithium aluminium hydride yields the chiral alkenes **37** and **38**. Ozonolysis of these derivatives, followed by a reductive work-up using dimethyl sulfide, provides enantiomerically pure (6*R*)-methylhexanal (**39**) and (6*S*)-methylhexanal (**40**). A Lewis acid catalyzed aldol condensation between the aldehydes and an acetylated Crimmins chiral auxiliary **41** yields both the (3*R*)- and (*3*S)-alcohols, which are separable by column chromatography. This approach provides enantiomerically pure 'activated fatty acids' **42** – **45**. It is possible to distinguish the (3*R*)- and (3*S*)-aldol products from their chemical shifts and coupling constants using ^{1}H-NMR.[137]

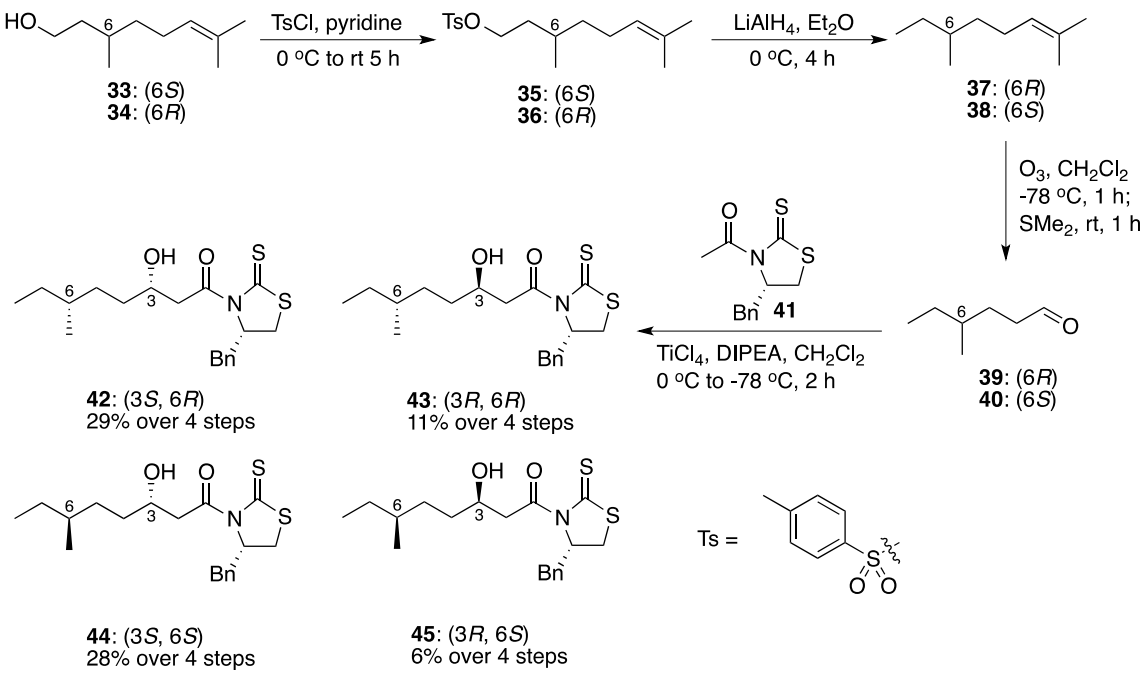

Scheme 2.1. Synthesis of four activated fatty acids for use in $TriA_1$ synthesis.

It appeared that it should be possible to distinguish the four possible tridecaptin A_1 lipid tail isomers using HPLC, as they are all diastereomers of each other. The $TriA_1$ peptide chain could be synthesized using solid phase peptide synthesis (Scheme 2.2). This is an extremely powerful method for the synthesis of peptides and its inventor, Robert Bruce Merrifield, was awarded the Nobel Prize in Chemistry for this discovery in 1984. In the Fmoc version, amino acids are used in which their α-amino group is protected with the base labile Fmoc group and any reactive side-chain functionalities are protected with acid-labile groups. The C-terminal amino acid is loaded onto a polystyrene bead, which allows sequential reactions to be performed on the resin bound amino acid without the need for purification. Excess reagents and waste are removed by filtration and washing the resin. In the first step of $TriA_1$ synthesis, the base-labile Fmoc group on resin bound alanine **46** is deprotected with piperidine (20% solution in

DMF). This yields amine **48** and fulvene **47**, which is UV active and can be used to monitor the progress of Fmoc-deprotection. Concurrently with this solid-phase reaction, Fmoc-D-*allo*-Ile-OH (**49**) is reacted with HATU to form activated ester **50**. This activated ester solution is then added to amine **48** and a new peptide (amide) bond is formed, yielding dipeptide **51**. These steps are repeated, substituting the necessary Fmoc-amino acids for **49** until the full peptide has been synthesized.

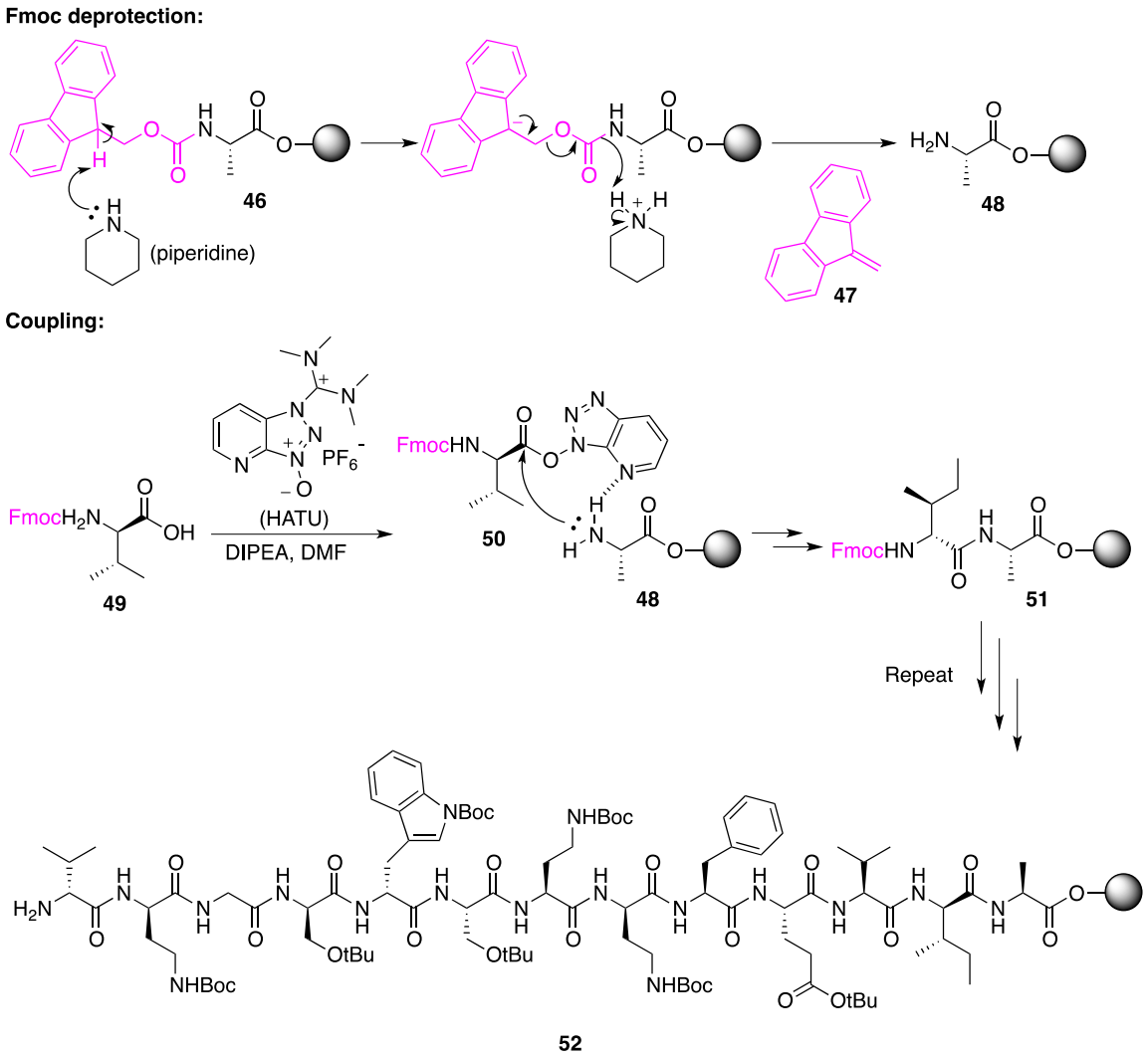

Scheme 2.2. Summary of the Fmoc-SPPS procedure.

The final step in the syntheses of the tridecaptin A_1 lipid tail isomers is *N*-terminal acylation with the appropriate activated fatty acid (Scheme 2.3). The standard approach to do this using compounds **42** – **45** would be to hydrolyze the fatty acids from the chiral auxiliary, protect the hydroxyl group, form an activated ester and couple this to the *N*-terminal D-Val. However, our group has shown that thiazolidinethiones are good leaving groups and are readily displaced with thiolates.[138] Therefore, this should also be possible with amines. Gentle stirring of resin bound $TriA_1$ **52** with one equivalent of activated fatty acid **45** for 24 h in CH_2Cl_2 yields the *N*-terminally acylated resin bound peptide in quantitative yields. Repeating this procedure with the other activated fatty acids and subsequent treatment of these resin bound peptides with a standard peptide cleavage cocktail yields the four possible $TriA_1$ lipid tail isomers **31** and **53** – **55**.

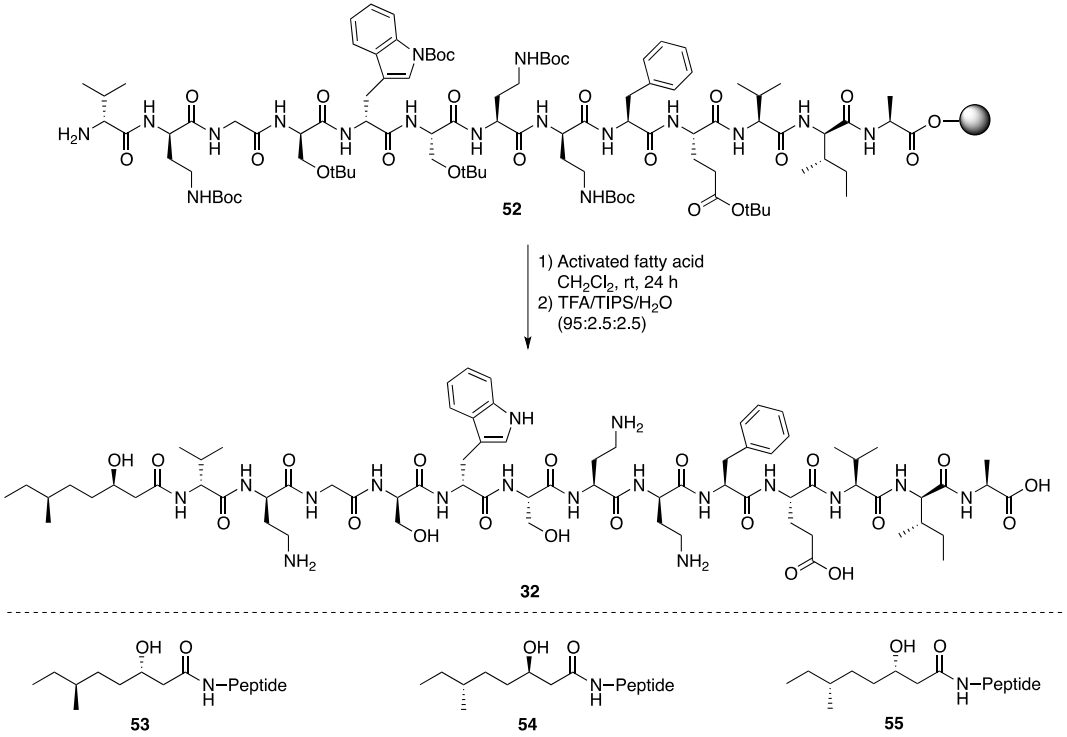

Scheme 2.3. Synthesis of $TriA_1$ lipid tail isomers.

2.1.2.2. Determination of the tridecaptin A_1 lipid tail stereochemistry

An equimolar amount of each $TriA_1$ lipid tail isomer was mixed with natural $TriA_1$ and analyzed by analytical HPLC using a C_{18} column (Fig. 2.2). Although this method easily identified the hydroxyl stereochemistry as 3*R*, it could not distinguish between the 3*R*,6*R* and 3*R*,6*S*-methyl analogues.

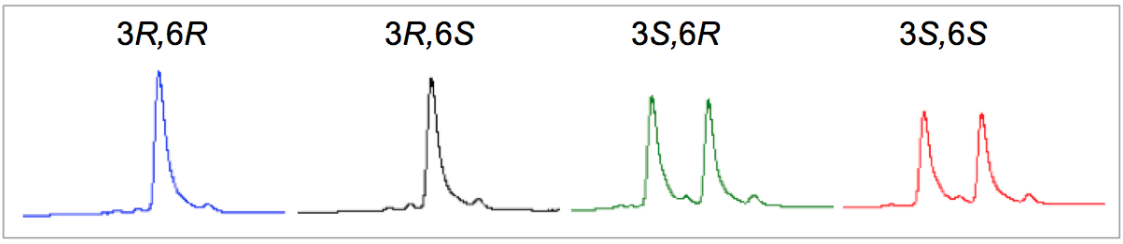

Figure 2.2. HPLC co-injection of natural $TriA_1$ with (3*R*,6*R*)-$TriA_1$ (blue), (3*R*,6*S*)-$TriA_1$ (black), (3*S*,6*R*)-$TriA_1$ (green), (3*S*,6*S*)-$TriA_1$ (red).

Therefore, ^{1}H-NMR analysis was used to determine the stereochemistry of the 6-methyl group (Fig. 2.3). A clear difference between the 6*R*- and 6*S*-methyl compounds was identified at the γ-position on the lipid tail, which is split into two signals for the (3*R*,6*R*) analogue but appears as one multiplet in the (3*R*,6*S*) analogue and natural $TriA_1$. Thus the stereochemistry of the tridecaptin A_1 lipid tail was unambiguously identified as (3*R*,6*S*). Branched-chain fatty acids (BFCAs) are biosynthesized from leucine, isoleucine and valine, with isoleucine yielding *anteiso*-fatty acids, as found in tridecaptin A_1.[139] The side-chain methyl group on isoleucine has an *S*-configuration and is consistent with the determined stereochemistry of the tridecaptin A_1 lipid tail, lending credence to our findings.

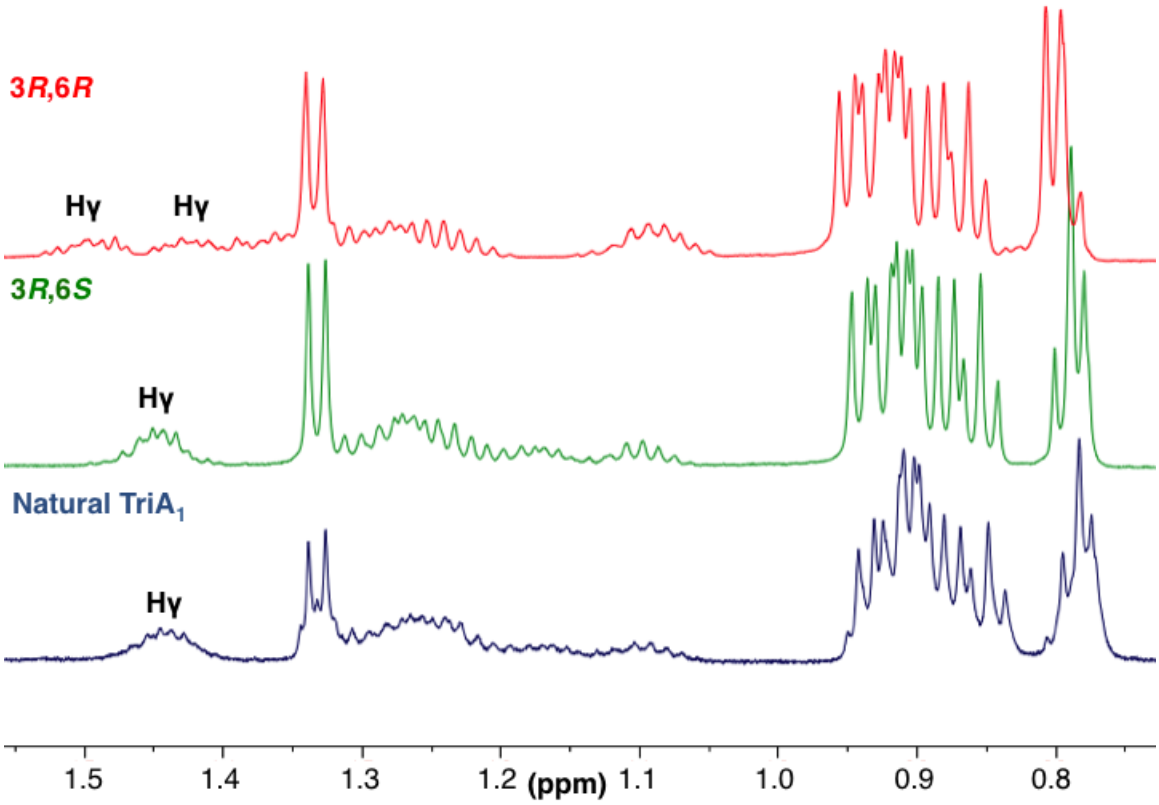

Figure 2.3. ^{1}H-NMR analysis of natural tridecaptin A_1 and the synthetic (3*R*,6*S*) and (3*R*,6*S*) lipid tail isomers.

2.1.3. Results and discussion – Tridecaptin B_1

2.1.3.1. Synthesis of the possible tridecaptin B_1 lipid tail isomers

Tridecaptin B_1 is *N*-terminally acylated with a 6-methyloctanoyl tail, containing just one chiral centre. Therefore, (6*S*)-methyloctanoic acid (**56**) and (6*R*)-methyloctanoic acid (**57**) were synthesized for structural elucidation purposes. The synthesis of both compounds starts with either (2*S*)-methylbutanol (**58**), which is commercially available, or (2*R*)-methylbutanol (**59**), which needed to be synthesized (Scheme 2.4). (2*R*)-methylbutanol (**59**) can be synthesized using a previously published literature

procedure.[140] (4*R*)-Benzyl-2-oxazolidinone (**60**) is first acylated with butanoyl chloride to yield oxazolidinone **61** in excellent yield. Subsequent methylation of **61** by treatment with NaHMDS, followed by MeI, yields enantiomerically pure oxazolidinone **62** in 69% yield. (2*R*)-Methylbutanol (**59**) is synthesized from **62** by treatment with $LiAlH_4$ and used directly in the synthesis of (6*R*)-methyloctanoic acid.

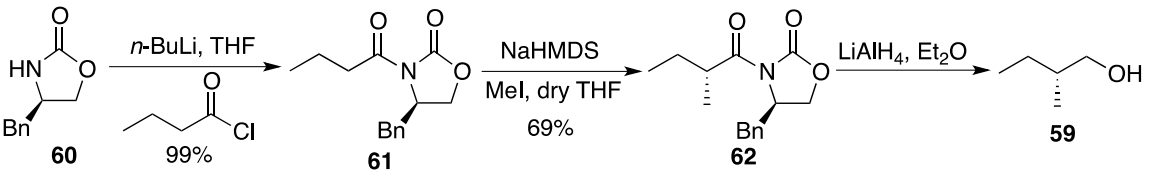

Scheme 2.4. Synthesis of (2*R*)-methylbutanol (**59**).

The 6-methyloctanoic acid enantiomers are synthesized in four steps from their respective 2-methylbutanol enantiomers (Scheme 2.5). Tosylation of (2*S*)-methylbutanol **58** gives tosylate **63** in good yield. A Grignard reaction is then used to extend the carbon chain using commercially available bromo dioxolane **65**, yielding acetal **66**. Deprotection of the acetal under acidic conditions, followed by oxidation of the resulting aldehyde by a Pinnick Oxidation, yields enantiomerically pure (6*S*)-methyloctanoic acid (**56**) in moderate yield. (6*S*)-methyloctanoic acid (**57**) is prepared using the same protocol.

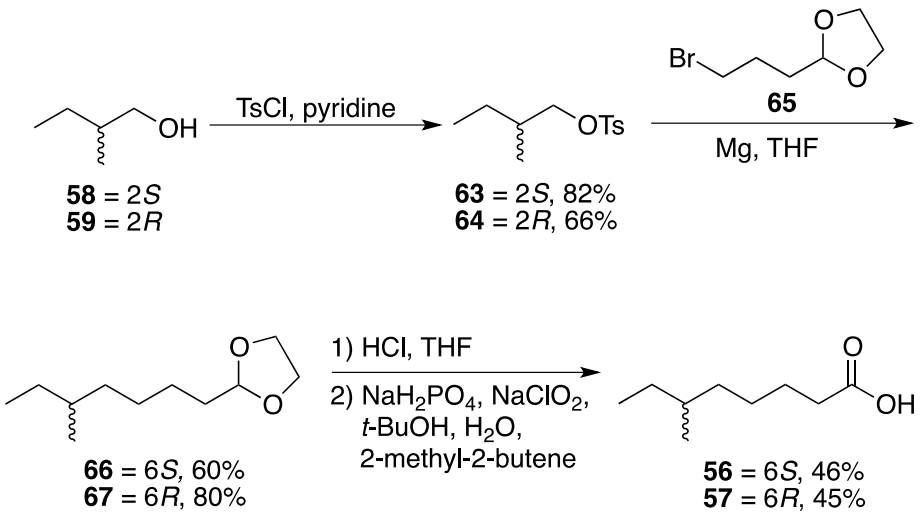

Scheme 2.5. Synthesis of both enantiomers of 6-methyloctanoic acid.

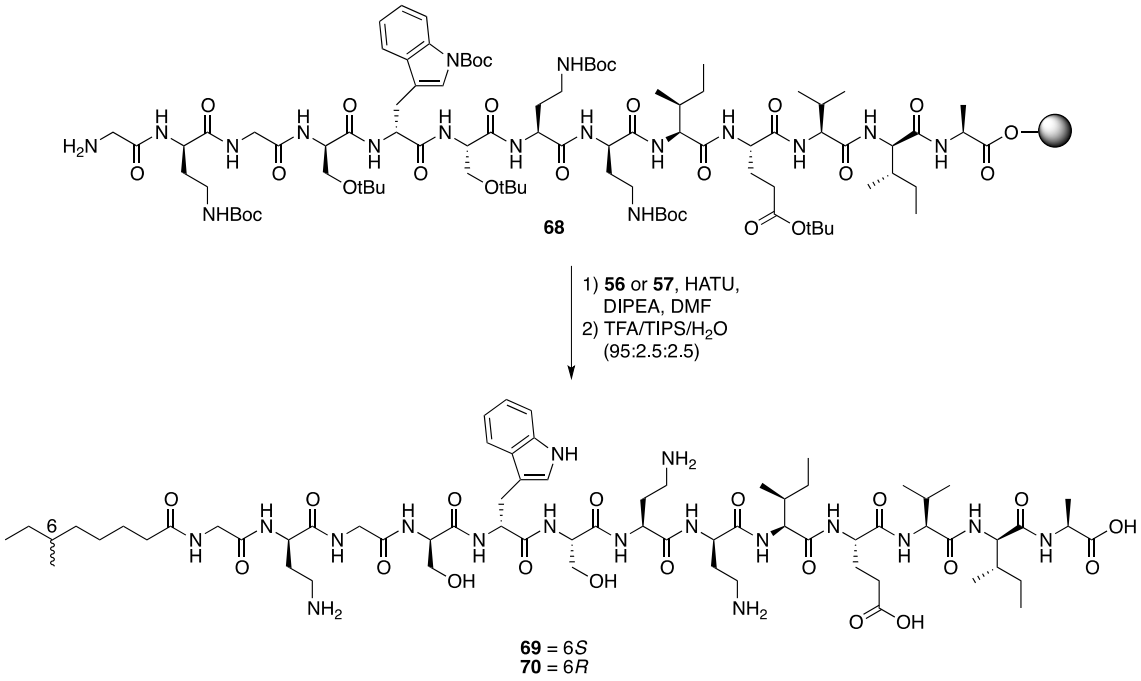

Scheme 2.6. Synthesis of $TriB_1$ lipid tail isomers.

The $TriB_1$ peptide chain is synthesized using Fmoc-SPPS. The *N*-terminus of resin bound $TriB_1$ (**68**) is acylated with either **56** or **57** by first activating the acids with

HATU and then coupling these activated esters to the *N*-terminal residue (Scheme 2.6). Subsequent treatment with TFA and purification by HPLC yields the $TriB_1$ lipid tail isomers **69** and **70**.

2.1.3.2. Analysis of Tridecaptin B_1 lipid tail isomers

Equimolar amounts of the synthetic standards, **69** and **70**, were mixed with natural tridecaptin B_1 and analyzed by HPLC, as described for $TriA_1$. The *R* and *S* isomers could not be distinguished by HPLC, therefore ^{1}H-NMR was used in an attempt to elucidate the stereochemistry. Unfortunately, these isomers were also not distinguishable by ^{1}H-NMR in a variety of solvents, including mixtures of D_2O, C_6D_5N, CD_3CN and d_6-DMSO. Although this method was successful for $TriA_1$, it has an *N*-terminal D-valine residue and a stereogenic 3-hydroxyl group. In contrast, the *N*-terminal residue on $TriB_1$ is glycine and there is no 3-hydroxyl group. It is likely that this additional 'chiral character' on $TriA_1$ allowed the methyl isomers to be distinguished by NMR. Therefore, an alternative method to elucidate the stereochemistry was sought.

2.1.3.3. Derivatization of Tridecaptin B_1 for stereochemical analysis

Our group previously attempted to elucidate the stereochemistry of the tridecaptin A_1 lipid tail by hydrolysis of the lipid tail from the natural peptide, chemical derivatization, and analysis by GCMS.[134] This approach was unsuccessful; however, it seemed that derivatizing the hydrolyzed lipid tail with a chiral compound could allow the resulting lipid tail derivatives to be distinguished by HPLC or ^{1}H-NMR. A literature search identified the Ohrui–Akasaka method as a possible procedure to determine the

stereochemistry of the $TriB_1$ lipid tail. In this approach, long chain chiral fatty acids are derivatized with a chiral anthracenyl derivative.[141] The 100% chiral gauche conformation of the resultant esters places methyl groups at stereogenic centres in close proximity to the anthracene ring, allowing separation of diastereomers by low temperature HPLC (−55 ^{o}C). The fluorescent anthracenyl group also allows for easy detection of very small amounts of material. Therefore, this approach was used to elucidate the stereochemistry of the $TriB_1$ lipid tail.

Chiral anthracenyl derivative **71** is synthesized in excellent yields from 2,3-anthracenedicarboxylic acid anhydride (**72**) and (1*R*,2*R*)-2-aminocyclohexanol (**73**) (Scheme 2.7). (6*S*)-Methyloctanoic acid (**56**) and (6*R*)-methyloctanoic acid (**57**) are derivatized with **71** to yield anthracenyl derivatives **74** and **75**, in good yields, respectively. Gratifyingly, the (6*S*)- and (6*R*)-esters were easily distinguished by comparing their methyl chemical shifts using ^{1}H-NMR. Hydrolysis of natural $TriB_1$ is achieved by heating the peptide at 90 °C in 6 M HCl for 2 hours, and the resulting fatty acid is extracted using Et_2O. This crude acid is coupled to alcohol **71** and the resulting ester compared to **74** and **75** by ^{1}H-NMR and low-temperature HPLC (Fig. 2.4). These results clearly demonstrated that the lipid tail on $TriB_1$ has a (6*S*)-methyl group. Furthermore, this is in agreement with the expected stereochemistry, assuming that the BCFA is derived from isoleucine.

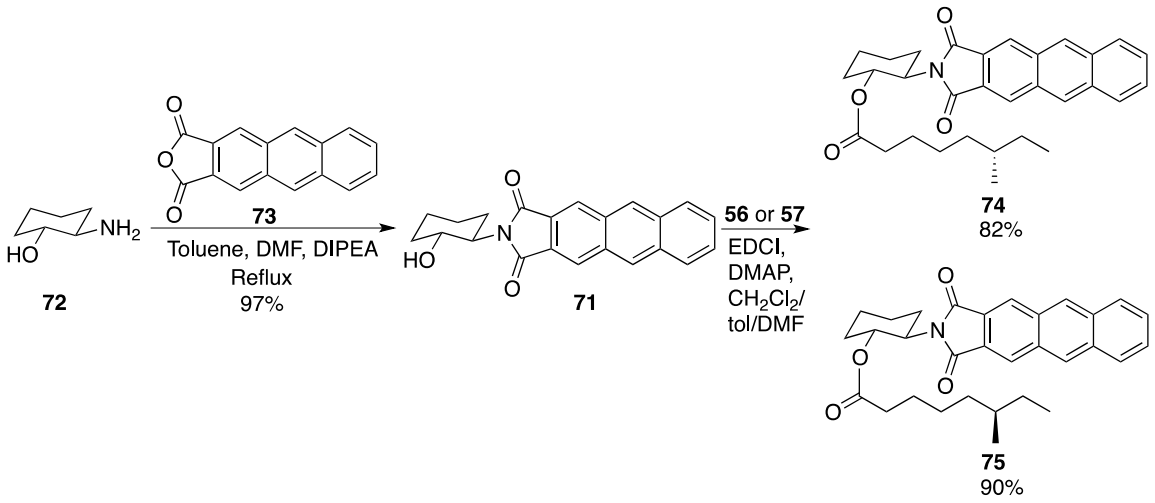

Scheme 2.7. Synthesis of anthracenyl derivatives for use as synthetic standards in determining the stereochemistry of the tridecaptin B_1 lipid tail.

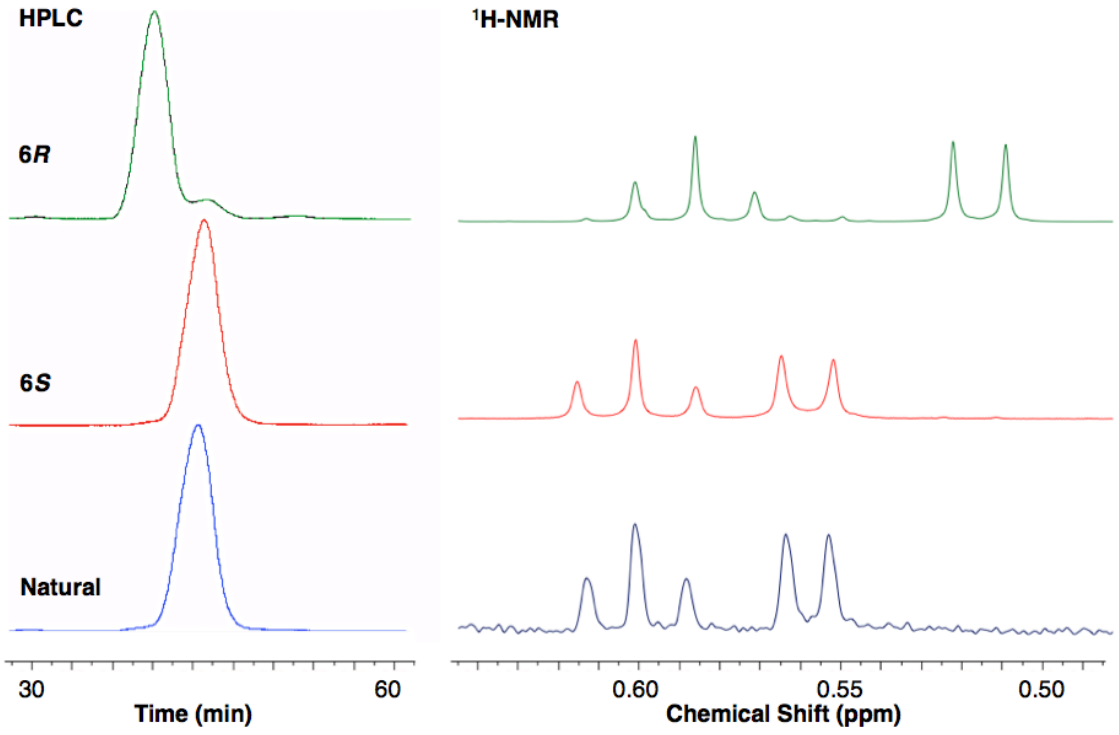

Figure 2.4. Analysis of the hydrolyzed and derivatized lipid tail from $TriB_1$ using HPLC and ^{1}H-NMR.

2.2. Cerexins

2.2.1. Project background

As part of our continued efforts to isolate and characterize new antimicrobial peptides, we decided to investigate the cerexin class of lipopeptides. Although these compounds are not new, there have been no further reports on them since the early isolation and structural characterization papers in the 1970's. Shoji and co-workers deposited the organism responsible for the production of the cerexins to the American Type Culture Collection (ATCC), therefore we obtained this strain for further study.

2.2.2. Results and discussion

2.2.2.1. Isolation of cerexin A_1

It was previously reported that cerexin A was isolated from *B. mycoides* ATCC 21929. This organism was obtained from ATCC and cultured to isolate antimicrobial compounds. Deferred-inhibition assays revealed that only compounds with activity against Gram-positive bacteria were produced, and *S. aureus* ATCC 6538 was identified as a suitable indicator strain. A 4 L culture was grown for 48 hours and the supernatants separated by centrifugation. An activity-guided purification approach using *S. aureus* ATCC 6538 as the indicator strain was used to isolate compounds with Gram-positive activity. The supernatant was first partially purified by HIC using Amberlite XAD 16 resin, which was subsequently washed with water, 20 % IPA, 40 % IPA and 80 % IPA + 0.1 % TFA. Gram-positive activity was only observed in the 80 % IPA wash. This fraction was concentrated and loaded onto a C_{18} solid phase extraction cartridge. The same wash cycle was repeated and once again the 80 % wash contained a

compound(s) with activity against *S. aureus*. Final purification was achieved by HPLC, with four major products identified with Gram-positive activity, P1 – P4 (Fig. 2.5). Analysis by high-resolution MS, tandem mass spectrometry (MS/MS), ^{1}H-NMR, TOCSY and NOESY identified the first fraction, P1, as cerexin A. The standard nomenclature of lipopeptides uses different letters when amino acids are changed and subscripted numbers when the lipid tail is changed within a structural class.[117] Therefore we have renamed this analogue cerexin A_1 ($CxnA_1$) (Fig 2.6). Although the structure of $CxnA_1$ has been previously reported, no effort had been reported to identify the stereochemistry of the β-hydroxy group on its lipid tail. Therefore, we decided to synthesize both possible lipid tail isomers of $CxnA_1$ to unambiguously assign its structure.

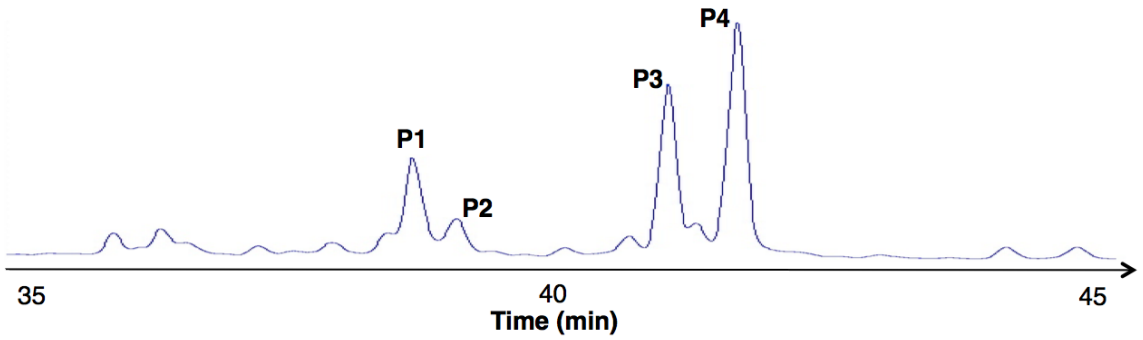

Figure 2.5. HPLC trace of supernatant from *B. mycoides* ATCC 21929.

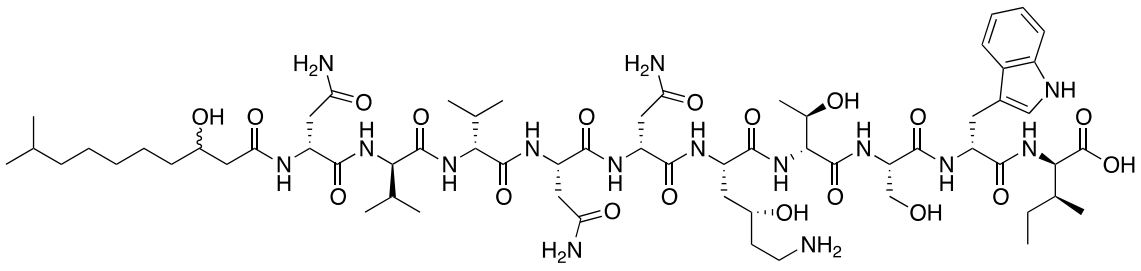

Figure 2.6. Structure of cerexin A_1 with unknown lipid tail stereochemistry.

2.2.2.2. Synthesis of orthogonally protected 4-*threo*-hydroxylysine

Cerexin A_1 contains the non-proteogenic amino acid 4-*threo*-hydroxylysine (4-Hyl), which is also found in collagen,[142] the glidobactins[143,144] and the cepafungins.[145,146] The synthesis of 4-Hyl derivative **76**, which can be used in Fmoc-SPPS, has been reported, therefore we used this procedure in our synthesis of $CxnA_1$.[147] This synthesis was completed with the assistance Mr. Richard Surgenor. Meldrum's acid is coupled to commercially available Boc-Asp-OtBu (**77**) using EDCI/DMAP conditions. The resulting product is refluxed in EtOAc, undergoing decarboxylation to yield an α-ketoketene, which then cyclizes to give ketone **78** in excellent yield. This intermediate is then reduced using $NaBH_4$ in AcOH and the resulting product recrystallized to yield diastereomerically pure alcohol **79** in moderate yield. Protection of the alcohol as a silyl ether proceeds smoothly; however, subsequent ring opening to give alcohol **81** is low yielding. Activation of alcohol **81** with MsCl, followed by substitution with NaN_3 yields azide **82**. Finally, deprotection of the Boc and tBu groups by treatment with TFA, followed by protection of the amine as an Fmoc carbamate yields amino acid **76**.

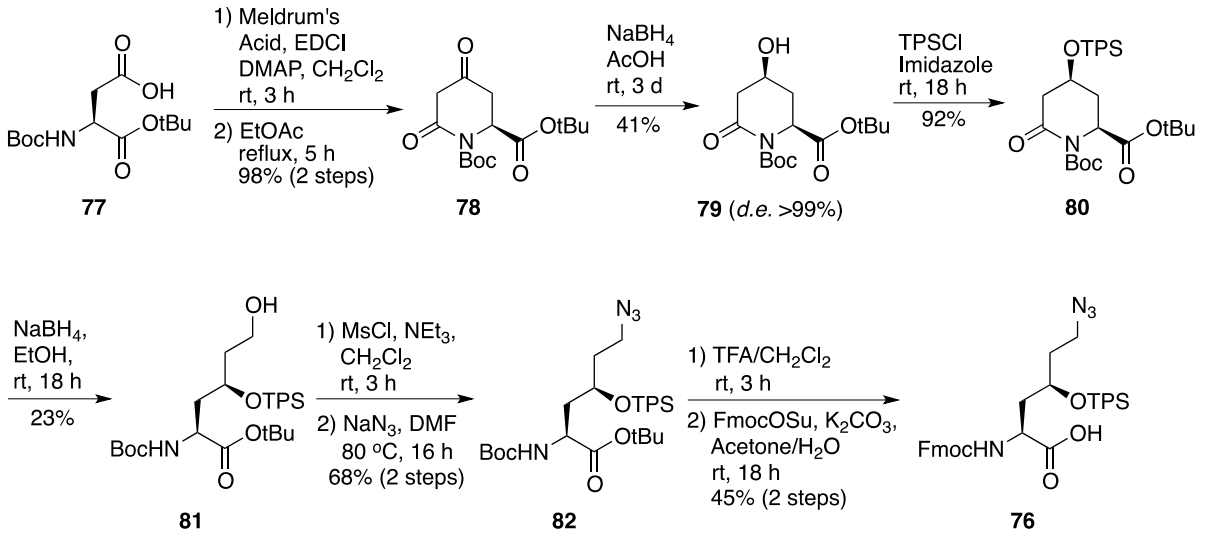

Scheme 2.8. Synthesis of orthogonally protected 4-Hyl analogue **76**.

2.2.2.3. Synthesis of activated fatty acids

Cerexin A_1 is acylated with a 3-hydroxy-9-methyldecanoyl chain. The same strategy employed for the synthesis of $TriA_1$ can be used to prepare both lipid tail isomers of $CxnA_1$. An aldol condensation between 7-methyoctanal (**83**) and acylated Crimmins auxiliary **41** (Scheme 2.9) yields the (3*S*)-alcohol **84** and the (3*R*)-alcohol **85**, which are separable by column chromatography.

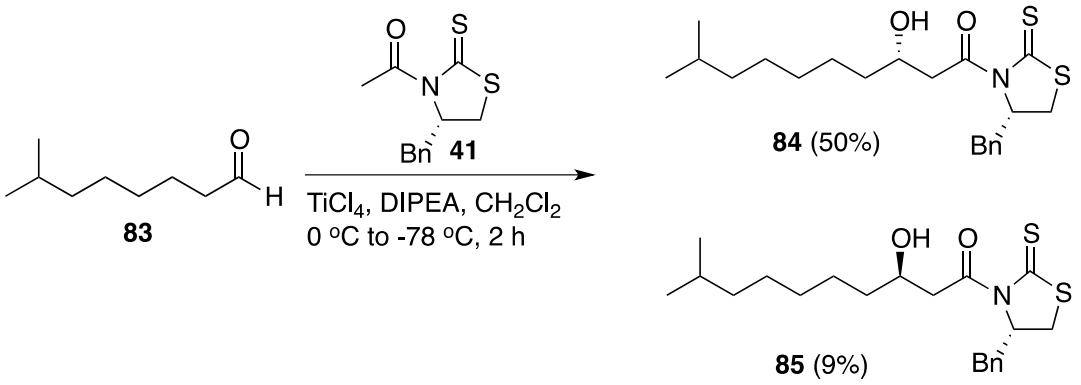

Scheme 2.9. Synthesis of activated fatty acids for $CxnA_1$ synthesis.

2.2.2.4. Synthesis of cerexin A_1 lipid tail isomers

The peptide chain of $CxnA_1$ is synthesized using standard Fmoc-SPPS chemistry to yield on resin peptide **86** (Scheme 2.10). Stirring the on-resin peptide with activated fatty acid **84** or **85** acylates the *N*-terminus with the desired lipid tail. The silyl protecting group of 4-Hyl is then removed by treatment with TBAF, followed by global deprotection and cleavage of the peptides from resin by treatment with TFA. Finally, the crude peptide is dissolved in phosphate buffer and the azide group reduced with TCEP, followed by purification by HPLC to yield the *R*-isomer **31** and *S*-isomer **87**.

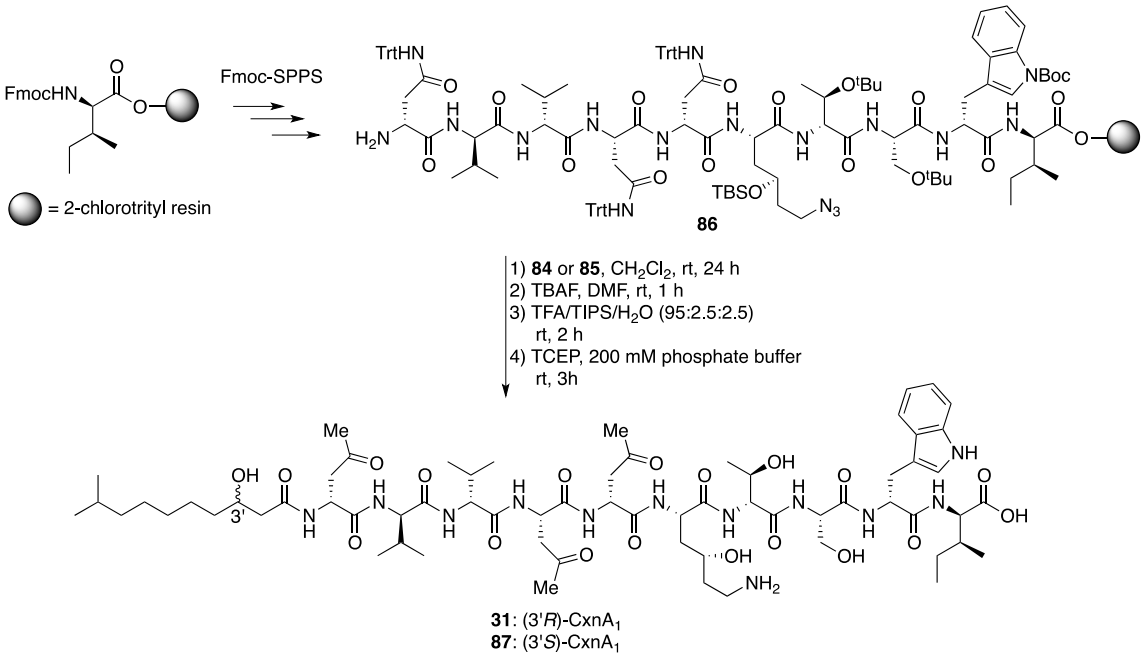

Scheme 2.10. Synthesis of $CxnA_1$ lipid tail isomers.

2.2.2.5. Elucidation of cerexin A_1 lipid tail stereochemistry

The $CxnA_1$ lipid tail isomers **31** and **87** were each mixed with natural $CxnA_1$ and co-injected onto a C_{18} HPLC column. In both cases only one peak was observed, therefore we turned to NMR analysis. Although small differences were visible between the natural $CxnA_1$ ^{1}H-NMR spectra and the ^{1}H-NMR spectra of the synthetic standards, we were not confident enough to use this to assign stereochemistry. Therefore, we turned to the Ohrui–Akasaka method previously used in our studies on tridecaptin B_1.

2.2.2.6. Derivatization of cerexin A_1 for stereochemical analysis

Although the Ohrui–Akasaka method has been almost exclusively used for the assignment of alkyl stereocentres in long chain fatty acids, we rationalized that derivatization of the alcohol on the $CxnA_1$ lipid tail would allow easy assignment of this

stereocentre. Thus, the appropriate synthetic standards were prepared from activated fatty acids **84** and **85** (Scheme 2.11). Hydrolysis of these compounds yields acids **88** and **89** in excellent yields. Methyl ester formation followed by coupling to commercially available carboxylic acid **90**, yields the (3*S*)- and (3*R*)-anthracenyl derivatives **91** and **92**. The lipid tail of $CxnA_1$ is hydrolyzed by heating the peptide at 90 ^oC in 6 M HCl for 2 hours, followed by extraction of the fatty acid with Et_2O. Following the steps outlined in scheme 2.11 yields the derivatized lipid tail, which can then be analyzed by ^1H-NMR.

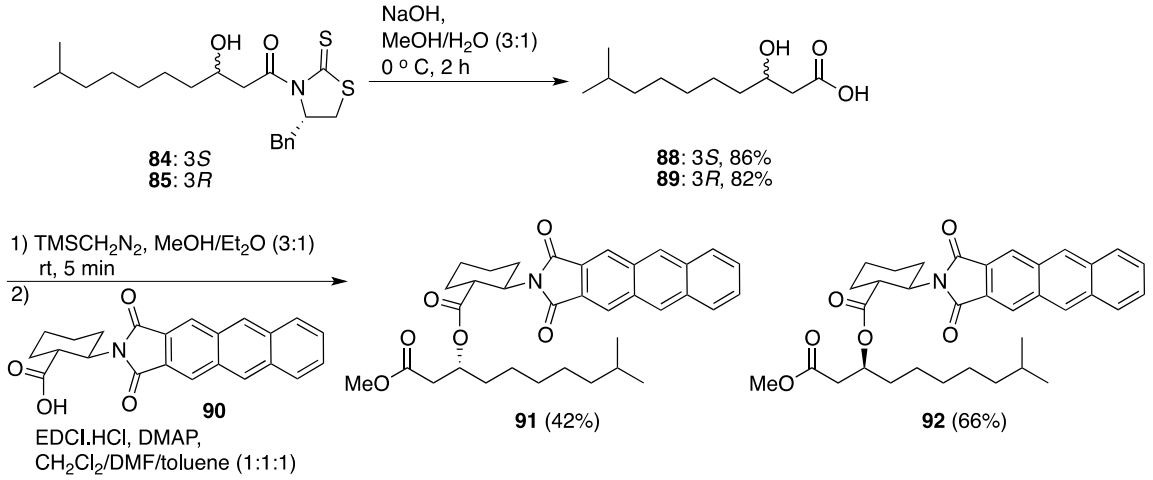

Scheme 2.11. Synthesis of synthetic standards for $CxnA_1$ lipid tail stereochemical analysis.

2.2.2.7. Elucidation of the cerexin A_1 lipid tail stereochemistry

The derivatized $CxnA_1$ lipid tail and synthetic standards **91** and **92** were analyzed by ^1H-NMR. Several differences were found between the (3*S*)- and (3*R*)- standards, but the most notable was in the methyl region of the spectra (Fig. 2.7). This clearly shows that

the stereochemistry of the 3-hydroxyl group on cerexin A_1's lipid tail has the *R*-configuration, which was also the case for tridecaptin A_1.

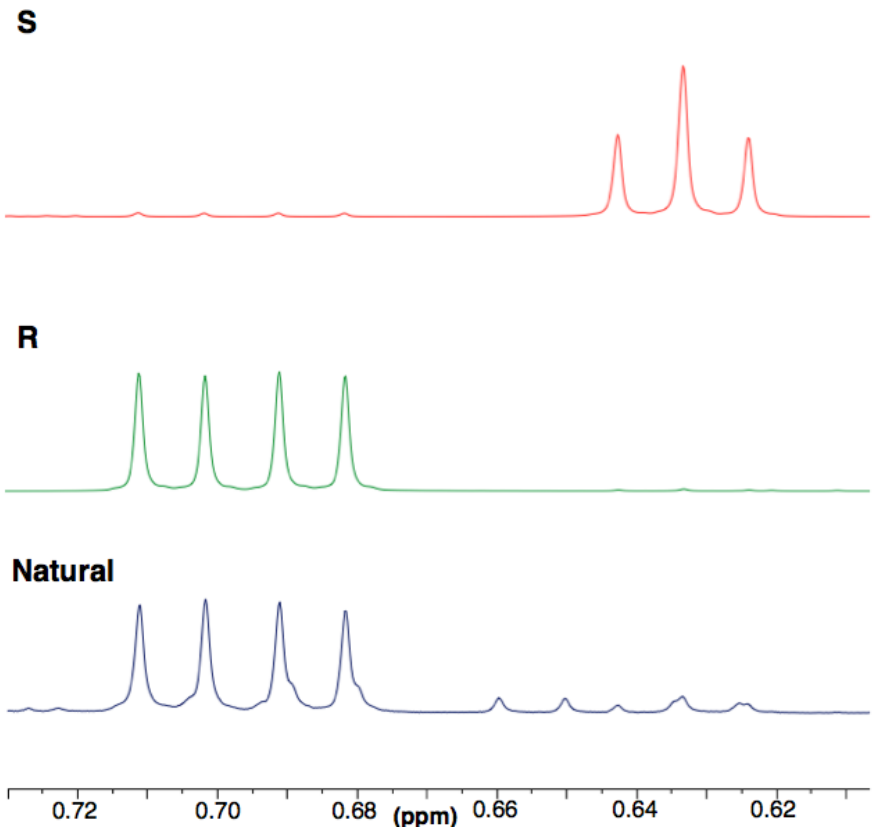

Figure 2.7. Determination of $CxnA_1$ lipid tail stereochemistry using the Ohrui–Akasaka method.

2.2.2.8. Characterization of other cerexin analogues produced by *B. mycoides* ATCC 21929

We next focused our attention on the identification of the other active compounds isolated from *B. mycoides* ATCC 21929 (P2 – P4, Fig. 2.5). High-resolution MS revealed that the molecular formulae of compounds relating to P2 (**93**), P3 (**94**) and P4 (**95**) differed from $CxnA_1$ by $+C_3H_2O_2$, $+C_4H_4O_3$ and $+C_4H_4O_2$ respectively (Table 2.2).

MS/MS analysis of **94** and **95** revealed that their lipid tail and amino acid sequence was identical to $CxnA_1$, with the exception of residue 6, which is 4-Hyl in $CxnA_1$. Compound **93** has a linear lipid tail that is one methylene shorter than the lipid tail on $CxnA_1$ and like compound **95**, has $+C_4H_4O_2$ on residue 6.

Compound	$[M+H]^+$	Molecular Formula	Difference with $CxnA_1$
$CxnA_1$ (**31**)	1374.7644	$C_{63}H_{104}N_{15}O_{19}$	N/A
93	1444.7694	$C_{66}H_{106}N_{15}O_{21}$	$+C_3H_2O_2$
94	1474.7808	$C_{67}H_{108}N_{15}O_{22}$	$+C_4H_4O_3$
95	1458.7860	$C_{67}H_{108}N_{15}O_{21}$	$+C_4H_4O_2$

Table 2.2. Comparison of cerexin analogues **93** – **95** with $CxnA_1$.

We therefore considered the possible modifications that could account for the extra mass units on residue 6 in these cerexin analogues. All known cerexins have either lysine or hydroxylysine at this position on the peptide chain. The side-chain amine on lysine is commonly modified in ribosomally and non-ribosomally synthesized peptides, therefore we considered that the extra mass units may result from modification of lysine or hydroxylysine in position 6. Recently, succinylation has been identified as a post-translational modification found in many ribosomally synthesized proteins.[148] To the best of our knowledge, only lysine succinylation in ribosomally synthesized peptides has been reported. Such a modification was found in unnatural thiocillin variants produced by pre-peptide gene replacement in a *B. cereus* strain.[149] When a threonine residue was replaced with lysine, products with +100.106 Da ($+C_4H_4O_3$) were identified that corresponded to succinylation of the lysine residue. We therefore considered that compound **94** might be succinylated $CxnA_1$.

To prove this hypothesis, peptide **94** was characterized using 2D-NMR experiments. The indole NH signal was used as an entry point and a combination of ^{1}H-^{1}H TOCSY and ^{1}H-^{1}H NOESY were used to fully assign all proton chemical shifts (Fig. 2.8). This data, in combination with the integration and multiplicity of the proton signals from the Hyl-ε-acyl group (Fig. 2.9), allowed unambiguous identification of the succinyl group.

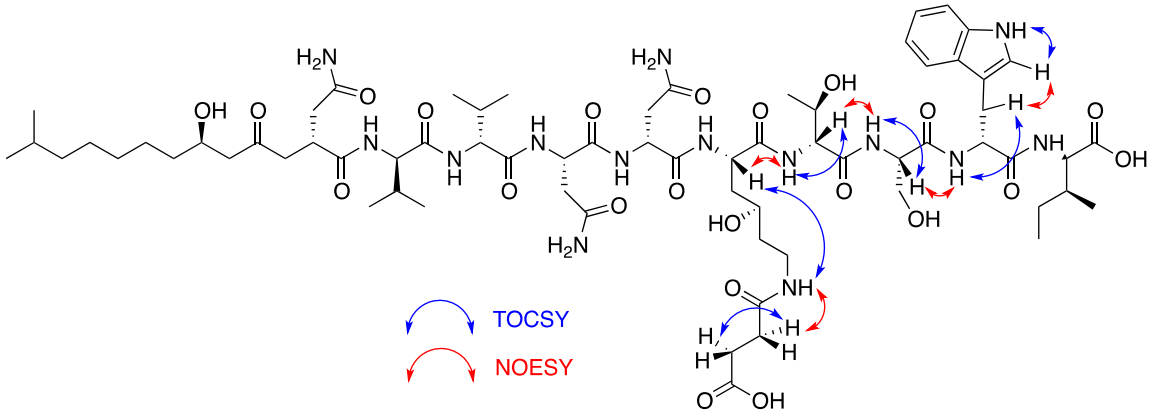

Figure 2.8. Key NOESY and TOCSY correlations allowing the complete structural assignment of $CxnE_1$.

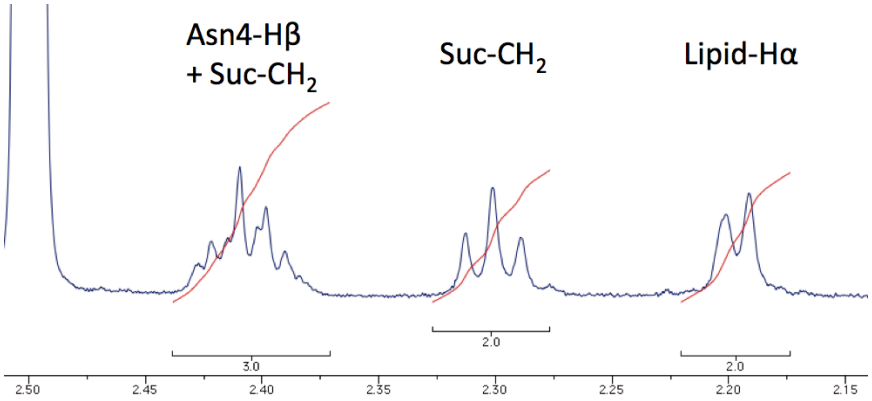

Figure 2.9. Zoom in of ^{1}H-NMR spectrum of $CxnE_1$ highlighting the signals resulting from the succinyl group. The chemical shift of both CH_2 signals, and the multiplicity (triplet) of the non-overlapping CH_2 confirm the presence of a succinyl group.

Furthermore, treatment of $CxnA_1$ with 100 equiv of succinic anhydride yielded a new succinylated product with an identical retention time to **94** (Fig. 2.10). Therefore, **94** has been designated as $CxnE_1$. This lead us to conclude that compounds **93** and **95**, which contain one less oxygen at residue 6, are composed of succinylated lysine (Fig. 2.11) and have been designated $CxnF_1$ and $CxnF_2$ respectively.

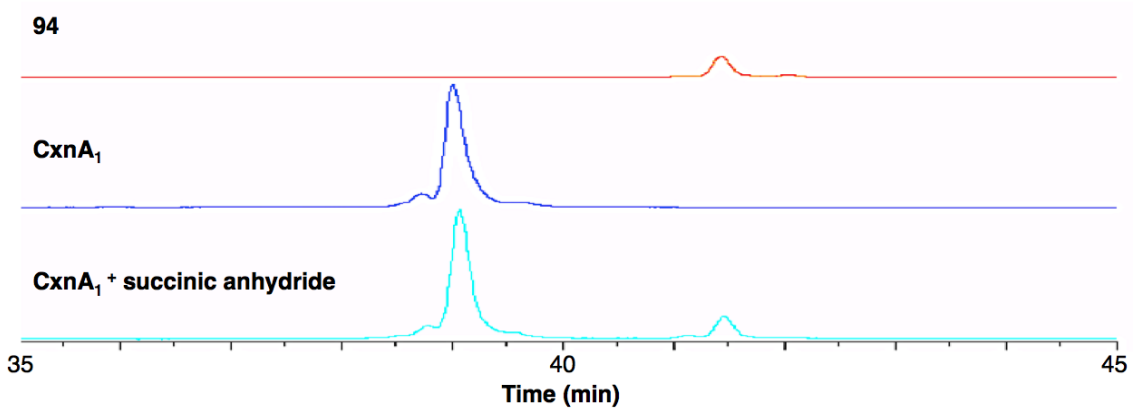

Figure 2.10. Succinylation of $CxnA_1$ shows compound **94** is succinylated $CxnA_1$.

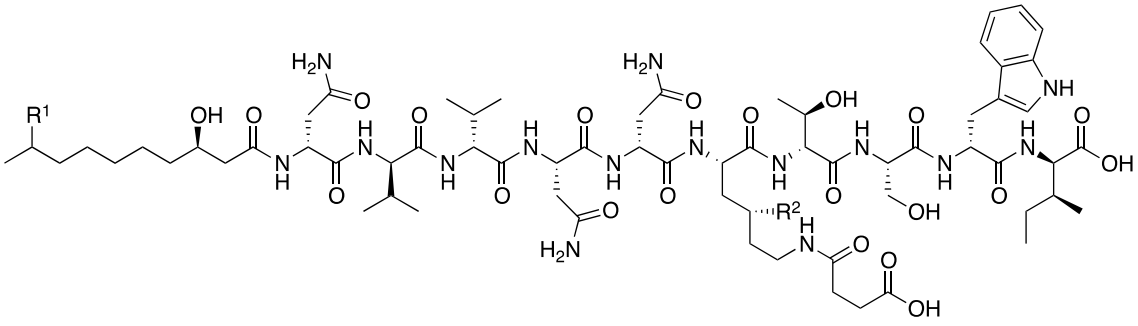

Figure 2.11. Structures of new cerexin analogues.

2.2.2.9. New synthesis of orthogonally protected 4-*threo*-hydroxylysine

2.2.2.9.1. Iodolactonization approach to hydroxylysine synthesis

During the synthesis of cerexin A_1, we rationalized that a shorter synthesis of an orthogonally protected 4-*threo*-hydroxylysine analogue, suitable for use in Fmoc-SPPS, should be possible. Previous studies have shown that kinetically controlled iodolactonizations of allylglycine (Agl) derivatives give predominantly *cis*-products, which upon ring opening would yield the desired *threo*-configuration.[150,151,152] Therefore, the synthesis of 4-*threo*-hydroxylysine using a kinetically controlled iodolactonization of allylglycine as the key step was attempted (Scheme 2.12).

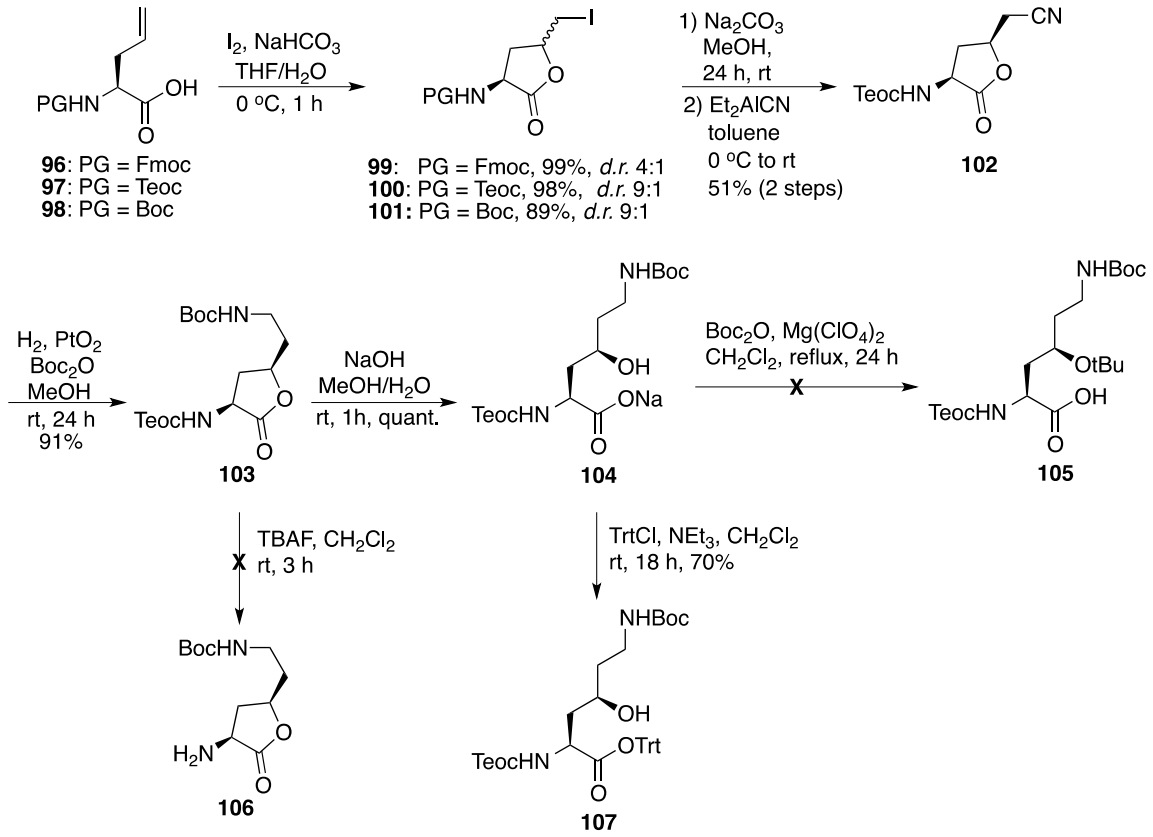

Scheme 2.12. Attempted synthesis of orthogonally protected *threo*-4-hydroxylysine via a kinetically controlled iodolactonization of allylglycine

We first used commercially available Fmoc-Agl-OH (**96**). Treatment of **96** with iodine and $NaHCO_3$ at 0 ^oC yields a 4:1 inseparable mixture of *cis*- and *trans*-iodolactones. Subsequent attempts to displace the iodine with NaCN resulted in Fmoc deprotection. Therefore a different starting material, Teoc-Agl-OH (**97**), was used. The Teoc protecting group is removed by treatment with TBAF, which can be performed in SPPS. A kinetically controlled iodolactonization of **97** yields an inseparable 9:1 mixture of *cis*- and *trans*-iodolactones **100,** with complete consumption of starting material. Multiple attempts were made to directly convert iodide **100** to nitrile **102**, however this material proved refractory to direct cyanation. Instead, methanolysis of iodolactone **100** yields an epoxy methyl ester, which is inseparable from unreacted starting material. Therefore, this intermediate is directly treated with Nagata's reagent (Et_2AlCN) in toluene. Rather than the expected methyl ester product, *cis*-lactone **102** is the product of this reaction. Presumably, the Lewis acid forms a six-membered ring by coordinating to the oxygen of the epoxide and carbonyl (Fig. 2.11). After cyanation of the epoxide, the resulting alkoxide ion will attack the carbonyl to give *cis*-lactone **102**. Reduction of nitrile **102** and concomitant protection as a Boc-carbamate yields *cis*-lactone **103** in excellent yield. Hydrolysis of **103** with sodium hydroxide yields alcohol **104**, which cannot be protonated to form the free acid as this undergoes rapid cyclization back to the five-membered ring. Unfortunately it was not possible to protect alcohol **104** as a *tert*-butyl ether, therefore attempts were made to protect it as a trityl ether. The protecting group on this position must be orthogonal to the Teoc group otherwise it may be deprotected upon Teoc deprotection on resin. Treatment of alcohol **104** did not yield the trityl ether, with the trityl ester **107** isolated as the main product. In a final attempt to

save this approach, deprotection of the Teoc-carbamate **103** was attempted for possible conversion to Fmoc-carbamate **106**. The free amine proved unstable and rapidly decomposed upon formation. Therefore, an alternative strategy to synthesize orthogonally protected *threo*-4-hydroxylysine was sought.

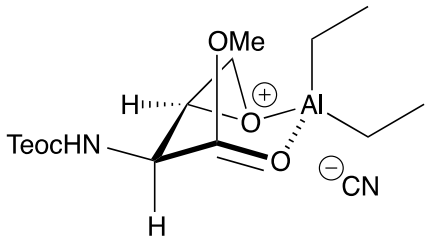

Figure 2.11. Proposed transition state for formation of *cis*-lactone **102**.

2.2.2.9.2. Reformatsky approach to hydroxylysine synthesis

A Reformatsky reaction is a common method to convert aldehydes to β-hydroxy esters. Although less common than the traditional Reformatsky reaction, it is possible to convert aldehydes directly to β-hydroxy nitriles using zinc and 2-bromoacetonitrile.[153] Thus, a Reformatsky type reaction was used as they key step in a new synthesis of orthogonally protected *threo*-4-hydroxylysine. This work was completed with the assistance of a summer student, Kevin Khey.[211]

Commercially available Boc-Asp-OtBu (**77**) is coupled to ethanethiol using DCC/DMAP conditions, to give thioester **108** in excellent yield (Scheme 2.13). The thioester is then reduced to aldehyde **109** in another excellent yielding reaction. Aldehyde **109** is treated with 2-bromoacetonitrile, zinc and TMSCl, followed by protection of the resulting β-hydroxy nitrile diastereomers as silyl ethers. This allowed much easier purification of the reaction products. The more polar diastereomer

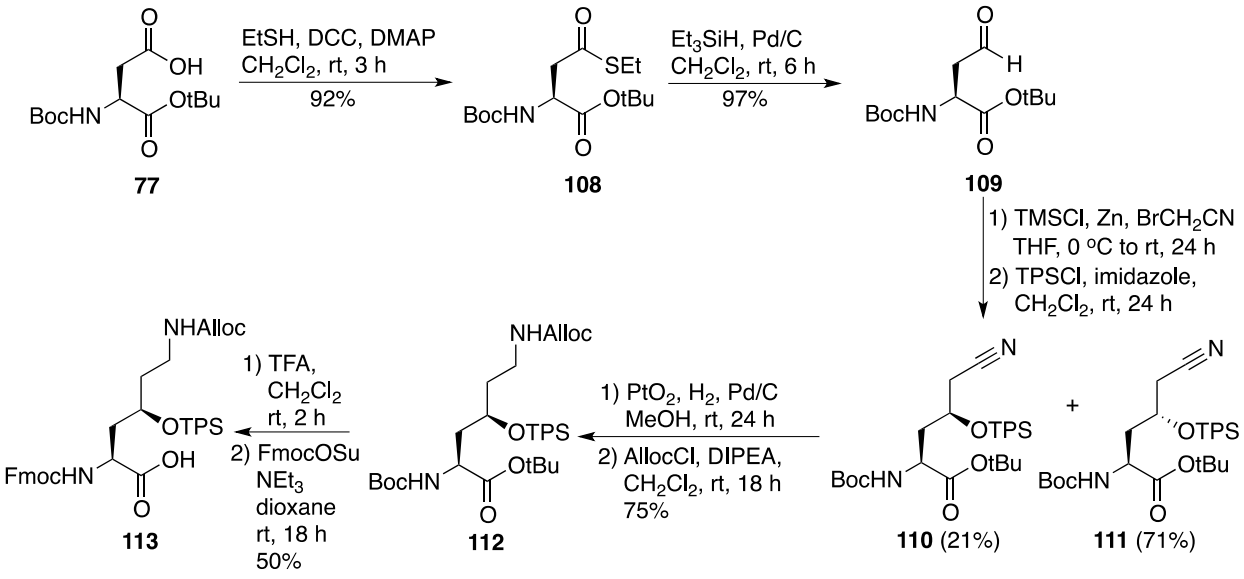

Scheme 2.13. Synthesis of orthogonally protected *threo*-4-hydroxylysine via a nitrile-Reformatsky reaction.

crystallized upon standing at ambient temperature for one week, therefore an X-ray crystal structure of this compound was obtained (Fig. 2.12). This allows the unambiguous assignment of the more polar diastereomer as *erythro*-silyl ether **111** and the less polar diastereomer as *threo*-silyl ether **110**. The overall yield for these two steps is 92% and the *threo:erythro* ratio is approximately 1:3. *Threo*-silyl ether **110** is reduced using Adam's catalyst and hydrogen, followed by protection of the resulting amine as an Alloc-carbamate. This protecting group can be orthogonally deprotected using palladium on resin.[154] Treatment with TFA removes the Boc and tBu groups and subsequent Fmoc protection of the resulting amine yields orthogonally protected *threo*-4-hydroxylysine **113** in good yields.

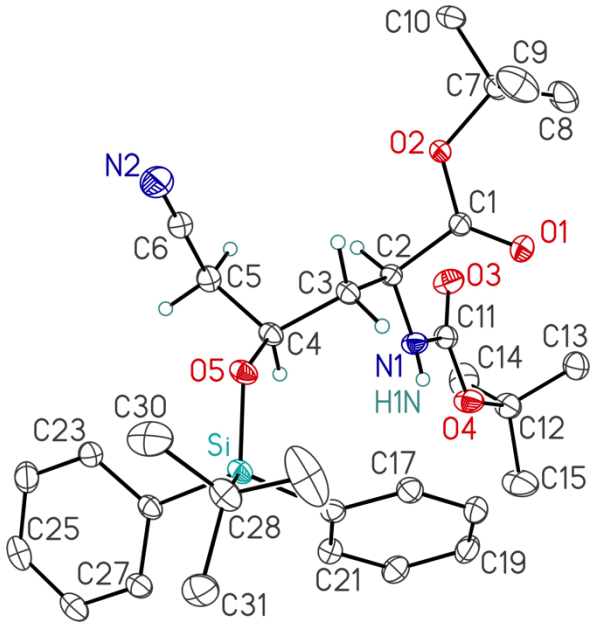

Figure 2.12. Crystal structure of compound **111**. Irrelevant hydrogens are omiited for clarity.

Overall, this approach is one step shorter than the literature procedure and offers the product in comparable yields. However, it also allows for the synthesis of orthogonally protected *erythro*-4-hydroxylysine. This isomer is found in the cepafungins and glidobactins, and we hope this new synthesis proves useful in other applications requiring 4-hydroxylysine analogues.

2.3. Conclusions

The work presented in this chapter highlights the power of chemical synthesis in allowing us to determine the absolute structure of natural products. In particular, we have shown that the previously reported Ohrui–Akasaka method for derivatizing chiral fatty acids is a rapid and reliable method for assigning the stereochemical configuration of lipopeptide lipid tails. A new procedure for the isolation of cerexin lipopeptides is also

reported. We have shown that in addition to producing the cerexin archetype, cerexin A_1, *B. mycoides* ATCC 21929 produces cerexin analogues, $CxnE_1$, $CxnF_1$ and $CxnF_2$. To the best of our knowledge, this is the first reported instance of succinylation in natural non-ribosomally synthesized peptides. A new synthesis of orthogonally protected *threo*-4-hydroxylysine and *erythro*-4-hydroxylysine is reported, which makes use of a nitrile-Reformatsky-type reaction as a key step. As a result of this work several tridecaptins and cerexin analogues were isolated/synthesized and subsequently used in structure-activity relationship studies, which are reported in chapter 3.

Chapter 3

Structure activity relationship studies on antimicrobial lipopeptides

3.1. Project background

During our structural elucidation of tridecaptin and cerexin lipopeptides, described in chapter 2 of this thesis, we synthesized and isolated several natural and unnatural analogues. Given the need for new classes of antibiotics, the antimicrobial activities of these compounds were characterized to determine if they would be good candidates for further *in vivo* studies.

3.2. Results and Discussion

3.2.1. SAR studies on tridecaptin A_1 lipid tail analogues

3.2.1.1. Antimicrobial activity of tridecaptin A_1 lipid tail stereoisomers

The antimicrobial activity of TriA_1 (**32**), (3*S*,6*S*)-TriA_1 (**53**), (3*R*,6*R*)-TriA_1 (**54**) and (3*S*,6*R*)-TriA_1 (**55**) were determined against a panel of Gram-positive (Table 3.1) and Gram-negative bacteria (Table 3.2). The strains selected are representative of clinically relevant pathogens. *E. faecalis* and *E. faecium* are members of the *Enterococcus* genus, which can cause urinary tract infections, meningitis, bacteremia, bacterial endocarditis and diverticulitis.[155,156] VRE is a particularly virulent strain that causes hospital-acquired infections. *Staphylococcus aureus* can cause a wide range of illnesses, including minor skin conditions like impetigo and life-threating diseases like pneumonia and meningitis.[157] Methicillin resistant *S. aureus* (MRSA) is the superbug archetype, which is resistant to most β-lactams. *Listeria monocytogenes* is a common

foodborne pathogen that causes listeriosis, which is estimated to cause 1600 illnesses and 260 deaths annually in the United States.[158] $TriA_1$ and its lipid tail stereoisomers have poor activity against these Gram-positive organisms.

	Activity (μg/mL)			
Analogue	***E. faecalis* ATCC 29212**	***S. aureus* ATCC 29213**	***L. monocytogenes* ATCC 15313**	***E. faecium* ATCC 19434**
$TriA_1$	>100	>100	50	>100
(3*S*,6*S*)-$TriA_1$	>100	>100	100	>100
(3*R*,6*R*)-$TriA_1$	>100	>100	100	>100
(3*S*,6*R*)-$TriA_1$	>100	>100	>100	>100

Table 3.1. $TriA_1$ lipid tail stereoisomers activity against Gram-positive bacteria.

Escherichia coli is the best-studied bacterium on the planet. Although most strains are fairly benign, some can cause serious foodborne illness, with *E. coli* O157:H7 being one of the most common.[159] *Salmonella enterica* is another species of Gram-negative bacteria that causes foodborne illness. *Campylobacter jejuni* was discussed in chapter 2 and the emergence of resistant strains may pose serious problems for future generations if left unchecked.[131] *Pseudomonas aeruginosa* is an opportunistic organism that causes a range of hospital-acquired infections. This is a particularly problematic pathogen as it contains an outer-membrane, multidrug efflux pumps and quite easily develops resistance against antibiotics.[160] *Klebsiella pneumoniae* causes several illnesses including pneumonia and serious hospital acquired infections. Carbapenem-resistant *Klebsiella pneumoniae* (CRKP) strains are particularly problematic as they are resistant to multiple classes of antibiotics, including aminoglycosides, fluoroquinolones and β-lactams.[57] These infections have an

associated mortality rate of over 50%.[58] *Acinetobacter baumannii* is another opportunistic pathogen that causes hospital acquired infections. More recently, carbapenemase-producing XMR strains of *Acinetobacter baumannii* have been found that are particularly adept at developing antibiotic resistance against antibiotics.[59]

Tridecaptin A_1 displays strong activity against most of these strains of Gram-negative bacteria, with the exception being *P. aeruginosa*. The typical error in MIC determination by broth-dilution assay is ±two-fold, therefore (3*S*,6*S*)-TriA_1 (**53**) and (3*R*,6*R*)-TriA_1 (**54**) have similar antimicrobial activities to TriA_1. This suggests that the stereochemical elements of the lipid tail are superfluous to the antimicrobial activity. Interestingly, the (3*S*,6*R*)-isomer **55**, in which both stereocentres are inverted, shows diminished activity relative to the natural peptide and may be due to a different arrangement of the peptide tertiary structure. The observation that the stereochemical elements on the lipid tail could be varied whilst retaining activity suggested that the chiral lipid tail could be replaced with a synthetically simpler analogue.

	Activity (μg/mL)					
Analogues	***E. coli* ATCC 25922**	***S. enterica* ATCC 13311**	***P. aeruginosa* ATCC 27853**	***C. jejuni* NCTC 11168**	***K. pneumoniae* ATCC 13883**	***A. baumannii* ATCC 19606**
32	3.13	6.25	50	1.56	3.13	12.5
53	6.25	6.25	50	1.56	6.25	25
54	3.13	6.25	50	3.13	6.25	12.5
55	12.5	25	100	3.13	12.5	50

Table 3.2. TriA_1 lipid tail stereoisomers activity against Gram-negative bacteria.

3.2.1.2. Synthesis and antimicrobial profiling of tridecaptin A_1 lipid tail analogues

The quantities of $TriA_1$ isolated from its producer strain are too low to be viable for large-scale production of the peptide (~2 mg/L). Although this could be optimized, chemical synthesis is an attractive alternative as it allows much larger quantities of the antimicrobial peptide to be obtained. However, the synthesis of the natural lipid tail of $TriA_1$ requires several linear steps from expensive chiral starting materials. Replacement of the chiral lipid tail with a structurally simpler and commercially available acyl chain would make tridecaptin A_1 more accessible for future studies. Therefore, a small library of lipid tail analogues was synthesized using Fmoc-SPPS and evaluated their antimicrobial activity against the strains listed in tables 3.1 and 3.2 (Fig. 3.1).[161]

To determine if the 3-hydroxyl and 6-methyl groups are required for activity, the octanamide analogue Oct-$TriA_1$ (**119**) was synthesized. This analogue fully retains the activity of the natural peptide against all organisms. Furthermore, Oct-$TriA_1$ is synthetically more accessible than $TriA_1$ and enables large quantities of peptide to be obtained for biological studies (~ 100 mg from 0.1 mmol resin). Encouraged by this result we then proceeded to test how the length of the lipid tail affects the antimicrobial activity of $TriA_1$. H-$TriA_1$ (**114**), an analogue with no lipid tail, is substantially less active than the natural peptide, typically requiring concentrations of 100 μg/mL or more to kill bacteria. Lipopeptides generally exert their bactericidal effect through lysis of the bacterial membrane. For the analogous polymyxins, this requires insertion of the lipid tail into the phospholipid bilayer, with unacylated polymyxin analogues showing no activity. [46] This is likely why H-$TriA_1$ also has limited antimicrobial activity.

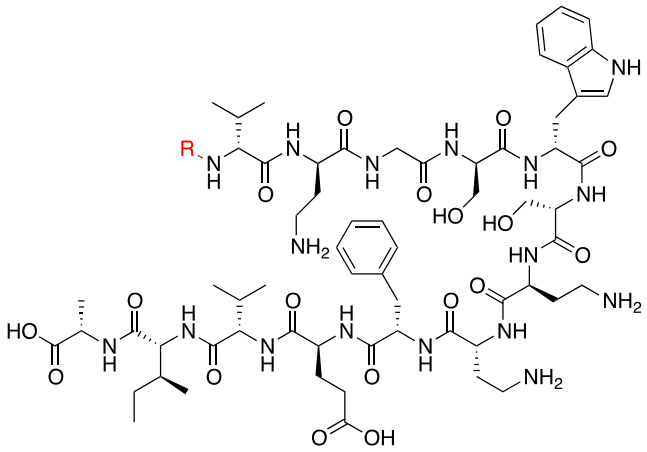

114: R = H; **115**: R = C(O)CH_3; **116**: R = C(O)C_3H_7; **117**: R = C(O)C_5H_{11};
118: R = C(O)C_6H_{13}; **119**: R = C(O)C_7H_{15}; **120**: R = C(O)C_8H_{17};
121: R = C(O)C_9H_{19}; **122**: R = C(O)$C_{10}H_{21}$; **123**: R = C(O)$C_{11}H_{23}$;
124: R = C(O)$C_{13}H_{27}$; **125**: R = C(O)$C_{15}H_{31}$; **126**: R = Fmoc;
127: R = Fpa; **128**: R = Apa; **129**: R = Aaa; **130**: R = PEG; **131**: R = Bio

Analogues	*E. coli*	*S. enterica*	*P. aeruginosa*	*C. jejuni*	*K. pneumoniae*	*A. baumannii*	*E. faecalis*	*S. aureus*	*L. monocytogenes*	*E. faecium*
TriA$_1$	3.13	6.25	50	1.56	3.13	12.5	>100	>100	50	>100
114	100	100	100	>100	50	>100	>100	>100	>100	>100
115	50	100	>100	100	50	>100	>100	>100	>100	>100
116	12.5	25	>100	12.5	25	100	>100	>100	>100	>100
117	3.13	6.25	50	3.13	3.13	25	>100	>100	100	>100
118	6.25	12.5	50	1.56	6.25	12.5	>100	>100	50	>100
119	3.13	6.25	25	0.78	3.13	12.5	100	100	25	50
120	12.5	6.25	100	0.78	12.5	50	100	100	25	100
121	6.25	12.5	>100	0.4	6.25	12.5	>100	>100	25	100
122	6.25	12.5	>100	0.4	6.25	12.5	>100	>100	25	100
123	12.5	50	>100	0.4	12.5	50	>100	>100	50	100
124	>100	>100	>100	12.5	>100	>100	>100	>100	>100	>100
125	>100	>100	>100	50	>100	>100	>100	>100	>100	>100
126	6.25	6.25	>100	0.78	6.25	12.5	50	100	12.5	25
127	6.25	>100	>100	1.56	100	>100	>100	>100	100	>100
128	6.25	12.5	>100	1.56	12.5	25	>100	>100	50	>100
129	6.25	6.25	50	1.56	12.5	12.5	50	50	25	50
130	>100	>100	>100	>100	>100	>100	>100	>100	>100	>100
131	50	50	>100	50	50	>100	>100	>100	>100	>100

Fig. 3.1. Activity of TriA$_1$ lipid tail analogues shown in μg/mL.

Analogues with a lipid tail shorter than C_6 or longer than C_{12} are also less active than the natural peptide, with the optimal length of the linear lipid tail in the C_8-C_{11} range. Shorter chains are likely less effective at disruption of the cell membrane whilst longer alkyl chains may result in lower activity due to poor solubility or micelle formation through hydrophobic interactions, preventing effective membrane disruption.

Previous SAR studies by our group on the two-component lantibiotic, lacticin 3147 A1 and A2, showed that a lacticin 3147 A2 analogue in which the *N*-terminal pentapeptide (13 linear step synthesis) is replaced with an Fmoc group retains its biological activity.[162] It was postulated that the Fmoc group retains the hydrophobic and planar character of the *N*-terminal pentapeptide. Fmoc-TriA_1 (**126**) was therefore synthesized and tested. The Fmoc analogue **126** retains activity against all the tested Gram-positive and Gram-negative organisms. However, it is possible that cleavage of the Fmoc-carbamate occurs *in vivo*, releasing a toxic benzofulvene moiety that causes the antimicrobial activity. Benzofulvene is a potent Michael-acceptor and could potentially react with a variety of cellular nucleophiles, leading to cell death. Therefore, Fpa-TriA_1 (**127**), which contains an analogous lipid tail with an amide rather than a carbamate linkage, was synthesized and tested. Fpa-TriA_1 cannot be *N*-terminally deprotected under basic conditions. This analogue retains activity against most of the Gram-negative organisms and suggests that the activity observed for Fmoc-TriA_1 is due to the lipid tail and not a cleaved side product. To further probe this hypothesis, Apa-TriA_1 (**128**) was synthesized and found to have comparable activity to the natural peptide.

Next, the importance of flexibility in the lipid tail was tested by synthesizing and testing Aaa-TriA_1 (**129**), which contains a carboxymethyladamantanyl lipid tail. Aaa-TriA_1 has comparable activity to the natural peptide against Gram-negative bacteria. Also, a PEGylated analogue of TriA_1, PEG-TriA_1 (**130**), in which the *N*-terminus is replaced with a triethylglycol analogue, was synthesized. PEGylation has been shown to be an effective strategy for increasing the solubility of drug molecules whilst retaining their activity.[163] PEG tails have the advantage of being soluble in both water and organic solvents and could therefore be an ideal lipid tail modification to improve TriA_1 solubility whilst retaining its hydrophobic character. Unfortunately, PEG-TriA1 was inactive against all organisms at the concentrations tested. The presence of heteroatoms in the lipid tail likely prevents effective interaction with the cell membrane or alters the conformation of the peptide, abolishing the antimicrobial activity. This effect is further highlighted by the lower activity of the biotin analogue **131**. Overall, this small library of lipid tail analogues shows that provided the hydrophobicity of the tail is maintained, and the carbon-chain length is not too long, the antimicrobial activity of the TriA_1 analogues is conserved.

3.2.1.3. Cytotoxicity and hemolytic activity of TriA_1 lipid tail analogues

The selective activity of TriA_1 against Gram-negative bacteria is a promising discovery, especially given the lack of new classes of antibiotics active against Gram-negative bacteria. However, a valid concern is that lipopeptides, which usually operate through a membrane-lysis mechanism, may also be toxic to human cells. Therefore, the hemolytic activities of TriA_1 and five lipid tail analogues, H-TriA_1 (**114**), But-TriA_1 (**116**),

Oct-TriA$_1$ (**119**), Laur-TriA$_1$ (**123**) and Fmoc-TriA$_1$ (**126**), were tested (Table 3.3). To be clinically useful, the concentration for hemolytic activity of a peptide should be substantially higher than its MIC against bacteria. Therefore, the extent of rabbit erythrocyte hemolysis was determined using a peptide concentration of 83 μg/mL, which is over 20-fold greater than the MIC of TriA$_1$ against most Gram-negative bacteria. H-TriA$_1$ and But-TriA$_1$, which have significantly lower antimicrobial activity than the natural peptide, show almost no hemolytic activity at the concentrations tested. A small increase in hemolytic activity was observed for TriA$_1$ (3.2%) and Oct-TriA$_1$ (4.7%) but considering this concentration is more than 20-fold greater than the MIC, this activity is negligible. In contrast, the C_{12} and Fmoc analogues caused substantial hemolysis and would be too toxic for *in vivo* use. Oct-TriA$_1$ was therefore chosen as our lead compound as it is the most active lipid tail analogue and has an MIC significantly lower than the concentrations required for hemolysis.

Analogue	**% Hemolysis at 83 μg/mL**
TriA$_1$ (**32**)	3.2
H-TriA$_1$ (**114**)	0.5
But-TriA$_1$ (**116**)	0.8
Oct-TriA$_1$ (**119**)	4.7
Laur-TriA$_1$ (**123**)	82.2
Fmoc-TriA$_1$ (**126**)	100.0

Table 3.3. Hemolytic activity of select TriA$_1$ lipid tail analogues.

To further assess the potential clinical applications of Oct-TriA$_1$, cytotoxicity data against human embryonic kidney cells (HEK 293) was obtained using an MTT assay. The MIC against HEK 293 cells is 100 μg/mL, which is significantly higher than the MIC of the peptide against bacteria. The combination of the strong activity of Oct-TriA$_1$

against Gram-negative bacteria and low cytotoxicity and hemolytic activity led us to test this analogue against more virulent strains of Gram-negative bacteria.

3.2.1.4. Activity of Oct-TriA$_1$ against MDR Gram-negative bacteria

The antimicrobial activity of Oct-TriA$_1$ against several MDR strains of Gram-negative bacteria was determined by our collaborators in the group of Professor Glen Armstrong at the University of Calgary (Table 3.4). *E. coli* O157:H7, one of the most dangerous strains of this species, causes severe food poisoning. The *Klebsiella* and *Enterobacter* strains are clinically isolated strains that are resistant to numerous antibiotics including β-lactams, aminoglycosides and fluoroquinolones. *Clostridium difficile* 630 is a multi-drug resistant and highly transmissible strain. Oct-TriA$_1$ displays excellent antimicrobial activity against the Gram-negative strains but is predictably less active against the Gram-positive *C. difficile* strain.

Organism	**MIC (μg/mL)**
E. coli O157:H7	0.43
K. pneumoniae KpCG	2.33
Enterobacter cloacae 849	0.43
Clostridium difficile 630	12.7

Table 3.4. Activity of Oct-TriA$_1$ against MDR bacteria.

3.2.1.5. Stability of Oct-TriA$_1$ to proteolytic cleavage

Proteases are enzymes that hydrolyze peptide bonds and can be particularly problematic for antimicrobial peptides, as cutting the peptide is likely to inhibit antimicrobial activity. To further evaluate Oct-TriA$_1$'s potential as a drug candidate, its stability against some common proteases found in the GI tract was determined. Trypsin

is a serine protease that cleaves peptides on the carboxyl side of positively charged amino acids lysine and arginine.[26] Chymotrypsin is also a serine protease and hydrolyzes peptide bonds on the carboxyl side of aromatic amino acids, including phenylalanine, tryptophan and tyrosine.[26] Pepsin is a member of the aspartate protease family and is found in the stomach. Pepsin typically cleaves peptide bonds between hydrophobic and aromatic amino acids.[26] The online tool PeptideCutter (Expasy) was used to assess where a ribosomal mimic of TriA$_1$, containing all L-amino acids, no lipid tail and Lys instead of Dab, would be cleaved by pepsin, trypsin and chymotrypsin.[164] Several potential cleavage sites were found (Fig. 3.2).

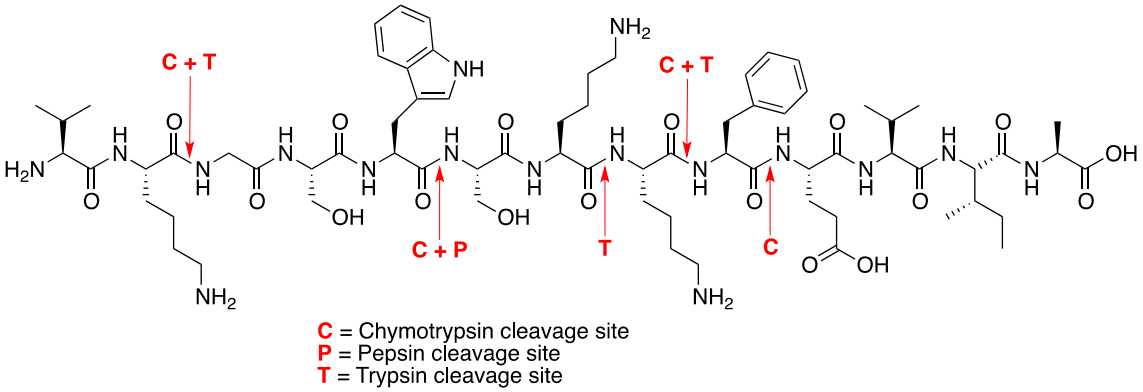

Figure 3.2. Predicted cleavage sites on ribosomal mimic of TriA$_1$.

Oct-TriA$_1$ was incubated under optimal enzymatic conditions with each protease for 18 hours; however, no decrease in antimicrobial activity (spot-on-lawn assay) or peptide degradation (LCMS) was observed. This suggests that Oct-TriA$_1$ could be orally active as it is not cleaved by the main GI tract proteases. Furthermore, it highlights the stability gained by *N*-terminal acylation and the presence of non-proteogenic amino acids in the peptides structure.

3.2.1.6. *In vivo* activity of Oct-TriA$_1$

Our final evaluation of the antimicrobial activity of Oct-TriA$_1$ was performed by our collaborators in the lab of Dr. Min Wu at the University of North Dakota. C57BL/6J mice were infected with *K. pneumoniae* by intranasal instillation and injected with Oct-TriA$_1$ through their tail vein (4 mg/kg body weight) one hour later. The survival rate of these mice was determined after seven days. All of the mice that were not treated with Oct-TriA$_1$ died by day five, whereas 75 % of the population treated with Oct-TriA$_1$ were still alive by seven days. Furthermore, after sacrificing the mice it was found that the colony forming units per mL of *K. pneumoniae* in the lungs of mice treated with Oct-TriA$_1$ was approximately three-fold lower than untreated animals. These results highlight the potential of Oct-TriA$_1$ as an antibiotic candidate.

3.2.2. Synergistic activity between H-TriA$_1$ and other antibiotics

3.2.2.1. Project background

An alternative approach to the treatment of Gram-negative bacteria is to sensitize their outer-membrane. This makes it more permeable, therefore bacteria are more susceptible to antibiotics normally blocked by the outer-membrane. Deacylation of the related lipopeptide polymyxin B with ficin results in removal of the lipid tail and the *N*-terminal amino acid, yielding the less toxic polymyxin B nonapeptide (PMBN). PMBN displays low antimicrobial activity; however, it acts synergistically with antibiotics normally reserved for the treatment of infections caused by Gram-positive bacteria.[165,166] Making Gram-negative bacteria more susceptible to antibiotics typically used for Gram-positive infections is an extremely attractive approach to tackling XMR

strains of Gram-negative bacteria, as it allows the continued use of existing classes of antibiotics. Recent work on the polymyxins has produced new derivatives explicitly for this purpose.[167,59]

3.2.2.2. Screening less active $TriA_1$ lipid tail analogues for synergy with rifampicin

The previous SAR studies on lipid tail analogues of $TriA_1$ identified three with significantly lower antimicrobial activities (≥50 μg/mL) than the natural peptide, H-$TriA_1$ (**114**), Ac-$TriA_1$ (**115**) and PEG-$TriA_1$ (**130**). These analogues were screened for synergistic activity with the RNA polymerase inhibitor rifampicin (**21**) against *E. coli* ATCC 25922 at sub-MIC concentrations of 12.5, 6.25, 3.13 and 1.56 μg/mL (Table 3.5). *Enterobacteriaceae*, and *Acinetobacter* and *Pseudomonas* species have a low susceptibility to rifampicin, but disruption of the outer-membrane increases the activity of this antibiotic. PEG-$TriA_1$ has no synergistic activity, while Bio-$TriA_1$ slightly decreases the MIC of rifampicin (eight-fold). H-$TriA_1$ displays excellent synergy with rifampicin, lowering the MIC 512-fold at 12.5 μg/mL and 64-fold at 6.25 μg/mL. Therefore, H-$TriA_1$ was used in subsequent synergistic studies. It is interesting to note that capping the *N*-terminus of $TriA_1$ significantly lowers its ability to sensitize Gram-negative bacteria. This may be due to the decreased electrostatic attraction between the positively charged peptide and the negatively charged outer-membrane.

Analogue	Rifampicin MIC at peptide concentrations (μg/mL)					MMD
	12.5	**6.25**	**3.13**	**1.56**	**0**	
PEG-TriA_1	1.56	1.56	3.13	3.13	3.13	2x
Bio-TriA_1	0.4	0.78	1.56	3.13	3.13	8x
H-TriA_1	0.012	0.1	0.78	0.78	6.25	512x

Table 3.5. Synergistic activity of TriA_1 analogues with rifampicin. MMD = Maximum MIC decrease.

3.2.2.3. Screening H-TriA_1 for synergy with other antibiotics

The synergistic activity of H-TriA_1 with ten other antibacterial agents was determined against a panel of Gram-negative bacteria (Table 3.6). [168] The antibiotics tested were penicillin (**1**), ampicillin (**2**), vancomycin (**7**), nisin (**8**), gallidermin (**9**), streptomycin (**12**), tetracycline (**17**), rifampicin (**21**), ciprofloxacin (**23**) and daptomycin (**25**). These antibiotics and their mechanisms of action are described in chapter 1. Penicillin G, ampicillin, ciprofloxacin, tetracycline and streptomycin have activity against both Gram-positive and Gram-negative bacteria; however, resistance mechanisms are common. Nisin, gallidermin, vancomycin and daptomycin are all too large to cross the outer-membrane.

Organism	Antibiotic	MIC at [H-TriA_1] (μg/mL)					MMD
		12.5	**6.25**	**3.13**	**1.56**	**0**	
E. coli ATCC 25922	Nisin	3.13	3.13	6.25	6.25	25	8x
	Gallidermin	6.25	6.25	6.25	12.5	100	16x
	Daptomycin	>500	>500	>500	>500	>500	*n.d.*
	Vancomycin	0.78	6.25	25	50	50	64x
	Rifampicin	0.012	0.1	0.78	0.78	6.25	512x
	Penicillin G	7.8	7.8	7.8	15.6	31.3	4x
	Tetracycline	0.2	0.2	0.2	0.39	0.39	2x
	Streptomycin	1.56	1.56	1.56	1.56	3.13	2x

	Ciprofloxacin	0.003	0.003	0.003	0.003	0.003	0
	Ampicillin	3.13	3.13	3.13	3.13	6.25	2x
E. coli DH5α	Nisin	3.13	6.25	6.25	6.25	12.5	4x
	Gallidermin	3.13	6.25	6.25	6.25	50	16x
	Daptomycin	500	>500	>500	>500	>500	*n.d.*
	Vancomycin	1.56	6.25	6.25	6.25	50	32x
	Rifampicin	0.012	0.2	0.39	0.39	6.25	512x
	Penicillin G	6.25	6.25	12.5	12.5	12.5	2x
	Tetracycline	0.1	0.1	0.1	0.1	0.1	0
	Streptomycin	0.1	0.1	0.1	0.1	0.1	0
	Ciprofloxacin	0.003	0.003	0.003	0.003	0.003	0
	Ampicillin	0.2	0.2	0.2	0.2	1.56	8x
S. enterica ATCC 13311	Nisin	12.5	12.5	25	25	50	4x
	Gallidermin	25	50	50	50	100	4x
	Daptomycin	>500	>500	>500	>500	>500	*n.d.*
	Vancomycin	6.25	25	12.5	50	100	16x
	Rifampicin	0.1	0.39	0.78	1.56	3.13	32x
	Penicillin G	1.56	1.56	3.13	3.13	12.5	8x
	Tetracycline	0.2	0.2	0.39	0.39	0.39	2x
	Streptomycin	3.13	3.13	6.25	6.25	6.25	2x
	Ciprofloxacin	0.003	0.003	0.003	0.003	0.006	2x
	Ampicillin	0.78	0.78	0.78	1.56	3.13	2x
C. jejuni NCTC 11168	Nisin	6.25	6.25	6.25	12.5	12.5	2x
	Gallidermin	3.13	6.25	6.25	6.25	12.5	4x
	Daptomycin	>500	>500	>500	>500	>500	*n.d.*
	Vancomycin	12.5	12.5	50	100	200	16x
	Rifampicin	0.1	1.56	12.5	12.5	12.5	128x
	Penicillin G	6.25	6.25	12.5	12.5	12.5	2x
	Tetracycline	0.024	0.024	0.024	0.024	0.024	0
	Streptomycin	1.56	1.56	1.56	1.56	1.56	0
	Ciprofloxacin	0.006	0.024	0.024	0.024	0.024	4x
	Ampicillin	6.25	6.25	6.25	12.5	12.5	2x
K. pneumoniae ATCC 13883	Nisin	0.78	3.13	3.13	6.25	12.5	16
	Gallidermin	1.56	3.13	3.13	6.25	50	16x
	Daptomycin	>500	>500	>500	>500	>500	*n.d.*
	Vancomycin	0.39	1.56	3.13	6.25	100	256x
	Rifampicin	0.006	0.024	0.024	0.03	3.13	512x
	Penicillin G	3.13	25	50	50	200	64x
	Tetracycline	0.78	0.78	0.78	0.78	1.56	2x

	Streptomycin	0.1	0.20	0.39	0.39	0.39	8x
	Ciprofloxacin	0.002	0.003	0.003	0.003	0.012	4x
	Ampicillin	50	100	100	250	250	5x
K. pneumoniae ATCC 700603	Vancomycin	31.3	31.3	62.5	62.5	250	8x
	Rifampicin	0.05	0.2	0.4	3.13	12.5	256x
A. baumannii ATCC 19606	Nisin	3.13	3.13	6.25	6.25	6.25	2x
	Gallidermin	12.5	12.5	12.5	12.5	12.5	0
	Daptomycin	>500	>500	>500	>500	>500	*n.d.*
	Vancomycin	3.13	12.5	25	50	50	16x
	Rifampicin	0.024	0.20	0.39	0.39	0.39	16x
	Penicillin G	31.25	125	125	250	500	16x
	Tetracycline	0.20	0.20	0.20	0.20	0.20	0
	Streptomycin	12.5	25	25	50	50	4x
	Ciprofloxacin	0.024	0.10	0.10	0.20	0.20	16x
	Ampicillin	31.25	62.5	125	250	500	16x
A. baumannii ATCC BAA-1605	Vancomycin	250	250	250	250	250	0
	Rifampicin	0.05	0.2	0.2	0.2	0.78	16

Table 3.5. Synergistic activity of H-TriA_1 with other antibiotics.

The largest synergistic effects are observed with rifampicin, showing a decrease in MIC of 512-fold against *E. coli* and *K. pneumoniae*, and a 128-fold decrease against *C. jejuni*. Moderate decreases of 32-fold and 16-fold are observed against *S. enterica* and *A. baumannii* respectively. There is also a strong synergistic effect between vancomycin and H-TriA_1, with a large MIC decrease of 256-fold against *K. pneumoniae*, 64- to 32-fold against *E. coli* and 16-fold against the other Gram-negative strains. Of particular note is the large decrease in MIC observed for vancomycin against *K. pneumoniae*, which normally has a high tolerance to this antibiotic (MIC = 100 µg/mL). This combination could therefore have potential for the treatment of CRKP infections, against which Oct-TriA_1 is also effective.

Surprisingly, moderate decreases in the MIC (4- to 16-fold) of the lantibiotics nisin and gallidermin were found against *E. coli*, *S. enterica*, *C. jejuni* and *K. pneumoniae*. This is unexpected as these lantibiotics are quite large peptides (Mw > 2 kDa). Given the low levels of resistance development observed for the lantibiotics and their low toxicity, a combination H-TriA_1 and nisin or gallidermin could be an excellent treatment strategy for Gram-negative infections. There is no synergy between daptomycin and H-TriA_1, which was not active at the highest concentration tested (500 µg/mL). The synergistic effects of the remaining antimicrobial agents, penicillin G, ampicillin, ciprofloxacin, tetracycline and streptomycin, range from small to moderate. Ciprofloxacin and ampicillin have similar MIC decreases (16-fold) to vancomycin and rifampicin against *A. baumannii*, which appears to be less susceptible to the synergistic action of H-TriA_1 than the other strains.

The top synergistic combinations (rifampicin/H-TriA1 and vancomycin/H-TriA_1) were also screened against more virulent strains of *K. pneumoniae* and *A. baumannii*. *K. pneumoniae* ATCC 700603 produces β-lactamase SHV-18 and is resistant to several β-lactams, cephalosporins and tetracycline. *A. baumannii* ATCC BAA-1605 is resistant to several β-lactams, cephalosporins, aminoglycosides and ciprofloxacin. A moderate MIC decrease of 8-fold was observed for vancomycin against the MDR *Klebsiella* strain; however excellent synergistic effects were observed with rifampicin, improving the MIC by 256-fold. No synergistic effect was observed against *A. baumannii* ATCC BAA-1605 with vancomycin and a 16-fold improvement was found with rifampicin.

3.2.2.4. Cytotoxicity and plasma stability studies with H-TriA_1

H-TriA1 has low hemolytic activity, causing 0.5% hemolysis at concentrations of 83 μg/mL (Table 3.3). To further assess the toxicity profile of H-TriA1, the toxicity against HEK293 cells was determined. TriA_1 inhibits all growth of these cells at 100 μg/mL, whereas H-TriA_1 is significantly less toxic, requiring 4000 μg/mL for the same effect. The cytotoxic concentration of H-TriA_1 against HEK293 cells is 320 times larger than the highest concentration used in the synergistic combinations (12.5 μg/mL) and suggests H-TriA_1 could be part of a clinically safe antibiotic combination.

H-TriA_1, like Oct-TriA_1, shows remarkable stability to GI tract proteases. To further highlight the excellent properties of H-TriA_1, its stability to human plasma was also assessed. Incubation of H-TriA_1 in plasma at 37 ^{o}C for 30 min shows no detectable degradation of the peptide. Furthermore, mixing H-TriA_1 with bovine serum albumin (BSA) has no effect on the synergistic activity, suggesting that it is unaffected by non-specific protein-binding.

3.2.3. Synthesis and evaluation of tridecaptin A_1 antibiotic conjugates

3.2.3.1. Project background

There is a clear and urgent need for new classes of antibiotics that target Gram-negative bacteria, and in particular those that show high levels of antibiotic resistance. We believe that the tridecaptins meet this need on two fronts. Agents like Oct-TriA_1 directly target Gram-negative bacteria and display strong activity against strains resistant to a host of standard antibiotics. In another approach, the inactive analogue H-TriA_1 sensitizes the outer-membrane of Gram-negative bacteria, making them more

susceptible to antibiotics typically used in the treatment of Gram-positive infections. Mixing two or more antibiotics to treat an infection is commonly known as combination therapy. A major advantage of this approach is that mixing antibiotics that have completely different modes of action will limit the ability of the bacteria to develop resistance mechanisms. For example, if they are resistant to a DNA gyrase inhibitor, it is unlikely that they will also be resistant to a ribosome inhibitor and peptidoglycan biosynthesis inhibitor. Therefore, the bacteria are killed and the resistance mechanism does not persist in the population.

An emerging strategy in combination therapy is the use of heterodimer antibiotics, wherein two different antibiotics are covalently linked together.[169] Potential advantages of this approach to treating bacterial infections are renewed activity against MDR bacteria, enhanced efficacy and duration *in vivo*, an expanded spectrum of activity and reduced development of resistance.[170] Therefore we envisaged that another possible use of the tridecaptins could be as carrier molecules of antibiotics through the outer-membrane. This is a "Trojan Horse" approach, wherein H-TriA_1 or Oct-TriA_1 disrupts the outer-membrane and carries its antibiotic cargo into the cell, where it then exerts its antimicrobial effect. This approach may offer some advantages over the synergistic combination of H-TriA_1 and other antibiotics. If both H-TriA_1 and the antibiotic do not reach the target bacteria *in vivo* there will be no synergistic effect, therefore conjugation would prevent this. Also, the moderate size of H-TriA_1 and its stability to proteases may prevent efflux of the antibiotic from the bacterial cell, as well as prevent it being degraded by targeting enzymes. However, there are also potential disadvantages. Covalently linking H-TriA_1 to an antibiotic may interfere with target binding, rendering it

inactive. The resulting conjugate may also get stuck on the outer-membrane if it is too large. Furthermore, there may be unpredictable cytotoxicity issues associated with the relatively large peptide-antibiotic conjugate. The use “delivery vehicles” to get antibiotics across the outer-membrane has been previously performed through covalent linkage of antibiotics to siderophores,[171,172] cell penetrating peptides[173,174] and polymers.[175]

3.2.3.2. Synthesis of azido Oct-TriA$_1$ and H-TriA$_1$ derivatives

The first stage in designing a peptide-antibiotic conjugate is identifying an appropriate linkage site on each compound. This must be in an area that is not involved in target receptor binding. TriA$_1$ has several possible linkage sites, including through the side chain amine of D-Dab2, Dab7 or D-Dab8, the C-terminus and the Glu10 side chain carboxylate. We suspected that the amines were vital for TriA$_1$ activity, so only the C-terminus and Glu10 were investigated as potential attachment sites. Two Oct-TriA$_1$ analogues, wherein carboxylates are individually replaced with amides, were synthesized by Fmoc-SPPS to determine the importance of these residues to the peptides antimicrobial activity.[214] Oct-TriA$_1$-NH$_2$ (**132A**) contains a C-terminal amide and in Oct-TriA$_1$(10Gln) (**132B**) the glutamic acid has been replaced with glutamine (Fig. 3.3). Both compounds retain full activity against *E. coli* ATCC 25922 cells, therefore Glu10 was chosen as the attachment site as it is most easily modified by Fmoc-SPPS.

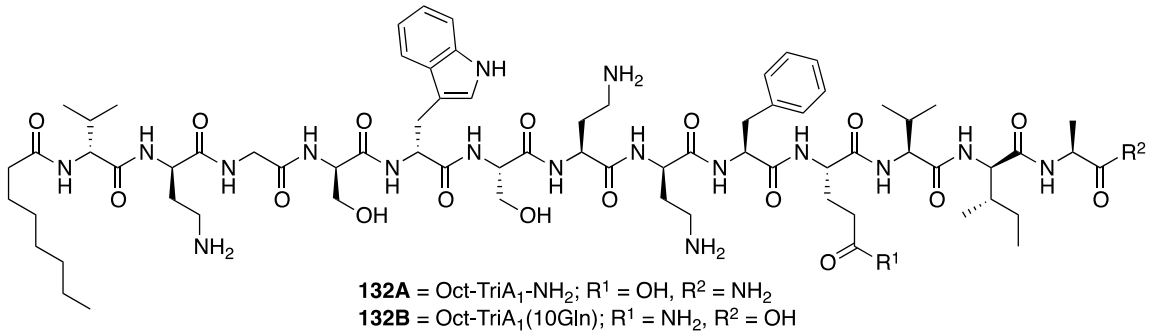

Fig. 3.3. Amide scan of Oct-TriA_1 carboxylic acids.

The attachment of a linker between the two components in a heterodimer is usually required, as this provides a degree of separation between them and reduces the chance that one will hinder the others receptor binding. Previous work by Breukink and coworkers found that a PEG_3 linker provided sufficient separation between the antibiotics in a nisin(1-12)-vancomycin hybrid, which displays activity against VRE.[176] Nisin(1-12) contains the 12 *N*-terminal residues of nisin, which bind to lipid II in a pyrophosphate cage. Therefore, we evaluated whether this would be a suitable linker for tridecaptin-drug conjugates.

Glutamic acid derivative **133**, which contains a PEG_3-linked azide on its side chain, was synthesized (Scheme 3.1). The azide allows attachment to alkyne containing antibiotics via copper assisted azide-alkyne cycloaddition (CuAAC), whose reaction conditions are compatible with multiple functional groups. The PEG_3-azide is attached to the side chain carboxylate of Fmoc-Glu-OtBu (**134**) using HATU as a coupling reagent. The resulting amide is then treated with TFA to remove the *tert*-butyl ester, yielding Fmoc amino acid **133** in 45% yield over 2 steps. This amino acid was used in

the solid phase synthesis of Oct-TriA$_1$ azide **135** and H-TriA$_1$ azide **136** (Fig. 3.4). Both peptides retained their activities against *E. coli* ATCC 25922.

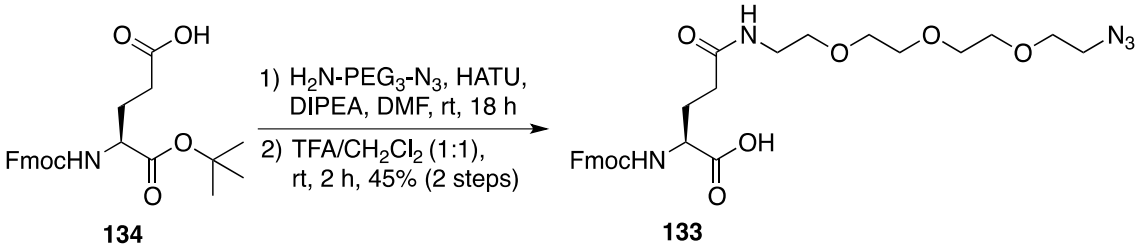

Scheme 3.1. Synthesis of Fmoc-Glu(10Gln(PEG$_3$N$_3$)) (**133**).

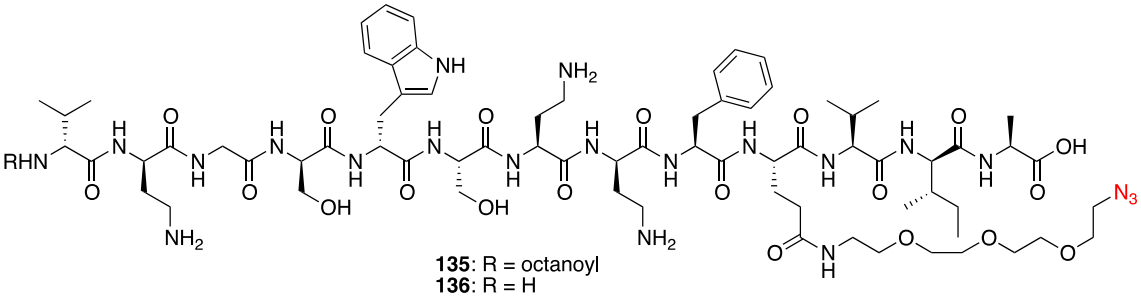

Figure 3.4. Oct-TriA$_1$ and H-TriA$_1$ azides.

3.2.3.3. Synthesis of alkyne containing antibiotics

Vancomycin (**7**), nisin (**8**), erythromycin (**14**), rifampicin (**21**) and daptomycin (**25**) were chosen for conjugation to the azido H-TriA$_1$ and Oct-TriA$_1$ peptides. Previous studies have shown that the carboxylic acid on vancomycin can be modified without loss of activity.[176] Treatment of vancomycin with propargylamine under HBTU coupling conditions yields vancomycin alkyne **137** in good yield (Scheme 3.2).[177] Another study found that modification of the nisin *N*-terminus negatively affects its activity.[178] Nisin contains only one carboxylic acid, on its C-terminus, and treatment of nisin with propargylamine under PyBOP coupling conditions yields nisin alkyne **138** in moderate

yield (Scheme 3.2).[179] Previous SAR studies have shown that the ketone functionality on erythromycin can be modified as an oxime ether without loss of activity.[180,181] Treatment of commercially available erythromycin A oxime (**139**) with propargyl bromide yields erythromycin alkyne **140** in 30% yield (Scheme 3.2). Recent studies have shown that the piperazine ring on rifampicin is vital for its activity,[182] therefore we chose to replace the methyl group on N4 with an alkyne group. First, 1-amino-4-propargyl piperazine (**141**) was synthesized in 3 steps from piperazine (**142**). Nitrosylation of **142** with $NaNO_2$ in 6M HCl yields nitrosopiperazine (**143**) in moderate yield, which is subsequently alkylated with propargyl bromide to give 1-nitroso-4-propargyl piperazine (**144**). Treatment of **144** with $LiAlH_4$ yields amine **141**, which is then reacted with commercially available rifaldehyde (**145**) to give rifampicin alkyne (**146**) in excellent yield. An alkyne functionality could be appended to daptomycin through one of its carboxylate groups or the ornithine side chain. The carboxylate groups in daptomycin are involved in calcium ion binding, which is essential for its antimicrobial activity, therefore the ornithine side chain was modified. Treatment of daptomycin with 4-pentynoic acid using HATU as a coupling reagent yields daptomycin alkyne **147** in moderate yields (Scheme 3.3). All antibiotic alkynes were found to retain comparable activity to the unmodified antibiotics.

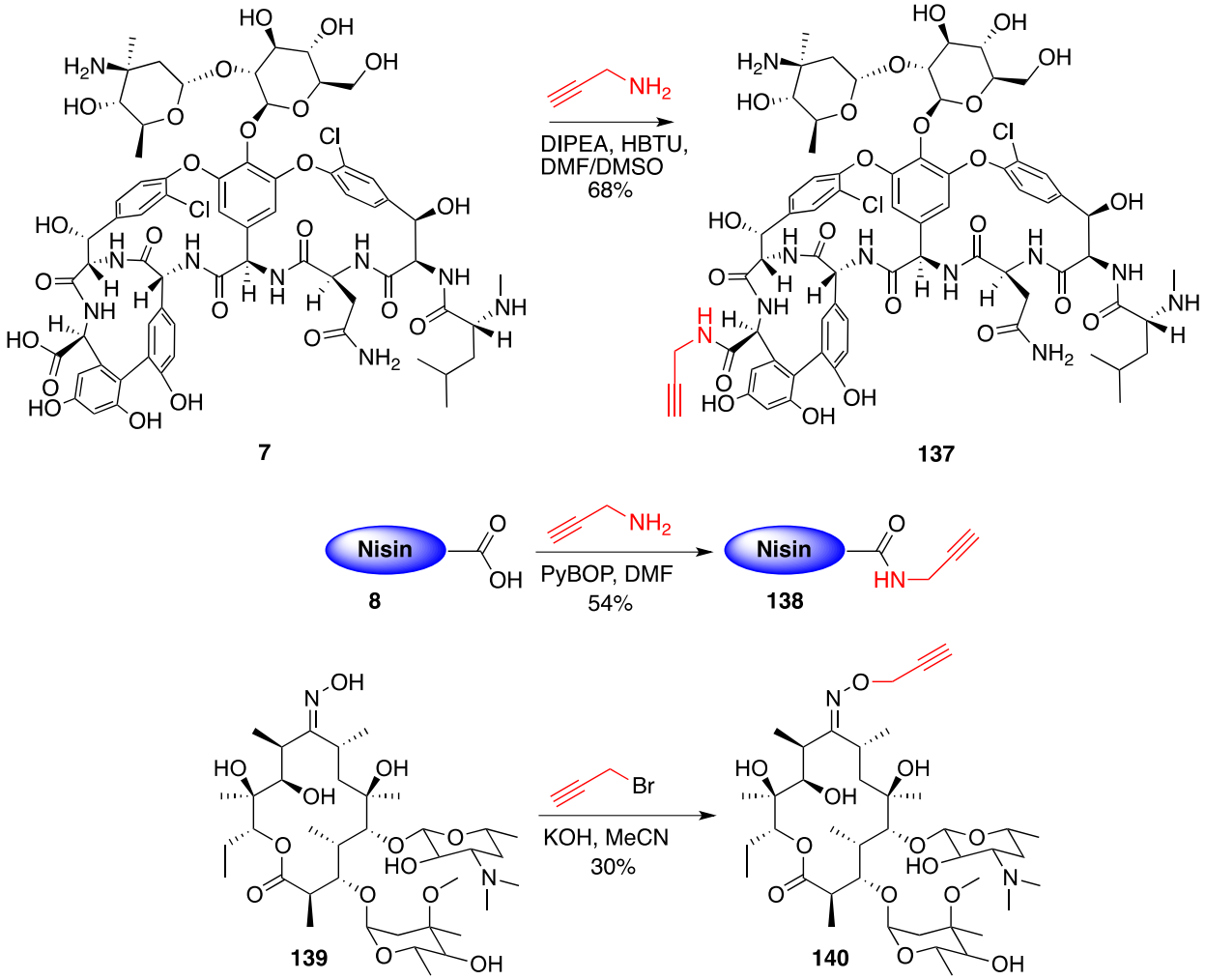

Scheme 3.2. Synthesis of vancomycin, nisin and erythromycin alkynes.

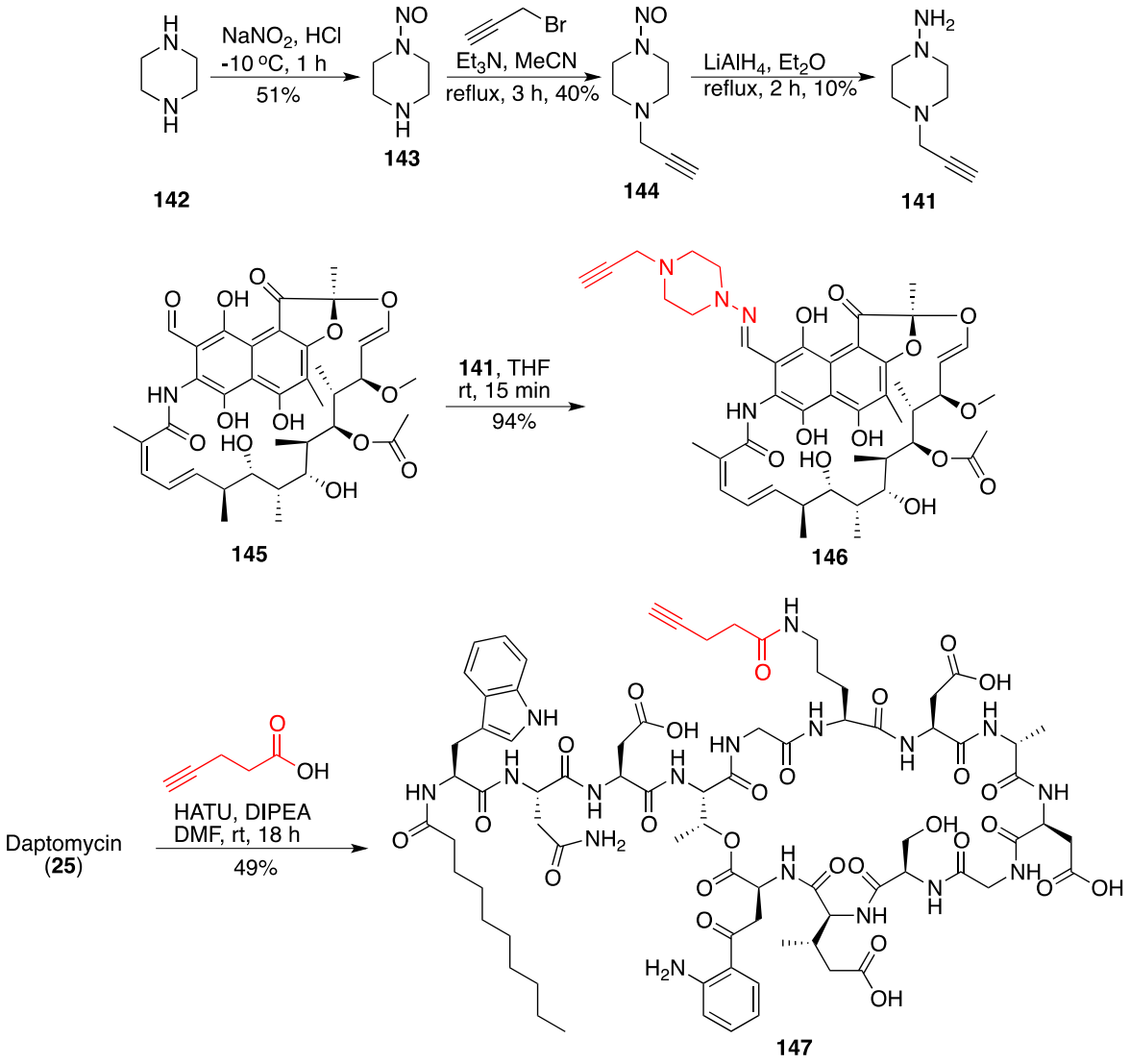

Scheme 3.3. Synthesis of rifampicin and daptomycin alkynes.

3.2.3.4. Synthesis Oct-TriA$_1$ and H-TriA$_1$ antibiotic conjugates

A previously reported CuACC procedure was used for the synthesis of the Oct-TriA$_1$ and H-TriA$_1$ antibiotic conjugates (Scheme 3.4).[183] The click-reactions between the peptide azides and nisin alkyne and daptomycin alkyne were unsuccessful, therefore these conjugates could not be carried forward for biological evaluation. The remaining conjugates were synthesized smoothly in moderate yields.

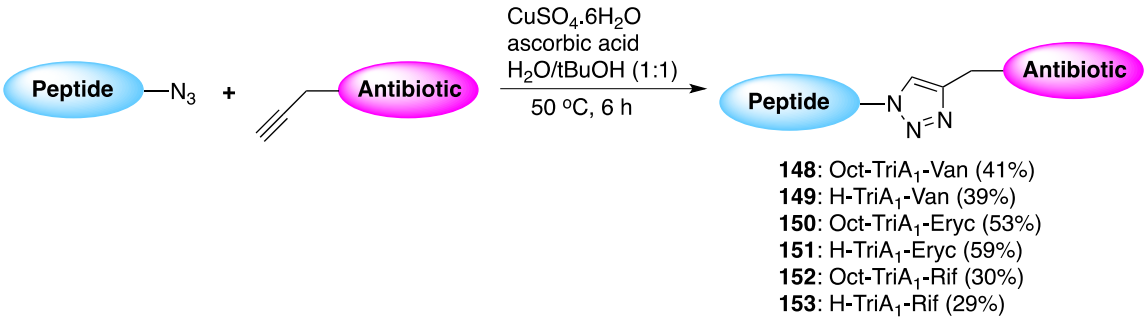

Scheme 3.4. Synthesis of peptide-antibiotic conjugates.

3.2.3.5. Antimicrobial testing of peptide-antibiotic conjugates

Conjugates **148** – **153** were tested against regular strains of the Gram-negative bacteria *E. coli*, *K. pneumoniae* and *A. baumannii*, as well as MDR strains of *K. pneumoniae* (ATCC 700603) and *A. baumannii* (ATCC BAA 1605) (Table 3.5). Unfortunately the activities of these compounds are not very promising. None of the Oct-TriA$_1$ conjugates have higher activity than Oct-TriA$_1$ alone against any of the organisms tested. Also, linking H-TriA$_1$ to vancomycin, erythromycin or rifampicin did not lead to enhanced activity compared to co-administration of the peptide and antibiotics. In some instances higher activity was observed with H-TriA$_1$-Van and H-TriA$_1$-Eryc in comparison to H-TriA$_1$, vancomycin or erythromycin alone. The activity of H-TriA$_1$-Van and H-TriA$_1$-Eryc is 4- to 8-fold higher than vancomycin or erythromycin alone against *E. coli* and the *A. baumannii* strains. However, this activity is still quite low, and given the effort required to synthesize these compounds, the synergistic combination of H-TriA$_1$ and these antibiotics is a much more attractive approach. A cleavable linker between the peptide and antibiotic may enhance activity of the conjugates. Replacement of the triazole ring with an ester would allow this functionality to be

hydrolyzed once it enters the cell, releasing the antibiotic. However, there was not enough time left in my graduate studies to try this approach.

	MIC (μM)				
Antibiotic	***E. coli* ATCC 25922**	***K. pneumoniae* ATCC 13883**	***K. pneumoniae* ATCC 700603**	***A. baumannii* ATCC 19606**	***A. baumannii* ATCC BAA 1605**
Oct-TriA$_1$	3.13	3.13	6.25	6.25	6.25
H-TriA$_1$	100	100	100	200	200
Vancomycin	200	200	250	200	200
Erythromycin	100	100	400	200	200
Rifampicin	6.25	12.5	25	0.4	0.78
H-TriA$_1$/Van	1.56	0.78	25	3.13	200
H-TriA$_1$/Eryc	3.13	0.4	200	12.5	200
H-TriA$_1$/Rif	0.05	0.0048	0.1	0.05	0.05
Oct-TriA$_1$-Van	12.5	100	25	25	50
Oct-TriA$_1$-Eryc	12.5	3.13	12.5	6.25	6.25
Oct-TriA$_1$-Rif	3.13	6.25	100	6.25	6.25
H-TriA$_1$-Van	25	100	200	25	25
H-TriA$_1$-Eryc	50	50	200	50	25
H-TriA$_1$-Rif	25	50	100	25	50

Table 3.6. Activity of peptide-antibiotic conjugates against Gram-negative strains.

3.2.3.6. *In vivo* testing of H-TriA$_1$-antibiotic conjugates

Although linking H-TriA$_1$ to vancomycin, erythromycin or rifampicin offered no advantages over co-administration of the peptide and antibiotics *in vitro*, they may offer some advantages *in vivo*. Therefore, the efficacy of these conjugates was determined against mice infected with *K. pneumoniae* (Fig. 3.5). This was performed by our collaborators in the lab of Dr. Min Wu at the University of North Dakota and the basic procedure is described in section 3.2.1.6. Rifampicin and vancomycin alone are both

effective treatments and there is no advantage gained by co-administering H-TriA$_1$ with these antibiotics, or linking them to H-TriA$_1$. In contrast, the activity of erythromycin is significantly improved *in vivo* by linking it to H-TriA$_1$. The number of viable *K. pneumoniae* colonies present in the lungs of these mice was also determined after the survival experiments. These results are consistent with the survival rate experiments, showing that out of the heterodimers, H-TriA$_1$-Eryc is the most effective treatment.

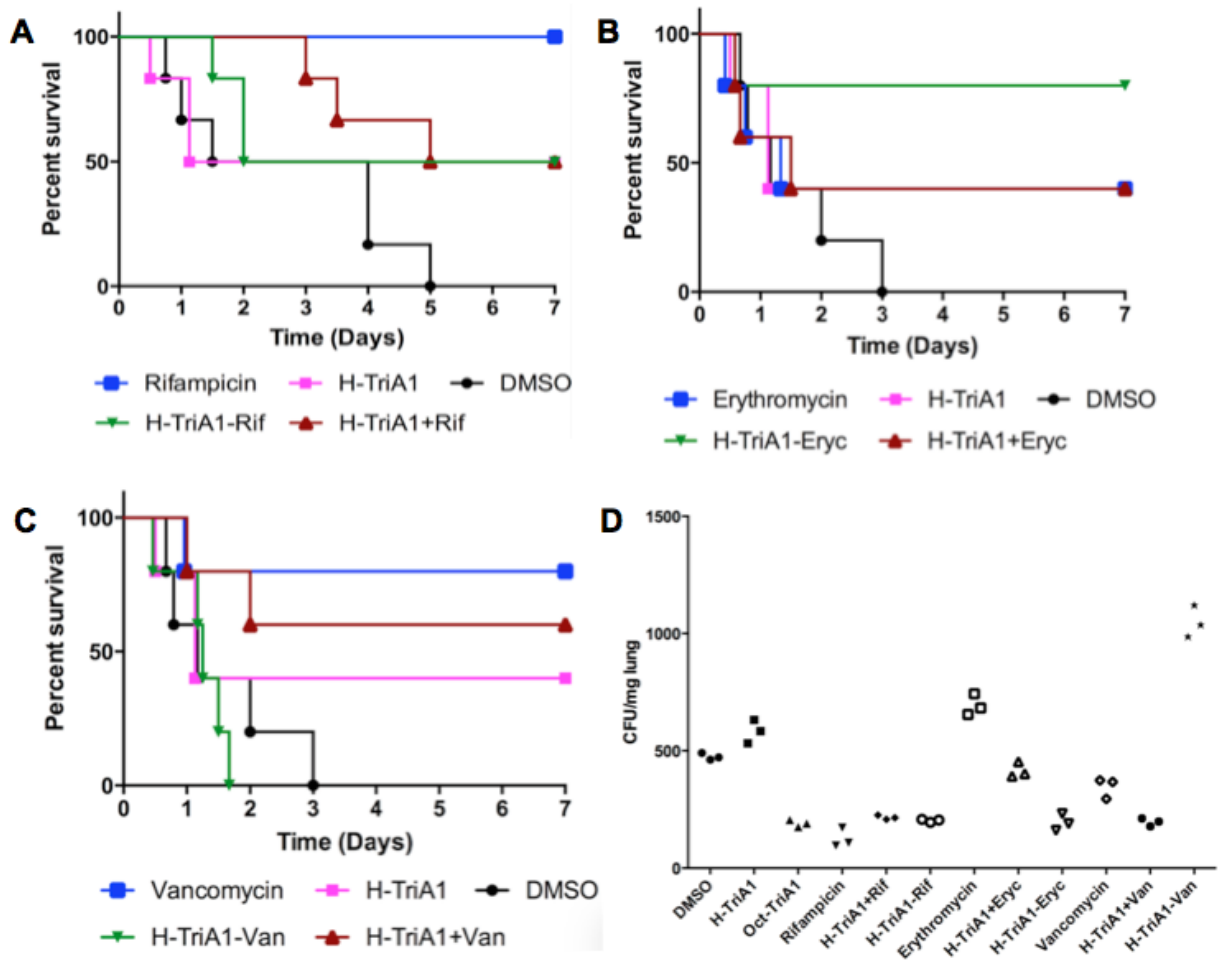

Figure 3.5. *In vivo* testing of antimicrobial compounds. Survival rates of mice treated with (A) rifampicin based treatments, (B) erythromycin based treatments and (C) vancomycin based treatments. (D) CFU count from excised lungs.

3.2.4. Alanine scan of Oct-TriA$_1$

3.2.4.1. Synthesis of Oct-TriA$_1$ analogues with single alanine substitutions

Replacement of individual residues of a peptide with alanine, followed by antimicrobial testing, reveals which residues are important to the peptides antimicrobial activity. A complete alanine scan was performed on Oct-TriA$_1$, in which L-amino acids were replaced with Ala and D- amino acids were replaced with D-Ala.[184] All peptides were synthesized using Fmoc-SPPS (Scheme 3.5).

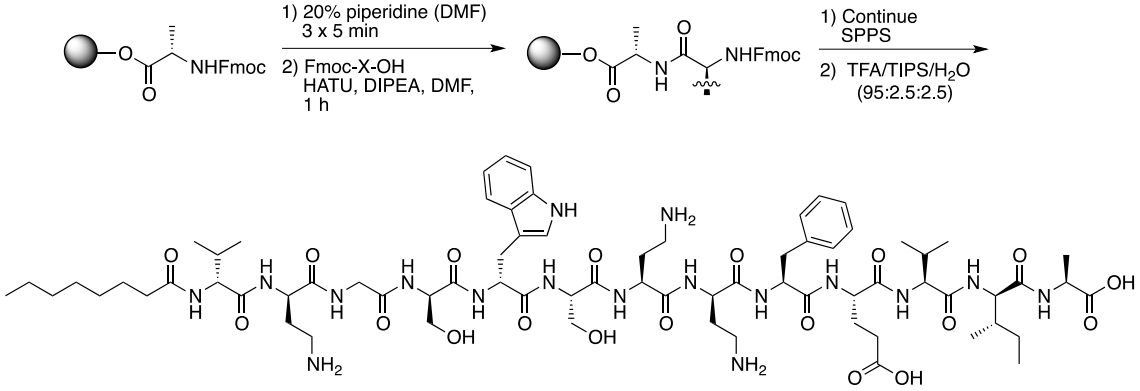

154: Oct-D-Ala-D-Dab-Gly-D-Ser-D-Trp-Ser-Dab-D-Dab-Phe-Glu-Val-D-*allo*-Ile-Ala-OH
155: Oct-D-Val-D-Ala-Gly-D-Ser-D-Trp-Ser-Dab-D-Dab-Phe-Glu-Val-D-*allo*-Ile-Ala-OH
156: Oct-D-Val-D-Dab-Ala-D-Ser-D-Trp-Ser-Dab-D-Dab-Phe-Glu-Val-D-*allo*-Ile-Ala-OH
157: Oct-D-Val-D-Dab-Gly-D-Ala-D-Trp-Ser-Dab-D-Dab-Phe-Glu-Val-D-*allo*-Ile-Ala-OH
158: Oct-D-Val-D-Dab-Gly-D-Ser-D-Ala-Ser-Dab-D-Dab-Phe-Glu-Val-D-*allo*-Ile-Ala-OH
159: Oct-D-Val-D-Dab-Gly-D-Ser-D-Trp-Ala-Dab-D-Dab-Phe-Glu-Val-D-*allo*-Ile-Ala-OH
160: Oct-D-Val-D-Dab-Gly-D-Ser-D-Trp-Ser-Ala-D-Dab-Phe-Glu-Val-D-*allo*-Ile-Ala-OH
161: Oct-D-Val-D-Dab-Gly-D-Ser-D-Ala-Ser-Dab-D-Ala-Phe-Glu-Val-D-*allo*-Ile-Ala-OH
162: Oct-D-Val-D-Dab-Gly-D-Ser-D-Trp-Ser-Dab-D-Dab-Ala-Glu-Val-D-*allo*-Ile-Ala-OH
163: Oct-D-Val-D-Dab-Gly-D-Ser-D-Trp-Ser-Dab-D-Dab-Phe-Ala-Val-D-*allo*-Ile-Ala-OH
164: Oct-D-Val-D-Dab-Gly-D-Ser-D-Trp-Ser-Dab-D-Dab-Phe-Glu-Ala-D-*allo*-Ile-Ala-OH
165: Oct-D-Val-D-Dab-Gly-D-Ser-D-Trp-Ser-Dab-D-Dab-Phe-Glu-Val-D-Ala-Ala-OH

Scheme 3.5. Synthesis of single alanine substitution Oct-TriA$_1$ analogues.

3.2.4.2. Antimicrobial testing of alanine scan Oct-TriA$_1$ analogues

Oct-TriA$_1$ analogues **154** – **165** were tested against a panel of Gram-positive and Gram-negative bacteria (Table 3.7). As expected, no Oct-TriA$_1$ analogues displayed strong activity against Gram-positive organisms, against which the parent peptide had

low activity. Analysis of the activity of the alanine-scan analogues against the Gram-negative bacteria was more revealing. Conservative substitutions of small and hydrophobic amino acids, including D-Val1, Gly3, D-Ser4, Ser6, and Val11, has little effect on the activity of the peptide. Also, substitution of Glu-10 with alanine does not affect activity, which mirrors our previous observation that a PEG_3-azide could be attached to Glu10 without lowering activity. Interestingly, substitution of D-*allo*-Ile12 with D-Ala decreases the activity 8-fold or greater against most of the Gram-negative organisms, correlating to the high hydrophobicity of this residue. Similarly, a large decrease is observed when the aromatic amino acids are replaced, with a 2- to 4-fold decrease in activity upon Phe9Ala substitution and an 8- to 16-fold decrease in activity upon D-Trp5 substitution. Replacement of D-Dab2 or Dab7 only decreases the activity 4-fold, however substitution of D-Dab8 with D-Ala abolishes the antimicrobial activity. Therefore, this residue must play a key role in the mechanism of action of tridecaptin A_1. Overall, these studies led us to conclude that D-Dab8 is vital for the activity of Oct-TriA_1 and D-*allo*-Ile12 and D-Trp5 are also important.

Analogues	*E. coli*	*S. enterica*	*P. aeruginosa*	*C. jejuni*	*K. pneumoniae*	*A. baumannii*	*E. faecalis*	*S. aureus*	*L. monocytogenes*	*E. faecium*
Oct-TriA$_1$	3.13	6.25	25	1.56	3.13	12.5	100	100	25	50
154	6.25	6.25	25	1.56	3.13	25	>100	>100	>100	>100
155	12.5	12.5	>100	12.5	6.25	>100	>100	>100	>100	>100
156	3.13	12.5	100	6.25	6.25	50	>100	>100	>100	>100
157	6.25	6.25	25	6.25	6.25	12.5	>100	>100	>100	>100
158	25	100	100	50	50	100	>100	>100	>100	>100
159	3.13	6.25	100	6.25	6.25	12.5	>100	>100	>100	>100
160	12.5	25	>100	12.5	12.5	25	>100	>100	>100	>100
161	>100	>100	>100	>100	>100	>100	>100	>100	>100	>100
162	12.5	12.5	50	6.25	12.5	100	>100	>100	>100	>100
163	6.25	6.25	12.5	3.13	6.25	25	>100	>100	25	>100
164	6.25	12.5	25	3.13	6.25	50	>100	>100	>100	>100
165	50	25	50	12.5	25	>100	>100	>100	>100	>100

Table 3.7. Antimicrobial activity of alanine-scan analogues in μg/mL.

3.2.5. SAR studies on cerexin analogues

During our structural elucidation of natural cerexins, several analogues were isolated and synthesized, including CxnA$_1$ (**31**), (3'*S*)-CxnA$_1$ (**87**), CxnF$_1$ (**93**), CxnE$_1$ (**94**) and CxnF$_2$ (**95**) (Fig. 3.6). To determine if *threo*-4-hydroxylysine is important for activity, analogues of CxnC$_1$ were also synthesized by Fmoc-SPPS. The activities of these peptides were then determined against a panel of Gram-positive and Gram-negative bacteria (Table 3.8).

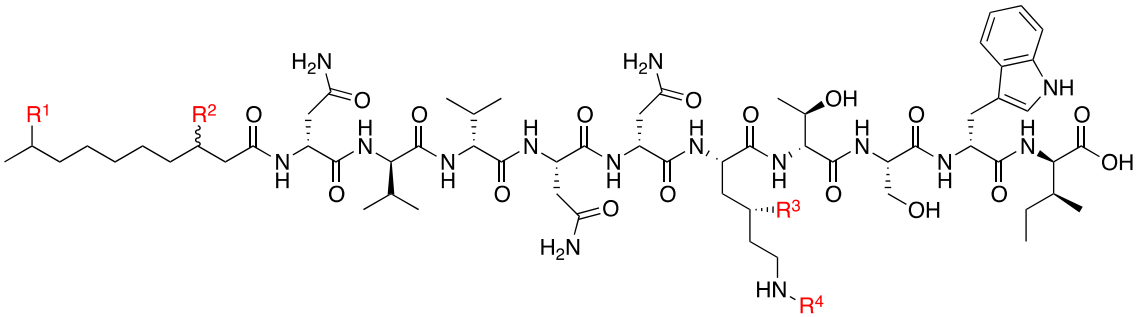

CxnA$_1$ (**31**): R^1 = CH$_3$, R^2 = (3*R*)-OH, R^3 = OH, R^4 = H
(3'*S*) CxnA$_1$ (**87**): R^1 = CH$_3$, R^2 = (3*R*)-OH, R^3 = OH, R^4 = H
CxnF$_1$ (**93**): R^1 = H, R^2 = (3*R*)-OH, R^3 = H, R^4 = succinyl
CxnE$_1$ (**94**): R^1 = CH$_3$, R^2 = (3*R*)-OH, R^3 = OH, R^4 = succinyl
CxnF$_2$ (**95**): R^1 = CH$_3$, R^2 = (3*R*)-OH, R^3 = H, R^4 = succinyl
(3'*R*) CxnC$_1$ (**166**): R^1 = CH$_3$, R^2 = (3*R*)-OH, R^3 = H, R^4 = H
(3'*S*) CxnC$_1$ (**167**): R^1 = CH$_3$, R^2 = (3*R*)-OH, R^3 = H, R^4 = H
Dec-CxnC$_1$ (**168**): R^1 = H, R^2 = (3*R*)-OH, R^3 = H, R^4 = H

Figure 3.6. Natural and synthetic cerexin analogues.

A limited amount of data is available on the antimicrobial activity of cerexin analogues and was determined by the agar dilution method, which is generally not as sensitive as broth-dilution assays.[121] These reports suggested that the cerexins have low activity against Gram-negative bacteria, a result corroborated by our results. Several Gram-positive organisms were screened and the low activity observed against *S. aureus* ATCC 6538 is representative for most strains. An exception is against strains of *B. subtilis*, for which moderate activity is observed. There is no notable difference between the *R*- and *S*-lipid tail isomers of CxnA$_1$ and CxnC$_1$. Also, like the tridecaptins, the hydroxyl group on the lipid tail is not necessary for antimicrobial activity. Substitution of hydroxylysine with lysine does not affect the activity either, showing that synthetically simpler cerexin analogues like Dec-CxnC$_1$ are just as effective as the natural peptides. In contrast, the succinylated cerexin analogues were inactive against *B. subtilus*. We postulated that succinylation may therefore be a self-protection mechanism, turned on

when the concentration of the cerexins gets too high to protect the producer strain. However, $CxnA_1$ is not active against its own producer strain at high concentrations, so there may be another reason for succinylating these compounds. Given the low antimicrobial activity of the cerexins, it is surprising that the producer strain makes such large quantities of these peptides. Efforts are currently underway in our group to further understand the function(s) and mode of action of these peptides.

	Activity (μg/mL)				
Analogue	*E. coli* ATCC 25922	*K. pneumoniae* ATCC 13383	*S. aureus* ATCC 6538	*B. subtilis* ORB 7664	*B. mycoides* ATCC 21929
$CxnA_1$	>500	>500	250	31.3	>500
(3'*S*)-$CxnA_1$	>500	>500	>500	62.5	>500
$CxnC_1$	>500	>500	250	31.3	>500
(3'*S*)-$CxnC_1$	>500	>500	>500	62.5	>500
Dec-$CxnC_1$	>500	>500	>500	62.5	>500
$CxnE_1$	>500	>500	>500	>500	>500
$CxnF_1$	>500	>500	>500	>500	>500
$CxnF_2$	>500	>500	>500	>500	>500

Table 3.8. Antimicrobial activity of cerexin analogues.

3.3. Conclusions

Tridecaptin A_1 shows selective and strong activity against Gram-negative bacteria. Replacement of the chiral lipid tail with octanoic acid yields Oct-$TriA_1$, which retains the full activity of the parent peptide. Oct-$TriA_1$ is active against multidrug resistant strains of Gram-negative bacteria that are resistant to many first choice antibiotics, including fluoroquinolones, aminoglycosides and β-lactams. Furthermore, it has low hemolytic activity and cytotoxicity and is stable to gastrointestinal proteases. The antimicrobial activity of Oct-$TriA_1$ persists *in vivo* and was used to successfully treat

Klebsiella pneumoniae infections in mice. We therefore believe that Oct-TriA_1 is an excellent antibiotic candidate.

An unacylated analogue of tridecaptin A_1, H-TriA_1, is practically inactive against Gram-negative bacteria, however administration of low concentrations of this peptide with other antibiotics substantially increases their activity against these organisms. This is particularly evident with rifampicin and vancomycin, whose activities against *K. pneumoniae* were raised over 100-fold. H-TriA_1 has extremely low cytotoxicity and hemolytic activity and is not degraded by proteases in human plasma. The use of H-TriA_1 as a sensitizer of Gram-negative bacteria to conventional Gram-positive antibiotics is important and could offer a solution to keep these antibiotics relevant in an age of increasing bacterial resistance.

An alanine scan of Oct-TriA_1 revealed three key residues responsible for antimicrobial activity, D-Trp5, D-Dab8 and D-*allo*-Ile12. Whilst we had previously postulated that TriA_1 is a regular lipopeptide that disrupts the membrane of Gram-negative bacteria by a generic-lysis mechanism, the observation that only one of the Dab residues is critical for activity suggests a chiral receptor may be involved in the mechanism of action. Furthermore, we found that Glu10 can act as a good anchor point for other molecules to TriA_1 without affecting the peptides activity. We were able to increase the activity of erythromycin *in vivo* by linking it to Glu10 on H-TriA_1, yielding H-TriA_1-Eryc, which has greater activity than a synergistic mixture of these compounds.

Finally, natural and synthetic cerexin analogues were screened for antimicrobial activity, and found only to show moderate activity against *B. subtilis*. This organism is not pathogenic to humans and the cerexins are therefore unlikely to ever become

antibiotics. However, it was interesting to note that cerexin analogues succinylated on the lysine/hydroxylysine residue had substantially lower activity against *B. subtilis*. As $CxnA_1$ is inactive against its own producer strain at very high concentrations, the observed succinylation is unlikely to be a protection mechanism. It is somewhat puzzling that *B. mycoides* goes through such effort to biosynthesize compounds with such a low spectrum of activity, thus presenting future Vederas group members with the challenge of elucidating the function of these peptides.

Chapter 4

Mechanistic studies on tridecaptin A_1

4.1. Background

The mode of action describes the cellular process inhibited by an antibiotic, whereas the mechanism of action describes how this inhibition is achieved at a molecular level. For example, vancomycins mode of action is inhibition of peptidoglycan biosynthesis, whereas its mechanism of action is sequestering lipid II by binding to D-Ala4 and D-Ala5 through a network of five hydrogen bonds.[72] It is important to understand exactly how an antibiotic works for a number of reasons. Identifying the molecular target and determining the structure of the antibiotic-receptor complex (e.g. X-ray crystallography or NMR) may allow the rational design of improved antimicrobial compounds. It also can help predict how it will behave *in vivo*. For example, knowing the binding site that an antibiotic occupies on the lysyl *t*RNA synthetase in *Plasmodium falciparum* enables us to compare this enzyme to its human counterpart and predict if it is also going to be inhibited and cause side effects. This chapter describes our work on elucidating both the mode of action and mechanism of action by which tridecaptin A_1 kills Gram-negative bacteria.

4.2. Mode-of-action studies

4.2.1. Growth kinetic measurements

Measuring the time taken for an antibiotic to exert its antimicrobial effect provides valuable information on the cellular process targeted by that compound.[185]

Bacteriostatic agents halt cell division but do not reduce the number of viable cells. They therefore must work in tandem with the bodies' immune system to clear bacterial infections. Antibiotics that target protein-synthesis and nucleic acid synthesis typically fall within this category. Bactericidal agents reduce the population of viable bacterial cells, and the time taken for a bactericidal agent to kill bacteria provides further information on its target. For example, the β-lactams, which inhibit peptidoglycan biosynthesis by binding to penicillin-binding proteins, require exposure times longer than three hours to exert their bactericidal effect. Cells exposed to β-lactams are unable to crosslink peptidoglycan, which is vital for cellular integrity; however, the crosslinks already in place before antibiotic exposure remain and if at this stage cells are transferred to fresh antibiotic free media, they resume normal growth. It is only after several hours and continuous peptidoglycan remodeling that the absence of crosslinks begins to take effect, leading to cell lysis. In contrast, agents that target the bacterial membrane typically kill bacteria within minutes. Therefore, the time taken for $TriA_1$ to kill *E. coli* cells was compared to the time taken by protein-synthesis inhibitor chloramphenicol, peptidoglycan biosynthesis inhibitor ampicillin and membrane targeting lipopeptide polymyxin B.

Optical density measurements of cells exposed to two times the MIC of these antibiotics were measured over three hours (Fig. 4.1). Cells exposed to $TriA_1$ grow at a reduced rate for approximately 20 minutes, at which point a steady decrease in the viable cell count occurs. Polymyxin B reduces the cell count immediately, while ampicillin displays an expected three-hour lag time common to β-lactam antibiotics. The bacteriostatic agent chloramphenicol does not reduce optical density.

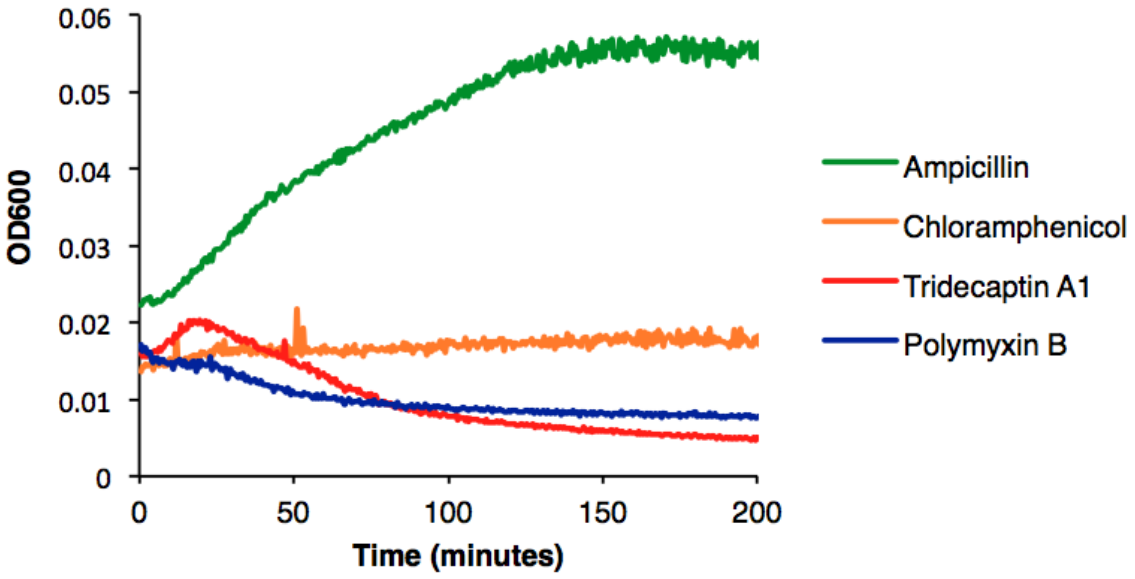

Figure 4.1. Comparison of $TriA_1$ to other antibiotics by growth kinetics of *E. coli*.

4.2.2. Time-Kill Assay

A complimentary approach to bacterial growth kinetics is a time-kill assay.[186] In this assay, bacteria are exposed to antibiotic concentrations ten times the MIC. At a set time point, an aliquot of bacterial cells are removed, diluted and plated onto an antibiotic free agar plate, which is grown overnight and the number of bacterial colonies counted. This is repeated at several time points to determine how long it takes an antibiotic to kill all cells. A time-kill assay was performed by Dr. Brandon Findlay with polymyxin B and $TriA_1$ (Fig. 4.2). $TriA_1$ shows slightly reduced cell viability after 15 minutes of exposure; however, a significant reduction is observed after 30 minutes and all cells are dead after 60 minutes. Polymyxin B acts much faster, significantly reducing the viable cell population after 5 minutes and killing all cells by 30 minutes. Taken together with the growth-kinetic assays, these results suggest that $TriA_1$ is a membrane targeting peptide, but does not act by a generic membrane-lysis mechanism like polymyxin B. This is

further supported by the fact that $TriA_1$ shows strong activity against Gram-negative bacteria, but is significantly less active against Gram-positive bacteria and mammalian cells. A general membrane lysis mode of action would not produce this selectivity.

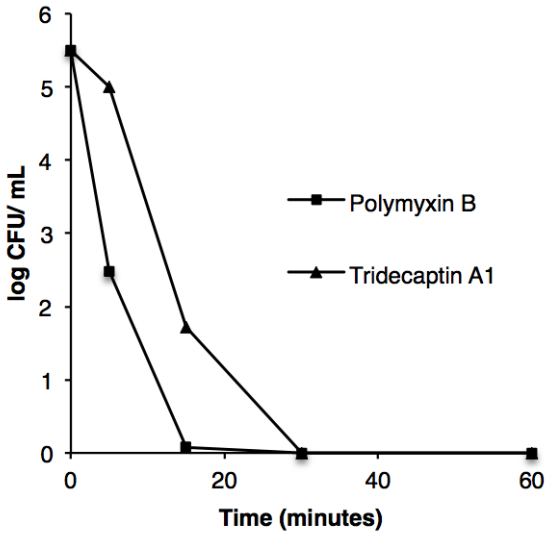

Figure 4.2. Time-kill assay of $TriA_1$ and polymyxin B against *E. coli* cells.

4.2.3 Outer-membrane disruption assay

In the $TriA_1$ mode of action, the first point of contact between the peptide and Gram-negative bacteria is the outer-membrane. Disruption of the outer-membrane in *E. coli* cells can be assessed using an ANS (**169**) uptake assay. The fluorescence of this hydrophobic dye increases when it enters more hydrophobic environments. Disruption of the outer-membrane allows increased access to hydrophobic regions of proteins and other biomolecules inside the cell, leading to an increase in fluorescence.[187] An ANS-uptake assay using *E. coli* ATCC 25922 shows that at concentrations at and above its MIC, $TriA_1$ disrupts the outer-membrane (Fig. 4.3). In contrast, the unacylated analogue

H-TriA_1 does not affect fluorescence, suggesting that the lipid tail is important for disrupting the outer-membrane. Like the polymyxins, the *N*-terminal lipid tail is likely required for permeation of the outer-membrane. However, this does not explain the observed synergy between H-TriA_1 and antibiotics like rifampicin and vancomycin. These large antibiotics are capable of crossing the outer-membrane in the presence of H-TriA_1, so it is surprising that ANS cannot. Therefore, we hypothesized that there may be a specific receptor on the outer-membrane that H-TriA_1 binds to induce this effect.

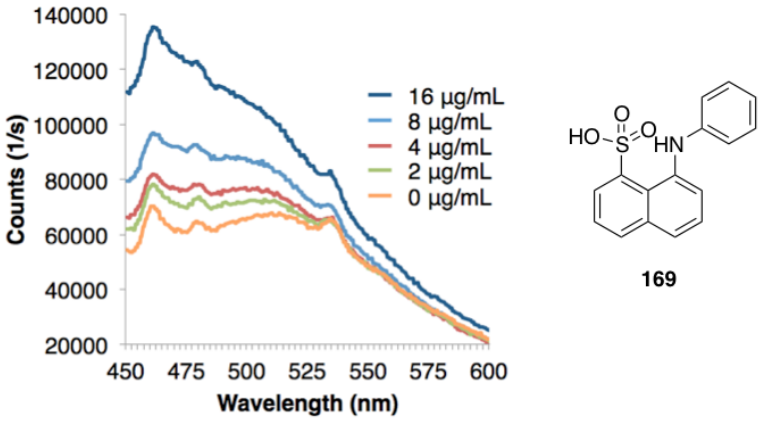

Figure 4.3. ANS uptake assay with TriA_1 treated *E. coli* cells.

4.2.4. Inner-membrane depolarization assay

Membrane depolarization studies are a common way to assess the effect of membrane-interacting antimicrobial compounds. DiBAC_4(3) (**170**) is a semi-permeable bisoxonol dye that allows the potassium gradient on the inner bacterial membrane to be visualized.[188] This negatively charged dye readily penetrates the outer-membrane, but accumulates on the exterior of the inner-membrane due to the high concentration of potassium ions there. Disruption of the inner-membrane disrupts the potassium

gradient, leading to dispersal of the dye, which then binds to hydrophobic proteins in the cytoplasm, causing an increase in fluorescence. Exposure of *E. coli* cells pretreated with $DiBAC_4(3)$ to $TriA_1$ (2xMIC) does not cause an increase in fluorescence (Fig. 4.4), suggesting it does not depolarize the inner-membrane. The observed decrease in fluorescence in Fig. 4.4 after $TriA_1$ addition is due to dilution of the reaction mixture when this solution is added. Subsequent addition of polymyxin B, which is known to depolarize the inner-membrane, resulted in a rapid increase in fluorescence, confirming the dye is functioning properly. This experiment was performed by Dr. Brandon Findlay.

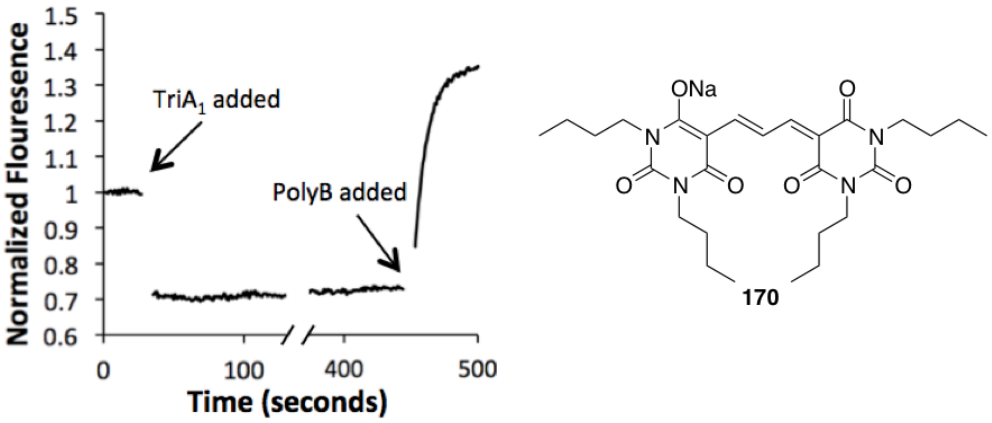

Figure 4.4. Membrane depolarization assay using $DiBAC_4(3)$.

4.2.5. Inner-membrane disruption assays

To determine if $TriA_1$ is lysing the inner-membrane, a membrane-disruption assay using the dye SYTOX green (**171**) was performed with *E. coli* cells by Dr. Brandon Findlay. SYTOX green is a fluorescent dye that binds to nucleic acids in the cytoplasm but cannot cross the inner-membrane.[189] The formation of large tears on the inner-membrane allows this dye to enter the cytoplasm and bind to nucleic acids, causing an increase in fluorescence. The formation of these large tears results in rapid cell death,

therefore SYTOX Green is known as a "live/dead" stain. Upon addition of $TriA_1$ to *E. coli* cells pretreated with SYTOX Green, a very gradual increase in fluorescence occurs, equivalent to an approximate doubling in fluorescence over five min (Fig. 4.5). In contrast, addition of the surfactant TritonX-100 leads to a much larger increase in fluorescence (> 6-fold) over the same period. The rate of increase in fluorescence correlates well with the rate of cell death observed in the time-kill assay, suggesting that fluorescence increases due to an increase in the number of dead cells, and that membrane tears are not an immediate effect of $TriA_1$ exposure.

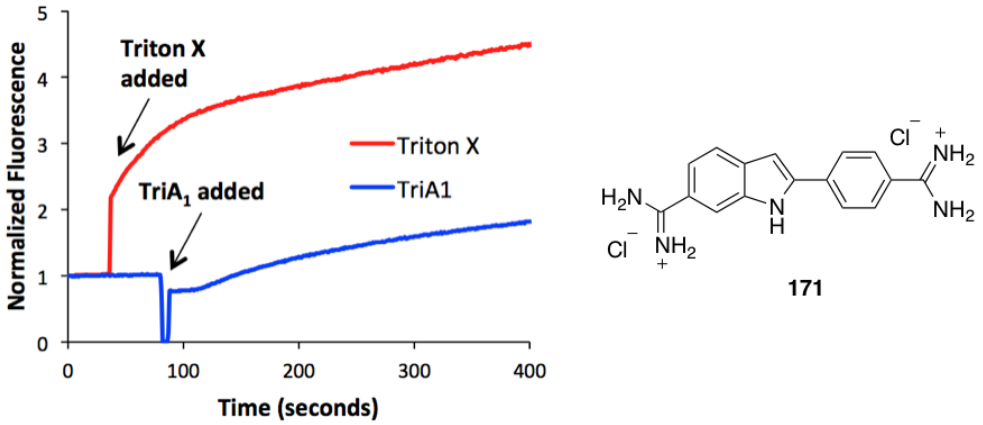

Figure 4.5. Membrane-disruption assay using SYTOX Green.

To further corroborate that $TriA_1$ is not directly killing *E. coli* by inner-membrane lysis, its ability to disrupt the inner-membrane of *E. coli* ML-35 cells was assessed using an ONPG assay (Fig. 4.6). *E. coli* ML-35 is a lactose permease deficient strain with constitutive cytoplasmic β-galactosidase activity.[190] Disruption of the inner-membrane releases the β-galactosidase, which can then cleave the *O*-nitrophenyl group from galactose derivative ONPG (**172**). This results in an absorbance increase at 405 nm

due to the *O*-nitrophenyl chromophore. When *E. coli* ML-35 cells pretreated with ONPG are exposed to $TriA_1$, a gradual increase in absorbance occurs over 15 min. In contrast, the lytic peptide mellitin results in a rapid increase in absorbance. These results further support our findings that $TriA_1$ does not immediately lyse the inner-membrane.

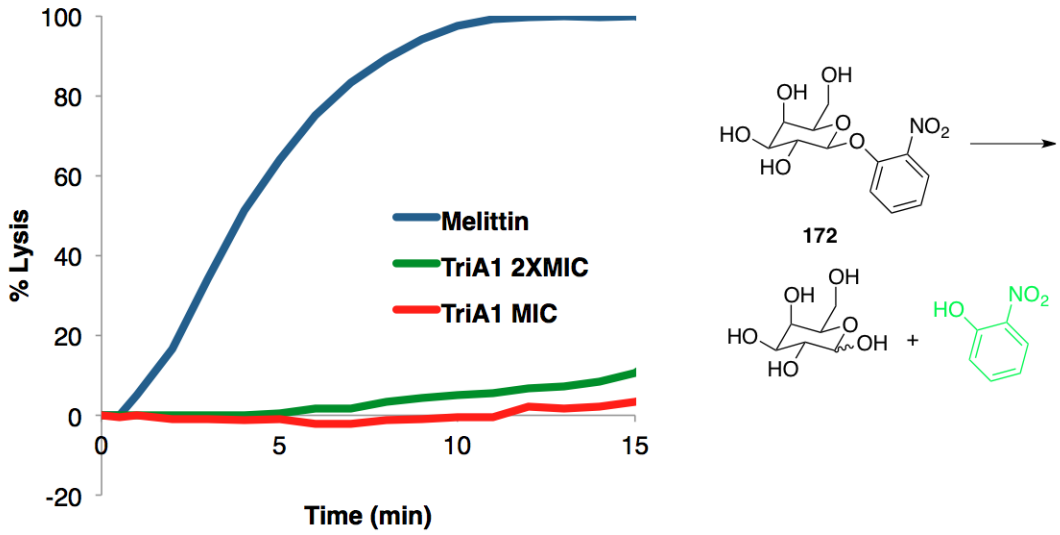

Figure 4.6. ONPG assay with $TriA_1$ treated *E. coli* cells.

4.2.6. Disruption of the proton-motive force

The rapid killing of *E. coli* cells observed in the time-kill assay stood in stark contrast to the lack of membrane activity observed with ONPG, SYTOX Green and $DiBAC_4(3)$. $TriA_1$ kills most cells by 30 minutes of exposure, therefore it does not inhibit protein-synthesis, nucleic acid synthesis or peptidoglycan biosynthesis. This rate of killing is highly suggestive of membrane attack and is further corroborated by the essential nature of the lipid tail on $TriA_1$ for antimicrobial activity and outer-membrane disruption. Therefore, we considered other membrane-targeting mechanisms that could give rise to the observed kill rate.

Bacteria use both protons and potassium ions to generate ATP via the proton-motive force, which occurs at the cytoplasmic membrane and is essential for cell growth.[191] The proton-motive force consists of two components, the electrical potential (ΔΨ) and the pH gradient (ΔpH). ΔΨ is the difference in electric potential between the interior and exterior of the membrane and is controlled by Na^+ and K^+ ion gradients. The ionophore valinomycin (**174**) binds selectively to K^+ ions and dissipates ΔΨ (Figure 4.7).[192] ΔpH is the difference in pH between the interior and exterior of the membrane and can be dissipated by the antibiotic nigericin (**173**), which is an antiporter of K^+ and H^+. Disruption of the proton-motive force is bactericidal, and while not a common mode of action, some antimicrobial compounds that inhibit the proton-motive force are known. For example, the bacteriocin subtilosin (**175**) has been shown to disrupt the proton-motive force in the Gram-positive bacterium *Gardnerella vaginalis*.[193] Therefore, we sought to determine if $TriA_1$ exerts its bactericidal effect by disruption of the proton-motive force.

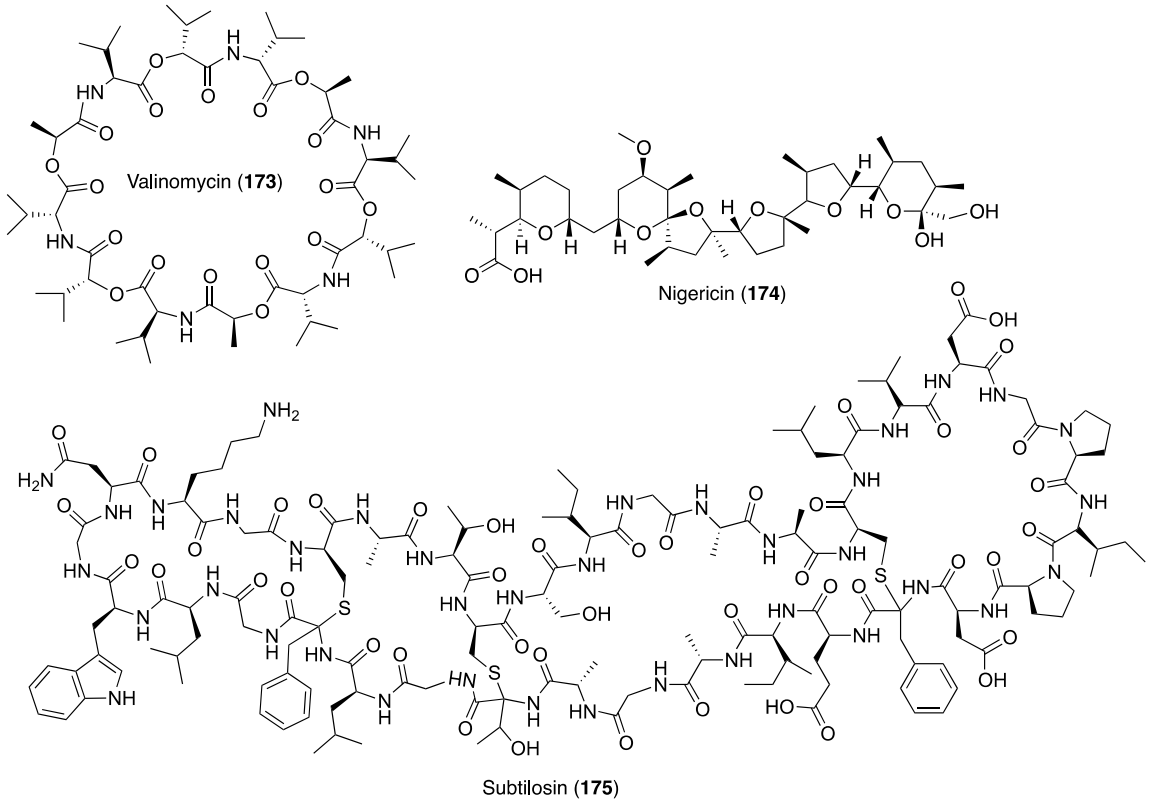

Figure 4.7. Antibiotics that target the proton-motive force.

To test this hypothesis, the pro-dye BCECF-AM (**176**) was adapted for use in Gram-negative bacteria. BCECF-AM is commonly used to measure the intracellular pH in mammalian cells.[194] It contains a fluorescein core and several acidic functionalities, all of which are protected as acetoxymethyl esters. These hydrophobic esters allow the dye to cross the cytoplasmic membrane, where it is then hydrolyzed by non-specific esterases, yielding the active dye BCECF (**177**) (Scheme 4.1). Depending on the pH, various degrees of protonation will exist, altering the electronic properties of the dye. BCECF has a p*K*a of 7 and a fluorescence decrease occurs as the pH drops from pH 8 to pH 6.

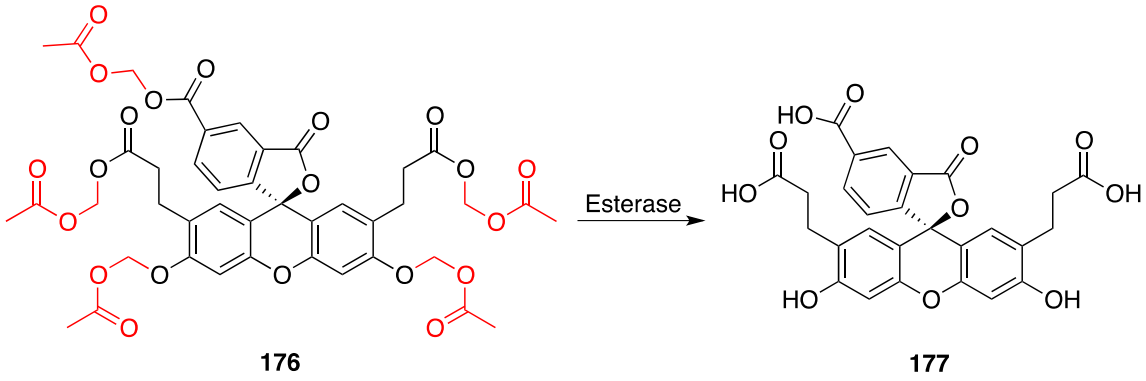

176 177

Scheme 4.1. Hydrolysis of BCECF-AM in the cytoplasm.

In this assay, *E. coli* cells are placed in a pH 6 buffer so that the cytoplasmic pH, which is typically pH 7.0 – 7.4, is higher than the external buffer. BCECF-AM cannot cross the outer-membrane, therefore *E. coli* cells must first be treated with EDTA to allow entry of this dye into the periplasm. EDTA chelates divalent cations (Ca^{2+}, Mg^{2+}, etc.) associated with the phosphate groups on LPS. This destabilizes LPS and leads to the loss of some LPS from the outer-membrane, exposing phospholipids and providing a permeation site for hydrophobic molecules.[195] Subsequent addition of glucose to the EDTA/BCECF-AM treated *E. coli* cells causes an increase in fluorescence due to an increase in cytosolic pH, confirming that the cells are actively respiring and that the dye is functioning properly (Fig. 4.8).[193]

To observe the effect of $TriA_1$ on the proton gradient, the electric potential is first dispersed by addition of valinomycin, resulting in a small increase in fluorescence. Subsequent addition of $TriA_1$ causes a rapid decrease in fluorescence, signifying a decrease in cytoplasmic pH due to the flow of protons from external buffer into the cytoplasm. A similar effect is observed upon addition of nigericin, suggesting that $TriA_1$ is dispersing the proton gradient on the inner-membrane of *E. coli* cells. As the proton

gradient is essential for ATP synthesis, which in turn is vital for powering many cellular processes, we propose that it is this disruption of the proton-motive force that allows $TriA_1$ to kill *E. coli*. These experiments were performed by Dr. Brandon Findlay.

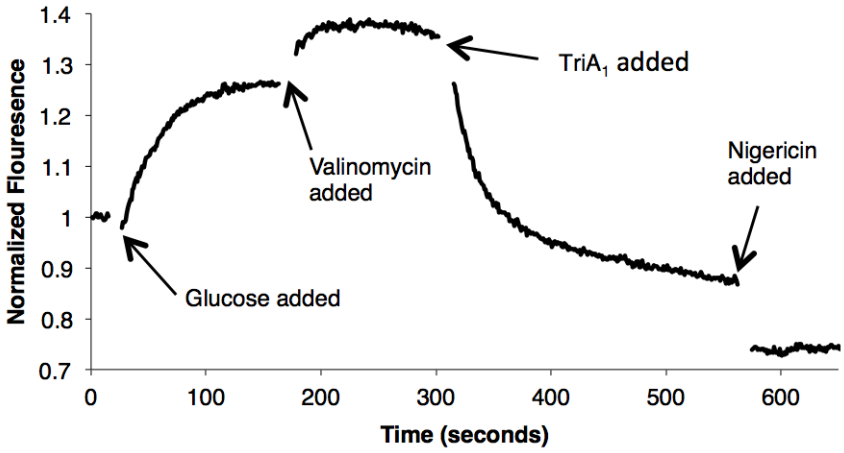

Figure 4.8. BCECF fluorescence from the cytoplasm of *E. coli* cells that are sequentially treated with glucose, valinomycin, tridecaptin A_1 and nigericin.

4.3. Mechanism of action studies

4.3.1. Analysis of the structure of tridecaptin A_1

Preliminary structural analysis of antimicrobial peptides can reveal a lot about their function. For example, polymyxin B contains five Dab residues, two hydrophobic amino acids and a lipid tail. Overall it has a +5 charge at physiological pH. Therefore, without knowing anything about its target, it is possible to predict that the high positive charge and amphiphilic nature of this peptide probably make it a membrane disrupter, given the overall negative charge of membranes. The toxicity to mammalian cells also arises from this high positive charge, as it allows the polymyxins to target both prokaryotic and eukaryotic cells. Analysis of the structure of $TriA_1$ also suggests a

membrane interaction, as it contains an *N*-terminal lipid tail, several hydrophobic amino acids and three Dab residues. However, the presence of a glutamic acid and C-terminal carboxylate mean it only has a +1 charge at physiological pH, which may limit its *in vivo* toxicity.

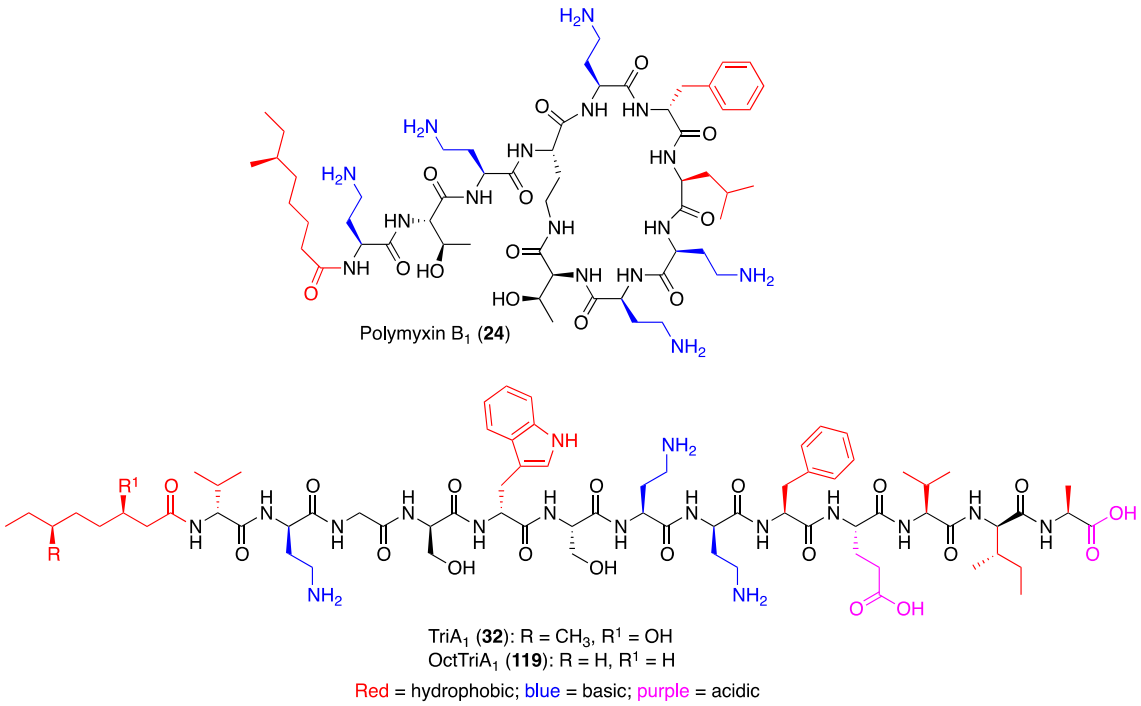

Figure 4.9. Hydrophobic, basic and acidic residues highlighted in the structures of tridecaptin A_1 and polymyxin B_1.

4.3.2. Alanine scan reveals key residues for Oct-TriA$_1$ activity

The alanine scan of Oct-TriA$_1$ described in chapter three determined the amino acids that were essential to the activity of this peptide (Fig. 4.10). The only essential residue is D-Dab8, whose substitution with alanine abolishes antimicrobial activity. D-Trp5 and D-*allo*-Ile12 are also important to the activity of TriA$_1$, resulting in an 8- to 16-fold loss in activity upon substitution.

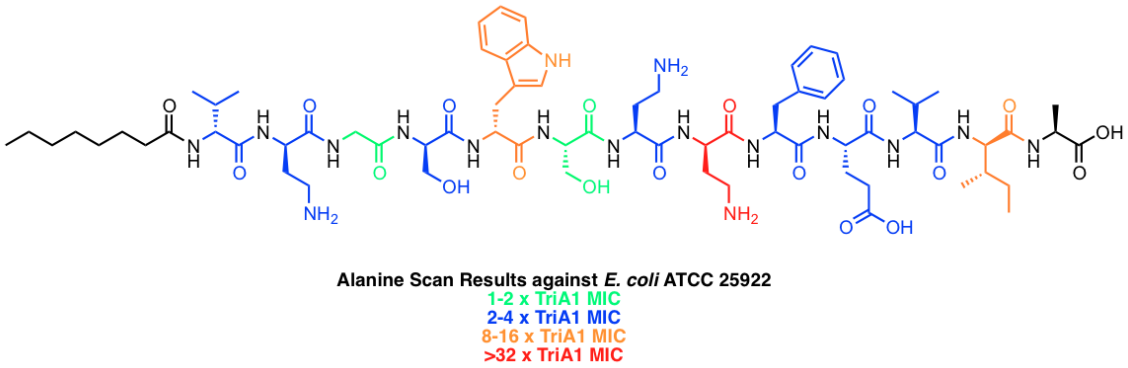

Figure 4.10. Difference in MICs of $TriA_1$ and alanine-scan analogues.

To further probe the decrease in activity upon substitution of certain amino acids, CD spectroscopy was used to analyze the structure of these analogues. $TriA_1$ is unstructured in both aqueous buffer and 50% trifluoroethanol, which is often used to induce structure in membrane targeting peptides (Fig. 4.11). In an attempt to more closely mimic the bacterial membrane, the CD spectra of tridecaptin analogues were measured in the presence of negatively charged phospholipid LUVs.[187] $TriA_1$ adopts a stable secondary structure in the presence of these LUVs, with a strong negative minimum at 196 nm and moderate positive maximum at 224 nm in the CD spectrum. This type of curve has been attributed to the poly-L-proline II helix adopted by positively charged polyproline chains and the extended helix structure observed in collagen.[196]

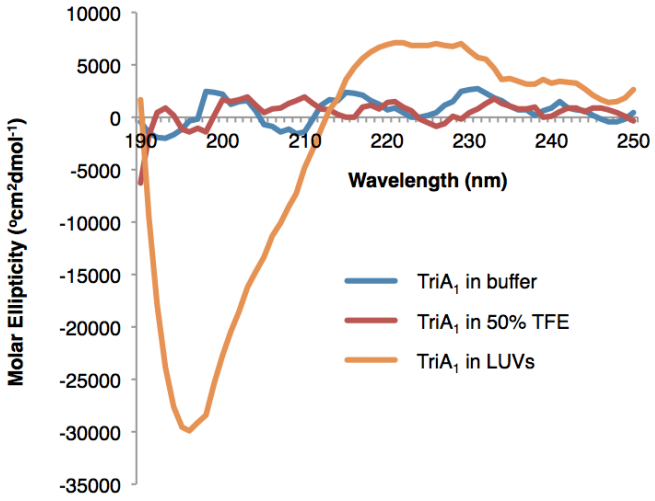

Figure 4.11. CD spectra of $TriA_1$ in different solvent systems.

The CD spectra of the alanine-scan analogues were recorded to correlate membrane structure and antimicrobial activity. All analogues are completely disordered in aqueous buffer and TFE, but many retain the structure of $TriA_1$ in the presence of LUVs (Fig. 4.12). In most cases the magnitude of the negative band at 194 nm directly relates to the activity of the peptide. Ala10 has the largest negative band, which may arise from the increased positive charge with substitution of L-Glu10 with alanine. Ala1, Ala4 and Ala6, have a similar spectrum to the natural peptide, whereas Ala3, Ala11 and Ala7, have a greatly reduced negative band, which correlates to a roughly 2- to 4-fold reduction in activity. Substitution of D-Dab8 with D-Ala, which significantly reduces antimicrobial activity, also prevents formation of the secondary structure adopted by the natural peptide. Substitution of D-Trp5 or D-*allo*-Ile12 had a similar affect. These results suggest that these three residues are important in adopting a stable secondary structure in membrane environments, and that this structure is related to the antimicrobial activity.

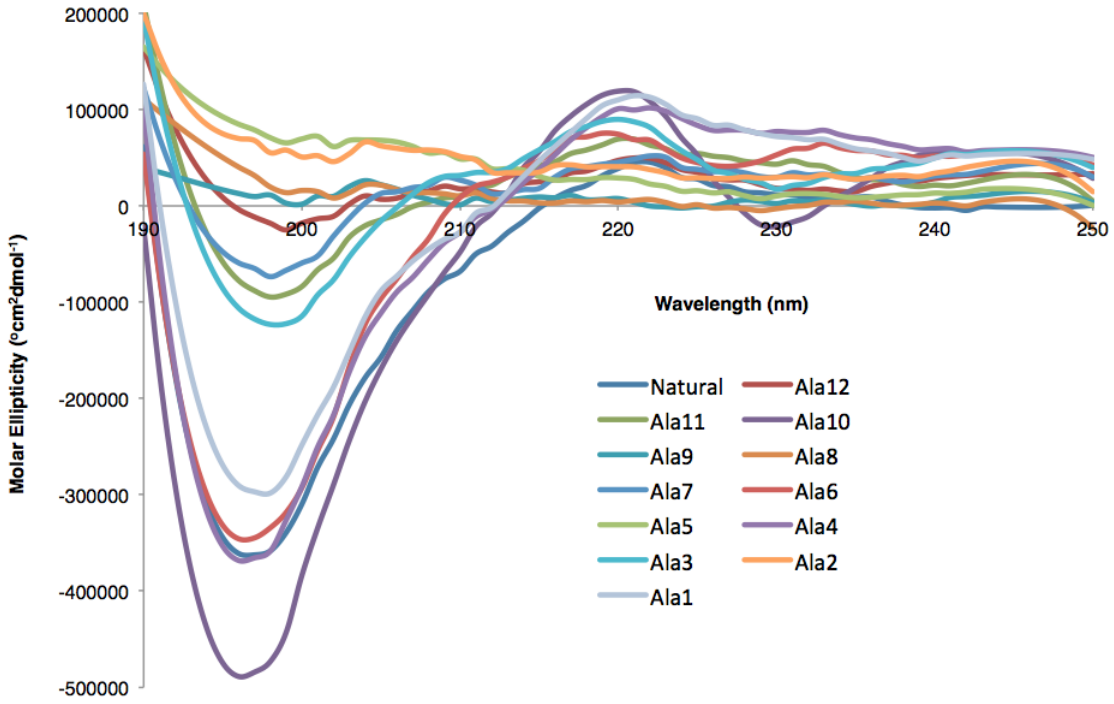

Figure 4.12. CD spectra of alanine-scan analogues in the presence of LUVs.

4.3.3. Synthesis and evaluation of the enantiomer of tridecaptin A_1

A common method to determine if a chiral interaction is involved in the mechanism of action of an antimicrobial compound is to synthesize and test its enantiomer. Therefore the enantiomer of Oct-TriA_1, *Ent*-TriA_1 (**206**), was synthesized using Fmoc-SPPS and tested against *E. coli* ATCC 25922 cells. *Ent*-TriA_1 is 4-fold less active than the natural peptide, suggesting that a chiral receptor is involved in the mechanism of action.

4.3.4. Lipopolysaccharide binding

Polymyxin B permeates the outer-membrane by first binding to the lipid A portion of lipopolysaccharide, followed by membrane insertion and passage into the periplasm.

Given the similarities between $TriA_1$ and polymyxin B, we decided to investigate if $TriA_1$ also binds to LPS. Isothermal titration calorimetry revealed that $TriA_1$, H-$TriA_1$ and *Ent*-$TriA_1$ bind to LPS from *E. coli* with similar affinities to polymyxin B (Fig. 4.13). The observation that H-$TriA_1$ binds to LPS provides a mechanistic rationale for the synergy observed between this peptide and vancomycin/rifampicin – H-$TriA_1$ binds to LPS and disrupts the outer-membrane, making it more permeable to these hydrophobic antibiotics. As the absence of the lipid tail does not effect LPS binding, it suggests that the lipid tail is either important for crossing the outer-membrane, or interacting with the inner-membrane. Furthermore, the observation that *Ent*-$TriA_1$ binds just as strongly to LPS as the natural peptide shows that there must be another chiral receptor that accounts for the difference in activity between *Ent*-$TriA_1$ and $TriA_1$.

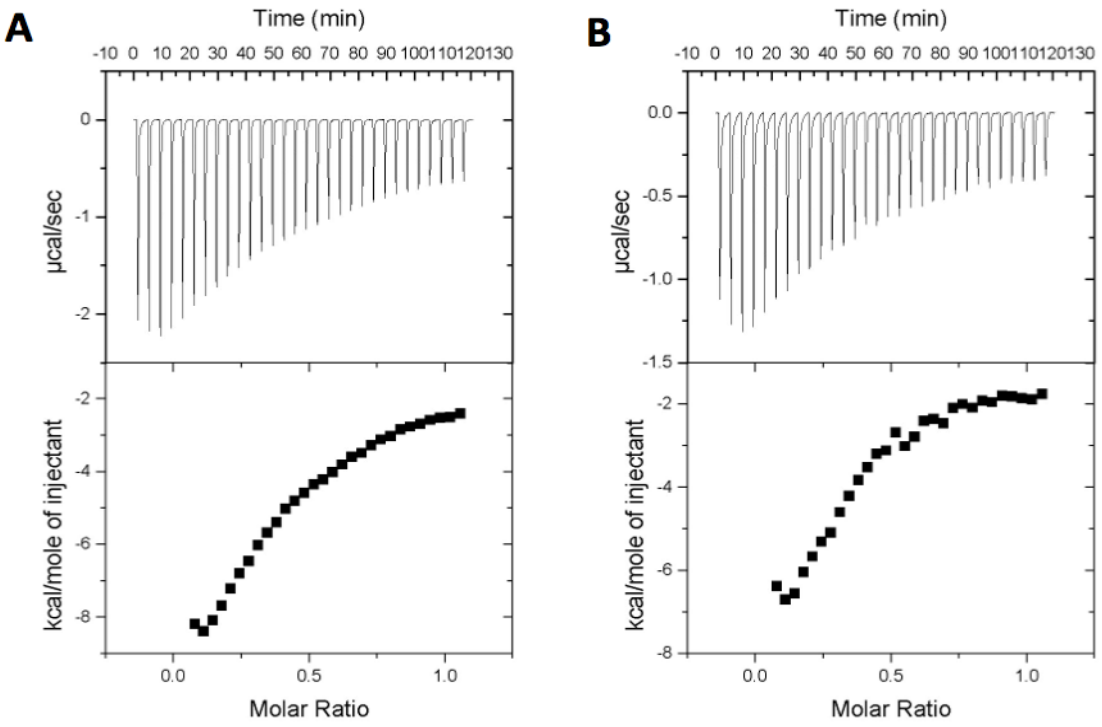

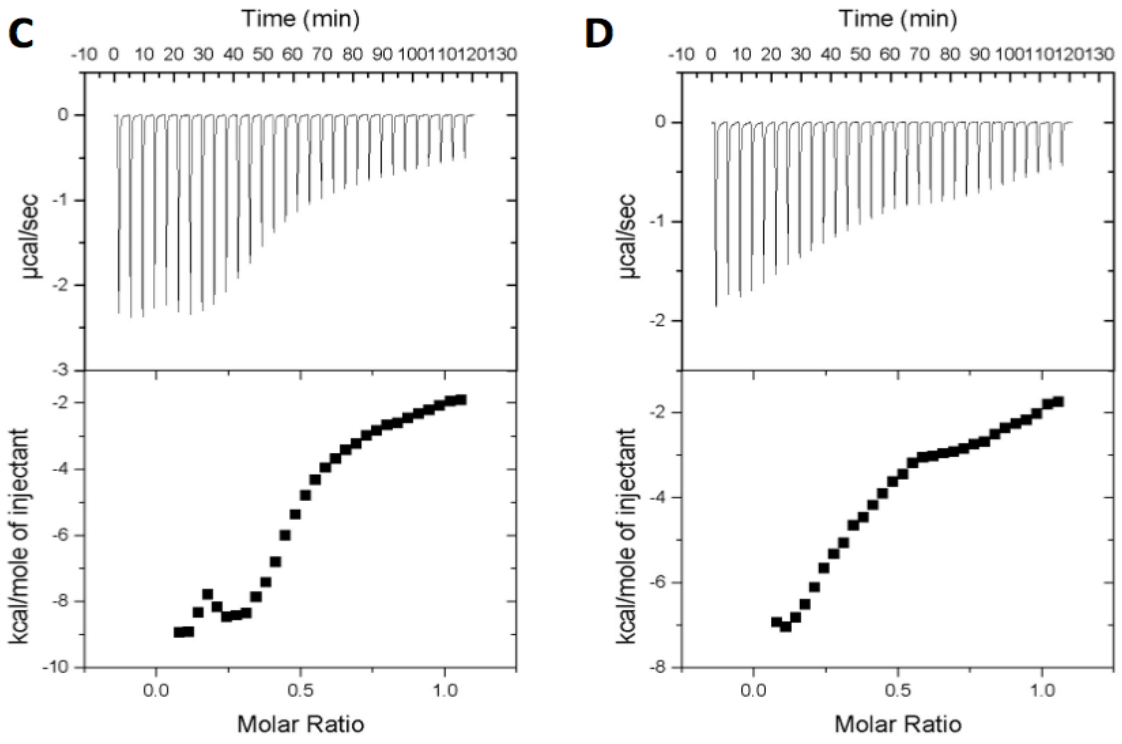

Figure 4.13. Binding of peptides to LPS from *E. coli*. (A) $TriA_1$, (B) *Ent*-$TriA_1$, (C) H-$TriA_1$ and (D) polymyxin B.

4.3.5. Identification of lipid II as the receptor on the inner-membrane

At this point one important question still remained about the mechanism of action of tridecaptin A_1. Mode-of-action studies suggested that it disrupts the proton-motive force; however, the enantiomer of $TriA_1$ is approximately 4-fold less active, meaning a chiral receptor is involved in the mechanism of action. This is not LPS, given the similar binding affinities of $TriA_1$ and *Ent*-$TriA_1$. Therefore, we concluded that the chiral receptor must be present on the inner-membrane. Given that several antimicrobial peptides bind to lipid II, and that prior to its elongation into peptidoglycan, lipid II is anchored to the exterior of the inner-membrane, we investigated if $TriA_1$ binds to lipid II.

The structure of lipid II differs slightly between Gram-positive and Gram-negative bacteria, namely on residue three of the pentapeptide portion. In Gram-negative bacteria, this amino acid is *meso*-diaminopimelic acid, whereas in most Gram-positive bacteria it is lysine (Fig. 4.14). A sample of Gram-negative lipid II (**178**) was purchased from the BaCWAN facility at the University of Warwick and tested for binding to $TriA_1$ using ITC (Fig. 4.15). $TriA_1$ binds strongly to Gram-negative lipid II in a 1:1 ratio. However, this discovery opened up another big question. Gram-positive bacteria also have lipid II on the exterior of their cytoplasmic membrane but $TriA_1$ is approximately 50-fold less active against these organisms. Therefore we also purchased Gram-positive lipid II (**179**) and were surprised to find that it showed little binding affinity to this analogue by ITC. This selective binding to Gram-negative lipid II would explain the difference in the activity of $TriA_1$ against Gram-positive and Gram-negative bacteria.

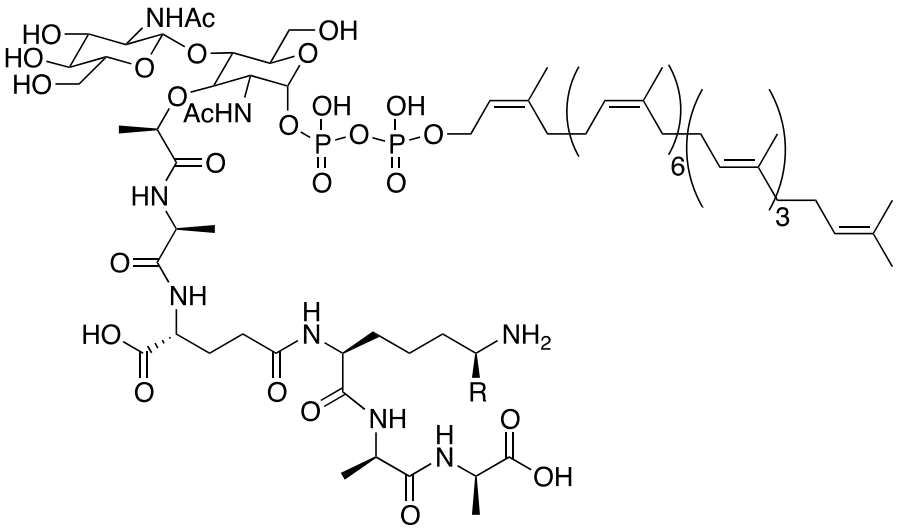

Gram-negative lipid II (**178**): R = COOH
Gram-positive lipid II (**179**): R = H

Figure 4.14. Structure of lipid II from Gram-negative and Gram-positive bacteria.

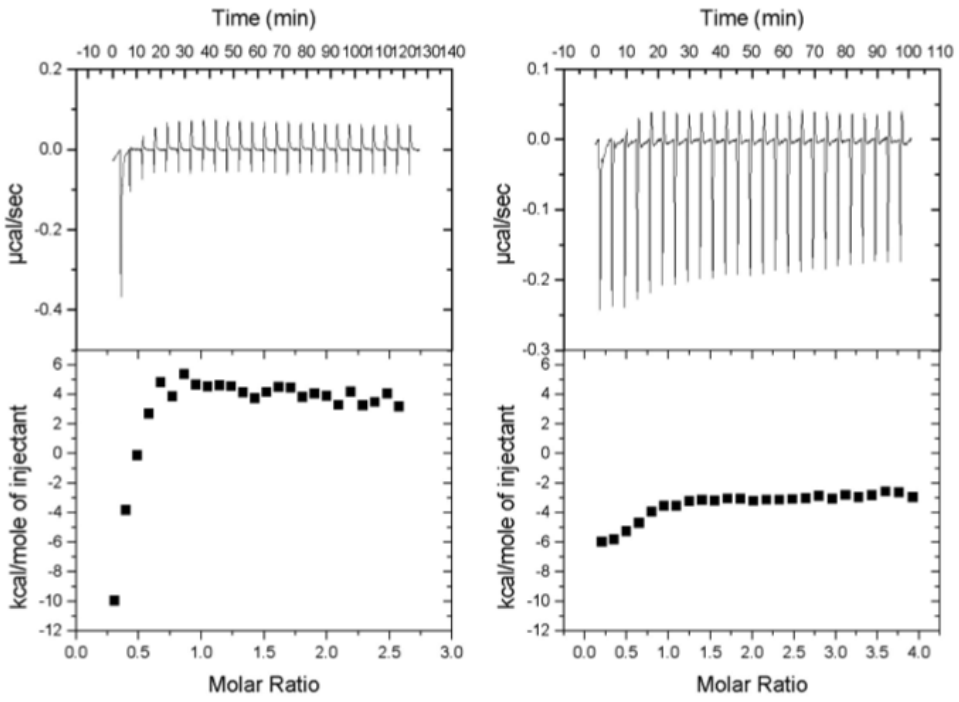

Figure 4.15. ITC isotherms from $TriA_1$ binding experiments with Gram-negative lipid II (left) and Gram-positive lipid II (right).

To the best of our knowledge, this is the first instance of an antimicrobial compound binding selectively to lipid II from Gram-negative bacteria. To further corroborate this discovery, an inhibition study was performed using a spot-on-lawn assay with *E. coli* (Fig. 4.16). The ITC data from Fig. 4.15 suggests that $TriA_1$ binds to Gram-negative lipid II in a 1:1 ratio. Therefore we rationalized that pre-mixing $TriA_1$ and Gram-negative lipid II would form a 1:1 complex, rendering $TriA_1$ inactive when applied to an agar plate containing *E. coli*. Pre-mixing $TriA_1$ with Gram-negative lipid II completely sequestered its activity against *E. coli*. Furthermore, performing the same experiment with Gram-positive lipid II had little effect on the zone of inhibition, further evidencing the selective interaction between $TriA_1$ and Gram-negative lipid II.

Figure 4.16. Spot-on-lawn assay with $TriA_1$ (left), $TriA_1$ + Gram-positive lipid II (middle) and $TriA_1$ + Gram-negative lipid II (right).

4.3.6. Linking lipid II binding to the $TriA_1$ mode of action

Having identified lipid II from Gram-negative bacteria as a binding partner of $TriA_1$, we next sought to link this observation to our proposed mode of action, disruption of the proton-motive force. Breukink and coworkers have previously used dye-leakage assays to show the importance of lipid II in the ability of nisin to form pores in model membranes.[197] In these experiments, LUVs containing a fluorescent dye are treated with nisin to assess pore formation, which releases the dye from the vesicles and causes a fluorescence increase. Incorporation of a small amount of lipid II into the surface of the LUVs substantially increases the ability of nisin to form pores, as would be expected as it binds to lipid II *in vivo*. Therefore, we devised a similar experiment to test if the presence of lipid II on the surface of LUVs increased the effectiveness of $TriA_1$ at forming small pores, which disrupt the proton-motive force. LUVs were constructed in which BCECF is encapsulated in the centre with an internal pH of 8, whilst the external buffer is pH 6. In this assay, the formation of pores will cause the internal pH to decrease as protons flow from the buffer into the vesicles, lowering fluorescence (Fig.

4.17). If Gram-negative lipid II is the receptor of $TriA_1$ on the inner-membrane, its presence on the surface of the LUVs should increase the ability of $TriA_1$ to form pores.

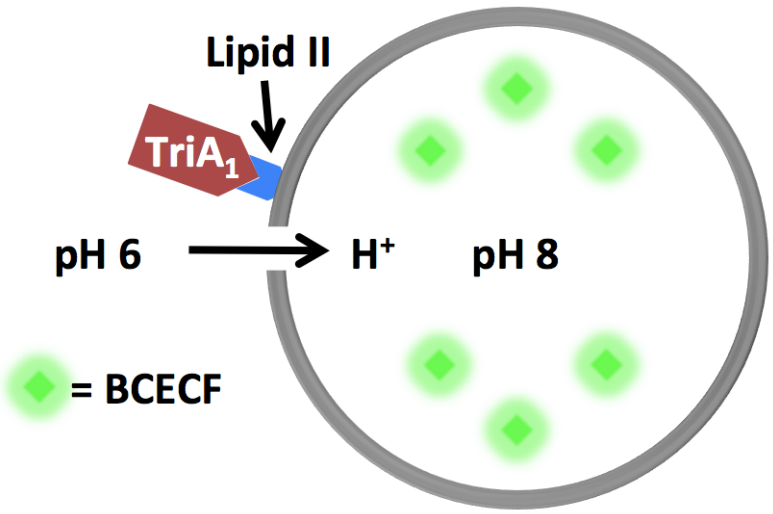

Figure 4.17. *In vitro* assay to assess the effect of lipid II on pore formation.

At this stage of our experiments we started using Oct-$TriA_1$ rather than $TriA_1$. It is synthetically more accessible, has identical activity to $TriA_1$ and also binds to LPS and Gram-negative lipid II. As the lipid tail on lipopeptides is typically embedded in the cell membrane, its identity rarely alters its mechanism of action. The addition of Oct-$TriA_1$ to LUVs doped with 1 mol% Gram-negative lipid II at concentrations mimicking the bacterial MIC causes a rapid decrease in fluorescence, signifying pore formation (Fig. 4.18). A much weaker decrease in fluorescence occurs with LUVs containing Gram-positive lipid II, which is only slightly greater than the decrease observed against vesicles lacking any lipid II. These studies confirm that Oct-TriA1 selectively recognizes Gram-negative lipid II and link this recognition to the observed antimicrobial activity against Gram-negative bacteria. This work was conducted by Dr. Brandon Findlay.

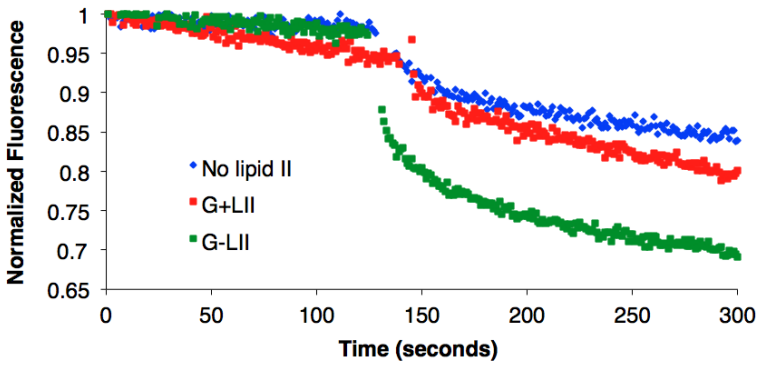

Figure 4.18. Fluorescence readings from LUV assays.

4.3.7. Synthesis of a lipid II analogue for NMR studies

Identification of the exact mechanism by which tridecaptin A_1 binds to lipid II may allow the rational design of peptidomimetics and will also help predict the likelihood of resistance development against this antimicrobial peptide. Two of the possible methods to observe this interaction are X-ray crystallography and NMR. Our group has extensive experience in the calculation of the 3D solution structures of peptides and proteins using NMR spectroscopy, therefore we envisaged using a similar approach to identify the binding mode of $TriA_1$ to Gram-negative lipid II. Natural lipid II contains an undecaprenyl (C_{55}) chain that can be problematic for NMR analysis. It has poor solubility in water and can make selection of a solvent system that is also applicable for $TriA_1$ difficult. Also, given its amphiphilic nature it is prone to micelle formation, which causes significant line broadening in NMR spectra. The numerous methyl and methylene signals from the C_{55} chain can also drown out other important signals from lipid II or $TriA_1$, making complete assignment of both compounds difficult.

To overcome these problems, the C_{55} tail can be replaced with a shorter terpene chain. Breukink and co-workers used a biosynthetic approach to prepare a Gram-

positive lipid II analogue containing an (*E*,*E*)-farnesyl terpene chain, which was subsequently used to determine the NMR solution structure of nisin in the presence of lipid II.[20] Lipid II was then docked into this structure to give a model of the nisin-lipid II complex. The length and geometry of the terpene tail was found not to affect the ability of nisin to bind to lipid II, presumably because it is embedded in the cell membrane.

VanNieuwenhze and coworkers performed the first total synthesis of this peptidoglycan precursor.[198,199] The biosynthetic approach to make lipid II relies on machinery from Gram-positive bacteria and therefore can only be used for Gram-positive lipid II analogues. Therefore we embarked on the synthesis of (*Z,Z*)-farnesyl Gram-negative lipid II (**180**) for our NMR studies based on the previously reported synthesis by VanNieuwenhze and coworkers.

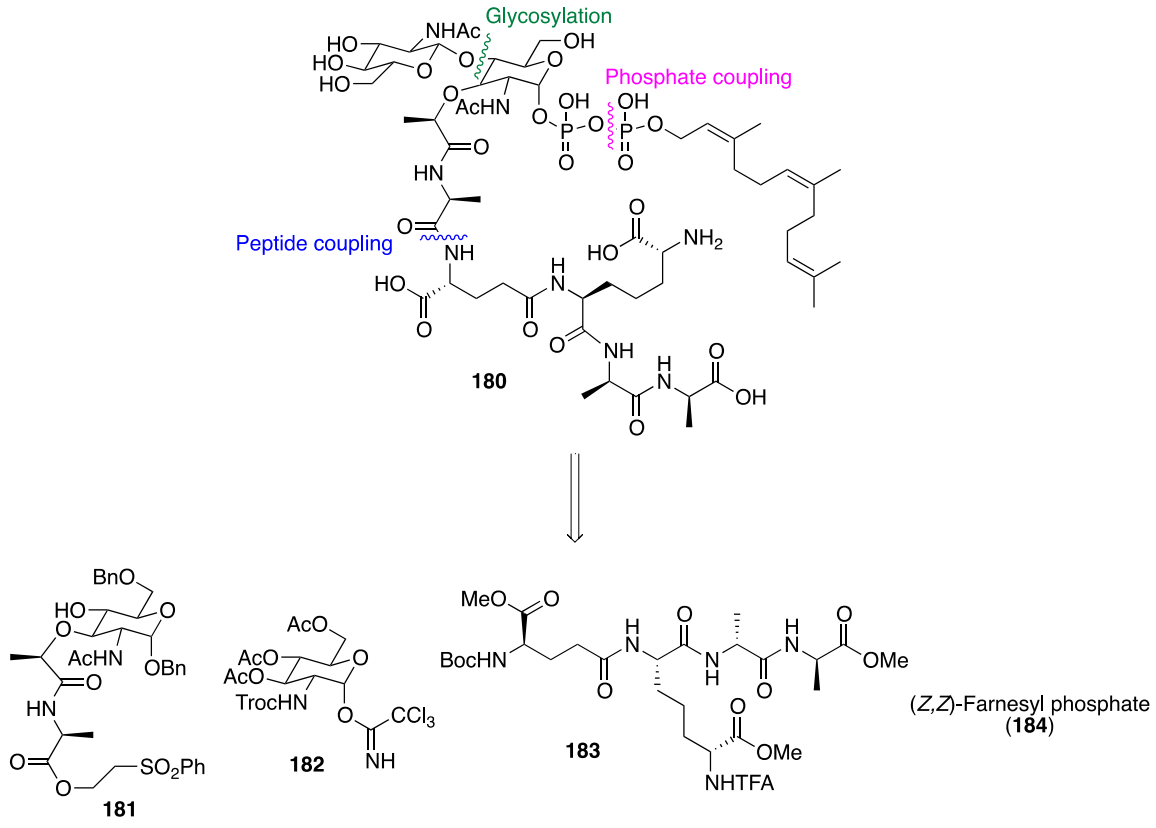

Scheme 4.2. Retrosynthetic analysis of lipid II analogue **180**.

The total syntheses of lipid II can be broken down into four linear syntheses, with each product then used to make lipid II (Scheme 4.2). Combination of glycosyl donor **181** with glycosyl acceptor **182** yields the disaccharide core, which can then be coupled to tetrapeptide **183** after protecting group manipulation. Given the sensitivity of the pyrophosphate bond, (*Z,Z*)-farnesyl phosphate (**184**) is added last to complete the lipid II synthesis.

Glycosyl donor **181** is synthesized in three steps from commercially available glycol **185** (Scheme 4.3). Treatment of **185** with L-chloropropionic acid, followed by coupling the resulting acid to alanine derivative **186** using CDMT/NMM conditions yields benzylidene **187** in excellent yield. Selective deprotection of the 4-hydroxyl group is then performed with TFA and TES to give glycosyl donor **181** in 62% yield.

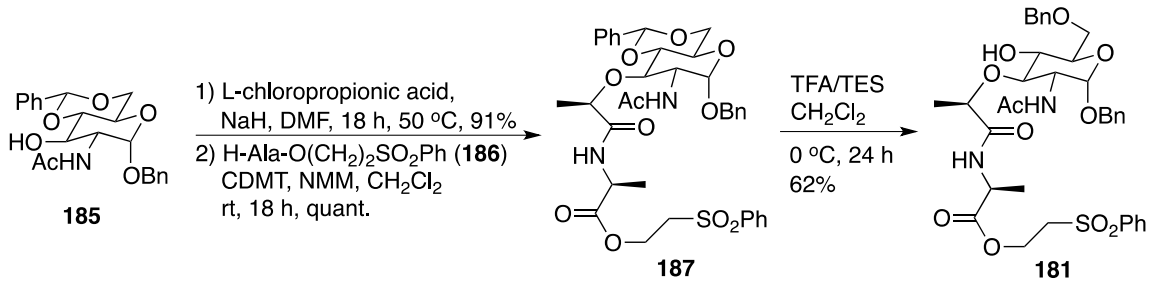

Scheme 4.3. Synthesis of glycosyl donor **181**.

Glycosyl acceptor **182** is synthesized in four steps from commercially available D-glucosamine (**188**) (Scheme 4.4). Protection of amine **188** as a Troc-carbamate, followed by global acetylation of the hydroxyl groups yields carbohydrate **189** in good yield. Selective deprotection of the anomeric position on **189** is achieved using hydrazine acetate and the resulting alcohol is reacted with Cl_3CCN and DBU as the base, to give glycosyl acceptor **182** in 42% yield over 2 steps.

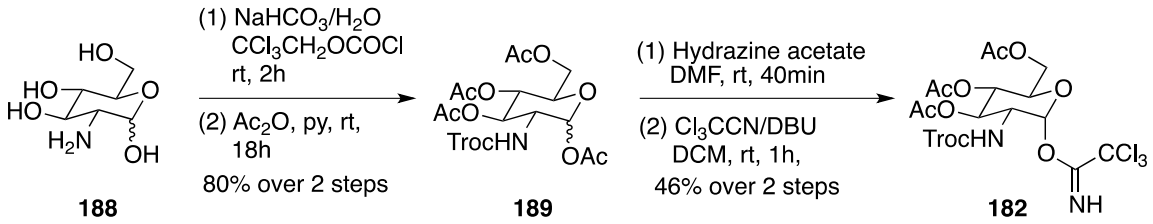

Scheme 4.4. Synthesis of glycosyl acceptor **182**.

The synthesis of tetrapeptide **183** first requires the synthesis of orthogonally protected *meso*-DAP **190**. This amino acid was synthesized using a modified literature procedure by another graduate student, Eva Rodriguez Lopez (Scheme 4.5).[200] Protection of the amine **191** with a trifluoroacetyl group, followed by methyl ester formation yields alkene **192** in 42% over 2 steps. Decarboxylative elimination of **193** yields vinylglycine derivative **194** in moderate yield. Alkenes **192** and **194** are then conjugated by cross-metathesis using Hoveyda-Grubbs 2nd generation catalyst to yield benzyl ester **195**, which is subsequently reduced with hydrogen over a palladium catalyst to give **190** in good yield.

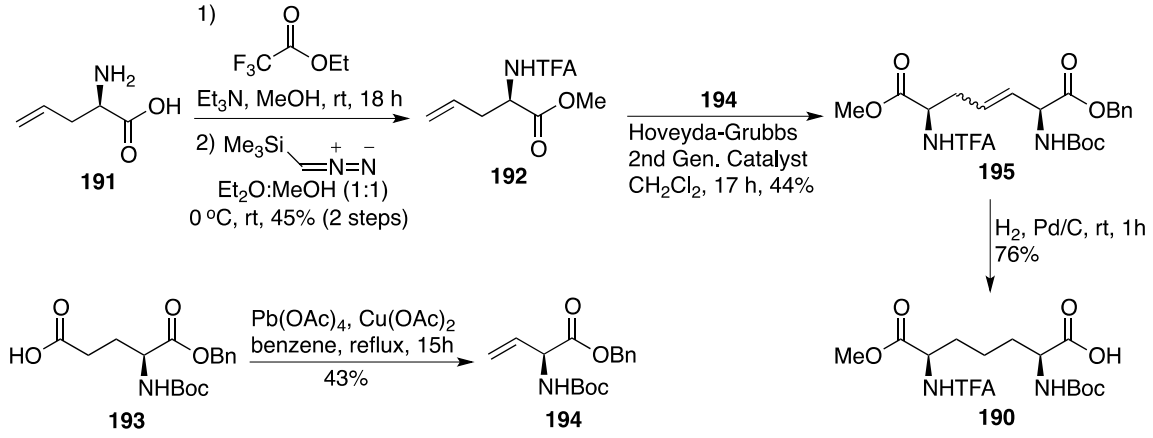

Scheme 4.5. Synthesis of orthogonally protected *meso*-DAP **190**.

Tetrapeptide **183** is synthesized in five steps using solution phase Boc-chemistry (Scheme 4.6). H-D-Ala-OMe (**196**) is coupled to Boc-D-Ala-OH (**197**) using HATU to yield Boc-dipeptide **198** in 75% yield. Deprotection of the Boc group on **198**, followed by coupling the resulting amine to *meso*-DAP **190** gives Boc-tripeptide **199** in good yield. Finally, deprotection of the Boc-carbamate on **199**, followed by coupling the resulting amine to Boc-D-Glu-OMe (**200**), yields tetrapeptide **183** in 91% yield.

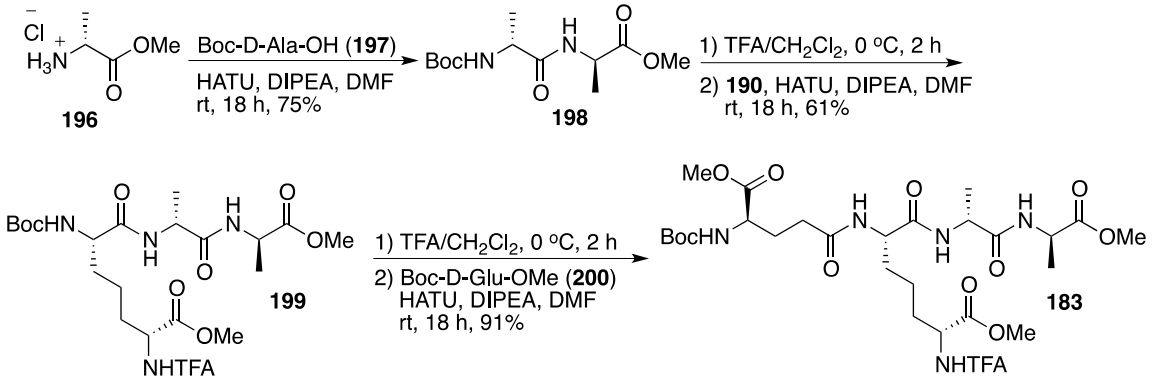

Scheme 4.6. Synthesis of tetrapeptide **183**.

With the key building blocks in hand, lipid II analogue **180** was then synthesized (Scheme 4.7). A TMSOTf catalyzed glycosylation between glycosyl donor **181** and glycosyl acceptor **182** yields disaccharide **201** in good yield. The benzyl ether at the 6-position on **201** is deprotected with $ZnCl_2$ and reprotected as an acetate ester. In the same pot, the Troc-carbamate is deprotected with zinc and reprotected as an acetamide to yield disaccharide **202** in 63% yield over two steps. Hydrogenolysis of benzyl ether **202**, followed by reaction with dibenzyl *N,N*-diethylphosphoramidite and oxidation of the resulting phosphite with H_2O_2 yields phosphate **203** in good yield. Deprotection of the ester on **203** with DBU yields a free acid, which is then coupled to the tetrapeptide (after

Boc deprotection) to give pentapeptidyl disaccharide **204** in 78% yield over two steps. Finally, the benzyl groups on **204** are removed with hydrogen over a palladium catalyst, followed by coupling the resulting phosphate to CDI activated (*Z,Z*)-farnesyl phosphate (**205**). Global deprotection is then performed with NaOH to yield lipid II analogue **180** in 25% yield over 3 steps.

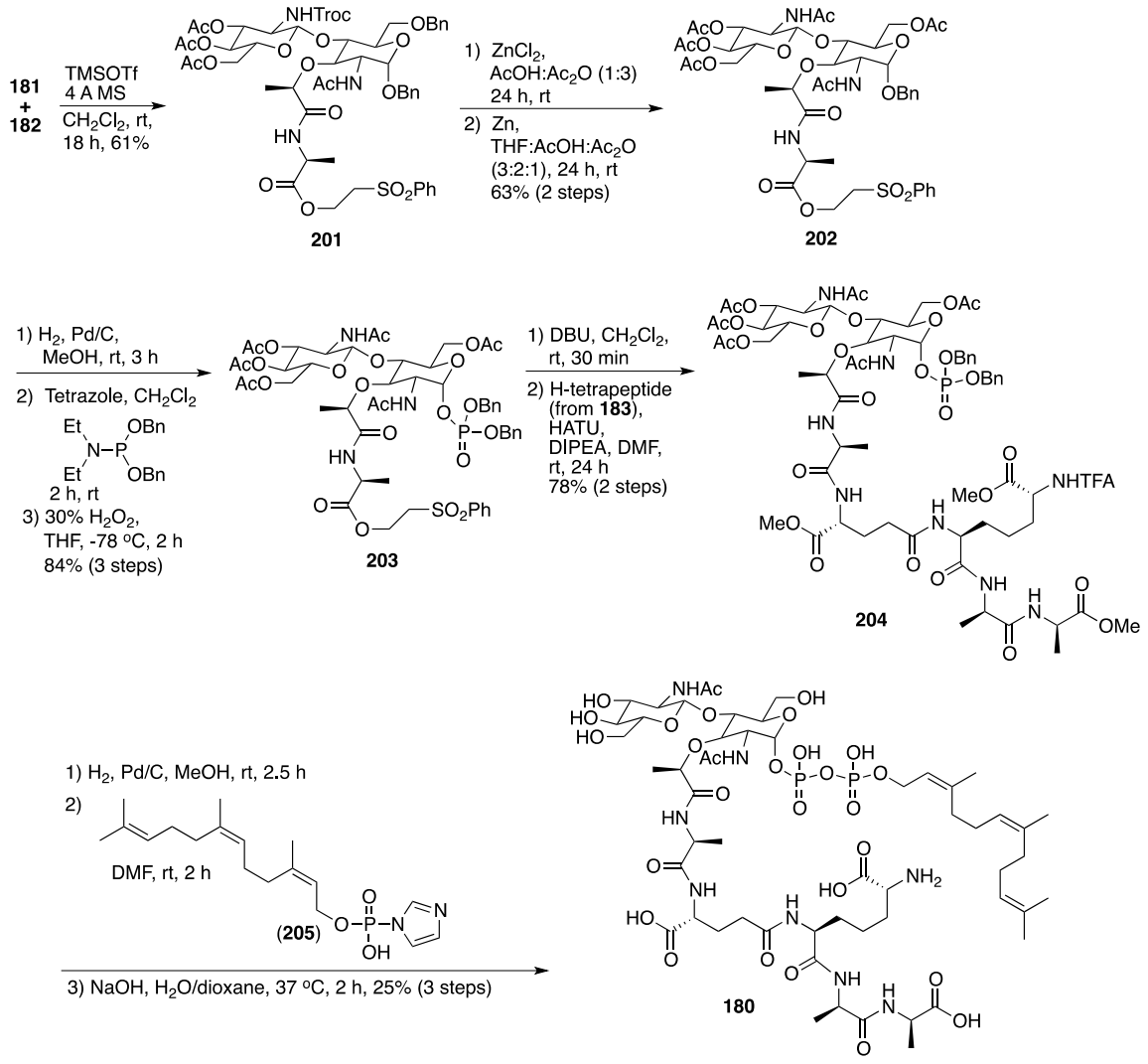

Scheme 4.7. Synthesis of (*Z*,*Z*)-farnesyl lipid II **180**.

4.3.8. Solution NMR structure of Oct-TriA_1 in DPC micelles

The CD experiments on the alanine-scan analogues (section 4.3.2) revealed that TriA_1 adopts a stable secondary structure in phospholipid vesicles, which is important for antimicrobial activity. We therefore embarked on calculating this structure to provide further insight into the mechanism of action of tridecaptin A_1. Deuterated DPC micelles are commonly used in peptide and protein NMR to mimic a bacterial membrane. Based on CD results, TriA_1 adopts a similar secondary structure in 180 mM DPC micelles to that in the presence of phospholipid LUVs, therefore this concentration of deuterated DPC was used in all NMR experiments. An NMR solvent composed of 90% H_2O and 10% D_2O was chosen as this minimizes deuterium washout of the backbone amide protons. TOCSY and NOESY allowed complete assignment of all proton chemical shifts in the peptide.

The 3D structure of the peptide was then calculated using CYANA.[201] As no lipid tail NOEs were found during the NMR assignments (likely because it is embedded in the membrane) the lipid tail was not included in the structure calculation. Along with chemical shift assignments, CYANA was provided with a list of NOE crosspeaks as distance restraints. With this input, CYANA was used to calculate 20 structures representative of Oct-TriA_1. The 20 calculated structures show excellent overlap, with a root-mean-square deviation (RMSD) between residues 3 and 11 of 0.20 ± 0.11 Å for backbone atoms (Fig. 4.19).

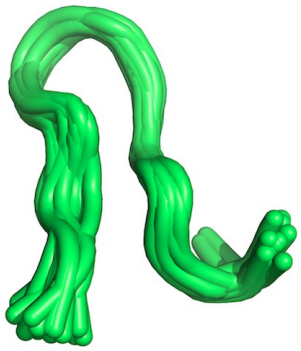

Figure 4.19. Overlay of 20 structures calculated by CYANA of Oct-TriA_1 in DPC micelles.

In the presence of DPC micelles, Oct-TriA_1 adopts an amphiphilic globular structure in which all hydrophobic residues reside on one face. There is also a π-stacking interaction between D-Trp5 and Phe9 stabilizing the loop. The hydrophobic face of Oct-TriA_1 likely sits in the bacterial membrane, whilst the more polar residues are exposed to solvent. We propose that at higher concentrations, this structure likely causes membrane lysis, and is responsible for killing Gram-positive bacteria, which lack the DAP of Gram-negative lipid II.

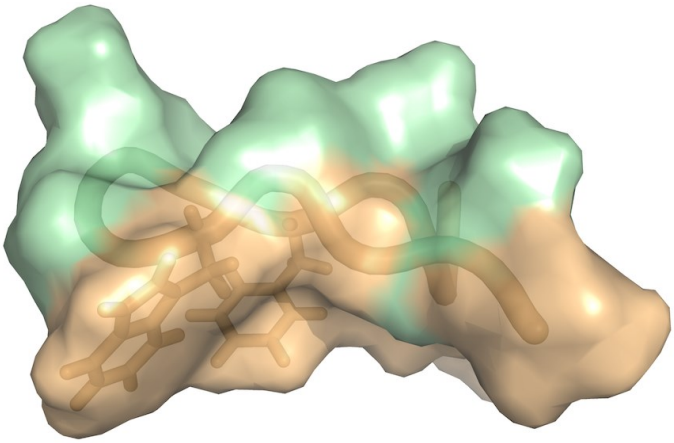

Figure 4.20. NMR solution structure of Oct-TriA_1 in DPC micelles. Hydrophobic residues are shown in orange, whereas all others are green.

4.3.9. NMR structure of Oct-TriA$_1$ in DPC micelles with lipid II

After calculation of the NMR solution structure of Oct-TriA$_1$ in DPC micelles, lipid II analogue **180** was fully characterized in the same solvent system. These two NMR solutions were mixed, giving a 1:1 mixture of Oct-TriA$_1$ and lipid II. Addition of lipid II analogue **180** to Oct-TriA$_1$ resulted in significant chemical shift changes in both Oct-TriA$_1$ and lipid II. In Oct-TriA$_1$, the most prominent changes were the amide chemical shifts of D-Dab8, Gly3, Phe 9 and Glu10 (Fig. 4.21).

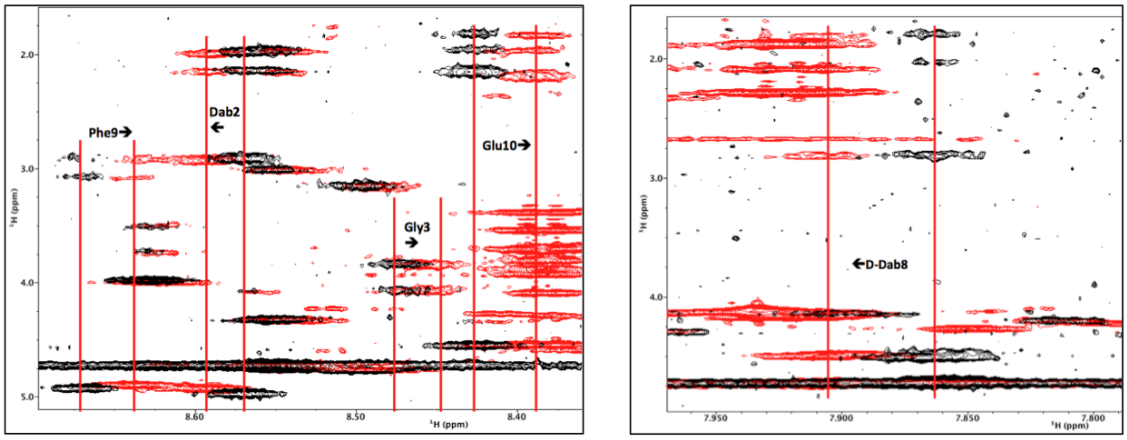

Figure 4.21. Overlay of the amide cross peak regions from the TOCSY spectra of Oct-TriA$_1$ in DPC micelles (black) and Oct-TriA$_1$ in DPC micelles with lipid II (red).

In lipid II analogue **180**, the largest chemical shift deviations occurred in the amide protons of D-γ-Glu2, Ala4 and Ala5 on the pentapeptide section (Fig. 4.22). This is indicative of a conformational change in both molecules and confirms they interact. Interestingly, the largest chemical shift change occurs on D-Dab8, which is the only essential residue for TriA$_1$ antimicrobial activity.

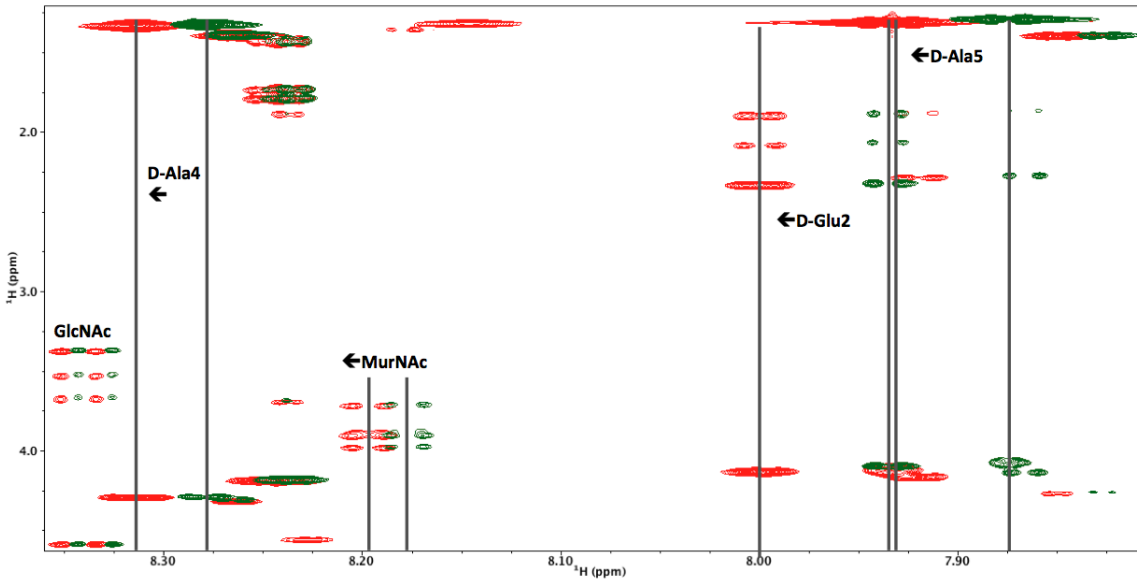

Figure 4.22. Overlay of the amide cross peak regions from the TOCSY spectra of Lipid II in DPC micelles (green) and lipid II in DPC micelles with Oct-TriA_1 (red).

The NMR solution structure of Oct-TriA_1 in DPC micelles containing Gram-negative lipid II was then calculated using CYANA. As with the previous NMR structure, the lipid tail was omitted from the structure calculation as no NOE cross peaks with other residues were found. 20 structures were calculated, which showed good overlap for the loop region, with an RMSD between residues 3 and 11 of 1.22 ± 0.51 Å for backbone atoms (Fig. 4.23). The variability shown at the N- and C-termini is due to an absence of NOE cross peaks found for these residues, which could mean they are embedded in the membrane.

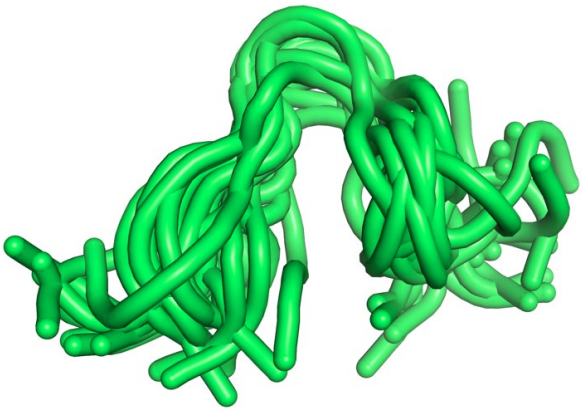

Figure 4.23. Overlay of 20 structures calculated by CYANA of Oct-TriA$_1$ in DPC micelles containing Gram-negative lipid II.

With lipid II present, Oct-TriA1 adopts a U-shaped structure that contains a hydrophobic face and is stabilized by a π-stacking interaction between D-Trp5 and Phe9, which is also present in Oct-TriA$_1$ when no lipid II is present. The most interesting feature of this structure is that D-Dab8, which is essential for the antimicrobial activity of the tridecaptins, is located right at the base of what appears to be a binding-pocket. The *N*-terminal D-Val residue, which contains the lipid tail, is on the hydrophobic face, supporting our prediction that the lipid tail is inserted into the membrane. The C-terminal alanine is also on this hydrophobic face and may explain the absence of NOE cross peaks found for the N- and C-termini.

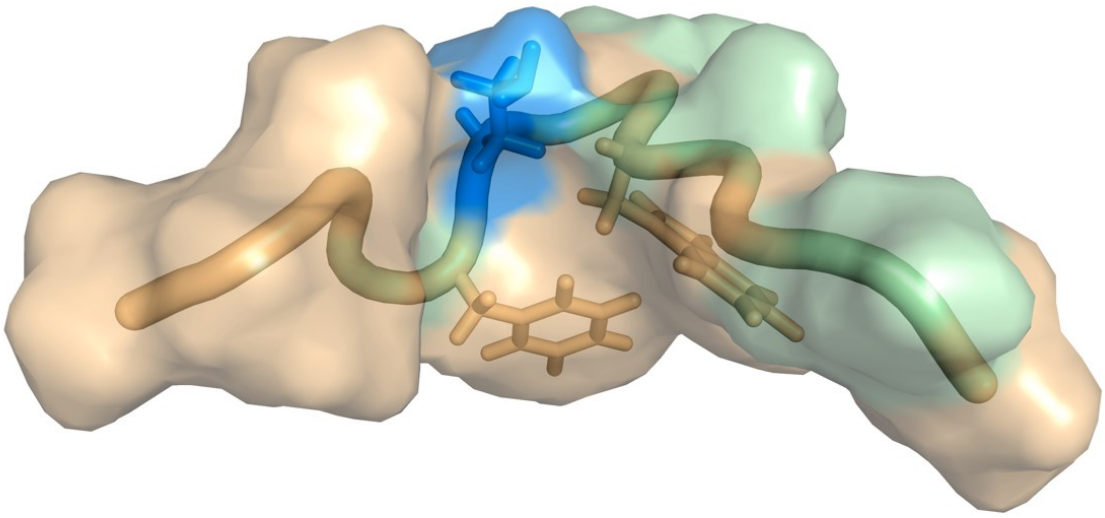

Figure 4.24. NMR solution structure of Oct-TriA$_1$ in DPC micelles containing Gram-negative lipid II. Hydrophobic residues are shown in orange, D-Dab8 is blue and all other residues are green.

4.3.10. Preliminary docking of lipid II into NMR structure of Oct-TriA$_1$

Lipid II was then docked into the NMR solution structure of Oct-TriA$_1$, calculated in the presence of lipid II, using AutoDock Vina.[202] Nine structures were calculated, with the top two having near identical conformations (Fig 4.25). The top hit is consistent with intra-molecular NOE cross peaks in lipid II, which are not present in the absence of Oct-TriA$_1$ (Fig. 4.25). This preliminary model shows that D-Trp5, Phe9 and D-Val1 (which contains the octanoyl tail) are in close proximity to the lipid II terpene chain (Fig. 4.26). The terpene tail of lipid II anchors it to the exterior of the inner-membrane, therefore this model is consistent with our hypothesis that these hydrophobic residues insert into the membrane during lipid II binding. There are four hydrogen bonds between Oct-TriA1 and lipid II in the proposed binding-pocket (Fig. 4.26).

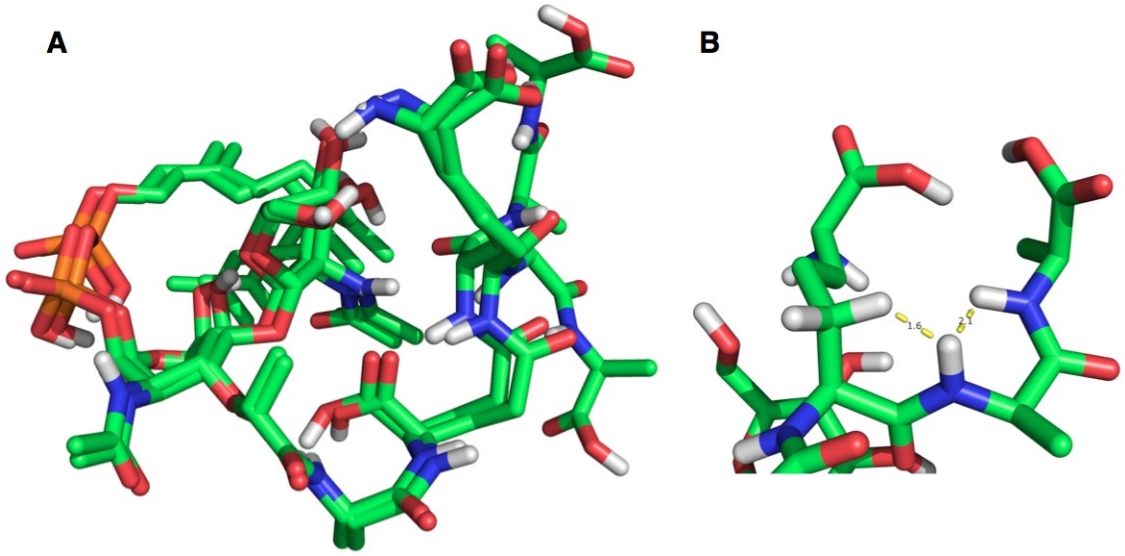

Figure 4.25. (A) Overlay of top docked lipid II structures and (B) intra-molecular NOEs consistent with docked structure (D-Ala4NH↔D-Ala5NH and DAP3Hβ).

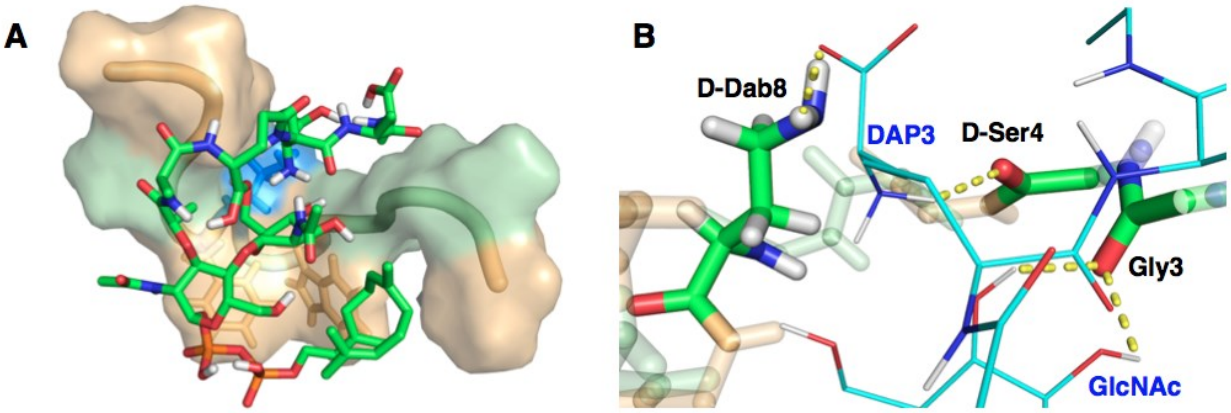

Figure 4.26. (A) Lipid II analogue **180** docked into Oct-TriA_1 and (B) inter-molecular hydrogen bonds within the complex.

The most notable of these inter-molecular hydrogen bonds is a 2.1 Å H-bond between the γ-amino group of D-Dab8 and the ε-carboxylate on DAP3 in lipid II, as this interaction perfectly describes all our experimental findings. When the D-Dab8 residue in

Oct-TriA_1 is replaced with alanine, the antimicrobial activity is drastically reduced (> 32-fold). When residue three of the pentapeptide on lipid II is DAP, as is common for Gram-negative bacteria, strong binding between Oct-TriA_1 and lipid II occurs. However, when this residue is Lys, as is common for most Gram-positive bacteria, very limited binding is observed. Therefore, the predicted interaction between D-Dab8 on TriA_1 and DAP3 on lipid II could be the key binding interaction that gives rise to the antimicrobial activity of the tridecaptins against Gram-negative bacteria. There are also H-bonds between the carbonyl of Gly3 and the 3- and 4-hydroxyls on GlcNAc. Like D-Dab8, Gly3 underwent a substantial amide chemical shift change upon addition of lipid II. Notably, the model does not show interactions between Oct-TriA_1 and the pyrophosphate moiety of lipid II, which is the common interaction between antimicrobial peptides and lipid II. ^{31}P-NMR was used to show that no change in the chemical shifts of the pyrophosphate occurred upon addition of Oct-TriA_1, confirming that the pyrophosphate is not involved in binding. To the best of our knowledge, this is the first reported instance of a lipid II-binding peptide that does not make use of a pyrophosphate cage. Further studies are currently being performed to develop a model of this complex using experimentally derived intramolecular NOEs.

4.4. Resistance development against tridecaptin A_1

The results from the mode-of-action and mechanism-of-action studies suggest that tridecaptin A_1 exerts its bactericidal effect by binding to lipid II on the inner-membrane and disrupting the proton-motive force. Lipid II is a late-stage intermediate in peptidoglycan-biosynthesis, and the proposed binding site for TriA_1 would be difficult for

bacteria to modify without affecting its subsequent processing by enzymes in the peptidoglycan-biosynthesis pathway. Furthermore, reorganization of bacterial-membrane compositions is not readily achieved through random evolution. One would therefore expect that resistance development against $TriA_1$ would be limited. To test this hypothesis, Dr. Brandon Findlay performed an *in vitro* evolution study, in which *E. coli* cells were continuously exposed to sub-MIC concentrations of Oct-$TriA_1$ or ciprofloxacin for one month. This experiment allows strains resistant to an antibiotic to become dominant over time, leading to a decrease in activity. During this one month experiment, the MIC of each antibiotic was determined daily (Fig. 4.27). Whereas an eight-fold loss of activity was observed for ciprofloxacin, no resistance development was observed against Oct-$TriA_1$, assuming the standard ± 2-fold error typical to MIC testing. Not only does this result fit well with our proposed mechanism of action, it also suggests that the tridecaptins are Gram-negative targeting antibiotics with limited potential for resistance development, an important find given the current problems of antibiotic resistance.

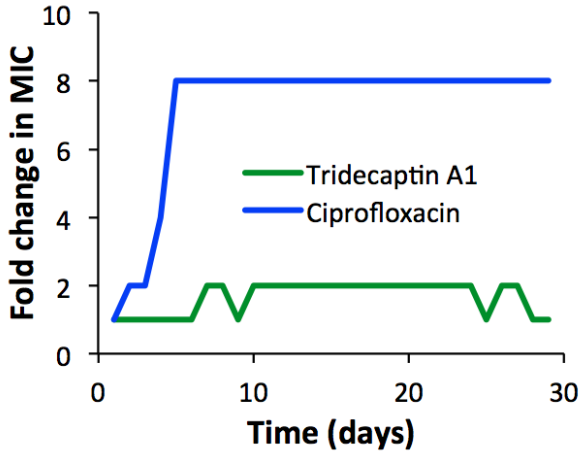

Figure 4.27. Resistance study with *E. coli* cells.

4.5. Conclusions

Tridecaptin A_1 is a novel antimicrobial lipopeptide that selectively targets Gram-negative bacteria and operates by a unique mode of action (Fig. 4.28).

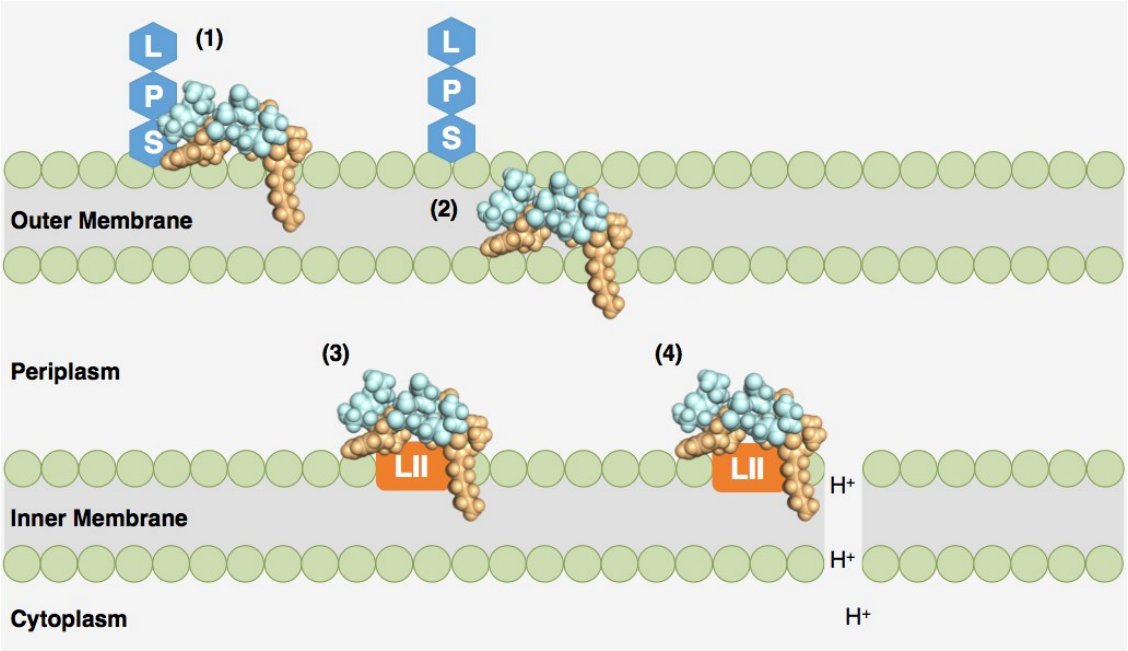

Figure 4.28. Summary of the mode of action of tridecaptin A_1. (1) $TriA_1$ binds to LPS; (2) $TriA_1$ permeates the outer-membrane; (3) $TriA_1$ binds to lipid II on the surface of the inner-membrane; (4) $TriA_1$ disrupts the proton-motive force.

It first binds to lipopolysaccharide on the surface of the outer-membrane, before permeating the outer-membrane and entering the periplasm. It then makes its way to the exterior of the inner-membrane and binds to lipid II. We have shown that tridecaptin A_1 binds selectively to Gram-negative lipid II, with the key interaction a hydrogen bond between the γ-amino group of D-2,4-adiaminobutyric acid 8 in tridecaptin A_1 and the ε-carboxylate of *meso*-diaminopimelic acid in lipid II. It is this selective binding to Gram-

negative lipid II that imparts the selectivity of tridecaptin A_1 against Gram-negative bacteria. Upon binding to lipid II, tridecaptin A_1 forms small pores that disrupt the proton-motive force. As this proton gradient is essential for the production of ATP, which powers many vital cellular processes, it leads to rapid cell death.

Chapter 5

Experimental procedures

5.1. General synthetic details

5.1.1. Reagents, solvents and purification

All commercially available reagents were purchased from Sigma-Aldrich Canada Ltd., Fisher Scientific Ltd., Alfa Aesar Ltd., Chem-Impex International Inc., Caledon, VWR International or TCI America and used without further purification unless otherwise stated. All solvents were of American Chemical Society (ACS) grade and were used without further purification unless otherwise stated. All anhydrous reactions were conducted under a positive pressure of argon using flame-dried glassware. Solvents for anhydrous reactions were distilled prior to use: CH_2Cl_2 and $CHCl_3$ were distilled over calcium hydride, tetrahydrofuran (THF) and diethyl ether were distilled over sodium with benzophenone as an indicator, and MeOH was distilled over magnesium. HPLC grade acetonitrile, *N,N*-dimethylformamide (DMF), 2-propanol (IPA), hexanes and MeOH were used without further purification. Commercially available ACS grade solvents (>99.0% purity) were used for column chromatography without further purification. Deionized water was obtained from a Milli-Q reagent water system (Millipore Co., Milford, MA). All reactions and fractions from column chromatography were monitored by thin layer chromatography (TLC) using glass plates with a UV fluorescent indicator (normal SiO_2, Merck 60 F254). One or more of the following methods were employed for visualization: UV absorption by fluorescence quenching, staining with phosphomolybdic acid in ethanol (10 g/100 mL), ninhydrin (ninhydrin:acetic acid:*n*-butanol/ 0.6 g:6 mL:200 mL) or

permanganate ($KMnO_4$:K_2CO_3:NaOH:H_2O/ 1.5 g:10 g:0.12 g:200 mL). Flash chromatography was performed using Merck type 60, 230-400 mesh silica gel. Preparative thin layer chromatography (TLC) purification was performed using plates purchased from Analtech (1000 or 500 microns). The removal of solvents *in vacuo* was performed via evaporation under reduced pressure using a Büchi rotary evaporator. Analytical scale high performance liquid chromatography (HPLC) was performed on one or more following systems: Varian ProStar chromatograph equipped with model 210 pump heads, a model 325 dual wavelength UV detector, and a Rheodyne 7725*i* injector fitted with a 500 µL sample loop; or a Gilson chromatograph equipped with model 322 pump heads, a model 171 diode array detector, a FC 203B fraction collector, and a Rheodyne 7725*i* injector fitted with a 1000 µL sample loop. Preparative and semi-preparative scale HPLC was performed on a Gilson chromatograph equipped with model 322 pump heads, a model UV/VIS-156 detector, and a GX-271 liquid handler. The columns used were Vydac C_{18} (5 µm, 4.6 x 250 mm), Vydac C_8 (5 µm, 10 x 250 mm), Phenomenex C_{18} (5 µm, 21.2 x 250 mm) and Develosil ODS-3 column (3 µm, 4.6 mm x 150 mm). All HPLC solvents were filtered and degassed before use.

5.1.2. Product Characterization

Optical rotations were measured on a Perkin Elmer 241 polarimeter with a microcell (10 cm, 1 mL) at ambient temperature and are reported in units of 10^{-1} deg cm^2 g^{-1}. All reported optical rotations were referenced against air and measured at the sodium D line (λ = 589.3 nm). Infrared spectra (IR) were recorded on either a Nicolet Magna 750 FT-IR spectrometer or a Nic-Plan FT-IR microscope. The term cast refers to the

evaporation of a solution on a NaCl plate. Nuclear magnetic resonance (NMR) spectra were recorded on a Varian Inova 600, Inova 500, Inova 400, Inova 300 or Unity 500 spectrometer at 27 °C. For ^{1}H (300, 400, 500 or 600 MHz) spectra, δ values were referenced to $CDCl_3$ (7.26 ppm), CD_2Cl_2 (5.32 ppm), CD_3OD (3.30 ppm), DMSO-d_6 (2.50 ppm), or D_2O (4.79 ppm) and for ^{13}C (75, 100, 125 or 150 MHz) spectra, δ values were referenced to $CDCl_3$ (77.0 ppm), CD_2Cl_2 (53.8 ppm), CD_3OD (49.0 ppm), or DMSO-d_6 (39.5 ppm). Reported splitting patterns are abbreviated as s = singlet, d = doublet, t = triplet, q = quartet, m = multiplet. Mass spectra (MS) were recorded on an Agilent Technologies 6220 oaTOF, a Kratos AEIMS-50, an Applied BioSystems Mariner BioSpectrometry Workstation, or a Perspective Biosystems VoyagerTM Elite MALDI-TOF MS using either α-cyano-4-hydroxycinnamic acid (CHCA) or 3,5-dimethoxy-4-hydroxycinnamic acid (sinapinic acid) as a matrix. LC MS/MS was performed on a Waters (Micromass) Q-TOF Premier. For MALDI-TOF MS, a typical sample preparation is described as follows. A solution of sample peptide (1 μL) in 0.1% TFA (aq.) is mixed in a 1:1 ratio (vol/vol) with a stock solution of sinapinic acid (10 mg/mL) in 50% acetonitrile containing 0.1% TFA (aq.). To prepare the sample plate, a sinapinic acid layer (0.7 μL; 10 mg/mL sinapinic acid in 3:2 acetone:MeOH) is pipetted onto a stainless steel target plate. The solvent is allowed to evaporate, leaving a thin layer of sinapinic acid on the surface of the plate. The sample matrix solution (0.6 μL) is then spotted onto the dried layer of sinapinic acid and allowed to dry.

5.1.3. General method for automated Fmoc solid phase peptide synthesis

Commercially available Fmoc protected amino acids and synthetic amino acids were

loaded onto the CEM Liberty 1 peptide synthesizer as 0.2 M DMF solutions. All amino acid subunits were coupled using 2-(1*H*-benzotriazole-1-yl)-1,1,3,3-tetramethyl-uroniumhexafluoro-phosphate (HBTU) and hydroxybenzotriazole (HOBt) as the activating agents and heated to 70 °C (50 °C for cysteines) for a 5 min coupling time. Removal of the Fmoc group was completed using piperidine in NMP and monitored by disappearance of the absorbance at 301 nm. Peptides were cleaved using a standard condition of TFA:TIPS:H_2O (95:2.5:2.5). Peptides were filtered through a plug of cotton or glass wool and the solvent was removed *in vacuo*. The crude peptide was then precipitated with cold ether until only a white solid remained and purified by HPLC. The product containing fractions were lyophilized to yield pure product.

5.1.4. General method for manual Fmoc solid phase peptide synthesis

Solid-phase peptide synthesis was performed on a 25 or 50 μmol scale using Fmoc chemistry on preloaded resin (ChemImpex). Reactions were performed in a custom-built 20 mL glass fritted column fitted with a T-joint and three-way T-bore teflon stopcock. The resin was pre-swollen in DMF (5 mL, 10 min) by bubbling with argon. Between deprotections and couplings the vessel was drained under argon pressure and washed with DMF (3 x 5 mL). The Fmoc group was removed by bubbling with 20% piperidine in DMF (3 x 5 mL x 5 min). The deprotection steps were monitored by UV absorbance. The next Fmoc-amino acid (5 equiv) was pre-activated by shaking with HATU (5 equiv) and DIPEA (10 equiv) in DMF (5 mL) for 5 min. The resin was bubbled with argon in the coupling solution for 1 h, drained and washed with DMF (3 x 5 mL). Appropriate deprotection and coupling steps were continued to complete the peptide

synthesis. The resin-bound peptide was washed with CH_2Cl_2 (3 x 5 mL) and dried under argon for 20 min. The resin was transferred to a screw top vial containing trifluoroacetic acid TFA:TIPS:H_2O (95:2.5:2.5, 5 mL) and gently shaken for 2 h. The cleavage solution was filtered and concentrated *in vacuo* and the crude peptide was precipitated with cold Et_2O. The crude peptide was dissolved in H_2O:MeCN (1:1, 5 mL) and purified by HPLC. The product containing fractions were lyophilized to yield pure products.

5.1.5. HPLC purification methods

Method 1: Gilson preparative system, Phenomenex C_{18} column, flow rate 10 mL/min, detected at 220 nm. Gradient: starting from 20% MeCN (0.1% TFA) and 80% water (0.1% TFA) for 5 min, ramping up to 55% MeCN over 30 min, then ramping up to 95% MeCN over 3 min, staying at 95% MeCN for 3 min, ramping down to 20% MeCN over 2 min, then staying at 20% MeCN for 5 min.

Method 2: Gilson analytical system, Vydac C_{18} column, flow rate 10 mL/min, detected at 220 nm. Gradient: starting from 20% MeCN (0.1% TFA) and 80% water (0.1% TFA) for 5 min, ramping up to 55% MeCN over 30 min, then ramping up to 95% MeCN over 3 min, staying at 95% MeCN for 3 min, ramping down to 20% MeCN over 2 min, then staying at 20% MeCN for 5 min.

Method 3: Gilson analytical system, Develosil ODS-3 column, column cooled to -55 ^{o}C by immersion in a dry-ice/acetone bath regulated with a Thermo Neslab CC-100 Immersion Chiller, flow rate 0.8 mL/min, detected at 370 nm. Isocratic flow maintained for 60 min.

Method 4: Gilson preparative system, Phenomenex C_{18} column, flow rate 10 mL/min, detected at 220 nm. Gradient: starting from 20% MeCN (0.1% TFA) and 80% water (0.1% TFA) for 5 min, ramping up to 25% MeCN over 10 min, then ramping up to 95% MeCN over 1 min, staying at 95% MeCN for 2 min, ramping down to 20% MeCN over 1 min, then staying at 20% MeCN for 3 min.

Method 5: Gilson preparative system, Phenomenex C_{18} column, flow rate 10 mL/min, detected at 220 nm. Gradient: starting from 10% MeCN (0.1% TFA) and 90% water (0.1% TFA), ramping up to 40% MeCN over 20 min, then ramping up to 95% MeCN over 1 min, staying at 95% MeCN for 2 min, ramping down to 20% MeCN over 1 min, then staying at 20% MeCN for 2 min.

Method 6: Gilson preparative system, Phenomenex C_{18} column, flow rate 5 mL/min, detected at 220 nm. Gradient: starting from 10% MeCN (0.04% AcOH) and 90% water (0.04% AcOH), ramping up to 40% MeCN over 10 min, then ramping up to 95% MeCN over 1 min, staying at 95% MeCN for 2 min, ramping down to 20% MeCN over 1 min, then staying at 20% MeCN for 2 min.

Method 7: Gilson preparative system, Phenomenex C_{18} column, flow rate 10 mL/min, detected at 220 nm. Gradient: starting from 40% MeCN (0.1% TFA) and 60% water (0.1% TFA), ramping up to 75% MeCN over 20 min, then 75% MeCN for 10 min, ramping down to 40% MeCN over 1 min, then staying at 40% MeCN for 1 min.

Method 8: Gilson preparative system, Phenomenex C_{18} column, flow rate 10 mL/min,

detected at 220 nm. Gradient: starting from 20% MeCN (0.1% TFA) and 80% water (0.1% TFA), ramping up to 50% MeCN over 30 min, then ramping up to 95% MeCN over 1 min, staying at 95% MeCN for 2 min, ramping down to 20% MeCN over 1 min, then staying at 20% MeCN for 1 min.

Method 9: Gilson preparative system, Phenomenex C_{18} column, flow rate 10 mL/min, detected at 220 nm. Gradient: starting from 10% MeCN (0.1% TFA) and 90% water (0.1% TFA), ramping up to 40% MeCN over 30 min, then ramping up to 95% MeCN over 1 min, staying at 95% MeCN for 2 min, ramping down to 20% MeCN over 1 min, then staying at 20% MeCN for 1 min.

Method 10: Gilson preparative system, Phenomenex C_{18} column, flow rate 10 mL/min, detected at 220 nm. Gradient: starting from 20% MeCN (0.1% TFA) and 90% water (0.1% TFA), ramping up to 95% MeCN over 30 min, staying at 95% MeCN for 5 min, ramping down to 20% MeCN over 1 min, then staying at 20% MeCN for 2 min.

Method 11: Gilson preparative system, Phenomenex C_{18} column, flow rate 10 mL/min, detected at 220 nm. Gradient: starting from 35% MeCN (0.1% TFA) and 65% water (0.1% TFA), ramping up to 95% MeCN over 30 min, staying at 95% MeCN for 5 min, ramping down to 20% MeCN over 1 min, then staying at 20% MeCN for 2 min.

5.2. General microbiology procedures

5.2.1. Bacterial growth conditions

All strains were grown from glycerol stocks stored at -80 ^{o}C. A small quantity of the appropriate glycerol stock was transferred to MHB (10 mL) and incubated at 37 ^{o}C overnight, with shaking at 225 rpm. The resulting suspension was then streaked on to a MHB hard agar plate and incubated overnight. Individual colonies were used for all experiments with bacteria.

5.2.2. Deferred-inhibition assays

An individual bacterial colony of the desired producer strain was used to inoculate MHB (~10 mL) and grown overnight at 37 ^{o}C, 225 rpm. A sterile tip was used placed into the culture and then used to pierce an MHB hard agar plate. The plate was grown overnight at 37 ^{o}C, 225 rpm. Cultures of the indicator strains were also grown overnight in MHB. The indicator strain suspension (100 µL) was added to molten MH soft agar (10 mL) at approx. 40 ^{o}C and poured on to the agar plate containing the overnight colony of the producer strain. These plates were then incubated at 37 ^{o}C overnight. Zones of inhibition indicated production of compounds active against the indicator strain.

5.2.3. Spot-on-lawn assays

An individual bacterial colony of the desired strain was used to inoculate MHB (~10 mL) and grown overnight at 37 ^{o}C, 225 rpm. The bacterial suspension (100 µL) was then added to molten MHB soft agar (10 mL) at approx. 40 ^{o}C and poured on to a MHB hard agar plate. The back of the plate was marked with equally spaced crosses to guide the

application of antibiotic solutions (no more than 12 per plate). Antibiotic solutions (10 µL) were added and allowed to evaporate. Plates were then incubated overnight and active compounds appeared as a zone of inhibition.

5.2.4. Microbroth dilution assays

All minimum inhibitory concentrations were determined using microbroth-dilution assays, according to Clinical and Standards Laboratory Institute (CLSI) guidelines. [203] Briefly, peptides were dissolved in MHB and serial dilutions made across a 96 well plate. Each well was inoculated with a suspension of the required bacterial strain to reach a final inoculum of 5×10^5 colony forming units per mL. The MIC was taken as the lowest concentration with no visible growth after 18 h.

5.2.5. Synergy assays

A modified broth-dilution assay in a 96-well plate was used to test for synergy between H-TriA_1 and a panel of 10 antibiotics, where row (A) is a sterility control; (B) antibiotic alone; (C) antibiotic in 12.5 µg/mL H-TriA_1; (D) antibiotic in 6.25 µg/mL H-TriA_1; (E) antibiotic in 3.13 µg/mL H-TriA_1; (F) antibiotic in 1.56 µg/mL H-TriA_1; (G) 12.5 µg/mL H-TriA_1 growth control and (H) growth control. MH broth (50 µL) was added to all wells in a 96-well plate. A solution of the desired antibiotic (4 x desired starting concentration) in MH broth (50 µL) was added to B1, C1, D1, E1 and F1 and serial dilutions were made across these rows. MH broth (50 µL) was added to rows A, B and H. A 25 µg/mL, 12.5 µg/mL, 6.25 µg/mL and 3.13 µg/mL solution (50 µL) of H-TriA_1 in MH broth was added to rows C, D, E and F respectively. A 25 µg/mL solution of H-TriA_1 in MH broth (50 µL)

was added to row G. Rows B-H were inoculated with 5 µL of bacterial suspension (see CLSI guidelines) so that the final concentration in each well was $5x10^5$ colony forming units per mL (CFU/mL). The MIC was measured as the lowest concentration of antibiotic required to prevent visible growth.

5.2.6. Hemolytic assays

The hemolytic activity of tridecaptin analogues was tested following a previously described method.[204] Defibrinated rabbit blood (1 mL; Hemostat Laboratories; Dixon, CA, USA), within 7 days of receipt, was diluted with PBS (19 mL) and mixed gently. This mixture was centrifuged (1000 *g*, 5 min, 4 °C) and the supernatant carefully removed. This was repeated three more times to remove free hemoglobin. The resulting pellet was gently resuspended in 19 mL of PBS. Aliquots of the blood solution (100 µL) were added to the wells of a 96-well plate. To these wells, 50 µL of a 250 µg/mL solution of tridecaptin analogue (in PBS) was added, and mixed gently by pipetting. Triton X-100 (50 µL of a 0.1% solution) was used as a positive control, while PBS (50 µL) was used as a blank. Each sample and control was tested in triplicate. The 96-well plate was then incubated at 37 °C for 30 min. The samples were gently mixed by pipetting, and 20 µL of each was added to 200 µL PBS, and once again gently mixed. The diluted samples were then centrifuged (13,000 rpm, 5 min) using a tabletop centrifuge. Supernatant (120 µL) from each sample was added to a new 96-well plate, and the absorbance was measured at 415 nm. Percent hemolysis of the peptides was calculated relative to Triton X-100, while the PBS negative control was used as a blank.

5.2.7. Cytotoxicity assays

A frozen dimethylsulfoxide (DMSO) stock of HEK 293 cells was thawed and diluted with media (Hyclone DMEM/High Glucose + 10 % fetal bovine serum; 10 mL). The cells were centrifuged and re-suspended in media (10 mL) in a 75 mL culture flask and grown at 37 °C for 48 h in a 5 % CO_2 incubator. The media was removed, cells were washed with phosphate buffered saline (PBS) solution (10 mL) and fresh media added (10 mL). After 48 h, the media was removed and cells were washed with PBS, followed by trypsinization by incubating with 0.0625 % trypsin in media (3 mL) for 5 min. The trypsinized suspension was added to media (8 mL) and centrifuged. The cell pellet was re-suspended in media (1 mL) and 100 μL was used to start a new culture or for a 3-[4,5-dimethylthiazol-2-yl]-2,5 diphenyl tetrazolium bromide (MTT) assay. Re-suspended cell pellet (100 μL) was diluted with media (10 mL). Cells were counted using a hemocytometer and the concentration was adjusted to $2.5x10^5$ cells/mL. The MTT assay was performed in a 96-well plate, with row (A) is a sterility control, (B), (C) and (D) peptide and (E) growth control. The suspension of HEK 293 cells (100 μL) was added to rows B-E and media (100 μL) was added to row A. The cells were incubated at 37 °C for 24 h. The media was replaced in all wells. A 16 mg/mL peptide solution (100 μL) was added to B1, C1 and D1 and serial dilutions were performed across each row. The plate was incubated for 48 h at 37 °C. A 2.5 mg/mL solution of thiazolyl blue tetrazolium bromide in PBS (20 μL) was added to all wells and the plate incubated for 3 h. The media was carefully removed from all wells and replaced with DMSO (100 μL). After 30 min, the absorbance at 570 nm was measured in each well. A graph of the absorbance vs. concentration was plotted and the MIC was determined as the lowest

concentration before absorbance increased from background values.

5.2.8. Protease-stability assays

These experiments were performed according to a previously reported procedure. [205] Freshly prepared sequencing grade trypsin or chymotrypsin (Hoffmann-La Roche Ltd., Mississauga, ON, Canada) in 1 mM HCl was used for digestion experiments. A protease solution (10 μM, 10 μL) was mixed with Oct-TriA_1 (100 μM, 100 μL) in 100 mM Tris-HCl buffer pH 7.8 for trypsin, 50 mM Tris-HCl buffer pH 7.8 plus 20 mM $CaCl_2$ for chymotrypsin or 100 mM HCl for pepsin. Reactions were incubated at 37 ^{o}C and a spot-on-lawn assay performed with 10 μL of the reaction volume after 1 h, 2 h and 18 h. The remaining solution was analyzed by HPLC method 2.

5.2.9. *In vivo* mouse assays

These experiments were performed in the lab of Dr. Wu. *K. pneumoniae* (*Kp*; American Type Culture Collection [ATCC] 43816 serotype II) was obtained from Dr. Miller (University of North Carolina, NC, USA) and was used for infection of mice. All animal procedures were approved by the Institutional Animal Care and Use Committee at the University of North Dakota. C57BL/6J mice were purchased from Harlan Laboratory (Indianapolis, IN, USA). Mice were housed in a temperature- and humidity-controlled environment, and had free access to food and water. Mice were randomly divided into a control group (n=4) and treated groups (n=4, per compound tested). The treated groups received peptide solutions in DMSO (2-4 mg/kg body weight, 50 μL) through tail vein injection one hour after being anesthesized with 40 mg/kg ketamine, and instilled with

1×10^5 colony-forming units (CFUs) of *Kp* by intranasal instillation. Survival was determined using a Kaplan–Meier curve. After bronchoalveolar lavage (BAL), the lung was excised for homogenization or fixed in 10% formalin.

5.2.10. Plasma-stability assays

An aliquot from a 1 mM solution of H-TriA_1 (10 µL) was added to human plasma (90 µL) and incubated at 37 ^oC for 0 min (control) or 30 min. After the desired time period, the sample was diluted with buffer (300 µL, 1:99 MeCN:H_2O + 0.1% TFA) and immediately loaded unto a C_{18} pipette column containing C_{18} silica (100 mg, Phenomonex Strata C_{18}-E, 55 µm, 70 A) that has been prewashed with EtOH (2 x 1mL) and H_2O (2 x 1 mL). The column was washed with buffer (3 x 100 µL) and H_2O (2 x 1 mL). The sample was delipidated with 4:6 *n*-butanol:diisopropyl ether (1 mL) and the peptide eluted with 9:1 MeOH:H_2O (1 mL). The elution fraction was concentrated *in vacuo* and redissolved in 1:9 MeCN:H_2O + 0.1% TFA (100 µL). The sample was further purified by Millipore C_{18} ziptip and analyzed by MALDI and LC MS/MS. The LC MS/MS data was processed using Mascot software to identify relevant peptide fragments. The percentage of peptide hydrolysis was estimated using the relative intensities of H-TriA_1 to fragmentation products by MALDI.

5.3. Structural characterization and isolation of peptides

5.3.1. HPLC co-injections of peptides

An aqueous solution of the synthetic peptide (100 µM, 100 µL) and natural peptide (100 µM, 100 µL) were mixed and analyzed by HPLC method 2.

5.3.2. HPLC analysis of $TriB_1$ lipid tail anthracenyl derivatives

Anthracenyl derivatives (50 µg) were dissolved in MeOH/MeCN/hexanes (300:200:5) (100 µL) and analyzed by HPLC method 3.

5.3.3. Isolation and purification of cerexin analogues

4L of MH broth was inoculated with a 10 mL overnight culture of *B. mycoides* ATCC 21929 in MH broth and shaken at 27 ^{o}C for 40 h. The cells were removed by centrifugation (10 000 rpm, 4 ^{o}C, 10 min) and the supernatants stored at 4 ^{o}C. Amberlite 16N resin (20 – 60 mesh, Sigma, 40G) was suspended in IPA and transferred to a column. The IPA was drained at 10 mL/min and the resin washed with dd H_2O (500 mL, 10 mL/min). The supernatant was then loaded on to the resin at 10 mL/min. The flow through was collected in a flask and the resin was washed sequentially with 250 mL of dd H_2O, 20% IPA, 40% IPA and 80% IPA + 0.1% TFA. 200 µL of each wash fraction was concentrated to approx. 20 µL and tested for activity against the *S. aureus* ATCC 6538. The activity containing fractions were then concentrated to ~30 mL. A C_{18}-SPE cartridge (Phenomenex) was washed with MeOH (50 mL) and dd H_2O (100 mL) at 10 mL/min. The concentrated activity containing fraction from the previous step was loaded on to the column at 3 mL/min and the flow through collected. The column was then washed sequentially with 50 mL of 30% EtOH, 40% IPA and 80% IPA + 0.1% TFA. Activity was tested and the activity containing fractions concentrated and purified by HPLC method 1.

5.3.4. Succinylation of cerexin A_1

Cerexin A_1 (0.35 mg, 25 μmol) was dissolved in phosphate buffer (10 mM, pH 6.5, 300 μL). A solution of succinic anhydride (1.25 mg, 1.25 mmol) in MeCN (200 μL) was then added and the mixture stirred at ambient temperature for 1 h. The mixture was then analyzed by HPLC method 1.

5.4. Mode-of-action procedures

5.4.1. Growth kinetic measurements

Experiment performed by Dr. Findlay. A single colony of *E. coli* DH5α was used to inoculate MHB (5 mL). This was grown with shaking at 225 rpm and 37 ^{o}C for 3.5 h. The resulting bacterial culture was diluted to 1x10^{6} CFU/mL in fresh MHB and mixed 1:1 with the antibiotics of interest in a 96 well plate. Final antibiotic concentrations varied from 64 to 0.125 μg/mL. The plate was then incubated at 37 ^{o}C overnight, with OD_{600} measurements taken every 0.5 s and agitation every 2 s. After incubation, the MIC of each antibiotic was determined by visual examination, and readings at 2x the MIC were used. The assay was repeated with a separate biological replicate.

5.4.2.Time-kill assays

Morphologically similar colonies of *E. coli* strain ATCC 25922 were suspended in MHB to a concentration of 1x10^{8} CFU/mL (compared to freshly prepared McFarland 0.5 standard) and diluted 1:100 with MHB. The resulting suspension was mixed 1:1 with either 50 μM tridecaptin A1 or 50 μM polymyxin B (approximately 10xMIC) and incubated at ambient temperature. After 5, 15, 30 and 60 min of incubation, 25 uL of

each culture was streaked onto a fresh agar plate and allowed to air dry. An untreated sample of cells at $1x10^8$ CFU/mL was used as a negative control. Plates were incubated overnight at 37 ^oC and the number of individual colonies counted at each time-point.

5.4.3. Outer-membrane-disruption assay

The ability of peptides to permeate the outer-membrane of *E. coli* ATCC 25922 cells was determined using the 8-anilinonaphthalene-1-sulfonic acid (ANS) uptake assay. A fully-grown overnight culture in MH broth was used to inoculate fresh broth to an OD_{600} of 0.05. Cells were grown to mid-log phase (OD_{600} ~ 0.3-0.8) and pelleted by centrifugation. Cells were washed with buffer (10 mM Tris, pH 7.4, 150 mM NaCl) and pelleted by centrifugation. Buffer was added to obtain at least 20 mL of a suspension of cells with an OD_{600} of 0.065. A constant concentration of 5 μM ANS in bacterial buffer suspension (2 mL) was used for all experiments and the concentration of $TriA_1$ and H-$TriA_1$ was varied. The peptide was added, and the fluorescence emission was measured after 10 min between 450 – 600 nm with excitation at 380 nm. The increase in fluorescence from blank readings was used to assess the penetration of the outer-membrane.

5.4.4. Membrane-depolarization assay with $DiBAC_4(3)$

Experiment performed by Dr. Findlay. Measurements were performed on a 75 XE PTI Fluorescence spectrophotometer. All slits were open 1 mm, and measurements were collected every second. Results were visualized in Felix32 analysis software, and analyzed in Microsoft Excel. For $DiBAC_4$ experiments, the excitation and emission

wavelengths on the fluorescence spectrometer were set to 492 nm and 515 nm respectively. Morphologically similar *E. coli* ATCC 25922 colonies were suspended in half-strength MHB to an OD_{600} of 0.45. The resulting suspension (75 µL) was mixed with $DiBAC_4$ (3 mg/L, 37.5 µL) and incubated at ambient temperature for 5 min. The mixture was then transferred to a 0.2 mL cuvette and tridecaptin A_1 was added to a final concentration of 6.25 µM. Readings were collected for five min, at which point the system was quenched by addition of polymyxin B (to a final concentration of 12.5 µM). Readings were repeated twice, and representative experiments are shown.

5.4.5. Inner-membrane-disruption assay with SYTOX Green

Experiment performed by Dr. Findlay. Measurements were performed on a 75 XE PTI Fluorescence spectrophotometer. All slits were open 1 mm, and measurements were collected every second. Results were visualized in Felix32 analysis software, and analyzed in Microsoft Excel. For SYTOX Green experiments, the excitation and emission wavelengths on the fluorescence spectrometer were set to 488 nm and 523 nm respectively. Morphologically similar *E. coli* ATCC 25922 colonies were suspended in MHB (75 µL) to an OD_{600} of 0.35. The resulting suspension was mixed with SYTOX Green (2.5 µM, 37.5 µL) and incubated at ambient temperature for 5 min. Tridecaptin A_1 was then added to a final concentration of 12.5 µM, with polymyxin B (12.5 µM final concentration) and Triton X-100 (0.25% final concentration) used as positive and negative control, respectively. Measurements were collected for 10 min. Representative examples from three technical replicates are shown.

5.4.6. Inner-membrane-disruption assay with ONPG

The ability of peptides to penetrate the inner-membrane of *E. coli* ML-35 cells was determined using an *o*-nitrophenyl-β-D-galactopyranoside (ONPG) assay. An overnight culture in MH broth was grown from a glycerol stock, and 100 μL was added to fresh broth (10 mL). Cells were grown for 3 h with shaking at 37 °C to mid-log phase (~2 x 10^{11} CFU/mL) and the suspension cooled to 0 °C. A 96-well plate was used for the ONPG assay, with row (A) is a blank; (B) positive control (mellitin) and (C) and (D) peptide. ONPG buffer (70 μL; 10 mM NaH_2PO_4, pH 7.4, 100 mM NaCl and 1.5 mM ONPG) and cell suspension (20 μL) were added to the first six wells in rows A – D. A 64 μg/mL solution of mellitin (10 μL) was added to row B. 10 μL of 40 x MIC, 20 x MIC, 10 x MIC, 5 x MIC, 2.5 x MIC and 1.25 x MIC peptide solutions was added to C1, C2, C3, C4, C5 and C6 respectively. The experiment was run in duplicate using D1-D6. A multichannel pipette was used to add the mellitin and peptide solutions as close in time as possible. After 15 min, the absorbance at 405 nm of each well was measured. The percentage of leakage was calculated for each peptide concentration taking the positive control as 100%.

5.4.7. *In vivo* assay of proton-motive force disruption

Experiment performed by Dr. Findlay. Measurements were performed on a 75 XE PTI Fluorescence spectrophotometer. All slits were open 1 mm, and measurements were collected every second. Results were visualized in Felix32 analysis software, and analyzed in Microsoft Excel. For BCECF experiments, the excitation and emission wavelengths on the fluorescence spectrometer were set to 500 nm and 522 nm

respectively. An *E. coli* ATCC 25922 glycerol stock was used to inoculate MHB (6 mL), which was grown overnight at 37 ^{o}C, 225 rpm. Cells were pelleted via centrifugation (16k g, 1 min) and washed with 50 mM potassium phosphate buffer (pH 6) and potassium phosphate buffer (50 mM, pH 6) containing EDTA (5 mM), before being re-suspended in the same phosphate-EDTA buffer (1 mL). BCECF-AM (1 mM, 20 µL) was added and cells incubated for 1 h at ambient temperature. This cell suspension was concentrated to 120 µL in the same phosphate-EDTA buffer and stored on ice for 4 h. An aliquot of the cell suspension (1 µL) was then added to fresh phosphate-EDTA buffer (200 µL) at ambient temperature. After the fluorescence stabilized, glucose was added (5 mM, 1 µL), and the signal allowed to stabilize. Valinomycin was then added (0.4 mM, 10 µL), followed 100 s later by the test compound. After the fluorescence signal stabilized, nigericin was added to quench (0.6 mM, 10 µL). Experiments shown are representative of results from three technical replicates.

5.4.8. Preparation of LUVs for CD experiments

POPC and POPG were purchased as 25 mg/mL solutions from Avanti Polar Lipids. The mini-extruder and membranes were also purchased from Avanti Polar Lipids. POPC (228 µL, 7.5 µmol) and POPG (77 µL, 2.5 µmol) were mixed and dried under an argon stream, followed by under high vacuum for 2 h. The film was hydrated with phosphate buffer (1 mL, 5 mM KH_2PO_4, pH 7.0) and vortexed for 30 s. The mixture was frozen using a dry ice bath, thawed with warm water and vortexed for 30 s. The freeze-thaw-vortex cycle was repeated twice. Passing the milky suspension through a 50-nm

polycarbonate membrane 10 times using a mini-extruder formed 50-nm LUVs. The phosphate concentration of the LUV solution was determined using the Stewart method.

5.4.9. CD spectroscopy

CD spectra were recorded on an OLIS DSM 17 CD spectrometer. Samples were added to a 0.4 mL quartz cuvette with 0.1 cm path length, measured from 190 – 250 nm at 20 ^{o}C and averaged over 5 scans. The peptide concentration remained constant at 20 μM for all experiments. The CD spectrum of phosphate buffer was subtracted from all spectra. For the vesicle experiments, 10 lipid equivalents (by phosphate concentration) were mixed thoroughly with the peptide solution before measuring. A digital filter of 15 was applied to CD spectra, which were converted to molar ellipticity units.

5.4.10. LPS binding experiments using ITC

Microcalorimetric experiments of peptide binding to LPS were performed on an MCS isothermal titration calorimeter (Microcal, Northampton, MA) at 37 ^{o}C. LPS from *E. coli* 055:B5 was purchased from Sigma-Aldrich (St. Louis, MO) and prepared as a 0.15 mM aqueous suspension in 20 mM HEPES (pH 7.0) buffer by suspension, sonication and temperature cycling between 5 ^{o}C and 70 ^{o}C. This suspension was stored at 4 ^{o}C for at least 12 h prior to use. 1 mM peptide solutions (polymyxin B, tridecaptin A_1, tridecaptin A_1 enantiomer and unacylated tridecaptin A_1) were prepared in the same buffer and all solutions were degassed prior to use by stirring under vacuum for 5 min at 37 ^{o}C. After thermal equilibration, aliquots of 10 uL of peptide solution were added every 5 min into the lipid-containing cell at 37 ^{o}C, which was stirred constantly and the ITC instrument

measured the heat of interaction after each injection. The change in heat rate during the titration steps was registered in real time and raw data were processed using the Origin® 7 software provided with the instrument. In control experiments, the corresponding peptide solution (or LPS solution) was injected into the buffer without LPS (or without peptide). Heats of dilution were significantly lower than instances of ligand-receptor binding.

5.4.11. Lipid II binding experiments using ITC

Microcalorimetric experiments of peptide binding to lipid II analogues were performed on an MCS isothermal titration calorimeter (Microcal, Northampton, MA) at 25 ^{o}C. G+LII (1 mg, 758 μM solution in 2:3:1 $CHCl_3$/MeOH/H_2O) and G-LII (1 mg, 501 μM solution in 2:3:1 $CHCl_3$/MeOH/H_2O) were purchased from the BaCWAN synthetic facility at the University of Warwick, UK. An aliquot of the required lipid II analogue was concentrated *in vacuo* and re-dissolved in 10 mM Tris-Cl and 150 mM NaCl (600 μL) to make a 150 μM solution. A 5 μM solution of tridecaptin A_1 (2 mL) was prepared in the same buffer. Samples were degassed by stirring under vacuum at 25 ^{o}C for 5 min prior to use. The lipid II analogue was titrated into tridecaptin A_1 (5 μM) using the following experimental conditions: temperature = 25°C, reference power = 17 μal/s, syringe-stirring speed = 300 rpm, number of injections = 25, injection volume = 10 μL, initial delay = 60 s and time between injections = 240 s. The change in heat rate during the titration steps was registered in real time and raw data were processed using the Origin® 7 software provided with the instrument. In control experiments, the corresponding peptide solution

(or lipid II solution) was injected into the buffer without lipid II (or without peptide). Heats of dilution were significantly lower than instances of ligand-receptor binding.

5.4.12. Inhibition studies on $TriA_1$ using a spot-on-lawn assay

An *E. coli* ATCC 25922 glycerol stock was used to inoculate MHB (10 mL), which was grown overnight at 37 ^{o}C, 225 rpm. The resulting suspension (100 µL) was used to inoculate freshly melted (37 ^{o}C) Mueller Hinton Agar (MHA) containing 0.75 % agarose (10 mL). This suspension was immediately poured on top of MHA containing 1.5 % agarose and allowed to solidify. Equally spaced marks were made on the back of the plate and used as guides to add 10 µL of each test solution. The plate was incubated overnight at 37 ^{o}C and active compounds were determined by a clear zone of inhibition on the plate. The following solutions were tested: 1) 50 µM $TriA_1$; 2) 50 µM G+LII; 3) 50 µM G-LII; 4) 100 µM $TriA_1$ + 100 µM G+LII and 5) 100 µM $TriA_1$ + 100 µM G-LII. Solutions 4 and 5 were incubated for 5 min at ambient temperature prior to testing. The positive control $TriA_1$ showed activity whereas the negative controls G-LII and G+LII showed no activity. Results shown are representative of results from three technical replicates.

5.4.13. Preparation of BCECF encapsulated LUVs

Experiment performed by Dr. Findlay. LUVs were prepared according to a previously reported literature procedure for the preparation of calcein filled vesicles.[190] 1,2-Dioleoyl-sn-glycero-3-phosphoethanolamine (DOPE) (16 mg) and 1,2-dioleoyl-sn-glycero-3-phospho-(1'-rac-glycerol) (DOPG) (4 mg) were dissolved in $CHCl_3$ (2 mL). If

necessary G+LII or G-LII was then added as a solution in 2:3:1 $CHCl_3$:MeOH:H_2O to 1 mol%. The solution was thoroughly mixed by shaking, then the solvent was removed under reduced pressure and the film dried in the dark under high vacuum overnight. The desiccated lipids were rehydrated with potassium phosphate buffer (50 mM, pH 8, 2 mL) and BCECF acid (2 mM, 10 µL). In dim light the solution was shaken thoroughly, vortexed and transferred to a 5 mL cryovial. The vial was frozen in liquid nitrogen, and thawed at 37 ^{o}C. The lipids were shaken thoroughly until finely suspended (vortexing was insufficient) and re-frozen. This process was repeated five times in total. The now finely dispersed vesicles were extruded 21 times (back and forth 10.5 times) through a lipid extruder (Avanti Polar Lipids, AL) containing a 100 nm pore. Non-encapsulated dye was removed by passing the pale yellow solution through a Sephadex G-50 size exclusion column (50 mM potassium phosphate buffer as eluent, pH 8). The vesicles were then stored in the dark on ice at 4 ^{o}C for further use. Total fluorescence decreased over time, but the vesicles retained activity for a minimum of three weeks at 4 ^{o}C. Fluorescence measurements were performed within three days of LUV preparation. Total phosphate concentration was determined using the Stewart method.

5.4.14. *In vitro* assay using BCECF LUVs

Experiment performed by Dr. Findlay. Measurements were performed on a 75 XE PTI Fluorescence spectrophotometer. All slits were open 1 mm, and measurements were collected every second. Results were visualized in Felix32 analysis software, and analyzed in Microsoft Excel. For BCECF experiments, the excitation and emission wavelengths on the fluorescence spectrometer were set to 500 nm and 522 nm

respectively. Freshly prepared lipid vesicles (10 µL) were added to potassium phosphate buffer (50 mM, pH 6, 2 mL). A small stir bar was needed to properly disperse the vesicles. The fluorescence was monitored for approximately 100 seconds to establish a baseline. Oct-TriA_1 was added, and fluorescence was monitored until stable. Triton X-100 (1%, 50 µL) was then added to quench fluorescence. Experiments shown are representative of results from three technical replicates.

5.4.15. NMR studies

Oct-TriA_1 and lipid II were dissolved separately in 600 µl of a 180 mM dodecylphosphocholine-d_{38} solution (10% D_2O/90% H_2O in 10 mM sodium phosphate buffer at pH 6). The final concentration was 4 mM for each compound. All spectra were referenced to the methylene protons in DPC at 1.52 ppm. One-dimensional (1D) ^{1}H-NMR and two-dimensional homonuclear (2D) $^1H^1$-H total correlation spectroscopy (TOCSY) and Nuclear Overhauser Effect spectroscopy (NOESY) experiments were acquired at 27 °C on a four channel 600 MHz Varian VNMRS spectrometer with a HCN z-axis pulsed-field gradient probe. The acquisition software used was VNMRJ 4.2A. Both TOCSY and NOESY experiments used a 8,000 Hz spectral window in both the directly and indirectly detected dimensions. A total of 512 experiments were used to define the indirectly detected dimension, with 32 and 64 scans for each experiment for the TOCSY and NOESY spectra, respectively, with a total of 4,882 real and imaginary points acquired in the directly detected dimension. A spin lock mix time of 250 ms was used for TOCSY spectra and a mix time of 150 ms was used for NOESY spectra. For all spectra, suppression of the water signal was achieved by presaturation during the

relaxation delay with the exception of the NOESY where saturation of the water peak was also applied during the mix time. NMRPipe [206] and NMRView [207] were used for data processing and analysis. All chemical shift assignments were performed manually. After complete spectral assignment of Oct-TriA$_1$ and the Gram-negative lipid II analogue, the solutions were mixed and the TOCSY and NOESY experiments repeated for the TriA$_1$-Lipid II complex.

5.4.16. Structure calculations

CYANA 2.1[201] was used to calculate the structure of Oct-TriA$_1$ in DPC micelles with and without lipid II using automatically assigned NOE cross peaks. Custom library files for non-canonical amino acids were created as follows: Diaminobutyric acid and D-allo-isoleucine (2*R*,3*S*) were drawn in Chemdraw, with the backbone nitrogen formylated and the backbone carboxylate converted to an amide ester. The resulting structures were then copied into Chemdraw 3D, and the three-dimensional structure was optimized via MM2 energy minimization. The formyl carbon was set to origin and the structure was then saved as a .pdb file. Using the cyana residue entries for lysine and isoleucine as templates, the coordinates derived from Chemdraw 3D were used to build library entries for the non-canonical amino acids in Cyana. To avoid formatting errors the coordinates were entered manually. Bond connectivity's and dihedral angles were determined via examination of the 2D residue structure, and averaging the coordinates of methyl and methylene protons created pseudoatoms. Chemical shifts (stored in the library file under CSTABLE) were estimated. Duplicating the cyana entry of the respective L-amino acid, then multiplying each value in the Z axis by -1 created D-amino

acid residues. The custom library files are available upon request. For Oct-TriA$_1$ in DPC micelles without lipid II, 211 crosspeak NOEs (94 short-range, 15 medium-range and 17 long-range) were used in the structure calculation. For Oct-TriA$_1$ with lipid II, 138 crosspeak NOEs (85 short-range and 17 medium-range) were used in the structure calculation. Seven cycles were done with 10,000 steps per cycle giving 20 structures. Coordinates for the structure of Oct-TriA$_1$ in DPC micelles without lipid II have been deposited in the PDB (2n5w) and the chemical shifts deposited to BMRB (accession number 25737). Coordinates for the structure of Oct-TriA$_1$ in DPC micelles with lipid II have been deposited in the PDB (2n5y) and the chemical shifts deposited to BMRB (accession number 25741). Structures were generated from the CYANA output .pdb files using MacPyMOL.[208] Out of the 20 structures calculated for Oct-TriA$_1$ in the presence of lipid II, the first had the highest target function (highlighted in blue) and was used in subsequent docking studies.

5.4.17. Docking studies

Before docking studies were performed, the *Z,Z*-farnesyl Gram-negative lipid II analogue was drawn in Avogadro (v. 1.1.1). This structure was then optimized using an energy minimization calculation with Force Field = UFF, Steps per Update = 4 and Algorithm = Steepest Descent. The energy minimized lipid II was saved as a .pdb file and used as the input ligand structure for docking studies. AutoDockTools (v. 1.5.6) was used to convert the .pdb file of the lipid II input to a .pdbqt file. The top Oct-TriA$_1$ structure from CYANA was used in for the docking studies. Non-bonded H-atoms were removed in MacPymol (v. 1.3r1) and the .pdb file converted to a .pdbqt format

using AutoDockTools (v. 1.5.6). The grid box function was used to obtain the necessary coordinates for the macromolecule (Oct-TriA_1) input file and the exhaustiveness was set to 5. *ZZ*-Farnesyl Gram-negative lipid II was then docked into Oct-TriA_1 using AutoDock Vina. The top two hits have nearly identical binding conformations and as the top hit had the lowest rmsd in it's conformational cluster, this was chosen as the docked lipid II structure. The final TriA_1-Lipid II complex was generated using MacPyMOL.

5.4.18. Development of resistance

Morphologically similar *E. coli* ATCC 25922 colonies were suspended in MHB to yield a cell suspension greater than 10^7 CFU/mL. 10 µL aliquots were then added to 1 mL test tubes containing doubling concentrations of either Oct-TriA_1 (0.375 to 12 mg/L) or ciprofloxacin (1 to 32 µg/L). Tubes were incubated at 37 ^oC, with shaking (225 rpm). After 24 hours, tubes were assessed for growth. The MIC was recorded, and 10 µL aliquots from the second highest antibiotic concentration that displayed growth (i.e. ¼ the MIC) were added to fresh media. The process was repeated for 1 month, with frozen stocks prepared every week.

5.5. Synthesis and characterization of compounds

(*S*)-3,7-Dimethyloct-6-enyl-4-methylbenzenesulfonate (35)

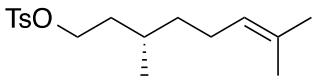

35

To an ice-cold solution of (*S*)-(+)-β-citronellol (3.00 g, 19.2 mmol, 1.0 equiv.) in pyridine (24 mL) was added TsCl (8.00 g, 42.1 mmol, 2.2 equiv.). This mixture was slowly

warmed to ambient temperature and stirred for another 4.5 h. H_2O (4 mL) and Et_2O (30 mL) were added and the two layers separated. The aqueous layer was cooled in an ice bath and 12 N HCl (30 mL) was added. The original organic layer was then added to this acidic solution. The layers were separated and the aqueous layer was extracted back with Et_2O (2 x 30 mL). The combined organic layer was sequentially washed with sat. $NaHCO_3$ (50 mL), H_2O (50 mL) and brine (50 mL), dried over Na_2SO_4, filtered and concentrated *in vacuo*, yielding **35** as a colourless oil. Spectral data were consistent with the previously reported literature compound.[209]

(*R*)-3,7-Dimethyloct-6-enyl-4-methylbenzenesulfonate (36)

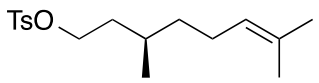

36

To an ice-cold solution of (*R*)-(+)-β-citronellol (3.00 g, 19.2 mmol, 1.0 equiv.) in pyridine (24 mL) was added TsCl (8.00 g, 42.1 mmol, 2.2 equiv.). This mixture was slowly warmed to ambient temperature and stirred for another 4.5 h. H_2O (4 mL) and Et_2O (30 mL) were added and the two layers separated. The aqueous layer was cooled in an ice bath and 12 N HCl (30 mL) was added. The original layer was then added to this acidic solution. The layers were separated and the aqueous layer was extracted back with Et_2O (2 x 30 mL). The combined organic layer was sequentially washed with sat. $NaHCO_3$ (50 mL), H_2O (50 mL) and brine (50 mL), dried over Na_2SO_4, filtered and concentrated *in vacuo*, yielding **36** as a colourless oil. Spectral data were consistent with the previously reported literature compound.[209]

(*R*)-2,6-Dimethyloct-2-ene (37)

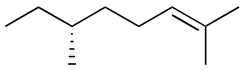

37

$LiAlH_4$ (0.93 g, 24.5 mmol, 1.3 equiv.) was added to a flame-dried flask under a blanket of argon, followed by the addition of Et_2O (25 mL). The resulting suspension was cooled in an ice bath, followed by the dropwise addition of a solution of **3** (19.2 mmol) in Et_2O (5 mL). The reaction mixture was stirred at 0 °C for 4 h and slowly quenched with H_2O. 1 M NaOH (25 mL) was added and the mixture was stirred for 10 min. The mixture was then filtered through a sintered glass funnel. The layers were separated and the aqueous layer was back-extracted with Et_2O (50 mL). The combined organic layer was sequentially washed with 1 M NaOH, H_2O and brine, dried over Na_2SO_4, filtered and concentrated *in vacuo*, yielding **37** as a colourless volatile liquid, which was used directly in the next step without further purification. Spectral data were consistent with the previously reported literature compound.[209]

(*S*)-2,6-Dimethyloct-2-ene (38)

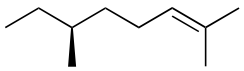

38

$LiAlH_4$ (0.93 g, 24.5 mmol, 1.3 equiv.) was added to a flame-dried flask under a blanket of argon, followed by the addition of Et_2O (25 mL). The resulting suspension was cooled in an ice bath, followed by the dropwise addition of a solution of **4** (19.2 mmol) in Et_2O (5 mL). The reaction mixture was stirred at 0 °C for 4 h and slowly quenched with H_2O. 1 M NaOH (25 mL) was added and the mixture was stirred for 10 min. The mixture was

then filtered through a sintered glass funnel. The layers were separated and the aqueous layer was back-extracted with Et_2O (50 mL). The combined organic layer was sequentially washed with 1 M NaOH, H_2O and brine, dried over Na_2SO_4, filtered and concentrated *in vacuo*, yielding **38** as a colourless volatile liquid, which was used directly in the next step without further purification. Spectral data were consistent with the previously reported literature compound.[209]

(*R*)-4-Methylhexanal (39)

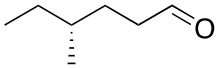

39

Compound **37** (19.2 mmol) was dissolved in CH_2Cl_2 (30 mL). This solution was cooled to -78 °C and ozone was bubbled through the solution until it turned blue. O_2 was then bubbled through the solution for 1 h, after which it was warmed to rt and stirred with dimethyl sulfide (1 mL) for 1 h. H_2O (20 mL) and pentane (25 mL) were added, separated and the aqueous layer extracted with pentane (2 x 25 mL). The combined organic layers were washed with H_2O and brine, dried over Na_2SO_4, filtered and concentrated *in vacuo* (keeping the temperature of water bath below 25 °C), yielding **39** as a colourless volatile liquid, which was used directly in the next step without further purification. Spectral data were consistent with the previously reported literature compound.[209]

(*S*)-4-Methylhexanal (40)

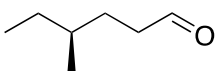

40

Compound **38** (19.2 mmol) was dissolved in CH_2Cl_2 (30 mL). This solution was cooled to -78 °C and ozone was bubbled through the solution until it turned blue. O_2 was then bubbled through the solution for 1 h, after which it was warmed to rt and stirred with dimethyl sulfide (1 mL) for 1 h. H_2O (20 mL) and pentane (25 mL) were added, separated and the aqueous layer extracted with pentane (2 x 25 mL). The combined organic layers were washed with H_2O and brine, dried over Na_2SO_4, filtered and concentrated *in vacuo* (keeping the temperature of water bath below 25 °C), yielding **40** as a colourless volatile liquid, which was used directly in the next step without further purification. Spectral data were consistent with the previously reported literature compound.[209]

(*S*)-1-(4-Benzyl-2-thioxothiazolidin-3-yl)ethanone (41)

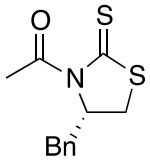

41

THF (24 mL) was added to a flame dried flask under a blanket of argon and cooled to 0 °C. NaH (60% wt in mineral oil, 0.20 g, 5.0 mmol, 1.0 equiv.) was added and stirred for 20 min. (*S*)-benzyl Crimmins chiral auxiliary (1.04 g, 5.0 mmol, 1.0 equiv.) was added and the mixture stirred at 0 °C for 1 h. Acetic anhydride (0.57 mL, 6.0 mmol, 1.2 equiv.) was then added and the mixture was stirred for a further 2 h. The reaction was

quenched by the addition of sat. NH_4Cl (10 mL). THF was removed *in vacuo* and EtOAc (30 mL) was added. The layers were separated and the organic layer was dried over Na_2SO_4, filtered and concentrated *in vacuo*. The crude product was purified by flash chromatography (silica gel, 8:1 hexanes : EtOAc), yielding **41** as a yellow solid (0.81 g, 65%). $[\alpha]_D^{25}$ 242.0 (*c* 0.40, $CHCl_3$); IR ($CDCl_3$, cast film) 3026, 2927, 1697, 1495, 1368 cm^{-1}; ^1H NMR ($CDCl_3$, 400 MHz): 7.37-7.28 (m, 5H, Ar-H), 5.41-5.36 (m, 1H, NCH), 3.39 (ddd, 1H, *J* = 11.5, 7.2, 1.1 Hz, SCHH), 3.23 (dd, 1H, *J* = 13.2, 3.8 Hz, PhCHH), 3.04 (dd, 1H, *J* = 13.2, 10.5 Hz, PhCHH), 2.89 (dd, 1H, *J* = 11.5, 0.7 Hz, SCHH), 2.80 (s, 3H, CH_3); ^{13}C NMR ($CDCl_3$, 125 MHz): δ 201.2, 170.3, 136.1, 129.1, 128.5, 126.8, 67.8, 36.3, 31.4, 26.7; HRMS (ES) Calcd for $C_{12}H_{13}NNaOS_2$ $[M+Na]^+$ 274.0331, found 274.0330.

General Procedure for Aldol Condensations

To a flame-dried flask under a blanket of argon was added a solution of **41** (1.71 g, 6.8 mmol, 1.0 equiv.) in CH_2Cl_2 (34 mL) and cooled to 0 °C. $TiCl_4$ (1.0 M in CH_2Cl_2, 6.80 mL, 6.8 mmol, 1.0 equiv.) was added and the resulting mixture stirred for 5 min at 0 °C. Upon cooling to -78 °C, DIPEA (1.18 mL, 6.8 mmol, 1.0 equiv.) was added and the mixture was stirred for 1 h at -78 °C. A solution of **39** (0.77 g, 6.8 mmol, 1.0 equiv.) in CH_2Cl_2 (6.6 mL) was then added dropwise. After stirring for another 1.5 h at the same temperature, the reaction was quenched by the addition of sat. NH_4Cl (10 mL). The layers were separated and the aqueous layer was extracted with CH_2Cl_2 (2 x 40 mL). The combined organic layers were dried over Na_2SO_4, filtered, concentrated *in vacuo* and purified by flash chromatography (silica gel, 6:1 then 4:1 hexanes : EtOAc), yielding

42 (0.72 g, 29% over 4 steps) and **43** (0.26 g, 11% over 4 steps) as yellow sticky oils. Using the same procedures, compounds **44** and **45** were synthesized in 28 % and 6 % yields, respectively, over 4 steps from compound **40**.

(3*S*,6*R*)-1-((*S*)-4-Benzyl-2-thioxothiazolidin-3-yl)-3-hydroxy-6-methyloctan-1-one (42)

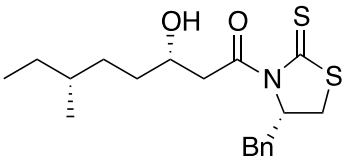

42

$[\alpha]_D$ 176.1° (*c* 0.48, $CHCl_3$); IR ($CHCl_3$, cast film) 3437, 2957, 2927, 2856, 1693, 1455, 1342 cm^{-1}; ^1H NMR ($CDCl_3$, 600 MHz): 7.37-7.26 (m, 5H, Ar-H), 5.43 (ddd, 1H, *J* = 10.5, 6.8, 3.8 Hz, -CHCH$_2$Ph), 4.15-4.10 (m, 1H, -CHOH), 3.66 (dd, 1H, *J* = 17.7, 2.2 Hz, -CHHC=O), 3.41 (dd, 1H, *J* = 11.5, 7.2 Hz, -CHHCS), 3.23 (dd, 1H, *J* = 13.3, 3.8 Hz, -CHHPh), 3.14 (dd, 1H, *J* = 17.7, 9.4 Hz, -CHHC=O), 3.06 (dd, 1H, *J* = 13.1, 10.6 Hz, -CHHPh), 2.91 (d, 1H, *J* = 11.5 Hz, -CHHCS), 2.70 (s, 1H, O-H), 1.57-1.45 (m, 3H), 1.40-1.30 (m, 2H), 1.21-1.11 (m, 2H), 0.91-0.85 (m, 6H, -CH$_2$CH$_3$, -CHCH$_3$); ^{13}C NMR ($CDCl_3$, 125 MHz): δ 201.4, 173.3, 136.4, 129.4, 128.9, 127.3, 68.3, 68.2, 46.0, 36.8, 34.3, 33.9, 32.3, 32.0, 29.4, 19.1, 11.4; HRMS (ES) Calcd for $C_{19}H_{27}NNaO_2S_2[M+Na]^+$ 388.1375, found 388.1369.

(3*R*,6*R*)-1-((*S*)-4-Benzyl-2-thioxothiazolidin-3-yl)-3-hydroxy-6-methyloctan-1-one (43)

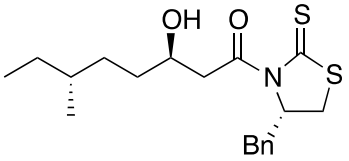

43

$[\alpha]_D$ 148.0° (*c* 0.15, $CHCl_3$); IR ($CHCl_3$, cast film) 3449, 2957, 2921, 2851, 1691, 1455, 1342 cm^{-1}; ^1H NMR ($CDCl_3$, 600 MHz): 7.36-7.34 (m, 2H, Ar-H), 7.29-7.27 (m, 3H, Ar-H), 5.41 (dd, 1H, *J* = 10.5, 6.6, 4.0 Hz), C<u>H</u>CH_2Ph), 4.06-4.00 (m, 1H, -C<u>H</u>OH), 3.46 (dd, 1H, *J* = 17.5, 9.3 Hz, -C<u>H</u>HC=O), 3.41 (ddd, 1H, *J* = 11.5, 7.2, 1.0 Hz, -C<u>H</u>HCS), 3.36 (dd, 1H, *J* = 17.5, 2.6 Hz, -CH<u>H</u>C=O), 3.24 (dd, 1H, *J* = 13.3, 4.0 Hz, -C<u>H</u>HPh), 3.11 (d, 1H, *J* = 4.1, O-<u>H</u>), 3.06 (dd, 1H, *J* = 13.3, 10.4 Hz, -CH<u>H</u>Ph), 2.92 (d, 1H, *J* = 11.6 Hz, -CH<u>H</u>CS), 1.57-1.45 (m, 3H), 1.40-1.30 (m, 2H), 1.21-1.11 (m, 2H), 0.91-0.85 (m, 6H, -CH_2C<u>H</u>$_3$, -CHC<u>H</u>$_3$); ^{13}C NMR ($CDCl_3$, 125 MHz): δ 201.5, 173.9, 136.4, 129.5, 129.0, 127.3, 69.0, 68.2, 45.5, 36.8, 34.4, 34.2, 32.3, 32.1, 29.3, 19.2, 11.4; HRMS (ES) Calcd for $C_{19}H_{27}NNaO_2S_2[M+Na]^+$ 388.1375, found 388.1369.

(3*S*,6*S*)-1-((*S*)-4-Benzyl-2-thioxothiazolidin-3-yl)-3-hydroxy-6-methyloctan-1-one (44)

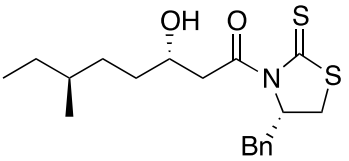

44

$[\alpha]_D$ 175.0° (*c* 0.97, CH_2Cl_2); IR (CH_2Cl_2, cast film) 3445, 2958, 2929, 2872, 1690, 1455, 1342 cm^{-1}; ^1H NMR ($CDCl_3$, 500 MHz): 7.37-7.25 (m, 5H, Ar-H), 5.1 (ddd, 1H, *J* = 10.5,

6.9, 3.8 Hz, C<u>H</u>CH_2Ph), 4.14-4.08 (m, 1H, -C<u>H</u>OH), 3.66 (dd, 1H, *J* = 17.7, 2.4 Hz, -C<u>H</u>HC=O), 3.40 (ddd, 1H, *J* = 11.5, 7.2, 0.9 Hz, -C<u>H</u>HCS), 3.22 (dd, 1H, *J* = 13.2, 3.8 Hz, -C<u>H</u>HPh), 3.13 (dd, 1H, *J* = 17.7, 9.4 Hz, -CH<u>H</u>C=O), 3.05 (dd, 1H, *J* = 13.2, 10.5 Hz, -CH<u>H</u>Ph), 2.90 (d, 1H, *J* = 11.6 Hz, -CH<u>H</u>CS), 1.57-1.46 (m, 3H), 1.40-1.33 (m, 2H), 1.20-1.12 (m, 2H), 0.90-0.86 (m, 6H, -CH_2C<u>H</u>$_3$, -CHC<u>H</u>$_3$); ^{13}C NMR ($CDCl_3$, 125 MHz): δ 201.4, 173.4, 136.4, 129.5, 129.0, 127.3, 68.3, 45.9, 36.9, 34.4, 34.0, 32.3, 32.0, 29.3, 19.2, 11.4; HRMS (ES) Calcd for $C_{19}H_{27}NNaO_2S_2$[M+Na]$^+$ 388.1375, found 388.1370.

(3*S*,6*R*)-1-((*S*)-4-Benzyl-2-thioxothiazolidin-3-yl)-3-hydroxy-6-methyloctan-1-one (45)

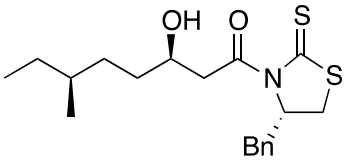

45

[α]$_D$ 176.1° (*c* 0.48, $CHCl_3$); IR ($CHCl_3$, cast film) 3437, 2957, 2927, 2856, 1693, 1455, 1342 cm^{-1}; ^{1}H NMR ($CDCl_3$, 600 MHz): 7.37-7.34 (m, 2H, Ar-<u>H</u>), 7.29-7.27 (m, 3H, Ar-<u>H</u>), 5.42 (ddd, 1H, *J* = 10.6, 6.9, 3.9 Hz, C<u>H</u>CH_2Ph), 4.04 (dtd, 1H, *J* = 9.5, 4.8, 2.4 Hz, -C<u>H</u>OH), 3.47 (dd, 1H, *J* = 17.7, 9.3 Hz, -C<u>H</u>HC=O), 3.41 (dd, 1H, *J* = 11.5, 7.2 Hz, -C<u>H</u>HCS), 3.35 (dd, 1H, *J* = 17.7, 2.6 Hz, -CH<u>H</u>C=O), 3.23 (dd, 1H, *J* = 13.3, 4.0 Hz, -C<u>H</u>HPh), 3.1 (s, 1H, O-<u>H</u>), 3.06 (dd, 1H, *J* = 13.2, 10.4 Hz, -CH<u>H</u>Ph), 2.91 (d, 1H, *J* = 11.6 Hz, -CH<u>H</u>CS), 1.64-1.57 (m, 1H), 1.50-1.43 (m, 1H), 1.39-1.26 (m, 4H), 1.19-1.13 (m, 1H), 0.91-0.85 (m, 6H, -CH_2C<u>H</u>$_3$, -CHC<u>H</u>$_3$); ^{13}C NMR ($CDCl_3$, 125 MHz): δ 201.4, 173.9, 136.4, 129.4, 128.9, 127.3, 68.3, 68.2, 45.5, 36.8, 34.3, 34.2, 32.2, 32.0, 29.4, 19.1, 11.3; HRMS (ES) Calcd for $C_{19}H_{27}NNaO_2S_2$[M+Na]$^+$ 388.1375, found 388.1369.

General Procedure for Coupling Activated Lipids to Resin-Bound H-TriA$_1$

Resin-bound H-TriA$_1$ (80 mg, 0.025 mmol) was stirred gently in a solution of the activated lipid (12 mg, 0.033 mmol) in CH_2Cl_2 (1 mL) at ambient temperature under argon for 24 h. The suspension was then filtered, washed with CH_2Cl_2 (5 x 5 mL) and dried under vacuum for 5 min. To simultaneously cleave the peptide from resin and remove side chain protecting groups, the dry resin was transferred to a screw-top vial containing TFA:TIPS:H_2O (95:2.5:2.5, 1 mL), and shaken for 2 h. The resin beads were removed via filtration through glass wool and the filtrate was concentrated *in vacuo*. The crude peptide was obtained by precipitation with cold Et_2O. The crude peptide was re-dissolved in H_2O/MeCN (3:1) containing 0.1 % TFA (aq) and purified by HPLC method 1.

(3*R*,6*S*)-Tridecaptin A$_1$ (32)

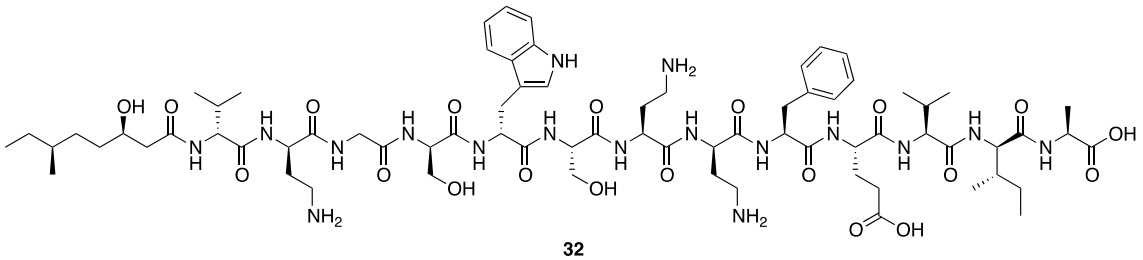

32

Peptide was isolated as a single peak using C_{18} HPLC (8.2 mg, 18 %). Retention time (HPLC method 2) = 33.83 min. ^{1}H NMR (D_2O, 600 MHz): δ 7.57 (d, 1H, *J* = 7.8 H, Trp5-ArH), 7.46 (d, 1H, *J* = 8.2 Hz, Trp5-ArH), 7.31 (t, 2H, *J* = 7.3 Hz, Phe9-ArH), 7.26 (t, 1H *J* = 7.4 Hz, Trp5-ArH), 7.21-7.19 (m, 4H, Trp5-ArH + Phe9-ArH), 7.11 (t, 1H, *J* = 7.5 Hz, Trp5-ArH), 4.67 (dd, 1H, *J* = 9.6, 5.8 Hz, Phe9-Hα), 4.61 (t, 1H, *J* = 7.3 Hz, Trp5-Hα), 4.44-4.42 (m, 2H, D-Dab2-Hα + D-Ser4-Hα), 4.35-4.22 (m, 5H, D-*allo*-Ile12-Hα + Dab7-

Hα + Glu10-Hα + D-Dab8-Hα + Ala13-Hα), 4.13-4.10 (m, 2H, Val11-Hα + Ser6-Hα), 4.05 (d, 1H, *J* = 7.2 Hz, D-Val1-Hα), 4.00-3.89 (m, 3H, Gly3-Hα + Lipid-Hβ), 3.75 (app. qd, 2H, *J* = 11.4, 5.5 Hz, D-Ser4-Hβ), 3.54 (dd, 1H, *J* = 11.4, 5.0 Hz, D-Ser4-Hβ), 3.30 (dd, 1H, *J* = 11.4, 5.5 Hz, D-Ser4-Hβ), 3.25 (d, 2H, *J* = 7.6 Hz, D-Trp5-Hβ), 3.17 (dd, 1H, *J* = 14.3, 5.7 Hz, Phe9-Hβ), 3.07-2.96 (m, 4H, D-Dab2-Hγ + Dab7-Hγ), 2.87 (dd, 1H, *J* = 14.0, 9.7 Hz, Phe9-Hβ), 2.73-2.68 (m, 1H, D-Dab8-Hγ), 2.62-2.57 (m, 1H, D-Dab8-Hγ), 2.47 (dd, 1H, *J* = 14.3, 5.3 Hz, Lipid-Hα), 2.41 (dd, 1H, *J* = 14.3, 8.1 Hz, Lipid-Hα), 2.33-2.29 (m, 2H, Glu10-Hγ + D-Dab2-Hβ), 2.21-2.15 (m, 2H, Dab2-Hβ + Dab7-Hβ), 2.08-1.78 (m, 9H, D-Val1-Hβ + Dab7-Hβ + D-Dab8-Hβ + Glu10-Hβ + Val11-Hβ + D-*allo*-Ile12-Hβ + Glu10-Hγ), 1.47-1.41 (m, 2H, Lipid-Hγ), 1.33 (d, 3H, *J* = 7.3 Hz, Ala13-Hβ), 1.50-1.19 (m, 7H, Lipid-Hδ, Hε, Hζ + D-*allo*-Ile12-Hγ), 0.94-0.84 (m, 15H, D-Val1-Hγ + Val11-Hγ + D-*allo*-Ile12-Hδ), 0.80-0.78 (m, 6H, Lipid-Hζ, Hη). MW calculated for $C_{73}H_{116}N_{17}O_{20}$ 1550.8577, found *high resolution* (FTICR-ESI-MS) 1550.8577 $(M+H)^+$.

(3*S*,6*S*)-Tridecaptin A_1 (53)

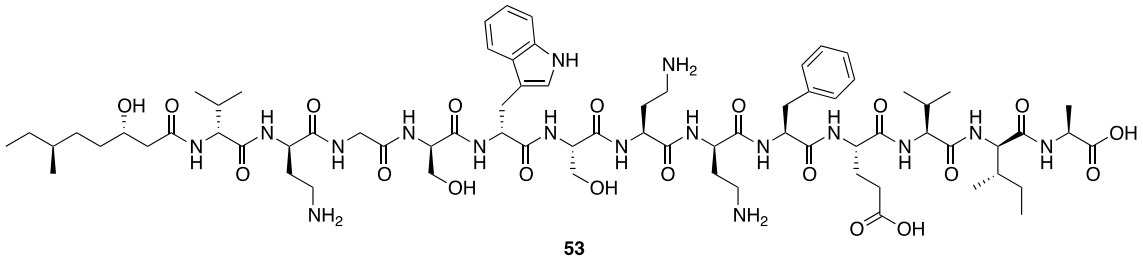

53

Peptide was isolated as a single peak using C_{18} HPLC (5.7 mg, 12 %). Retention time (HPLC method 2) = 32.62 min. ^{1}H NMR (D_2O, 600 MHz): δ 7.57 (d, 1H, *J* = 8.2 H, Trp5-ArH), 7.46 (d, 1H, *J* = 8.2 Hz, Trp5-ArH), 7.31 (t, 2H, *J* = 7.3 Hz, Phe9-ArH), 7.26 (t, 1H *J* = 7.2 Hz, Trp5-ArH), 7.21-7.19 (m, 3H, Trp5-ArH + Phe9-ArH), 7.11 (t, 1H, *J* = 7.5 Hz,

Trp5-ArH), 4.67 (dd, 1H, *J* = 9.7, 5.8 Hz, Phe9-Hα), 4.62 (t, 1H, *J* = 7.3 Hz, Trp5-Hα), 4.44-4.41 (m, 2H, D-Dab2-Hα + D-Ser4-Hα), 4.35-4.26 (m, 4H, D-*allo*-Ile12-Hα + Dab7-Hα + Glu10-Hα + D-Dab8-Hα), 4.22 (q, 1H, *J* = 7.0 Hz, Ala13-Hα) 4.13-4.10 (m, 2H, Val11-Hα + Ser6-Hα), 4.04 (d, 1H, *J* = 7.3 Hz, D-Val1-Hα), 3.92-3.89 (m, 3H, Gly3-Hα + Lipid-Hβ), 3.74 (app. qd, 2H, *J* = 11.7, 5.4 Hz, D-Ser4-Hβ), 3.54 (dd, 1H, *J* = 11.5, 5.1 Hz, D-Ser4-Hβ), 3.30 (dd, 1H, *J* = 11.5, 5.6 Hz, D-Ser4-Hβ), 3.25 (d, 2H, *J* = 7.5 Hz, D-Trp5-Hβ), 3.17 (dd, 1H, *J* = 14.1, 5.5 Hz, Phe9-Hβ), 3.08-2.96 (m, 4H, D-Dab2-Hγ + Dab7-Hγ), 2.87 (dd, 1H, *J* = 14.2, 10.0 Hz, Phe9-Hβ), 2.73-2.68 (m, 1H, D-Dab8-Hγ), 2.61-2.56 (m, 1H, D-Dab8-Hγ), 2.41 (m, 2H, Lipid-Hα), 2.32-2.27 (m, 2H, Glu10-Hγ + D-Dab2-Hβ), 2.21-2.14 (m, 2H, Dab2-Hβ + Dab7-Hβ), 2.08-1.80 (m, 9H, D-Val1-Hβ + Dab7-Hβ + D-Dab8-Hβ + Glu10-Hβ + Val11-Hβ + D-*allo*-Ile12-Hβ + Glu10-Hγ), 1.50-1.19 (m, 10H, Ala13-Hβ + Lipid-Hγ, Hδ, Hε, Hζ + D-*allo*-Ile12-Hγ), 1.10-1.02 (m, 2H, Lipid-Hδ, Hζ), 0.96-0.85 (m, 15H, D-Val1-Hγ + Val11-Hγ + D-*allo*-Ile12-Hδ), 0.81-0.78 (m, 6H, Lipid-Hζ, Hη). MW calculated for $C_{73}H_{116}N_{17}O_{20}$ 1550.8577, found *high resolution* (FTICR-ESI-MS) 1550.8580 $(M+H)^+$.

(3*R*,6*R*)-Tridecaptin A_1 (54)

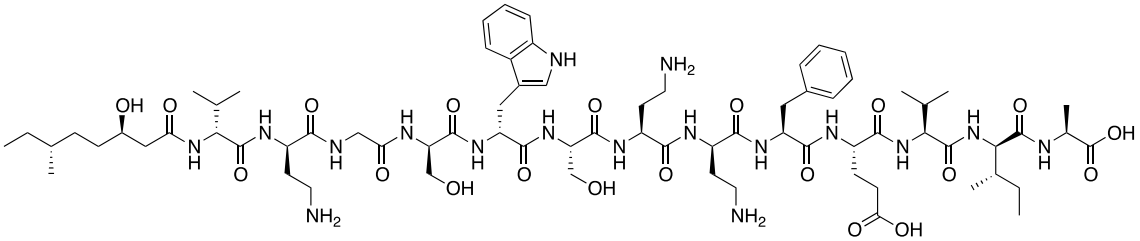

54

Peptide was isolated as a single peak using C_{18} HPLC (8.6 mg, 18 %). Retention time (HPLC method 2) = 34.11 min. ^{1}H NMR (D_2O, 600 MHz): δ 7.59 (d, 1H, *J* = 8.0 H, Trp5-

ArH), 7.48 (d, 1H, *J* = 8.2 Hz, Trp5-ArH), 7.32 (t, 2H, *J* = 7.2 Hz, Phe9-ArH), 7.26 (t, 1H *J* = 7.3 Hz, Trp5-ArH), 7.22-7.20 (m, 4H, Trp5-ArH + Phe9-ArH), 7.12 (t, 1H, *J* = 7.3 Hz, Trp5-ArH), 4.66 (dd, 1H, *J* = 9.5, 5.7 Hz, Phe9-Hα), 4.63 (t, 1H, *J* = 7.4 Hz, Trp5-Hα), 4.46-4.43 (m, 2H, D-Dab2-Hα + D-Ser4-Hα), 4.35-4.27 (m, 4H, D-*allo*-Ile12-Hα + Dab7-Hα + Glu10-Hα + D-Dab8-Hα), 4.24 (q, 1H, *J* = 5.7 Hz, Ala13-Hα), 4.15-4.11 (m, 2H, Val11-Hα + Ser6-Hα), 4.07 (d, 1H, *J* = 7.2 Hz, D-Val1-Hα), 3.97-3.88 (m, 3H, Gly3-Hα + Lipid-Hβ), 3.76 (app. qd, 2H, *J* = 11.2, 5.5 Hz, D-Ser4-Hβ), 3.56 (dd, 1H, *J* = 11.4, 5.0 Hz, D-Ser4-Hβ), 3.32 (dd, 1H, *J* = 11.5, 5.5 Hz, D-Ser4-Hβ), 3.26 (d, 2H, *J* = 7.4 Hz, D-Trp5-Hβ), 3.18 (dd, 1H, *J* = 14.1, 5.6 Hz, Phe9-Hβ), 3.08-2.97 (m, 4H, D-Dab2-Hγ + Dab7-Hγ), 2.87 (dd, 1H, *J* = 13.9, 9.9 Hz, Phe9-Hβ), 2.73-2.68 (m, 1H, D-Dab8-Hγ), 2.62-2.57 (m, 1H, D-Dab8-Hγ), 2.49 (dd, 1H, *J* = 14.2, 5.3 Hz, Lipid-Hα), 2.41 (dd, 1H, *J* = 14.3, 8.0 Hz, Lipid-Hα), 2.34-2.29 (m, 2H, Glu10-Hγ + D-Dab2-Hβ), 2.23-2.15 (m, 2H, Dab2-Hβ + Dab7-Hβ), 2.08-1.78 (m, 9H, D-Val1-Hβ + Dab7-Hβ + D-Dab8-Hβ + Glu10-Hβ + Val11-Hβ + D-*allo*-Ile12-Hβ + Glu10-Hγ), 1.50-1.19 (m, 10H, Lipid-Hγ, Hδ, Hε, Hζ + D-*allo*-Ile12-Hγ + Ala13-Hβ), 1.13-1.05 (m, 2H, Lipid-Hδ, Hζ), 0.96-0.85 (m, 15H, D-Val1-Hγ + Val11-Hγ + D-*allo*-Ile12-Hδ), 0.81-0.78 (m, 6H, Lipid-Hζ, Hη). MW calculated for $C_{73}H_{116}N_{17}O_{20}$ 1550.8577, found *high resolution* (FTICR-ESI-MS) 1550.8577 $(M+H)^+$.

(3*S*,6*R*)-Tridecaptin A_1 (55)

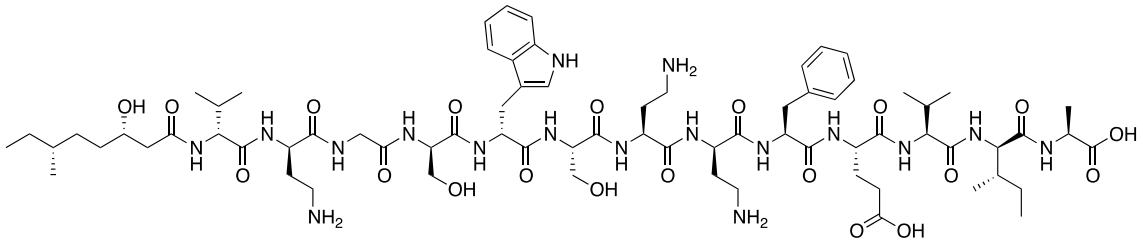

55

Peptide was isolated as a single peak using C_{18} HPLC (5.0 mg, 11 %). Retention time (HPLC method 2) = 32.70 min. ^{1}H NMR (D_2O, 600 MHz): δ 7.57 (d, 1H, *J* = 8.2 H, Trp5-ArH), 7.46 (d, 1H, *J* = 8.2 Hz, Trp5-ArH), 7.40-7.25 (m, 4H, Trp5-ArH + Phe9-ArH), 7.21-7.19 (m, 3H, Trp5-ArH + Phe9-ArH), 7.11 (t, 1H, *J* = 7.6 Hz, Trp5-ArH), 4.67 (dd, 1H, *J* = 9.1, 6.1 Hz, Phe9-Hα), 4.62 (t, 1H, *J* = 7.2 Hz, Trp5-Hα), 4.44-4.41 (m, 2H, D-Dab2-Hα + D-Ser4-Hα), 4.35-4.21 (m, 5H, D-*allo*-Ile12-Hα + Dab7-Hα + Glu10-Hα + D-Dab8-Hα + Ala13-Hα), 4.13-4.10 (m, 2H, Val11-Hα + Ser6-Hα), 4.04 (d, 1H, *J* = 7.5 Hz, D-Val1-Hα), 3.92-3.89 (m, 3H, Gly3-Hα + Lipid-Hβ), 3.74 (app. qd, 2H, *J* = 11.7, 5.4 Hz, D-Ser4-Hβ), 3.54 (dd, 1H, *J* = 11.5, 5.1 Hz, Ser6-Hβ), 3.30 (dd, 1H, *J* = 11.3, 5.2 Hz, Ser6-Hβ), 3.23 (d, 2H, *J* = 7.3 Hz, D-Trp5-Hβ), 3.17 (dd, 1H, *J* = 14.4, 5.8 Hz, Phe9-Hβ), 3.08-2.96 (m, 4H, D-Dab2-Hγ + Dab7-Hγ), 2.87 (dd, 1H, *J* = 13.9, 9.8 Hz, Phe9-Hβ), 2.73-2.68 (m, 1H, D-Dab8-Hγ), 2.52-2.47 (m, 1H, D-Dab8-Hγ), 2.41 (d, 1H, *J* = 6.5 Hz, Lipid-Hα), 2.32-2.30 (m, 2H, Glu10-Hγ + D-Dab2-Hβ), 2.20-2.14 (m, 2H, Dab2-Hβ + Dab7-Hβ), 2.08-1.80 (m, 9H, D-Val1-Hβ + Dab7-Hβ + D-Dab8-Hβ + Glu10-Hβ + Val11-Hβ + D-*allo*-Ile12-Hβ + Glu10-Hγ), 1.45-1.39 (m, 2H, Lipid-Hγ), 1.33-1.04 (m, 12H, Ala13-Hβ + Lipid-Hδ, Hε, Hζ + D-*allo*-Ile12-Hγ), 0.94-0.77 (m, 21H, D-Val1-Hγ + Val11-Hγ + D-*allo*-Ile12-Hδ, Lipid-Hζ, Hη). MW calculated for $C_{73}H_{116}N_{17}O_{20}$ 1550.8577, found *high resolution* (FTICR-ESI-MS) 1550.8587 $(M+H)^+$.

(*R*)-4-Benzyl-3-butyryloxazolidin-2-one (61)

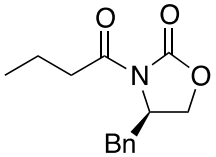

61

(*R*)-4-benzyloxazolidin-2-one (**60**) (10.0 g, 56.4 mmol) was dissolved in dry THF (80 mL) and cooled to -78 ^{o}C under argon. 2.5 M *n*-BuLi (25.1 mL, 62.6 mmol) was added drop wise over 30 min and the reaction mixture stirred for a further 30 min. Butyryl chloride (7.1 mL, 81.3 mmol) was then added and the reaction stirred for 30 min at -78 °C and another 30 min at ambient temperature. The reaction was quenched by the addition of saturated NH_4Cl (50 mL) and extracted with CH_2Cl_2 (3 × 50 mL). The combined organic extracts were washed with 1 M NaOH (40 mL) and brine (40 mL), dried over anhydrous Na_2SO_4 and concentrated *in vacuo*. The crude oil was purified by flash column chromatography (SiO_2, 4:1 hexanes:EtOAc) to yield the product as a pale yellow oil (13.8 g, 99%). $[\alpha]_D^{25}$ = -56.4 (*c* = 1.0 g/100mL, $CHCl_3$); IR ($CHCl_3$ cast) 3029, 2965, 2934, 2876, 1783, 1701 cm^{-1}; ^{1}H NMR ($CDCl_3$, 500 MHz): δ 7.37-7.34 (m, 2H, meta-ArH), 7.31-7.29 (m, 1H, para-ArH), 7.24-7.22 (m, 2H, ortho-ArH), 4.72-4.67 (m, 1H, NC<u>H</u>), 4.23-4.17 (m, 2H, C<u>H$_2$</u>Ph), 3.32 (dd, 1H, *J* = 13.4, 3.3 Hz, OC<u>H</u>H), 3.01-2.87 (m, 2H, NC(O)C<u>H$_2$</u>), 2.79 (dd, 1H, *J* = 13.4, 9.6 Hz, OCH<u>H</u>), 1.81-1.70 (m, 2H, C<u>H$_2$</u>CH$_3$), 1.05 (t, 3H, *J* = 7.4 Hz, CH$_2$C<u>H$_3$</u>); ^{13}C NMR ($CDCl_3$, 125 MHz): δ 173.2, 153.5, 135.4, 129.4, 129.0, 127.3, 66.2, 55.1, 38.0, 37.4, 17.7, 13.7; HRMS (ES) Calcd for $C_{14}H_{17}NO_3Na$ $[M+Na]^+$ 270.1101, found 270.1098.

(*R*)-4-Benzyl-3-((*R*)-2-methylbutanoyl)oxazolidin-2-one (62)

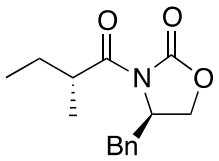

62

Oxazolidinone **61** was dissolved in THF (80 mL) and cooled to -78 ^{o}C under argon. 1 M NaHMDS (67.0 mL, 67.0 mmol) was added via syringe over 5 min and the reaction stirred for 30 min. MeI (8.60 mL, 138 mmol) was then added and the reaction stirred for a further 3 h. Brine (50 mL) and CH_2Cl_2 (80 mL) were added and the reaction warmed to ambient temperature with stirring. The phases were separated and the aqueous layer was diluted with H_2O (50 mL) and extracted with CH_2Cl_2 (2 × 50 mL). The combined organic extracts were dried over anhydrous Na_2SO_4, concentrated *in vacuo* and purified by flash column chromatography (SiO_2, 9:1 hexanes:EtOAc) to yield the product as a colourless oil (10.1 g, 69%). $[\alpha]_D^{25}$ = -69.1 (*c* = 1.0 g/100mL, $CHCl_3$); IR ($CHCl_3$ cast) 3030, 2969, 2934, 2877, 1781, 1698 cm^{-1}; ^{1}H NMR ($CDCl_3$, 500 MHz): δ 7.37-7.34 (m, 2H, meta-ArH), 7.31-7.28 (m, 1H, para-ArH), 7.24-7.23 (m, 2H, ortho-ArH), 4.73-4.68 (m, 1H, NC<u>H</u>), 4.24-4.17 (m, 2H, C<u>H$_2$</u>Ph), 3.70-3.63 (m, 1H, NC(O)C<u>H</u>), 3.29 (dd, 1H, *J* = 13.4, 3.2 Hz, OC<u>H</u>H), 2.79 (dd, 1H, *J* = 13.4, 9.6 Hz, OCH<u>H</u>), 1.80 (ddt, 2H, *J* = 14.1, 7.1 Hz, CH$_2$C<u>H</u>H), 1.50 (ddt, 2H, *J* = 14.0, 7.0 Hz, CH$_2$C<u>H</u>H), 1.25 (d, 3H, *J* = 6.9 Hz, CHC<u>H$_3$</u>), 0.95 (t, 3H, *J* = 7.4 Hz, CH$_2$C<u>H$_3$</u>); ^{13}C NMR ($CDCl_3$, 125 MHz): δ 177.2.2, 153.1, 135.4, 129.5, 129.0, 127.3, 66.0, 55.4, 39.2, 37.9, 26.4, 16.9, 11.7; HRMS (ES) Calcd for $C_{15}H_{19}NNaO_3$ $[M+Na]^+$ 284.1257, found 284.1259.

(2*R*)-Methylbutanol (59)

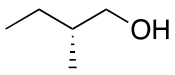

59

Oxazolidin-2-one **62** (10.1 g, 38.6 mmol) was dissolved in Et_2O (70 mL) and cooled to -20 ^{o}C. $LiAlH_4$ (4.4 g, 115.9 mmol) was added in parts and the reaction was stirred at 0

^{o}C for 2 h. H_2O (10 mL) was added and the reaction mixture stirred at ambient temperature for 15 min. The mixture was then filtered through celite and the celite washed with Et_2O (4 x 100 mL). The combined organic extracts were washed with brine (100 mL), dried over anhydrous Na_2SO_4 and concentrated by rotary evaporator at 0 ^{o}C to approximately 10 mL. This crude alcohol was used in the next step without purification.

(2*S*)-Methylbutyltosylate (63)

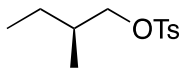

63

(2*S*)-Methylbutanol (5.0 g, 57.0 mmol) was dissolved in pyridine (100 mL). Tosyl chloride (21.6 g, 113 mmol) was added and the resulting solution stirred at ambient temperature for 16 h. The reaction was diluted with H_2O (300 mL) and Et_2O (300 mL) and the organic phase separated. The aqueous phase was washed with Et_2O (2 x 150 mL) and the combined organic extracts washed with H_2O (100 mL), dried over anhydrous Na_2SO_4 and concentrated *in vacuo* to yield tosylate **63** as a colourless oil (11.2 g, 82%). $[\alpha]_D^{25}$ = 4.78 (*c* = 1.1 g/100mL, $CHCl_3$); IR ($CHCl_3$ cast) 2966, 2934, 2879, 1361 cm^{-1}; ^{1}H NMR ($CDCl_3$, 500 MHz): δ 7.79 (d, 2H, *J* = 8.5 Hz, ortho-ArH), 7.34 (d, 2H, *J* = 7.9 Hz, meta-ArH), 3.88 (dd, 1H, *J* = 9.4, 5.90, OC<u>H</u>H), 3.81 (dd, 1H, *J* = 9.4, 6.40, OCH<u>H</u>), 2.45 (s, 3H, ArC<u>H</u>$_3$), 1.75-1.66 (m, 1H, C<u>H</u>CH_2O), 1.44-1.34 (m, 1H, C<u>H</u>HCH_3), 1.20-1.09 (m, 1H, CH<u>H</u>CH_3), 0.88 (d, 3H, *J* = 6.8 Hz, CHC<u>H</u>$_3$), 0.83 (t, 3H, *J* = 7.5 Hz, CH_2C<u>H</u>$_3$); ^{13}C NMR ($CDCl_3$, 125 MHz): δ 144.7, 133.4, 129.9, 128.0, 75.0, 34.5, 25.6, 21.8, 16.1, 11.1; HRMS (ES) Calcd for $C_{12}H_{18}NaO_3S$ $[M+Na]^+$ 265.0869,

found 265.0867.

(2*R*)-Methylbutyltosylate (64)

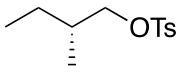

64

Product was isolated as a colourless oil (5.45 g, 66%). $[\alpha]_D^{25}$ = -4.3 (*c* = 1.1 g/100mL, $CHCl_3$); IR ($CHCl_3$ cast) 2966, 2934, 2879, 1360 cm^{-1}; ^1H NMR ($CDCl_3$, 500 MHz): δ 7.79 (d, 2H, *J* = 8.3 Hz, ortho-ArH), 7.34 (d, 2H, *J* = 7.4 Hz, meta-ArH), 3.83 (dd, 1H, *J* = 9.38, 5.90, OC<u>H</u>H), 3.77 (dd, 1H, *J* = 9.38, 6.40, OCH<u>H</u>), 2.40 (s, 3H, ArC<u>H</u>$_3$), 1.66 (ddt, 1H, *J* = 13.1, 6.6 Hz, C<u>H</u>CH_2O), 1.38-1.30 (m, 1H, C<u>H</u>HCH_3), 1.14-1.05 (m, 1H, CH<u>H</u>CH_3), 0.83 (d, 3H, *J* = 6.8 Hz, CHC<u>H</u>$_3$), 0.78 (t, 3H, *J* = 7.5 Hz, CH_2C<u>H</u>$_3$); ^{13}C NMR ($CDCl_3$, 125 MHz): δ 144.7, 133.3, 129.9, 128.0, 74.9, 34.4, 25.5, 21.7, 16.0, 11.0; HRMS (ES) Calcd for $C_{12}H_{18}NaO_3S$ $[M+Na]^+$ 265.0869, found 265.0868.

2-(1-(6*S*)-Methyloctyl)-1,3-dioxolane (66)

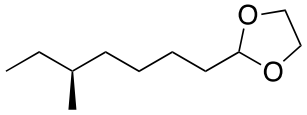

66

Magnesium turnings were removed from the oven and ground with a mortar and pestle. The magnesium (0.54 g, 22.0 mmol) was then added to a flame-dried flask under argon and suspended in dry THF (6 mL). A small crystal of I_2 was added and the mixture refluxed until the brown colour disappeared. The flask was then removed from the oil bath and the bromo dioxolane (1.52 mL, 11.0 mmol) added slowly. Upon initiation of the reaction, the addition was adjusted to maintain a smooth reflux. The mixture was then

heated to reflux for 3 h and cooled to ambient temperature. The Grignard reagent was titrated using the I_2/LiCl method[210] and found to have a concentration of 1 M. In a separate flask, tosylate **63** (0.5 g, 2.1 mmol) and anhydrous $CuCl_2$ (24 mg, 0.11 mmol) were dissolved in dry THF (6 mL) under argon and cooled to – 10 ^oC. The Grignard solution (1 M in THF, 2.5 mL, 2.5 mmol) was added dropwise and the resulting brown solution stirred at ambient temperature for 2 h. The mixture was diluted with saturated NH_4Cl (5 mL) and washed with Et_2O (3 x 10 mL). The combined organic extracts were washed with brine, dried over anhydrous Na_2SO_4, concentrated *in vacuo* and purified by flash column chromatography (SiO_2, 9:1 hexanes:EtOAc) to yield the product as a colourless oil (235 mg, 60%). $[\alpha]_D^{25}$ = 6.98 (*c* = 0.55 g/100mL, $CHCl_3$); IR ($CHCl_3$ cast) 2957, 2928, 2875 cm^{-1}; ^1H NMR ($CDCl_3$, 500 MHz): δ 4.84 (t, 1H, *J* = 4.90, OC<u>H</u>O), 3.97-3.93 (m, 2H, OCH<u>H</u>), 3.87-3.83 (m, 2H, OC<u>H</u>H), 1.67-1.64 (m, 2H, OCHC<u>H</u>$_2$), 1.42-1.28 (m, 7H), 1.13-1.09 (m, 2H, C<u>H</u>$_2$CH$_3$), 0.86-0.83 (m, 6H, 2 x CH_3); ^{13}C NMR ($CDCl_3$, 125 MHz): δ 104.9, 65.0, 36.6, 34.4, 34.1, 29.6, 27.2, 24.6, 19.4, 11.5.

2-(1-(6*R*)-methyloctyl)-1,3-dioxolane (67)

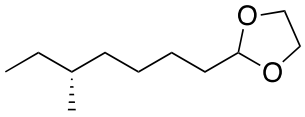

67

Product isolated as a colourless oil (0.65 g, 85%). $[\alpha]_D^{25}$ = -7.02 (*c* = 0.55 g/100mL, $CHCl_3$); IR ($CHCl_3$ cast) 2957, 2928, 2875 cm^{-1}; ^1H NMR ($CDCl_3$, 500 MHz): δ 4.84 (t, 1H, *J* = 4.90, OC<u>H</u>O), 3.97-3.95 (m, 2H, OCH<u>H</u>), 3.85-3.83 (m, 2H, OC<u>H</u>H), 1.67-1.63 (m, 2H, OCHC<u>H</u>$_2$), 1.46-1.25 (m, 7H), 1.16-1.07 (m, 2H, C<u>H</u>$_2$CH$_3$), 0.86-0.83 (m, 6H, 2 x CH_3); ^{13}C NMR ($CDCl_3$, 125 MHz): δ 104.9, 65.0, 36.6, 34.4, 34.1, 29.6, 27.2, 24.6,

19.3, 11.5.

(6*S*)-Methyloctanoic acid (56)

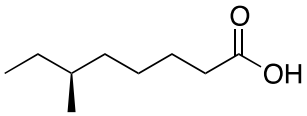

56

Dioxolane **66** (186 mg, 1.0 mmol) was dissolved in THF (10 mL) and 1 M HCl (10 mL) and stirred at 50 ^{o}C for 5 h. The reaction mixture was then added to a stirring solution of sat. $NaHCO_3$ (30 mL) and the organic layer separated. The aqueous layer was washed with CH_2Cl_2 (3 x 15 mL) and the combined organic extracts washed with brine (30 mL), dried over anhydrous Na_2SO_4 and concentrated *in vacuo*. The crude fragrant aldehyde (1.0 mmol) was then dissolved in *t*-BuOH (5 mL) and H_2O (1 mL) and stirred at ambient temperature. 1-Methyl-2-butene (3.18 mL, 30.0 mmol), NaH_2PO_4 (360 mg, 3.0 mmol) and $NaClO_2$ (181 mg, 2.0 mmol) were added sequentially and the resulting yellow solution stirred at ambient temperature for 1 h. A solution of sat. NH_4Cl (5 mL) and CH_2Cl_2 (30 mL) were added and the organic layer separated. The aqueous layer was washed with CH_2Cl_2 (2 x 10 mL) and the combined organic extracts dried over anhydrous Na_2SO_4 and concentrated *in vacuo*. The crude reaction was purified by flash column chromatography (SiO_2, 9:1 hexanes:EtOAc + 0.1 % AcOH) to yield (6*S*)-Methyloctanoic acid (**3**) as a colourless liquid (73 mg, 46 %). $[\alpha]_D^{25}$ = 7.38 (*c* = 1.0 g/100mL, $CHCl_3$), lit[140] $[\alpha]_D^{25}$ = -7.9 (*c* = 0.9 g/100mL, $CHCl_3$); IR ($CHCl_3$ cast) 2961, 2931, 2874, 1711 cm^{-1}; ^{1}H NMR ($CDCl_3$, 500 MHz): δ 2.39-2.37 (m, 2H, C(O)C$\underline{H}_2$), 1.66-1.54 (m, 2H, C(O)CH$_2$C$\underline{H}_2$), 1.36-1.08 (m, 9H), 0.87-0.84 (m, 6H, 2 x CH_3); ^{13}C NMR ($CDCl_3$, 125 MHz): δ 180.4, 36.4, 34.4 (2 overlapping signals), 29.6, 26.8, 25.4, 19.3,

11.5; HRMS (ES) Calcd for $C_9H_{17}O_2$ $[M-H]^-$ 157.1234, found 157.1232.

(6*R*)-Methyloctanoic acid (57)

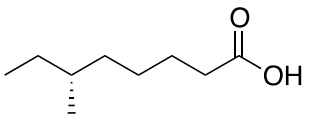

57

$[\alpha]_D^{25}$ = -5.38 (*c* = 1.0 g/100mL, $CHCl_3$), lit[140] $[\alpha]_D^{25}$ = -5.7 (*c* = 0.8 g/100mL, $CHCl_3$); IR ($CHCl_3$ cast) 2961, 2932, 2874, 1711 cm^{-1}; ^1H NMR ($CDCl_3$, 500 MHz): δ 2.36 (t, 2H, *J* = 7.5, C(O)C$\underline{H_2}$), 1.67-1.57 (m, 2H, C(O)CH_2C$\underline{H_2}$), 1.39-1.28 (m, 5H), 1.15-1.09 (m, 2H, C$\underline{H_2}CH_3$), 0.86-0.84 (m, 6H, 2 x CH_3); ^{13}C NMR ($CDCl_3$, 125 MHz): δ 180.4, 36.3, 34.3 (2 overlapping signals), 29.6, 26.7, 25.2, 19.3, 11.5; HRMS (ES) Calcd for $C_9H_{17}O_2$ $[M-H]^-$ 157.1234, found 157.1234.

(6*S*)-TriB$_1$ (69)

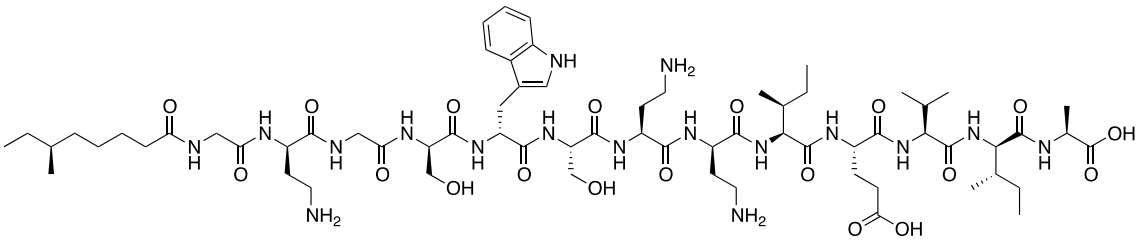

69

Product eluted at 31.1 min (HPLC method 2) and was isolated as a white powder (7 mg, 19%). ^1H NMR (D_2O, 600 MHz): δ 7.57 (d, 1H, *J* = 8.1 Hz, D-Trp5-ArH), 7.46 (d, 1H, *J* = 8.1 Hz, D-Trp5-ArH), 7.21-7.19 (m, 2H, D-Trp5-ArH), 7.11 (t, 1H, *J* = 7.1 Hz, D-Trp5-ArH), 4.63-4.60 (1H, m, D-Trp5-Hα), 4.46-4.44 (m, 1H, D-Ser4-Hα), (m, 2H, D-Dab2-Hα + D-Dab8-Hα), 4.36-4.31 (m, 3H, Dab7-Hα + Glu10-Hα + D-alle12-Hα), 4.22-4.18 (m, 1H, Ala13-Hα), 4.16-4.10 (m, 3H, Ser6-Hα + Ile9-Hα + Val11-Hα), 3.90 (s, 2H, Gly3-

Hα), 3.88 (s, 2H, Gly1-Hα), 3.80-3.73 (m, 2H, D-Ser4-Hβ), 3.56-3.54 (m, 1H, Ser6-Hβ), 3.30-3.25 (m, 3H, D-Trp5-Hβ + Ser6-Hβ), 3.06-2.94 (m, 6H, D-Dab2-Hγ + Dab7-Hγ + D-Dab8-Hγ), 2.36-1.79 (m, 15H, Lipid-Hα + D-Dab2-Hβ + Dab7-Hβ + D-Dab8-Hβ + Ile9-Hβ + Glu10-Hβ + Glu10-Hγ + Val11-Hβ + D-aIle12-Hβ), 1.53-1.47 (m, 2H, Lipid-Hβ), 1.41-0.99 (m, 14H, Lipid-Hγ, Hδ, Hε, Hζ + Ile9-Hγ + D-aIle12-Hγ Ala13-Hβ), 0.92-0.75 (m, 24H, Lipid-Hζ, Hη + Ile9- Hγ, Hδ + Val11-Hγ + D-aIle12-Hγ, Hδ). HRMS (ES) Calcd for $C_{67}H_{112}N_{17}O_{19}$ $[M+H]^+$ 1458.8315, found 1458.8327.

(6'*R*)-TriB$_1$ (70)

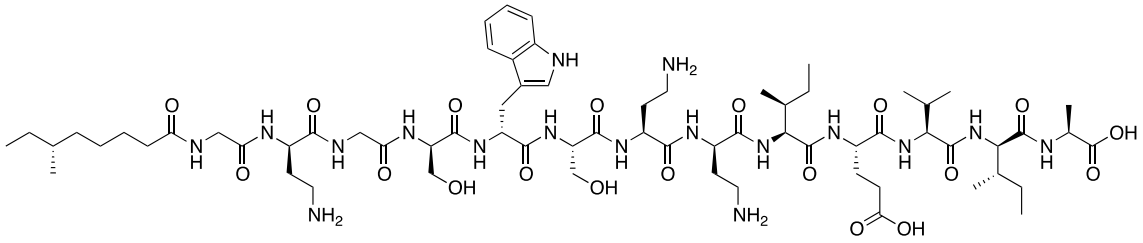

70

Product eluted at 31.1 min (HPLC method 2) and was isolated as a white powder (8 mg, 22%). ^{1}H NMR (D_2O, 600 MHz): ^{1}H NMR (D_2O, 600 MHz): δ 7.57 (d, 1H, *J* = 8.1 Hz, D-Trp5-ArH), 7.47 (d, 1H, *J* = 8.1 Hz, D-Trp5-ArH), 7.22-7.19 (m, 2H, D-Trp5-ArH), 7.12 (t, 1H, *J* = 7.4 Hz, D-Trp5-ArH), 4.62 (1H, t, *J* = 7.3 Hz, D-Trp5-Hα), 4.45 (t, 1H, *J* = 5.1 Hz, D-Ser4-Hα), 4.43-4.39 (m, 2H, D-Dab2-Hα + D-Dab8-Hα), 4.37-4.32 (m, 3H, Dab7-Hα + Glu10-Hα + D-aIle12-Hα), 4.22-4.18 (m, 1H, Ala13-Hα), 4.15-4.11 (m, 3H, Ser6-Hα + Ile9-Hα + Val11-Hα), 3.90 (s, 2H, Gly3-Hα), 3.88 (s, 2H, Gly1-Hα), 3.80-3.73 (m, 2H, D-Ser4-Hβ), 3.56-3.54 (m, 1H, Ser6-Hβ), 3.30-3.25 (m, 3H, D-Trp5-Hβ + Ser6-Hβ), 3.06-2.94 (m, 6H, D-Dab2-Hγ + Dab7-Hγ + D-Dab8-Hγ), 2.36-1.79 (m, 15H, Lipid-Hα + D-Dab2-Hβ + Dab7-Hβ + D-Dab8-Hβ + Ile9-Hβ + Glu10-Hβ + Glu10-Hγ + Val11-Hβ + D-

alle12-Hβ), 1.53-1.47 (m, 2H, Lipid-Hβ), 1.41-0.99 (m, 14H, Lipid-Hγ, Hδ, Hε, Hζ + Ile9-Hγ + D-alle12-Hγ Ala13-Hβ), 0.92-0.75 (m, 24H, Lipid-Hζ, Hη + Ile9- Hγ, Hδ + Val11-Hγ + D-alle12-Hγ, Hδ). HRMS (ES) Calcd for $C_{67}H_{112}N_{17}O_{19}$ $[M+H]^+$ 1458.8315, found 1458.8322.

(1*R*, 2*R*)-2-(2,3-Anthracenedicarboximido)cyclohexanol (71)

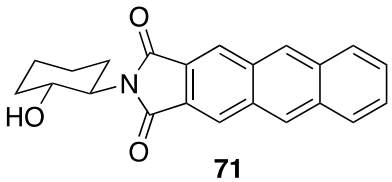

71

This compound was synthesized according to a modified literature procedure.[141] 2,3-Anthracenedicarboxylic acid anhydride (**73**) (100 mg, 0.403 mmol) was added to dry toluene (35 mL) and heated to reflux (oil bath, 140 ^oC). A solution of (1*R*,2*R*)-2-aminocyclohexanol (**72**) (65 mg, 0.564 mmol) in dry DMF (10 mL) was added to the reaction mixture, at which point all solids dissolved. Dry DIPEA (3 mL) was then added and the resulting solution refluxed for 16 h. Most of the solvent (35 mL) was then removed using a Dean-Stark tube and the resulting solution cooled to ambient temperature. EtOAc (70 mL) was added and the resulting solution washed with 0.2 M NaOH (50 mL), 0.2 M HCl (50 mL) and saturated $NaHCO_3$ (50 mL). The organic phase was then dried over anhydrous Na_2SO_4 and concentrated *in vacuo* to yield alcohol **71** as a yellow powder (135 mg, 97%). $[\alpha]_D^{25}$ = -34.99 (*c* = 0.212 g/100mL, DMF); IR ($CHCl_3$ cast) 3525, 2926, 2856, 1764, 1699 cm^{-1}; ^1H NMR (d_6-DMSO, 500 MHz): δ 8.87 (s, 2H, H8), 8.59 (s, 2H, H7), 8.15-8.13 (m, 2H, H10), 7.64-7.63 (m, 2H, H9), 4.93 (d, 1H, *J* = 4.72 Hz, OH), 4.12-4.06 (m, 1H, H1), 3.84 (ddd, 1H, *J* = 12.8, 9.7, 3.4 Hz, H2),

2.14-2.06 (m, 1H, H3(eq)), 1.96-1.90 (m, 1H, H6(eq)), 1.73-1.64 (m, 3H, H3(ax) + H4(eq) + H4(ax)), 1.32-1.17 (m, 3H, H6(ax) + H5(eq) + H5(ax)); ^{13}C NMR (d_6-DMSO, 125 MHz): δ 167.5, 132.6, 131.6, 129.9, 128.3, 127.5, 126.6, 125.0, 67.6, 57.3, 34.7, 28.2, 25.0, 24.2; HRMS (ES) Calcd for $C_{22}H_{20}NO_3$ $[M+H]^+$ 346.1438, found 346.1432.

(1*R*,2*R*)-1-((6*S*)-Methyloctyl)-2-(2,3-anthracenedicarboximido) cyclohexanoate (74)

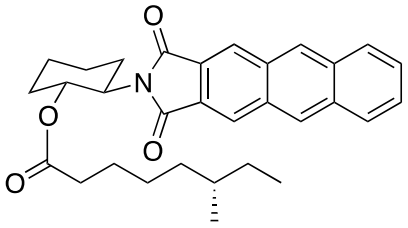

74

(6*S*)-Methyloctanoic acid (**56**) (6.0 mg, 37.9 µmol) and EDCI.HCl (12.0 mg, 62.6 µmol) were dissolved in a 1:1:1 mixture of dry CH_2Cl_2, toluene and DMF (0.9 mL). Alcohol **71** (14.4 mg, 41.7 µmol) was added, followed by DMAP (1.5 mg, 12.2 µmol). The resulting cloudy yellow solution was stirred at ambient temperature for 16 h, clarifying as the reaction progressed. The reaction mixture was diluted with EtOAc (9 mL) and washed with sat. $NaHCO_3$ (5 mL), 10% citric acid (5 mL), water (5 mL) and brine (5 mL), dried over anhydrous Na_2SO_4 and concentrated *in vacuo*. The crude product was dissolved in CH_2Cl_2 (0.5 mL) and purified by preparatory TLC (Analtech Silica Gel GF, 20 x 20 cm, 500 microns), eluting with 2:1 hexanes:EtOAc. The product eluted as a thin yellow band (R_f ~ 0.6) and was isolated as a yellow solid (15 mg, 82%). $[\alpha]_D^{25}$ = -29.46 (*c* = 0.30 g/100mL, DMF); IR ($CHCl_3$ cast) 2928, 2859, 1772, 1731, 1707 cm^{-1}; ^{1}H NMR ($CDCl_3$, 500 MHz): δ 8.63 (s, 2H, Anth9, Anth10), 8.49 (s, 2H, Anth5, Anth8), 8.10-8.07 (m, 2H, Anth2, Anth3), 7.63-7.60 (m, 2H, Anth1, Anth4), 5.57 (ddd, 1H, *J* = 10.7, 4.7, 4.7 Hz,

NCH), 4.31 (ddd, 1H, *J* = 12.6, 10.5, 4.3 Hz, OCH), 2.48 (dddd, 1H, *J* = 13.0, 13.0, 13.0, 3.4 Hz, OCHCH(eq)), 2.26-2.21 (m, 1H, NCHCH(eq)), 2.09 (t, 2H, *J* = 7.5 Hz, lipid-Hα), 1.93-1.81 (m, 3H, OCHCH(ax) + $OCHCH_2CH$(eq) + $NCHCH_2CH$(eq)), 1.57-1.26 (m, 5H, NCHCH(ax) + $NCHCH_2CH$(ax) + $OCHCH_2CH$(ax) + lipid-Hβ), 1.05-0.66 (m, 7H, lipid-Hγ, Hδ, Hε, Hζ), 0.60 (t, 3H, *J* = 7.4 Hz, Lipid-Hη), 0.56 (d, 3H, *J* = 6.5 Hz, Lipid-Hζ); ^{13}C NMR ($CDCl_3$, 125 MHz): δ173.2, 167.8, 133.4, 132.2, 130.2, 128.6, 127.6, 126.5, 125.9, 71.7, 54.3, 36.2, 34.7, 34.1, 31.9, 29.4, 28.7, 26.5, 25.5, 25.3, 24.1, 19.0, 11.3; HRMS (ES) Calcd for $C_{31}H_{35}NNaO_4$ $[M+Na]^+$ 508.2458, found 508.2448.

(1*R*,2*R*)-1-((6*R*)-methyloctyl)-2-(2,3-anthracenedicarboximido) cyclohexanoate (75)

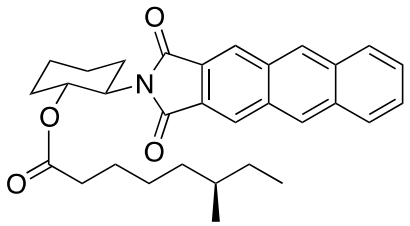

75

Product isolated as a yellow solid (16.5 mg, 90%). $[\alpha]_D^{25}$ = -37.39 (*c* = 0.30 g/100mL, DMF); IR ($CHCl_3$ cast) 2929, 2859, 1764, 1731, 1706 cm^{-1}; ^{1}H NMR ($CDCl_3$, 500 MHz): δ 8.61 (s, 2H, Anth9, Anth10), 8.48 (s, 2H, Anth5, Anth8), 8.08-8.06 (m, 2H, Anth2, Anth3), 7.62-7.60 (m, 2H, Anth1, Anth4), 5.57 (ddd, 1H, *J* = 10.7, 4.7, 4.7 Hz, NCH), 4.31 (ddd, 1H, *J* = 12.6, 10.5, 4.2 Hz, OCH), 2.48 (dddd, 1H, *J* = 13.0, 13.0, 13.0, 3.4 Hz, OCHCH(eq)), 2.25-2.21 (m, 1H, NCHCH(eq)), 2.14-2.04 (m, 2H, lipid-Hα), 1.91-1.82 (m, 3H, OCHCH(ax) + $OCHCH_2CH$(eq) + $NCHCH_2CH$(eq)), 1.59-1.20 (m, 5H, NCHCH(ax) + $NCHCH_2CH$(ax) + $OCHCH_2CH$(ax) + lipid-Hβ), 1.05-0.67 (m, 7H, lipid-Hγ, Hδ, Hε, Hζ), 0.59 (t, 3H, *J* = 7.4 Hz, Lipid-Hη), 0.52 (d, 3H, *J* = 6.5 Hz, Lipid-Hζ); ^{13}C

NMR ($CDCl_3$, 125 MHz): δ173.1, 167.8, 133.4, 132.1, 130.1, 128.6, 127.6, 126.5, 125.9, 71.7, 54.3, 36.1, 34.7, 34.0, 31.9, 29.4, 28.6, 26.5, 25.5, 25.3, 24.1, 18.9, 11.3; HRMS (ES) Calcd for $C_{31}H_{36}NO_4$ $[M+H]^+$ 486.2639, found 486.2639.

Hydrolysis of tridecaptin B_1 and derivatisation of resulting methyloctanoate

Tridecaptin B_1 (3 mg, 2.06 μmol) was dissolved in 6M HCl (4 mL) and stirred at 110 ^oC for 3 h in a pressure tube. The reaction mixture was then cooled to ambient temperature and extracted with Et_2O (3 x 5 mL). The organic layer was dried over anhydrous Na_2SO_4 and concentrated *in vacuo* to yield crude 6-methyloctanoic acid (assumed 2.06 μmol). This residue was dissolved in a dry 1:1:1 mixture of CH_2Cl_2/toluene/DMF (150 μL) and to this solution was added EDCI.HCl (1.2 mg, 6.17 μmol), alcohol **71** (2.1 mg, 6.17 μmol) and DMAP (0.2 mg, 1.64 μmol). The resulting yellow solution was stirred at ambient temperature for 22 h and then loaded directly on to a preparatory TLC plate (Analtech Silica Gel GF, 20 x 20 cm, 500 microns) and eluted with 2:1 hexanes:EtOAc. The product eluted as a thin yellow band (R_f = 0.60) and was isolated as a yellow oil (300 μg, 30% over 2 steps). This product was dissolved in $CDCl_3$ (300 μL) and analysed by ^{1}H-NMR for comparison with **74** and **75**. HPLC analysis was then performed using method 3.

Di-*tert*-butyl-(2*S*)-4,6-dioxo-1,2-piperidinedicarboxylate (78)

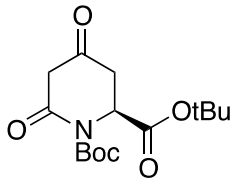

78

To a solution of Boc-Asp-O^{t}Bu (5.00 g, 17.3 mmol) in dry CH_2Cl_2 (70.0 mL) under argon were added EDCI.HCl (4.97 g, 25.9 mmol), DMAP (3.16 g, 25.9 mmol) and Meldrum's acid (2.49 g, 17.3 mmol) sequentially at 0 ^{o}C with stirring. The resultant orange solution was allowed to equilibrate to ambient temperature and was stirred for 3 h, after which time the reaction mixture was transferred to a separatory funnel and washed with 1N $KHSO_4$ (2 x 70 mL). The organic phase was then isolated and dried over anhydrous Na_2SO_4, and the solvent removed by rotary evaporation to yield a green residue. The residue was subsequently dissolved in EtOAc, heated to 85 ^{o}C in an oil bath and left to reflux overnight. After allowing the solution to cool to ambient temperature the mixture was washed with 1N $KHSO_4$ (2 x 70 mL) and brine (70 mL). The organic phase was collected and dried over Na_2SO_4, before concentrating in vacuo to produce a dark green solid. The crude product was finally purified by flash column chromatography on silica gel using EtOAc (100 %) as the eluent to afford the pure product as a powdery white solid (5.30 g, 98%). $[\alpha]^{20}_{D}$ + 91.6 (*c* 1.00, $CHCl_3$); IR (KBr disc): 3200, 2980, 2934, 1731; ^{1}H-NMR ($CDCl_3$, 400 MHz): δ 5.05 (dd, 1H, *J* = 6.9, 2.1 Hz, Hα), 3.51 (d, 1H, *J* = 19.5 Hz, Hδ), 3.36 (d, 1H, *J* = 19.5 Hz, Hδ), 3.02 (dd, 1H, *J* = 17.7, 1.9 Hz, Hβ), 2.82 (dd, 1H, *J* = 6.9, 17.7 Hz, Hβ), 1.54 (s, 9H, tBu), 1.50 (s, 9H, tBu); ^{13}C-NMR ($CDCl_3$, 125 MHz): δ 200.3, 169.1, 165.5, 151.4, 84.8, 84.1, 54.8, 50.6, 41.1, 28.1, 28.0; HRMS (ESI^{+}) calcd. for $C_{15}H_{23}NNaO_6$ ($[M+Na]^{+}$) 336.1418; found 336.1419.

Di-*tert*-butyl (*2S*,4*S*)-4-hydroxy-6-oxo-1,2-piperidinedicarboxylate (79)

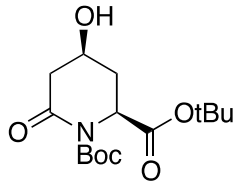

79

Ketone **78** (5.30 g, 16.9 mmol) was placed in a flame dried, argon filled round-bottomed flask equipped with a stirring bar. The solid was then dissolved in freshly distilled CH_2Cl_2 (85.1 mL) and the contents cooled to 0 ^oC. At this temperature, 10 % (v/v) AcOH (9.45 mL) was slowly added to the stirred solution via hypodermic syringe. After 5 min of stirring, sodium borohydride (1.45 g, 38.3 mmol) was added carefully to the reaction vessel over a period of 3 min to avoid vigorous effervescence. After addition of the reducing agent, the flask was sealed with a vented Teflon cap and the solution was left to stir for three days. After this time the cloudy yellow solution was quenched with water (100 mL) at 0 ^oC and was left to stir for a further 10 min. The contents of the reaction vessel were then partitioned, and the organic phase was concentrated in vacuo yielding a yellow solid. This solid was redissolved in EtOAc (100 mL), and was washed with saturated $NaHCO_3$ (100 mL), water (100 mL) and brine (100 mL). The isolated organic phase was then dried over anhydrous Na_2SO_4 and the solvent removed in vacuo to produce a yellow solid. The crude product was transferred to a beaker where it was purified by recrystallization from hot CH_2Cl_2. On complete dissolution of the solid in the minimum amount of hot solvent, diisopropyl ether was added until incipient turbidity was observed. The solution was allowed to cool to ambient temperature and then 0 ^oC before filtering the solid under vacuum. Using the same technique, additional material was recovered by further recrystallization of the orange/brown mother liquor. The

product was isolated as a white crystalline solid (2.24 g, 41 %, de >99 %). $[\alpha]^{20}_{D}$ – 24.5 (*c* 1.00, $CHCl_3$); IR ($CHCl_3$ cast): 3492, 2980, 2933, 1774, 1726; ^{1}H-NMR ($CDCl_3$, 400 MHz): δ 4.65 (dd, 1H, *J* = 6.67, 2.86 Hz, Hα), 4.26 (m, 1H, Hγ), 2.78 (ddd, 1H, *J* = 17.3, 5.0, 0.7 Hz, Hδ), 2.64 (ddd, 1H, *J* = 17.3, 4.3, 1.9 Hz, Hδ), 2.40 (m, 1H, Hβ), 2.23 (ddd, 1H, *J* = 14.2, 3.0, 2.9 Hz, Hβ), 1.99 (d, 1H, *J* = 4.9 Hz, OH), 1.52 (s, 9H, tBu), 1.47 (s, 9H, tBu); ^{13}C-NMR ($CDCl_3$, 125 MHz): δ 171.2, 168.5, 147.8, 83.5, 82.5, 64.3, 56.2, 43.3, 33.0, 28.0, 27.8; HRMS (ESI^+) calcd. for $C_{15}H_{25}NNaO_6$ ($[M+Na]^+$) 338.1574; found 338.1574.

Di-*tert*-butyl-(2*S*,4*S*)-4-[(*tert*-butyldiphenylsilyl)oxy]-6-oxo-1,2-piperidinedicarboxylate (80)

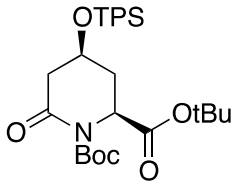

80

Imidazole (1.93 g, 28.4 mmol) and *tert*-butyl(chloro)diphenyl silane (3.90 g) were added to a solution of alcohol **79** (2.24 g, 7.10 mmol) in anhydrous CH_2Cl_2 (100 mL) at 0 ^{o}C. On addition of all components, the reaction mixture was warmed to ambient temperature and stirred for 16 h. The solvent was then removed from the mixture under reduced pressure, and was directly replaced with EtOAc (100 mL). The resultant solution was then extracted with 1 N $KHSO_4$ (100 mL), water (100 mL) and brine (100 mL). The isolated organic phase was dried over Na_2SO_4, and the filtrate was concentrated in vacuo to yield the crude product, which was finally purified by flash column chromatography using 6:1 hexanes/EtOAc as the eluent. The pure product was

isolated as a colourless oil (3.61 g, 92 %). $[\alpha]^{20}_{D}$ – 17.1 (*c* 1.00, $CHCl_3$); IR ($CHCl_3$ cast): 3072, 3049, 2979, 2932, 2893, 2859, 1782, 1727; ^{1}H-NMR ($CDCl_3$, 400 MHz): δ 7.63 (m, 4H, Ar-H), 7.40 (m, 6H, Ar-H), 4.30 (dd, 1H, *J* = 8.3, 6.6 Hz, Hα), 4.02 (m, 1H, Hγ), 2.65 (ddd, 1H, *J* = 16.6, 5.4, 2.0 Hz, Hδ), 2.53 (dd, 1H, $H_δ$), 2.26 (m, 1H, *J* = 16.6, 9.2 Hz, Hβ), 2.02 (m, 1H, Hβ), 1.47 (s, 9H, tBu), 1.45 (s, 9H, tBu), 1.07 (s, 9H, tBu); ^{13}C-NMR ($CDCl_3$, 125 MHz): δ 170.0, 168.7, 152.0, 135.7, 133.4, 133.1, 130.0, 127.8, 83.6, 82.3, 65.0, 56.6, 44.1, 34.8, 29.0 27.9, 26.9, 19.0; HRMS (ESI^+) calcd. for $C_{31}H_{43}NNaO_6Si$ ($[M+Na]^+$) 576.2752; found 576.2749.

tert-Butyl-(2*S*,4*S*)-2-[(_tert_-butoxycarbonyl)amino]-4-[(_tert_-butyldiphenylsilyl)oxy]-6-hydroxyhexanoate (81)

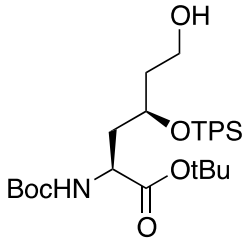

81

Lactam **80** (3.38 g, 6.09 mmol) was dissolved in anhydrous EtOH (47.6 mL) in a flame dried, argon filled round-bottomed flask. The contents were cooled to 0 ^{o}C, at which temperature sodium borohydride (1.15 g, 30.5 mmol) was added portion-wise to the reaction vessel. The cloudy solution was allowed to equilibrate to ambient temperature and stir overnight. The reaction was then quenched by the addition of water (548 µL, 30.5 mmol), and the solution was stirred for a further 10 min at ambient temperature. The solvent was removed by rotary evaporation at reduced pressure, and the resultant

residue was dissolved in EtOAc (50 mL) and partitioned with water (50 mL). The aqueous phase was further extracted with EtOAc (30 mL), and the combined organic phases were washed with brine (50 mL), and then dried over anhydrous Na_2SO_4. The solvent was removed by rotary evaporation, and the crude product was subject to purification by flash column chromatography on silica gel using 2:1 hexanes/EtOAc as the eluent. The product was isolated as a colourless oil (0.77 g, 23 %). $[\alpha]^{20}_D$ + 5.04 (*c* 1.00, $CHCl_3$); IR ($CHCl_3$ cast): 2976, 2931, 2858, 1718; ^{1}H-NMR ($CDCl_3$, 500 MHz): δ 7.70 (m, 4H, Ar-H), 7.41 (m, 6H, Ar-H), 5.28 (bd, 1H, *J* = 6.2 Hz, NH), 4.06 (m, 2H, Hα + Hγ), 3.56 (m, 2H, Hε), 1.95 (m, 2H, Hβ), 1.75 (m, 2H, Hδ), 1.67 (m, 1H, OH), 1.43 (s, 9H, tBu), 1.36 (s, 9H, tBu), 1.06 (s, 9H, tBu); ^{13}C-NMR ($CDCl_3$, 125 MHz): 171.7, 155.4, 135.9, 135.8, 133.7, 133.3, 129.9, 129.8, 127.8, 127.7, 81.6, 79.5, 69.7, 59.1, 52.0, 38.4, 38.3, 28.3, 28.0, 27.0, 19.3; HRMS (ESI^+) calcd. for $C_{31}H_{48}NO_6Si$ ($[M+H]^+$) 558.3245; found 558.3236.

tert-Butyl-(2*S*,4*S*)-6-Azido-2-[(_tert_-butoxycarbonyl)-amino]-4-[(_tert_-butyldiphenylsilyl)oxy]hexanoate (82)

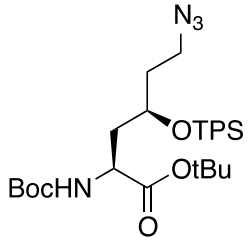

82

DIPEA (332 µL, 1.91 mmol) was added to a stirred solution of alcohol **81** (0.71 g, 1.27 mmol) in CH_2Cl_2 (21 mL) at ambient temperature. On cooling the solution to 0 ^oC, methanesulfonyl chloride (148 µL, 1.91 mmol) was added dropwise over 30 s via

hypodermic syringe. The solution was then left to return to ambient temperature and stir for 2 h. After this time, the reaction was quenched with water (11.5 µL, 0.64 mmol) and the solvent was then removed in vacuo, and directly replaced with EtOAc (21.2 mL). The organic phase was transferred to a separatory funnel where the solution was treated with consecutive washings of 1N $KHSO_4$ (21.2 mL), water (21.2 mL), $NaHCO_3$ (21.2 mL) and brine (21.2 mL). The isolated organic phase was then dried over Na_2SO_4, and the filtrate was concentrated in vacuo. The colourless residue was dissolved in DMF (10.6 mL), and was transferred to a round-bottomed flask equipped with a stirring bar. Sodium azide (0.247 g, 3.81 mmol) was added to the stirred solution, which was then fitted with a condenser before heating to 80 ^oC for 16 h. The reaction mixture was cooled to ambient temperature, quenched with water (30 mL) and left to stir for a further 5 min. EtOAc (90 mL) was added to the biphasic mixture which was then transferred to a separating funnel where the layers were partitioned. The aqueous phase was further extracted with EtOAc (2 x 40 mL). The combined organic fractions were subsequently treated with brine, dried over anhydrous Na_2SO_4 and concentrated in vacuo. The crude product was purified by flash column chromatography on silica gel using 9:1 hexanes/EtOAc as the eluent to yield a colourless oil (0.50 g, 68%). $[\alpha]^{20}_D$ – 9.45 (*c* 1.00, $CHCl_3$); IR ($CHCl_3$ cast): 2977, 2933, 2858, 2097, 1716; ^{1}H-NMR ($CDCl_3$, 500 MHz): δ 7.68 (m, 4H, Ar-H), 7.42 (m, 6H, Ar-H), 5.19 (bd, 1H, *J* = 6.4 Hz, NH), 4.12 (m, 1H, Hα), 3.95 (m, 1H, Hα), 3.17 (t, 2H, Hε), 1.92 (m, 2H, Hβ), 1.72 (m, 2H, Hδ), 1.43 (s, 9H, ^{t}Bu), 1.38 (s, 9H, ^{t}Bu), 1.06 (s, 9H, ^{t}Bu); ^{13}C-NMR ($CDCl_3$, 125 MHz): 171.6, 155.3, 135.9, 135.8, 133.6, 133.1, 129.9, 127.8, 81.7, 79.6, 69.0, 51.9, 47.6, 38.7, 35.3, 28.4, 27.9, 27.0, 19.3; HRMS (ESI^+) calcd. for $C_{31}H_{46}N_4O_5Si$ ($[M+H]^+$) 583.3310; found

583.3301.

(2*S*,4*R*)-6-Azido-4-[*tert*-butyldiphenylsilyl)oxy]-2-[(9*H*-flouren-9-ylmethoxy)carbonyl]aminohexanoic Acid (76)

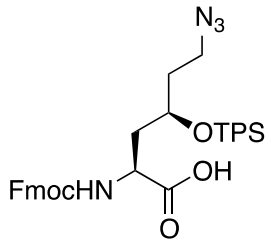

76

To a stirred solution of azide **82** (6.55 g, 0.755 mmol) in CH_2Cl_2 (4.4 mL) at 0 ^oC, was added TFA (6.55 g, 4.40 mL, 57.5 mmol) via hypodermic syringe. The solution was then warmed to reach ambient temperature and stirred for 3 h. The solvent was removed by rotary evaporation and coevaporated with toluene (2 x 4 mL) and Et_2O (4 mL). The concentrated residue was dissolved in acetone (11 mL) and potassium carbonate solution (0.21 M, 11 mL) was subsequently added until a pH ≈ 9 was achieved. Fmoc-OSu (0.306 g, 0.907 mmol) was dissolved in 2 mL acetone, and was then transferred to the reaction vessel. A small additional amount of acetone (approx. 3 mL) was also added to the solution to ensure complete dissolution of all reaction components. After being left to stir overnight, the acetone was removed carefully by rotary evaporation, and the resulting mixture was acidified using 6M HCl until the pH ≈ 2. The aqueous solution was extracted with EtOAc (3 x 20 mL) and the combined organic layers were dried over sodium sulphate, and concentrated in vacuo. The crude product was subject to purification by column chromatography on silica gel using 9:1 CH_2Cl_2/acetone to yield an off-white foam (0.22 g, 45%). $[\alpha]^{20}_D$ + 5.62 (*c* 1.00, MeOH); IR ($CHCl_3$ cast): 3305,

2961, 1545; ^{1}H-NMR ($CDCl_3$, 400 MHz): δ 7.77 (m, 2H, Ar-H), 7.66 (m, 6H, Ar-H), 7.56 (m, 2H, Ar-H), 7.39 (m, 6H, Ar-H), 7.29 (m, 2H, Ar-H), 5.43 (bd, 1H, *J* = 6.5 Hz, NH), 4.45 (m, 1H, Fmoc-CH_2), 4.35 (m, 1H), 4.29 (app. s, 1H, Fmoc-CH), 4.19 (t, 1H, *J* = 5.9 Hz, Hα), 4.00 (m, 1H, Hγ), 3.17 (t, 2H, *J* = 6.5 Hz, Hε), 2.00 (m, 2H, Hβ), 1.75 (m, 2H, Hd), 1.06 (s, 9H, tBu); ^{13}C-NMR ($CDCl_3$, 125 MHz): 144.3, 143.7, 141.5, 141.3, 135.9, 135.8, 133.4, 132.7, 130.2, 130.0, 127.9, 127.8, 127.7, 127.1, 125.1, 124.7, 120.0, 68.4, 67.1, 65.2, 50.4, 47.5, 47.1, 37.2, 35.1, 27.0, 19.3; HRMS (ESI^+) calcd. for $C_{37}H_{40}N_4NaO_5Si$ ($[M+Na]^+$) 671.2666; found 671.2650.

(3*S*)-1-((*S*)-4-Benzyl-2-thioxothiazolidin-3-yl)-3-hydroxy-10-methyldecan-1-one (84)

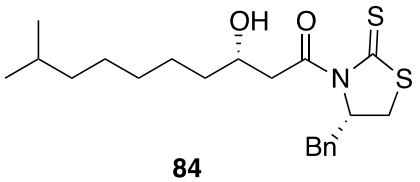

84

Acetate **41** (0.85 g, 3.38 mmol) was placed in a flame dried, argon filled round bottomed flask where it was then dissolved in freshly distilled CH_2Cl_2 (16.9 mL). The solution was cooled to 0 ^{o}C and left to stir before the addition of 1M $TiCl_4$ (3.38 mL, 3.38 mmol, CH_2Cl_2 solution) via hypodermic syringe. The bright orange solution was then stirred for a further 5 min before subsequent cooling to –78 ^{o}C. At this temperature, DIPEA (0.43 g, 0.589 mL, 3.38 mmol) was added, and the resultant dark red mixture was left to stir for another 90 min. A solution of 7-methyloctanal (**83**) (0.48 g, 3.38 mmol) in CH_2Cl_2 (3.30 mL) was added drop wise over 30 s to the reaction mixture, which was then left to stir for a further 90 min. After this time, the solution was quenched by the addition of saturated aqueous ammonium chloride (5.00 mL) at -78 ^{o}C. After allowing the solution

to reach ambient temperature, the layers were separated, and the aqueous phase was further extracted with CH_2Cl_2 (2 x 40 mL). The combined organic fractions were then dried over anhydrous Na_2SO_4, and were concentrated by rotary evaporation at reduced pressure. The crude product was initially purified by flash column chromatography using 9:1 hexanes/EtOAc as the eluent, followed by a 6:1 mixture of the same solvents. The product containing fractions were collected and concentrated in vacuo to yield the product as a yellow crystalline solid (0.66 mg, 50%). $[\alpha]^{20}_D$ + 151.89 (*c* 1.00, $CHCl_3$); IR ($CHCl_3$ cast): 3462, 3027, 2927, 2855, 1692; ^{1}H-NMR ($CDCl_3$, 500 MHz): δ 7.35 (m, 2H, Ar-H), 7.28 (m, 3H, Ar-H), 5.41 (m, 1H, NC<u>H</u>), 4.14 (m, 1H, Hβ), 3.65 (dd, 1H, *J* = 17.5, 2.2 Hz, Hα), 3.40 (ddd, 1H, *J* = 11.4, 7.2, 0.9 Hz, NC(S)SC<u>H</u>HCHBn), 3.22 (dd, 1H, *J* = 13.2, 4.0 Hz, PhC<u>H</u>H), 3.12 (dd, 1H, *J* = 17.8, 9.5 Hz, Hα), 3.05 (dd, 1H, *J* = 13.2, 10.5 Hz, PhCH<u>H</u>), 2.90 (d, 1H, *J* = 11.2 Hz, NC(S)SCH<u>H</u>CHBn), 2.69 (bs, 1H, -O<u>H</u>), 1.62-1.43 (m, 4H, Hδ + Hε), 1.38-1.25 (m, 5H, Hζ + Hη + Hθ), 1.19-1.15 (m, 2H, Hγ), 0.87 (s, 3H, C<u>H</u>$_3$), 0.86 (s, 3H, C<u>H</u>$_3$); ^{13}C-NMR ($CDCl_3$, 125 MHz); 201.4, 173.4, 136.4, 129.5, 129.0, 127.3, 68.3, 67.9, 45.9, 39.0, 36.9, 36.4, 32.1, 29.8, 28.0, 27.3, 25.6, 22.7; HRMS (ESI^+) calcd. for $C_{21}H_{31}NNaO_2S_2$ $[M+Na]^+$ 416.1688; found 416.1686.

(3*R*)-1-((*S*)-4-Benzyl-2-thioxothiazolidin-3-yl)-3-hydroxy-10-methyldecan-1-one (85)

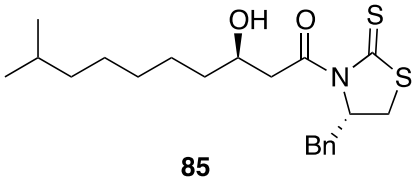

85

Isolated as a yellow solid (0.12 g, 9%) and is minor product from the synthesis of **84.** $[\alpha]^{20}_D$ + 87.56 (*c* 1.00, $CHCl_3$); IR ($CHCl_3$ cast): 3438, 3363, 3027, 2927, 2856, 1689;

^{1}H-NMR ($CDCl_3$, 500 MHz): 7.36-7.26 (m, 5H, Ar-H), 5.42 (m, 1H, -NC<u>H</u>), 4.08-4.03 (m, 1H, Hβ), 3.46 (dd, 1H, *J* = 17.5, 9.3 Hz, NC(S)SC<u>H</u>HCHBn), 3.41 (ddd, 1H, *J* = 11.6, 7.3, 0.9 Hz, NC(S)SCH<u>H</u>CHBn), 3.34 (dd, 1H, *J* = 17.6, 2.6 Hz, Hα), 3.23 (dd, 1H, *J* = 13.4, 4.0 Hz, PhC<u>H</u>H), 3.08-3.03 (m, 2H, PhCH<u>H</u> + O<u>H</u>), 2.91 (d, 1H, *J* = 11.6 Hz, NC(S)SCH<u>H</u>CHBn), 1.55 (m, 4H, Hδ + Hε), 1.30 (m, 5H, Hζ + Hη + Hθ), 1.16 (m, 2H, Hγ), 0.87 (s, 3H, C<u>H</u>$_3$), 0.86 (s, 3H, C<u>H</u>$_3$); ^{13}C-NMR ($CDCl_3$, 500 MHz); 201.5, 173.9, 136.4, 129.5, 128.9, 127.3, 68.5, 68.3, 45.5, 39.0, 36.8, 36.7, 32.1, 29.8, 28.0, 27.3, 25.5, 22.7; HRMS (ESI$^+$) calcd. for $C_{21}H_{31}NNaO_2S_2$ $[M+Na]^+$ 416.1688; found 416.1688.

(3*R*)-CxnA$_1$ (31)

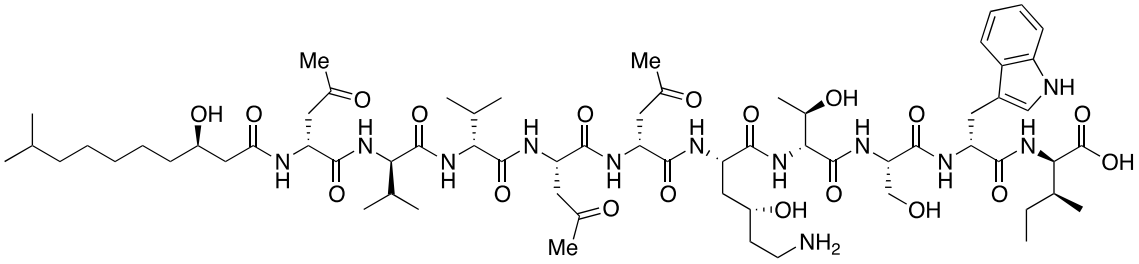

31

Product eluted at 38.7 min (HPLC method 1) and was isolated as a white powder (10.5 mg from 4L culture). HRMS (ES) Calcd for $C_{63}H_{104}N_{15}O_{19}$ $[M+H]^+$ 1374.7627, found 1374.7644.

(3*S*)-CxnA$_1$ (87)

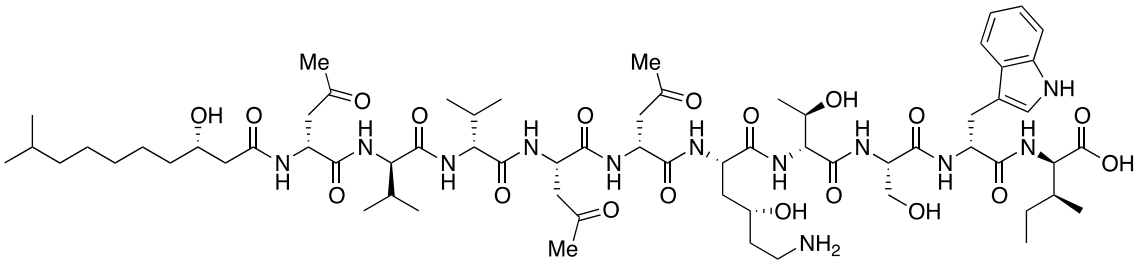

87

Resin-bound peptide **86** (0.025 mmol) was stirred gently in a solution of the activated lipid (2 equiv) in CH_2Cl_2 (1 mL) at ambient temperature under argon for 24 h. The suspension was then filtered and washed with CH_2Cl_2 (5 X 5 mL). The resin bound peptide was then bubbled in DMF (1 mL) and TBAF (100 equiv) for 1 h to remove the silyl protecting group. The resin was then filtered and washed with DMF (3 x 1 mL) and CH_2Cl_2 (3 x 1 mL) and dried by vacuum filtration for 5 min. The dry resin was transferred to a screw-top vial containing TFA:TIPS:H_2O (95:2.5:2.5, 1 mL), and shaken for 2 h. The resin beads were removed via filtration through glass wool and the filtrate was concentrated *in vacuo*. The crude peptide (assume 0.025 mmol) was dissolved in phosphate buffer (200 mM, pH = 7.5, 10 mL) and to this solution was added TCEP (62.5 mg, 0.25 mmol). The resulting solution was stirred at ambient temperature for 1 h and purified by HPLC method 1. Product eluted at 38.7 min and was isolated as a white powder (1 mg, 3% overall yield). HRMS (ES) Calcd for $C_{63}H_{104}N_{15}O_{19}$ $[M+H]^+$ 1374.7627, found 1374.7644.

(3*R*)-Hydroxy-9-methyldecanoic acid (88)

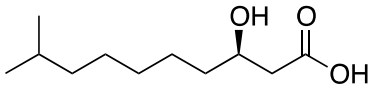

88

Thiazolidinone **85** (50 mg, 0.127 mmol) was dissolved in THF (2.2 mL) and cooled to 0 ^{o}C. A solution of LiOH.H_2O (10.7 mg, 0.254 mmol) in H_2O (0.8 mL) was added and the reaction stirred at 0 ^{o}C for 2 h. 1M HCl (2 mL) was added and the reaction mixture extracted with EtOAc (3 x 5 mL). The combined organic were dried over anhydrous Na_2SO_4 and concentrated *in vacuo*. The crude product was purified by column chromatography (SiO_2, 3:1 hexanes:EtOAc + 0.1% AcOH) to yield the acid as a colourless oil (21 mg, 82%). $[\alpha]_D^{25}$ = -17.00 (*c* = 1.00 g/100mL, $CHCl_3$); IR ($CHCl_3$ cast) 2953, 2929, 2857, 1713; ^{1}H NMR ($CDCl_3$, 500 MHz): δ 4.06-4.00 (m, 1H, Hβ), 2.58 (dd, 1H, *J* = 16.6, 3.0 Hz, Hα), 2.48 (dd, 1H, *J* = 16.6, 9.0 Hz, Hα'), 1.59-1.41 (m, 4H, Hγ + 2xHδ + Hθ), 1.38-1.26 (m, 5H, Hγ' + 2Hε + 2Hζ), 1.18-1.14 (m, 2H, 2Hη), 0.86 (d, 6H, *J* = 6.2 Hz, 6Hι); ^{13}C NMR ($CDCl_3$, 125 MHz): δ 177.7, 68.2, 41.2, 39.1, 36.7, 29.9, 28.1, 27.4, 25.6, 22.8; HRMS (ES) Calcd for $C_{11}H_{21}O_3$ $[M-H]^-$ 201.1496, found 201.1492.

(3*S*)-Hydroxy-9-methyldecanoic acid (89)

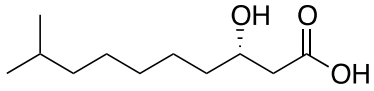

89

Thiazolidinone **84** (50 mg, 0.127 mmol) was dissolved in THF (2.2 mL) and cooled to 0 ^{o}C. A solution of LiOH.H_2O (10.7 mg, 0.254 mmol) in H_2O (0.8 mL) was added and the reaction stirred at 0 ^{o}C for 2 h. 1M HCl (2 mL) was added and the reaction mixture

extracted with EtOAc (3 x 5 mL). The combined organic were dried over anhydrous Na_2SO_4 and concentrated *in vacuo*. The crude product was purified by column chromatography (SiO_2, 3:1 hexanes:EtOAc + 0.1% AcOH) to yield the acid as a colourless oil (22 mg, 86%). $[\alpha]_D^{25}$ = +11.50 (*c* = 1.00 g/100mL, $CHCl_3$); IR ($CHCl_3$ cast) 2953, 2929, 2857, 1713; ^{1}H NMR ($CDCl_3$, 500 MHz): ^{1}H NMR ($CDCl_3$, 500 MHz): δ 4.06-4.00 (m, 1H, Hβ), 2.60-2.52 (m, 1H, Hα), 2.50-2.40 (m, 1H, Hα'), 1.58-1.40 (m, 4H, Hγ + 2xHδ + Hθ), 1.37-1.26 (m, 5H, Hγ' + 2Hε + 2Hζ), 1.18-1.13 (m, 2H, 2Hη), 0.86 (d, 6H, *J* = 6.2 Hz, 6Hι); ^{13}C NMR ($CDCl_3$, 125 MHz): δ 178.1, 68.3, 41.4, 39.1, 36.8, 29.9, 28.2, 27.5, 25.7, 22.9; HRMS (ES) Calcd for $C_{11}H_{21}O_3$ $[M-H]^-$ 201.1496, found 201.1491.

(*R*)-1-Methoxy-9-methyl-1-oxodecan-3-yl-2-(1*H*-naphtho[2,3-*f*]isoindol-2(3*H*)-yl)cyclohexanecarboxylate (91)

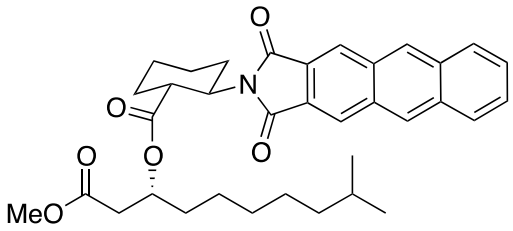

91

Acid **88** (10 mg, 0.05 mmol), EDCI.HCl was dissolved in a 3:1 mixture of Et_2O and MeOH (1 mL) and stirred at rt. TMS diazomethane (~3 equiv) was added drop wise until a yellow colour persisted and TLC showed complete consumption of the acid starting material. AcOH (14 µL, 0.25 mmol) was added to quench excess TMS diazomethane and the reaction concentrated by rotary evaporator and dried over high vacuum for 1 h. The resulting oil was dissolved in a dry 1:1:1 mixture of CH_2Cl_2:toluene:DMF (1.5 mL)

and EDCI.HCl (14.4 mg, 0.075 mmol), DMAP (1.2 mg, 0.01 mmol) and alcohol **90** (21 mg, 0.055 mmol) were sequentially added. The resulting yellow solution was stirred overnight and diluted with EtOAc (10 mL). This solution was washed with saturated $NaHCO_3$ (5 mL), 10% citric acid (5 mL), water (5 mL) and brine (5 mL). The organic phase was then dried over anhydrous Na_2SO_4 and concentrated *in vacuo*. The crude product was dissolved in CH_2Cl_2 (0.5 mL) and purified by preparatory TLC (Analtech Silica Gel GF, 20 x 20 cm, 500 microns), eluting with 2:1 hexanes:EtOAc, to yield ester **91** as a yellow solid (12 mg, 42%). $[\alpha]_D^{25}$ = -12.40 (*c* = 0.5 g/100mL, $CHCl_3$); IR ($CHCl_3$ cast) 2931, 2859, 1740, 1706; ^{1}H NMR ($CDCl_3$, 500 MHz): 8.62 (s, 2H, Anth9, Anth10), 8.47 (s, 2H, Anth5, Anth8), 8.08-8.07 (m, 2H, Anth2, Anth3), 7.62-7.60 (m, 2H, Anth1, Anth4), 5.10-5.07 (m, 1H, lipid-Hβ), 4.48 (td, 1H, *J* = 11.9, 3.9 Hz, NC<u>H</u>), 3.57 (td, 1H, *J* = 11.8, 3.4 Hz, C(O)C<u>H</u>), 3.43 (s, 3H, OMe), 2.43 (dd, 1H, *J* = 15.3, 8.0 Hz, lipid-Hα), 2.32 (dd, 1H, *J* = 15.3, 5.1 Hz, lipid-Hα'), 2.24-2.16 (m, 2H, NCHC<u>H(eq)</u> + C(O)CHC<u>H(eq)</u>), 1.93-1.81 (m, 3H, OCHC<u>H(ax)</u> + $OCHCH_2C$<u>H(eq)</u> + $NCHCH_2C$<u>H(eq)</u>), 1.55-1.23 (m, 8H, NCHC<u>H(ax)</u> + $NCHCH_2C$<u>H(ax)</u> + $OCHCH_2C$<u>H(ax)</u> + lipid-2Hγ, 2Hδ, Hθ), 1.10-0.88 (m, 6H, lipid-2Hε, 2Hζ, 2Hη), 0.71 (d, 3H, *J* = 6.6 Hz, Hι), 0.69 (d, 3H, *J* = 6.6 Hz, Hι'); ^{13}C NMR ($CDCl_3$, 125 MHz): δ 173.0, 170.7, 167.7, 133.4, 132.2, 130.1, 128.6, 127.6, 126.9, 125.7, 70.6, 68.2, 51.6, 45.4, 39.1, 38.9, 34.3, 30.2, 29.7, 29.5, 27.9, 25.5, 25.4, 24.9, 22.8, 22.6; HRMS (ES) Calcd for $C_{35}H_{41}NNaO_6$ $[M+Na]^+$ 594.2826, found 594.2824.

(*S*)-1-Methoxy-9-methyl-1-oxodecan-3-yl-2-(1*H*-naphtho[2,3-*f*]isoindol-2(3*H*)-yl)cyclohexanecarboxylate (92)

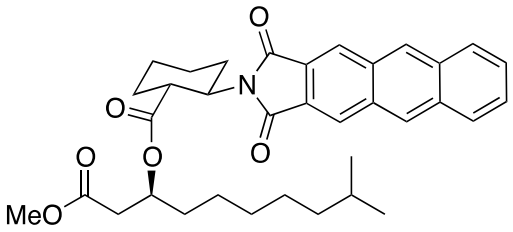

92

Acid **89** (10 mg, 0.05 mmol), EDCI.HCl was dissolved in a 3:1 mixture of Et_2O and MeOH (1 mL) and stirred at rt. TMS diazomethane (~3 equiv) was added drop wise until a yellow colour persisted and TLC showed complete consumption of the acid starting material. AcOH (14 µL, 0.25 mmol) was added to quench excess TMS diazomethane and the reaction concentrated by rotary evaporator and dried over high vacuum for 1 h. The resulting oil was dissolved in a dry 1:1:1 mixture of CH_2Cl_2:toluene:DMF (1.5 mL) and EDCI.HCl (14.4 mg, 0.075 mmol), DMAP (1.2 mg, 0.01 mmol) and alcohol **90** (21 mg, 0.055 mmol) were sequentially added. The resulting yellow solution was stirred overnight and diluted with EtOAc (10 mL). This solution was washed with saturated $NaHCO_3$ (5 mL), 10% citric acid (5 mL), water (5 mL) and brine (5 mL). The organic phase was then dried over anhydrous Na_2SO_4 and concentrated *in vacuo*. The crude product was dissolved in CH_2Cl_2 (0.5 mL) and purified by preparatory TLC (Analtech Silica Gel GF, 20 x 20 cm, 500 microns), eluting with 2:1 hexanes:EtOAc, to yield ester **91** as a yellow solid (15 mg, 66%). $[\alpha]_D^{25}$ = -13.16 (*c* = 0.5 g/100mL, $CHCl_3$); IR ($CHCl_3$ cast) 2930, 2862, 1747, 1704; ^{1}H NMR ($CDCl_3$, 500 MHz): ^{1}H NMR ($CDCl_3$, 500 MHz): 8.61 (s, 2H, Anth9, Anth10), 8.47 (s, 2H, Anth5, Anth8), 8.08-8.06 (m, 2H, Anth2, Anth3), 7.62-7.60 (m, 2H, Anth1, Anth4), 5.10-5.06 (m, 1H, lipid-Hβ), 4.48 (td, 1H, *J* =

11.9, 3.8 Hz, NCH), 3.57-3.52 (m, 4H, C(O)CH + OMe), 2.43-2.36 (m, 2H, lipid-Hα), 2.25-2.19 (m, 1H, NCHCH(eq)), 2.15-2.12 (m, 1H, C(O)CHCH(eq)), 1.91-1.81 (m, 3H, OCHCH(ax) + $OCHCH_2CH$(eq) + $NCHCH_2CH$(eq)), 1.55-1.23 (m, 8H, NCHCH(ax) + $NCHCH_2CH$(ax) + $OCHCH_2CH$(ax) + lipid-2Hγ, 2Hδ, Hθ), 1.10-0.88 (m, 6H, lipid-2Hε, 2Hζ, 2Hη), 0.63 (t, 6H, *J* = 6.5 Hz, Hι); ^{13}C NMR ($CDCl_3$, 125 MHz): δ 173.2, 170.8, 167.6, 133.4, 132.2, 130.1, 128.6, 127.6, 126.7, 125.8, 70.4, 68.2, 51.8, 45.4, 39.1, 38.9, 36.7, 34.1, 30.0, 29.9, 29.5, 28.1, 27.7, 25.6, 25.4, 24.9, 22.8, 22.6; HRMS (ES) Calcd for $C_{35}H_{41}NNaO_6$ $[M+Na]^+$ 594.2827, found 594.2824.

CxnF$_1$ (93)

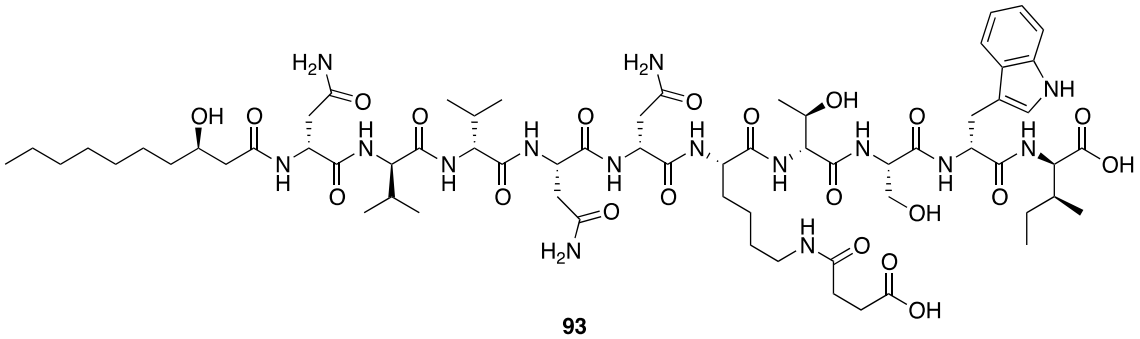

93

Product eluted at 39.1 min (HPLC method 1) and was isolated as a white powder (4.5 mg from 4L culture). HRMS (ES) Calcd for $C_{63}H_{104}N_{15}O_{19}$ $[M+H]^+$ 1444.7682, found 1444.7694.

CxnE$_1$ (94)

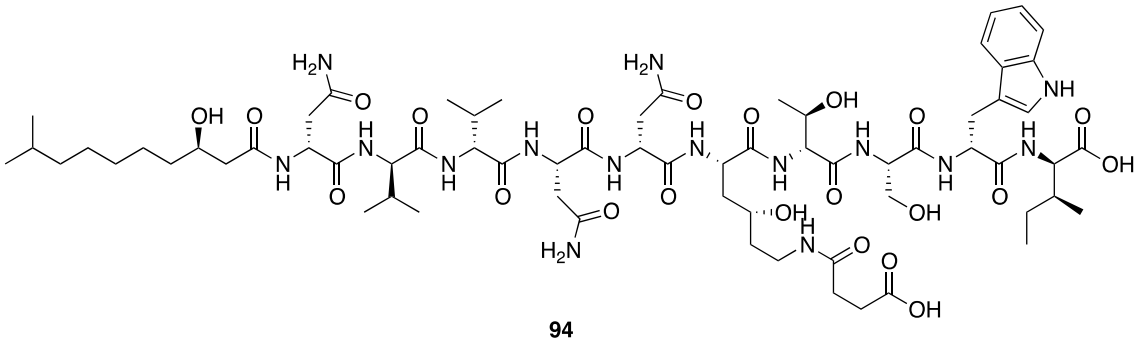

94

Product eluted at 41.0 min (HPLC method 1) and was isolated as a white powder (15 mg from 4L culture). HRMS (ES) Calcd for $C_{63}H_{104}N_{15}O_{19}$ $[M+H]^+$ 1474.7788, found 1474.7808.

CxnF$_2$ (95)

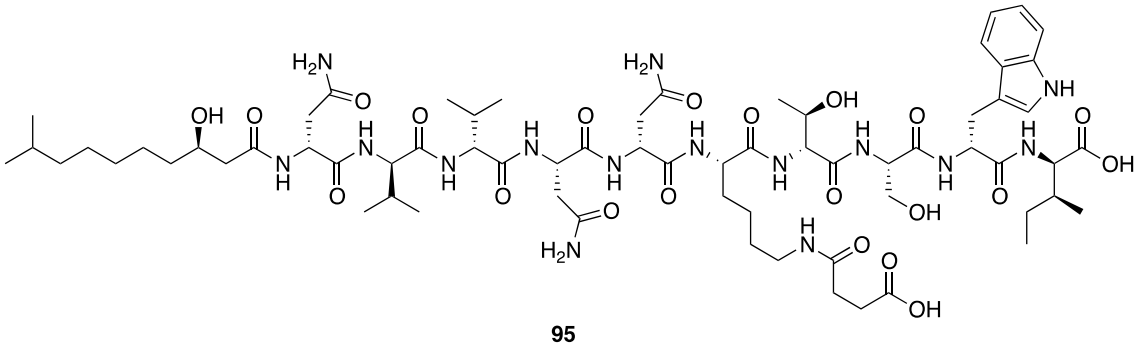

95

Product eluted at 41.6 min (HPLC method 1) and was isolated as a white powder (39 mg from 4L culture). HRMS (ES) Calcd for $C_{63}H_{104}N_{15}O_{19}$ $[M+H]^+$ 1458.7840, found 1458.7860.

(9*H*-Fluoren-9-yl)methyl-(3*S*)-5-(iodomethyl)-2-oxotetrahydrofuran-3-ylcarbamate (99)

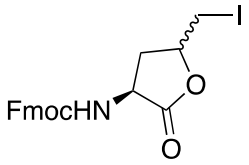

99

Fmoc-L-Agl-OH (**96**) (1.01 g, 3.0 mmol) was dissolved in THF (30 mL) and 1 M $NaHCO_3$ (30 mL). This solution was cooled to 0 ^oC and a 0.6 M solution of iodine in THF (15 mL) was added drop wise over 10 min. The reaction was stirred for 1 h and quenched with saturated sodium sulphite (20 mL). Water (50 mL) and $CHCl_3$ (100 mL) were added and the organic layer separated and washed with sat. $NaHCO_3$ (50 mL) and brine (50 mL). The organic extract was then dried over anhydrous Na_2SO_4 and concentrated *in vacuo* to yield an inseparable 4:1 mixture of the *cis*- and *trans*-lactones (1.35 g, 99%).

2-(Trimethylsilyl)ethyl-(3*S*)-5-(iodomethyl)-2-oxotetrahydrofuran-3-ylcarbamate (100)

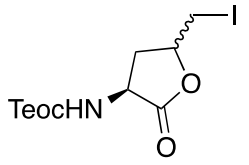

100

Teoc-L-Agl-OH (**97**) (710 mg, 2.74 mmol) was dissolved in THF (30 mL) and 1 M $NaHCO_3$ (30 mL). This solution was cooled to 0 ^oC and a 0.6 M solution of iodine in THF (15 mL) was added drop wise over 10 min. The reaction was stirred for 1 h and quenched with saturated sodium sulphite (20 mL). Water (50 mL) and $CHCl_3$ (100 mL)

were added and the organic layer separated and washed with sat. $NaHCO_3$ (50 mL) and brine (50 mL). The organic extract was then dried over anhydrous Na_2SO_4 and concentrated *in vacuo* to yield the product as a 9:1 mixture of *cis* and *trans* isomers (785 mg, 74%).

tert-Butyl-(3*S*)-5-(iodomethyl)-2-oxotetrahydrofuran-3-ylcarbamate (101)

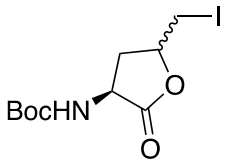

101

Boc-L-Agl-OH (**98**) (4.41 g, 20.5 mmol) was dissolved in THF (250 mL) and 1 M $NaHCO_3$ (200 mL). This solution was cooled to 0 ^oC and a 0.6 M solution of iodine in THF (50 mL) was added drop wise over 10 min. The reaction was stirred for 1 h and quenched with saturated sodium sulphite (100 mL). Water (100 mL) and $CHCl_3$ (600 mL) were added and the organic layer separated and washed with sat. $NaHCO_3$ (300 mL) and brine (200 mL). The organic extract was then dried over anhydrous Na_2SO_4 and concentrated *in vacuo* to yield the product as a 9:1 mixture of *cis* and *trans* isomers (6.20 mg, 89%).

2-(Trimethylsilyl)ethyl-(3*S*)-5-(cyanomethyl)-2-oxotetrahydrofuran-3-ylcarbamate (102)

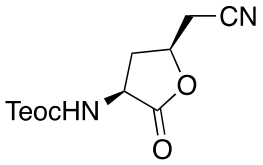

102

Iodolactone **100** (4.00 g, 10.4 mmol) and finely powdered Na_2CO_3 (3.31 g, 31.2 mmol) were added to anhydrous MeOH (45 mL) under Ar in a flame-dried flask and stirred at 40 ^oC for 22 h. The pH was adjusted to 7.5 with 0.25 M HCl and the MeOH removed by rotary evaporator. H_2O (20 mL) and EtOAc (50 mL) were added and the aqueous layer washed twice with EtOAc (2 x 50 mL). The combined organic extracts were dried over anhydrous Na_2SO_4 and concentrated *in vacuo*. The resulting crude epoxide (~10.4 mmol) was co-evaporated with anhydrous toluene (3 x 50 mL), dissolved in anhydrous toluene and cooled to 0 ^oC. Et_2AlCN (1 M tol soln, 31.2 mL, 31.2 mmol) was added drop wise over 15 min and the resulting amber solution stirred at ambient temperature for 18 h. The reaction mixture was then added to an ice-cold solution of stirring saturated $NaHCO_3$ (150 mL). EtOAc (150 mL) was added and the mixture stirred for 15 min. The aqueous phase extracted with EtOAc (2 x 100 mL) and the combined organic extracts dried over anhydrous Na_2SO_4 and concentrated *in vacuo*. The crude residue was purified by flash column chromatography to yield nitrile **102** as a yellow oil (1.5 g, 51%). ^1H NMR ($CDCl_3$, 500 MHz): 5.48-5.40 (m, 1H, NH), 4.66 (dq, 1H, *J* = 10.4, 5.3 Hz, Hγ), 4.52-4.47 (m, 1H, Hα), 4.18 (t, 2H, $OC\underline{H_2}$), 2.94-2.84 (m, 3H, Hδ + Hβ), 2.11 (dd, 1H, *J* = 22.7, 11.6 Hz, Hβ'), 1.01-0.97 (m, 2H, $SiC\underline{H_2}$), 0.03 (s, 9H, TMS); ^{13}C NMR ($CDCl_3$, 125 MHz): δ 173.2, 156.4, 115.3, 71.7, 64.3, 51.3, 34.8, 23.8, 17.8, -1.39; HRMS (ES) Calcd for $C_{12}H_{20}N_2NaO_4Si$ $[M+Na]^+$ 307.1085, found 307.1080.

Lactone (103)

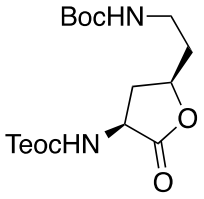

103

Nitrile **102** (1.00 g, 3.52 mmol) was dissolved in anhydrous MeOH (60 mL) at 0 ^{o}C. To this solution was added Boc_2O (1.54 g, 7.04 mmol) and PtO_2 (160 mg, 0.70 mmol). The resulting suspension was stirred under a H_2 atmosphere for 72 h and filtered through celite (10 g). The celite was washed with MeOH (3 x 50 mL) and the filtrate concentrated *in vacuo*. The crude product was purified by column chromatography (SiO_2, 2:1 Hexanes:EtOAc) to yield the product was a colourless oil (1.24 g, 91%). $[\alpha]_D^{25}$ = 20.54 (*c* = 1.0 g/100mL, $CHCl_3$); IR ($CHCl_3$ cast) 3346, 2954, 1784, 1695; ^{1}H NMR ($CDCl_3$, 500 MHz): 5.25-5.16 (m, 1H, Teoc-NH), 4.80-4.73 (m, 1H, Boc-NH), 4.51-4.45 (m, 1H, Hγ), 4.45-4.40 (m, 1H, Hα), 4.18 (t, 2H, OC$\underline{H_2}$), 3.31-3.27 (m, 2H, Hε), 2.84 (ddd, 1H, *J* = 12.7, 8.1, 4.8 Hz, Hβ), 2.03-1.83 (m, 3H, Hβ' + Hδ), 1.43 (s, 9H, tBu), 1.01-0.97 (m, 2H, SiC$\underline{H_2}$), 0.03 (s, 9H, TMS); ^{13}C NMR ($CDCl_3$, 125 MHz): δ 174.5, 156.5, 156.1, 79.7, 76.3, 64.1, 51.7, 37.3, 36.5, 35.7, 28.5, 17.8, -1.36; HRMS (ES) Calcd for $C_{17}H_{33}N_2O_6Si$ $[M+H]^+$ 389.2107, found 389.2102.

(2*S*,4*R*)-Trityl-6-(*tert*-butoxycarbonylamino)-4-hydroxy-2-((2-(trimethylsilyl)ethoxy) carbonylamino)hexanoate (107)

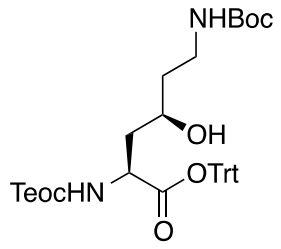

107

Lactone **103** (32 mg, 82.4 μmol) was dissolved in MeOH (150 μL) and H_2O (50 μL) and stirred at ambient temperature. NaOH (3.3 mg, 82.4 μmol) was added and the resulting solution stirred for 1 h. The reaction mixture was concentrated *in vacuo*, azetroped with toluene (3 x 500 μL), re-dissolved in anhydrous MeOH (500 μL) and concentrated *in vacuo* to yield sodium salt **104** as a white solid (quant.). The crude sodium salt was dissolved in anhydrous CH_2Cl_2 (500 μL). Trityl chloride (25 mg, 90.7 μmol), DMAP (2 mg, 16.5 μmol) and NEt_3 (18 μL, 123.6 μmol) were added and the resulting mixture stirred at ambient temperature for 18 h. The reaction mixture was then concentrated *in vacuo* and purified by column chromatography (SiO_2, 2:1 hexanes:EtOAc) to yield the unwanted trityl ester as a lovely white foam (70%). ^{1}H NMR ($CDCl_3$, 500 MHz): 5.70 (d, 1H, *J* = 6.3 Hz, Teoc-NH), 5.00-4.95 (m, 1H, Boc-NH), 4.70-4.65 (m, 1H, Hα), 4.29 (br s, 1H, OH), 4.17-4.15 (m, 2H, OC$\underline{H_2}$), 3.60-3.54 (m, 1H, Hγ), 3.43-3.37 (m, 1H, Hε), 3.12-3.05 (m, 1H, Hε'), 2.01-1.97 (m, 1H, Hβ), 1.59-1.49 (m, 3H, Hβ' + Hδ), 1.42 (s, 9H, tBu), 0.99-0.96 (m, 2H, SiC$\underline{H_2}$), 0.03 (s, 9H, TMS); ^{13}C NMR ($CDCl_3$, 125 MHz): δ 170.4, 157.7, 156.7, 142.8, 128.4, 127.9, 127.6, 91.6 79.5, 66.1, 64.0, 52.2, 40.3, 38.1, 37.1, 28.5, 17.8, -1.36; HRMS (ES) Calcd for $C_{36}H_{49}N_2O_7Si$ $[M+H]^+$ 649.3309, found 649.3315.

(*S*)-*tert*-Butyl-2-(*tert*-butoxycarbonylamino)-4-(ethylthio)-4-oxobutanoate (108)

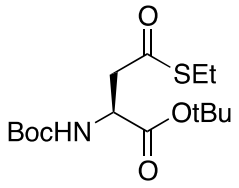

108

Boc-Asp-OtBu (**77**) (4.50 g, 15.6 mmol) was dissolved in dry CH_2Cl_2 (30 mL). DCC (3.86 g, 18.7 mmol), ethanethiol (3.4 mL, 46.5 mmol), and DMAP (0.20 g, 1.6 mmol) were added, and the reaction was stirred at ambient temperature for 2 h. The mixture then was filtered through celite, and concentrated *in vacuo*. The crude product was purified by flash chromatography (SiO_2, 9:1 hexanes:EtOAc) to yield thioester **108** as a pale yellow oil that crystallizes upon standing (4.78 g, 92%). $[\alpha]_D^{25}$ = 19.22 (*c* = 1.0 g/100 mL, $CHCl_3$); IR ($CHCl_3$ cast) 3378, 2978, 2933, 1720, 1498, 1368, 1253, 1157 cm^{-1}; ^1H NMR ($CDCl_3$, 500 MHz): δ 5.40 (d, 1H, *J* = 7.5 Hz, NH), 4.43-4.40 (m, 1H, Hα), 3.14 (dd, 1H, *J* = 16.4, 4.5 Hz, Hβ), 3.03 (dd, 1H, *J* = 16.2, 4.5 Hz, Hβ), 2.94-2.83 (m, 2H, $SC\underline{H}_2$), 1.45 (s, 9H, tBu), 1.44 (s, 9H, tBu), 1.24 (t, 3H, *J* = 7.5 Hz, $SCH_2C\underline{H}_3$); ^{13}C NMR ($CDCl_3$, 125 MHz): δ 197.1, 169.9, 155.5, 82.5, 80.0, 51.1, 45.8, 28.5, 28.0, 23.6, 14.8; HRMS (ES) Calcd for $C_{15}H_{28}NO_5S$ $[M+H]^+$ 334.1683, found 334.1681.

(*S*)-*tert*-Butyl-2-(*tert*-butoxycarbonylamino)-4-oxobutanoate (109)

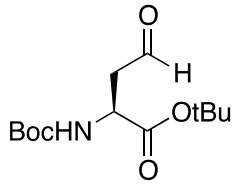

109

To a solution of thioester **108** (10.67 g, 32.0 mmol) in dry CH_2Cl_2 (35 mL), Pd/C (0.40 g) and Et_3SiH (15.3 mL, 96.0 mmol) were added, and the reaction was stirred at ambient temperature for 6 h. The mixture was then filtered through celite and concentrated *in vacuo*. The crude product was purified by flash chromatography (SiO_2, 85:15 hexanes:EtOAc) to yield aldehyde **109** as a pale yellow oil that crystallizes upon standing (8.53 g, 97%). $[\alpha]_D^{25}$ = 29.09 (*c* = 1.0 g/100 mL, $CHCl_3$); IR ($CHCl_3$ cast) 3370, 2979, 2934, 1722, 1503, 1369, 1156, 1056, 847 cm^{-1}; ^1H NMR ($CDCl_3$, 400 MHz): δ 9.73 (s, 1H, C(O)H), 5.35 (d, 1H, *J* = 6.4 Hz, NH), 4.50-4.45 (m, 1H, Hα), 3.00 (dd, 1H, *J* = 17.8, 5.2 Hz, Hβ), 2.93 (dd, 1H, *J* = 17.8, 5.6 Hz, Hβ), 1.45 (s, 9H, tBu), 1.44 (s, 9H, tBu); ^{13}C NMR ($CDCl_3$, 125 MHz): δ 199.5, 170.1, 155.5, 82.9, 80.2, 49.5, 46.5, 28.5, 28.0; HRMS (ES) Calcd for $C_{13}H_{23}NNaO_5$ $[M+Na]^+$ 296.1468, found 296.1470.

General procedure for the Reformatsky reaction

Zinc (5.37 g, 82.1 mmol), TMSCl (1.42 mL, 11.2 mmol), and dry THF (40 mL) were added sequentially to a flame dried two-necked flask under argon. The mixture was stirred and refluxed for 30 min then removed from heat. Bromoacetonitrile (5.17 mL, 74.6 mmol) in dry THF (40 mL) was added at a rate to maintain smooth reflux. The mixture was stirred for 15 min then cooled to ambient temperature. The Reformatsky reagent was titrated using the I_2/LiCl method[210] and determined to have a concentration of 0.50 M. In a separate flask, aldehyde **109** (3.02 g, 11.0 mmol) was dissolved in dry THF (50 mL) under argon and cooled to 0 °C. The Reformatsky reagent (0.50 M in THF, 57.6 mL, 28.8 mmol) was added drop wise over 30 min, and the reaction was stirred at 0 °C for 6 h, then ambient temperature for 10 h. The mixture was quenched with H_2O

(10 mL), concentrated *in vacuo* then partitioned in EtOAc (100 mL), saturated NH_4Cl (50 mL), and brine (50 mL). The aqueous layer was washed with EtOAc (2 x 100 mL), and the combined organic extracts were dried over anhydrous Na_2SO_4 and concentrated *in vacuo*. The crude mixture of alcohol diastereomers was dissolved in dry CH_2Cl_2 (200 mL) and cooled to 0 °C. Imidazole (3.00 g, 44.0 mmol) and TPSCl (5.72 mL, 22.0 mmol) were added, and the reaction was stirred at ambient temperature for 24 h. The mixture was then concentrated *in vacuo*, dissolved in EtOAc (200 mL), and washed with 1M $KHSO_4$ (100 mL), H_2O (100 mL), and brine (100 mL). The organic extract was dried under anhydrous Na_2SO_4, concentrated *in vacuo*, and purified by flash chromatography (SiO_2, 6:1 hexane:EtOAc) to yield *threo*-silyl ether **110** as a white solid (1.26 g, 21% over 2 steps) and *erythro*-silyl ether **111** as a pale yellow oil that crystallized upon standing (4.43 g, 71% over 2 steps).

(5*S*,7*S*)-*tert*-Butyl-5-(cyanomethyl)-2,2,11,11-tetramethyl-9-oxo-3,3-diphenyl-4,10-dioxa-8-aza-3-siladodecane-7-carboxylate (110)

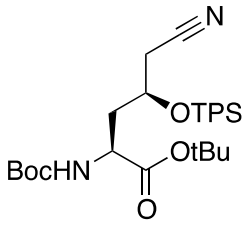

110

$[\alpha]_D^{25}$ = -0.84 (*c* = 1.0 g/100mL, $CHCl_3$); IR ($CHCl_3$ cast) 3357, 2977, 2933, 2860, 1717, 1368, 1153, 1112 cm^{-1}; ^1H NMR ($CDCl_3$, 500 MHz): δ 7.72-7.66 (m, 4H, ArH), 7.49-7.38 (m, 6H, ArH), 4.94 (d, 1H, *J* = 8.0 Hz, NH), 4.15-4.11 (m, 1H, Hα), 4.05-4.03 (m, 1H, Hγ), 2.40-2.38 (m, 2H, Hδ), 2.19-2.13 (m, 1H, Hβ), 1.97-1.90 (m, 1H, Hβ), 1.43 (s, 9H,

tBu), 1.39 (s, 9H, tBu), 1.08 (s, 9H, Si-tBu); ^{13}C NMR ($CDCl_3$, 125 MHz): δ 171.1, 155.6, 135.9, 135.88, 135.3, 134.9, 129.8, 128.1, 128.0, 127.9, 117.3, 82.7, 80.1, 66.6, 50.9, 40.3, 28.3, 28.1, 27.0, 26.7, 24.9, 19.4, 19.2; HRMS (ES) Calcd for $C_{31}H_{44}N_2NaO_5Si$ $[M+Na]^+$ 575.2912, found 575.2909.

(5*R*,7*S*)-*tert*-Butyl-5-(cyanomethyl)-2,2,11,11-tetramethyl-9-oxo-3,3-diphenyl-4,10-dioxa-8-aza-3-siladodecane-7-carboxylate (111)

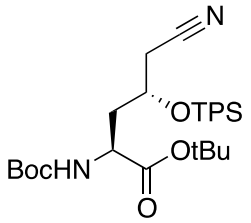

111

$[\alpha]_D^{25}$ = 9.02 (*c* = 1.50 g/100mL, $CHCl_3$); IR ($CHCl_3$ cast) 3429, 2961, 2932, 2896, 2858, 1708, 1368, 1154, 1113 cm^{-1}; ^{1}H NMR ($CDCl_3$, 500 MHz): δ 7.73-7.65 (m, 4H, ArH), 7.48-7.36 (m, 6H, ArH), 4.72 (d, 1H, *J* = 8.0 Hz, NH), 4.02-3.98 (m, 2H, Hα + Hɣ), 2.66 (dd, 1H, *J* = 15.7, 3.5 Hz, Hβ), 2.53 (dd, 1H, *J* = 17.4, 4.5 Hz, Hβ), 2.20 (t, 2H, *J* = 11.0 Hz, Hδ), 1.70 (t, 1H, *J* = 11.0 Hz, Hδ), 1.43 (s, 9H, tBu), 1.35 (s, 9H, tBu), 1.08 (s, 9H, Si-tBu); ^{13}C NMR ($CDCl_3$, 125 MHz): δ 171.1, 155.6, 135.9, 135.3, 134.9, 129.8, 128.1, 128.0, 127.9, 117.3, 82.7, 80.1, 66.6, 50.9, 40.3, 28.3, 28.1, 27.0, 26.7, 24.9, 19.4, 19.2; HRMS (ES) Calcd for $C_{31}H_{48}N_3O_5Si$ $[M+NH_4]^+$ 570.3358, found 570.3356.

(6*S*,8*R*)-*tert*-Butyl-8-(*tert*-butyldiphenylsilyloxy)-2,2-dimethyl-4,12-dioxo-3,13-dioxa-5,11-diazahexadec-15-ene-6-carboxylate (112)

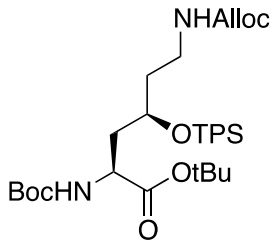

112

Silyl ether **110** (0.51 g, 0.93 mmol) was dissolved in dry 10:1 MeOH (5.6 mL)/$CHCl_3$ (0.6 mL). PtO_2 (0.11 g, 0.47 mmol) was added, and the mixture was stirred under H_2 at ambient temperature for 24 h. The mixture was then filtered through celite and concentrated *in vacuo* to yield the free amine as a white solid. The amine was dissolved in dry CH_2Cl_2 (6.9 mL) and cooled to 0 ^oC. DIPEA (0.65 mL, 3.72 mmol) and allylchloroformate (0.30 mL, 2.79 mmol) were then added. The reaction was stirred at ambient temperature for 24 h and concentrated *in vacuo*. The crude product was purified by flash chromatography (SiO_2 5:1 hexane:EtOAc) to yield carbamate **112** as a colourless oil (0.45 g, 75% over 2 steps). $[\alpha]_D^{25}$ = 9.92 (*c* = 1.0 g/100mL, $CHCl_3$); IR ($CHCl_3$ cast) 3348, 2977, 2932, 2858, 1718, 1521, 1367, 1152 cm^{-1}; ^1H NMR ($CDCl_3$, 500 MHz): δ 7.70-7.68 (m, 4H, ArH), 7.44-7.34 (m, 6H, ArH), 5.91-5.82 (m, 1H, C<u>H</u>=CH_2), 5.38 (d, 1H, *J* = 7.0 Hz, NH), 5.26 (d, 1H, *J* = 17.1, CH=C<u>H</u>H), 5.19 (d, 1H, *J* = 10.5, CH=C<u>H</u>H), 4.56-4.42 (m, 2H, Alloc O<u>CH_2</u>), 4.28-4.13 (m, 2H, Alloc NH + Hα), 3.91-3.85 (m, 1H, Hɣ), 3.16-3.08 (m, 1H, Hε), 2.98-2.91 (m, 1H, Hε'), 1.95-1.88 (m, 2H, Hβ), 1.66-1.55 (m, 2H, Hδ), 1.44 (s, 9H, tBu), 1.39 (s, 9H, tBu), 1.06 (s, 9H, Si-tBu); ^{13}C NMR ($CDCl_3$, 125 MHz): δ 172.1, 156.5, 155.7, 136.1, 133.4, 133.2, 130.2, 130.0,

128.0, 127.9, 117.6, 81.6, 79.5, 69.2, 65.6, 52.2, 38.3, 37.2, 28.6, 28.2, 27.2, 19.6; HRMS (ES) Calcd for $C_{35}H_{53}N_2O_7Si$ $[M+H]^+$ 641.3617, found 641.3611.

(5*S*,7*R*)-7-(*tert*-Butyldiphenylsilyloxy)-1-(9*H*-fluoren-9-yl)-3,11-dioxo-2,12-dioxa-4,10-diazapentadec-14-ene-5-carboxylic acid (113)

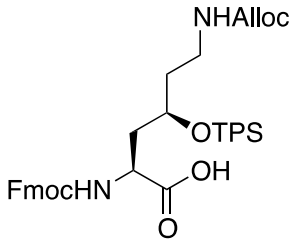

113

Boc-carbamate **112** (0.36 g, 0.55 mmol) was dissolved in dry CH_2Cl_2 (3.5 mL) and TFA (3.5 mL, 45.7 mmol) and stirred at ambient temperature for 2 h. The reaction mixture was then concentrated *in vacuo* and co-evaporated with toluene (3 x 3.5 mL). The resulting oil was dissolved in dry THF (3 mL), and the solution's pH adjusted to pH 8 with triethylamine (0.23 mL, 1.65 mmol). FmocOSu (0.22 g, 0.66 mmol) was then added and the reaction stirred at ambient temperature for 24 h. The reaction mixture was then acidified with AcOH (0.09 mL, 1.65 mmol), concentrated *in vacuo*, and purified by flash chromatography (SiO_2, 95:5 CH_2Cl_2:acetone + 1% AcOH) to yield Hyl derivative **113** as a white solid (0.18 g, 47% over 2 steps). $[\alpha]_D^{25}$ = 45.12 (*c* = 0.8 g/100mL, $CHCl_3$); IR ($CHCl_3$ cast) 3337, 3072, 3018, 2932, 2858, 1714, 1524, 1240, 1111, 759 cm^{-1}; ^1H NMR ($CDCl_3$, 500 MHz): δ7.75-7.27 (m, 18H, ArH), 6.07 (s, 1H, NH), 5.82-5.76 (m, 1H, Alloc C<u>H</u>=CH_2), 5.19-5.11 (m, 2H, J = 17.4, 10.0 Hz, Alloc CHC<u>H_2</u>), 4.45-3.88 (m, 8H, Alloc NH + Alloc OC<u>H_2</u> + Fmoc C<u>H_2</u> + Fmoc C<u>H</u> + Hα + Hɣ), 3.16-3.03 (m, 1H, Hε), 2.96-2.88 (m, 1H, Hε'), 2.12-2.01 (s, 2H, Hβ), 1.66-1.55 (s, 2H, Hδ), 1.05 (s, 9H, Si-tBu); ^{13}C NMR

($CDCl_3$, 125 MHz): δ 156.8, 144.1, 144.0, 141.4, 135.9, 134.1, 133.1, 132.8, 130.0, 129.9, 127.9, 127.8, 127.2, 125.4, 120.1, 117.7, 68.4, 67.3, 65.8, 47.3, 37.2, 27.1, 19.4; HRMS (ES) Calcd for $C_{41}H_{45}N_2O_7Si$ $[M-H]^-$ 705.3002, found 705.3014.

H-TriA$_1$-OH (114)

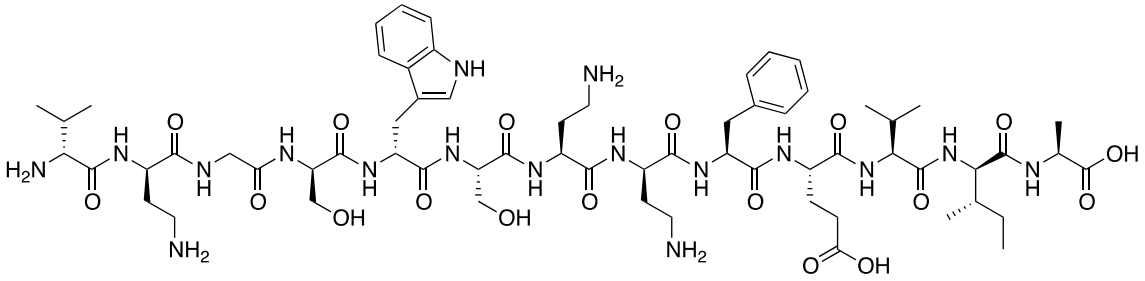

114

Peptide was isolated as a single peak using C_{18} HPLC (17.7 mg, 38%). Retention time (HPLC method 2) = 17.66 min. ^{1}H NMR (D_2O, 600 MHz): δ 7.57 (d, 1H, *J* = 7.9 Hz, Trp5-ArH), 7.46 (d, 1H, *J* = 8.2 Hz, Trp5-ArH), 7.31 (m, 3H, Trp5-ArH + Phe9-ArH), 7.21-7.19 (m, 4H, Trp5-ArH + Phe9-ArH), 7.11 (t, 1H, *J* = 7.4 Hz, Trp5-ArH), 4.68 (dd, 1H, *J* = 9.6, 5.9 Hz, Phe9-Hα), 4.63 (t, 1H, *J* = 7.3 Hz, Trp5-Hα), 4.52-4.49 (m, 1H, D-Ser4-Hα), 4.45 (t, 1H, *J* = 5.5 Hz, D-Dab2-Hα), 4.35-4.21 (m, 5H, D-*allo*-Ile12-Hα + Dab7-Hα + Glu10-Hα + D-Dab8-Hα + Ala13-Hα), 4.13-4.10 (m, 2H, Val11-Hα + Ser6-Hα), 3.90 (app. q, 2H, *J* = 13.0 Hz, Gly3-Hα), 3.85-3.80 (m, 1H, D-Val1-Hα), 3.73 (app. tt, 2H, *J* = 12.6, 6.3 Hz, D-Ser4-Hβ), 3.52 (dd, 1H, *J* = 11.5, 5.1 Hz, Ser6-Hβ), 3.29 (dd, 1H, *J* = 11.5, 5.6 Hz, Ser6-Hβ), 3.24 (d, 2H, *J* = 7.7 Hz, D-Trp5-Hβ), 3.17 (dd, 1H, *J* = 14.2, 5.7 Hz, Phe9-Hβ), 3.12-2.95 (m, 4H, D-Dab2-Hγ + Dab7-Hγ), 2.87 (dd, 1H, *J* = 13.9, 9.8 Hz, Phe9-Hβ), 2.73-2.67 (m, 1H, D-Dab8-Hγ), 2.62-2.55 (m, 1H, D-Dab8-Hγ), 2.32-2.30 (m, 2H, Glu10-Hγ + D-Dab2-Hβ), 2.23-1.75 (m, 11H, D-Dab2-Hβ + Dab7-Hβ + D-Val1-Hβ + Dab7-Hβ + D-Dab8-Hβ + Glu10-Hβ + Val11-Hβ + D-*allo*-Ile12-Hβ + Glu10-

Hγ), 1.37-1.27 (m, 5H, Ala13-Hβ + D-*allo*-Ile12-Hγ), 0.94-0.77 (m, 18H, D-Val1-Hγ + Val11-Hγ + D-*allo*-Ile12-Hγ, Hδ). MW calculated for $C_{64}H_{100}N_{17}O_{18}$ 1394.7427, found *high resolution* (FTICR-ESI-MS) 1394.7421 $(M+H)^+$.

Ac-TriA_1-OH (115)

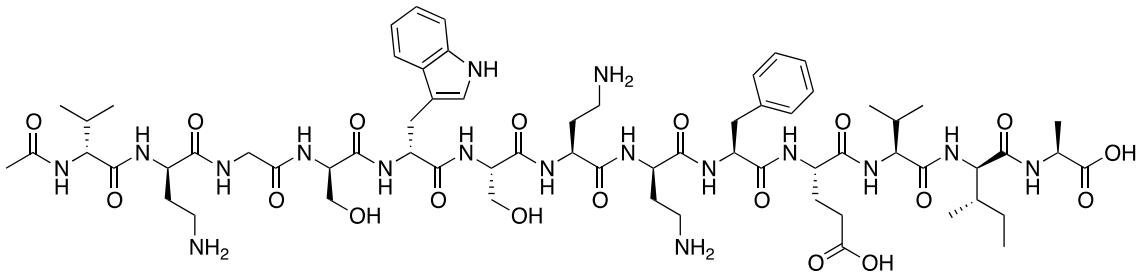

115

Peptide was isolated as a single peak using C_{18} HPLC (8.1 mg, 45 %). Retention time (HPLC method 2) = 21.43 min. ^{1}H NMR (D_2O, 600 MHz): δ 7.57 (d, 1H, *J* = 8.0 Hz, Trp5-ArH), 7.46 (d, 1H, *J* = 8.2 Hz, Trp5-ArH), 7.32-7.25 (m, 3H, Trp5-ArH + Phe9-ArH), 7.21-7.19 (m, 4H, Trp5-ArH + Phe9-ArH), 7.11 (t, 1H, *J* = 7.5 Hz, Trp5-ArH), 4.67 (dd, 1H, *J* = 9.7, 5.8 Hz, Phe9-Hα), 4.61 (t, 1H, *J* = 7.3 Hz, Trp5-Hα), 4.47-4.42 (m, 2H, D-Ser4-Hα + D-Dab2-Hα), 4.35-4.21 (m, 5H, D-*allo*-Ile12-Hα + Dab7-Hα + Glu10-Hα + D-Dab8-Hα + Ala13-Hα), 4.13-4.10 (m, 2H, Val11-Hα + Ser6-Hα), 4.00 (d, 1H, *J* = 7.6 Hz, D-Val1-Hα), 3.89 (app. q, 2H, *J* = 13.1 Hz, Gly3-Hα), 3.74 (app. qd, 2H, *J* = 11.3, 5.5 Hz, D-Ser4-Hβ), 3.53 (dd, 1H, *J* = 11.5, 5.0 Hz, Ser6-Hβ), 3.30 (dd, 1H, *J* = 11.4, 5.6 Hz, Ser6-Hβ), 3.25 (d, 2H, *J* = 7.5 Hz, D-Trp5-Hβ), 3.17 (dd, 1H, *J* = 14.1, 5.7 Hz, Phe9-Hβ), 3.10-2.99 (m, 4H, D-Dab2-Hγ + Dab7-Hγ), 2.88 (dd, 1H, *J* = 14.2, 9.7 Hz, Phe9-Hβ), 2.70 (ddd, 1H, *J* = 12.7, 10.5, 5.3 Hz, D-Dab8-Hγ), 2.59 (ddd, 1H, *J* = 12.7, 10.4, 5.9 Hz, D-Dab8-Hγ), 2.32-2.30 (m, 2H, Glu10-Hγ + D-Dab2-Hβ), 2.21-2.14 (m, 2H, D-Dab2-Hβ + Dab7-Hβ), 2.09-1.78 (m, 12H, Lipid-CH_3, D-Val1-Hβ + Dab7-Hβ + D-Dab8-Hβ + Glu10-

Hβ + Val11-Hβ + D-*allo*-Ile12-Hβ + Glu10-Hγ), 1.37-1.27 (m, 4H, Ala13-Hβ + D-*allo*-Ile12-Hγ), 1.25-1.18 (m, 1H, D-*allo*-Ile12-Hγ), 0.94-0.84 (m, 18H, D-Val1-Hγ + Val11-Hγ + D-*allo*-Ile12-Hδ). MW calculated for $C_{66}H_{102}N_{17}O_{19}$ 1436.7532, found *high resolution* (FTICR-ESI-MS) 1436.7537 $(M+H)^+$.

But-TriA_1-OH (116)

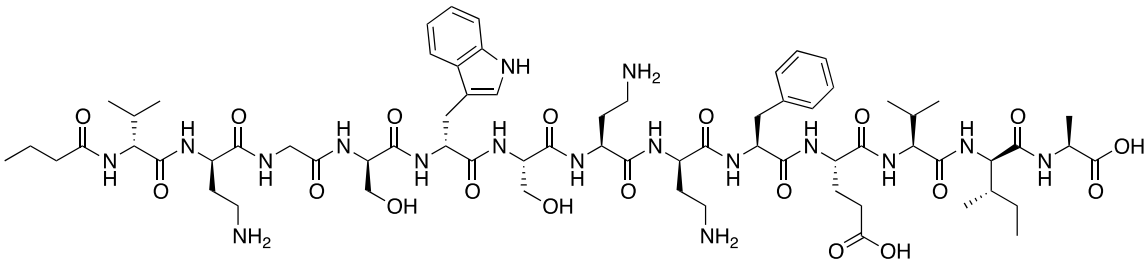

116

Peptide was isolated as a single peak using C_{18} HPLC (5.8 mg, 32 %). Retention time (HPLC method 2) = 24.83 min. ^{1}H NMR (D_2O, 600 MHz): δ 7.57 (d, 1H, *J* = 8.0 Hz, Trp5-ArH), 7.46 (d, 1H, *J* = 8.2 Hz, Trp5-ArH), 7.32-7.25 (m, 3H, Trp5-ArH + Phe9-ArH), 7.21-7.19 (m, 4H, Trp5-ArH + Phe9-ArH), 7.11 (t, 1H, *J* = 7.5 Hz, Trp5-ArH), 4.67 (dd, 1H, *J* = 9.7, 5.8 Hz, Phe9-Hα), 4.61 (t, 1H, *J* = 7.4 Hz, Trp5-Hα), 4.45-4.42 (m, 2H, D-Ser4-Hα + D-Dab2-Hα), 4.35-4.20 (m, 5H, D-*allo*-Ile12-Hα + Dab7-Hα + Glu10-Hα + D-Dab8-Hα + Ala13-Hα), 4.13-4.10 (m, 2H, Val11-Hα + Ser6-Hα), 4.01 (d, 1H, *J* = 7.6 Hz, D-Val1-Hα), 3.89 (app. q, 2H, *J* = 13.0 Hz, Gly3-Hα), 3.74 (app. qd, 2H, *J* = 11.3, 5.5 Hz, D-Ser4-Hβ), 3.54 (dd, 1H, *J* = 11.4, 5.0 Hz, Ser6-Hβ), 3.30 (dd, 1H, *J* = 11.4, 5.6 Hz, Ser6-Hβ), 3.25 (d, 2H, *J* = 7.5 Hz, D-Trp5-Hβ), 3.17 (dd, 1H, *J* = 14.1, 5.7 Hz, Phe9-Hβ), 3.08-2.96 (m, 4H, D-Dab2-Hγ + Dab7-Hγ), 2.87 (dd, 1H, *J* = 14.0, 9.7 Hz, Phe9-Hβ), 2.71 (ddd, 1H, *J* = 12.7, 10.5, 5.3 Hz, D-Dab8-Hγ), 2.59 (ddd, 1H, *J* = 12.7, 10.4, 5.9 Hz, D-Dab8-Hγ), 2.32-2.14 (m, 6H, Glu10-Hγ + D-Dab2-Hβ + D-Dab2-Hβ + Dab7-Hβ + Lipid-

Hα), 2.09-1.80 (m, 9H, D-Val1-Hβ + Dab7-Hβ + D-Dab8-Hβ + Glu10-Hβ + Val11-Hβ + D-*allo*-Ile12-Hβ + Glu10-Hγ), 1.55 (sextet, 2H, *J* = 7.4 Hz, Lipid-Hβ), 1.32-1.28 (m, 4H, Ala13-Hβ + D-*allo*-Ile12-Hγ), 1.24-1.19 (m, 1H, D-*allo*-Ile12-Hγ), 0.94-0.84 (m, 21H, D-Val1-Hγ + Val11-Hγ + D-*allo*-Ile12-Hγ, Hδ, Lipid-CH_3). MW calculated for $C_{68}H_{106}N_{17}O_{19}$ 1464.7845, found *high resolution* (FTICR-ESI-MS) 1464.7848 $(M+H)^+$.

Hex-TriA_1-OH (117)

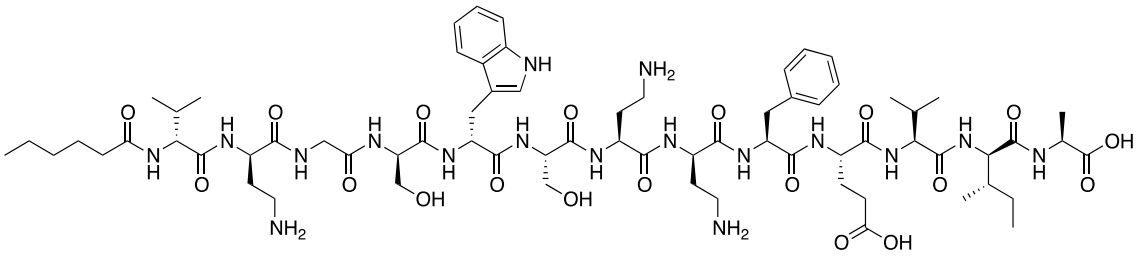

117

Peptide was isolated as a single peak using C_{18} HPLC (7.1 mg, 38 %). Retention time (HPLC method 2) = 29.72 min. ^{1}H NMR (D_2O, 600 MHz): δ 7.57 (d, 1H, *J* = 8.0 Hz, Trp5-ArH), 7.46 (d, 1H, *J* = 8.2 Hz, Trp5-ArH), 7.32-7.26 (m, 3H, Trp5-ArH + Phe9-ArH), 7.21-7.19 (m, 4H, Trp5-ArH + Phe9-ArH), 7.11 (t, 1H, *J* = 7.5 Hz, Trp5-ArH), 4.67 (m, 1H, Phe9-Hα), 4.61 (t, 1H, *J* = 7.4 Hz, Trp5-Hα), 4.44-4.42 (m, 2H, D-Ser4-Hα + D-Dab2-Hα), 4.35-4.22 (m, 5H, D-*allo*-Ile12-Hα + Dab7-Hα + Glu10-Hα + D-Dab8-Hα + Ala13-Hα), 4.13-4.10 (m, 2H, Val11-Hα + Ser6-Hα), 4.01 (d, 1H, *J* = 7.6 Hz, D-Val1-Hα), 3.89 (s, 2H, Gly3-Hα), 3.74 (app. qd, 2H, *J* = 11.7, 5.5 Hz, D-Ser4-Hβ), 3.54 (dd, 1H, *J* = 11.4, 5.0 Hz, Ser6-Hβ), 3.30 (dd, 1H, *J* = 11.4, 5.5 Hz, Ser6-Hβ), 3.25 (d, 2H, *J* = 7.3 Hz, D-Trp5-Hβ), 3.17 (dd, 1H, *J* = 13.9, 5.8 Hz, Phe9-Hβ), 3.07-2.96 (m, 4H, D-Dab2-Hγ + Dab7-Hγ), 2.87 (dd, 1H, *J* = 13.4, 9.9 Hz, Phe9-Hβ), 2.73-2.68 (m, 1H, D-Dab8-Hγ), 2.61-2.57 (m, 1H, D-Dab8-Hγ), 2.34-2.14 (m, 6H, Glu10-Hγ + D-Dab2-Hβ + D-Dab2-Hβ

+ Dab7-Hβ + Lipid-Hα), 2.09-1.80 (m, 9H, D-Val1-Hβ + Dab7-Hβ + D-Dab8-Hβ + Glu10-Hβ + Val11-Hβ + D-*allo*-Ile12-Hβ + Glu10-Hγ), 1.53 (sextet, 2H, *J* = 7.4 Hz, Lipid-Hβ), 1.32-1.19 (m, 9H, Ala13-Hβ + D-*allo*-Ile12-Hγ + Lipid-Hγ, Hδ), 0.94-0.80 (m, 21H, D-Val1-Hγ + Val11-Hγ + D-*allo*-Ile12-Hγ, Hδ, Lipid-CH_3). MW calculated for $C_{70}H_{111}N_{17}O_{19}$ 1492.8158, found *high resolution* (FTICR-ESI-MS) 1492.8162 $(M+H)^+$.

Hep-TriA_1-OH (118)

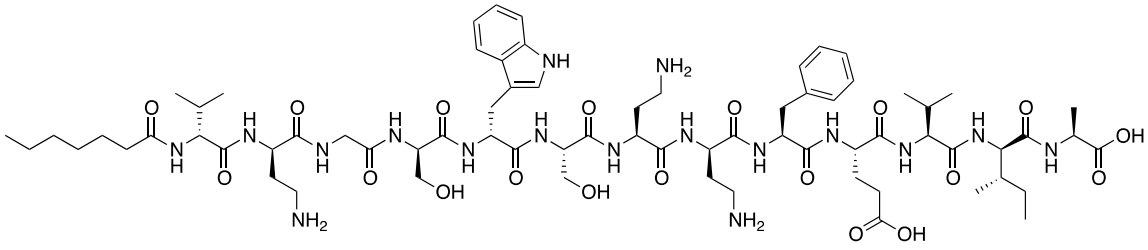

118

Peptide was isolated as a single peak using C_{18} HPLC (3.5 mg, 23.2 %). Retention time (HPLC method 2) = 22.79 min. ^{1}H NMR (D_2O, 600 MHz): δ 7.57 (d, 1H, *J* = 8.1 Hz, Trp5-ArH), 7.46 (d, 1H, *J* = 8.2 Hz, Trp5-ArH), 7.32-7.25 (m, 4H, Trp5-ArH + Phe9-ArH), 7.21-7.19 (m, 3H, Trp5-ArH + Phe9-ArH), 7.11 (t, 1H, *J* = 7.4 Hz, Trp5-ArH), 4.67 (dd, *J* = 9.8, 5.5 Hz, 1H, Phe9-Hα), 4.61 (t, 1H, *J* = 7.4 Hz, Trp5-Hα), 4.45-4.41 (m, 2H, D-Ser4-Hα + D-Dab2-Hα), 4.35-4.21 (m, 5H, D-*allo*-Ile12-Hα + Dab7-Hα + Glu10-Hα + D-Dab8-Hα + Ala13-Hα), 4.13-4.10 (m, 2H, Val11-Hα + Ser6-Hα), 4.01 (d, 1H, *J* = 7.6 Hz, D-Val1-Hα), 3.89 (s, 2H, Gly3-Hα), 3.74 (app. qd, 2H, *J* = 11.8, 5.4 Hz, D-Ser4-Hβ), 3.54 (dd, 1H, *J* = 11.6, 5.1 Hz, Ser6-Hβ), 3.30 (dd, 1H, *J* = 11.4, 5.6 Hz, Ser6-Hβ), 3.25 (d, 2H, *J* = 7.7 Hz, D-Trp5-Hβ), 3.17 (dd, 1H, *J* = 14.0, 5.7 Hz, Phe9-Hβ), 3.07-2.97 (m, 4H, D-Dab2-Hγ + Dab7-Hγ), 2.87 (dd, 1H, *J* = 14.1, 9.9 Hz, Phe9-Hβ), 2.71 (app. td, 1H, *J* = 11.5, 4.4 Hz, D-Dab8-Hγ), 2.59 (app. td, 1H, *J* = 10.7, 5.5 Hz, D-Dab8-Hγ), 2.34-2.14

(m, 6H, Glu10-Hγ + D-Dab2-Hβ + D-Dab2-Hβ + Dab7-Hβ + Lipid-Hα), 2.09-1.80 (m, 9H, D-Val1-Hβ + Dab7-Hβ + D-Dab8-Hβ + Glu10-Hβ + Val11-Hβ + D-*allo*-Ile12-Hβ + Glu10-Hγ), 1.54-1.48 (m, 2H, Lipid-Hβ), 1.33-1.19 (m, 11H, Ala13-Hβ + D-*allo*-Ile12-Hγ + Lipid-Hγ, Hδ, Hε), 0.94-0.80 (m, 21H, D-Val1-Hγ + Val11-Hγ + D-*allo*-Ile12-Hγ, Hδ, Lipid-CH_3). MW calculated for $C_{71}H_{112}N_{17}O_{19}$ 1506.8315, found *high resolution* (FTICR-ESI-MS) 1506.8331 $(M+H)^+$.

Oct-TriA_1-OH (119)

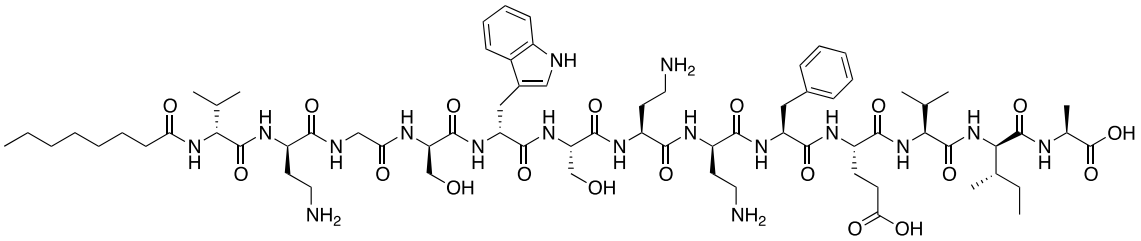

119

Peptide was isolated as a single peak using C_{18} HPLC (17.5 mg, 46 %). Retention time (HPLC method 2) = 35.98 min. ^{1}H NMR (D_2O, 600 MHz): δ 7.57 (d, 1H, *J* = 7.9 Hz, Trp5-ArH), 7.46 (d, 1H, *J* = 8.6 Hz, Trp5-ArH), 7.32-7.25 (m, 3H, Trp5-ArH + Phe9-ArH), 7.21-7.19 (m, 4H, Trp5-ArH + Phe9-ArH), 7.11 (t, 1H, *J* = 7.4 Hz, Trp5-ArH), 4.69-4.66 (m, 1H, Phe9-Hα), 4.62 (t, 1H, *J* = 8.2 Hz, Trp5-Hα), 4.45-4.41 (m, 2H, D-Ser4-Hα + D-Dab2-Hα), 4.34-4.24 (m, 5H, D-*allo*-Ile12-Hα + Dab7-Hα + Glu10-Hα + D-Dab8-Hα + Ala13-Hα), 4.13-4.10 (m, 2H, Val11-Hα + Ser6-Hα), 4.01 (d, 1H, *J* = 7.5 Hz, D-Val1-Hα), 3.89 (s, 2H, Gly3-Hα), 3.78-3.71 (m, 2H, D-Ser4-Hβ), 3.56-3.53 (m, 1H, Ser6-Hβ), 3.31-3.29 (m, 1H, Ser6-Hβ), 3.26 (d, 2H, *J* = 6.7 Hz, D-Trp5-Hβ), 3.18-3.15 (m, 1H, Phe9-Hβ), 3.07-2.96 (m, 4H, D-Dab2-Hγ + Dab7-Hγ), 2.89-2.86 (m, 1H, Phe9-Hβ), 2.73-2.68 (m, 1H, D-Dab8-Hγ), 2.61-2.57 (m, 1H, D-Dab8-Hγ), 2.34-2.14 (m, 6H, Glu10-Hγ + D-

Dab2-Hβ + Dab7-Hβ + Lipid-Hα), 2.09-1.79 (m, 9H, D-Val1-Hβ + Dab7-Hβ + D-Dab8-Hβ + Glu10-Hβ + Val11-Hβ + D-*allo*-Ile12-Hβ + Glu10-Hγ), 1.54-1.48 (m, 2H, Lipid-Hβ), 1.34-1.17 (m, 13H, Ala13-Hβ + D-*allo*-Ile12-Hγ + Lipid-Hγ, Hδ, Hε, Hζ), 0.94-0.79 (m, 21H, D-Val1-Hγ + Val11-Hγ + D-*allo*-Ile12-Hγ, Hδ, Lipid-CH_3). MW calculated for $C_{72}H_{114}N_{17}O_{19}$ 1520.8471, found *high resolution* (FTICR-ESI-MS) 1520.8471 $(M+H)^+$.

Non-TriA_1-OH (120)

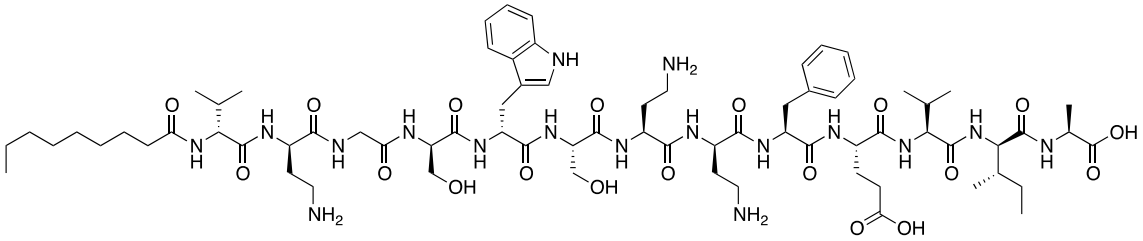

120

Peptide was isolated as a single peak using C_{18} HPLC (10 mg, 65 %). Retention time (HPLC method 2) = 35.15 min. ^{1}H NMR (D_2O + 10 % CD_3OD, 600 MHz, solvent suppression at 4.724 and 3.249 ppm): δ 7.55 (d, 1H, *J* = 7.6 Hz, Trp5-ArH), 7.44 (d, 1H, *J* = 8.3 Hz, Trp5-ArH), 7.29-7.23 (m, 3H, Trp5-ArH + Phe9-ArH), 7.18-7.16 (m, 4H, Trp5-ArH + Phe9-ArH), 7.09 (t, 1H, *J* = 7.7 Hz, Trp5-ArH), 4.75.4.77 (m, 1H, Phe9-Hα), 4.60-3.57 (m, Trp5-Hα), 4.42-4.39 (m, 2H, D-Ser4-Hα + D-Dab2-Hα), 4.32-4.16 (m, 5H, D-*allo*-Ile12-Hα + Dab7-Hα + Glu10-Hα + D-Dab8-Hα + Ala13-Hα), 4.11-4.08 (m, 2H, Val11-Hα + Ser6-Hα), 3.99-3.97 (m, 1H, D-Val1-Hα), 3.87 (s, 2H, Gly3-Hα), 3.78-3.71 (m, 2H, D-Ser4-Hβ), 3.61-3.51 (m, 2H, Ser6-Hβ), 3.18-3.15 (m, 1H, Phe9-Hβ), 3.03-2.95 (m, 4H, D-Dab2-Hγ + Dab7-Hγ), 2.87-2.81 (m, 1H, Phe9-Hβ), 2.73-2.68 (m, 1H, D-Dab8-Hγ), 2.61-2.57 (m, 1H, D-Dab8-Hγ), 2.29-2.11 (m, 6H, Glu10-Hγ + D-Dab2-Hβ + Dab7-Hβ + Lipid-Hα), 2.05-1.74 (m, 9H, D-Val1-Hβ + Dab7-Hβ + D-Dab8-Hβ + Glu10-Hβ +

Val11-Hβ + D-*allo*-Ile12-Hβ + Glu10-Hγ), 1.51-1.47 (m, 2H, Lipid-Hβ), 1.30-1.13 (m, 15H, Ala13-Hβ + D-*allo*-Ile12-Hγ + Lipid-Hγ, Hδ, Hε, Hζ, Hη), 0.93-0.78 (m, 21H, D-Val1-Hγ + Val11-Hγ + D-*allo*-Ile12-Hγ, Hδ, Lipid-CH_3). MW calculated for $C_{73}H_{116}N_{17}O_{19}$ 1534.8628, found *high resolution* (FTICR-ESI-MS) 1534.8623 $(M+H)^+$.

Dec-TriA_1-OH (121)

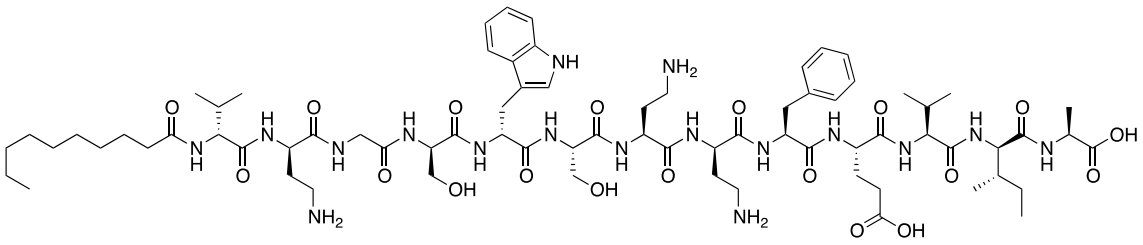

121

Peptide was isolated as a single peak using C_{18} HPLC (5.1 mg, 26 %). Retention time (HPLC method 2) = 41.28 min. ^{1}H NMR (D_2O + 10 % CD_3OD, 600 MHz): δ 7.67 (d, 1H, *J* = 7.7 Hz, Trp5-ArH), 7.57 (d, 1H, *J* = 7.8 Hz, Trp5-ArH), 7.43-7.37 (m, 3H, Trp5-ArH + Phe9-ArH), 7.32-7.30 (m, 4H, Trp5-ArH + Phe9-ArH), 7.21 (t, 1H, *J* = 7.1 Hz, Trp5-ArH), 4.81-4.76 (m, 1H, Phe9-Hα), 4.75-4.70 obscured by solvent (m, 1H, Trp5-Hα), 4.59-4.50 (m, 2H, D-Ser4-Hα + D-Dab2-Hα), 4.48-4.37 (m, 5H, D-*allo*-Ile12-Hα + Dab7-Hα + Glu10-Hα + D-Dab8-Hα + Ala13-Hα), 4.29-4.22 (m, 2H, Val11-Hα + Ser6-Hα), 4.15 (d, 1H, *J* = 7.1 Hz, D-Val1-Hα), 4.01 (app. q, 2H, *J* = 13.2 Hz, Gly3-Hα), 3.90-3.81 (m, 2H, D-Ser4-Hβ), 3.75-3.69 (m, 1H, Ser6-Hβ), 3.47-3.42 (m, 1H, Ser6-Hβ), 3.40-3.30 (m, 2H, D-Trp5-Hβ), 3.30-3.25 (m, 1H, Phe9-Hβ), 3.18-3.06 (m, 4H, D-Dab2-Hγ + Dab7-Hγ), 3.03-2.97 (m, 1H, Phe9-Hβ), 2.87-2.81 (m, 1H, D-Dab8-Hγ), 2.79-2.74 (m, 1H, D-Dab8-Hγ), 2.50-1.90 (m, 15H, Glu10-Hγ + D-Dab2-Hβ + Dab7-Hβ + Lipid-Hα + D-Val1-Hβ + D-Dab8-Hβ + Glu10-Hβ + Val11-Hβ + D-*allo*-Ile12-Hβ), 1.67-1.60 (m, 2H, Lipid-Hβ), 1.47-

1.27 (m, 15H, Ala13-Hβ + D-*allo*-Ile12-Hγ + Lipid-Hγ, Hδ, Hε, Hζ, Hη), 1.08-0.92 (m, 21H, D-Val1-Hγ + Val11-Hγ + D-*allo*-Ile12-Hγ, Hδ, Lipid-CH_3). MW calculated for $C_{74}H_{118}N_{17}O_{19}$ 1548.8484, found *high resolution* (FTICR-ESI-MS) 1548.8794 $(M+H)^+$.

Undec-TriA_1-OH (122)

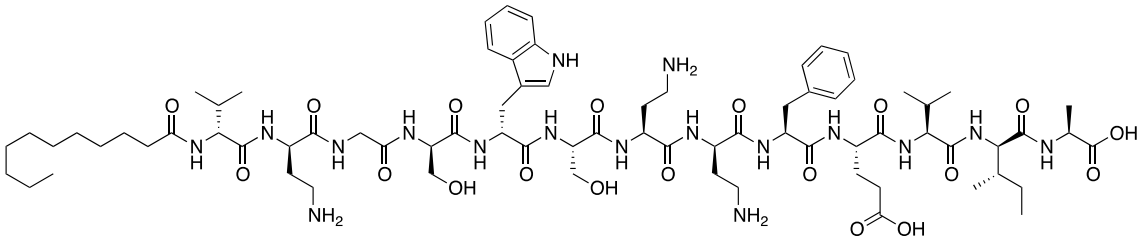

122

Peptide was isolated as a single peak using C_{18} HPLC (9 mg, 57.6 %). Retention time (HPLC method 2) = 44.20 min. ^{1}H NMR (D_2O + 10 % CD_3OD, 600 MHz): δ 7.53 (d, 1H, *J* = 8.0 Hz, Trp5-ArH), 7.41 (d, 1H, *J* = 8.0 Hz, Trp5-ArH), 7.28-7.21 (m, 3H, Trp5-ArH + Phe9-ArH), 7.16-7.13 (m, 4H, Trp5-ArH + Phe9-ArH), 7.07-7.05 (m, 1H, Trp5-ArH), 4.65-4.62 (m, 1H, Phe9-Hα), 4.59-4.56 (m, 1H, Trp5-Hα), 4.42-4.36 (m, 2H, D-Ser4-Hα + D-Dab2-Hα), 4.31-4.22 (m, 5H, D-*allo*-Ile12-Hα + Dab7-Hα + Glu10-Hα + D-Dab8-Hα + Ala13-Hα), 4.08-4.06 (m, 2H, Val11-Hα + Ser6-Hα), 3.98-3.95 (m, 1H, D-Val1-Hα), 3.86-3.84 (m, 2H, Gly3-Hα), 3.77-3.72 (m, 2H, D-Ser4-Hβ), 3.70-3.68 (m, 1H, Ser6-Hβ), 3.54-3.50 (m, 1H, Ser6-Hβ), 3.40-3.30 (m, 2H, D-Trp5-Hβ), 3.30-3.25 (m, 1H, Phe9-Hβ), 3.18-3.06 (m, 4H, D-Dab2-Hγ + Dab7-Hγ), 2.85-2.81 (m, 1H, Phe9-Hβ), 2.71-2.65 (m, 1H, D-Dab8-Hγ), 2.60-2.54 (m, 1H, D-Dab8-Hγ), 2.31-2.33 (m, 6H, Glu10-Hγ + D-Dab2-Hβ + Dab7-Hβ + Lipid-Hα), 2.04-1.77 (m, 9H, D-Val1-Hβ + Dab7-Hβ + D-Dab8-Hβ + Glu10-Hβ + Val11-Hβ + D-*allo*-Ile12-Hβ + Glu10-Hγ), 1.52-1.45 (m, 2H, Lipid-Hβ), 1.32-1.13 (m, 19H, Ala13-Hβ + D-*allo*-Ile12-Hγ + Lipid-Hγ, Hδ, Hε, Hζ, Hη, Hθ, Hι), 0.91-0.75

(m, 21H, D-Val1-Hγ + Val11-Hγ + D-*allo*-Ile12-Hγ, Hδ, Lipid-CH_3). MW calculated for $C_{75}H_{120}N_{17}O_{19}$ 1562.8941, found *high resolution* (FTICR-ESI-MS) 1562.8955 $(M+H)^+$.

Laur-TriA_1-OH (123)

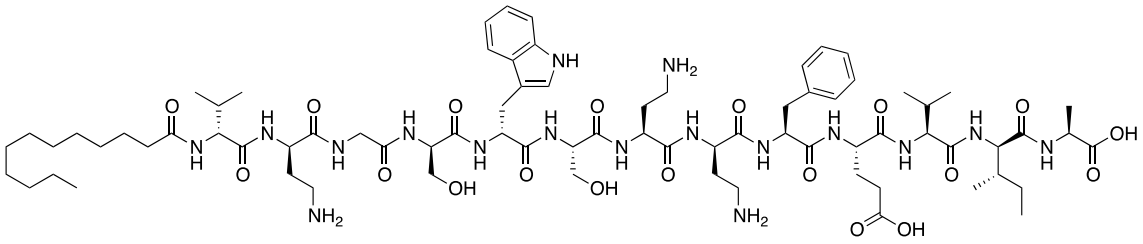

123

Peptide was isolated as a single peak using C_{18} HPLC (3.0 mg, 20 %). Retention time (HPLC method 2) = 47.68 min. ^{1}H NMR (D_2O + 10 % CD_3OD, 600 MHz): δ 7.51 (d, 1H, *J* = 8.0 Hz, Trp5-ArH), 7.38 (d, 1H, *J* = 8.0 Hz, Trp5-ArH), 7.25-7.19 (m, 3H, Trp5-ArH + Phe9-ArH), 7.15-7.11 (m, 3H, Trp5-ArH + Phe9-ArH), 7.04-7.02 (m, 1H, Trp5-ArH), 4.63-4.61 (m, 1H, Phe9-Hα), 4.57-4.54 (m, 1H, Trp5-Hα), 4.41-4.34 (m, 2H, D-Ser4-Hα + D-Dab2-Hα), 4.30-4.21 (m, 5H, D-*allo*-Ile12-Hα + Dab7-Hα + Glu10-Hα + D-Dab8-Hα + Ala13-Hα), 4.06-4.03 (m, 2H, Val11-Hα + Ser6-Hα), 3.96-3.94 (m, 1H, D-Val1-Hα), 3.88-3.50 (m, 2H, Gly3-Hα + D-Ser4-Hβ + Ser6-Hβ + D-Trp5-Hβ), 3.10-3.07 (m, 1H, Phe9-Hβ), 3.01-2.92 (m, 4H, D-Dab2-Hγ + Dab7-Hγ), 2.83-2.79 (m, 1H, Phe9-Hβ), 2.68-2.64 (m, 1H, D-Dab8-Hγ), 2.58-2.54 (m, 1H, D-Dab8-Hγ), 2.29-2.09 (m, 6H, Glu10-Hγ + D-Dab2-Hβ + Dab7-Hβ + Lipid-Hα), 2.01-1.76 (m, 9H, D-Val1-Hβ + Dab7-Hβ + D-Dab8-Hβ + Glu10-Hβ + Val11-Hβ + D-*allo*-Ile12-Hβ + Glu10-Hγ), 1.49-1.43 (m, 2H, Lipid-Hβ), 1.32-1.13 (m, 21H, Ala13-Hβ + D-*allo*-Ile12-Hγ + Lipid-Hγ, Hδ, Hε, Hζ, Hη, Hθ, Hι, Hκ), 0.89-0.73 (m, 21H, D-Val1-Hγ + Val11-Hγ + D-*allo*-Ile12-Hγ, Hδ, Lipid-CH_3). MW

calculated for $C_{76}H_{122}N_{17}O_{19}$ 1576.9097, found *high resolution* (FTICR-ESI-MS) 1576.9102 $(M+H)^+$.

Myr-TriA_1-OH (124)

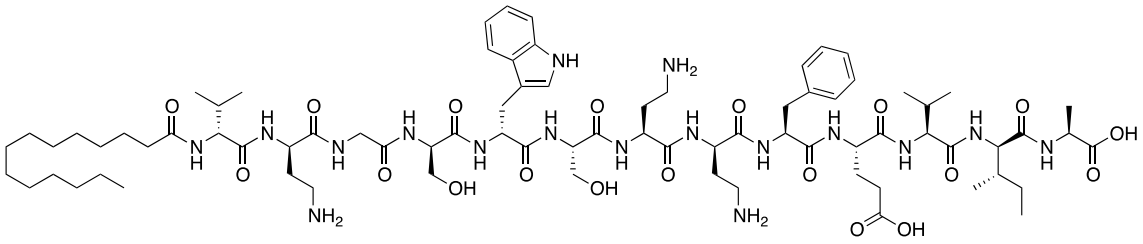

124

Peptide was isolated as a single peak using C_{18} HPLC (3.2 mg, 20 %). Retention time (HPLC method 2) = 51.60 min. MS/MS: *m/z* 203.1 (y2), 302.2 (y3), 431.2 (y4), 678.3 (y6), 778.3 (y7), 865.4 (y8), 1195.5 (y11), 310.3 (b1), 410.3 (b2), 467.3 (b3), 554.3 (b4), 1027.5 (b8), 1174.5 (b9), 1303.6 (b10), 1402.7 (b11), 1515.9 (b12), 282.3 (a1), 526.4 (a4), 712.4 (a5). MW calculated for $C_{78}H_{126}N_{17}O_{19}$ 1604.9410, found *high resolution* (FTICR-ESI-MS) 1604.9417 $(M+H)^+$.

Palm-TriA_1-OH (125)

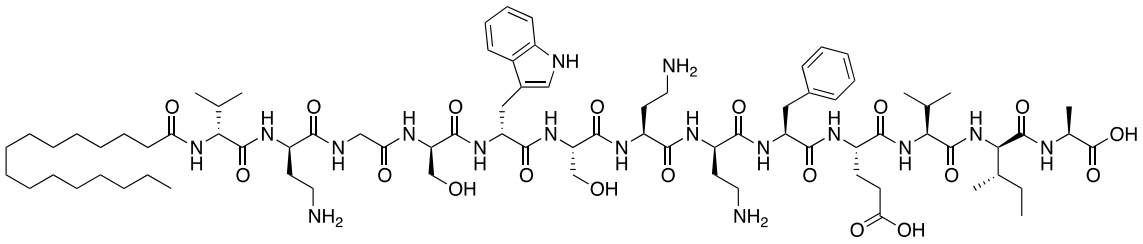

125

Peptide was isolated as a single peak using C_{18} HPLC (1.0 mg, 9 %). Retention time (HPLC method 2) = 52.80 min. MS/MS: *m/z* 302.2 (y2), 431.2 (y4), 578.5 (y5), 678.3 (y6), 778.3 (y7), 865.4 (y8), 1051.5 (y9), 1195.5 (y11), 1295.5 (y12), 338.3 (b1), 438.3

(b2), 495.4 (b3), 582.4 (b4), 1055.6 (b8), 1202.7 (b9), 1331.7 (b10), 1430.7 (b11), 310.3 (a1), 554.4 (a4), 740.4 (a5). MW calculated for $C_{80}H_{130}N_{17}O_{19}$ 1632.9723, found *high resolution* (FTICR-ESI-MS) 1632.9718 $(M+H)^+$.

Fmoc-TriA_1-OH (126)

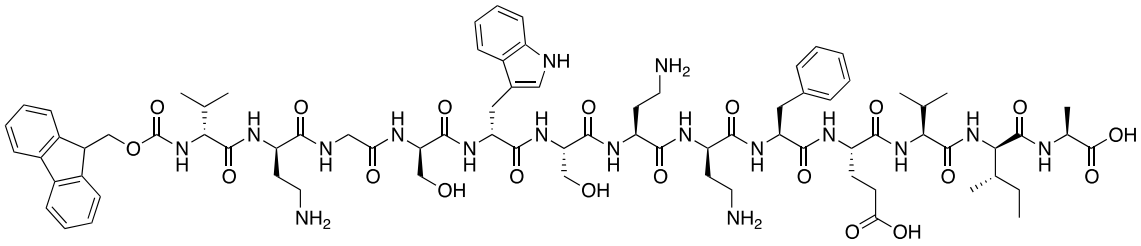

126

Peptide was isolated as a single peak using C_{18} HPLC (10 mg, 19 %). Retention time (HPLC method 2) = 38.59 min. MS/MS: *m/z* 203.1 (y2), 302.2 (y3), 431.2 (y4), 578.3 (y5), 678.3 (y6), 778.4 (y7), 865.4 (y8), 1051.4 (y9), 1138.4 (y10), 1195.5 (y11), 1295.5 (y12), 422.2 (b2), 479.2 (b3), 566.2 (b4), 752.3 (b5), 839.3 (b6), 1039.4 (b8), 1186.5 (b9), 1315.5 (b10), 1414.6 (b11), 294.2 (a1), 538.2 (a4), 724.3 (a5), 1386.5 (a11). MW calculated for $C_{79}H_{110}N_{17}O_{20}$ 1616.8108, found *high resolution* (FTICR-ESI-MS) 1616.8088 $(M+H)^+$.

Fpa-TriA_1-OH (127)

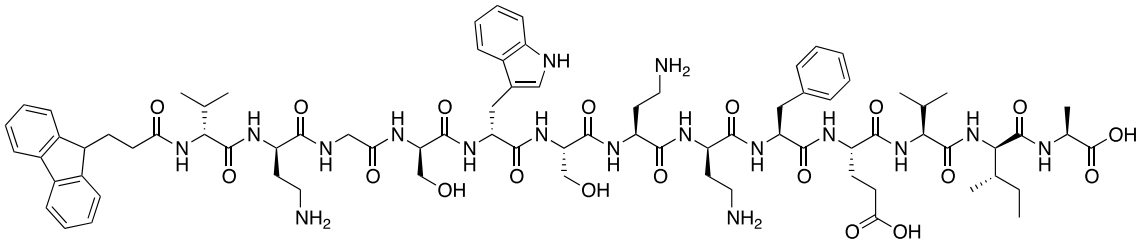

127

Peptide was isolated as a single peak using C_{18} HPLC (6.4 mg, 32 %). Retention time (HPLC method 2) = 37.94 min. MS/MS: *m/z* 203.1 (y2), 302.2 (y3), 431.2 (y4), 578.3 (y5), 678.3 (y6), 778.4 (y7), 865.4 (y8), 1051.4 (y9), 1138.4 (y10), 1195.5 (y11), 1295.5 (y12), 320.2 (b1), 564.2 (b4), 750.3 (b5), 837.4 (b6), 1037.4 (b8), 1184.4 (b9), 1313.5 (b10), 1412.6 (b11), 1525.7 (b12), 292.2 (a1), 536.2 (a4), 722.3 (a5), 1497.6 (a12). MW calculated for $C_{80}H_{112}N_{17}O_{19}$ 1614.8315, found *high resolution* (FTICR-ESI-MS) 1614.8297 $(M+H)^+$.

Anth-TriA_1-OH (128)

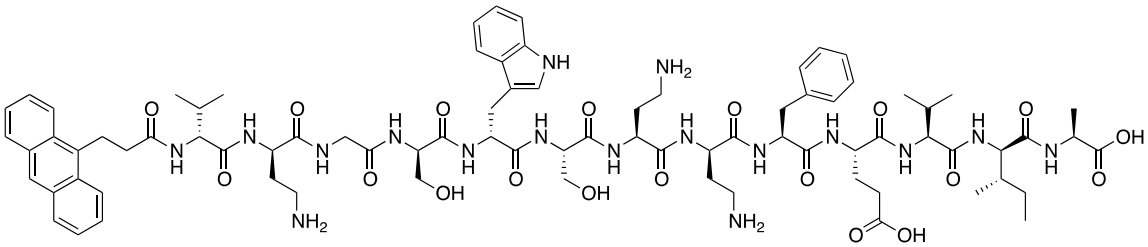

128

Peptide was isolated as a single peak using C_{18} HPLC (5.5 mg, 16 %). Retention time (HPLC method 2) = 39.88 min. ^{1}H NMR (D_2O + 10 % CD_3OD, 600 MHz): δ 7.51-7.02 (m, 18H, Trp5-ArH + Phe9-ArH + Anth-ArH), 4.65-4.61 (m, 1H, Phe9-Hα), 4.55 (t, 1H, *J* = 7.3 Hz, Trp5-Hα), 4.39-4.18 (m, 7H, D-Ser4-Hα + D-Dab2-Hα + D-*allo*-Ile12-Hα + Dab7-Hα + Glu10-Hα + D-Dab8-Hα + Ala13-Hα), 4.09-4.06 (m, 2H, Val11-Hα + Ser6-Hα), 3.89-3.86 (m, 3H, D-Val1-Hα + Gly3-Hα), 3.70-3.63 (m, 2H, D-Ser4-Hβ), 3.56-3.53 (m, 1H, Ser6-Hβ), 3.30-3.10 obscured by MeOH (m, 4H, Ser6-Hβ + D-Trp5-Hβ + Phe9-Hβ), 3.01-2.91 (m, 4H, D-Dab2-Hγ + Dab7-Hγ), 2.87-2.79 (m, 1H, Phe9-Hβ), 2.70-2.64 (m, D-Dab8-Hγ), 2.59-2.54 (m, 1H, D-Dab8-Hγ), 2.28-2.10 (m, 6H, Glu10-Hγ + D-Dab2-Hβ + D-Dab2-Hβ + Dab7-Hβ + Anth-Hα), 2.01-1.75 (m, 9H, D-Val1-Hβ + Dab7-Hβ + D-

Dab8-Hβ + Glu10-Hβ + Val11-Hβ + D-*allo*-Ile12-Hβ + Glu10-Hγ), 1.29-1.12 (m, 5H, Ala13-Hβ + D-*allo*-Ile12-Hγ), 0.90-0.80 (m, 18H, D-Val1-Hγ + Val11-Hγ + D-*allo*-Ile12-Hγ, Hδ, Lipid-CH_3). MW calculated for $C_{71}H_{112}N_{17}O_{19}$ 1506.8315, found *high resolution* (FTICR-ESI-MS) 1506.8331 $(M+H)^+$.

Aaa-TriA_1-OH (129)

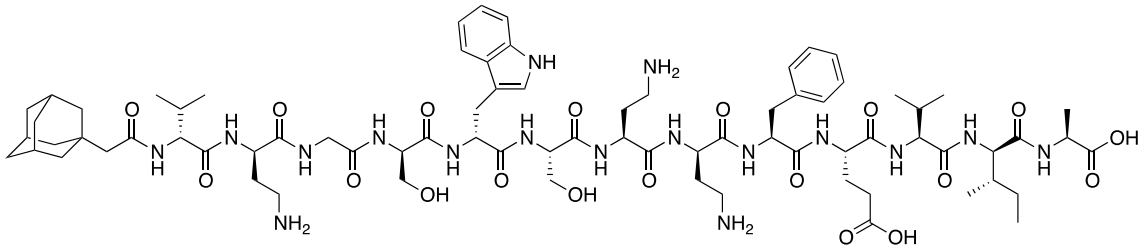

129

Peptide was isolated as a single peak using C_{18} HPLC (9.2 mg, 58.6 %). Retention time (HPLC method 2) = 36.77 min. MS/MS: *m/z* 203.1 (y2), 302.2 (y3), 431.2 (y4), 578.3 (y5), 678.3 (y6), 778.4 (y7), 865.4 (y8), 1051.4 (y9), 1195.5 (y11), 1295.5 (y12), 276.2 (b1), 376.3 (b2), 433.3 (b3), 520.3 (b4), 706.3 (b5), 793.3 (b6), 993.3 (b8), 1140.5 (b9), 1296.6 (b10), 1368.7 (b11), 1481.8 (b12), 248.2 (a1), 348.2 (a2) 492.3 (a4), 678.3 (a5), 765.3 (a6), 865.4 (a7), 1453.8 (a12). MW calculated for $C_{76}H_{116}N_{17}O_{19}$ 1570.8628, found *high resolution* (FTICR-ESI-MS) 1570.8615 $(M+H)^+$.

PEG-TriA_1-OH (130)

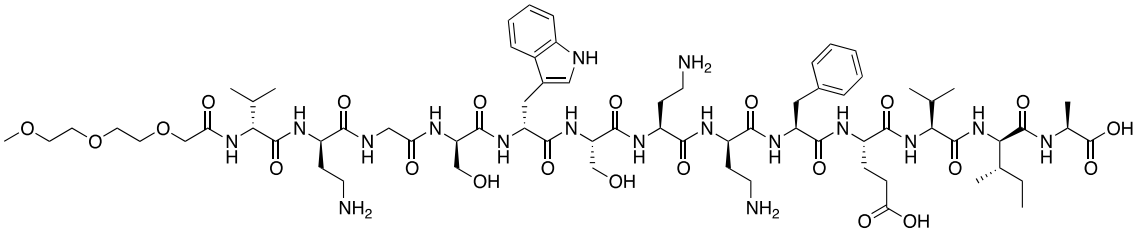

130

Peptide was isolated as a single peak using C_{18} HPLC (8.0 mg, 51.4 %). Retention time (HPLC method 2) = 23.02 min. ^{1}H NMR (D_2O, 600 MHz): δ 7.57 (d, 1H, *J* = 7.8 Hz, Trp5-ArH), 7.46 (d, 1H, *J* = 8.2 Hz, Trp5-ArH), 7.32-7.25 (m, 3H, Trp5-ArH + Phe9-ArH), 7.21-7.19 (m, 4H, Trp5-ArH + Phe9-ArH), 7.11 (t, 1H, *J* = 7.5 Hz, Trp5-ArH), 4.68 (dd, 1H, *J* = 9.8, 5.7 Hz, Phe9-Hα), 4.62 (t, 1H, *J* = 7.4 Hz, Trp5-Hα), 4.48-4.42 (m, 2H, D-Ser4-Hα + D-Dab2-Hα), 4.35-4.26 (m, 4H, D-*allo*-Ile12-Hα + Dab7-Hα + Glu10-Hα + D-Dab8-Hα), 4.19 (q, 1H, *J* = 7.3, Ala13-Hα), 4.14-4.08 (m, 4H, Val11-Hα + Ser6-Hα + PEG-Hα), 3.89 (app. q, 2H, *J* = 13.9 Hz, Gly3-Hα), 3.77-3.53 (m, 10H, D-Val1-Hα + D-Ser4-Hβ + PEG-OCH_2 + Ser6-Hβ), 3.31 (m, 4H, PEG-CH_3 + Ser6-Hβ), 3.25 (d, 2H, *J* = 8.8 Hz, D-Trp5-Hβ), 3.18 (dd, 1H, *J* = 14.0, 5.0 Hz, Phe9-Hβ), 3.08-2.96 (m, 4H, D-Dab2-Hγ + Dab7-Hγ), 2.87 (dd, 1H, *J* = 13.9, 9.8 Hz, Phe9-Hβ), 2.72-2.68 (m, 1H, D-Dab8-Hγ), 2.61-2.56 (m, 1H, D-Dab8-Hγ), 2.32-2.26 (m, 2H, Glu10-Hγ + D-Dab2-Hβ), 2.21-1.78 (m, 11H, D-Dab2-Hβ + Dab7-Hβ + D-Val1-Hβ + Dab7-Hβ + D-Dab8-Hβ + Glu10-Hβ + Val11-Hβ + D-*allo*-Ile12-Hβ + Glu10-Hγ), 1.31-1.19 (m, 5H, Ala13-Hβ + D-*allo*-Ile12-Hγ), 0.96-0.84 (m, 18H, D-Val1-Hγ + Val11-Hγ + D-*allo*-Ile12-Hγ, Hδ). MW calculated for $C_{71}H_{112}N_{17}O_{22}$ 1554.8162, found *high resolution* (FTICR-ESI-MS) 1554.8137 $(M+H)^+$.

Bio-TriA_1-OH (131)

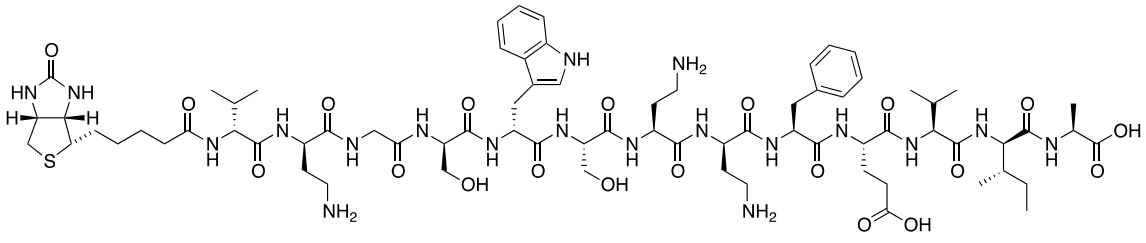

131

Peptide was isolated as a single peak using C_{18} HPLC (8.3 mg, 51.0 %). Retention time (HPLC method 2) = 22.87 min. ^{1}H NMR (D_2O, 600 MHz): δ 7.57 (d, 1H, *J* = 8.5 Hz, Trp5-ArH), 7.46 (d, 1H, *J* = 8.2 Hz, Trp5-ArH), 7.32-7.25 (m, 3H, Trp5-ArH + Phe9-ArH), 7.21-7.19 (m, 4H, Trp5-ArH + Phe9-ArH), 7.11 (t, 1H, *J* = 7.5 Hz, Trp5-ArH), 4.67 (dd, 1H, *J* = 9.5, 5.3 Hz, Phe9-Hα), 4.62 (t, 1H, *J* = 7.1 Hz, Trp5-Hα), 4.50-4.48 (m, 1H, Biotin-NHC*H*CH_2-) 4.45-4.41 (m, 2H, D-Ser4-Hα + D-Dab2-Hα), 4.35-4.26 (m, 5H, D-*allo*-Ile12-Hα + Dab7-Hα + Glu10-Hα + D-Dab8-Hα + Biotin-NHC*H*CH-), 4.22-4.18 (m, 1H, Ala13-Hα), 4.13-4.10 (m, 2H, Val11-Hα + Ser6-Hα), 4.01 (d, 1H, *J* = 7.5 Hz, D-Val1-Hα), 3.89 (s, 2H, Gly3-Hα), 3.75 (app. qd, 2H, *J* = 12.0, 5.4 Hz, D-Ser4-Hβ), 3.55 (dd, 1H, *J* = 11.5, 6.2 Hz, Ser6-Hβ), 3.31 (dd, 1H, *J* = 11.2, 5.3 Hz, Ser6-Hβ), 3.25 (d, 2H, *J* = 6.9 Hz, D-Trp5-Hβ), 3.19-3.16 (m, 2H, Phe9-Hβ + Biotin-NHCHC*H*), 3.07-2.97 (m, 4H, D-Dab2-Hγ + Dab7-Hγ), 2.90-2.85 (m, 2H, Phe9-Hβ + Biotin-NHCHC*H*H), 2.73-2.68 (m, 2H, D-Dab8-Hγ + Biotin-NHCHCH*H*), 2.61-2.56 (m, 1H, D-Dab8-Hγ), 2.32-1.78 (m, 14H, Glu10-Hγ + D-Dab2-Hβ + Dab7-Hβ + D-Val1-Hβ + D-Dab8-Hβ + Glu10-Hβ + D-*allo*-Ile12-Hβ + Biotin-NHC(O)C*H*$_2$-), 1.64-1.44 (m, 4H, Biotin-NHC(O)CH_2C*H*$_2$$CH_2$C*H*$_2$-), 1.34-1.19 (m, 7H, Ala13-Hβ + D-*allo*-Ile12-Hγ + Biotin-NHC(O)CH_2CH_2C*H*$_2$-), 0.96-0.84 (m, 18H, D-Val1-Hγ + Val11-Hγ + D-*allo*-Ile12-Hγ, Hδ). MW calculated for $C_{74}H_{114}N_{19}O_{20}S$ 1620.8203, found *high resolution* (FTICR-ESI-MS) 1620.8191 $(M+H)^+$.

Oct-TriA_1-NH_2 (132A)

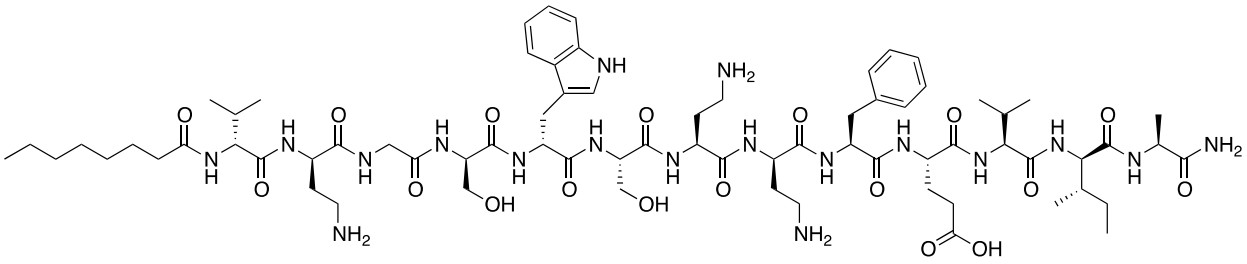

132A

Peptide was isolated as a single peak using C_{18} HPLC (47 mg, 31%). Retention time (HPLC method 1) = 40.9 min. MW calculated for $C_{72}H_{115}N_{18}O_{18}$ 1519.8637, found *low resolution* (MALDI) 1519.9 $(M+H)^+$.

Oct-TriA_1(10Gln) (132B)

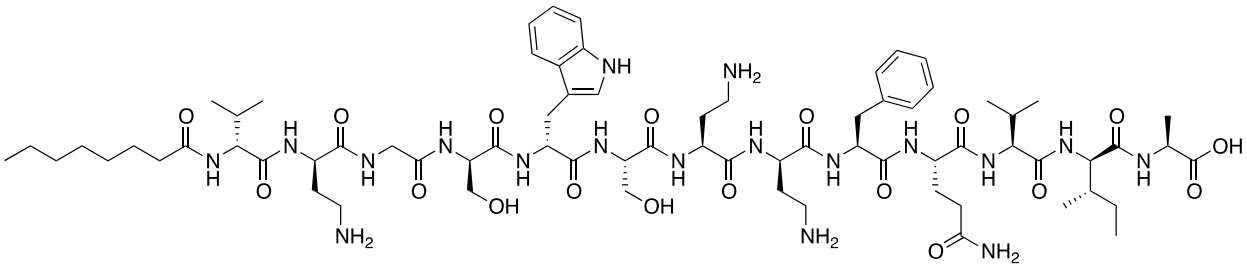

132B

Peptide was isolated as a single peak using C_{18} HPLC (65 mg, 43%). Retention time (HPLC method 1) = 41.0 min. MW calculated for MW calculated for $C_{72}H_{115}N_{18}O_{18}$ 1519.8637, found *low resolution* (MALDI) 1519.9 $(M+H)^+$.

Fmoc-Glu(10Gln(PEG_3N_3))-OH (133)

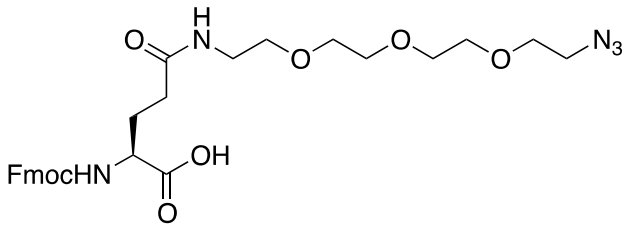

133

Fmoc-Glu-OtBu (1.00 g, 2.35 mmol) was dissolved in dry DMF (15 mL) and cooled to 0 ^oC. DIPEA (0.5 mL, 2.84 mmol) and HATU (1.08 g, 2.84 mmol) were then added. A solution of H_2N-PEG_3-N_3 (0.56 mL, 2.84 mmol) in dry DMF (5 mL) was then added and the reaction stirred at ambient temperature for 18 h. The reaction mixture was concentrated *in vacuo* and redissolved in EtOAc (100 mL). This solution was washed with 10% citric acid (50 mL), saturated $NaHCO_3$ (50 mL) and brine (50 mL), dried over anhydrous Na_2SO_4 and concentrated *in vacuo*. The resulting oil was dissolved in CH_2Cl_2 (10 mL) and TFA (10 mL) and stirred at ambient temperature for 3 h. The reaction mixture was then concentrated *in vacuo* and purified by column chromatography (SiO_2, EtOAc to 9:1 EtOAc/MeOH) to yield acid **133** as a colourless oil (0.73 g, 45% over 2 steps). $[\alpha]_D^{25}$ = 6.03 (*c* = 0.6 g/100mL, EtOAc); IR ($CHCl_3$ cast) 3324, 3067, 2877, 2109, 1721 cm^{-1}; ^1H NMR ($CDCl_3$, 500 MHz): δ 7.76 (d, 2H, *J* = 7.5 Hz, Fmoc-ArH), 7.60 (t, 2H, *J* = 7.0 Hz, Fmoc-ArH), 7.39 (t, 2H, *J* = 7.5 Hz, Fmoc-ArH), 7.31 (t, 2H, *J* = 7.4 Hz, Fmoc-ArH), 6.63-6.57 (m, 1H, $OCH_2CH_2N\underline{H}$), 6.01 (d, 1H, *J* = 6.8 Hz, Fmoc-NH), 4.41-4.34 (m, 3H, Hα + Fmoc-CH_2), 4.21 (t, 1H, *J* = 7.1 Hz, Fmoc-CH), 3.64-3.61 (m, 10H, 5x$OC\underline{H}_2$), 3.56 (t, 2H, *J* = 4.9 Hz, $OC\underline{H}_2CH_2NH$), 3.52-3.41 (m, 2H, $OCH_2C\underline{H}_2NH$), 3.36 (t, 2H, *J* = 5.0 Hz, $C\underline{H}_2N_3$), 2.51-2.37 (m, 2H, Hγ), 2.23-2.08 (m, 2H Hβ); HRMS (ES) Calcd for $C_{28}H_{35}N_5NaO_8$ $[M+Na]^+$ 592.2378, found 592.2371.

Oct-TriA$_1$(10Gln(PEG$_3$N$_3$))-OH (135)

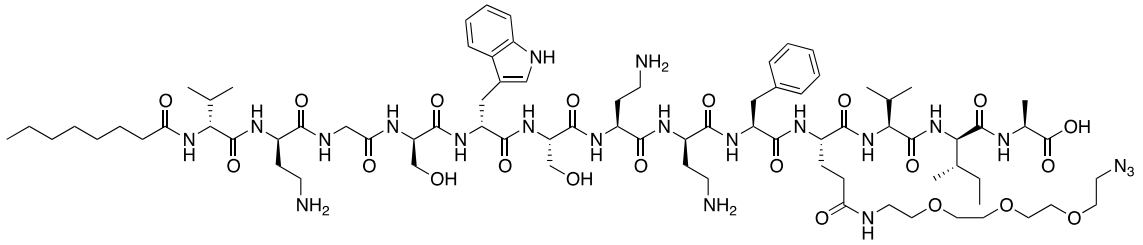

135

Peptide was isolated as a single peak using C_{18} HPLC (6 mg, 14%). Retention time (HPLC method 1) = 47.0 min. HRMS (ES) Calcd for $C_{80}H_{131}N_{21}O_{21}$ 860.9909, found 860.9894 $(M+2H)^{2+}$.

H-TriA$_1$(10Gln(PEG$_3$N$_3$))-OH (136)

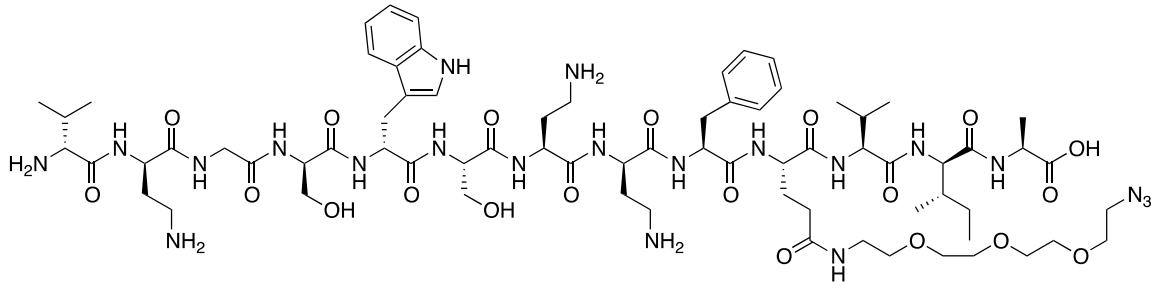

136

Peptide was isolated as a single peak using C_{18} HPLC (9 mg, 23%). Retention time (HPLC method 1) = 31.5 min. HRMS (ES) Calcd for $C_{72}H_{115}N_{21}O_{20}$ 1594.8700, found 1594.8693 $(M+H)^{+}$.

Vancomycin alkyne (137)

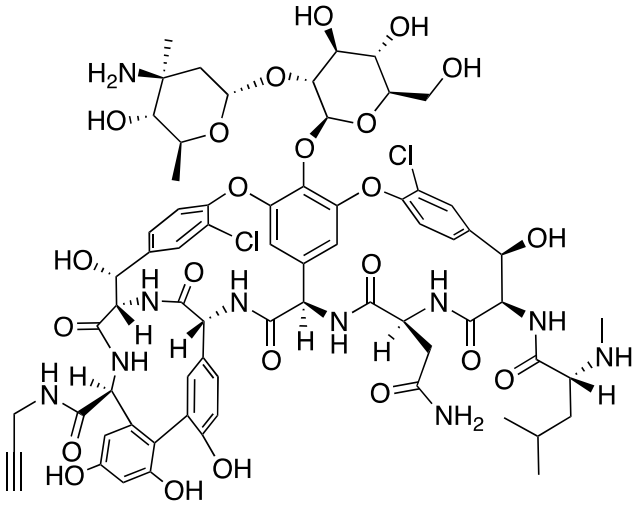

137

Vancomycin.HCl.2H_2O (115 mg, 75.6 µmol) was dissolved in dry DMSO (1 mL) and dry DMF (1 mL). Molecular sieves were added (320 mg, 4 Å) and the solution left to stand at ambient temperature for 1 h. The molecular sieves were removed and propargylamine.HCl (14 mg, 151.1 µmol) was added. The mixture was cooled to 0 ^{o}C and HBTU (43 mg, 113.4 µmol) and DIPEA (80 µL, 435.5 µmol) were added. The reaction mixture was warmed to ambient temperature and stirred overnight. The mixture was concentrated *in vacuo*, dissolved in 1:1 H_2O:MeCN, purified by HPLC method 4 and lyophilized to yield the product as a white solid (76.5 mg, 68%). Retention time (HPLC method 4) = 9.0 min. HRMS (ES) Calcd for $C_{69}H_{78}Cl_2N_{10}O_{23}$ $[M+H]^+$ 1484.4618, found 1484.4618.

Nisin alkyne (138)

Nisin (24 mg, 7.2 µmol) was dissolved in DMF (300 µL). Propargylamine (34 µL, 527.0 µmol) and PyBOP (11 mg, 21.5 µmol) were added to the resulting solution and stirred at

RT for 2 h. The reaction mixture was neutralized with 1 M HCl (6 drops), concentrated *in vacuo*, re-dissolved in 1:1 H_2O/MeCN (2 mL) and purified by HPLC method 5. The product containing fractions were pooled, concentrated, frozen and lyophilized to yield the product as a white fluffy powder (13 mg, 54%). Retention time (HPLC method 5) = 17.2 min. HRMS (ES) Calcd for $C_{146}H_{236}N_{43}O_{36}S_7$ $[M+3H]^{3+}$ 1130.5329, found 1130.5328.

Erythromycin Alkyne (140)

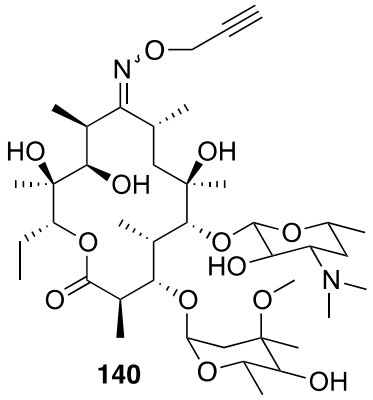

140

To a solution of Erythromycin A, 9-O-oxime (100 mg, 0.133 mmol) in acetonitrile (1.2 mL) was added propargyl bromide (80% solution in toluene, 18.4 µL, 0.165 mmol) and KOH (13 mg, 0.21 mmol). The reaction mixture was stirred at ambient temperature for 3 h, followed by the addition of $CHCl_3$ (2 mL). The resulting mixture was filtrated through a millipore filter disk, concentrated *in vacuo* and redissolved in 1:1 MeCN/H_2O (3 mL). The product was purified by HPLC method 6. Product containing fractions, were pooled, concentrated, frozen and lyophilized to yield the product as a white fluffy powder (31 mg, 30%). Product eluted over several min by HPLC. HRMS (ES) Calcd for $C_{40}H_{71}N_2O_3$ $[M+H]^+$ 787.4956, found 787.4956.

1-Nitrosopiperazine (143)

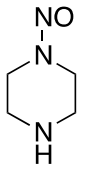

143

Piperazine (**142**) (5.16 g, 60 mmol) was dissolved in 6M HCl (36 mL) and cooled to -10 ^{o}C. A solution of $NaNO_2$ (4.14 g, 60 mmol) in H_2O (72 mL) was added slowly by addition funnel over 1h. The reaction mixture was adjusted to pH 10 with 3 M NaOH and extracted with $CHCl_3$ (2 x 100 mL). The combined organic extracts were dried over anhydrous Na_2SO_4, concentrated *in vacuo* and purified by flash column chromatography (SiO_2, 8% MeOH in CH_2Cl_2) to yield the product as a yellow oil (3.56 g, 51%). IR (Neat film) 3333, 2957, 2925, 2827, 2743 cm^{-1}; ^{1}H NMR ($CDCl_3$, 500 MHz): δ 4.21 (dd, 2H, *J* = 5.1 Hz, $CH_{(eq)}NNO$), 3.80 (dd, 2H, *J* = 5.5 Hz, $CH_{(ax)}NNO$), 3.06 (dd, 2H, *J* = 5.3 Hz, $CH_{(eq)}NH$), 2.81 (dd, 2H, *J* = 5.3 Hz, $CH_{(ax)}NH$); ^{13}C NMR ($CDCl_3$, 125 MHz): δ 51.1, 46.6, 45.1, 40.8; HRMS (ES) Calcd for $C_4H_{10}N_3O$ $[M+H]^+$ 116.0818, found 116.0819.

1-Nitroso-4-propargylpiperazine (144)

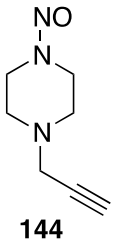

144

1-Nitrosopiperazine (**143**) (400 mg, 3.47 mmol) and propargyl bromide (520 mg of 80% solution in toluene, 3.47 mmol) were dissolved in anhydrous MeCN (10 mL) and NEt_3 (0.97 mL, 6.94 mmol). The reaction mixture was refluxed for 3 h and concentrated *in*

vacuo. The crude was then dissolved in 10% NaOH and extracted with CH_2Cl_2 (2 x 10 mL). The organic phase was dried over anhydrous Na_2SO_4, concentrated *in vacuo* and purified by column chromatography (SiO_2, 8% MeOH in CH_2Cl_2) to yield the product as an orange oil (210 mg, 40%). IR (Neat film) 3278, 2925, 2822; ^{1}H NMR (500 MHz; $CDCl_3$): δ 4.29 (t, 2H, *J* = 5.3 Hz, NONCH(eq)), 3.87 (t, 2H, *J* = 5.5 Hz, NONCH(ax)), 3.38 (d, 2H, *J* = 2.4 Hz, C<u>H</u>$_2$CCH), 2.77 (t, 2H, *J* = 5.3 Hz, NCH(eq)), 2.53 (t, 2H, *J* = 5.5 Hz, NCH(ax)), 2.27 (t, 1H, *J* = 2.4 Hz, CH_2C<u>C</u>H); ^{13}C NMR ($CDCl_3$, 125 MHz): δ 77.8, 74.1, 52.0, 50.5, 49.6, 46.7, 39.3; HRMS (ES) Calcd for $C_7H_{12}N_3O$ $[M+H]^+$ 154.0975, found 154.0974.

1-Amino-4-propargylpiperazine (141)

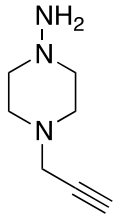

141

$LiAlH_4$ (0.79 g, 20.8 mmol) was added to a flame dried RBF, suspended in anhydrous Et_2O (15 mL) and stirred vigourously. A solution of **144** (1.60 mg, 10.4 mmol) in anhydrous Et_2O (5 mL) was added and the reaction mixture refluxed for 2 h. The reaction mixture was then cooled, quenched with 2 M HCl and filtered through celite. The celite was subsequently washed with 2M HCl (100 mL) and the filtrate adjusted to pH 10 with 10% NaOH. The aqueous phase was extracted with CH_2Cl_2 (3 x 100 mL) and the organic phase dried over anhydrous Na_2SO_4 and concentrated *in vacuo*. The crude product was purified by column chromatography (SiO_2, 10% MeOH in CH_2Cl_2) to

yield alkyne **141** as an off-white solid (135 mg, 10%). IR (Neat film) 3290, 3212, 2940, 2913, 2814, 1602; ^{1}H NMR ($CDCl_3$, 500 MHz): δ 3.29 (d, 2H, *J* = 2.4 Hz, $C\underline{H_2}CCH$), 3.20-3.00 (m, 2H), 2.80-2.60 (m, 6H), 2.24 (t, 1H, *J* = 2.4 Hz, $CH_2C\underline{C}H$); ^{13}C NMR ($CDCl_3$, 125 MHz): δ 78.7, 73.4, 59.3, 51.7, 46.5; HRMS (ES) Calcd for $C_7H_{13}N_3$ $[M]^+$ 139.1110, found 139.1110.

Rifampicin alkyne (146)

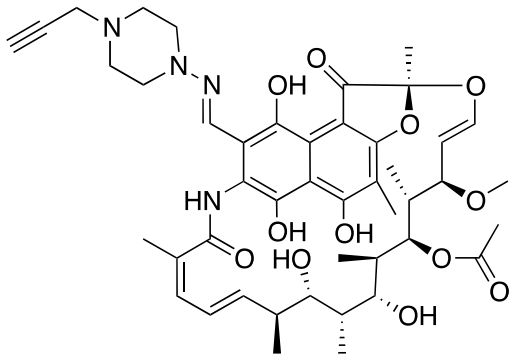

146

Rifaldehyde (**145**) (100 mg, 0.138 mmol) was suspended in dry THF (0.5 mL). Piperazine **141** (19 mg, 0.138 mmol) was added and the reaction stirred vigourously for 15 min. The reaction was then diluted with CH_2Cl_2 (7 mL) and washed with 5.5 mL of a solution of ascorbic acid (2.0 g) in 3:1 H_2O/brine (40 mL). The aqueous phase was then extracted with CH_2Cl_2 (7 mL) and the combined CH_2Cl_2 extracts dried over anhydrous Na_2SO_4 and concentrated *in vacuo* to yield rifampicin alkyne (**146**) as a red solid (110 mg, 94%). HRMS (ES) Calcd for $C_{45}H_{57}N_4O_{12}$ $[M-H]^-$ 845.3978, found 845.3977.

Daptomycin alkyne (147)

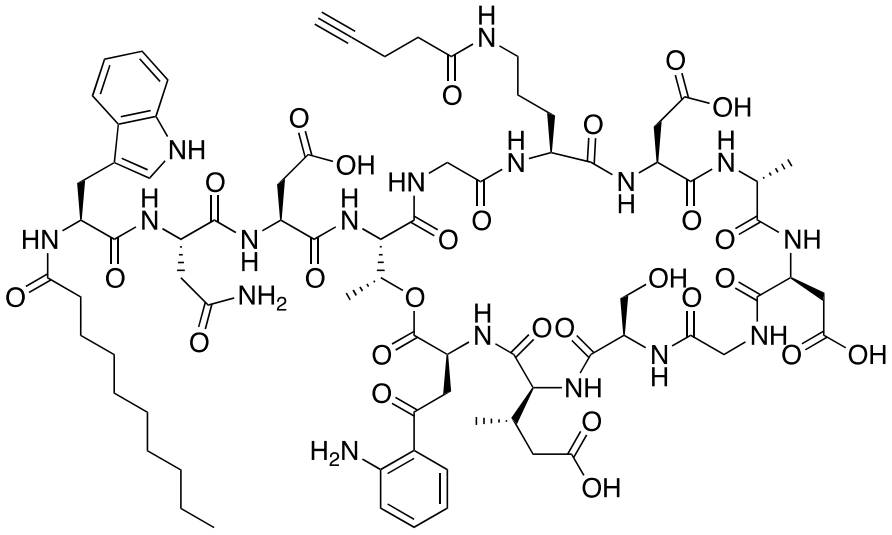

147

4-Pentynoic acid (73 mg, 74.0 μmol) was dissolved in dry DMF (1 mL) and cooled to 0 ^{o}C. HATU (24 mg, 61.7 μmol) and DIPEA (54 μL, 308.7 μmol) were added and the solution stirred at 0 ^{o}C for 15 min under argon. A suspension of daptomycin (100 mg, 61.7 μmol) in dry DMF (1 mL) was added and the solution stirred at ambient temperature overnight. The reaction mixture was concentrated *in vacuo*, redissolved in 1:1 H_2O:MeCN (10 mL) and purified by HPLC method 7. The product was isolated as a white powder (45 mg, 49%). Retention time (HPLC method 7) = 14.0 min. HRMS (ES) Calcd for $C_{77}H_{107}N_{17}O_{27}$ $[M+2H]^{2+}$ 850.8756, found 850.8745.

General click chemistry procedure

The peptide azide (2.5 μmol) and alkyne (7.5 μmol) were dissolved in 1:1 H_2O/tBuOH (125 μL). A 100 mM solution of $CuSO_4$ (15 μL, 1.5 μmol) and freshly prepared 500 mM solution of ascorbic acid (12 μL, 6.0 μmol) were added and the reaction mixture stirred at 50 ^{o}C until reaction complete consumption of the azide starting material by observed

using MALDI. The click product was then purified by HPLC.

Oct-TriA$_1$-Van (148)

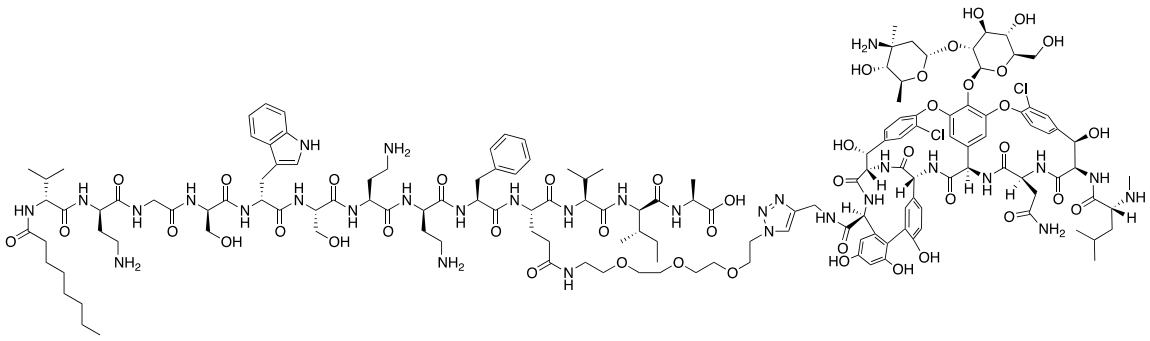

148

Purified by HPLC method 1 to yield conjugate **148** as a white solid (3.3 mg, 41%). HRMS (ES) Calcd for $C_{149}H_{210}Cl_2N_{31}O_{44}$ $[M+3H]^{3+}$ 1069.1503, found 1069.1499.

H-TriA$_1$-Van (149)

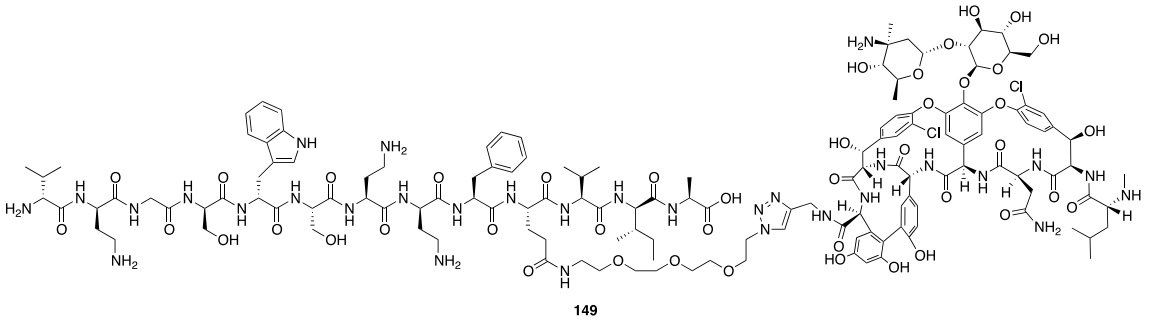

149

Purified by HPLC method 1 to yield conjugate **149** as a white solid (3.0 mg, 39%). HRMS (ES) Calcd for $C_{141}H_{196}Cl_2N_{31}O_{43}$ $[M+3H]^{3+}$ 1027.1155, found 1027.1156.

Oct-TriA$_1$-Eryc (150)

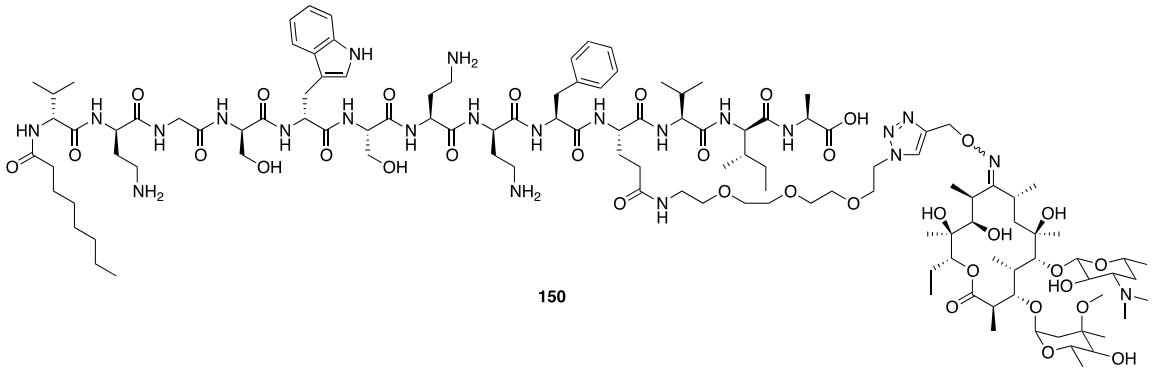

150

Purified by HPLC method 1 to yield conjugate **150** as a white solid (3.3 mg, 53%). HRMS (ES) Calcd for $C_{120}H_{202}N_{23}O_{34}$ $[M+3H]^{3+}$ 836.4923, found 836.4905.

H-TriA$_1$-Eryc (151)

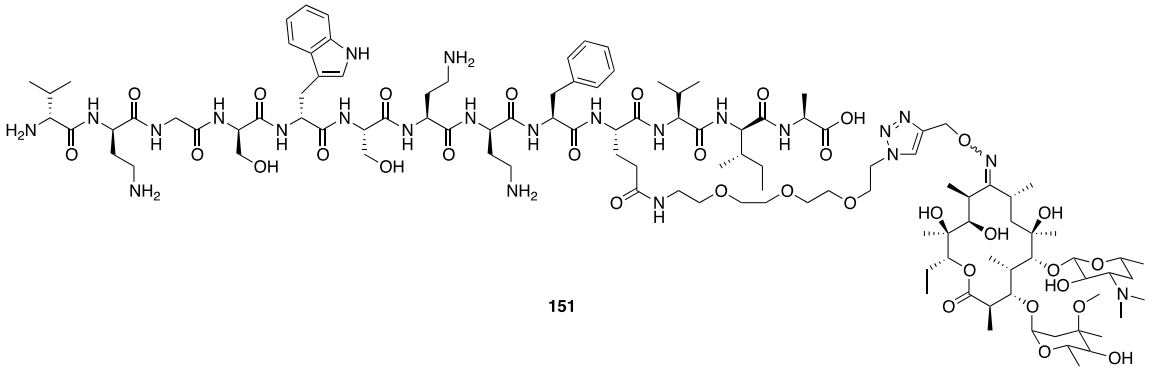

151

Purified by HPLC method 1 to yield conjugate **151** as a white solid (3.5 mg, 59%). HRMS (ES) Calcd for $C_{112}H_{187}N_{23}O_{33}$ $[M+2H]^{2+}$ 1191.1825, found 1191.1819.

Oct-TriA$_1$-Rif (152)

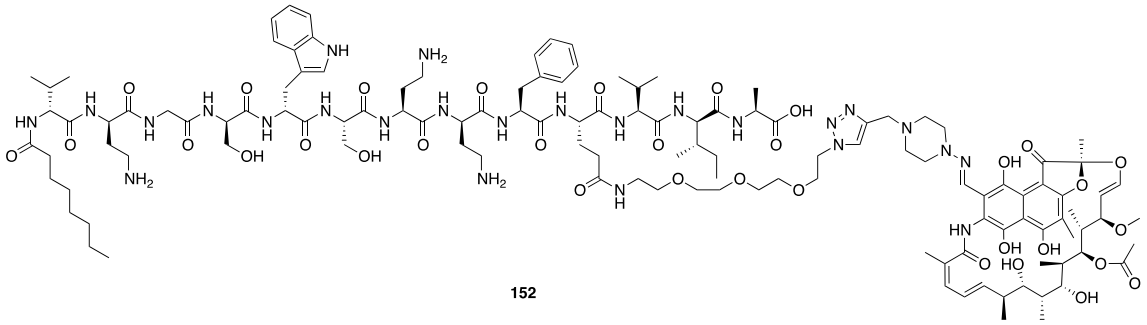

152

Purified by HPLC method 1 to yield conjugate **152** as a white solid (1.9 mg, 30%). HRMS (ES) Calcd for $C_{125}H_{188}N_{25}O_{33}$ $[M+3H]^{3+}$ 855.7928, found 855.7907.

H-TriA$_1$-Rif (153)

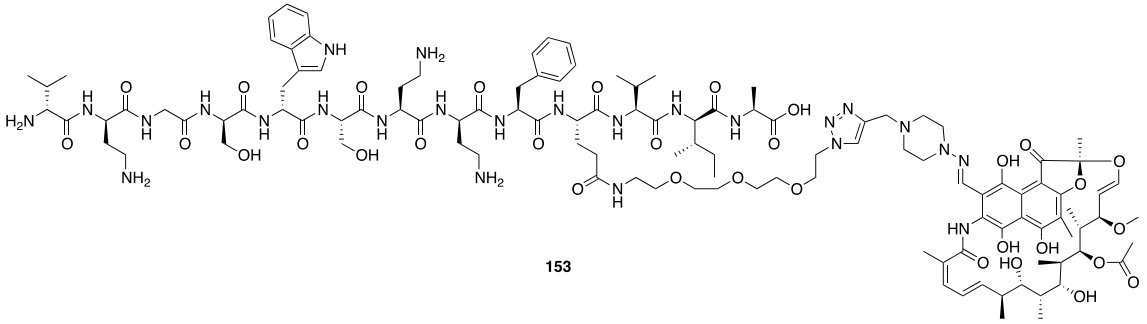

153

Purified by HPLC method 1 to yield conjugate **153** as a white solid (1.7 mg, 29%). HRMS (ES) Calcd for $C_{117}H_{174}N_{25}O_{32}$ $[M+3H]^{3+}$ 813.7580, found 813.7563.

Oct-TriA_1(Ala1) (154)

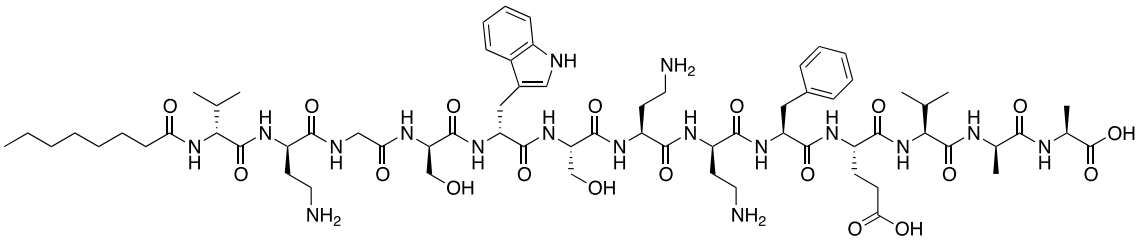

154

Peptide was isolated as a single peak using C_{18} HPLC (2.3 mg, 3.1 %). Retention time (HPLC method 2) = 39.8 min. ^{1}H NMR (D_2O, 600 MHz): δ 7.57 (d, 1H, *J* = 8.0 Hz, D-Trp5-ArH), 7.46 (d, 1H, *J* = 8.2 Hz, D-Trp5-ArH), 7.32-7.25 (m, 3H, Phe9-ArH), 7.21-7.19 (m, 4H, D-Trp5-ArH + Phe9-ArH), 7.11 (t, 1H, *J* = 7.5 Hz, D-Trp5-ArH), 4.69-4.66 (m, 1H, Phe9-Hα), 4.62 (t, 1H, *J* = 7.1 Hz, D-Trp5-Hα), 4.45-4.41 (m, 2H, D-Ser4-Hα + D-Dab2-Hα), 4.35-4.25 (m, 4H, D-*allo*-Ile12-Hα + Dab7-Hα + Glu10-Hα + D-Dab8-Hα), 4.22-4.16 (m, 2H, Ala1-Hα + Ala13-Hα), 4.13-4.10 (m, 2H, Val11-Hα + Ser6-Hα), 3.89 (s, 2H, Gly3-Hα), 3.78-3.71 (m, 2H, D-Ser4-Hβ), 3.54 (dd, 1H, *J* = 11.8, 4.8 Hz, Ser6-Hβ), 3.31 (dd, 1H, *J* = 11.4, 5.4 Hz, Ser6-Hβ), 3.25 (d, 2H, *J* = 7.4 Hz, D-Trp5-Hβ), 3.20-3.15 (m, 1H, Phe9-Hβ), 3.07-2.96 (m, 4H, D-Dab2-Hγ + Dab7-Hγ), 2.89-2.84 (m, 1H, Phe9-Hβ), 2.73-2.68 (m, 1H, D-Dab8-Hγ), 2.61-2.56 (m, 1H, D-Dab8-Hγ), 2.29-2.14 (m, 6H, Glu10-Hγ + D-Dab2-Hβ + Dab7-Hβ + Lipid-Hα), 2.08-1.78 (m, 8H, Dab7-Hβ + D-Dab8-Hβ + Glu10-Hβ + Val11-Hβ + D-*allo*-Ile12-Hβ + Glu10-Hγ), 1.54-1.49 (m, 2H, Lipid-Hβ), 1.33-1.29 (m, 8H, Ala1-Hβ + Ala13-Hβ + D-*allo*-Ile12-Hγ), 1.25-1.17 (m, 8H, Lipid-Hγ, Hδ, Hε, Hζ), 0.94-0.92 (m, 6H, Val11-Hγ), 0.87-0.84 (m, 6H, D-*allo*-Ile12-Hγ, Hδ), 0.80-0.78 (m, 3H, Lipid-CH_3). MW calculated for $C_{72}H_{114}N_{17}O_{19}$ 1491.8086, found *high resolution* (ESI-MS) 498.2767 $(M+3H)^{3+}$, calculated 498.2768.

Oct-TriA$_1$(Ala2) (155)

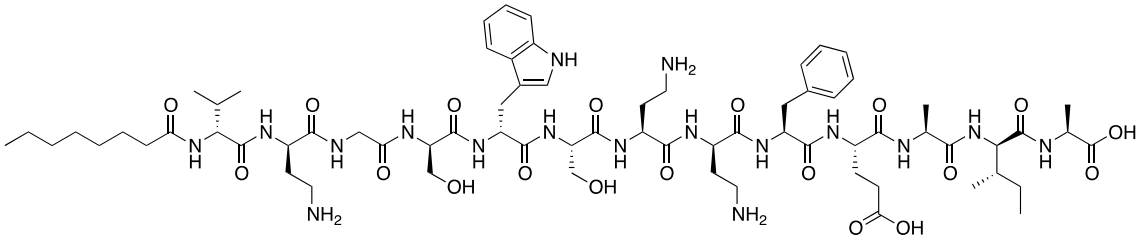

155

Peptide was isolated as a single peak using C_{18} HPLC (3.0 mg, 4.0 %). Retention time (HPLC method 2) = 49.8 min. MW calculated for $C_{71}H_{110}N_{16}O_{19}$ 1490.8133, found *high resolution* (ESI-MS) 746.4132 $(M+2H)^{2+}$, calculated 746.4139.

Oct-TriA$_1$(Ala3) (156)

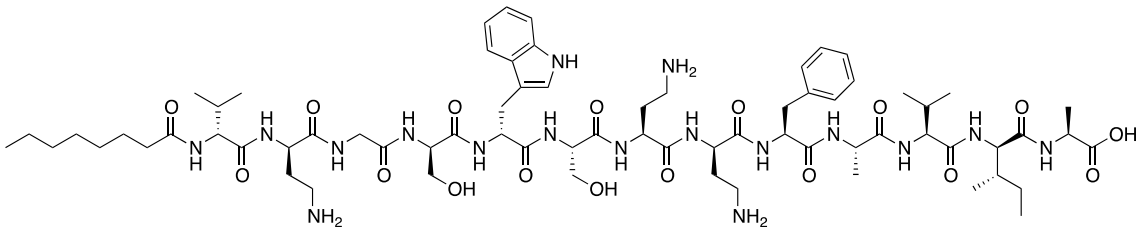

156

Peptide was isolated as a single peak using C_{18} HPLC (2.3 mg, 3.0 %). Retention time (HPLC method 2) = 39.8 min. ^{1}H NMR (D_2O, 600 MHz): δ 7.57 (d, 1H, *J* = 7.9 Hz, D-Trp5-ArH), 7.46 (d, 1H, *J* = 8.4 Hz, D-Trp5-ArH), 7.32-7.25 (m, 3H, Phe9-ArH), 7.21-7.18 (m, 4H, D-Trp5-ArH + Phe9-ArH), 7.11 (t, 1H, *J* = 7.5 Hz, D-Trp5-ArH), 4.69-4.67 (m, 1H, Phe9-Hα), 4.60 (t, 1H, *J* = 7.4 Hz, D-Trp5-Hα), 4.44-4.38 (m, 2H, D-Ser4-Hα + D-Dab2-Hα), 4.34-4.25 (m, 5H, D-*allo*-Ile12-Hα + Dab7-Hα + Glu10-Hα + D-Dab8-Hα + Ala13-Hα), 4.19-4.15 (m, 1H, Ala3-Hα), 4.12-4.10 (m, 2H, Val11-Hα + Ser6-Hα), 3.98 (d, 1H, *J* = 7.2 Hz, D-Val1-Hα), 3.79-3.70 (m, 2H, D-Ser4-Hβ), 3.55-3.52 (m, 1H, Ser6-Hβ), 3.29-3.24 (m, 3H, Ser6-Hβ + D-Trp5-Hβ), 3.20-3.16 (m, 1H, Phe9-Hβ), 3.06-2.96

(m, 4H, D-Dab2-Hγ + Dab7-Hγ), 2.88-2.84 (m, 1H, Phe9-Hβ), 2.73-2.68 (m, 1H, D-Dab8-Hγ), 2.60-2.55 (m, 1H, D-Dab8-Hγ), 2.30-2.14 (m, 6H, Glu10-Hγ + D-Dab2-Hβ + Dab7-Hβ + Lipid-Hα), 2.08-1.80 (m, 9H, D-Val1-Hβ + Dab7-Hβ + D-Dab8-Hβ + Glu10-Hβ + Val11-Hβ + D-*allo*-Ile12-Hβ + Glu10-Hγ), 1.52-1.46 (m, 2H, Lipid-Hβ), 1.33-1.15 (m, 16H, Ala3-Hβ + Ala13-Hβ + D-*allo*-Ile12-Hγ + Lipid-Hγ, Hδ, Hε, Hζ), 0.95-0.84 (m, 18H, D-Val1-Hγ + Val11-Hγ + D-*allo*-Ile12-Hγ, Hδ), 0.80-0.77 (m, 1H, Lipid-CH_3). MW calculated for $C_{73}H_{115}N_{17}O_{19}$ 1533.8555, found *high resolution* (ESI-MS) 512.2922 $(M+3H)^{3+}$, calculated 512.2924.

Oct-TriA_1(Ala4) (157)

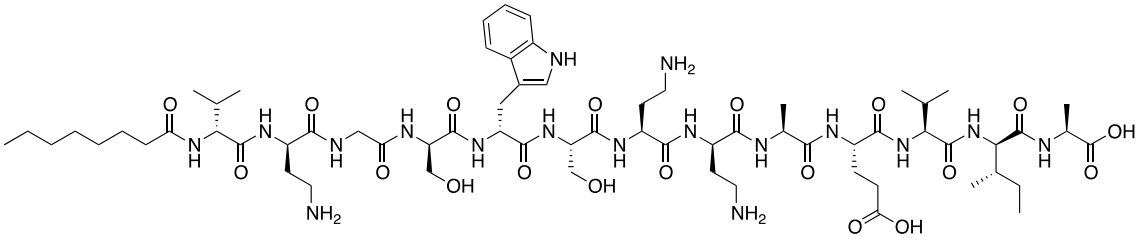

157

Peptide was isolated as a single peak using C_{18} HPLC (2.6 mg, 3.5 %). Retention time (HPLC method 2) = 43.8 min. ^{1}H NMR (D_2O, 600 MHz): δ 7.57 (d, 1H, *J* = 7.9 Hz, D-Trp5-ArH), 7.46 (d, 1H, *J* = 8.2 Hz, D-Trp5-ArH), 7.32-7.25 (m, 3H, Phe9-ArH), 7.21-7.19 (m, 4H, D-Trp5-ArH + Phe9-ArH), 7.11 (t, 1H, *J* = 7.5 Hz, D-Trp5-ArH), 4.66 (dd, 1H, *J* = 9.6, 5.8 Hz, Phe9-Hα), 4.58 (t, 1H, *J* = 7.3 Hz, D-Trp5-Hα), 4.42 (dd, 1H, *J* = 9.0, 5.2 Hz, D-Dab2-Hα), 4.35-4.25 (m, 5H, D-*allo*-Ile12-Hα + Dab7-Hα + Glu10-Hα + D-Dab8-Hα + Ala13-Hα), 4.18 (q, 1H, *J* = 7.3 Hz, Ala4-Hα), 4.12-4.10 (m, 2H, Val11-Hα + Ser6-Hα), 4.00 (d, 1H, *J* = 7.9 Hz, D-Val1-Hα), 3.88-3.81 (m, 2H, Gly3-Hα), 3.51 (dd, 1H, *J* = 11.4, 4.5 Hz, Ser6-Hβ), 3.27-3.17 (m, 4H, Ser6-Hβ + D-Trp5-Hβ + Phe9-Hβ),

3.07-2.97 (m, 4H, D-Dab2-Hγ + Dab7-Hγ), 2.86 (dd, 1H, *J* = 14.3, 10.2 Hz, Phe9-Hβ), 2.23-2.67 (m, 1H, D-Dab8-Hγ), 2.60-2.55 (m, 1H, D-Dab8-Hγ), 2.30-2.17 (m, 6H, Glu10-Hγ + D-Dab2-Hβ + Dab7-Hβ + Lipid-Hα), 2.08-1.80 (m, 9H, D-Val1-Hβ + Dab7-Hβ + D-Dab8-Hβ + Glu10-Hβ + Val11-Hβ + D-*allo*-Ile12-Hβ + Glu10-Hγ), 1.55-1.50 (m, 2H, Lipid-Hβ), 1.33-1.17 (m, 16H, Ala4-Hβ + Ala13-Hβ + D-*allo*-Ile12-Hγ + Lipid-Hγ, Hδ, Hε, Hζ), 0.95-0.79 (m, 21H, D-Val1-Hγ + Val11-Hγ + D-*allo*-Ile12-Hγ, Hδ, Lipid-CH_3). MW calculated for $C_{72}H_{113}N_{17}O_{18}$ 1503.8450, found *high resolution* (ESI-MS) 502.2899 $(M+3H)^{3+}$, calculated 502.2899.

Oct-TriA_1(Ala5) (158)

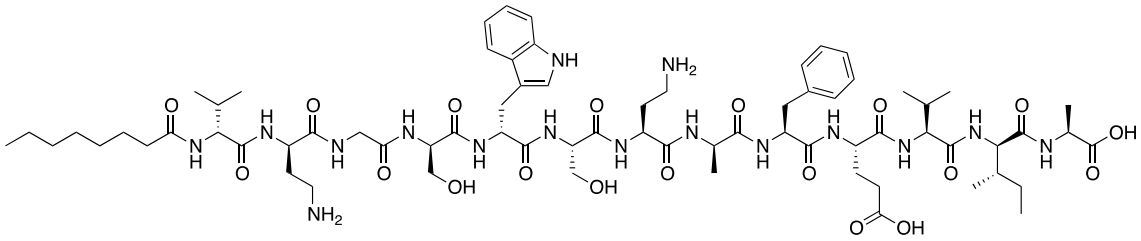

158

Peptide was isolated as a single peak using C_{18} HPLC (7.0 mg, 10.0 %). Retention time (HPLC method 2) = 37.7 min. ^{1}H NMR (D_2O, 600 MHz): δ 7.33 (t, 2H, *J* = 7.3 Hz, Phe9-ArH), 7.28 (t, 1H, *J* = 7.33 Hz, Phe9-ArH), 7.23 (d, 2H, *J* = 7.4 Hz, Phe9-ArH), 4.70 (dd, 1H, *J* = 9.5, 5.6 Hz, Phe9-Hα), 4.46-4.40 (m, 3H, D-Ser4-Hα + D-Dab2-Hα + Ser6-Hα), 4.34-4.24 (m, 5H, D-*allo*-Ile12-Hα + Dab7-Hα + Glu10-Hα + D-Dab8-Hα + Ala13-Hα), 4.22 (q, 1H, *J* = 7.3 Hz, Ala5-Hα +), 4.11 (d, 1H, *J* = 7.8 Hz, D-Val1-Hα), 4.01 (d, 1H, *J* = 7.5 Hz, D-Val1-Hα), 3.96 (s, 2H, Gly3-Hα), 3.89-3.83 (m, 2H, D-Ser4-Hβ), 3.79-3.76 (m, 2H, Ser6-Hβ), 3.21 (dd, 2H, *J* = 14.2, 5.5 Hz, Phe9-Hβ), 3.09-2.99 (m, 4H, D-Dab2-Hγ + Dab7-Hγ), 2.91 (dd, 2H, *J* = 14.0, 9.9 Hz, Phe9-Hβ), 2.74-2.69 (m, 1H, D-Dab8-Hγ),

2.61-2.56 (m, 1H, D-Dab8-Hγ), 2.36-2.16 (m, 6H, Glu10-Hγ + D-Dab2-Hβ + Dab7-Hβ + Lipid-Hα), 2.10-1.80 (m, 9H, D-Val1-Hβ + Dab7-Hβ + D-Dab8-Hβ + Glu10-Hβ + Val11-Hβ + D-*allo*-Ile12-Hβ + Glu10-Hγ), 1.57-1.52 (m, 2H, Lipid-Hβ), 1.33-1.20 (m, 16H, Ala5-Hβ + Ala13-Hβ + D-*allo*-Ile12-Hγ + Lipid-Hγ, Hδ, Hε, Hζ), 0.96-0.80 (m, 21H, D-Val1-Hγ + Val11-Hγ + D-*allo*-Ile12-Hγ, Hδ, Lipid-CH_3). MW calculated for $C_{64}H_{108}N_{16}O_{19}$ 1404.7977, found *high resolution* (ESI-MS) 469.2734 $(M+3H)^{3+}$, calculated 469.2732.

Oct-TriA_1(Ala6) (159)

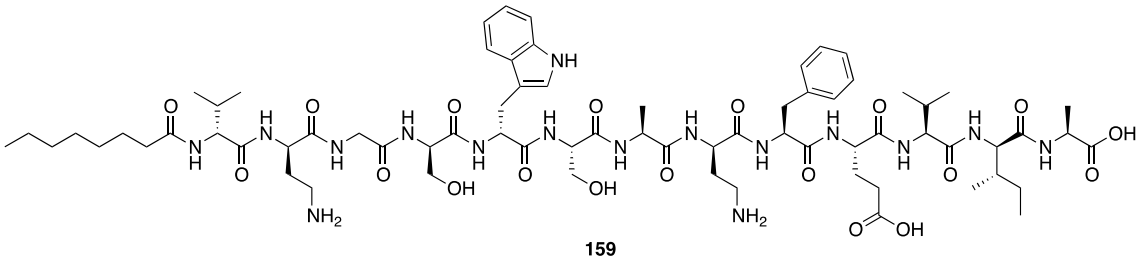

159

Peptide was isolated as a single peak using C_{18} HPLC (3.3 mg, 4.4 %). Retention time (HPLC method 2) = 44.4 min. ^{1}H NMR (D_2O, 600 MHz): δ 7.57 (d, 1H, *J* = 8.3 Hz, D-Trp5-ArH), 7.45 (d, 1H, *J* = 6.9 Hz, D-Trp5-ArH), 7.31-7.25 (m, 3H, Phe9-ArH), 7.21-7.17 (m, 4H, D-Trp5-ArH + Phe9-ArH), 7.11 (t, 1H, *J* = 7.3 Hz, D-Trp5-ArH), 4.69-4.66 (m, 1H, Phe9-Hα), 4.56 (t, 1H, *J* = 7.9 Hz, D-Trp5-Hα), 4.45-4.41 (m, 2H, D-Ser4-Hα + D-Dab2-Hα), 4.35-4.25 (m, 4H, D-*allo*-Ile12-Hα + Glu10-Hα + D-Dab8-Hα + Ala13-Hα), 4.16 (q, 1H, *J* = 7.4 Hz, Ala6-Hα), 4.10 (d, 1H, *J* = 7.4 Hz, Val11-Hα), 4.02-3.99 (m, 2H, D-Val1-Hα + Dab7-Hα), 3.89 (s, 2H, Gly3-Hα), 3.77-3.74 (m, 2H, D-Ser4-Hβ), 3.24-3.18 (m, 3H, D-Trp5-Hβ + Phe9-Hβ), 3.07-2.96 (m, 4H, D-Dab2-Hγ + Dab7-Hγ), 2.87-2.83 (m, 1H, Phe9-Hβ), 2.73-2.69 (m, 1H, D-Dab8-Hγ), 2.60-2.56 (m, 1H, D-Dab8-Hγ), 2.28-1.82 (m, 15H, Glu10-Hγ + D-Dab2-Hβ + Lipid-Hα + D-Val1-Hβ + Dab7-Hβ + D-Dab8-Hβ +

Glu10-Hβ + Val11-Hβ + D-*allo*-Ile12-Hβ), 1.54-1.49 (m, 2H, Lipid-Hβ), 1.34-1.14 (m, 13H, Ala13-Hβ + D-*allo*-Ile12-Hγ + Lipid-Hγ, Hδ, Hε, Hζ), 1.01 (d, 3H, *J* = 7.0 Hz, Ala6-Hβ), 0.96-0.78 (m, 18H, D-Val1-Hγ + Val11-Hγ + D-*allo*-Ile12-Hγ, Lipid-CH_3). MW calculated for $C_{72}H_{113}N_{17}O_{18}$ 1503.8450, found *high resolution* (ESI-MS) 502.2893 $(M+3H)^{3+}$, calculated 502.2889.

Oct-TriA_1(Ala7) (160)

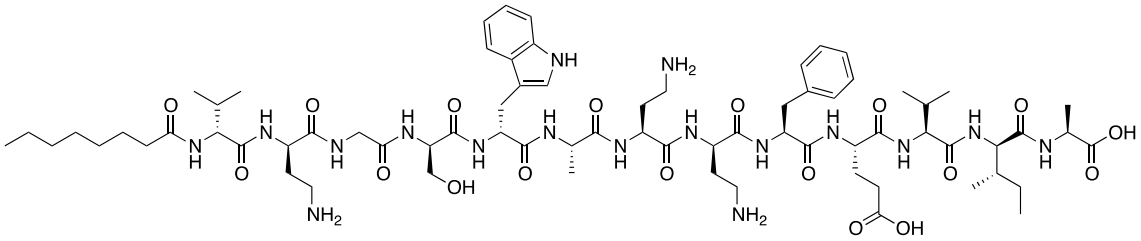

160

Peptide was isolated as a single peak using C_{18} HPLC (1.0 mg, 1.3 %). Retention time (HPLC method 2) = 47.0 min. MALDI MS/MS was used for characterisation due to the poor water solubility of the peptide (see supporting information). MW calculated for $C_{71}H_{110}N_{16}O_{19}$ 1490.8133, found *high resolution* (ESI-MS) 746.4132 $(M+2H)^{2+}$, calculated 746.4139.

Oct-TriA_1(Ala8) (161)

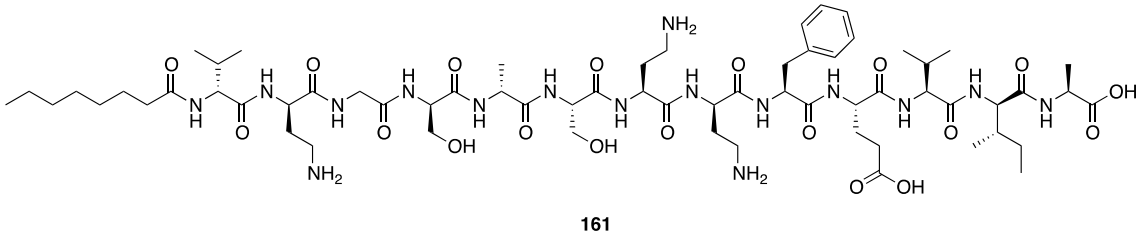

161

Peptide was isolated as a single peak using C_{18} HPLC (3.4 mg, 4.6 %). Retention time (HPLC method 2) = 48.9 min. MALDI MS/MS was used for characterisation due to the

poor water solubility of the peptide (see supporting information). MW calculated for $C_{71}H_{110}N_{16}O_{19}$ 1490.8133, found *high resolution* (ESI-MS) 746.4132 $(M+2H)^{2+}$, calculated 746.4139.

Oct-TriA_1(Ala9) (162)

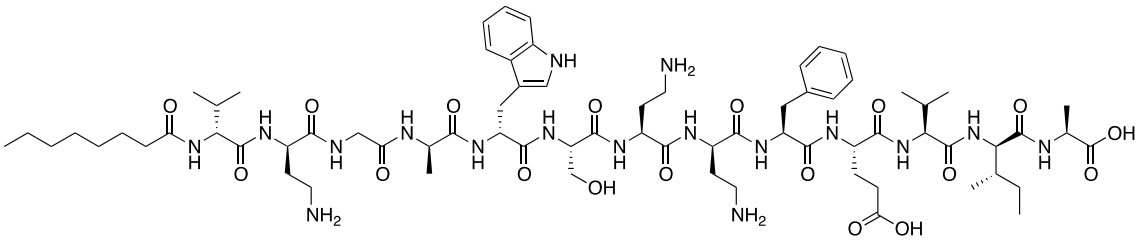

162

Peptide was isolated as a single peak using C_{18} HPLC (4.0 mg, 5.5 %). Retention time (HPLC method 2) = 38.2 min. ^{1}H NMR (D_2O, 600 MHz): δ 7.58 (d, 1H, *J* = 8.1 Hz, D-Trp5-ArH), 7.47 (d, 1H, *J* = 8.2 Hz, D-Trp5-ArH), 7.22-7.19 (m, 2H, D-Trp5-ArH), 7.12 (t, 1H, *J* = 7.5 Hz, D-Trp5-ArH), 4.62 (t, 1H, *J* = 7.0 Hz, D-Trp5-Hα), 4.45-4.41 (m, 2H, D-Ser4-Hα + D-Dab2-Hα), 4.39-4.35 (m, 2H, Dab7-Hα + Glu10-Hα), 4.33 (d, 1H, *J* = 5.6 Hz, D-*allo*-Ile12-Hα), 4.30-4.27 (m, 2H, D-Dab8-Hα + Ala13-Hα), 4.21-4.16 (m, 2H, Ala9-Hα + Ser6-Hα), 4.12 (d, 1H, *J* = 7.7 Hz, Val11-Hα), 4.01 (d, 1H, *J* = 7.5 Hz, D-Val1-Hα), 3.89 (m, 2H, Gly3-Hα), 3.80-3.73 (m, 2H, D-Ser4-Hβ), 3.54 (dd, 1H, *J* = 11.4, 4.9 Hz, Ser6-Hβ), 3.30 (dd, 1H, 11.3, 6.0 Hz, Ser6-Hβ), 3.26 (d, 2H, *J* = 7.3 Hz, D-Trp5-Hβ), 3.08-2.95 (m, 6H, D-Dab2-Hγ + Dab7-Hγ + D-Dab8-Hγ), 2.37-1.86 (m, 15H, Glu10-Hγ + D-Dab2-Hβ + Dab7-Hβ + Lipid-Hα + D-Val1-Hβ + D-Dab8-Hβ + Glu10-Hβ + Val11-Hβ + D-*allo*-Ile12-Hβ), 1.54-1.50 (m, 2H, Lipid-Hβ), 1.33-1.18 (m, 16H, Ala9-Hβ + Ala13-Hβ + D-*allo*-Ile12-Hγ + Lipid-Hγ, Hδ, Hε, Hζ), 0.92-0.79 (m, 21H, D-Val1-Hγ + Val11-Hγ + D-

allo-Ile12-Hγ, Hδ, Lipid-CH_3). MW calculated for $C_{66}H_{109}N_{17}O_{19}$ 1443.8086, found *high resolution* (ESI-MS) 482.2767 $(M+3H)^{3+}$, calculated 482.2768.

Oct-TriA_1(Ala10) (163)

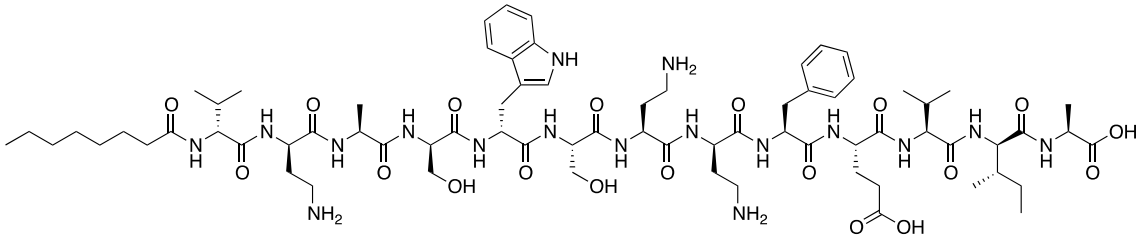

163

Peptide was isolated as a single peak using C_{18} HPLC (7.0 mg, 9.6 %). Retention time (HPLC method 2) = 41.6 min. ^{1}H NMR (D_2O, 600 MHz): δ 7.57 (d, 1H, *J* = 8.0 Hz, D-Trp5-ArH), 7.46 (d, 1H, *J* = 8.2 Hz, D-Trp5-ArH), 7.33-7.25 (m, 3H, Phe9-ArH), 7.21-7.19 (m, 4H, D-Trp5-ArH + Phe9-ArH), 7.11 (t, 1H, *J* = 7.1 Hz, Trp5-ArH), 4.69 (dd, 1H, *J* = 10.2, 5.7 Hz, Phe9-Hα), 4.61 (t, 1H, *J* = 7.4 Hz, D-Trp5-Hα), 4.44-4.41 (m, 2H, D-Ser4-Hα + D-Dab2-Hα), 4.34-4.25 (m, 4H, D-*allo*-Ile12-Hα + Dab7-Hα + D-Dab8-Hα + Ala13-Hα), 4.20 (q, 1H, *J* = 7.3 Hz, Ala10-Hα) 4.12-4.09 (m, 2H, Val11-Hα + Ser6-Hα), 4.01 (d, 1H, *J* = 7.6 Hz, D-Val1-Hα), 3.89 (s, 2H, Gly3-Hα), 3.74 (qd, 2H, *J* = 12.4, 5.5 Hz, D-Ser4-Hβ), 3.54 (dd, 1H, *J* = 11.5, 5.0 Hz, Ser6-Hβ), 3.29 (dd, 1H, *J* = 11.5, 5.5 Hz, Ser6-Hβ), 3.24 (d, 2H, *J* = 7.4 Hz, D-Trp5-Hβ), 3.20 (dd, 1H, *J* = 14.2, 5.4 Hz, Phe9-Hβ), 3.07-2.96 (m, 4H, D-Dab2-Hγ + Dab7-Hγ), 2.86 (dd, 1H, *J* = 14.4, 10.3 Hz, Phe9-Hβ), 2.69-2.64 (m, 1H, D-Dab8-Hγ), 2.58-2.53 (m, 1H, D-Dab8-Hγ), 2.30-2.09 (m, 4H, D-Dab2-Hβ + Dab7-Hβ + Lipid-Hα), 2.09-1.79 (m, 8H, D-Val1-Hβ + Dab7-Hβ + D-Dab8-Hβ + Val11-Hβ + D-*allo*-Ile12-Hβ + Glu10-Hγ), 1.56-1.50 (m, 2H, Lipid-Hβ), 1.32-1.16 (m, 16H, Ala10-Hβ + Ala13-Hβ + D-*allo*-Ile12-Hγ + Lipid-Hγ, Hδ, Hε, Hζ), 0.94-0.84 (m, 18H,

D-Val1-Hγ + Val11-Hγ + D-*allo*-Ile12-Hγ, Hδ), 0.81-0.78 (m, 3H, Lipid-CH_3). MW calculated for $C_{70}H_{111}N_{17}O_{17}$ 1461.8344, found *high resolution* (ESI-MS) 488.2855 $(M+3H)^{3+}$, calculated 488.2854.

Oct-TriA_1(Ala11) (164)

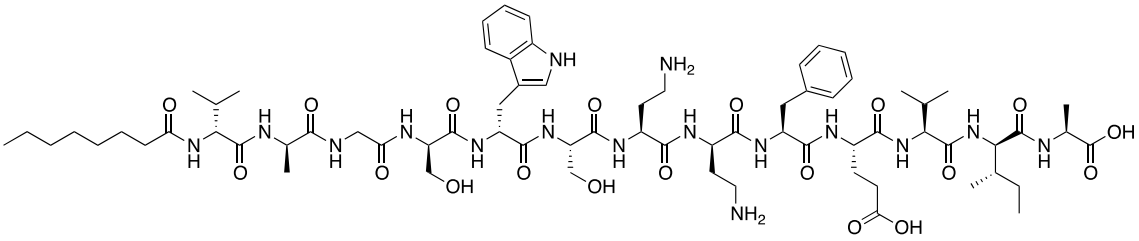

164

Peptide was isolated as a single peak using C_{18} HPLC (6.7 mg, 9.0 %). Retention time (HPLC method 2) = 39.1 min. ^{1}H NMR (D_2O, 600 MHz): δ 7.57 (d, 1H, *J* = 8.0 Hz, D-Trp5-ArH), 7.46 (d, 1H, *J* = 8.2 Hz, D-Trp5-ArH), 7.32-7.25 (m, 3H, Phe9-ArH), 7.21-7.19 (m, 4H, D-Trp5-ArH + Phe9-ArH), 7.11 (t, 1H, *J* = 7.6 Hz, D-Trp5-ArH), 4.66 (dd, 1H, *J* = 9.1, 6.2 Hz, Phe9-Hα), 4.61 (t, 1H, *J* = 7.4 Hz, D-Trp5-Hα), 4.44-4.41 (m, 2H, D-Ser4-Hα + D-Dab2-Hα), 4.34-4.26 (m, 5H, D-*allo*-Ile12-Hα + Dab7-Hα + Glu10-Hα + D-Dab8-Hα + Ala13-Hα), 4.20 (q, 1H, *J* = 7.8 Hz, Ala11-Hα), 4.13-4.11 (m, 1H, Ser6-Hα), 4.01 (d, 1H, *J* = 7.5 Hz, D-Val1-Hα), 3.89 (s, 2H, Gly3-Hα), 3.75 (ddd, 2H, *J* = 17.8, 11.9, 6.3 Hz, D-Ser4-Hβ), 3.54 (dd, 1H, *J* = 11.0, 4.7 Hz, Ser6-Hβ), 3.31 (dd, 1H, *J* = 11.3, 5.3 Hz, Ser6-Hβ), 3.25 (d, 2H, *J* = 7.5 Hz, D-Trp5-Hβ), 3.17 (dd, 1H, *J* = 13.9, 5.8 Hz, Phe9-Hβ), 3.07-2.96 (m, 4H, D-Dab2-Hγ + Dab7-Hγ), 2.90 (dd, 1H, *J* = 14.5, 10.5 Hz, Phe9-Hβ), 2.74-2.70 (m, 1H, D-Dab8-Hγ), 2.64-2.59 (m, 1H, D-Dab8-Hγ), 2.32-2.13 (m, 6H, Glu10-Hγ + D-Dab2-Hβ + Dab7-Hβ + Lipid-Hα), 2.09-1.79 (m, 9H, D-Val1-Hβ + Dab7-Hβ + D-Dab8-Hβ + Glu10-Hβ + Val11-Hβ + D-*allo*-Ile12-Hβ + Glu10-Hγ), 1.54-

1.50 (m, 2H, Lipid-Hβ), 1.36-1.16 (m, 16H, Ala11-Hβ + Ala13-Hβ + D-*allo*-Ile12-Hγ + Lipid-Hγ, Hδ, Hε, Hζ), 0.91-0.78 (m, 15H, D-Val1-Hγ + D-*allo*-Ile12-Hγ, Hδ, Lipid-CH_3). MW calculated for $C_{70}H_{109}N_{17}O_{19}$ 1491.8086, found *high resolution* (ESI-MS) 498.2768 $(M+3H)^{3+}$, calculated 498.2768.

Oct-TriA_1(Ala2) (165)

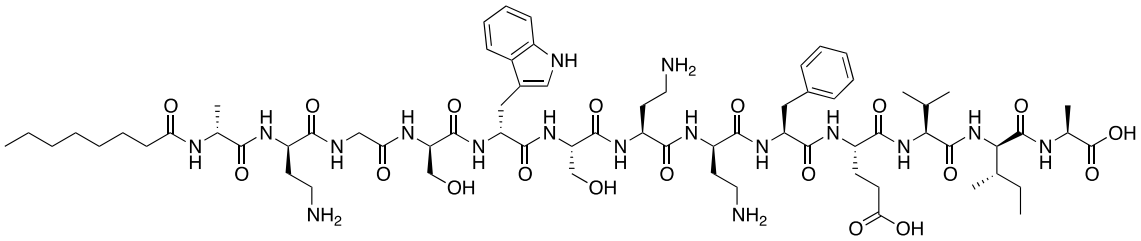

165

Peptide was isolated as a single peak using C_{18} HPLC (2.2 mg, 3.0 %). Retention time (HPLC method 2) = 37.0 min. ^{1}H NMR (D_2O, 600 MHz): δ 7.57 (d, 1H, *J* = 7.8 Hz, D-Trp5-ArH), 7.46 (d, 1H, *J* = 8.2 Hz, D-Trp5-ArH), 7.32-7.25 (m, 3H, Phe9-ArH), 7.21-7.18 (m, 4H, D-Trp5-ArH + Phe9-ArH), 7.11 (t, 1H, *J* = 7.4 Hz, D-Trp5-ArH), 4.67 (dd, 1H, *J* = 9.6, 5.7 Hz, Phe9-Hα), 4.62 (t, 1H, *J* = 7.4 Hz, D-Trp5-Hα), 4.45-4.41 (m, 2H, D-Ser4-Hα + D-Dab2-Hα), 4.35-4.26 (m, 4H, Dab7-Hα + Glu10-Hα + D-Dab8-Hα + Ala13-Hα), 4.17 (q, 1 H, *J* = 7.2, D-Ala12-Hα), 4.12 (t, 1H, *J* = 4.9 Hz, Ser6-Hα), 4.01-3.99 (m, 2H, D-Val1-Hα + Val11-Hα), 3.89 (s, 2H, Gly3-Hα), 3.75 (ddd, 2H, *J* = 17.6, 11.6, 6.0 Hz, D-Ser4-Hβ), 3.54 (dd, 1H, *J* = 11.2, 4.9 Hz, Ser6-Hβ), 3.31 (dd, 1H, *J* = 11.1, 5.4 Hz, Ser6-Hβ), 3.24 (d, 2H, *J* = 7.2 Hz, D-Trp5-Hβ), 3.17 (dd, 1H, *J* = 14.0, 5.6, Phe9-Hβ), 3.07-2.96 (m, 4H, D-Dab2-Hγ + Dab7-Hγ), 2.87 (dd, 1H, *J* = 13.7, 9.9 Hz, Phe9-Hβ), 2.73-2.68 (m, 1H, D-Dab8-Hγ), 2.61-2.57 (m, 1H, D-Dab8-Hγ), 2.34-2.14 (m, 6H, Glu10-Hγ + D-Dab2-Hβ + Dab7-Hβ + Lipid-Hα), 2.09-1.79 (m, 9H, D-Val1-Hβ + Dab7-Hβ + D-

Dab8-Hβ + Glu10-Hβ + Val11-Hβ + D-*allo*-Ile12-Hβ + Glu10-Hγ), 1.56-1.49 (m, 2H, Lipid-Hβ), 1.36-1.15 (m, 13H, D-Ala12-Hβ + Ala13-Hβ + Lipid-Hγ, Hδ, Hε, Hζ), 0.95-0.89 (m, 12H, D-Val1-Hγ + Val11-Hγ), 0.82-0.78 (m, 3H, Lipid-CH_3). MW calculated for $C_{69}H_{107}N_{17}O_{19}$ 1477.7929, found *high resolution* (ESI-MS) 493.6049 $(M+3H)^{3+}$, calculated 493.6049.

3*R*-CxnC$_1$ 166

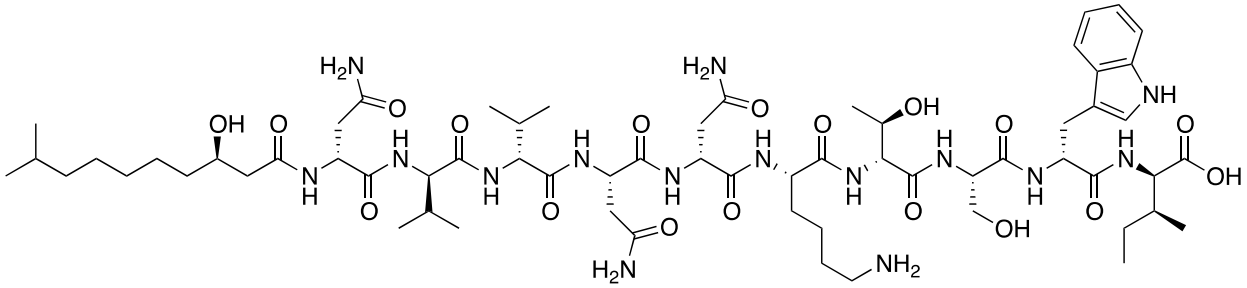

166

Purified by HPLC method 1 to yield peptide as a white solid (6.6 mg, 19%). MALDI (low res) Calcd for $C_{63}H_{105}N_{15}O_{18}$ $[M+H]^+$ 1358.7684, 1358.8.

3*S*-CxnC$_1$ 167

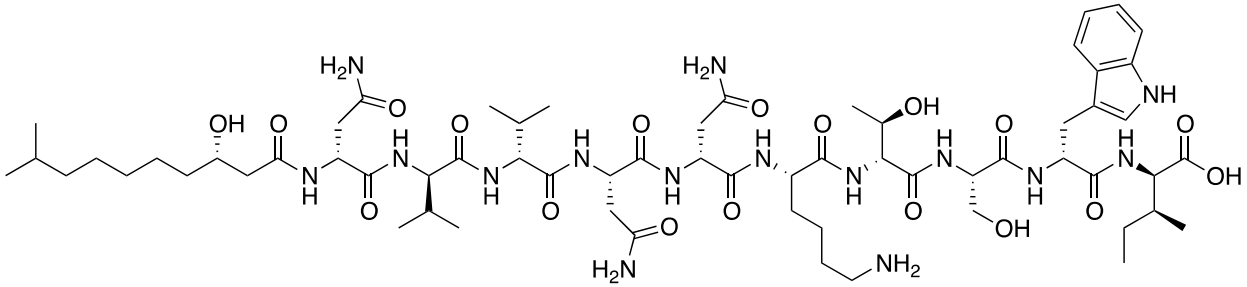

167

Purified by HPLC method 1 to yield peptide as a white solid (4.0 mg, 12%). MALDI (low res) Calcd for $C_{63}H_{105}N_{15}O_{18}$ $[M+H]^+$ 1358.7684, 1358.8.

Dec-CxnC$_1$ 168

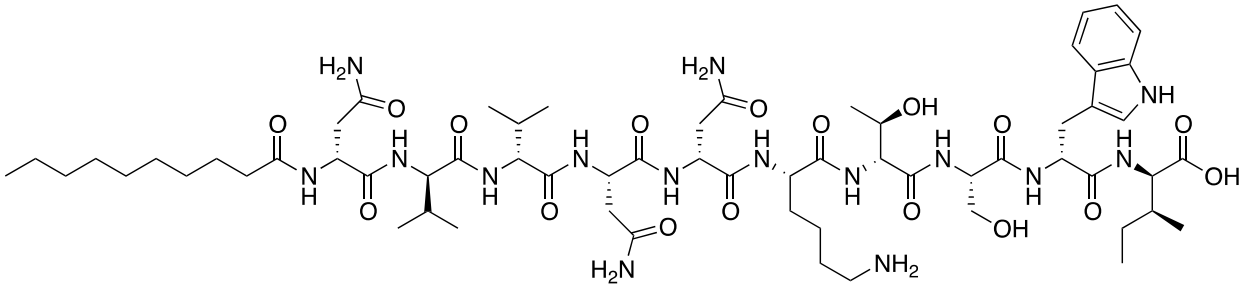

168

Purified by HPLC method 1 to yield peptide as a white solid (4.0 mg, 12%). MALDI (low res) Calcd for $C_{63}H_{104}N_{15}O_{17}$ $[M+H]^+$ 1342.7735, 1342.8.

***Ent*-TriA$_1$ (206)**

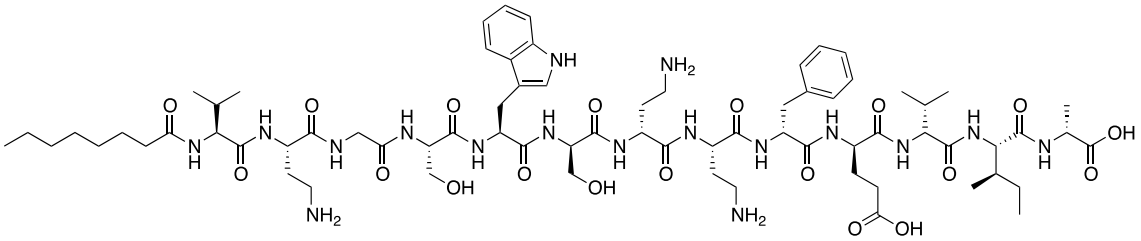

206

Peptide was isolated as a single peak using C_{18} HPLC (17 mg, 44.7 %). Retention time (HPLC method 2) = 43.3 min. ^{1}H NMR (D_2O, 600 MHz): δ 7.57 (d, 1H, *J* = 7.9 Hz, D-Trp5-ArH), 7.46 (d, 1H, *J* = 8.6 Hz, D-Trp5-ArH), 7.32-7.25 (m, 3H, Phe9-ArH), 7.21-7.19 (m, 4H, D-Trp5-ArH + Phe9-ArH), 7.11 (t, 1H, *J* = 7.4 Hz, D-Trp5-ArH), 4.69-4.66 (m, 1H, Phe9-Hα), 4.62 (t, 1H, *J* = 8.2 Hz, D-Trp5-Hα), 4.45-4.41 (m, 2H, D-Ser4-Hα + D-

Dab2-Hα), 4.34-4.24 (m, 5H, D-*allo*-Ile12-Hα + Dab7-Hα + Glu10-Hα + D-Dab8-Hα + Ala13-Hα), 4.13-4.10 (m, 2H, Val11-Hα + Ser6-Hα), 4.01 (d, 1H, *J* = 7.5 Hz, D-Val1-Hα), 3.89 (s, 2H, Gly3-Hα), 3.78-3.71 (m, 2H, D-Ser4-Hβ), 3.56-3.53 (m, 1H, Ser6-Hβ), 3.31-3.29 (m, 1H, Ser6-Hβ), 3.26 (d, 2H, *J* = 6.7 Hz, D-Trp5-Hβ), 3.18-3.15 (m, 1H, Phe9-Hβ), 3.07-2.96 (m, 4H, D-Dab2-Hγ + Dab7-Hγ), 2.89-2.86 (m, 1H, Phe9-Hβ), 2.73-2.68 (m, 1H, D-Dab8-Hγ), 2.61-2.57 (m, 1H, D-Dab8-Hγ), 2.34-2.14 (m, 6H, Glu10-Hγ + D-Dab2-Hβ + Dab7-Hβ + Lipid-Hα), 2.09-1.79 (m, 9H, D-Val1-Hβ + Dab7-Hβ + D-Dab8-Hβ + Glu10-Hβ + Val11-Hβ + D-*allo*-Ile12-Hβ + Glu10-Hγ), 1.54-1.48 (m, 2H, Lipid-Hβ), 1.34-1.17 (m, 13H, Ala13-Hβ + D-*allo*-Ile12-Hγ + Lipid-Hγ, Hδ, Hε, Hζ), 0.94-0.79 (m, 21H, D-Val1-Hγ + Val11-Hγ + D-*allo*-Ile12-Hγ, Hδ, Lipid-CH_3). MW calculated for $C_{72}H_{114}N_{17}O_{19}$ 1520.8471, found *high resolution* (FTICR-ESI-MS) 1520.8471 $(M+H)^+$.

(2*S*)-2-(Phenylsulfonyl)ethyl-2-((2*R*)-2-(7-acetamido-6-(benzyloxy)-2-phenylhexahydropyrano[3,2-*d*][1,3]dioxin-8-yloxy)propanamido)propanoate (187)

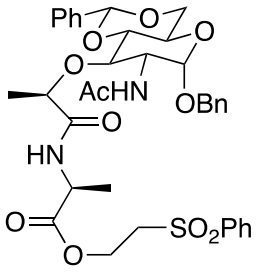

187

Glycol **185** (Carbosynth, UK) (7.00 g, 17.5 mmol) was suspended in dry dioxane (100 mL) and sodium hydride (60% dispersion in mineral oil, 4.90 g, 122.5 mmol) was added in parts at ambient temperature. The suspension was stirred at 50 ^oC for 1 h and cooled to 0 ^oC. Note, it is essential that the reaction mixture be cooled to 0 ^oC to prevent epimerization of L-chloropropionic acid. Once sufficiently cold, a solution of L-

chloropropionic acid (5.00 g, 46.1 mmol) in dry dioxane (20 mL) was added dropwise over 10 min. The reaction mixture was then warmed to ambient temperature and stirred for 18 h. The solvents were removed by rotary evaporator and the resulting solid stirred vigorously in brine (100 mL) at 4 ^{o}C for 1 h. The suspension was then filtered and the solid washed sparingly with cold water. The solid was dried overnight in a vacuum oven (50 ^{o}C), re-suspended in 60:39:1 MeOH:CH_2Cl_2: triethylamine (200 mL) and stirred for 5 min. The mixture was then filtered through celite and concentrated *in vacuo* to yield the muramic acid ammonium salt as a white foam (9.11 g, 91%), which was used directly in the next step without further purification. The muramic acid derivative (3.00 g, 5.24 mmol) was dissolved in CH_2Cl_2 (40 mL) and cooled to 0 ^{o}C. 2-Chloro-4,6-dimethoxy-1,3,5-triazine (1.10 g, 6.29 mmol) and *N*-methylmorpholine (0.58 mL, 5.24 mmol) were added and the mixture stirred at 0 ^{o}C for a further 45 min. Alanine-2-(phenylsulfonyl)-ethyl ester (1.62 g, 6.29 mmol) was then added and the reaction gradually warmed to ambient temperature and stirred for 18 h. The resulting cloudy solution was diluted with CH_2Cl_2 (30 mL) and washed with 1M HCl (100 mL) and brine (100 mL). The organic phase was dried over anhydrous sodium sulfate and concentrated *in vacuo* to yield **187** as a white solid (3.90 g, quant.). $[\alpha]_D^{25}$ = 92.48 (*c* = 0.85 g/100mL, CH_2Cl_2); IR (CH_2Cl_2 cast) 3378, 3064, 2984, 2930, 1748, 1660 cm^{-1}; ^{1}H NMR ($CDCl_3$, 500 MHz) δ 7.95 – 7.87 (m, 2H, ArH), 7.69 – 7.63 (m, 1H, ArH), 7.56 (t, *J* = 7.8 Hz, 2H, ArH), 7.50 – 7.43 (m, 2H, ArH), 7.41 – 7.25 (m, 8H, ArH), 6.93 (d, *J* = 7.1 Hz, 1H, Ala1-NH), 6.16 (d, *J* = 8.9 Hz, 1H, AcNH), 5.57 (s, 1H, $O_2C\underline{H}$), 4.95 (d, *J* = 3.8 Hz, 1H, H1), 4.71 (d, *J* = 11.8 Hz, 1H, PhC$\underline{H}$H), 4.52 – 4.38 (m, 3H, PhCH$\underline{H}$ + OC$\underline{H_2}$), 4.30 (td, *J* = 9.3, 3.9 Hz, 1H, H2), 4.24 (dd, *J* = 10.2, 4.8 Hz, 1H, H6), 4.17 (t, *J* = 7.2 Hz, 1H, Ala1-Hα), 4.07 (q, *J* =

6.7 Hz, 1H, OC<u>H</u>), 3.87 (m, 1H, H5), 3.77 (t, *J* = 10.3 Hz, 1H, H6), 3.72 – 3.60 (m, 2H, H3 + H4), 3.42 (ddd, *J* = 14.6, 6.6, 5.5 Hz, 2H, SC<u>H</u>$_2$), 1.93 (s, 3H, Ac), 1.37 (d, *J* = 6.8 Hz, 3H, MurNAc-CH_3), 1.29 (d, *J* = 7.2 Hz, 3H, Ala1-Hβ); ^{13}C NMR ($CDCl_3$, 125 MHz) δ 173.12, 171.91, 170.65, 137.20, 136.85, 134.21, 129.59, 129.19, 128.82, 128.48, 128.44, 128.37, 128.21, 126.07, 101.60, 97.67, 81.66, 78.64, 78.34, 77.37, 70.29, 68.99, 63.32, 58.16, 55.09, 53.15, 48.10, 23.59, 19.51, 17.33. HRMS (ES) Calcd for $C_{36}H_{42}N_2NaO_{11}S$ $[M+Na]^+$ 733.2402, found 733.2403.

Glycosyl donor (181)

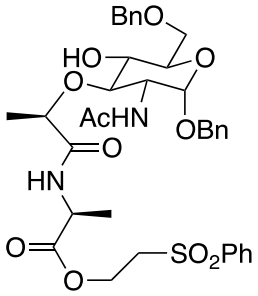

181

Benzylidene **187** (3.46 g, 4.87 mmol) was dissolved in CH_2Cl_2 (50 mL) and cooled to 0 ^oC. Triethylsilane (3.63 mL, 24.34 mmol) was added, followed by TFA (1.86 mL, 24.34 mmol) dropwise. The solution was stirred at 0 ^oC for 5 h and another portion of TFA (1.12 mL, 14.60 mmol) was added. The reaction was stirred for a further 19 h at 0 ^oC and diluted with CH_2Cl_2 (50 mL). Saturated sodium bicarbonate (50 mL) was slowly added and the aqueous layer extracted with CH_2Cl_2. The combined organic extracts were washed with brine (50 mL), dried over anhydrous sodium sulfate and concentrated *in vacuo*. The crude product was purified by column chromatography (silica, gradient: 0% - 3% MeOH in CH_2Cl_2) to yield the product as a white foam (2.10 g, 62%). $[\alpha]_D^{25}$ =

79.43 (*c* = 0.80 g/100mL, CH_2Cl_2); IR (CH_2Cl_2 cast) 3288, 3064, 2983, 2928, 1748, 1658 cm^{-1}; ^1H NMR ($CDCl_3$, 500 MHz) δ 7.94 – 7.85 (m, 2H, ArH), 7.69 – 7.63 (m, 1H, ArH), 7.57 (t, *J* = 7.7 Hz, 2H, ArH), 7.41 – 7.22 (m, 9H, ArH), 6.92 (d, *J* = 7.2 Hz, 1H, Ala1-NH), 6.10 (d, *J* = 9.0 Hz, 1H, AcNH), 4.92 (d, *J* = 3.6 Hz, 1H, H1), 4.71 (d, *J* = 11.8 Hz, 1H, PhC<u>H</u>H), 4.65 – 4.54 (m, 2H, $PhCH_2$), 4.49 – 4.34 (m, 3H, PhCH<u>H</u> + OCH_2), 4.29 – 4.17 (m, 2H, H2 + Ala1-Hα), 4.13 (t, *J* = 6.7 Hz, 1H, OCH), 4.07 (q, *J* = 6.7 Hz, 1H, OCH), 3.80 (dd, *J* = 9.5, 4.6 Hz, 1H, H5), 3.74 (dd, *J* = 10.3, 4.5 Hz, 1H, H6), 3.72 – 3.65 (m, 2H, H3 + H4), 3.53 (dd, *J* = 10.5, 8.7 Hz, 1H, H6), 3.39 (ddd, *J* = 9.2, 6.6, 5.5 Hz, 2H, SCH_2), 3.01 (s, 1H, OH), 1.90 (s, 3H, Ac), 1.40 (d, *J* = 6.7 Hz, 3H, MurNAc-CH_3), 1.30 (d, *J* = 7.2 Hz, 3H, Ala1-HB); ^{13}C NMR ($CDCl_3$, 125 MHz) δ 173.09, 171.97, 170.46, 139.25, 137.90, 137.15, 134.24, 129.60, 128.72, 128.59, 128.32, 128.31, 128.18, 127.94, 127.81, 97.23, 80.61, 77.93, 73.84, 71.72, 70.57, 70.30, 69.98, 58.15, 55.06, 52.64, 48.01, 23.51, 19.15, 17.25; HRMS (ES) Calcd for $C_{36}H_{44}N_2O_{11}S$ $[M+H]^+$ 735.2558, found 735.2546.

Glycosyl acceptor (182)

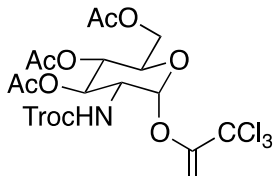

182

D-Glucosamine (**188**) (10.00 g, 46.4 mmol) and sodium bicarbonate (7.80 g, 92.8 mmol) were dissolved in water (120 mL) and stirred vigorously for 5 min. 2,2,2-Trichloroethoxycarbonyl chloride (7.65 mL, 55.6 mmol) was added dropwise and the solution stirred at ambient temperature for 2 h, over which time a white precipitate

formed. The suspension was filtered, washed with water and dried by lyophilization (24 h) to give a white flocculent solid. This solid was dissolved in dry pyridine (100 mL) and acetic anhydride (50 mL) and stirred at ambient temperature for 18 h. The reaction mixture was concentrated *in vacuo* and co-evaporated with toluene (3 x 50 mL). The resulting oily residue was dissolved in $CHCl_3$ (100 mL) and washed with 1M HCl (100 mL). The aqueous phase was back extracted with $CHCl_3$ (2 x 100 mL) and the combined organic extracts washed with brine (50 mL). The organic phase was then dried over anhydrous sodium sulfate and concentrated *in vacuo* to yield 1,3,4,6-tetra-*O*-acetyl-2-troc-D-glucosamine (**189**) (19.42 g, 80%) as a white solid. **2** (10 g, 19.3 mmol) was dissolved in dry DMF (100 mL) and to this solution was added hydrazine acetate (2.11 g, 23.0 mmol). The reaction mixture was stirred at ambient temperature for 40 min, diluted with EtOAc (100 mL) and washed with water (100 mL), saturated sodium bicarbonate (100 mL) and water (100 mL). The combined aqueous phases were back extracted with EtOAc (100 mL) and the combined organic extracts washed with brine, dried over anhydrous sodium sulfate and concentrated *in vacuo*. The resulting yellow oil was dissolved in CH_2Cl_2 (100 mL) and trichloroacetonitrile (19.2 mL, 191.3 mmol). 1,8-Diazabicycloundec-7-ene (0.57 mL, 3.83 mmol) was added and the reaction mixture stirred at ambient temperature for 90 min and concentrated *in vacuo*. The crude reaction mixture was purified by flash column chromatography (silica, 2:1 hexanes:EtOAc + 0.1% triethylamine) to yield the product as a white foam (5.5 g, 46%). $[\alpha]_D^{25}$ = 76.1 (*c* = 1.1 g/100mL, CH_2Cl_2); IR ($CHCl_3$ cast) 3317, 2957, 1750 cm^{-1}; ^1H NMR ($CDCl_3$, 500 MHz) δ 8.80 (s, 1H, acetimidate-NH), 6.43 (d, *J* = 3.6 Hz, 1H, H1), 5.35 (dd, *J* = 10.8, 9.5 Hz, H3), 5.25 (t, *J* = 9.9 Hz, H4), 5.19 (d, *J* = 9.3 Hz, Troc-NH),

4.75 – 4.67 (m, 2H, Troc-CH_2), 4.29 (m, 2H, H2 + H6), 4.16 – 4.09 (m, 2H, H5 + H6), 2.07 (m, 9H, 3 x OCH_3); ^{13}C NMR ($CDCl_3$, 125 MHz) δ 171.01, 170.44, 169.12, 160.28, 154.00, 95.11, 94.44, 90.54, 74.56, 70.18, 67.27, 61.28, 53.80, 20.57, 20.47; HRMS (ES) Calcd for $C_{17}H_{20}Cl_6N_2NaO_{10}$ $[M+Na]^+$ 644.9141, found 644.9137.

Boc-D-Ala-D-Ala-OMe (198)

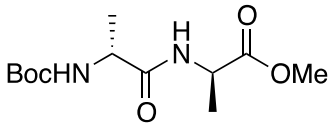

198

H-D-Ala-OMe.HCl (5.00 g, 35.8 mmol), Boc-D-Ala-OH (6.78 g, 35.8 mmol) and HATU (13.60 g, 35.8 mmol) were dissolved in dry DMF (175 mL) and cooled to 0 ^oC. DIPEA (6.25 mL, 107.4 mmol) was added and the reaction stirred at ambient temperature for 18 h. The solution was then concentrated *in vacuo*, re-dissolved in EtOAc (200 mL) and washed with 0.5 M HCl (100 mL), saturated sodium bicarbonate (100 mL) and brine (100 mL). The organic phase was then dried over anhydrous sodium sulfate and concentrated *in vacuo* to yield Boc-dipeptide **198** as a white foam (7.37 g, 75%). $[\alpha]_D^{25}$ = 26.18 (*c* = 0.75 g/100mL, CH_2Cl_2); IR (CH_2Cl_2 cast) 3310, 3073, 2980, 2937, 1747, 1663 cm^{-1}; ^1H NMR ($CDCl_3$, 400 MHz) δ 6.67 (m, 1H, D-Ala5NH), 5.03 (m, 1H, D-Ala4NH), 4.56 (app. pentet, *J* = 7.2 Hz, 1H, D-Ala5Hα), 4.17 (m, 1H, D-Ala4Hα), 3.74 (s, 3H, D-Ala5-OMe), 1.44 (m, 9H, Boc), 1.39 (d, *J* = 7.1 Hz, 3H, D-Ala5Hβ), 1.35 (d, *J* = 7.1 Hz, 3H, D-Ala4Hβ). ^{13}C NMR ($CDCl_3$, 125 MHz) δ 173.32, 172.30, 52.59, 48.15, 28.43, 18.50, 18.41; HRMS (ES) Calcd for $C_{12}H_{22}N_2NaO_5$ $[M+Na]^+$ 297.1421, found 297.1420.

Boc-DAP(TFA, OMe)-D-Ala-D-Ala-OMe (199)

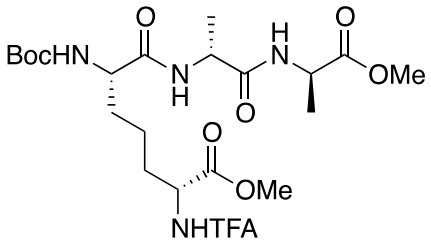

199

Boc-dipeptide **198** (507 mg, 1.85 mmol) was dissolved in CH_2Cl_2 (6 mL) and cooled to 0 ^oC. TFA (6 mL) was added and the resulting solution stirred for 3 h and concentrated *in vacuo*. The resulting oil was co-evaporated with toluene (3 x 10 mL) and dried under high vacuum for 30 min. During this time, DAP **190** (740 mg, 1.85 mmol) and HATU (703 mg, 1.85 mmol) were dissolved in dry DMF (10 mL) and cooled to 0 ^oC. DIPEA (0.5 mL, 2.87 mmol) was added and the resulting yellow solution stirred at 0 ^oC for 15 min. The deprotected dipeptide (1.85 mmol) was dissolved in dry DMF (7 mL) and DIPEA (0.5 mL, 2.87 mmol) and this solution was added to the DAP **190** solution. The resulting solution was stirred for 18 h at ambient temperature and concentrated *in vacuo*. The resulting oil was re-dissolved in EtOAc (30 mL) and washed with 0.5 M HCl (20 mL), saturated sodium bicarbonate (20 mL) and brine (20 mL). The organic phase was then dried over anhydrous sodium sulfate and concentrated *in vacuo* to yield Boc-tripeptide **199** as a white solid (630 mg, 61%). $[\alpha]_D^{25}$ = -3.33 (*c* = 0.6 g/100mL, CH_2Cl_2); IR (CH_2Cl_2 cast) 3298, 3077, 2980, 2929, 1746, 1723, 1656 cm^{-1}; ^1H NMR ($CDCl_3$, 500 MHz) δ 6.70 (d, *J* = 7.4 Hz, 1H, D-Ala4NH), 6.67 – 6.57 (m, 1H, D-Ala5NH), 5.07 (m, 1H, DAP3γNH), 4.66 – 4.47 (m, 3H, DAP3Hε + D-Ala4NHα + D-Ala5NHα), 4.07 (m, 1H, DAP3Hα), 3.79 (s, 3H, -OMe), 3.75 (s, 3H, -OMe), 2.00-1.91 (m, 1H, DAP3Hδ), 1.93 – 1.71 (m, 2H, DAP3Hδ + DAP3Hβ), 1.73 – 1.53 (m, 2H, DAP3Hβ + DAP3Hγ), 1.42 (m,

16H, DAP3Hβ + Boc + D-Ala4Hβ + D-Ala5Hβ). ^{13}C NMR ($CDCl_3$, 125 MHz) δ 173.23, 171.69, 171.53, 171.24, 53.08, 52.67, 52.61, 49.01, 48.33, 31.98, 31.42, 28.39, 21.35, 18.30; HRMS (ES) Calcd for $C_{22}H_{35}F_3N_4NaO_9$ $[M+Na]^+$ 579.2248, found 579.2242.

Boc-D-γ-Glu(OMe)-DAP(TFA, OMe)-D-Ala-D-Ala-OMe (183)

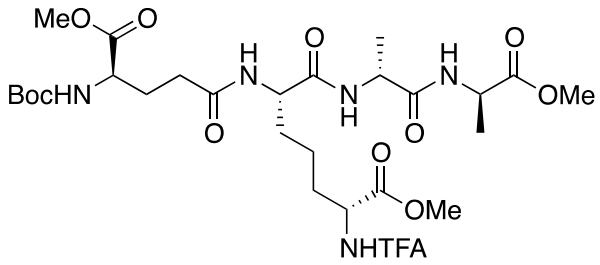

183

Boc-tripeptide **199** (610 mg, 1.1 mmol) was dissolved in CH_2Cl_2 (5 mL) and cooled to 0 ^oC. TFA (5 mL) was added and the resulting solution stirred for 3 h and concentrated *in vacuo*. The resulting oil was co-evaporated with toluene (3 x 5 mL) and dried under high vacuum for 30 min. During this time, Boc-D-Glu-OMe (288 mg, 1.1 mmol) and HATU (418 mg, 1.1 mmol) were dissolved in dry DMF (6 mL) and cooled to 0 ^oC. DIPEA (0.29 mL, 1.65 mmol) was added and the resulting yellow solution stirred at 0 ^oC for 15 min. The deprotected tripeptide (1.1 mmol) was dissolved in dry DMF (5 mL) and DIPEA (0.29 mL, 1.65 mmol) and this solution was added to the Boc-D-Glu-OMe solution. The resulting solution was stirred for 18 h at ambient temperature and concentrated *in vacuo*. The resulting oil was re-dissolved in EtOAc (30 mL) and washed with 0.5 M HCl (20 mL), saturated sodium bicarbonate (20 mL) and brine (20 mL). The organic phase was then dried over anhydrous sodium sulfate and concentrated *in vacuo* to yield Boc-tetrapeptide **183** as a white solid (690 mg, 91%). ^{1}H NMR (DMSO-d_6, 600 MHz) δ 9.79 (d, J = 7.5 Hz, 1H, DAP3εNH), 8.20 (m, 2H, D-Ala4NH + D-Ala5NH), 7.99 (d, J = 7.6 Hz,

1H, DAP3αNH), 7.22 (d, *J* = 7.7 Hz, 1H, D-Glu2NH), 4.36 – 4.17 (m, 4H, DAP3Hα + DAP3Hε + D-Ala4Hα + D-Ala5Hα), 3.94 (m, 1H, D-Glu2Hα), 3.70 – 3.56 (m, 9H, 3 x OMe), 2.26 – 2.11 (m, 2H, D-Glu2Hγ), 1.94 – 1.67 (m, 4H, D-Glu2Hβ + DAP3Hδ), 1.59 (m, 1H, DAP3Hβ), 1.48 (m, 1H, DAP3Hβ), 1.43 – 1.13 (m, 17H, DAP3Hγ + Boc + D-Ala4Hβ + D-Ala5Hβ).

Troc-Disaccharide (201)

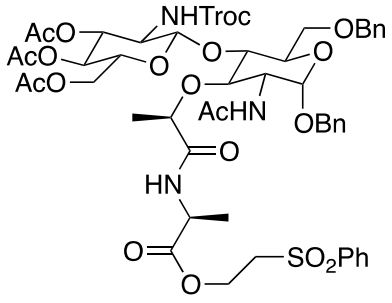

201

4 Å molecular sieves (MS) (15 g) in a round-bottomed flask were heated under vacuum with a Bunsen burner for approximately 5 min and left to cool at ambient temperature. The flask was depressurized with argon and directly used in the reaction. A solution of glycol **181** (2.00g, 2.81 mmol) in dry CH_2Cl_2 (30 mL) was added to the flask containing 4 Å MS under argon and the suspension gently stirred. Trimethylsilyl triflate (0.3 mL, 2.81 mmol) was added, followed by a solution of acetimidate **182** (5.26 g, 8.42 mmol) in dry CH_2Cl_2 (30 mL). The resulting suspension was stirred at ambient temperature overnight. The reaction mixture was decanted and the solution diluted with CH_2Cl_2 (50 mL). The organic solution was washed with saturated sodium bicarbonate (75 mL) and brine (100 mL) and dried over anhydrous sodium sulfate. The solution was concentrated *in vacuo* and purified by flash column chromatography (silica, gradient: 1:1 EtOAc:hexane –

EtOAc – 19:1 EtOAc:MeOH) to yield the product as a white foam (2.00 g, 61%). $[\alpha]_D^{25}$ = 28.96 (*c* = 0.6 g/100mL, CH_2Cl_2); IR (CH_2Cl_2 cast) 3358, 3282, 3064, 2926, 1751, 1661 cm^{-1}; ^1H NMR ($CDCl_3$, 500 MHz) δ 7.98 – 7.87 (m, 2H, ArH), 7.70 – 7.62 (m, 1H, ArH), 7.61 – 7.42 (m, 6H, ArH), 7.38 – 7.23 (m, 6H, ArH), 6.84 (d, *J* = 7.5 Hz, 1H, Ala1NH), 6.53 (d, *J* = 7.4 Hz, 1H, MurNAc-NH), 5.09 (d, *J* = 3.6 Hz, 1H, MurNAc-H1), 4.97 (t, *J* = 9.6 Hz, 1H, GlcNAc-H4), 4.87 (d, *J* = 12.0 Hz, 1H, MurNAc-1-C*H*HPh), 4.76 (m, 2H, GlcNAc-H3 + Troc-C*H*H), 4.60 (m, 2H, Troc-CH*H* + MurNAc-6-CH*H*Ph), 4.50 – 4.39 (m, 2H, OC*H*H + MurNAc-6-C*H*HPh), 4.35 (m, 2H, OCH*H* + MurNAc-1-C*H*HPh), 4.28 – 4.03 (m, 5H, MurNAc-H2 + MurNAc-C*H*O + GlcNAc-H1 + GlcNAc-H6 + Ala1Hα), 3.98 (dd, *J* = 12.3, 2.2 Hz, 1H, GlcNAc-H6), 3.91 (t, *J* = 9.5 Hz, 1H, MurNAc-H3), 3.68 (dd, *J* = 10.9, 2.4 Hz, 1H, MurNAc-H6), 3.62 (dt, *J* = 10.1, 2.3 Hz, 1H, MurNAc-H4), 3.55 (td, *J* = 10.2, 8.4 Hz, 1H, MurNAc-H5), 3.49 – 3.33 (m, 4H, CH_2S + GlcNAc-H2 + GlcNAc-H5), 2.05 – 1.94 (m, 9H, 3 x Ac), 1.90 (s, 3H, Ac), 1.34 (d, *J* = 6.7 Hz, 3H, Ala1Hβ), 1.25 (dd, *J* = 9.7, 7.2 Hz, 3H, MurNAc-CH_3). ^{13}C NMR ($CDCl_3$, 125 MHz) δ 173.47, 171.93, 170.79, 170.54, 170.41, 169.53, 154.25, 139.37, 137.45, 137.27, 134.18, 129.54, 129.24, 128.67, 128.26, 128.23, 100.13, 97.26, 95.74, 77.73, 75.78, 74.60, 73.89, 72.28, 71.32, 70.53, 70.40, 68.42, 67.27, 61.58, 58.24, 56.31, 55.04, 53.75, 47.83, 23.38, 20.75, 18.44, 17.63; HRMS (ES) Calcd for $C_{51}H_{62}Cl_3N_3NaO_{20}S$ $[M+Na]^+$ 1196.2605, found 1196.2585.

Acetyl-Disaccharide (202)

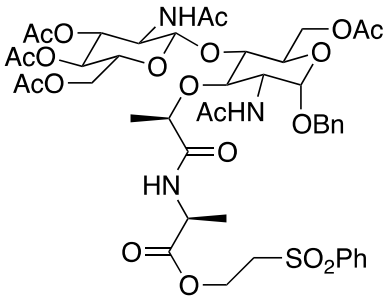

202

The troc-disaccharide **201** (4.0 g, 3.4 mmol) was dissolved in acetic anhydride and AcOH (2:1, 23 mL) and to this solution was added a solution of anhydrous $ZnCl_2$ (4.6 g, 34.0 mmol) in Ac_2O and AcOH (2:1, 11 mL). The reaction mixture was stirred for 24 h at ambient temperature, at which point zinc dust (8.9 g, 136.0 mmol) and a mixture of THF, Ac_2O and AcOH (3:2:1, 54 mL) were added. The reaction was stirred for a further 24 h at ambient temperature and filtered through celite, washed with EtOAc, and concentrated *in vacuo*. The resulting residue was co-evaporated with toluene (2 x 20 mL) and re-dissolved in EtOAc (100 mL). The organic layer was washed with saturated sodium bicarbonate (2 x 50 mL), water (2 x 50 mL) and brine (50 mL) and dried over anhydrous sodium sulfate and concentrated *in vacuo*. The crude product was purified by flash column chromotography (silica, 2% MeOH in EtOAc) to yield the product as a white foam (2.13 g, 63%). $[\alpha]_D^{25}$ = 28.96 (*c* = 0.6 g/100mL, CH_2Cl_2); IR (CH_2Cl_2 cast) 3358, 3282, 3064, 2926, 1751, 1661 cm^{-1}; ^1H NMR ($CDCl_3$, 500 MHz) δ 7.97 – 7.86 (m, 2H, *ortho*-ArH), 7.72 – 7.63 (m, 1H, *para*-ArH), 7.57 (m, 2H, *meta*-ArH), 7.38 – 7.24 (m, 5H, Bn-ArH), 7.16 (d, *J* = 7.6 Hz, 1H, MurNAc-NH), 6.84 (d, *J* = 6.8 Hz, 1H, Ala1NH), 6.02 (d, *J* = 9.5 Hz, 1H, GlcNAc-NH), 5.17 – 5.06 (m, 2H, MurNAc-H1 + GlcNAc-H3), 4.64 (d, *J* = 12.1 Hz, 1H, MurNAc-1-C*H*HPh), 4.49 (d, *J* = 12.1 Hz, 1H, MurNAc-1-

C*H*HPh), 4.46 – 4.22 (m, 6H, OCH_2 + MurNAc-C*H*O + GlcNAc-H1 + GlcNAc-H6 + MurNAc-H6), 4.19 – 4.14 (m, 1H, MurNAc-H6), 4.12 (q, *J* = 7.1 Hz, 1H, GlcNAc-H6), 4.09 – 3.97 (m, 3H, GlcNAc-H2 + MurNAc-H2 + MurNAc-H3), 3.78 (d, *J* = 5.2 Hz, MurNAc-H5), 3.62 - 3.54 (m, 2H, GlcNAc-H5 + MurNAc-H4), 3.36 (m, 2H, CH_2S), 2.14 (s, 3H), 2.05 – 1.97 (m, 6H), 1.95 (s, 3H), 1.93 (s, 3H), 1.37 (d, *J* = 6.7 Hz, 3H, MurNAc-CH_3), 1.29 (d, *J* = 7.2 Hz, 3H, Ala1Hβ). ^{13}C NMR ($CDCl_3$, 500 MHz) δ 173.85, 172.01, 171.36, 171.06, 170.91, 170.75, 170.72, 169.42, 139.29, 137.44, 134.22, 129.57, 128.62, 128.24, 128.14, 128.01, 100.42, 97.08, 76.15, 75.77, 72.63, 71.98, 70.44, 69.66, 68.23, 62.40, 61.76, 60.53, 58.16, 55.03, 54.77, 53.72, 47.99, 23.38, 23.32, 21.13, 20.77, 20.75, 20.74, 18.49, 17.47. HRMS (ES) Calcd for $C_{45}H_{59}N_3NaO_{20}S$ $[M+Na]^+$ 1016.3305, found 1016.3293.

Disaccharidyl phosphate (203)

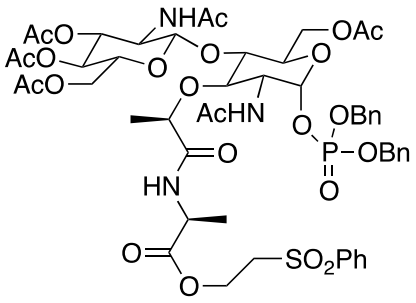

203

Benzyl ether **202** (1.50 g, 1.51 mmol) was dissolved in THF and MeOH (4:1, 45 mL) and added to a degassed suspension of 10% palladium on charcoal (2.70 g, 2.54 mmol) in the same solvent (30 mL). The reaction mixture was stirred under a hydrogen atmosphere for 3 h and filtered through a thin layer of celite. The celite was washed with CH_2Cl_2 (200 mL), the filtrate concentrated *in vacuo* and the resulting oil precipitated

from ether and hexanes (1:1, 40 mL). The precipitate was filtered and dried to yield the lactol as a white solid (1.35 g, 99%). This was dissolved in anhydrous CH_2Cl_2 (10 mL) and added rapidly via syringe to a vigorously stirred suspension of tetrazole (0.53 g, 7.50 mmol) and dibenzyl N,N'-diethylphosphoramidite (1.35 mL, 4.50 mmol) in anhydrous CH_2Cl_2 (10 mL) under argon at ambient temperature. The reaction mixture became homogeneous within a few min. After 2 h, the mixture was diluted with CH_2Cl_2 (10 mL) and washed with saturated sodium bicarbonate (5 mL), water (5mL) and brine (5 mL). The organic solution was dried over anhydrous sodium sulfate and concentrated *in vacuo* to yield a colourless oil, which was precipitated from ether and hexanes (1:1, 40 mL) to yield the phosphite as a white solid. The product was dissolved in THF (30 mL) and cooled to -78 °C. Hydrogen peroxide (50%, 1.63 mL) was added dropwise via syringe to the vigorously stirred solution. After the addition was complete, the ice bath was removed and the mixture was allowed to warm to ambient temperature over 2 h. The reaction mixture was then diluted with ice-cold saturated sodium sulfite (5 mL), followed by EtOAc (10 mL), and stirred for 5 min. The organic layer was dried over anhydrous sodium sulfate and concentrated *in vacuo* to yield phosphate **21** as a white solid (1.46 g, 84%). $[\alpha]_D^{25}$ = 2.93 (*c* = 0.45 g/100mL, CH_2Cl_2); IR (CH_2Cl_2 cast) 3278, 3066, 2982, 1747, 1666 cm^{-1}; ^1H NMR (DMSO-d_6, 500 MHz) δ 8.67 (d, *J* = 4.6 Hz, 1H, NHAc), 8.40 (d, *J* = 7.0 Hz, 1H, NHAc), 8.07 (d, *J* = 9.0 Hz, 1H, NHAc), 7.92 – 7.80 (m, 2H, *ortho*-ArH), 7.76 – 7.72 (m, 1H, *para*-ArH), 7.67 – 7.59 (m, 2H, *meta*-ArH), 7.44 – 7.27 (m, 10H, 2 x Bn-ArH), 5.81 (dd, *J* = 6.4, 3.1 Hz, H1, MurNAc-H1), 5.24 (t, *J* = 9.9 Hz, 1H, GlcNAc-H3), 5.13 – 4.95 (m, 4H, 2 x CH_2Ph), 4.91 (t, *J* = 9.8 Hz, 1H, GlcNAc-H4), 4.72 (dd, *J* = 16.2, 7.5 Hz, 1H, GlcNAc-H1), 4.60 (d, *J* = 6.7 Hz, 1H, MurNAc-

C*H*O), 4.40 – 4.18 (m, 3H, MurNAc-H6 + GlcNAc-H6 + OC*H*H), 4.13 – 3.95 (m, 4H, MurNAc-H6 + GlcNAc-H6 + OC*H*H + Ala1Hα), 3.87 – 3.71 (m, 4H, GlcNAc-H2 + GlcNAc-H5 + MurNAc-H3 + MurNAc-H5), 3.65 – 3.56 (m, 3H, MurNAc-H2 + SCH_2), 3.42 (dd, *J* = 10.9, 8.7 Hz, 1H, MurNAc-H4), 2.03 – 1.87 (m, 12H, 4 x Ac), 1.75 (s, 3H, Ac), 1.69 (s, 2H, Ac), 1.29 (d, *J* = 6.7 Hz, 3H, MurNAc-CH_3), 1.11 (d, *J* = 7.3 Hz, 3H, AlaHβ); ^{13}C NMR (DMSO-d_6, 125 MHz) δ 174.48, 171.35, 169.91, 169.83, 169.56, 169.30, 139.26, 135.76, 133.93, 129.39, 128.43, 128.38, 128.36, 128.33, 127.93, 127.84, 127.70, 127.65, 127.62, 99.60, 75.97, 75.75, 73.89, 72.34, 70.74, 70.43, 68.69, 68.46, 68.42, 68.30, 66.36, 61.63, 57.92, 53.65, 47.35, 40.02, 39.95, 39.85, 39.78, 39.69, 39.61, 39.52, 39.44, 39.35, 39.19, 39.02, 22.61, 22.38, 20.53, 20.38, 20.27, 18.96, 16.52; HRMS (ES) Calcd for $C_{52}H_{66}N_3NaO_{23}PS$ $[M+Na]^+$ 1186.3438, found 1186.3416.

Pentapeptidyl disaccharide (204)

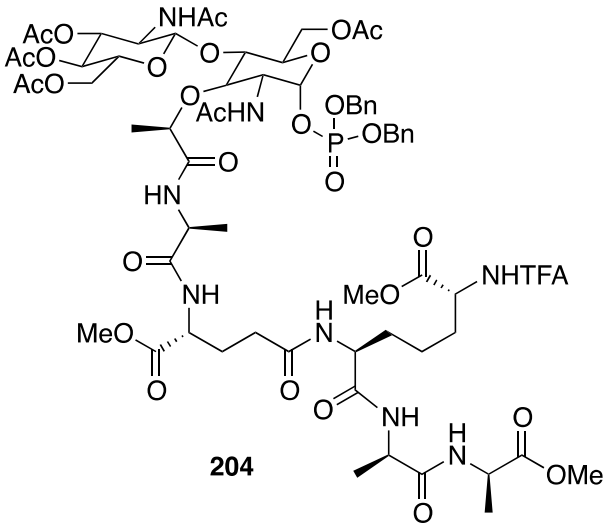

204

The Boc-Tetrapeptide **183** (194 mg, 0.283 mmol) was dissolved in CH_2Cl_2 (2 mL) and TFA (2 mL) and stirred at ambient temperature for 3 h. The reaction mixture was then

concentrated *in vacuo* and co-evaporated with toluene (2 x 2 mL) and precipitated with cold ether (6 mL) to yield the peptide TFA salt as an off-white solid (0.283 mmol). Concurrent with the start of the Boc-deprotection, the disaccharidyl ester (194 mg, 0.258 mmol) was dissolved in dry CH_2Cl_2 (2 mL) and stirred at ambient temperature under argon. A solution of Diazabicycloundec-7-ene (38.6 µL, 0.258 mmol) in dry CH_2Cl_2 (1 mL) was added drop wise over 2 min and stirred for a further 30 min. The reaction mixture was diluted with CH_2Cl_2 (7 mL), washed with 1 M HCl (5 mL) and brine (5 mL), dried over anhydrous sodium sulfate and concentrated *in vacuo*. The oil was dried under high vac for 2 h to yield the acid as a white solid (260 mg, 0.255 mmol). The acid was dissolved in dry DMF (2 mL) and cooled to 0 ^{o}C with an ice-bath. HATU (108 mg, 0.283 mmol), followed by DIPEA (45 µL, 0.258 mmol) was added and the resulting yellow solution stirred for 5 min. The peptide TFA salt was dissolved in dry DMF (1 mL) and DIPEA (90 µL, 0.516 mmol) and the resulting solution added at once to the activated ester. A further 2 equivalents of DIPEA (90 µL, 0.516 mmol) was added to change to pH to 8.0. The ice-bath was removed and the reaction stirred at ambient temperature for 24 h. The reaction mixture was then concentrated *in vacuo* and re-dissolved in $CHCl_3$ and IPA (9:1, 10 mL) and washed with 1 M HCl (5 mL) and saturated sodium bicarbonate (5 mL). Both aqueous washes were back-extracted with $CHCl_3$ (5 mL) and the combined organic extracts washed with brine (2 x 5 mL), dried over anhydrous sodium sulfate and concentrated *in vacuo*. The crude product with precipitated from Et_2O to yield the pentapeptidyl disaccharide **204** as off-white solid (316 mg, 78%), which was used directly in the next step without further purification. HRMS (ES) Calcd for $C_{67}H_{92}F_3N_8NaO_{30}P$ $[M+Na]^+$ 1599.5507, found 1599.5485.

Synthesis of *ZZ*-Farnesyl Gram-negative lipid II (180)

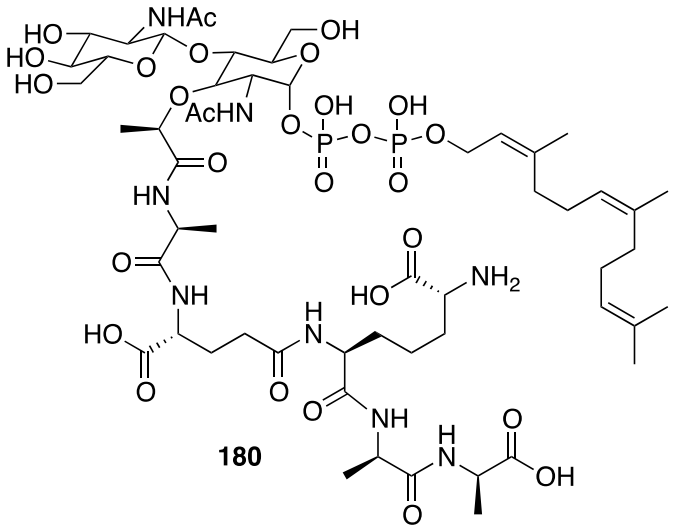

180

Dibenzyl phosphate **204** (79 mg, 50 μmol) was dissolved in anhydrous MeOH (10 mL) and the flask flushed with argon. Pd/C (10 % w/w, 167 mg, 157 μmol) was added and the resulting suspension stirred under a H_2 pressurized atmosphere for 2.5 h. The suspension was then filtered through celite (5 g), which was washed with MeOH (2 x 10 mL). Pyridine (2 mL) was added to the filtrate, which was then concentrated *in vacuo* and dried by high vacuum for 16 h to yield the sugar phosphate salt as a white solid. (*Z,Z*)-farnesyl phosphate (24 mg, 0.05 mmol) was suspended in dry DMF (1 mL) to form a cloudy suspension. Carbonyl diimidazole (41 mg, 0.25 mmol) was added and the resulting clear solution stirred for 2 h. Excess carbonyl diimidazole was destroyed by the addition of dry MeOH (8.1 μL, 0.20 mmol) and stirring continued for 45 min. Excess MeOH was removed by rotary evaporator and a solution of the sugar phosphate (0.05 mmol) in dry DMF (1 mL) was added to this solution. The resulting solution was stirred for 72 h under argon at ambient temperature and concentrated *in vacuo*. The crude diphosphate was dissolved in dioxane (1 mL) and a solution of sodium hydroxide (40

mg, 1 mmol) in water (1 mL) was added. The resulting solution was stirred at 37 ^{o}C for 2 h. The resulting mixture was centrifuged and purified by HPLC: column = GraceVydac Protein and Peptide C_{18} 100 mm column 10 micron; flow-rate = 10 mL/min, UV = 220 nm, method = 100 % 50 mM NH_4HCO_3(aq) to 100 % MeOH over 30 min. Product containing fractions (determined by ESI-MS) were frozen and lyophilized to yield *ZZ*-farnesyl Gram-negative lipid II (**180**) as a fluffy white power (17 mg, 25%).

5.6. NMR data for CYANA calculations

5.6.1. Oct-TriA_1 in DPC micelles

Residue	Chemical Shift (ppm)				
	Amide NH	**Hα**	**Hβ**	**Hγ**	**Other**
D-Val1	7.69	4.30	2.08	0.89	NA
D-Dab2	8.57	4.96	2.14, 1.97	2.91	NA
Gly3	8.47	4.06, 3.83	NA	NA	NA
D-Ser4	8.13	4.87	3.62	NA	NA
D-Trp5	8.50	4.75	3.14	NA	E1 = 10.52, D1 = 7.24, Z2 = 7.32, H2 = 7.02, Z3 = 6.95, E3 = 7.50,
Ser6	8.63	3.97	3.72, 3.50	NA	NA
Dab7	8.55	4.31	2.15, 1.96	3.00	NA
D-Dab8	7.86	4.50	2.03, 1.79	2.80	NA
Phe9	8.67	4.92	3.06, 2.91	NA	D1, D2, Z = 7.21, E1, E2 = 7.14
Glu10	8.43	4.54	1.92, 1.82	2.15	NA
Val11	8.24	4.55	1.87	0.91	NA
D-alle12	8.14	4.09	1.31	OBS	OBS
Ala13	7.90	4.13	1.29	NA	NA

NA = not applicable, OBS = obscured.

5.6.2. 180 in DPC micelles

Residue	Chemical Shift (ppm)				
	Amide NH	**Hα**	**Hβ**	**Hγ**	**Other**
GlcNAc	8.38	NA	NA	NA	H1 = 4.54 , H2 = 3.52, H3 = 3.70, H4 = 3.53, H5 = 3.38, H6 = 3.53, Ac = 2.01
MurNAc	8.19	NA	NA	NA	H1 = 5.45, H2 = 3.71, H3 = 3.98, H4 = 3.90, H5 = 3.53, H6 = 3.38, Ac = 2.01, OC*H* = 4.42, CH_3 = 1.38
Ala1	8.27	4.30	1.38	NA	NA
D-Glu2	7.94	4.09	2.32	2.06, 1.88	NA
DAP3	8.24	4.18	1.88, 1.79	1.43	Hδ = 1.73, Hε = 3.68
D-Ala4	8.28	4.29	1.32	NA	NA
D-Ala5	7.88	4.08	1.29	NA	NA
Farnesyl	NA	NA	NA	NA	C1-H = 4.41, C2-H = 5.43, C3-CH_3 = 1.73, C4-H = 2.11, C5-H = 2.07, C6-H = 5.16, C7-CH_3 = 1.66, C8-H = 2.02, C9-H = 2.02, C10-H = 5.11, C11-CH_3 = 1.64, 1.59

NA = not applicable.

5.6.3. Oct-TriA_1 in DPC micelles with 180

Residue					
	Amide NH	**Hα**	**Hβ**	**Hγ**	**Other**
D-Val1	7.71	4.29	2.10	0.90	NA
D-Dab2	8.59	4.92	2.15, 1.99	2.93	NA
Gly3	8.45	4.07, 3.84	NA	NA	NA
D-Ser4	8.15	4.85	3.64	NA	NA
D-Trp5	8.48	4.76	3.15	NA	E1 = 10.52, D1 = 7.25, Z2 = 7.41, H2 = 7.02, Z3 = 6.95, E3 = 7.50,
Ser6	8.62	3.99	3.74, 3.50	NA	NA
Dab7	8.55	4.32	2.15, 1.98	3.01	NA
D-Dab8	7.90	4.49	2.04, 1.80	2.82	NA
Phe9	8.64	4.89	3.08, 2.91	NA	D1, D2, Z = 7.21, E1, E2 = 7.14
Glu10	8.39	4.54	1.96, 1.83	2.17, 2.20	NA
Val11	8.23	4.55	1.96	0.91	NA
D-*a*lle12	8.15	4.12	1.31	OBS	OBS
Ala13	7.92	4.11	1.30	NA	NA

NA = not applicable, OBS = obscured.

5.6.4. 180 in DPC micelles with Oct-TriA_1

Residue	Chemical Shift (ppm)				
	Amide NH	**Hα**	**Hβ**	**Hγ**	**Other**
GlcNAc	8.38	NA	NA	NA	H1 = 4.54 , H2 = 3.54, H3 = 3.71, H4 = 3.53, H5 = 3.38, H6 = 3.53, Ac = 1.96
MurNAc	8.20	NA	NA	NA	H1 = 5.46, H2 = 3.72, H3 = 3.98, H4 = 3.90, H5 = 3.53, H6 = 3.38, Ac = 2.01, OC*H* = 4.42, CH_3 = 1.37
Ala1	8.26	4.31	1.39	NA	NA
D-Glu2	8.00	4.13	2.33	2.08, 1.89	NA
DAP3	8.24	4.18	1.88, 1.79	1.43	Hδ = 1.73, Hε = 3.70
D-Ala4	8.32	4.29	1.33	NA	NA
D-Ala5	7.94	4.11	1.31	NA	NA
Farnesyl	NA	NA	NA	NA	C1-H = 4.42, C2-H = 5.43, C3-CH_3 = 1.72, C4-H = 2.10, C5-H = 2.06, C6-H = 5.15, C7-CH_3 = 1.66, C8-H = 2.01, C9-H = 2.01, C10-H = 5.09, C11-CH_3 = 1.64, 1.58

NA = not applicable, OBS = obscured.

Chapter 6

References

(1) Lynch, D. B.; Jeffery, I. B.; Cusack, S.; O'Connor, E. M.; O'Toole, P. W. *Interdiscip Top Gerontol* **2015**, *40*, 141-154.

(2) Gilbert, J. A. *Genome Biol* **2015**, *16*, 97.

(3) Chaudet, M. M.; Allen, J. L.; Rose, D. R. *Protein Expr Purif* **2012**, *86*, 135-141.

(4) Sun, W.; Roland, K. L.; Curtiss, R. *J Infect Dev Ctries* **2011**, *5*, 614-627.

(5) Morens, D. M.; Taubenberger, J. K.; Fauci, A. S. *J Infect Dis* **2008**, *198*, 962-970.

(6) Fleming, A. *Bull World Health Organ* **2001**, *79*, 780-790.

(7) Butler, M. S.; Blaskovich, M. A.; Cooper, M. A. *J Antibiot* **2013**, *66*, 571-591.

(8) Park, K. S.; Ki, C. S.; Lee, N. Y. *Ann Lab Med* **2015**, *35*, 404-409.

(9) O'Shea, R.; Moser, H. E. *J Med Chem* **2008**, *51*, 2871-2878.

(10) Silver, L. L. *Expert Opin Drug Discov* **2008**, *3*, 487-500.

(11) Silver, L. L. *Clin Microbiol Rev* **2011**, *24*, 71-109.

(12) Typas, A.; Banzhaf, M.; Gross, C. A.; Vollmer, W. *Nat Rev Microbiol* **2012**, *10*, 123-136.

(13) Kong, K. F.; Schneper, L.; Mathee, K. *APMIS* **2010**, *118*, 1-36.

(14) Mandal, S. M.; Roy, A.; Mahata, D.; Migliolo, L.; Nolasco, D. O.; Franco, O. L. *J Antibiot* **2014**, *67*, 771-775.

(15) Stone, K. J.; Strominger, J. L. *Proc Natl Acad Sci U S A* **1971**, *68*, 3223-3227.

(16) Parenti, F.; Cavalleri, B. *J Antibiot* **1989**, *42*, 1882-1883.

(17) McIntyre, J. J.; Bull, A. T.; Bunch, A. W. *Biotechnol Bioeng* **1996**, *49*, 412-420.

(18) Perkins, H. R. *Biochem J* **1969**, *111*, 195-205.

(19) Lohans, C. T.; Vederas, J. C. *J Antibiot (Tokyo)* **2014**, *67*, 23-30.

(20) Hsu, S. T.; Breukink, E.; Tischenko, E.; Lutters, M. A.; de Kruijff, B.; Kaptein, R.; Bonvin, A. M.; van Nuland, N. A. *Nat Struct Mol Biol* **2004**, *11*, 963-967.

(21) Breukink, E.; Wiedemann, I.; van Kraaij, C.; Kuipers, O. P.; Sahl, H. G.; de Kruijff, B. *Science* **1999**, *286*, 2361-2364.

(22) Brötz, H.; Josten, M.; Wiedemann, I.; Schneider, U.; Götz, F.; Bierbaum, G.; Sahl, H. G. *Mol Microbiol* **1998**, *30*, 317-327.

(23) Kahan, F. M.; Kahan, J. S.; Cassidy, P. J.; Kropp, H. *Ann N Y Acad Sci* **1974**, *235*, 364-386.

(24) Eschenburg, S.; Priestman, M.; Schönbrunn, E. *J Biol Chem* **2005**, *280*, 3757-3763.

(25) Neuhaus, F. C.; Lynch, J. L. *Biochemistry* **1964**, *3*, 471-480.

(26) Berg, J. M.; Tymoczko, J. L.; Stryer, L. Biochemistry, 5th Edition, New York: W. H. Freeman; **2002**.

(27) Mukhtar, T. A.; Wright, G. D. *Chem Rev* **2005**, *105*, 529-542.

(28) Demirci, H.; Murphy IV, F.; Murphy, E.; Gregory, S. T.; Dahlberg, A. E.; Jogl, G. *Nat Commun* **2013**, *4*, 1355.

(29) Douthwaite, S. *Nucl Acids Res* **1992**, *20*, 4717-4720.

(30) Usary, J.; Champney, W. S. *Mol Microbiol* **2001**, *40*, 951-962.

(31) Ippolito, J. A.; Kanyo, Z. F.; Wang, D.; Franceschi, F. J.; Moore, P. B.; Steitz, T. A.; Duffy, E. M. *J Med Chem* **2008**, *51*, 3353-3356.

(32) Davidovich, C.; Bashan, A.; Auerbach-Nevo, T.; Yaggie, R. D.; Gontarek, R. R.; Yonath, A. *Proc Natl Acad Sci U S A* **2007**, *104*, 4291-4296.

(33) Pioletti, M.; Schlünzen, F.; Harms, J.; Zarivach, R.; Glühmann, M.; Avila, H.; Bashan, A.; Bartels, H.; Auerbach, T.; Jacobi, C. *EMBO J* **2001**, *20*, 1829-1839.

(34) Jonker, H. R. A.; Ilin, S.; Grimm, S. K.; Wöhnert, J.; Schwalbe, H. *Nucl Acids Res* **2007**, *35*, 441-454.

(35) Silvian, L. F.; Wang, J.; Steitz, T. A. *Science* **1999**, *285*, 1074-1077.

(36) Oblak, M.; Kotnik, M.; Solmajer, T. *Curr Med Chem* **2007**, *14*, 2033-2047.

(37) Mariani, R.; Maffioli, S. I. *Curr Med Chem* **2009**, *16*, 430-454.

(38) Lewis, R. J.; Singh, O. M.; Smith, C. V.; Skarzynski, T.; Maxwell, A.; Wonacott, A. J.; Wigley, D. B. *EMBO J* **1996**, *15*, 1412-1420.

(39) Campbell, E. A.; Korzheva, N.; Mustaev, A.; Murakami, K.; Nair, S.; Goldfarb, A.; Darst, S. A. *Cell* **2001**, *104*, 901-912.

(40) Bax, B. D.; Chan, P. F.; Eggleston, D. S.; Fosberry, A.; Gentry, D. R.; Gorrec, F.; Giordano, I.; Hann, M. M.; Hennessy, A.; Hibbs, M.; Huang, J.; Jones, E.; Jones, J.; Brown, K. K.; Lewis, C. J.; May, E. W.; Saunders, M. R.; Singh, O.; Spitzfaden, C. E.; Shen, C.; Shillings, A.; Theobald, A. J.; Wohlkonig, A.; Pearson, N. D.; Gwynn, M. N. *Nature* **2010**, *466*, 935-940.

(41) Artsimovitch, I.; Seddon, J.; Sears, P. *Clin Infect Dis* **2012**, *55 Suppl 2*, S127-31.

(42) Zhang, Y. M.; Rock, C. O. *J Lipid Res* **2009**, *50 Suppl*, S115-9.

(43) Coates, A. R.; Hu, Y. *Trends Pharmacol Sci* **2008**, *29*, 143-150.

(44) Wu, X.; Hurdle, J. G. *Antibiotics: Targets, Mechanisms and Resistance*, New York: John Wiley and Sons; **2014**.

(45) Kift, E. V.; Maartens, G.; Bamford, C. *S Afr Med J* **2014**, *104*, 183-186.

(46) Velkov, T.; Thompson, P. E.; Nation, R. L.; Li, J. *J Med Chem* **2010**, *53*, 1898-

1916.

(47) Straus, S. K.; Hancock, R. E. *Biochim Biophys Acta* **2006**, *1758*, 1215-1223.

(48) Lakshmanan, M.; Xavier, A. S. *J Young Pharm* **2013**, *5*, 112-115.

(49) Tago, Y.; Imai, M.; Ihara, M.; Atofuji, H.; Nagata, Y.; Yamamoto, K. *J Mol Biol* **2005**, *351*, 299-308.

(50) Blattner, F. R.; Plunkett, G.; Bloch, C. A.; Perna, N. T.; Burland, V.; Riley, M.; Collado-Vides, J.; Glasner, J. D.; Rode, C. K.; Mayhew, G. F.; Gregor, J.; Davis, N. W.; Kirkpatrick, H. A.; Goeden, M. A.; Rose, D. J.; Mau, B.; Shao, Y. *Science* **1997**, *277*, 1453-1462.

(51) Paphitou, N. I. *Int J Antimicrob Agents* **2013**, *42 Suppl*, S25-8.

(52) Azeredo da Silveira, S.; Perez, A. *Expert Rev Anti Infect Ther* **2015**, *13*, 531-533.

(53) Lewis, K. *Nat Rev Drug Discov* **2013**, *12*, 371-387.

(54) Kirby, W. M. *J Clin Invest* **1945**, *24*, 170-174.

(55) Bellamy, W. D.; Klimek, J. W. *J Bacteriol* **1948**, *55*, 153-160.

(56) Tzouvelekis, L. S.; Markogiannakis, A.; Psichogiou, M.; Tassios, P. T.; Daikos, G. L. *Clin Microbiol Rev* **2012**, *25*, 682-707.

(57) Gasink, L. B.; Edelstein, P. H.; Lautenbach, E.; Synnestvedt, M.; Fishman, N. O. *Infect Control Hosp Epidemiol* **2009**, *30*, 1180-1185.

(58) Cantón, R.; Akóva, M.; Carmeli, Y.; Giske, C. G.; Glupczynski, Y.; Gniadkowski, M.; Livermore, D. M.; Miriagou, V.; Naas, T.; Rossolini, G. M.; Samuelsen, Ø.; Seifert, H.; Woodford, N.; Nordmann, P.; European, N. O. C. *Clin Microbiol Infect* **2012**, *18*, 413-431.

(59) Vaara, M.; Fox, J.; Loidl, G.; Siikanen, O.; Apajalahti, J.; Hansen, F.; Frimodt-

Møller, N.; Nagai, J.; Takano, M.; Vaara, T. *Antimicrob Agents Chemother* **2008**, *52*, 3229-3236.

(60) Brown, A. G.; Butterworth, D.; Cole, M.; Hanscomb, G.; Hood, J. D.; Reading, C.; Rolinson, G. N. *J Antibiot* **1976**, *29*, 668-669.

(61) Brock, J.; Tallman, G. *Pipeline or pipe dream: New antibiotics for multidrug-resistant gram-negative bacilli*, *Infectious Disease News*, **December 2013**.

(62) Cain, B. D.; Norton, P. J.; Eubanks, W.; Nick, H. S.; Allen, C. M. *J Bacteriol* **1993**, *175*, 3784-3789.

(63) El Ghachi, M.; Bouhss, A.; Blanot, D.; Mengin-Lecreulx, D. *J Biol Chem* **2004**, *279*, 30106-30113.

(64) Cao, M.; Helmann, J. D. *J Bacteriol* **2002**, *184*, 6123-6129.

(65) Podlesek, Z.; Comino, A.; Herzog-Velikonja, B.; Zgur-Bertok, D.; Komel, R.; Grabnar, M. *Mol Microbiol* **1995**, *16*, 969-976.

(66) Bernard, R.; Guiseppi, A.; Chippaux, M.; Foglino, M.; Denizot, F. *J Bacteriol* **2007**, *189*, 8636-8642.

(67) Lis, M.; Kuramitsu, H. K. *Infect Immun* **2003**, *71*, 1938-1943.

(68) Manson, J. M.; Keis, S.; Smith, J. M.; Cook, G. M. *Antimicrob Agents Chemother* **2004**, *48*, 3743-3748.

(69) Fiedler, W.; Rotering, H. *J Biol Chem* **1988**, *263*, 14684-14689.

(70) Pollock, T. J.; Thorne, L.; Yamazaki, M.; Mikolajczak, M. J.; Armentrout, R. W. *J Bacteriol* **1994**, *176*, 6229-6237.

(71) Arias, C. A.; Murray, B. E. *Nat Rev Microbiol* **2012**, *10*, 266-278.

(72) Walsh, C. T. *Science* **1993**, *261*, 308-309.

(73) Meziane-Cherif, D.; Saul, F. A.; Haouz, A.; Courvalin, P. *J Biol Chem* **2012**, *287*, 37583-37592.

(74) Draper, L. A.; Cotter, P. D.; Hill, C.; Ross, R. P. *Microbiol Mol Biol Rev* **2015**, *79*, 171-191.

(75) Castañeda-García, A.; Blázquez, J.; Rodríguez-Rojas, A. *Antibiotics* **2013**, *2*, 217-236.

(76) Kadner, R. J.; Winkler, H. H. *J Bacteriol* **1973**, *113*, 895-900.

(77) Tsuruoka, T.; Yamada, Y. *J Antibiot* **1975**, *28*, 906-911.

(78) Kim, D. H.; Lees, W. J.; Kempsell, K. E.; Lane, W. S.; Duncan, K.; Walsh, C. T. *Biochemistry* **1996**, *35*, 4923-4928.

(79) Rigsby, R. E.; Fillgrove, K. L.; Beihoffer, L. A.; Armstrong, R. N. *Methods Enzymol* **2005**, *401*, 367-379.

(80) Russell, R. R. *J Bacteriol* **1972**, *111*, 622-624.

(81) Cáceres, N. E.; Harris, N. B.; Wellehan, J. F.; Feng, Z.; Kapur, V.; Barletta, R. G. *J Bacteriol* **1997**, *179*, 5046-5055.

(82) Feng, Z.; Barletta, R. G. *Antimicrob Agents Chemother* **2003**, *47*, 283-291.

(83) Springer, B.; Kidan, Y. G.; Prammananan, T.; Ellrott, K.; Böttger, E. C.; Sander, P. *Antimicrob Agents Chemother* **2001**, *45*, 2877-2884.

(84) Karlowsky, J. A.; Hoban, D. J.; Zelenitsky, S. A.; Zhanel, G. G. *J Antimicrob Chemother* **1997**, *40*, 371-376.

(85) Edgar, R.; Bibi, E. *J Bacteriol* **1997**, *179*, 2274-2280.

(86) Shaw, K. J.; Rather, P. N.; Hare, R. S.; Miller, G. H. *Microbiol Rev* **1993**, *57*, 138-163.

(87) Petinaki, E.; Guérin-Faublée, V.; Pichereau, V.; Villers, C.; Achard, A.; Malbruny, B.; Leclercq, R. *Antimicrob Agents Chemother* **2008**, *52*, 626-630.

(88) Bozdogan, B.; Berrezouga, L.; Kuo, M. S.; Yurek, D. A.; Farley, K. A.; Stockman, B. J.; Leclercq, R. *Antimicrob Agents Chemother* **1999**, *43*, 925-929.

(89) Brisson-Noël, A.; Courvalin, P. *Gene* **1986**, *43*, 247-253.

(90) Leclercq, R. *Clin Infect Dis* **2002**, *34*, 482-492.

(91) Weisblum, B. *Antimicrob Agents Chemother* **1995**, *39*, 577-585.

(92) Long, K. S.; Vester, B. *Antimicrob Agents Chemother* **2012**, *56*, 603-612.

(93) Böck, A.; Turnowsky, F.; Högenauer, G. *J Bacteriol* **1982**, *151*, 1253-1260.

(94) Pringle, M.; Poehlsgaard, J.; Vester, B.; Long, K. S. *Mol Microbiol* **2004**, *54*, 1295-1306.

(95) Speer, B. S.; Shoemaker, N. B.; Salyers, A. A. *Clin Microbiol Rev* **1992**, *5*, 387-399.

(96) Jones, C. S.; Osborne, D. J.; Stanley, J. *Mol Cell Probes* **1992**, *6*, 313-317.

(97) McMurry, L. M.; Levy, S. B. *Gram-positive pathogens. ASM Press, Washington, DC* **2000**, 660-677.

(98) Taylor, D. E.; Chau, A. *Antimicrob Agents Chemother* **1996**, *40*, 1-5.

(99) Speer, B. S.; Bedzyk, L.; Salyers, A. A. *J Bacteriol* **1991**, *173*, 176-183.

(100) Yang, W.; Moore, I. F.; Koteva, K. P.; Bareich, D. C.; Hughes, D. W.; Wright, G. D. *J Biol Chem* **2004**, *279*, 52346-52352.

(101) Kuiper, E. G.; Conn, G. L. *J Biol Chem* **2014**, *289*, 26189-26200.

(102) Cundliffe, E.; Thompson, J. *Nature* **1979**, *278*, 859-861.

(103) Thompson, J.; Schmidt, F.; Cundliffe, E. *J Biol Chem* **1982**, *257*, 7915-7917.

(104) Cameron, D. M.; Thompson, J.; Gregory, S. T.; March, P. E.; Dahlberg, A. E. *Nucl Acids Res* **2004**, *32*, 3220-3227.

(105) Seah, C.; Alexander, D. C.; Louie, L.; Simor, A.; Low, D. E.; Longtin, J.; Melano, R. G. *Antimicrob Agents Chemother* **2012**, *56*, 1916-1920.

(106) Vickers, A. A.; Chopra, I.; O'Neill, A. J. *Antimicrob Agents Chemother* **2007**, *51*, 4484-4485.

(107) Deguchi, T.; Fukuoka, A.; Yasuda, M.; Nakano, M.; Ozeki, S.; Kanematsu, E.; Nishino, Y.; Ishihara, S.; Ban, Y.; Kawada, Y. *Antimicrob Agents Chemother* **1997**, *41*, 699-701.

(108) Goldstein, B. P. *J Antibiot (Tokyo)* **2014**, *67*, 625-630.

(109) Stamm, L. V.; Bergen, H. L.; Shangraw, K. A. *Antimicrob Agents Chemother* **2001**, *45*, 2973-2974.

(110) Olaitan, A. O.; Morand, S.; Rolain, J. M. *Front Microbiol* **2014**, *5*, 643.

(111) Raetz, C. R.; Reynolds, C. M.; Trent, M. S.; Bishop, R. E. *Annu Rev Biochem* **2007**, *76*, 295-329.

(112) Padilla, E.; Llobet, E.; Doménech-Sánchez, A.; Martínez-Martínez, L.; Bengoechea, J. A.; Albertí, S. *Antimicrob Agents Chemother* **2010**, *54*, 177-183.

(113) Bayer, A. S.; Mishra, N. N.; Chen, L.; Kreiswirth, B. N.; Rubio, A.; Yang, S. J. *Antimicrob Agents Chemother* **2015**, *59*, 4930-4937.

(114) Bayer, A. S.; Schneider, T.; Sahl, H. G. *Ann N Y Acad Sci* **2013**, *1277*, 139-158.

(115) Kraljevic, S.; Stambrook, P. J.; Pavelic, K. *EMBO Rep* **2004**, *5*, 837-842.

(116) Pirri, G.; Giuliani, A.; Nicoletto, S. F.; Pizzuto, L.; Rinaldi, A. C. *Cent Eur J Biol* **2009**, *4*, 258-273.

(117) Cochrane, S. A.; Vederas, J. C. *Med Res Rev* **2014**, doi: 10.1002/med.21321.

(118) Finking, R.; Marahiel, M. A. *Annu Rev Microbiol* **2004**, *58*, 453-488.

(119) Murai, A.; Amino, Y.; Ando, T. *J Antibiot* **1985**, *38*, 1610-1613.

(120) Shoji, J.; Hinoo, H. *J Antibiot* **1975**, *28*, 60-63.

(121) Shoji, J.; Hinoo, H.; Wakisaka, Y.; Koizumi, K.; Mayama, M. *J Antibiot* **1975**, *28*, 56-59.

(122) Shoji, J.; Kato, T.; Matsumoto, K.; Takahashi, Y.; Mayama, M. *J Antibiot* **1976**, *29*, 1281-1285.

(123) Shoji, J.; Kato, T. *J Antibiot* **1975**, *28*, 764-769.

(124) Shoji, J.; Kato, T.; Sakazaki, R. *J Antibiot* **1976**, *29*, 1268-1274.

(125) Shoji, J.; Kato, T. *J Antibiot* **1976**, *29*, 1275-1280.

(126) Shoji, J.; Kato, T.; Terabe, S.; Konaka, R. *J Antibiot* **1979**, *32*, 313-319.

(127) Kato, T.; Hinoo, H.; Shoji, J. *J Antibiot* **1978**, *31*, 652-661.

(128) Kato, T.; Sakazaki, R.; Hinoo, H.; Shoji, J. *J Antibiot* **1979**, *32*, 305-312.

(129) Abriouel, H.; Franz, C. M.; Ben Omar, N.; Gálvez, A. *FEMS Microbiol Rev* **2011**, *35*, 201-232.

(130) Svetoch, E. A.; Stern, N. J.; Eruslanov, B. V.; Kovalev, Y. N.; Volodina, L. I.; Perelygin, V. V.; Mitsevich, E. V.; Mitsevich, I. P.; Pokhilenko, V. D.; Borzenkov, V. N.; Levchuk, V. P.; Svetoch, O. E.; Kudriavtseva, T. Y. *J Food Prot* **2005**, *68*, 11-17.

(131) Zhao, S.; Young, S. R.; Tong, E.; Abbott, J. W.; Womack, N.; Friedman, S. L.; McDermott, P. F. *Appl Environ Microbiol* **2010**, *76*, 7949-7956.

(132) van Belkum, M. J.; Lohans, C. T.; Vederas, J. C. *Genome Announc* **2015**, *3*,

(133) Lohans, C. T.; Huang, Z.; van Belkum, M. J.; Giroud, M.; Sit, C. S.; Steels, E. M.; Zheng, J.; Whittal, R. M.; McMullen, L. M.; Vederas, J. C. *J Am Chem Soc* **2012**, *134*, 19540-19543.

(134) Lohans, C. T.; van Belkum, M. J.; Cochrane, S. A.; Huang, Z.; Sit, C. S.; McMullen, L. M.; Vederas, J. C. *ChemBioChem* **2014**, *15*, 243-249.

(135) Cochrane, S. A.; Lohans, C. T.; van Belkum, M. J.; Bels, M. A.; Vederas, J. C. *Org Biomol Chem* **2015**, *13*, 6073-6081.

(136) Akasaka, K.; Tamogami, S.; Beeman, R. W.; Mori, K. *Tetrahedron* **2011**, *67*, 201-209.

(137) Hodge, M. B.; Olivo, H. F. *Tetrahedron* **2004**, *60*, 9397-9403.

(138) Gao, Z.; Wang, J.; Norquay, A. K.; Qiao, K.; Tang, Y.; Vederas, J. C. *J Am Chen Soc* **2013**, *135*, 1735-1738.

(139) de Mendoza, D.; Schujman, G.; Aguilar, P. *Bacillus subtilis and its closest relatives: from genes to cells. ASM Press, Washington, DC* **2002**, 43-55.

(140) Yang, Z.; Jin, X.; Guaciaro, M.; Molino, B. F. *J Org Chem* **2012**, *77*, 3191-3196.

(141) Akasaka, K.; Ohrui, H. *Biosci Biotechnol Biochem* **1999**, *63*, 1209-1215.

(142) Mizuno, K.; Adachi, E.; Imamura, Y.; Katsumata, O.; Hayashi, T. *Micron* **2001**, *32*, 317-323.

(143) Oka, M.; Nishiyama, Y.; Ohta, S.; Kamei, H.; Konishi, M.; Miyaki, T.; Oki, T.; Kawaguchi, H. *J Antibiot* **1988**, *41*, 1331-1337.

(144) Oka, M.; Yaginuma, K.; Numata, K.; Konishi, M.; Oki, T.; Kawaguchi, H. *J Antibiot* **1988**, *41*, 1338-1350.

(145) Terui, Y.; Nishikawa, J.; Hinoo, H.; Kato, T.; Shoji, J. *J Antibiot* **1990**, *43*, 788-

795.

(146) Shoji, J.; Hinoo, H.; Kato, T.; Hattori, T.; Hirooka, K.; Tawara, K.; Shiratori, O.; Terui, Y. *J Antibiot* **1990**, *43*, 783-787.

(147) Marin, J.; Didierjean, C.; Aubry, A.; Casimir, J. R.; Briand, J. P.; Guichard, G. *J Org Chem* **2004**, *69*, 130-141.

(148) Zhang, Z.; Tan, M.; Xie, Z.; Dai, L.; Chen, Y.; Zhao, Y. *Nat Chem Biol* **2011**, *7*, 58-63.

(149) Bowers, A. A.; Acker, M. G.; Young, T. S.; Walsh, C. T. *J Am Chem Soc* **2012**, *134*, 10313-10316.

(150) Guillerm, D.; Lavrador, K.; Guillerm, G. *Synth Commun* **1995**, *25*, 877-882.

(151) Chenault, H. K.; Dahmer, J.; Whitesides, G. M. *J Am Chem Soc* **1989**, *111*, 6354-6364.

(152) Pattarozzi, M.; Zonta, C.; Broxterman, Q. B.; Kaptein, B.; De Zorzi, R.; Randaccio, L.; Scrimin, P.; Licini, G. *Org Lett* **2007**, *9*, 2365-2368.

(153) Zheng, J.; Yu, Y.; Shen, Y. *Synt Commun* **1990**, *20*, 3277-3282.

(154) Liu, W.; Chan, A. S.; Liu, H.; Cochrane, S. A.; Vederas, J. C. *J Am Chem Soc* **2011**, *133*, 14216-14219.

(155) Fisher, K.; Phillips, C. *Microbiol* **2009**, *155*, 1749-1757.

(156) Ryan, K. J.; Ray, C. G. *Sherris medical microbiology: an introduction to infectious diseases*. 4th Edition, New York: McGraw-Hill Medical, **2004**.

(157) Liu, G. Y. *Pediatr Res* **2009**, *65*, 71R-77R.

(158) Scallan, E.; Hoekstra, R. M.; Angulo, F. J.; Tauxe, R. V.; Widdowson, M. A.; Roy, S. L.; Jones, J. L.; Griffin, P. M. *Emerg Infect Dis* **2011**, *17*, 7-15.

(159) Karch, H.; Tarr, P. I.; Bielaszewska, M. *Int J Med Microbiol* **2005**, *295*, 405-418.

(160) Poole, K. *Clin Microbiol Infect* **2004**, *10*, 12-26.

(161) Cochrane, S. A.; Lohans, C. T.; Brandelli, J. R.; Mulvey, G.; Armstrong, G. D.; Vederas, J. C. *J Med Chem* **2014**, *57*, 1127-1131.

(162) Pattabiraman, V. R.; McKinnie, S. M.; Vederas, J. C. *Angew Chem Int Ed* **2008**, *47*, 9472-9475.

(163) Veronese, F. M.; Mero, A. *BioDrugs* **2008**, *22*, 315-329.

(164) Gasteiger, E.; Hoogland, C.; Gattiker, A.; Wilkins, M. R.; Appel, R. D.; Bairoch, A. *Protein identification and analysis tools on the ExPASy server*; Springer: 2005;

(165) Vaara, M.; Vaara, T. *Nature* **1983**, *303*, 526-528.

(166) Viljanen, P.; Vaara, M. *Antimicrob Agents Chemother* **1984**, *25*, 701-705.

(167) Vaara, M.; Siikanen, O.; Apajalahti, J.; Fox, J.; Frimodt-Møller, N.; He, H.; Poudyal, A.; Li, J.; Nation, R. L.; Vaara, T. *Antimicrob Agents Chemother* **2010**, *54*, 3341-3346.

(168) Cochrane, S. A.; Vederas, J. C. *Int J Antimicrob Agents* **2014**, *44*, 493-499.

(169) Meunier, B. *Acc Chem Res* **2008**, *41*, 69-77.

(170) Long, D. D.; Marquess, D. G. *Future Med Chem* **2009**, *1*, 1037-1050.

(171) Yoganathan, S.; Sit, C. S.; Vederas, J. C. *Org Biomol Chem* **2011**, *9*, 2133-2141.

(172) Ji, C.; Miller, P. A.; Miller, M. J. *J Am Chem Soc* **2012**, *134*, 9898-9901.

(173) Meng, J.; Da, F.; Ma, X.; Wang, N.; Wang, Y.; Zhang, H.; Li, M.; Zhou, Y.; Xue, X.; Hou, Z.; Jia, M.; Luo, X. *Antimicrob Agents Chemother* **2015**, *59*, 914-922.

(174) Schmidt, N. W.; Deshayes, S.; Hawker, S.; Blacker, A.; Kasko, A. M.; Wong, G. C. *ACS Nano* **2014**, *8*, 8786-8793.

(175) Sharma, R.; Singla, N.; Mehta, S.; Gaba, T.; Rawal, R. K.; Rao, H. S.; Bhardwaj, T. R. *Mini Rev Med Chem* **2015**, *15*, 751-761.

(176) Arnusch, C. J.; Bonvin, A. M.; Verel, A. M.; Jansen, W. T.; Liskamp, R. M.; de Kruijff, B.; Pieters, R. J.; Breukink, E. *Biochemistry* **2008**, *47*, 12661-12663.

(177) Sundram, U. N.; Griffin, J. H. *J Org Chem* **1995**, *60*, 1102-1103.

(178) Bonev, B. B.; Breukink, E.; Swiezewska, E.; De Kruijff, B.; Watts, A. *FASEB J* **2004**, *18*, 1862-1869.

(179) Slootweg, J. C.; van der Wal, S.; Quarles van Ufford, H. C.; Breukink, E.; Liskamp, R. M.; Rijkers, D. T. *Bioconjug Chem* **2013**, *24*, 2058-2066.

(180) Kawashima, Y.; Yamada, Y.; Asaka, T.; Misawa, Y.; Kashimura, M.; Morimoto, S.; Ono, T.; Nagate, T.; Hatayama, K.; Hirono, S. *Chem Pharm Bull* **1994**, *42*, 1088-1095.

(181) Lee, Y.; Choi, J. Y.; Fu, H.; Harvey, C.; Ravindran, S.; Roush, W. R.; Boothroyd, J. C.; Khosla, C. *J Med Chem* **2011**, *54*, 2792-2804.

(182) Pyta, K.; Przybylski, P.; Klich, K.; Stefańska, J. *Org Biomol Chem* **2012**, *10*, 8283-8297.

(183) Gogoi, K.; Mane, M. V.; Kunte, S. S.; Kumar, V. A. *Nucleic Acids Res* **2007**, *35*, e139.

(184) Cochrane, S. A.; Findlay, B.; Vederas, J. C.; Ratemi, E. S. *ChemBioChem* **2014**, *15*, 1295-1299.

(185) Schneider, T.; Kruse, T.; Wimmer, R.; Wiedemann, I.; Sass, V.; Pag, U.; Jansen, A.; Nielsen, A. K.; Mygind, P. H.; Raventós, D. S.; Neve, S.; Ravn, B.; Bonvin, A. M.; De Maria, L.; Andersen, A. S.; Gammelgaard, L. K.; Sahl, H. G.; Kristensen,

H. H. *Science* **2010**, *328*, 1168-1172.

(186) Lin, G.; Ednie, L. M.; Appelbaum, P. C. *Antimicrobial Agents Chemother* **2010**, *54*, 2258-2261.

(187) Thennarasu, S.; Lee, D. K.; Tan, A.; Prasad Kari, U.; Ramamoorthy, A. *Biochim Biophys Acta* **2005**, *1711*, 49-58.

(188) Li, T.; Jiang, L.; Chen, H.; Zhang, X. *J Mol Neurosci* **2008**, *35*, 289-295.

(189) Langsrud, S.; Sundheim, G. *J Appl Bacteriol* **1996**, *81*, 411-418.

(190) Pate, M.; Blazyk, J. *Methods Mol Med* **2008**, *142*, 155-173.

(191) Mazurkiewicz, P.; Driessen, A. J.; Konings, W. N. *Curr Issues Mol Biol* **2005**, *7*, 7-21.

(192) Ahmed, S.; Booth, I. R. *Biochem J* **1983**, *212*, 105-112.

(193) Noll, K. S.; Sinko, P. J.; Chikindas, M. L. *Probiotics Antimicrob Proteins* **2011**, *3*, 41-47.

(194) Molenaar, D.; Abee, T.; Konings, W. N. *Biochim Biophys Acta* **1991**, *1115*, 75-83.

(195) Vaara, M. *Microbiol Rev* **1992**, *56*, 395-411.

(196) Greenfield, N. J. *Nat Protoc* **2006**, *1*, 2876-2890.

(197) Wiedemann, I.; Breukink, E.; van Kraaij, C.; Kuipers, O. P.; Bierbaum, G.; de Kruijff, B.; Sahl, H. G. *J Biol Chem* **2001**, *276*, 1772-1779.

(198) Saha, S. L.; Van Nieuwenhze, M. S.; Hornback, W. J.; Aikins, J. A.; Blaszczak, L. C. *Org Lett* **2001**, *3*, 3575-3577.

(199) VanNieuwenhze, M. S.; Mauldin, S. C.; Zia-Ebrahimi, M.; Winger, B. E.; Hornback, W. J.; Saha, S. L.; Aikins, J. A.; Blaszczak, L. C. *J Am Chem Soc* **2002**, *124*, 3656-3660.

(200) Lebar, M. D.; Lupoli, T. J.; Tsukamoto, H.; May, J. M.; Walker, S.; Kahne, D. *J Am Chem Soc* **2013**, *135*, 4632-4635.

(201) Güntert, P. *Methods Mol Biol* **2004**, *278*, 353-378.

(202) Trott, O.; Olson, A. J. *J Comput Chem* **2010**, *31*, 455-461.

(203) Wiegand, I.; Hilpert, K.; Hancock, R. E. *Nat Protoc* **2008**, *3*, 163-175.

(204) Tang, W.; van der Donk, W. A. *Nat Chem Biol* **2013**, *9*, 157-159.

(205) Waseh, S.; Hanifi-Moghaddam, P.; Coleman, R.; Masotti, M.; Ryan, S.; Foss, M.; MacKenzie, R.; Henry, M.; Szymanski, C. M.; Tanha, J. *PLoS One* **2010**, *5*, e13904.

(206) Delaglio, F.; Grzesiek, S.; Vuister, G. W.; Zhu, G.; Pfeifer, J.; Bax, A. *J Biomol NMR* **1995**, *6*, 277-293.

(207) Johnson, B. A. *Methods Mol Biol* **2004**, *278*, 313-352.

(208) Seeliger, D.; de Groot, B. L. *J Comput Aided Mol Des* **2010**, *24*, 417-422.

(209) Mori, K.; Harashima, S. *Liebigs Annalen der Chemie* **1993**, *1993*, 391-401.

(210) Krasovskiy, A.; Knochel, P. *Synthesis* **2006**, 890-891.

(211) Cochrane, S. A.; Surgenor, Surgenor, R. R.; Khey, K. M. W.; Vederas, J. C. *Org Lett* **2015**, *17*, 5428-5431.

(212) Cochrane, S. A.; Huang, Z.; Vederas, J. C. *Org Biomol Chem* **2013**, *11*, 630-639.

(213) Kwon, M.; Cochrane, S. A.; Vederas, J. C.; Ro, D. K. *FEBS Lett* **2014**, *588*, 4597-4603.

(214) Cochrane, S. A.; Li, X.; He, S.; Yu, M.; Wu, M.; Vederas, J. C. *J Med Chem* **2015**, DOI: 10.1021/acs.jmedchem.5b01578.

Appendix

Investigation of the ring-closing metathesis of peptides in water

This work has been reproduced from the original article in Organic and Biomolecular Chemistry with permission from the Royal Society of Chemistry.[A1]

A.1. Project background

Disulfide bonds are common in naturally occurring peptides and often play an important role in their correct folding, stability and biological activity.[A2-A6] Two examples are the mammalian hormone oxytocin (**A1**), which controls mammary and uterine smooth muscle contraction,[A7-A8] and the orally active analgesic crotalphine (**A2**), isolated from the venom of the South American rattlesnake *Crotalus durissus terrificus* (Fig. A.1).[A9-A11]

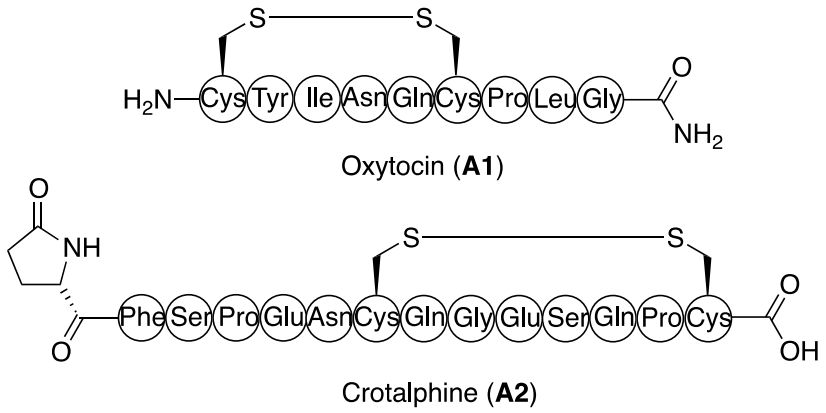

Figure A.1. Structure of oxytocin (**A1**) and crotalphine (**A2**).

As disulfide bonds are susceptible to reduction to free thiols, which can result in scrambling of bridges and loss of activity, there is considerable interest in replacement of these moieties in peptides with more stable linkages.[A12-18] Ring-closing metathesis (RCM) in peptides allows for the replacement of disulfide bridges with a dicarba bridge.[A19-A28] The resulting stapled peptides are more stable than the natural analogues and many examples have been shown to retain their biological activity.[A22-A28] Solution-phase RCM of peptides has been mostly limited to hydrophobic peptides in organic solvents.[A29-A30] The RCM of resin bound peptides is an alternative to the solution phase process, but aggregation of the peptide chain with the resin or peptide complexation to the catalyst can hinder the reaction.[A31-A34] The RCM of unprotected peptides in an aqueous environment is an attractive strategy.[A35] Peptides generally have high solubility in water, and performing these reactions in aqueous media could allow cyclizations to be performed that are not possible on-resin. A major drawback with this approach is the insolubility of commercially available ruthenium-based metathesis catalysts and the competing catalyst decomposition pathways in water.[A36-A37] It is possible to chemically modify ruthenium catalysts to solubilize them in water, however this requires a series of chemical steps to make appropriate ligands.[A38-A40]

Lipshutz and co-workers have reported the use of aqueous micelles as media to achieve cross-metathesis (CM) and RCM on small organic molecules.[A41-42] Several common detergents including sodium dodecyl sulfate (SDS) and Triton X-100 were used at critical micelle concentrations to perform CM reactions using 2% Grubbs 2nd generation catalyst in moderate yields.[A41] Davis and co-workers have also reported a novel system for aqueous CM.[A44-A45] A mutant of the serine protease subtilisin *Bacillus*

lentus containing *S*-allyl cysteine (Sac) at position 156 successfully underwent CM in high yields with a number of substrates using 200 equivalents Hoveyda-Grubbs 2nd generation catalyst (HGII) and 10000 equivalents $MgCl_2$ in water with 30 % t-BuOH as a co-solvent. The authors found that Mg^{2+} is required for success of this reaction, presumably to disrupt non-productive chelation between the catalyst and protein. They proposed that the sulfur atom in the allyl sulfide coordinates to the ruthenium centre of the catalyst and brings the reactive alkene moieties of the protein and substrate into close proximity, thereby enhancing the rate of reaction and competing with non-productive chelation to the protein. This method was also used by Schultz and co-workers to perform RCM on a large protein bearing adjacent genetically encoded *O*-crotylserine residues.[A46]

The micellar systems can potentially protect the insoluble catalyst from decomposition by water by sequestration inside the micelle (Fig. A.2). The alkene chains could then enter the lipophilic environment for RCM. Given that oxytocin (**A1**) is positively charged and crotalphine (**A2**) is negatively charged at neutral pH, polar head groups on the micelle could affect the RCM of these peptides. Three commercially available detergents were therefore selected for study at their critical micelle concentrations; (1) anionic SDS, (2) neutral Triton X-100 and (3) cationic cetyl trimethylammonium bromide (CTAB). In addition, 30 % t-BuOH was used in a non-micellar solvent system. The Hoveyda-Grubbs 2nd generation catalyst was chosen for these reactions as it displays superior air and moisture stability compared to other commercially available catalysts.

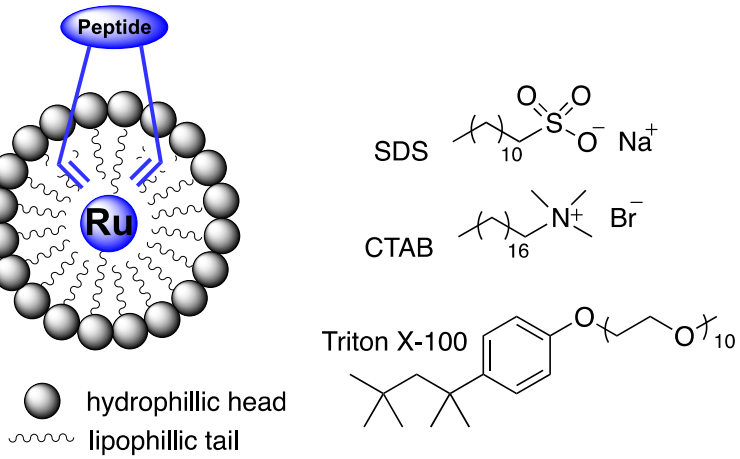

Figure A.2. Use of micelles for aqueous ring closing metathesis.

All peptides were synthesized using standard Fmoc solid-phase peptide synthesis (SPPS). Several variants were selected to test the influence of chain length and of heteroatoms in the alkene-bearing side chain (Fig. A.3). The replacement of cysteines in oxytocin and crotalphine with allylglycine (Agl) affords analogues that have sulfur replaced directly with a methylene unit upon cyclization. *S*-Allylcysteine (Sac) and *O*-allylserine (Oas) containing peptides allow catalyst coordination effects to be probed. Pentenylglycine (Pgl) incorporation can probe the effect of chain length.

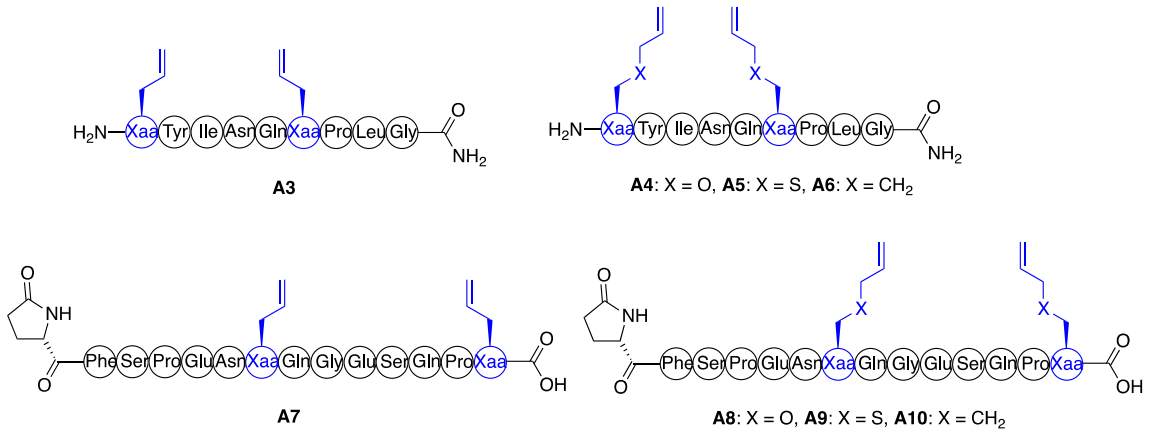

Figure A.3. Proposed oxytocin and crotalphine analogues to study aqueous ring-closing metathesis.

A.2. Results and Discussion

A.2.1. Synthesis of alkene containing amino acids

The syntheses of alkene bearing amino acids Fmoc-Pgl-OH (**A11**), Fmoc-Oas-OH (**A12**) and Fmoc-Sac-OH (**A13**) are shown in Scheme A.1. The asymmetric synthesis of Fmoc-Pgl-OH was accomplished using the chiral Ni(II) Schiff-base method reported by Belokon *et al*.[A46] Benzylation of (*S*)-proline (**A14**) followed by halogen substitution of the *in situ* generated acyl chloride **A15** with 2-aminobenzophenone (**A16**) yields the ligand (*S*)-BPB (**A17**) in 54% yield over 2 steps. Complexation between (*S*)-BPB, glycine and $Ni(NO_3)_2$ under basic conditions yields the Ni(II) Schiff-base (*S*)-Gly-Ni-BPB (**A18**) in moderate yield. A diastereoselective alkylation reaction between 5-bromo-1-pentene and **A18**, followed by acidic hydrolysis liberates amino acid **A20**. Subsequent protection of the free amine as an Fmoc-carbamate gives Fmoc-Pgl-OH (**A11**) in good yield. Fmoc-Oas-OH (**A12**) is synthesized from commercially available Boc-Ser-OH (**A21**) in 3 steps. Selective allylation of the hydroxyl unit, followed by acidic

Boc cleavage and re-protection as an Fmoc-carbamate yields Fmoc-Oas-OH (**A12**) in 73% overall yield. Commercially available H-Sac-OH (**A23**) is protected as an Fmoc-carbamate to give Fmoc-Sac-OH (**A13**).

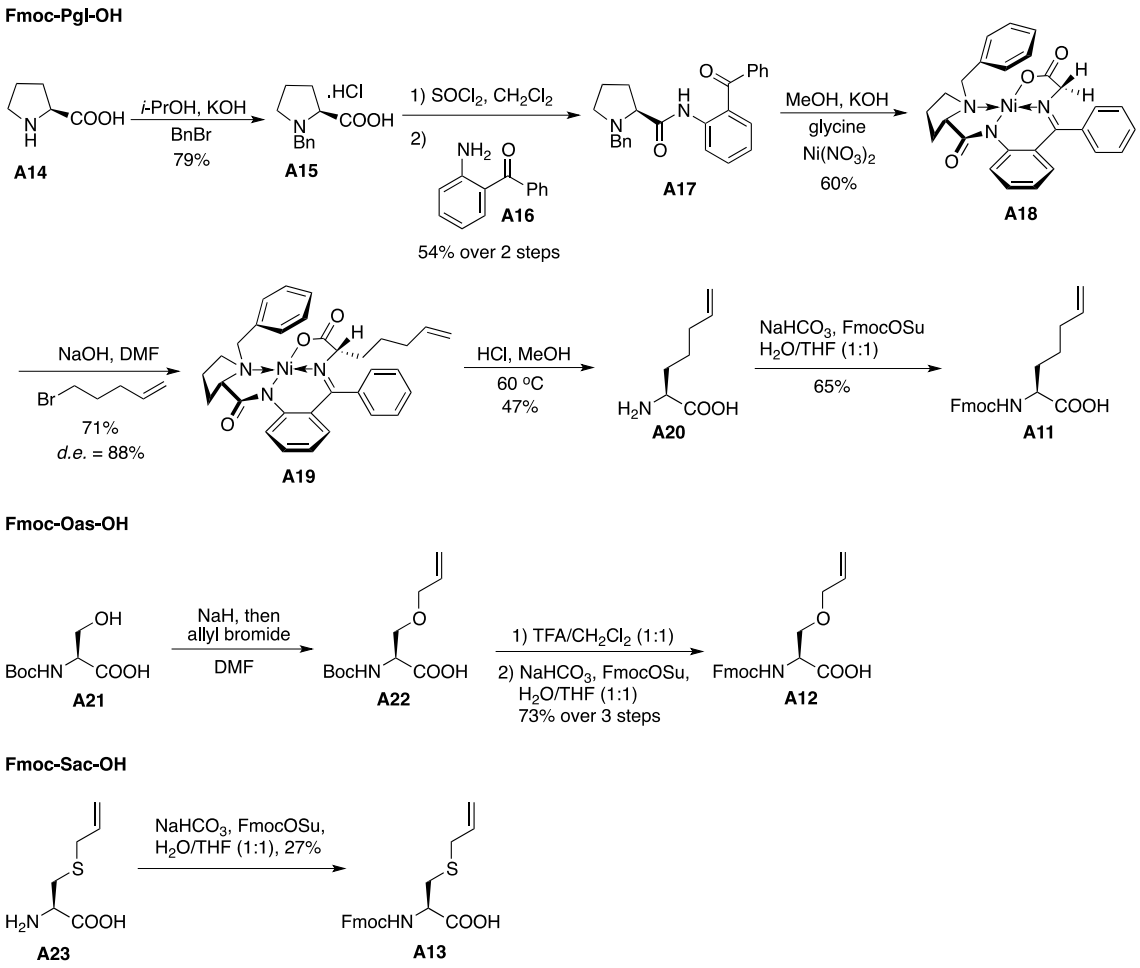

A.2.2. On-resin ring closing metathesis of peptides

The RCM of oxytocin and crotalphine analogues were first performed on-resin for comparison with the latter aqueous reactions. The resin bound Fmoc-protected peptides are refluxed in CH_2Cl_2 with 20 mol% HGII for 24 h, followed by the addition of DMSO (50 equiv relative to the catalyst loading) and stirred for a further 12 h at ambient

temperature. Deprotection of the Fmoc-carbamate, acidic cleavage from resin and HPLC purification are then performed. The RCM of resin bound Agl oxytocin analogue **A3** proceeds in 50% yield. The resulting 1:1 mixture of *cis*- and *trans*-isomers is separable by HPLC. The resin bound oxytocin analogues **A3** – **A6** undergo complete conversion to the desired cyclic products as an inseparable mixture of *cis/trans* isomers. Attempts to cyclize the crotalphine analogues on-resin were unsuccessful, presumably due to complexation between the catalyst and amide backbone and/or hydrophobic protecting groups of the peptides.

A.2.3. Aqueous ring-closing metathesis of peptides

Our efforts were then directed towards the RCM of fully unprotected oxytocin and crotalphine analogues in water. RCM reactions failed to proceed for any analogues when CTAB or Triton X-100 were used as additives. MALDI analysis showed some product formation in the 8.2 mM SDS system for the Pgl, Oas and Sac analogues, however product was not successfully isolated from this system. We therefore directed our attention to the use of 30 % t-BuOH as a co-solvent.

We first focused on the RCM of the Agl analogues **A3** and **A7** as the resulting olefin bridge is an isostere of a disulfide-bond. Initial attempts to perform RCM on these analogues using stoichiometric amounts of HGII at 37 °C were unsuccessful. Performing the reaction at higher temperatures (up to 80 °C) had no effect on the reaction. The loading of HGII was then increased to 50 equiv but MALDI analysis after 24 h revealed only the formation of ruthenium-peptide adducts. Davis and co-workers observed a similar problem in their cross-metathesis reactions on proteins, which was

circumvented by adding a large excess of $MgCl_2$ (10000 equiv) to disrupt non-productive chelation. Even with the addition of 10000 equiv $MgCl_2$, no reaction occurred in our case.

To determine if the failure of Agl analogues to cyclize in aqueous media is due to side chain length, the Pgl analogues **A6** and **A10** were examined. Cyclic products were detected by MALDI when the reactions were performed in the t-BuOH system using 50 equiv HGII, however the isolated yields are typically less than 1%. Lower loadings of HGII gave no product and higher loadings did not increase the yield. The major products are ruthenium-peptide adducts and addition of excess MgCl2 has little effect on disrupting the non-productive chelation. Trace amounts of a side-product 14 Da higher in mass than the RCM product are formed. Comparison of the LC MS/MS spectra of the isolated +14 Da side-product with synthetic standard **A24** showed that a piperidine ring had been formed at the *N*-terminus, possibly by a hydroamination reaction between the *N*-terminal amine and a ruthenium carbene on residue 1 (Fig. 4).

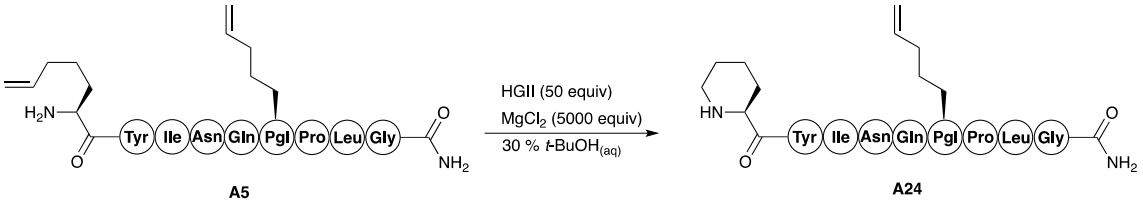

Figure 4. Side-product from aqueous RCM of **A5**.

The role of a heteroatom within the alkene side-chain was then studied by examining the Oas and Sac analogues. The Oas analogues **A4** and **A8** displayed similar reactivity to the Pgl analogues. A +14 Da side product was also detected in the

RCM of oxytocin analogue **A4**, presumably analogous to the Pgl oxytocin side-product **A24**. The peptide analogues containing *S*-allylcysteine underwent remarkably faster and cleaner reactions than all the other analogues (Scheme A.2). The crotalphine analogue **A9** undergoes RCM with 50 mol% HGII in 63% isolated yield. It is important to note that this reaction failed on-resin. Initial attempts to cyclize oxytocin analogue **A5** failed because it decomposed rapidly upon exposure to HGII. Protection of the *N*-terminus as an Fmoc-carbamate (**A25**) allows Sac oxytocin to undergo complete conversion (78% isolated yield) to the desired cyclic product in 3 h using 50 mol% HGII. The enhanced reactivity of *S*-allyl containing peptides is in full agreement with the results of Davis and co-workers. The ability to perform these cyclizations using sub-stoichiometric amounts of HGII allows the cost-effective synthesis of valuable biologically relevant peptide analogues in milligram quantities.

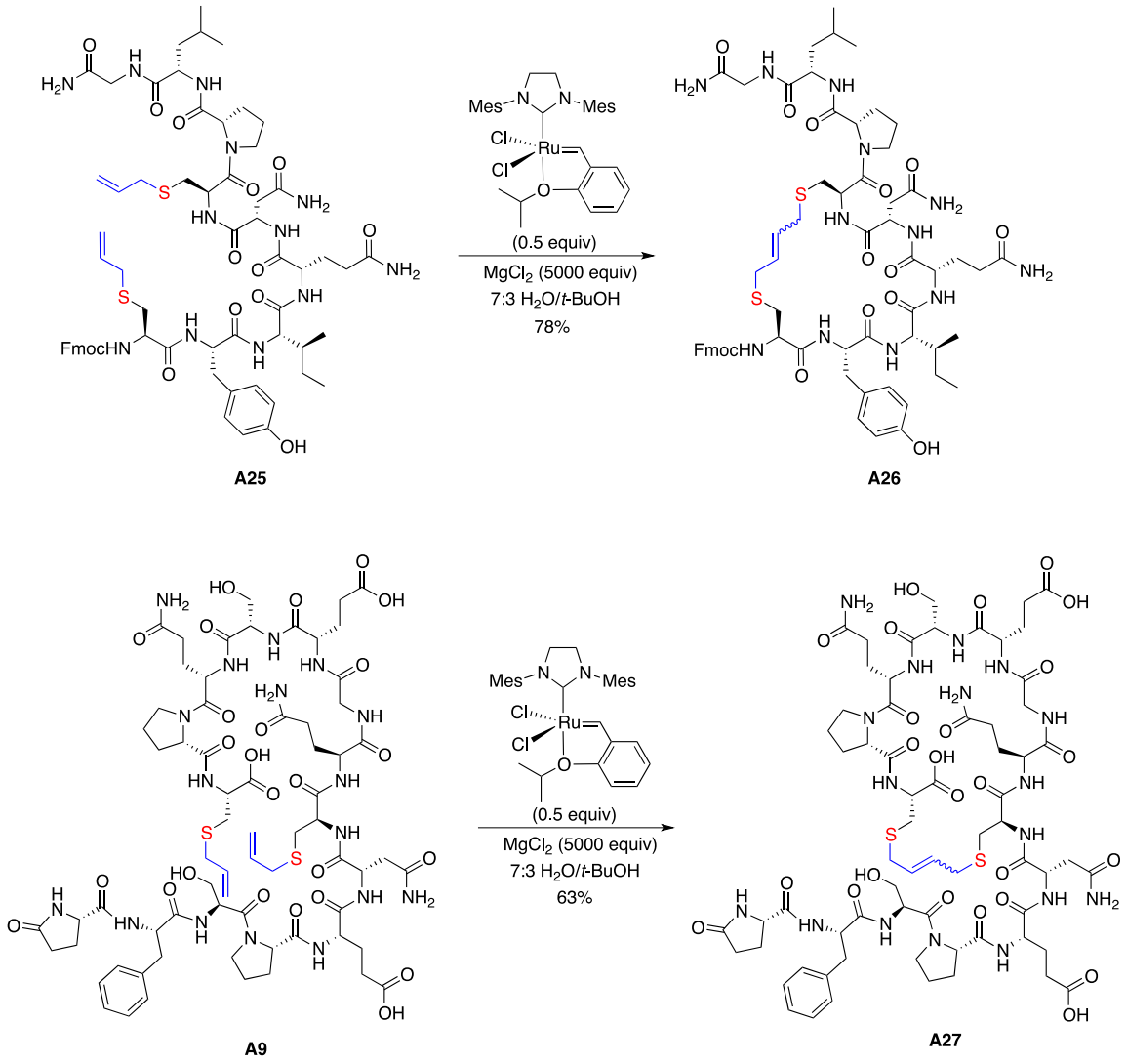

Scheme A.2. RCM of Sac containing peptides in t-BuOH system.

A.2.4. Alternative allyl sulfide containing amino acid investigation

The enhanced reactivity of the sulfur containing analogues led us to synthesize linear peptides **A28** and **A29** (Scheme A.3). The alkene amino acid, Fmoc-SAgl-OH (**A30**) is synthesized from commercially available Fmoc-Agl-OH (**A31**) in 3 steps. Protection of **A31** as methyl ester **A32**, followed by a cross-metathesis reaction with allyl methyl sulfide yields alkene **A33** in good yields. Subsequent ester hydrolysis using

Pascal's conditions[A47] gives Fmoc-SAgl-OH (**A30**). This unnatural amino acid is analogous to *S*-allyl cysteine with the positions of the sulfur and alkene switched. Performing RCM on these analogues would yield the same cyclic products as the RCM of **A3** and **A7**. We hoped the sacrificial allyl sulfide would facilitate aqueous RCM through coordination between the ruthenium in the catalyst and sulfur on the side chain. Attempts to perform the RCM of resin bound **A28** and **A29** failed with only the linear starting materials recovered. The aqueous reactions were also unsuccessful. Analysis of the MALDI spectra after 24 h revealed only ruthenium-peptide adducts, suggesting that the chain length of the alkene side chain is also an important factor in aqueous RCM. This is highlighted by comparison of the reactivity of the Agl, Pgl and Oas analogues. Agl analogues **A3** and **A7** also formed ruthenium-peptide adducts but failed to cyclize, whereas both the Pgl and Oas analogues underwent RCM, albeit in low yields, in the t-BuOH system.

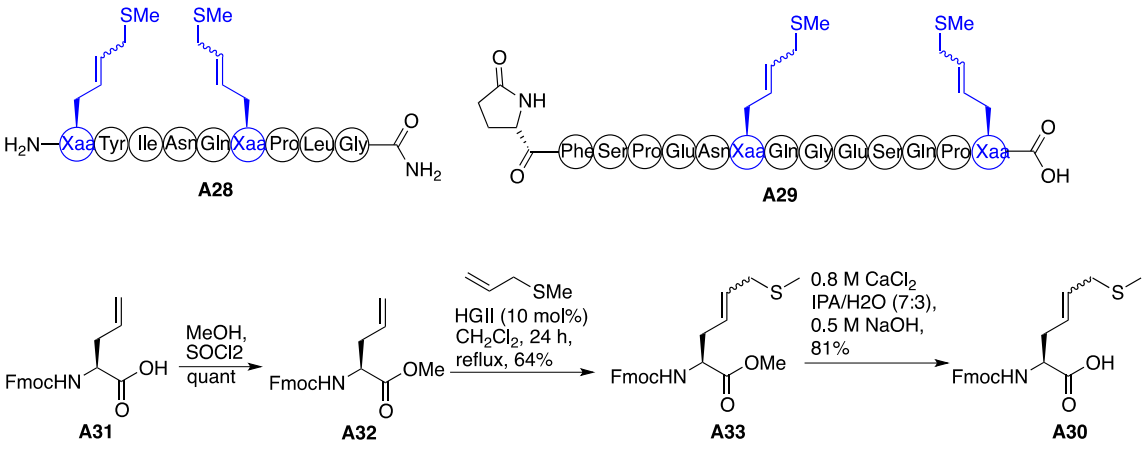

Scheme A.3. Sacrificial sulfide peptides and amino acid **A30** synthesis.

A.3. Conclusions

The RCM of oxytocin analogues containing allylglycine, pentenylglycine, O-allylserine or S-allylcysteine can be achieved in good to excellent yields on-resin. None of the crotalphine analogues could be cyclized by this method. *S*-allylcysteine analogues of oxytocin and crotalphine also undergo efficient RCM in water containing excess $MgCl_2$ and 30 % t-BuOH as a co-solvent. The addition of $MgCl_2$ is vital to disrupt non-productive chelation between the resulting ruthenium-carbene and other coordinating heteroatoms on the peptide. The sulfur atom within S-allylcysteine drastically improved the efficiency of RCM compared to pentenylglycine and *O*-allylserine analogues. This methodology provides an alternative to the on-resin cyclization of *S*-allylcysteine, which is particularly attractive in instances where on-resin cyclization is not possible.

A.4. Experimental procedures

A.4.1. General synthetic information

Peptide synthesis

All peptides were synthesized on a CEM Liberty 1 Microwave Peptide Synthesizer. Solid phase synthesis was carried out on a 0.1 mmol scale using Fmoc chemistry on Rink Amide NovaGel^{TM} resin (0.63 mmol/g loading) for oxytocin analogues, 2-chlorotrityl resin (0.80 mmol/g loading) for 7,14-Sac-crotalphine and 7,14-X-crotalphine, and Wang resin (0.65 mmol/g loading) for the remaining crotalphine analogues. Commercially available asymmetrically protected amino acids and synthesized amino acids were loaded on the peptide synthesizer as 0.2 M DMF solutions. All amino acid subunits were

coupled using O-benzotriazole-N,N,N',N'-tetramethyl-uronium-hexafluoro-phosphate (HBTU) as the activating agent and heated at 70 ^{o}C (50 ^{o}C for cysteines) for a 5 min coupling time. Fmoc residues were deprotected using a 20 % solution of piperidine in DMF and the dibenzofulvene adduct absorption monitored at 301 nm using a UV monitor.

General procedure for cleavage and purification of peptides

To simultaneously cleave the peptide from resin and remove side chain protecting groups a solution of TFA:TIPS:H_2O (95:2.5:2.5) was added to the resin-bound peptide for 2 h. The resin beads were removed via filtration through glass wool and the filtrate was concentrated *in vacuo*. The crude peptide was obtained by precipitation with cold Et_2O. The crude peptide was then dissolved in 10 mL water and purified by HPLC. The following HPLC methods were used for purification. Oxytocin analogues prep-scale (Method A): Zorbax C_8, flow rate 10mL/min, detected at 220 nm. Gradient: Starting from 10% MeCN (0.1% TFA) and 90% water (0.1% TFA) for 5 min, ramping up to 55% MeCN over 20 min, staying at 55% MeCN for 10 min, ramping up to 95% MeCN over 4 min, staying at 95% MeCN for 1 min, ramping down to 10% MeCN over 2 min and staying at 10% MeCN for 3 min. Crotalphine analogues prep-scale (Method B): Phenomenex C_{18} column, flow rate 10 mL/min, detected at 220nm. Gradient: Starting from 5% MeCN (0.1% TFA) and 95% water (0.1% TFA) for 5 min, ramping up to 40% MeCN over 25 min, then ramping up to 95% MeCN over 5 min, staying at 95% MeCN for 5min, ramping down to 5% MeCN over 1 min, then staying at 5% MeCN for 5 min. Oxytocin analogues analytical-scale (Method C): Analytical C_{18} column, flow rate

1.0mL/min, detected at 220nm. Gradient: Starting from 10% MeCN (0.1% TFA) and 90% water (0.1% TFA) for 5 min, ramping up to 55% MeCN over 20 min, staying at 55% MeCN for 10 min, ramping up to 95% MeCN over 4 min, ramping down to 10% MeCN over 2 min and staying at 10% MeCN for 1 min. Crotalphine analogues prep-scale (Method D): Vydac C_{18} column, flow rate 1.0 mL/min, detected at 220nm. Gradient: Starting from 5% MeCN (0.1% TFA) and 95% water (0.1% TFA) for 5 min, ramping up to 40% MeCN over 25 min, then ramping up to 95% MeCN over 5 min, staying at 95% MeCN for 5min, ramping down to 5% MeCN over 1 min, then staying at 5% MeCN for 5 min. Semi-Prep method (Method E): Vydac C_{18} (5 μm, 10 x 250 mm) 5.0 mL/min, detected at 220nm. Gradient: Starting from 10% MeCN (0.1% TFA) and 90% water (0.1% TFA) for 5 min, ramping up to 40% MeCN over 20 min, ramping up to 95% MeCN over 4 min, staying at 95% MeCN for 1 min, ramping down to 10% MeCN over 2 min and staying at 10% MeCN for 3 min. The peptide was collected, concentrated *in vacuo* to remove acetonitrile and lyophilized to give the final product.

Procedure for loading amino acids onto 2-chlorotrityl resin

In a manual SPPS vessel 2-chlorotrityl resin (190 mg, 0.15 mmol) was bubbled with argon in CH_2Cl_2 for 15 min. The resin was then filtered and transferred to a screw-top vial. Diisopropylethyl amine (DIPEA) (0.21 mL, 1.2 mmol) and Fmoc-L-Sac-OH (206 mg, 0.6 mmol) were dissolved in CH_2Cl_2 (3 mL) and added to the resin. The resulting slurry was shaken for 2.5 h, filtered and washed with CH_2Cl_2 (3 x 10 mL). The resin was then capped bubbled with argon in MeOH/DIPEA/ CH_2Cl_2 (10:5:85) for 15 min. The solution

was removed by filtration and the resin then washed with DMF (3 x 10 mL) and CH_2Cl_2 (3 x 10 mL) and dried under argon.

Procedure for loading amino acids onto Wang resin

A 3-necked round bottom flask equipped with a stirring bar was flame dried and cooled in a desiccator under argon. The amino acid (10.0 equiv.) was dissolved in dry CH_2Cl_2 and cooled to 0 ^oC. Diisopropylcarbodiimide (DIC) (5.0 equiv.) was added and the reaction was stirred at 0 ^oC for 20 min. The reaction mixture was then concentrated *in vacuo* and re-dissolved in DMF (10 mL). Wang resin (1.0 equiv.) was added to a manual SPPS vessel and washed with CH_2Cl_2 (2 x 5 mL) and DMF (5 mL). The resin was pre-swollen by bubbling with argon in DMF (5 mL) for 1 h and filtered. The activated anhydride solution was added to the resin followed by 4-dimethylaminopyridine (DMAP) (0.1 equiv.) and bubbled with argon for 2 h. The solvent was removed by filtration and the resin washed with DMF (3 x 5 mL). The resin was then capped by bubbling with argon in 20 % acetic anhydride in DMF (10 mL) for 15 min and filtered. The resin was washed with DMF (3 x 5 mL) and CH_2Cl_2 (3 x 5 mL) and dried under argon.

General procedure for RCM on-resin

To a flame-dried 10 mL round-bottomed flask equipped with a magnetic stirring bar and flushed with argon was added linear Fmoc-1,6-Sac-oxytocin on rink amide resin (110 mg, 0.03 mmol). The resin was suspended in CH_2Cl_2 (5 mL) and Hoveyda-Grubbs 2nd generation catalyst (4.4 mg, 20 mol%) was added. The resulting suspension was

refluxed with gentle stirring under argon for 24 h and cooled to ambient temperature. DMSO (0.02 mL) was added and the reaction stirred for a further 12 h. The resin was then filtered through a manual SPPS vessel and washed successively with MeOH and CH_2Cl_2. A small amount of resin was cleaved using TFA/TIPS/H_2O (95:2.5:2.5) to confirm cyclization had occurred. Fmoc-deprotection was performed by bubbling the resin in a solution of 20 % piperidine in DMF (3 x 10 mL x 5 min) with argon. The resin was washed with DMF (3 x 10 mL), DCM (3 x 10 mL) and dried under argon. The peptide was then cleaved from resin using TFA/TIPS/H_2O (95:2.5:2.5), filtered, concentrated *in vacuo* and precipitated with cold ether. The crude peptide was dissolved in water (4 mL) and acetonitrile (2 mL) and purified by HPLC (Method E).

General procedure for RCM in the *t*-BuOH system

Fmoc-1,6-Sac-oxytocin **3d'** (1.0 mg, 0.8 μmol) and $MgCl_2.6H_2O$ (813 mg, 4.0 mmol) were dissolved in Milli-Q H_2O (7.0 mL) and stirred at ambient temperature. A solution of Hoveyda-Grubbs 2nd Generation Catalyst (0.25 mg, 0.4 μmol) in *t*-BuOH (3.0 mL) was then added and the resulting solution stirred at 37 ^{o}C. The reaction progress was monitored by MALDI and after 3 h the starting material had been completely consumed. The product was then purified by prep-scale C_8 HPLC using Method A. The product containing fractions were pooled, concentrated and lyophilized to yield cyclized Fmoc-1,6-Sac-oxytocin as a fluffy white powder (0.8 mg, 78%).

General procedure for RCM in the micellar system

Hoveyda-Grubbs 2nd Generation Catalyst (12.5 mg, 20.0 μmol) was suspended in 8.2 mM SDS (10.0 mL) and stirred for 10 min. 1,6-Oas-oxytocin (1.0 mg, 1.0 μmol) and $MgCl_2.6H_2O$ (1.0 g, 5.0 mmol) were then added and the resulting green micellar solution stirred at 37 ^oC for 24 h. The reaction mixture was washed with CH_2Cl_2 (3 x 10 mL) and the resulting colourless solution was diluted with Milli-Q water (10.0 mL). The reaction mixture was passed through a prep-scale C_8 HPLC using Method A.

A.4.2 Product characterization

1,6-Agl-oxytocin (A3)

Peptide was isolated as a single peak using C_8 HPLC Method A (16 mg, 16%). Retention time (Method C) = 15.8 min. ^1H NMR (D_2O, 500 MHz): δ 7.10 (d, 2H, *J* = 8.0 Hz, Tyr Ar-H), 6.81 (d, 2H, *J* = 8.0 Hz, Tyr Ar-H), 5.84-5.62 (m, 2H, C<u>H</u>=CH_2), 5.28-5.12 (m, 4H, C<u>H</u>=CH_2), 4.70-4.60 (m, 3H), 4.44-4.38 (m, 1H), 4.33-4.26 (m, 1H), 4.21-4.19 (m, 1H), 4.08-4.02 (m, 2H), 3.88 (app. q, 2H, *J* = 14.4 Hz), 3.80-3.72 (m, 1H), 3.70-3.62 (m, 1H), 3.00-2.90 (m, 2H), 2.78 (dd, 1H, *J* = 15.7, 5.2 Hz), 2.70 (dd, 1H, *J* = 15.7, 8.1 Hz), 2.64-2.60 (m, 2H), 2.55-2.50 (m, 1H), 2.43-2.36 (m, 2H), 2.32 (t, 1H, *J* = 7.7 Hz), 2.28-2.23 (m, 2H), 2.08-1.86 (m, 7H), 1.76-1.56 (m, 6H), 1.46-1.36 (m, 1H), 1.16-1.14 (m, 1H), 0.92-0.80 (m, 12H). MW calculated for $C_{47}H_{73}N_{12}O_{12}$ 997.5465, found *high resolution* (FTICR-ESI-MS) 997.5461 $(M+H)^+$.

1,6-Pgl-oxytocin (A4)

Peptide was isolated as a single peak using C_8 HPLC Method A (16 mg, 16%). Retention time (Method C) = 19.0 min. ^{1}H NMR (D_2O, 500 MHz): δ 7.20 (d, 2H, *J* = 8.1 Hz, Tyr Ar-H), 6.90 (d, 2H, *J* = 8.2 Hz, Tyr Ar-H), 6.00-5.82 (m, 2H, C<u>H</u>=CH_2), 5.14-5.06 (m, 4H, C<u>H</u>=CH_2), 4.77-4.71 (m, 2H), 4.68-4.62 (m, 1H), 4.48 (t, 1H, *J* = 7.0 Hz), 4.42-4.35 (m, 1H), 4.25 (t, 1H, *J* = 7.3 Hz), 4.12 (d, 1H, *J* = 8.7 Hz), 4.06 (t, 1H, *J* = 6.4 Hz), 3.96 (app. q, 2H, *J* = 15.6 Hz), 3.90-3.82 (m, 1H), 3.75-3.68 (m, 1H), 3.10-2.00 (m, 2H), 2.88 (dd, 1H, *J* = 15.5, 5.7 Hz), 2.80 (dd, 1H, *J* = 15.5, 8.2 Hz), 2.40 (t, 2H, *J* = 7.8 Hz), 2.37-2.31 (m, 1H), 2.28-1.40 (m, 27 H), 1.22-1.14 (m, 1H), 1.16-0.87 (m, 12H). MW calculated for $C_{51}H_{81}N_{12}O_{12}$ 1053.6078, found *high resolution* (FTICR-ESI-MS) 1053.6086 $(M+H)^+$.

1,6-Oas-oxytocin (A5)

Peptide was isolated as a single peak using C_8 HPLC Method A (15 mg, 15%). Retention time (Method C) = 18.1 min. ^{1}H NMR (D_2O, 500 MHz): δ 7.10 (d, 2H, *J* = 8.2 Hz, Tyr Ar-H), 6.81 (d, 2H, *J* = 8.3 Hz, Tyr Ar-H), 5.94-5.82 (m, 2H, C<u>H</u>=CH_2), 5.35-5.22 (m, 4H, C<u>H</u>=CH_2), 4.84 (app. t, 1H, *J* = 5.7 Hz), 4.70 (dd, 1H, *J* = 7.9, 5.8 Hz), 4.66 (app. t, 1H, *J* = 7.8 Hz), 4.41 (dd, 1H, *J* = 8.4, 6.0 Hz), 4.34-4.29 (m, 1H), 4.24-4.39 (m, 2H), 4.08-4.00 (m, 5H), 3.94-3.75 (m, 7H), 3.72-3.66 (m, 2H), 2.98 (d, 1H, *J* = 7.6 Hz), 2.80 (dd, 1H, *J* = 15.5, 5.5 Hz), 2.72 (dd, 2H, *J* = 15.4, 8.0 Hz), 2.33 (app. t, 2H, *J* = 7.8 Hz), 2.30-2.24 (m, 1H), 2.08-1.90 (m, 6H), 1.78-1.58 (m, 5H), 1.44-1.36 (m, 1H), 1.14-1.04 (m, 1H), 0.92-0.80 (m, 12H). MW calculated for $C_{49}H_{77}N_{12}O_{14}$ 1057.5677, found *high resolution* (FTICR-ESI-MS) 1057.5675 $(M+H)^+$.

1,6-Sac-oxytocin (A6)

Peptide was isolated as a single peak using C_8 HPLC Method A (15 mg, 14%). Retention time (Method C) = 18.6 min. ^{1}H NMR (D_2O, 500 MHz): δ 7.02 (d, 2H, *J* = 8.4 Hz, Tyr Ar-H), 6.82 (d, 2H, *J* = 8.2 Hz, Tyr Ar-H), 5.76-5.86 (m, 2H, C<u>H</u>=CH_2), 5.14-5.24 (m, 4H, C<u>H</u>=CH_2), 4.78 (t, 1H, *J* = 7.2 Hz), 4.70-4.64 (m, 2H), 4.41 (dd, 1H, *J* = 8.3, 5.5 Hz), 4.34-4.29 (m, 1H), 4.21 (dd, 1H, *J* = 9.2, 5.4 Hz), 4.15 (t, 1H, *J* = 6.4 Hz), 4.04 (d, 1H, *J* = 8.6 Hz), 3.89 (app. q, 2H, *J* = 21.3 Hz), 3.80-3.72 (m, 2H), 3.22 (d, 2H, *J* = 7.1 Hz), 3.18 (d, 2H, *J* = 7.1 Hz), 3.00 (d, 2H, *J* = 7.7 Hz), 2.97-2.92 (m, 3H), 2.83-2.77 (m, 1H), 2.78-2.66 (m, 2H), 2.34 (t, 2H, *J* = 7.6 Hz), 2.31-2.34 (m, 1H), 2.10-1.92 (m, 6H), 1.78-1.58 (m, 5H), 1.42-1.36 (m, 1H), 1.14-1.04 (m, 1H), 0.98-0.80 (m, 12H). MW calculated for $C_{49}H_{77}N_{12}O_{12}S_2$ 1089.5220, found *high resolution* (FTICR-ESI-MS) 1089.5217 $(M+H)^+$.

7,14-Agl-crotalphine (A7)

Peptide was isolated as a single peak using C_{18} HPLC Method B (20 mg, 13%). Retention time (Method D) = 20.9 min. ^{1}H NMR (D_2O, 600 MHz): δ 7.37-7.23 (m, 5H, Phe-ArH), 5.84-5.71 (m, 2H, C<u>H</u>=CH_2), 5.22-5.10 (m, 4H, C<u>H</u>=CH_2), 4.73-4.68 (m, 1H), 4.65 (dd, 1H, *J* = 9.1, 4.9 Hz), 4.46-4.24 (m, 9H), 3.94 (s, 2H), 3.86-3.72 (m, 5H), 3.72-3.62 (m, 3H), 3.16 (dd, 1H, *J* = 13.8, 6.6 Hz), 3.01 (dd, 1H, *J* = 13.8, 9.0 Hz), 2.84 (dd, 1H, *J* = 16.2, 7.8 Hz), 2.75 (dd, 1H, *J* = 15.6, 7.2 Hz), 2.64-1.72 (m, 33H). MW calculated for $C_{66}H_{94}N_{17}O_{25}$ 1524.6601, found *high resolution* (FTICR-ESI-MS) 1524.6591 $(M+H)^+$.

7,14-Pgl-crotalphine (A8)

Peptide was isolated as a single peak using C_{18} HPLC Method B (15 mg, 10%). Retention time (Method D) = 25.3 min. ^{1}H NMR (D_2O, 600 MHz): δ 7.37-7.23 (m, 5H, Phe-ArH), 5.90-5.80 (m, 2H, C<u>H</u>=CH_2), 5.08-4.95 (m, 4H, C<u>H</u>=CH_2), 4.78-4.60 (m, 3H), 4.45-4.37 (m, 4H), 4.30-4.23 (m, 4H), 3.96-3.64 (m, 9H), 3.17 (dd, 1H, *J* = 13.8, 6.6 Hz), 3.01 (dd, 1H, *J* = 13.8, 9.0 Hz), 2.86 (dd, 1H, *J* = 15.6, 6.6 Hz), 2.76 (dd, 1H, *J* = 15.6, 7.2 Hz), 2.48-1.66 (m, 35H), 1.50-1.36 (m, 4H). MW calculated for $C_{70}H_{102}N_{17}O_{25}$ 1580.7227, found *high resolution* (FTICR-ESI-MS) 1580.7229 $(M+H)^+$.

7,14-Oas-crotalphine (A9)

Peptide was isolated as a single peak using C_{18} HPLC Method B (21 mg, 13%). Retention time (Method D) = 21.9 min. ^{1}H NMR (D_2O, 600 MHz): δ 7.32-7.18 (m, 5H, Phe-ArH), 5.90-5.80 (m, 2H, C<u>H</u>=CH_2), 5.28-5.14 (m, 4H, C<u>H</u>=CH_2), 4.72-4.64 (m, 2H), 4.62-4.58 (m, 1H), 4.53 (t, 1H, *J* = 4.2 Hz), 4.41 (t, 1H, *J* = 5.4 Hz), 4.46-4.36 (m, 3H), 4.36-4.30 (m, 1H), 4.28-4.26 (m, 1H), 4.20 (dd, 1H, *J* = 9.0, 4.2 Hz), 4.06-3.60 (m, 18H), 3.01 (dd, 1H, *J* = 13.8, 6.6 Hz), 2.95 (dd, 1H, *J* = 13.8, 9.0 Hz), 2.81 (dd, 1H, *J* = 16.2, 6.6 Hz), 2.73 (dd, 1H, *J* = 16.2, 7.2 Hz), 2.49-1.70 (m, 27H), 1.67-1.75 (m, 1H). MW calculated for $C_{68}H_{98}N_{17}O_{27}$ 1584.6813, found *high resolution* (FTICR-ESI-MS) 1584.6831 $(M+H)^+$.

7,14-Sac-crotalphine (A10)

Peptide was isolated as a single peak using C_{18} HPLC Method B (20 mg, 12%). Retention time (Method D) = 24.1 min. ^{1}H NMR (D_2O, 600 MHz): δ 7.38-7.24 (m, 5H,

Phe-ArH), 5.85-5.75 (m, 2H, C<u>H</u>=CH_2), 5.21-5.13 (m, 4H, C<u>H</u>=CH_2), 4.68-4.66 (m, 1H), 4.54-4.20 (m, 5H), 4.39 (t, 1H, *J* = 6.0 Hz), 4.31 (dd, 2H, *J* = 4.8, 3.6 Hz), 4.25 (dd, 1H, *J* = 9.6, 4.8 Hz), 3.98-3.66 (m, 10H), 3.19 (dd, 4H, *J* = 18.0, 7.2 Hz), 3.16-3.70 (m, 8H), 2.52-1.74 (m, 27H), 1.80-1.75 (m, 1H). MW calculated for $C_{68}H_{98}N_{17}O_{25}S_2$ 1616.6356, found *high resolution* (FTICR-ESI-MS) 1616.6342 $(M+H)^+$.

(*S*)-1-Benzylpyrrolidine-2-carboxylic acid hydrochloride ((*S*)-BP.HCl) (A15)

(*S*)-Proline (**A14**) (17.3 g, 0.12 mol) and KOH pellets (25.4 g, 0.45 mol) were suspended in *i*-PrOH (100 mL) and stirred vigorously at 40 ^oC until complete dissolution. Benzyl bromide (21.4 mL, 0.18 mol) was then added drop wise over 30 min. The orange suspension was stirred at 40 ^oC for a further 6 h and acidified to pH 5 with 6M HCl. The reaction mixture was filtered through a glass fritted filter funnel and the remaining solid washed thoroughly with CH_2Cl_2. The filtrate was then concentrated *in vacuo* to yield a viscous orange oil. Addition of minimal cold acetone lead to the precipitation of the desired product, which was filtered, washed with cold acetone and dried in a vacuum oven to yield (*S*)-BP.HCl **A15** as a white powder (18.9 g, 79%). $[\alpha]_D$ -24.3° (*c* 0.70, H_2O); IR ($CHCl_3$ cast) 3046, 2991, 2969, 2884, 1632 cm^{-1}; ^1H NMR ($CDCl_3$, 400 MHz): δ 8.80 (br s, 1H, COO<u>H</u>), 7.41-7.36 (m, 5H, Ar-H), 4.32 (d, 1H, *J* = 12.7 Hz, PhC<u>H</u>H), 4.12 (d, 1H, *J* = 12.7 Hz, PhCH<u>H</u>), 3.80-3.70 (m, 1H, Pro-H_δ), 3.68-3.54 (m, 1H, Pro-H_α), 2.90-2.84 (m, 1H, Pro-H_δ), 2.40-2.12 (m, 2H, Pro-H_β), 2.08-1.80 (m, 2H, Pro-H_γ); ^{13}C NMR ($(CD_3)_2SO$, 125 MHz): δ 172.2, 135.9, 129.6, 128.3, 127.7, 65.9, 57.2, 52.8, 28.5, 22.7; HRMS (ES) Calcd for $C_{12}H_{14}NO_2[M-H]^-$ 204.1030, found 204.1031.

(*S*)-*N*-(2-benzoylphenyl)-1-benzylpyrrolidine-2-carboxamide ((*S*)-BPB) (17)

(*S*)-BP.HCl (**15**) (6.00 g, 29.2 mmol) was suspended in freshly distilled CH_2Cl_2 (40 mL), stirred under argon at ambient temperature for 5 min and then cooled to -25 ^oC. Thionyl chloride (2.54 mL, 35.0 mmol) was added over 5 min, the reaction mixture warmed to -10 ^oC until all solids dissolved and then cooled to -25 ^oC. A solution of 2-aminobenzophenone (**16**) (6.90 g, 35.0 mmol) in CH_2Cl_2 (40 mL) was then added to the reaction mixture and stirred at ambient temperature for 16 h. A solution of Na_2CO_3 (5.88 g, 55.5 mmol) in water (30 mL) was then added in parts to the green reaction mixture at 0 ^oC. The resulting orange suspension was stirred at 0 ^oC for 5 min at which point it was diluted with CH_2Cl_2 (50 mL) and filtered through a glass fritted filter funnel. The aqueous phased was washed with CH_2Cl_2 (3 x 30 mL) and the combined organic extracts were dried over anhydrous sodium sulfate, filtered and concentrated *in vacuo*. The crude orange oil was purified by flash chromatography (silica gel, 4:1 hexanes / EtOAc) to yield (*S*)-BPB **17** as an orange powder (6.10 g, 54%). $[\alpha]_D$ -131.8° (*c* 0.50, CH_2Cl_2); IR ($CHCl_3$ cast) 3261, 3061, 3028, 2970, 2874, 2808, 1690, 1644 cm^{-1}; ^1H NMR ($(CD_3)_2SO$, 400 MHz): δ 8.28 (d, 1H, Ar-H), 7.76-7.70 (m, 2H, Ar-H), 7.70-7.64 (m, 1H, Ar-H), 7.62-7.52 (m, 3H, Ar-H), 7.49-7.73 (m, 1H, Ar-H), 7.33-7.26 (m, 2H, Ar-H), 7.22-7.06 (m, 4H, Ar-H), 3.73 (dd, 1H, *J* = 12.9, 2.2 Hz, PhC<u>H</u>H), 3.52 (dd, 1H, *J* = 12.9, 2.3 Hz, PhCH<u>H</u>), 3.20-3.13 (m, 1H, Pro-H_α), 3.00-2.92 (m, 1H, Pro-H_δ), 2.38-2.30 (m, 1H, Pro-H_δ), 2.16-2.02 (m, 1H, Pro-H_β), 1.74-1.52 (m, 3H, Pro-H_β, H_γ); ^{13}C NMR ($(CD_3)_2SO$, 125 MHz): δ 197.3, 173.7, 138.7, 138.3, 138.1, 133.4, 133.3, 132.0, 129.4, 129.0, 128.4, 127.4, 126.7, 123.3, 121.6, 67.8, 59.4, 53.9, 30.6, 24.1; HRMS (ES) Calcd for $C_{25}H_{25}N_2O_2[M+H]^+$ 385.1911, found 385.1907.

Nickel(II)(*R*,*E*)-(1-benzylpyrrolidine-2-carbonyl)(2-((carboxylatomethylimino)(phenyl)methyl)phenyl)amide((*S*)-Gly-Ni-BPB) (A18)

(*S*)-BPB (**A17**) (3.00 g, 7.8 mmol), nickel (II) nitrate hexahydrate (4.54 g, 15.6 mmol) and glycine (2.92 g, 39.0 mmol) were dissolved in MeOH (70 mL) at 45 ^{o}C and the green solution was stirred under argon. A solution of KOH (3.06 g, 54.6 mmol) in MeOH (30 mL) was then added and the resulting brown suspension was stirred at 60 ^{o}C for 1 h. The reaction mixture was then cooled to 0 ^{o}C and neutralized with AcOH (3.13 mL, 54.6 mmol). The resulting solution was concentrated *in vacuo* and the crude residue washed several times with water, which was removed be decantation. The crude residue was then purified by flash chromatography (silica gel, 3:1 hexanes / EtOAc $\rightarrow$ 9:1 EtOAc / *i*-PrOH) to yield (*S*)-Gly-Ni-BPB (**A18**) as a red solid (2.33 g, 60%). $[\alpha]_D$ +2076.9° (*c* 0.60, CH_2Cl_2); IR ($CHCl_3$ cast) 3053, 2975, 1674, 1638 cm^{-1}; ^1H NMR ($CDCl_3$, 400 MHz): δ 8.30 (d, 1H, *J* = 8.8 Hz, Ar-H), 8.07 (d, 2H, *J* = 7.1 Hz, Ar-H), 7.58-7.47 (m, 3H, Ar-H), 7.58-7.40 (m, 2H, Ar-H), 7.31 (dd, 1H, *J* = 7.4, 7.4 Hz, Ar-H), 7.21 (dd, 1H, 7.2, 7.2 Hz, Ar-H), 7.10 (d, 1H, *J* = 7.2 Hz, Ar-H), 7.20-6.95 (m, 1H, Ar-H), 6.80 (d, 1H, *J* = 7.0 Hz, Ar-H), 6.75-6.68 (m, 1H, Ar-H), 4.49 (d, 1H, *J* = 12.7 Hz, PhC<u>H</u>H), 3.83-3.64 (m, 4H, PhC<u>H</u>H, Pro-H_δ, Gly-H_α), 3.52-3.42 (m, 1H, Pro-H_α), 3.42-3.28 (m, 1H, Pro-H_δ), 2.62-2.53 (m, 1H, Pro-H_β), 2.36-2.50 (m, 1H, Pro-H_β), 2.21-2.02 (m, 2H, Pro-H_γ); ^{13}C NMR ($CDCl_3$, 125 MHz): δ 181.4, 177.3, 171.7, 142.6, 134.7, 133.3, 133.2, 132.2, 131.8, 129.8, 129.6, 129.4, 129.1, 128.9, 126.3, 125.7, 125.2, 124.3, 120.9, 69.9, 63.1, 61.3, 57.5, 30.8, 23.7; HRMS (ES) Calcd for $C_{27}H_{25}N_3O_3NaNi[M+Na]^+$ 520.1142, found 520.1149.

Nickel(II)((*R*)-1-benzylpyrrolidine-2-carbonyl)(2-((*E*)-((*S*)-1-carboxylatohex-5-enylimino)(phenyl)methyl)phenyl)amide ((*S,S*)-Pgl-Ni-BPB) (A19)

(*S*)-Gly-Ni-BPB (**A8**) (4.00g, 8.0 mmol) and finely ground NaOH (3.20 g, 80.0 mmol) were added to an argon purged flask. DMF (32 mL) was added at once and the reaction mixture was stirred for 5 min. 5-Bromo-pent-1-ene (0.92 mL, 7.8 mmol) was then added at once and the reaction was stirred vigorously for another 5 min. The reaction mixture was then quenched with a mixture of 5% AcOH (320 mL) and benzene (160 mL). The resulting emulsion was filtered through celite, washed with brine (200 mL), dried over anhydrous sodium sulfate, filtered and concentrated *in vacuo* to yield a crude red solid which was purified by flash chromatography (silica gel, 98:2 EtOAc / *i*-PrOH) to yield (*S,S*)-Pgl-Ni-BPB (**A19**) as a red solid (3.80 g, 84%). $[\alpha]_D$ +2547.5° (*c* 0.50, CH_2Cl_2); IR ($CHCl_3$ cast) 3060, 2924, 1676, 1639 cm^{-1}; ^1H NMR ($CDCl_3$, 600 MHz): δ 8.14 (d, 1H, *J* = 8.6 Hz, Ar-H), 8.05 (d, 2H, *J* = 7.4 Hz, Ar-H), 7.52-7.47 (m, 2H, Ar-H), 7.47-7.42 (m, 1H, Ar-H), 7.35 (dd, 2H, *J* = 7.4 Hz, 7.4 Hz, Ar-H), 7.28-7.24 (m, 1H, Ar-H), 7.19 (dd, 1H, *J* = 7.4, 7.4 Hz, Ar-H), 7.14 (dd, 1H, *J* = 7.4, 7.4 Hz, Ar-H), 6.92 (d, 1H, *J* = 7.5 Hz, Ar-H), 6.68-6.61 (m, 2H, Ar-H), 5.77-5.68 (m, 1H, C<u>H</u>=CH_2), 5.20-4.93 (m, 2H, CH=C<u>H_2</u>), 4.54 (d, 1H, *J* = 12.7 Hz, PhC<u>H</u>H), 3.96-3.88 (m, 1H, pGly-H_α), 3.60-3.51 (m, 3H, PhCH<u>H</u>, Pro-H_δ), 3.49-3.44 (m, 1H, Pro-H_α), 2.73-2.81 (m, 1H, Pro-H_β), 2.57-2.48 (m, 1H, Pro-H_β), 2.28-2.18 (m, 1H, pGly-H_β), 2.18-2.10 (m, 1H, Pro-H_γ), 2.10-1.88 (m, 4H, Pro-H_γ, pGly-H_β, pGly-H_δ), 1.76-1.61 (m, 2H, pGly-H_β, pGly-H_δ); ^{13}C NMR ($CDCl_3$, 125 MHz): δ 180.4, 179.4, 170.4, 142.2, 137.8, 133.8, 133.3, 133.2, 132.2, 131.6, 129.7, 128.9, 128.9, 127.6, 127.2, 126.5, 123.7, 120.8, 115.3, 70.4, 70.2, 63.1, 56.9,

34.8, 33.3, 30.8, 24.7, 23.7; HRMS (ES) Calcd for $C_{32}H_{33}N_3O_3NaNi[M+Na]^+$ 588.1768, found 588.1769.

(*S*)-2-aminohept-6-enoic acid (Pgl) (A20)

A solution of (*S,S*)-Pgl-Ni-BPB (**A19**) (3.80g, 6.7 mmol) in MeOH (14 mL) and CH_2Cl_2 (7 mL) was added drop wise to a solution of 3M HCl (14 mL) and MeOH (14 mL) at 60 ^oC and stirred at 60 ^oC for 1 h. The resulting green solution was then concentrated *in vacuo* and co-evaporated with water (10 mL) and concentrated NH_4OH (10 mL). The crude residue washed with CH_2Cl_2 (3 X 50 mL) and then dissolved in water (100 mL). This solution was then concentrated *in vacuo* to approximately 10 mL and loaded unto an ion-exchange column (DOWEX 50Wx2-200 resin), which was pre-washed with water to neutral pH. The column was eluted with water to pH 7 and then with NH_4OH/water (4:1) (10 X 50 mL). Fractions containing the amino acid were determined by ninhydrin staining on a silica TLC plate, combined, concentrated to approximately 10 mL and further purified by the aforementioned method. The fractions containing amino acid were concentrated and lyophilized overnight to yield pentenylglycine (Pgl) (**20**) as a fluffy white solid (450 mg, 47%). $[\alpha]_D$ +15.12° (*c* 1.02, H_2O); IR (KBr disc) 2940, 1580 cm^{-1}; ^1H NMR (D_2O, 400 MHz): δ 5.87 (dddd, 1H, *J* = 17.2, 10.4, 6.7, 6.7 Hz, C<u>H</u>=CH_2), 5.10-5.00 (m, 2H, CH=C<u>H_2</u>), 3.71 (app. t, 1H, *J* = 6.1 Hz, H_α), 2.10 (app. q, 2H, *J* = 7.1 Hz, H_β), 1.88-1.81 (m, 2H, H_δ), 1.51-1.41 (m, 2H, H_γ); ^{13}C NMR (D_2O, 125 MHz): δ 169.8, 133.4, 109.8, 49.5, 27.2, 24.7, 18.3; HRMS (ES) Calcd for $C_7H_{12}NO_2$ $[M-H]^-$ 142.0874, found 142.0873.

(*S*)-2-(((9*H*-fluoren-9-yl)methoxy)carbonylamino)hept-6-enoic acid (Fmoc-Pgl-OH) (A11)

(*S*)-Pentenylglycine (**A20**) (450 mg, 3.1 mmol) and $NaHCO_3$ (791 mg, 9.4 mmol) were dissolved in water (30 mL) and stirred at ambient temperature. A solution of FmocOSu (1.17 g, 3.5 mmol) in THF (30 mL) was then added to the aqueous solution and stirring was continued for an additional 2 h at ambient temperature. The reaction mixture was acidified to pH 1 with 6 M HCl and extracted with EtOAc (4 x 30 mL). The organic phase was dried over anhydrous sodium sulfate, filtered, concentrated *in vacuo* and purified by flash chromatography (silica gel, 97:2:1 CH_2Cl_2 : *i*-PrOH : AcOH), yielding Fmoc-L-Pgl-OH (**A11**) as a white solid (744 mg, 65%). $[\alpha]_D$ -2.4° (*c* 0.5, MeOH); IR ($CHCl_3$ cast) 3317, 3067, 2928, 1718, 1522 cm^{-1}; ^1H NMR ($CDCl_3$, 600 MHz): δ 7.64 (d, 2H, *J* = 7.3 Hz, Fmoc-H), 7.61-7.52 (m, 2H, Fmoc-H), 7.40 (t, 2H, *J* = 7.2 Hz, Fmoc-H), 7.30 (t, 2H, *J* = 7.2 Hz, Fmoc-H), 5.81-5.68 (m, 1H, C<u>H</u>=CH_2), 5.23 (d, 1H, *J* = 8.2 Hz, NH), 5.02 (d, 1H, *J* = 17.1 Hz, CH=C<u>H</u>H), 4.98 (d, 1H, *J* = 10.0 Hz, CH=CH<u>H</u>), 4.56-4.38 (m, 3H, Fmoc CHC<u>H_2</u>, Cys-H_α), 4.23 (t, 1H, *J* = 6.7 Hz, Fmoc C<u>H</u>CH_2), 2.16-2.04 (2H, m, C<u>H_2</u>CH=CH_2), 1.96-1.88 (m, 1H, H_β), 1.76-1.66 (m, 1H, H_β), 1.56-1.42 (m, 2H, H_γ); ^{13}C NMR ($CDCl_3$, 125 MHz): δ 177.2, 156.0, 143.7 (d, rotamers), 141.3, 137.7, 127.7, 127.1, 125.0, 120.0, 115.3, 67.1, 53.6, 47.2, 33.1, 31.7, 24.5; HRMS (ES) Calcd for $C_{22}H_{23}NO_4Na[M+Na]^+$ 388.1519, found 388.1514.

(*S*)-3-(allyloxy)-2-(*tert*-butoxycarbonylamino)propanoic acid (A22)

NaH (2.44 g of a 60% oil dispersion, 61.0 mmol) was suspended in 20 mL of DMF and cooled to 0 ^oC with stirring. A solution of Boc-L-Ser-OH (**A21**) (5.00 g, 24.0 mmol) in

DMF (40 mL) was then added drop wise to the NaH suspension over 30 min using an addition funnel. Allyl bromide (2.0 mL, 24.0 mmol) was then added and the reaction mixture warmed to ambient temperature and stirred for an additional 3 h. The reaction mixture was concentrated *in vacuo* and the resulting residue dissolved in water (40 mL) and washed with EtOAc (2 x 20 mL). The aqueous phase was then acidified to pH 1 with the addition of 6 M HCl and extracted with EtOAc (2 X 40 mL). The organic washings were combined, dried over anhydrous sodium sulfate, filtered and concentrated *in vacuo* to yield crude Boc-L-Oas-OH (**A22**) as a yellow oil that was used in the next step without further purification.

(*S*)-2-(((9*H*-fluoren-9-yl)methoxy)carbonylamino)-3-(allyloxy)propanoic acid (Fmoc-Oas-OH) (A12)

Boc-L-Oas-OH (**A22**) (5.90 g, 24.0 mmol) was dissolved in CH_2Cl_2 (120 mL) and TFA (120 mL) and stirred for 2 h at ambient temperature. The reaction mixture was then concentrated *in vacuo*, co-evaporated with toluene (3 x 10 mL) and the resulting orange TFA salt was dissolved in water (120 mL). $NaHCO_3$ (6.03 g, 120.0 mmol) was added and the solution was stirred at ambient temperature. A solution of FmocOSu (8.90 g, 26.4 mmol) in THF (120 mL) was then added to the aqueous solution and stirring was continued for an additional 2 h at ambient temperature. The reaction mixture was acidified to pH 1 with 6 M HCl and extracted with EtOAc (6 x 50 mL). The organic phase was dried over anhydrous sodium sulfate, filtered, concentrated *in vacuo* and purified by flash chromatography (silica gel, 97:2:1 CH_2Cl_2 : *i*-PrOH : AcOH), yielding Fmoc-L-Oas-OH (**A12**) as a white solid (6.42 g, 73% for 3 steps). $[\alpha]_D$ 10.6° (*c* 0.78, CH_2Cl_2); IR

($CHCl_3$ cast) 3376, 3063, 1766, 1668, 1543 cm^{-1}; ^1H NMR ($CDCl_3$, 600 MHz): δ 7.77 (d, 2H, *J* = 7.5 Hz, Fmoc-H), 7.63-7.50 (m, 2H, Fmoc-H), 7.40 (t, 2H, *J* = 7.4 Hz, Fmoc-H), 7.32 (t, 2H, *J* = 7.4 Hz, Fmoc-H), 5.86 (m, 1H, C<u>H</u>=CH_2), 5.69 (d, 1H, *J* = 7.9 Hz, NH), 5.28 (d, 1H, *J* = 17.3 Hz, CH=CH<u>H</u>), 5.70 (d, 1H, *J* = 10.5 Hz, CH=CH<u>H</u>), 4.58-4.56 (m, 1H, Ser-H_α), 4.46 (dd, 1H, *J* = 10.5, 7.2, Fmoc CHC<u>H</u>H), 4.37 (dd, 1H, *J* = 10.5, 7.4, Fmoc CHCH<u>H</u>), 4.25 (t, 1H, *J* = 7.2 Hz, Fmoc C<u>H</u>CH_2), 4.04 (2H, d, *J* = 5.4 Hz, C<u>H_2</u>CH=CH_2), 3.96 (dd, 1H, *J* = 9.5, 2.9, Ser-H_β), 3.72 (dd, 1H, *J* = 9.7, 3.4, Ser-H_β); ^{13}C NMR ($CDCl_3$, 125 MHz): δ 175.1, 156.2, 143.7 (d, rotamers), 141.3, 133.7, 127.7, 127.1, 125.1, 120.0, 118.0, 72.5, 69.4, 67.3, 54.2, 47.1; HRMS (ES) Calcd for $C_{21}H_{21}NO_5Na[M+Na]^+$ 390.1312, found 390.1307.

(*R*)-2-(((9*H*-fluoren-9-yl)methoxy)carbonylamino)-3-(allylthio)propanoic acid (Fmoc-Sac-OH) (A13)

S-allyl-L-cysteine (Sac) (**A23**) (2.00 g, 12.4 mmol) and $NaHCO_3$ (3.13 g, 37.2 mmol) were dissolved in water (60 mL) and stirred at ambient temperature. A solution of FmocOSu (4.59 g, 13.6 mmol) in THF (60 mL) was then added to the aqueous solution and stirring was continued for an additional 2 h at ambient temperature. The reaction mixture was acidified to pH 1 with 6 M HCl and extracted with EtOAc (4 x 30 mL). The organic phase was dried over anhydrous sodium sulfate, filtered, concentrated *in vacuo* and purified by flash chromatography (silica gel, 97:2:1 CH_2Cl_2 : *i*-PrOH : AcOH), yielding Fmoc-L-Sac-OH (**A13**) as a white solid (1.30 g, 27%). $[\alpha]_D$ -12.2° (*c* 1.00, CH_2Cl_2); IR ($CHCl_3$ cast) 3325, 3065, 1685, 1532 cm^{-1}; ^1H NMR ($CDCl_3$, 600 MHz): δ 7.77 (d, 2H, *J* = 7.6 Hz, Fmoc-H), 7.62-7.60 (m, 2H, Fmoc-H), 7.40 (t, 2H, *J* = 7.4 Hz,

Fmoc-H), 7.31 (t, 2H, *J* = 7.5 Hz, Fmoc-H), 5.76-5.73 (m, 1H, C<u>H</u>=CH_2), 5.64 (d, 1H, *J* = 7.8 Hz, NH), 5.13 (m, 2H, CH=C<u>H_2</u>), 4.60-4.66 (m, 1H, Cys-H_α), 4.44-4.46 (m, 2H, Fmoc CHC<u>H_2</u>), 4.24 (1H, t, *J* = 7.1 Hz, Fmoc C<u>H</u>CH_2), 3.15 (2H, d, *J* = 7.1 Hz, C<u>H_2</u>CH=CH_2), 3.04 (dd, 1H, *J* = 14.2, 4.5, Cys-H_β), 2.94 (dd, 1H, *J* = 14.0, 4.5 Hz, Cys-H_β); ^{13}C NMR ($CDCl_3$, 125 MHz): δ 175.4, 155.9, 143.6 (d, rotamers), 141.3, 133.5, 127.8, 127.1, 125.0, 120.0, 118.2, 67.4, 53.4, 47.1, 35.3, 32.5; HRMS (ES) Calcd for $C_{21}H_{21}NO_4SNa[M+Na]^+$ 406.1083, found 406.1079.

1-Pip-6-Pgl-oxytocin (A24)

Peptide was isolated as a single peak using C_8 HPLC Method A (4 mg, 4%). This was used as a standard to confirm the identity of the hydroamination side-product by LC MS/MS comparison. Retention time (Method C) = 17.4 min. ^{1}H NMR (D_2O, 500 MHz): δ 7.10 (d, 2H, *J* = 8.3 Hz, Tyr Ar-H), 6.80 (d, 2H, *J* = 8.3 Hz, Tyr Ar-H), 5.85 (ddt, 1H, *J* = 17.1, 10.4, 6.6 Hz, C<u>H</u>=CH_2), 5.06 (d, 1H, *J* = 17.3, CH=C<u>H</u>H), 5.00 (d, 1H, *J* = 10.3, CH=CH<u>H</u>), 4.66 (dd, 1H, *J* = 7.8, 6.0 Hz), 4.62 (t, 1H, *J* = 7.8 Hz), 4.58 (dd, 1H, *J* = 8.9, 4.9 Hz), 4.40 (dd, 1H, *J* = 8.1, 5.9 Hz), 4.29 (dd, 1H, *J* = 9.5, 4.9 Hz), 4.20 (t, 1H, *J* = 7.3 Hz), 4.06 (d, 1H, *J* = 8.6 Hz), 3.94-3.82 (m, 4H), 3.80-3.75 (m, 1H), 3.66-3.60 (m, 1H), 3.44 (d, 1H, *J* = 12.7 Hz), 3.02 (td, 1H, *J* = 12.4, 2.1 Hz), 2.97 (d, 2H, 7.8 Hz), 2.79 (dd, 1H, *J* = 15.5, 5.8 Hz), 2.71 (dd, 1H, *J* = 15.5, 8.0 Hz), 2.37-2.22 (m, 4H), 2.19-2.13 (m, 1H), 2.11-1.84 (m, 11 H), 1.80-1.56 (m, 10H), 1.51-1.37 (m, 3H), 1.16-1.08 (m, 1H), 0.96-0.79 (m, 12H). MW calculated for $C_{50}H_{79}N_{12}O_{12}$ 1039.5935, found *high resolution* (FTICR-ESI-MS) 1039.5931 $(M+H)^+$.

Fmoc-1,6-Sac-oxytocin (A25)

Peptide was isolated as a single peak using C_8 HPLC Method A (4 mg, 3%). Retention time (Method C) = 27.2 min. MW calculated for $C_{64}H_{87}N_{12}O_{14}S_2$ 1311.5906, found *high resolution* (FTICR-ESI-MS) 1311.5918 $(M+H)^+$.

Cyclized Fmoc-1,6-Sac-oxytocin (A26)

Peptide was isolated as mixture of isomers C_8 HPLC Method A. Retention time (Method C) = 25.6 min. MW calculated for $C_{62}H_{83}N_{12}O_{14}S_2$ 1283.5588, found *high resolution* (FTICR-ESI-MS) 1283.5593 $(M+H)^+$.

Cyclized 7,14-Sac-crotalphine (A27)

Peptide was isolated as a mixture of isomers using C_{18} HPLC Method B. Retention time (Method D) = 17.7 min. ^{1}H NMR (D_2O, 500 MHz): δ 7.37-7.22 (m, 5H, Phe-ArH), 5.63-5.54 (m, 2H, RC<u>H</u>=C<u>H</u>R'), 4.55-4.38 (m, 6H), 4.33-4.27 (m, 1H), 4.25 (dd, 1H, *J* = 9.3, 4.7 Hz), 4.05-4.00 (m, 1H), 3.98-3.66 (m, 9H), 3.16 (dd, 2H, *J* = 14.1, 6.5 Hz), 3.05-2.75 (m, 7H), 2.50-1.90 (m, 25H), 1.81-1.75 (m, 1H). MW calculated for $C_{66}H_{94}N_{17}O_{25}S_2$ 1588.6043, found *high resolution* (FTICR-ESI-MS) 1588.6053 $(M+H)^+$.

Fmoc-1,6-X-oxytocin (A28)

Peptide was isolated as a single peak using C_{18} HPLC Method E (4.5 mg, 0.03 mmol scale, 13%). Retention time (Method C) = 19.4 min. ^{1}H NMR (D_2O, 600 MHz): δ 7.10 (d, 2H, *J* = 8.7 Hz, Tyr Ar-H), 6.81 (d, 2H, *J* = 8.5 Hz, Tyr Ar-H), 5.14-5.24 (m, 4H, CR<u>H</u>=CR'<u>H</u>), 4.68-4.60 (m, 2H), 4.41-4.39 (m, 1H), 4.32-4.29 (m, 1H), 4.23-4.20 (m,

1H), 4.07-4.05 (m, 2H), 3.89 (app. q, 2H, *J* = 15.8 Hz), 3.77-3.62 (m, 2H), 3.13-3.08 (m, 2H), 2.97 (d, 2H, *J* = 7.7 Hz), 2.82-2.50 (m, 6H), 2.43-2.40 (m, 1H), 2.35-2.32 (m, 2H), 2.28-2.23 (m, 1H), 2.06-1.89 (m, 7H), 1.73-1.59 (m, 4H), 1.45-1.41 (m, 1H), 1.14-1.08 (m, 1H), 0.98-0.80 (m, 12H). MW calculated for $C_{51}H_{80}N_{12}O_{12}S_2$ 1117.5538, found *high resolution* (HRMS-ESI-MS) 1117.5533 $(M+H)^+$.

7,14-X-crotalphine (A29)

Peptide was isolated as a single peak using C_{18} HPLC Method B (8 mg, 0.03 mmol sacle, 12%). Retention time (Method D) = 25.3 min. ^{1}H NMR (D_2O, 600 MHz): δ 7.36-7.24 (m, 5H, Phe-ArH), 5.63-5.49 (m, 4H, RCH=CHR'), 4.71 (t, 1H, *J* = 6.7 Hz), 4.66 (dd, 1H, *J* = 9.0, 4.8 Hz), 4.45-4.42 (m, 2H), 4.41-4.37 (m, 2H), 4.34-4.28 (m, 3H), 4.25 (dd, 1H, *J* = 9.3, 4.7 Hz), 3.92-3.96 (m, 2H), 3.85-3.64 (m, 7H), 3.16 (dd, 1H, *J* = 13.8, 7.0 Hz), 3.09 (dd, 2H, *J* = 15.3, 6.9 Hz), 3.01 (dd, 1H, *J* = 13.8, 9.0 Hz), 2.84 (dd, 1H, *J* = 15.8, 6.1 Hz), 2.76 (dd, 1H, *J* = 15.8, 7.6 Hz), 2.60-1.90 (m, 35H), 1.79-1.75 (m, 1H). MW calculated for $C_{70}H_{99}N_{17}O_{25}S_2$ 820.8225, found *high resolution* (HRMS-ESI-MS) 820.8222 $(M-2H)^{-2}$.

(*S*)-methyl-2-(((9*H*-fluoren-9-yl)methoxy)carbonylamino)pent -4-enoate (A32)

Fmoc-L-Agl-OH (**A31**) (1.00 g, 2.96 mmol) was dissolved in MeOH (7 mL) and cooled to 0 °C. TMSCl (1.2 mL, 9.28 mmol) was added and the resulting solution stirred at 0 °C for 1 h and then at ambient temperature for 16 h. The reaction mixture was concentrated *in vacuo* and re-suspended in EtOAc (10 mL) and water (10 mL). The layers were separated and the water extracted with EtOAc (2 x 10 mL). The EtOAc

fractions were combined, washed with brine (5 mL), dried over anhydrous sodium sulfate, filtered and concentrated *in vacuo* to yield the methyl ester **A32** as a white solid (1.04 g, quant.) $[\alpha]_D$ +7.80° (*c* 0.40, CH_2Cl_2); IR (KBr disc) 3340, 3067, 2952, 1724, 1526 cm^{-1}; ^1H NMR ($CDCl_3$, 600 MHz): δ 7.77 (d, 2H, *J* = 7.5, Fmoc-H), 7.6 (m, 2H, Fmoc-H), 7.41 (app. t, 2H, *J* = 7.4, Fmoc-H), 7.33 (app. t, 2H, *J* = 7.3, Fmoc-H), 5.74-5.68 (m, 1H, C<u>H</u>=CH_2), 5.35-5.34 (m, 1H, NH), 5.17-5.13 (m, 2H, CH=C<u>H_2</u>), 4.53-4.49 (m, 1H, Fmoc-C<u>H</u>CH_2), 4.41-4.40 (m, 2H, Fmoc-CHC<u>H_2</u>), 4.26-4.23 (m, 1H, H_α), 3.74 (s, 3H, OC<u>H_3</u>), 2.63-2.52 (m, 2H, H_β); ^{13}C NMR ($CDCl_3$, 125 MHz): δ 172.2, 155.7, 143.9, 143.8, 141.3, 132.1, 127.7, 127.1, 125.1, 120.0, 119.4, 67.1, 53.3, 52.4, 47.2, 36.8; HRMS (ES) Calcd for $C_{21}H_{21}NO_4Na$ $[M+Na]^+$ 374.1357, found 374.1363.

(*S*)-methyl-2-(((9*H*-fluoren-9-yl)methoxy)carbonylamino)-6-(methylthio)hex-4-enoate (A33)

Fmoc-L-Agl-OMe (**A32**) (1.00 g, 2.85 mmol) was added to a flame-dried flask under a blanket of argon and dissolved in dry CH_2Cl_2 (12 mL, 0.25 M). Allyl methyl sulfide (0.62 mL, 5.70 mmol) was added, followed by the addition of Hoveyda-Grubbs 2nd generation catalyst (182 mg, 10 mol %) in parts to avoid excessive effervescence. The resulting green solution was refluxed under argon for 24 h, concentrated *in vacuo* and purified by column chromatography (silica gel, 7:1 hexanes / EtOAc) to yield methyl ester **A33** as a yellow oil and mixture of *E*/*Z* isomers (750 mg, 64%). $[\alpha]_D$ +21.97° (*c* 0.83, CH_2Cl_2); IR (KBr disc) 3335, 3065, 2951, 1722, 1520 cm^{-1}; ^1H NMR ($CDCl_3$, 500 MHz): δ 7.77 (d, 2H, *J* = 7.5, Fmoc-H), 7.6 (m, 2H, Fmoc-H), 7.40 (app. t, 2H, *J* = 7.5, Fmoc-H), 7.32 (app. t, 2H, *J* = 7.5, Fmoc-H), 5.55-5.36 (m, 2H, RC<u>H</u>=C<u>H</u>R'), 5.32 (d, 1H, *J* = 8.0 Hz,

NH), 4.48-4.44 (m, 1H, Fmoc-C<u>H</u>CH_2), 4.40 (d, 2H, *J* = 7.1 Hz, Fmoc-CHC<u>H_2</u>), 4.23 (t, *J* = 7.0 Hz, 1H, H_α), 3.76-3.74 (m, 3H, OC<u>H_3</u>), 3.11-3.02 (m, 2H, H_ε), 2.64-2.49 (m, 2H, H_β), 2.04-2.00 (m, 3H, SC<u>H_3</u>); ^{13}C NMR ($CDCl_3$, 125 MHz): δ 172.2, 155.7, 143.9, 143.8, 141.3, 130.9, 127.7, 127.1, 126.3, 125.1, 120.0, 67.1, 53.5, 52.5, 47.2, 35.7, 35.3, 30.0, 14.4; HRMS (ES) Calcd for $C_{23}H_{25}NO_4SNa$ $[M+Na]^+$ 434.1385, found 434.1385.

(*S*)-2-(((9*H*-fluoren-9-yl)methoxy)carbonylamino)-6-(methylthio)hex-4-enoic acid (Fmoc-X-OH) (A30)

Methyl ester **19** (680 mg, 1.65 mmol) was dissolved in CH_2Cl_2 (2 mL), *i*-PrOH (22.5 mL) and water (10.5 mL). $CaCl_2.2H_2O$ (4.11 mg, 28.0 mmol) was then added and the reaction mixture stirred until all solids had dissolved. 0.5 M NaOH (6.8 mL) was added and the resulting suspension stirred for 75 min at ambient temperature. The reaction mixture was concentrated to remove *i*-PrOH, acidified to pH 1 with 6M HCl (~ 25 drops) and washed with EtOAc (2 x 40 mL). The EtOAc extracts were combined, dried over anhydrous Na_2SO_4, filtered and concentrated *in vacuo* to yield the Fmoc amino acid **20** as a white solid (530 mg, 81 %). $[\alpha]_D$ +13.31° (*c* 0.40, CH_2Cl_2); IR (KBr disc) 3313, 3065, 2916, 1721, 1523 cm^{-1}; ^{1}H NMR ($CDCl_3$, 400 MHz): δ 7.77 (d, 2H, *J* = 7.5, Fmoc-H), 7.6 (m, 2H, Fmoc-H), 7.40 (app. t, 2H, *J* = 7.3, Fmoc-H), 7.32 (app. t, 2H, *J* = 7.4, Fmoc-H), 5.62-5.40 (m, 2H, RC<u>H</u>=C<u>H</u>R'), 5.30 (d, 1H, *J* = 8.0 Hz, NH), 4.57-4.40 (m, 3H, Fmoc-C<u>H</u>CH_2, Fmoc-CHC<u>H_2</u>), 4.23 (t, *J* = 6.6 Hz, 1H, H_α), 3.13-3.04 (m, 2H, H_ε), 2.62-2.53 (m, 2H, H_β), 2.04-1.98 (m, 3H, SC<u>H_3</u>); ^{13}C NMR ($CDCl_3$, 125 MHz): δ 175.8, 155.9, 143.8, 143.7, 141.3, 131.2, 127.8, 127.1, 126.0, 125.1, 120.0, 67.2, 53.3, 47.1,

35.7, 35.0, 14.4; HRMS (ES) Calcd for $C_{22}H_{23}NO_4SNa$ $[M+Na]^+$ 420.1240, found 420.1233.

Cyclized *cis*-1,6-Agl-oxytocin (A34)

The stereochemistry was determined to be *cis* by comparison of the alkene splitting pattern with previously published spectra.[7a] Peptide was isolated as a single peak using C_{18} HPLC Method E (0.7 mg, 0.03 mmol scale, 2.4% overall yield). Retention time (Method C) = 15.5 min. ^{1}H NMR (D_2O, 600 MHz): δ 7.20 (d, 2H, *J* = 8.4 Hz, Tyr Ar-H), 6.9 (d, 2H, *J* = 8.4 Hz, Tyr Ar-H), 5.68-5.64 (m, 1H, RC<u>H</u>=CHR'), 5.60-5.56 (m, 1H, RC<u>H</u>=CHR'), 4.64-4.62 (m, 1H), 4.44-4.42 (m, 2H), 4.31-4.26 (m, 3H), 4.08-4.04 (m, 2H), 3.90 (m, 2H), 3.73-3.60 (m, 2H), 3.17 (dd, 1H, *J* = 14.4, 6.1 Hz), 3.00 (m, dd, 1H, *J* = 14.3, 8.6 Hz), 2.87-2.71 (m, 6H), 2.53-2.47 (m, 2H), 2.43-2.26 (m, 6H), 2.09-1.89 (m, 9H), 1.70-1.60 (m, 5H), 1.27-1.20 (m, 1H), 0.94-0.87 (m, 12H). MW calculated for $C_{45}H_{69}N_{12}O_{12}$ 969.5152, found *high resolution* (FTICR-ESI-MS) 969.5144 $(M+H)^+$.

Cyclized *trans*-1,6-Agl-oxytocin (A35)

The stereochemistry was determined to be *trans* by comparison of the alkene splitting pattern with previously published spectra.[7a] Peptide was isolated as a single peak using C_{18} HPLC Method E (0.8 mg, 0.03 mmol scale, 2.8% overall yield). Retention time (Method C) = 16.0 min. ^{1}H NMR (D_2O, 600 MHz): δ 7.21 (d, 2H, *J* = 8.5 Hz, Tyr Ar-H), 6.9 (d, 2H, *J* = 8.4 Hz, Tyr Ar-H), 5.65 (dt, 1H, *J* = 15.1, 7.4 Hz, RC<u>H</u>=CHR'), 5.53 (dt, 1H, *J* = 14.7, 7.4 Hz, RCH=C<u>H</u>R'), 4.71-4.68 (m, 1H), 4.64-4.62 (m, 1H), 4.44-4.41 (m, 1H), 4.31-4.28 (m, 1H), 4.13-4.10 (m, 2H), 4.00 (d, 1H, *J* = 6.2 Hz), 3.90 (app. q, 2H, *J* =

17.6 Hz), 3.73-3.60 (m, 2H), 3.14 (dd, 1H, *J* = 14.4, 7.1 Hz), 3.04-2.95 (m, 2H), 2.79-2.71 (m, 2H), 2.64-2.59 (m, 1H), 2.55-2.50 (m, 1H), 2.45-2.27 (m, 6H), 2.11-1.98 (m, 5H), 1.92-1.85 (m, 2H), 1.70-1.60 (m, 5H), 1.39-1.34 (m, 1H), 1.16-1.13 (m, 1H), 0.94-0.87 (m, 12H). MW calculated for $C_{45}H_{69}N_{12}O_{12}$ 969.5153, found *high resolution* (FTICR-ESI-MS) 969.5144 $(M+H)^+$.

Cyclized 1,6-Pgl-oxytocin (A36)

Peptide was isolated as a mixture of isomers using C_8 HPLC Method A (1.5 mg, 0.03 mmol scale, 5% overall yield). Retention time (Method C) = 16.9 min. ^{1}H NMR (D_2O, 600 MHz): δ 7.20 (d, 2H, *J* = 8.6 Hz, Tyr Ar-H), 6.84 (d, 2H, *J* = 8.6 Hz, Tyr Ar-H), 5.53-5.49 (m, 1H, RC<u>H</u>=CHR'), 5.45-5.40 (m, 1H, RC<u>H</u>=CHR'), 4.89-5.87 (m, 1H), 4.52-4.50 (m, 1H), 4.44-4.42 (m, 1H), 4.29-4.27 (m, 1H), 4.15-4.13 (m, 1H), 3.97-3.81 (m, 6H), 3.67-3.62 (m, 1H), 3.10 (dd, 1H, *J* = 14.3, 6.3 Hz), 3.04 (dd, 1H, *J* = 16.8, 4.1 Hz), 2.92 (dd, 1H, *J* = 14.2, 9.0 Hz), 2.78 (dd, 1H, *J* = 16.2, 10.2 Hz), 2.42-2.24 (m, 4H), 2.08-1.53 (m, 27 H), 1.50-1.40 (m, 2H), 1.29-1.21 (m, 2H), 0.93-0.87 (m, 12H). MW calculated for $C_{49}H_{77}N_{12}O_{12}$ 1025.5778, found *high resolution* (FTICR-ESI-MS) 1025.5781 $(M+H)^+$.

Cyclized 1,6-Oas-oxytocin (A37)

Peptide was isolated as a mixture of isomers using C_8 HPLC Method A (2.5 mg, 0.03 mmol scale, 8% overall yield). Retention time (Method C) = 16.6 min. ^{1}H NMR (D_2O, 600 MHz): δ 7.20 (d, 2H, *J* = 8.5 Hz, Tyr Ar-H), 6.85 (d, 2H, *J* = 8.4 Hz, Tyr Ar-H), 5.77-5.70 (m, 2H, RC<u>H</u>=C<u>H</u>R'), 4.85-4.80 (m, 2H), 4.46-4.43 (m, 1H), 4.31-4.28 (m, 2H), 4.16-3.97 (m, 9H), 3.93-3.69 (m, 9H), 3.15 (dd, 1H, *J* = 14.5, 5.6 Hz), 3.00-2.92 (m, 2H),

2.82 (dd, 1H, *J* = 16.0, 10.0 Hz), 2.43-2.27 (m, 5H), 2.06-1.91 (m, 6H), 1.68-1.59 (m, 5H), 1.42-1.39 (m, 1H), 1.22-1.15 (m, 1H), 0.94-0.82 (m, 12H). MW calculated for $C_{47}H_{73}N_{12}O_{14}$ 1029.5364, found *high resolution* (FTICR-ESI-MS) 1029.5360 $(M+H)^+$.

Cyclized 1,6-Sac-oxytocin (A38)

Peptide was isolated as a mixture of isomers using C_8 HPLC Method A (2 mg, 0.03 mmol scale, 6%). Retention time (Method C) = 18.0 min. ^{1}H NMR (D_2O, 600 MHz): δ 7.21 (d, 2H, *J* = 8.5 Hz, Tyr Ar-H), 6.86 (d, 2H, *J* = 8.6 Hz, Tyr Ar-H), 5.66-5.60 (m, 2H, RC<u>H</u>=C<u>H</u>R'), 4.84-4.80 (m, 1H), 4.46 (dd, 1H, *J* = 8.6, 5.2 Hz), 4.32 (dd, 1H, *J* = 10.0, 4.5 Hz), 4.16 (t, 1H, *J* = 6.1 Hz), 4.12 (dd, 1H, *J* = 8.5, 5.4 Hz), 4.03 (d, 1H, *J* = 6.0 Hz), 3.90 (app. q, 2H, *J* = 21.5 Hz), 3.82-3.72 (m, 2H), 3.26-3.14 (m, 4H), 3.12-3.08 (m, 1H), 3.01-2.92 (m, 5H), 2.83-2.76 (m, 2H), 2.41-2.26 (m, 4H), 2.07-1.89 (m, 8H), 1.87-1.81 (m, 1H), 1.71-1.59 (m, 4H), 1.42-1.35 (m, 1H), 1.21-1.15 (m, 1H), 0.95-0.86 (m, 12H). MW calculated for $C_{47}H_{73}N_{12}O_{12}S_2$ 1061.4907, found *high resolution* (FTICR-ESI-MS) 1061.4905 $(M+H)^+$.

Cyclized 7,14-Pgl-crotalphine (A39)

Peptide was isolated as a mixture of isomers peak using C_{18} HPLC Method B. Retention time (Method D) = 20.8 min. MW calculated for $C_{68}H_{98}N_{17}O_{25}$ 1552.6901, found *high resolution* (FTICR-ESI-MS) 1552.6916 $(M+H)^+$.

Cyclized 7,14-Oas-crotalphine (A40)

Peptide was isolated as a mixture of isomers using C_{18} HPLC Method B. Retention time (Method D) = 18.6 min. MW calculated for $C_{66}H_{94}N_{17}O_{27}$ 1556.6500, found *high resolution* (FTICR-ESI-MS) 1556.6479 $(M+H)^+$.

A.5. References

A1 Woycechowsky, K. J.; Raines, R. T. *Curr. Opin. Chem. Biol*. **2000**, *4*, 533–539.

A2 Daly, N. L.; Rosengren, K. J.; Craik, D. J. Adv. *Drug Delivery Rev*. **2009**, *61*, 918–930.

A3 Walewska, A.; Skalicky, J. J.; Davis, D.R.; Zhang, M. M.; Lopez-Vera, E.; Watkins, M.; Han, T. S.; Yoshikami, D.; Olivera, B. M.; Bulaj, G. *J. Am. Chem. Soc.* **2008**, *130*, 14280–14286.

A4 Almeida, A. M.; Li, R.; Gellman, S. H. *J. Am. Chem. Soc.* **2012**, *134*, 75-78.

A5 Liu, H.; Boudreau, M. A.; Zheng, J.; Whittal, R. M.; Austin, P.; Roskelley, C. D.; Roberge, M.; Andersen, R. J.; Vederas, J. C. *J. Am. Chem. Soc*. **2010**, *132*, 1486–1487.

A6 Lehninger, A. L.,; Nelson, D. L.,; Cox, M., *Principles of Biochemistry*, 2nd ed.; Worth Publishers, Inc.: New York, New York, 1993; pp 750-752.

A7 Sweetman, S. C. *Martindale: The Complete Drug Reference*, 34th ed.; Pharmaceutical Press: London, 2004.

A8 Gutierrez, V. P.; Zambelli, V. O.; Picolo, G.; Chacur, M.; Sampaio, S. C.; Brigatte, P.; Konno, K.; Cury, Y. Behavioural Pharmacol. **2012**, *23*, 14–24.

A9 Konno, K.; Picolo, G.; Gutierrez, V. P.; Brigatte, P.; Zambelli, V. O.; Camargo, A. C. M.; Cury, Y. *Peptides* **2008**, *29*, 1293-1304.

A10 Huang, Z.; Derksen, D. J.; Vederas, J. C. *Org. Lett.* **2010**, *12*, 2282-2285.

A11 Knerr, P.J.; Tzekou, A.; Ricklin, D.; Qu, H.; Chen, H.; van der Donk, W. A.; Lambris, J. D. *ACS Chem. Biol*. **2011**, *6*, 753–760 and references therein.

A12 Binder, J. B.; Raines, R. T. *Curr. Opin. Chem. Biol.* **2008**, *12*, 767–773.

A13 Liskamp, R. M. J.; Rijkers, D. T. S.; Kruijtzer, J. A. W.; Kemmink, J. *ChemBioChem* **2011**, *12*, 1626-1653.

A14 Holland-Nell, K.; Meldal, M. *Angew. Chem. Int. Ed*. **2011**, *50*, 5204-5206.

A15 Malcor, J.-D.; Payrot, N.; David, M.; Faucon, A.; Abouzid, K.; Jacquot, G.; Floquet, N.; Debarbieux, F.; Rougon, G.; Martinez, J.; Khrestchatisky, M.; Vlieghe, P.; Lisowski, V. *J. Med. Chem*. **2012**, *55*, 2227-2241.

A16 de Araujo, A. D.; Mobli, M.; King, G. F.; Alewood, P. F. *Angew. Chem. Int. Ed.* **2012**, DOI: 10.1002/anie.201204229.

A17 Dekan, Z.; Vetter, I.; Daly, N. L.; Craik, D. J.; Lewis, R. J.; Alewood, P. F. *J. Am. Chem. Soc.* **2011**, *133*, 15866-15869.

A18 Miller, S. J.; Blackwell, H. E.; Grubbs, R. H. *J. Am. Chem. Soc.* **1996**, *118*, 9606-9614.

A19 Williams, R. M.; Liu, J. *J. Org. Chem.* **1998**, *63*, 2130-2132.

A20 Gao, Y.; Lane-Bell, P.; Vederas, J. C. *J. Org. Chem.* **1998**, *63*, 2133-2143.

A21 Stymiest, J. L.; Mitchell, B. F.; Wong S.; Vederas, J. C. *Org. Lett.* **2003**, *5*, 47-49.

A22 Stymiest, J. L.; Mitchell, B. F.; Wong, S.; Vederas, J. C. *J. Org. Chem.* **2005**, *70*, 7799-7809.

A23 Hossain, M. A.; Rosengren, K. J.; Zhang, S.; Bathgate, R. A. D.; Tregear, G. W.; van Lierop, B. J.; Robinson, A. J.; Wade, J. D. *Org. Biomol. Chem.* **2009**, *7*, 1547-1553.

A24 Andersson, H.; Demaegdt, H.; Johnsson,A.; Vauquelin, G.; Lindeberg, G.; Hallberg, M.; Érdélyi, M.; Karlén; Hallberg, A. *J. Med. Chem.* **2011**, *54*, 3779-3792.

A25 Mulder, M. P. C.; Kruijtzer, J. A. W.; Breukink, E. J.; Kemmink, J.; Pieters, R. J.; Liskamp, R. M. J. *Bioorg. Med. Chem*. **2011**, *19*, 6505-6517.

A26 García-Aranda, M. I.; Marrero, P.; Gautier, B.; Martín-Martínez, M.; Inguimbert, N.; Vidal, M.; García-López, M. T.; Jiménez, M. A.; González-Muñiz, R.; Pérez de Vega, M. *J. Bioorg. Med. Chem.* **2011**, *19*, 1978-1986.

A27 Pérez de Vega, M. J.; García-Aranda, M. I.; González-Muñiz, R. *Med. Res. Rev*. **2011**, *31*, 677-715.

A28 Henchey, L. K.; Jochim, A. L.; Arora, P. S. *Curr. Opin. Chem. Biol.* **2008**, *12*, 692-697.

A29 Reichwein, J. F.; Versluis, C.; Liskamp, R. M. J. *J. Org. Chem.* **2000**, *65*, 6187-6195.

A30 Schafmeister, C. E.; Po, J.; Verdine, G. L. *J. Am. Chem. Soc.* **2000**, *122*, 5891-5892.

A31 Schmiedeberg, N.; Kessler, H.; *Org. Lett.* **2002**, *4*, 59-62. (b) Jarvo, E. R.; Copeland, G. T.; Papaioannou, N.; Bonitatebus, P. J., Jr.; Miller, S. J. *J. Am. Chem. Soc.* **1999**, *121*, 11638-11643.

A32 Baron, A.; Verdié, P.; Martinez, J.; Lamaty, F. J. Org. Chem. **2011**, *76*, 766-772.

A33 Heapy, A. M.; Williams, G. M.; Fraser, J. D.; Brimble, M. A. *Org. Lett.* **2012**, *14*, 878-881.

A34 Derksen, D. J.; Stymiest, J. L.; Vederas, J. C. *J. Am. Chem. Soc*. **2006**, *128*, 14252-14253.

A35 Dinger, M. B.; Mol, J. C. *Organometallics* **2003**, *22*, 1089-1095.

A36 Dinger, M. B.; Mol, J. C. *Eur. J. Inorg. Chem.* **2003**, 2827-2823.

A37 Lynn, D. M.; Mohr, B.; Grubbs, R. H.; Henling, L. M.; Day, M. W. *J. Am. Chem. Soc.* **2000**, *122*, 6601-6609.

A38 Hong, S. H.; Grubbs, R. H. *J. Am. Chem. Soc.* **2006**, *128*, 3508-3509.

A39 Jordan, J. P.; Grubbs, R. H. *Angew. Chem. Int. Ed.* **2007**, *46*, 5152-5155.

A40 Lipshutz, B. H.; Aguinaldo, G. T.; Ghorai, S.; Voigtritter, K. *Org. Lett.* **2008**, *10*, 1325-1328.

A41 Lipshutz, B. H.; Ghorai, S.; Leong, W. W. Y.; Taft, B. R. *J. Org. Chem.* **2011**, *76*, 5061-5073.

A42 Lin, Y. A.; Chalker, J. M.; Floyd, N.; Bernardes, G. J. L.; Davis, B. G. *J. Am. Chem. Soc.* **2008**, *130*, 9642-9643.

A43 Lin, Y. A.; Chalker, J. M.; Davis, B. G. *ChemBioChem* **2009**, *10*, 959-969.

A44 Lin, Y. A.; Chalker, J. M.; Davis, B. G. *J. Am. Chem. Soc.* **2010**, *132*, 16805-16811.

A45 Ai, H.; Shen, W.; Brustad, E.; Schultz, P. G. *Angew. Chem. Int. Ed.* **2010**, *49*, 935-937.

A46 Belokon, Y. N.; Tararov, V. I.; Maleev, V. I.; Savel'eva, T. F.; Ryzhov, M. G. *Tetrahedron Asymmetry* **1998**, *9*, 4249-5252.

A47 Pascal, R.; Sola, R. *Tetrahedron Lett.* **1998**, *39*, 5031-5034.